

February 2009

Revision 0

# MAGNASTOR<sup>®</sup>

(Modular Advanced Generation  
Nuclear All-purpose STORAGE)

---

## FINAL SAFETY ANALYSIS REPORT

Docket No. 72-1031



List of Effective Pages

Chapter 1

Page 1-i ..... Revision 0  
Page 1-1 ..... Revision 0  
Page 1.1-1 thru 1.1-4..... Revision 0  
Page 1.2-1 ..... Revision 0  
Page 1.3-1 thru 1.3-15..... Revision 0  
Page 1.4-1 ..... Revision 0  
Page 1.5-1 ..... Revision 0  
Page 1.6-1 thru 1.6-2..... Revision 0  
Page 1.7-1 thru 1.7-2..... Revision 0  
Page 1.8-1 ..... Revision 0

16 drawings (see Section 1.8)

Chapter 2

Page 2-i thru 2-ii ..... Revision 0  
Page 2-1 ..... Revision 0  
Page 2.1-1 thru 2.1-5..... Revision 0  
Page 2.2-1 thru 2.2-7..... Revision 0  
Page 2.3-1 thru 2.3-8..... Revision 0  
Page 2.4-1 thru 2.4-7..... Revision 0  
Page 2.5-1 ..... Revision 0  
Page 2.6-1 thru 2.6-2..... Revision 0

Chapter 3

Page 3-i thru 3-viii ..... Revision 0  
Page 3-1 ..... Revision 0  
Page 3.1-1 thru 3.1-5..... Revision 0  
Page 3.2-1 thru 3.2-2..... Revision 0  
Page 3.3-1 ..... Revision 0  
Page 3.4-1 thru 3.4-26..... Revision 0  
Page 3.5-1 thru 3.5-27..... Revision 0  
Page 3.6-1 thru 3.6-12..... Revision 0  
Page 3.7-1 thru 3.7-70..... Revision 0  
Page 3.8-1 thru 3.8-10..... Revision 0  
Page 3.9-1 thru 3.9-2..... Revision 0  
Page 3.10-1 ..... Revision 0  
Page 3.10.1-1 thru 3.10.1-27..... Revision 0  
Page 3.10.2-1 thru 3.10.2-27..... Revision 0  
Page 3.10.3-1 thru 3.10.3-23..... Revision 0  
Page 3.10.4-1 thru 3.10.4-14..... Revision 0  
Page 3.10.5-1 thru 3.10.5-2..... Revision 0  
Page 3.10.6-1 thru 3.10.6-36..... Revision 0

Page 3.10.7-1 thru 3.10.7-2..... Revision 0  
Page 3.10.8-1 thru 3.10.8-8..... Revision 0  
Page 3.10.9-1 thru 3.10.9-11..... Revision 0

Chapter 4

Page 4-i thru 4-iv ..... Revision 0  
Page 4-1 ..... Revision 0  
Page 4.1-1 thru 4.1-6..... Revision 0  
Page 4.2-1 ..... Revision 0  
Page 4.3-1 ..... Revision 0  
Page 4.4-1 thru 4.4-59..... Revision 0  
Page 4.5-1 thru 4.5-2..... Revision 0  
Page 4.6-1 thru 4.6-4..... Revision 0  
Page 4.7-1 thru 4.7-2..... Revision 0  
Page 4.8-1 ..... Revision 0  
Page 4.8.1-1 thru 4.8.1-10..... Revision 0  
Page 4.8.2-1 thru 4.8.2-8..... Revision 0  
Page 4.8.3-1 thru 4.8.3-9..... Revision 0

Chapter 5

Page 5-i thru 5-viii ..... Revision 0  
Page 5-1 ..... Revision 0  
Page 5.1-1 thru 5.1-6..... Revision 0  
Page 5.2-1 thru 5.2-11..... Revision 0  
Page 5.3-1 thru 5.3-6..... Revision 0  
Page 5.4-1 thru 5.4-5..... Revision 0  
Page 5.5-1 thru 5.5-17..... Revision 0  
Page 5.6-1 thru 5.6-13..... Revision 0  
Page 5.7-1 thru 5.7-3..... Revision 0  
Page 5.8-1 ..... Revision 0  
Page 5.8.1-1 thru 5.8.1-4..... Revision 0  
Page 5.8.2-1 thru 5.8.2-13..... Revision 0  
Page 5.8.3-1 thru 5.8.3-31..... Revision 0  
Page 5.8.4-1 thru 5.8.4-30..... Revision 0  
Page 5.8.5-1 thru 5.8.5-9..... Revision 0  
Page 5.8.6-1 thru 5.8.6-2..... Revision 0  
Page 5.8.7-1 thru 5.8.7-41..... Revision 0  
Page 5.8.8-1 thru 5.8.8-56..... Revision 0  
Page 5.8.9-1 thru 5.8.9-64..... Revision 0  
Page 5.8.10-1 thru 5.8.10-5..... Revision 0  
Page 5.8.11-1 thru 5.8.11-42..... Revision 0  
Page 5.8.12-1 thru 5.8.12-3..... Revision 0

List of Effective Pages (cont'd)

Chapter 6

Page 6-i thru 6-iv ..... Revision 0  
Page 6-1 ..... Revision 0  
Page 6.1-1 thru 6.1-6..... Revision 0  
Page 6.2-1 thru 6.2-5..... Revision 0  
Page 6.3-1 thru 6.3-9..... Revision 0  
Page 6.4-1 thru 6.4-8..... Revision 0  
Page 6.5-1 thru 6.5-7..... Revision 0  
Page 6.6-1 ..... Revision 0  
Page 6.7-1 ..... Revision 0  
Page 6.7.1-1 thru 6.7.1-37..... Revision 0  
Page 6.7.2-1 thru 6.7.2-5..... Revision 0  
Page 6.7.3-1 thru 6.7.3-16..... Revision 0  
Page 6.7.4-1 thru 6.7.4-44..... Revision 0  
Page 6.7.5-1 thru 6.7.5-7..... Revision 0  
Page 6.7.6-1 thru 6.7.6-17..... Revision 0  
Page 6.7.7-1 thru 6.7.7-27..... Revision 0

Chapter 7

Page 7-i ..... Revision 0  
Page 7-1 ..... Revision 0  
Page 7.1-1 thru 7.1-6..... Revision 0  
Page 7.2-1 thru 7.2-2..... Revision 0  
Page 7.3-1 ..... Revision 0  
Page 7.4-1 ..... Revision 0

Chapter 8

Page 8-i thru 8-ii ..... Revision 0  
Page 8-1 ..... Revision 0  
Page 8.1-1 thru 8.1-3..... Revision 0  
Page 8.2-1 ..... Revision 0  
Page 8.3-1 thru 8.3-15..... Revision 0  
Page 8.4-1 ..... Revision 0  
Page 8.5-1 thru 8.5-2..... Revision 0  
Page 8.6-1 thru 8.6-2..... Revision 0  
Page 8.7-1 thru 8.7-2..... Revision 0  
Page 8.8-1 thru 8.8-4..... Revision 0  
Page 8.9-1 ..... Revision 0  
Page 8.10-1 thru 8.10-7..... Revision 0  
Page 8.11-1 thru 8.11-3..... Revision 0  
Page 8.12-1 thru 8.12-3..... Revision 0  
Page 8.13-1 thru 8.13-17..... Revision 0

Chapter 9

Page 9-i ..... Revision 0  
Page 9-1 thru 9-2..... Revision 0  
Page 9.1-1 thru 9.1-17..... Revision 0  
Page 9.2-1 thru 9.2-2..... Revision 0  
Page 9.3-1 thru 9.3-3..... Revision 0

Chapter 10

Page 10-i ..... Revision 0  
Page 10-1 ..... Revision 0  
Page 10.1-1 thru 10.1-20..... Revision 0  
Page 10.2-1 thru 10.2-3..... Revision 0  
Page 10.3-1 thru 10.3-2..... Revision 0

Chapter 11

Page 11-i ..... Revision 0  
Page 11-1 ..... Revision 0  
Page 11.1-1 thru 11.1-2..... Revision 0  
Page 11.2-1 ..... Revision 0  
Page 11.3-1 thru 11.3-6..... Revision 0  
Page 11.4-1 ..... Revision 0  
Page 11.5-1 ..... Revision 0

Chapter 12

Page 12-i ..... Revision 0  
Page 12-1 ..... Revision 0  
Page 12.1-1 thru 12.1-7..... Revision 0  
Page 12.2-1 thru 12.2-20..... Revision 0  
Page 12.3-1 thru 12.3-2..... Revision 0

Chapter 13

Page 13-i ..... Revision 0  
Page 13-1 ..... Revision 0  
Page 13A-i ..... Revision 0  
Page 13A-1..... Revision 0  
Page 13B-i..... Revision 0  
Page 13B-1..... Revision 0  
Page 13C-i..... Revision 0  
Page 13C-1 thru 13C-23 ..... Revision 0

**List of Effective Pages (cont'd)**

Chapter 14

Page 14-i ..... Revision 0  
Page 14-1 thru 14-2..... Revision 0  
Page 14.1-1 thru 14.1-7..... Revision 0  
Page 14.2-1 ..... Revision 0

Chapter 15

Page 15-i ..... Revision 0  
Page 15-1 ..... Revision 0  
Page 15.1-1 ..... Revision 0  
Page 15.2-1 thru 15.2-4..... Revision 0  
Page 15.3-1 ..... Revision 0

## Chapter 1 General Description

### Table of Contents

|       |   |       |
|-------|---|-------|
| 1     | GENERAL DESCRIPTION.....                      | 1-1   |
| 1.1   | Terminology .....                             | 1.1-1 |
| 1.2   | Introduction .....                            | 1.2-1 |
| 1.3   | General Description of MAGNASTOR.....         | 1.3-1 |
| 1.3.1 | MAGNASTOR Components.....                     | 1.3-1 |
| 1.3.2 | Operational Features .....                    | 1.3-6 |
| 1.4   | MAGNASTOR Contents .....                      | 1.4-1 |
| 1.5   | Identification of Agents and Contractors..... | 1.5-1 |
| 1.6   | Generic Concrete Cask Arrays.....             | 1.6-1 |
| 1.7   | References.....                               | 1.7-1 |
| 1.8   | License Drawings.....                         | 1.8-1 |

### List of Figures

|              |   |        |
|--------------|---|--------|
| Figure 1.3-1 | Major Component Configuration for Loading the Concrete Cask ..... | 1.3-9  |
| Figure 1.3-2 | TSC and Basket.....   | 1.3-10 |
| Figure 1.3-3 | Concrete Cask .....   | 1.3-11 |
| Figure 1.6-1 | Typical ISFSI Storage Pad Layout .....                            | 1.6-2  |

### List of Tables

|             |   |        |
|-------------|---|--------|
| Table 1.3-1 | Design Characteristics .....                                | 1.3-12 |
| Table 1.3-2 | Physical Design Parameters of the TSC and Fuel Baskets..... | 1.3-13 |
| Table 1.3-3 | TSC Fabrication Specification Summary .....                 | 1.3-14 |
| Table 1.3-4 | Concrete Cask Fabrication Specification Summary .....       | 1.3-15 |

## 1 GENERAL DESCRIPTION

This Safety Analysis Report (SAR) describes the NAC International Inc. (NAC) MAGNASTOR<sup>®</sup> System for the storage of spent fuel. It demonstrates that MAGNASTOR satisfies the requirements of the U.S. Nuclear Regulatory Commission (NRC) for spent nuclear fuel storage as prescribed in Title 10 of the Code of Federal Regulations, Part 72 (10 CFR 72) [1] and NUREG-1536 [2]. MAGNASTOR is a canister-based system that accommodates both the storage and transport of Pressurized Water Reactor (PWR) and Boiling Water Reactor (BWR) spent fuel.

The principal components of MAGNASTOR are:

- transportable storage canister (TSC)
- concrete cask
- transfer cask

The TSC is designed and fabricated to meet the requirements for storage in the concrete cask, for transport in a transport cask and to be compatible with the U.S. Department of Energy planning for permanent disposal in a Mined Geological Disposal System. The TSC incorporates a welded closure to preclude the loss of contents and to preserve the general health and safety of the public during long-term storage of spent fuel.

In long-term storage, the TSC is installed in a concrete cask, which provides structural protection and radiation shielding, as well as natural convection cooling. The concrete cask also provides protection during storage for the TSC under adverse environmental conditions.

The transfer cask is used to move the TSC between the workstations during TSC loading and preparation activities. It is also used to transfer the TSC to or from the concrete cask and to a transport cask.

This SAR is formatted in accordance with NRC Regulatory Guide 3.61 [4], except that Chapter 8, Materials Evaluation, is added in accordance with the requirement of Interim Staff Guidance (ISG)-15 [5], with the subsequent renumbering of the remaining chapters. The terminology used in this report is presented in Section 1.1. The term TSC refers to both the PWR and BWR TSCs where the discussion is common to both configurations. Discussion of features unique to the PWR and BWR configurations is addressed in subsections, as appropriate, within each chapter.

## 1.1 Terminology

This section lists and defines the terms used in this SAR.

### Adapter Plate

A carbon steel plate assembly positioned on the top of the concrete cask and used to align the transfer cask. It supports the operating mechanism for opening and closing the transfer cask shield doors.

### Assembly Average Fuel Enrichment

Value calculated by averaging the  $^{235}\text{U}$  wt % enrichment over the entire fuel region ( $\text{UO}_2$ ) of an individual fuel assembly, including axial blankets, if present.

### Assembly Defect

Any change in the physical as-built condition of the assembly, with the exception of normal in-reactor changes such as elongation from irradiation growth or assembly bow. Example of assembly defects include: (a) missing rods, (b) broken or missing grids or grid straps (spacer), and (c) missing or broken grid springs, etc. An assembly with a defect is damaged only if it cannot meet its fuel-specific and system-related functions.

### Breached Spent Fuel Rod

Spent fuel with cladding defects that permit the release of gas from the interior of the fuel rod. A fuel rod breach may be a minor defect (i.e., hairline crack or pinhole), allowing the rod to be classified as undamaged, or be a gross breach requiring a damaged fuel classification.

### Burnup

Amount of energy generated during irradiation – measured in MWd/MTU.

### Assembly Average Burnup

Value calculated by averaging the burnup over the entire fuel region ( $\text{UO}_2$ ) of an individual fuel assembly, including axial blankets, if present.

### Peak Average Rod Burnup

Value calculated by averaging the burnup in any rod over the length of the rod, then using the highest burnup calculated as the peak average rod burnup.

### Concrete Cask

A concrete cylinder that holds the TSC during storage. The concrete cask is formed around a steel inner liner and base and is closed by a lid.

### Base

A carbon steel weldment incorporating the air inlets and the pedestal that supports the TSC inside of the concrete cask.

### Lid

A thick concrete and carbon steel closure for the concrete cask. The lid precludes access to the TSC and provides radiation shielding.

### Liner

A carbon steel shell that forms the inside diameter of the concrete cask. The liner serves as the inner form during concrete pouring and provides radiation shielding and structural protection for the TSC.

### Standoffs (Channels)

Carbon steel weldments attached to the liner that assist in centering the TSC in the concrete cask and supporting the TSC and its contents in a nonmechanistic tip-over event.

### Confinement System

The components of the TSC assembly that retain the spent fuel during storage.

### Contents

Up to 37 PWR fuel assemblies or up to 87 BWR fuel assemblies. The fuel assemblies are confined in a TSC. Non-fuel hardware may be inserted into PWR fuel assemblies and BWR fuel assemblies may include channels.

### Damaged Fuel

Spent nuclear fuel (SNF) that cannot fulfill its fuel-specific or system-related function. Spent fuel is classified as damaged under the following conditions.

- 1) There is visible deformation of the rods in the SNF assembly.  
Note: This is not referring to the uniform bowing that occurs in the reactor; this refers to bowing that significantly opens up the lattice spacing.
- 2) Individual fuel rods are missing from the assembly and the missing rods are not replaced by a solid dummy rod that displaces a volume equal to, or greater than, the original fuel rod.
- 3) The SNF assembly has missing, displaced or damaged structural components such that:
  - 3.1) Radiological and/or criticality safety is adversely affected (e.g., significantly changed rod pitch); or
  - 3.2) The assembly cannot be handled by normal means (i.e., crane and grapple); or
  - 3.3) The assembly contains fuel rods with damaged or missing grids, grid straps, and/or grid springs producing an unsupported length greater than 60 inches.Note: Assemblies with the following structural defects meet MAGNASTOR system-related functional requirements and are, therefore, classified as undamaged: Assemblies with missing or damaged grids, grid straps and/or grid springs resulting in an unsupported fuel rod length not to exceed 60 inches.
- 4) Any SNF assembly that contains fuel rods for which reactor operating records (or other records or tests) cannot support the conclusion that they do not contain gross breaches.  
Note: Breached fuel rods with minor cladding defects (i.e., pinhole leaks or hairline cracks that will not permit significant release of particulate matter from the spent fuel rod) meet MAGNASTOR system-related functional requirements and are, therefore, classified as undamaged.



- 5) The SNF assembly is no longer in the form of an intact fuel bundle (e.g., consists of or contains debris such as loose fuel pellets or rod segments).

#### Factor of Safety

An analytically determined value defined as the allowable stress or displacement of a material divided by its calculated stress or displacement.

#### Fuel Basket (Basket)

The structure inside the TSC that provides structural support, criticality control, and heat transfer paths for the fuel assemblies.

#### Developed Cell

A basket opening formed by either four fuel tubes or fuel tubes and basket weldments. Fuel assemblies are loaded into the developed cells.

#### Fuel Tube

A carbon steel tube with a square cross-section. Fuel assemblies are loaded into the fuel tubes. A fuel tube may have neutron absorber material attached on its interior faces.

#### Neutron Absorber

A borated aluminum metal matrix or composite with neutron absorption capability.

#### Grossly Breached Spent Fuel Rod

A breach in the spent fuel cladding that is larger than a pinhole or hairline crack. A gross cladding breach may be established by visual examination with the capability to determine if the fuel pellet can be seen through the cladding, or through a review of reactor operating records indicating the presence of heavy metal isotopes.

#### Intact Fuel (Assembly or Rod)

Any fuel that can fulfill all fuel-specific and system-related functions and that is not breached.

#### MAGNASTOR (Modular Advanced Generation, Nuclear, All-purpose STORAGE)

The high-capacity system designed for safe, long-term spent fuel storage at a power reactor site or at an independent spent fuel storage installation.

#### Spent Nuclear Fuel (or Spent Fuel)

Irradiated fuel assemblies with the same configuration as when originally fabricated, consisting generally of the end fittings, fuel rods, guide tubes, and integral hardware. For PWR fuel, a thimble plug, an in-core instrument thimble, a burnable poison rod insert, or a control element assembly (CEA) is considered to be a component of standard fuel. For BWR fuel, the channel is considered to be integral hardware. Solid filler rods, burnable poison rods, burnable poison rod assemblies, thimble plugs, control element assemblies and stainless steel rod inserts may be inserted in PWR fuel assemblies.

## Transfer Cask

A shielded device used to lift and handle the TSC during fuel loading and closure operations, as well as to transfer the TSC in/out of the concrete cask during storage or in/out of a transport cask. The transfer cask includes two lifting trunnions and two shield doors that can be opened to permit the vertical transfer of the TSC.

### Trunnions

Two low-alloy steel components used to lift the transfer cask in a vertical orientation via a lifting assembly.

## TSC (Transportable Storage Canister)

The stainless steel cylindrical shell, bottom-end plate, closure lid, closure ring, and redundant port covers that contain the fuel basket structure and the spent fuel contents.

### Closure Lid

A thick, stainless steel disk installed directly above the fuel basket following fuel loading. The closure lid provides the confinement boundary for storage and operational shielding during TSC closure.

### Drain and Vent Ports

Penetrations located in the closure lid to permit draining, drying, and helium backfilling of the TSC.

### Port Cover

The stainless steel plates covering the vent and drain ports that are welded in place following draining, drying, and backfilling operations.

### Closure Ring

A stainless steel ring welded to the closure lid and TSC shell to provide a double weld redundant sealing closure of the TSC satisfying 10 CFR 72.236(e) requirements.

## Undamaged Fuel

Spent nuclear fuel that can meet all fuel-specific and system-related functions. Undamaged fuel is spent nuclear fuel that is not Damaged Fuel, as defined herein, and does not contain assembly structural defects that adversely affect radiological and/or criticality safety. As such, undamaged fuel may contain:

- a) Breached spent fuel rods (i.e, rods with minor defects up to hairline cracks or pinholes), but cannot contain grossly breached fuel rods;
- b) Grid, grid strap and/or grid spring damage, provided that the unsupported length of the fuel rod does not exceed 60 inches.

## 1.2 Introduction

MAGNASTOR is a spent fuel dry storage system consisting of a concrete cask and a welded stainless steel TSC with a welded closure to safely store spent fuel. The TSC is stored in the central cavity of the concrete cask. The concrete cask provides structural protection, radiation shielding, and internal airflow paths that remove the decay heat from the TSC contents by natural air circulation. MAGNASTOR is designed and analyzed for a 50-year service life.

The loaded TSC is moved to and from the concrete cask using the transfer cask. The transfer cask provides radiation shielding during TSC closure and preparation activities. The TSC is transferred into the concrete cask by positioning the transfer cask with the loaded TSC on top of the concrete cask, opening the shield doors, and lowering the TSC into the concrete cask. Figure 1.3-1 depicts the major components of MAGNASTOR in such a configuration.

MAGNASTOR is designed to safely store up to 37 PWR or up to 87 BWR spent fuel assemblies in separate fuel basket assemblies. These capacities, combined with enhanced operational features, assure that MAGNASTOR reduces the time required and the personnel dose received on a per-assembly basis when placing spent fuel into dry storage. The fuel specifications and parameters that establish the design basis for the PWR and BWR fuel assemblies are presented in Chapter 2. The spent fuel considered in the design includes fuel assemblies that have different overall lengths. The PWR and BWR fuel assembly populations are divided into two groups based on fuel assembly length, and are accommodated by two different lengths of TSCs. The concrete cask and transfer cask are a fixed height and can accommodate both lengths of TSC. The designations and corresponding lengths of the TSCs are shown on the License Drawings.

For PWR fuel, the inclusion of nonfuel assembly hardware can increase an assembly's overall length, resulting in the need to use the longer TSC. Spacers may be used in a given TSC to allow loading of fuel that is significantly shorter than the TSC length. The BWR fuel assembly groups are evaluated for the effects of the zirconium alloy channel that surrounds the fuel assembly in reactor operations. Fuel assembly channel effects are addressed in both the thermal heat transfer and criticality analyses. BWR assembly channels are included in the assembly weight assigned to each basket opening in the structural analysis. The mass associated with the channel is conservatively neglected from the material homogenization in the shielding analysis.

The system design and analyses are in accordance with 10 CFR 72, ANSI/ANS 57.9 [6], the applicable sections of the ASME Boiler and Pressure Vessel Code (ASME Code), and the American Concrete Institute (ACI) code [7]. The analyses demonstrate that MAGNASTOR meets the regulatory requirements of 10 CFR 72 and the guidance of NUREG-1536 [2].

### 1.3 General Description of MAGNASTOR

MAGNASTOR provides for the long-term storage of PWR and BWR fuel assemblies as listed in Chapter 2. During long-term storage, the system provides an inert environment, passive structural shielding, cooling and criticality control, and a welded confinement boundary. The structural integrity of the system precludes the release of contents in any of the design basis normal conditions and off-normal or accident events, thereby assuring public health and safety during use of the system.

#### 1.3.1 MAGNASTOR Components

The design and operation of the principal components of MAGNASTOR and the associated auxiliary equipment are described in this section. The design characteristics of the principal components of the system are presented in Table 1.3-1.

This list shows the auxiliary equipment generally needed to use MAGNASTOR.

- automated, remote, and /or manual welding equipment to perform TSC field closure welding operations
- an engine-driven or towed frame or a heavy-haul trailer to move the concrete cask to and from the storage pad and to position the concrete cask on the storage pad
- draining, drying, helium backfill, and water cooling systems for preparing the TSC and contents for storage
- hydrogen monitoring equipment to confirm the absence of explosive or combustible gases during TSC closure welding
- an adapter plate and a hydraulic supply system
- a lifting yoke for lifting and handling the transfer cask and rigging equipment for lifting and handling system components

In addition to these items, the system requires utility services (electric, helium, air, clean borated water, etc.), standard torque wrenches, tools and fittings, and miscellaneous hardware.

##### 1.3.1.1 Transportable Storage Canister (TSC)

Two lengths of TSCs accommodate all evaluated PWR and BWR fuel assemblies. The TSC is designed for transport per 10 CFR 71 [3]. The load conditions in transport produce higher stresses in the TSC than are produced during storage conditions, except for TSC lifting. Consequently, transport load conditions establish the design basis for the TSC and, therefore, the TSC design is conservative with respect to storage conditions.

The stainless steel TSC assembly holds the fuel basket structure and confines the contents (see Figure 1.3-2). The TSC is defined as the confinement boundary during storage. The welded closure lid, closure ring, and redundant port covers prevent the release of contents under normal conditions and off-normal or accident events. The fuel basket assembly provides the structural support and a heat transfer path for the fuel assemblies, while maintaining a subcritical configuration for all of the evaluated normal conditions and off-normal or accident events.

The major components of the TSC assembly are the shell, base plate, closure lid, closure ring, and redundant port covers for the vent and drain ports, which provide the confinement boundary during storage. The TSC component dimensions and materials of fabrication are provided in Table 1.3-1. The TSC overall dimensions and design parameters for the two lengths of TSCs are provided in Table 1.3-2.

The TSC consists of a cylindrical stainless steel shell with a welded stainless steel bottom plate at its closed end and a 9-in thick stainless steel closure lid at its open end. The stainless steel shell and bottom plate are dual-certified Type 304/304L. The closure lid, closure ring and port covers are Type 304 stainless steel. A fuel basket assembly is placed inside the TSC. The closure lid is positioned inside the TSC on the lifting lugs above the basket assembly following fuel loading. After the closure lid is placed on the TSC, the TSC is moved to a workstation, and the closure lid is welded to the TSC. After nondestructive examination and pressure testing of the closure lid weld, the closure ring is welded to the closure lid and TSC shell. The vent and drain ports are penetrations through the lid, which provide access for auxiliary systems to drain, dry, and backfill the TSC. The drain port has a threaded fitting for installing the drain tube. The drain tube extends the full length of the TSC and ends in a sump in the bottom plate. The vent port also provides access to the TSC cavity for draining, drying, and backfilling operations. Following completion of backfilling, the inner port covers at the vent and drain ports are installed and welded in place. The final surface of the inner port cover weld is visually and nondestructively examined. The inner vent and drain port cover welds are then helium leak tested to verify the absence of helium leakage past the port cover welds. The outer port covers are then installed and welded, and the final weld surfaces are nondestructively examined.

The TSC is designed, fabricated, and inspected to the requirements of the ASME Boiler and Pressure Vessel Code (ASME Code), Section III, Division 1, Subsection NB [8], except as noted in the Alternatives to the ASME Code as provided in Table 2.1-2.

Refer to Table 1.3-3 for a summary of the TSC fabrication requirements.

### 1.3.1.2 Fuel Baskets

Each TSC contains either a PWR or BWR fuel basket, which positions and supports the stored fuel. As described in the following sections, the design of the basket is similar for the PWR and BWR configurations. The fuel basket for each fuel type is designed, fabricated, and inspected to the requirements of the ASME Code, Section III, Division 1, Subsection NG [9], except as noted in Table 2.1-2.

The structural components of both the PWR and BWR baskets are fabricated from ASME SA537, Class 1, carbon steel. To minimize corrosion and preclude significant generation of combustible gases during fuel loading, the assembled basket is coated with electroless nickel plating using an immersion process. Following coating, the neutron absorber panels and the stainless steel retainers are installed on the basket structure as shown on the License Drawings. The principal dimensions and materials of fabrication of the fuel basket are provided in Table 1.3-1.

Both fuel basket designs minimize horizontal surfaces that could entrain water and provide an open path for water flow to the drain tube and sump in the bottom of the TSC. The fuel baskets are supported from the baseplate by 3-in high spacers at the corner of the fuel tubes enabling the TSC to fill and drain evenly.

Spacers may be used to limit the movement of the spent fuel assemblies during storage or in subsequent transport operations.

#### PWR Fuel Basket

The PWR fuel basket design is an arrangement of square fuel tubes held in a right-circular cylinder configuration using support weldments that are bolted to the outer fuel tubes. The design parameters for the two lengths of PWR fuel baskets are provided in Table 1.3-2.

Fuel tubes support an enclosed neutron absorber sheet on up to four interior sides of the fuel tube. The neutron absorber panels, in conjunction with minimum TSC cavity water boron levels, provide criticality control in the basket. Each neutron absorber panel is covered by a sheet of stainless steel to protect the material during fuel loading and to keep it in position. The neutron absorber and stainless steel cover are secured to the fuel tube using weld posts located across the width and along the length of the fuel tube.

Each PWR fuel basket has a capacity of 37 fuel assemblies in an aligned configuration. Square tubes are assembled in an array where the tubes function as independent fuel positions and as sidewalls for the adjacent fuel positions in what is called a developed cell array. Consequently, the 37 fuel positions are developed using only 21 tubes. The array is surrounded by weldments

that serve both as sidewalls for some perimeter fuel positions and as the structural load path from the array to the TSC shell wall. Each PWR basket fuel tube has a nominal 8.86-in square opening. Each developed cell fuel position has a nominal 8.76-in square opening.

### **BWR Fuel Basket**

The BWR fuel basket design is an arrangement of square fuel tubes held in a right-circular cylinder configuration using support weldments that are bolted to the outer fuel tubes. The design parameters for the two lengths of BWR fuel baskets are provided in Table 1.3-2.

Each fuel tube supports an enclosed neutron absorber sheet on up to four interior sides of the fuel tube, which provides criticality control in the basket. The neutron absorber is covered by a sheet of stainless steel to protect the material during fuel loading and to keep it in position. The neutron absorber and stainless steel cover are secured to the fuel tube using weld posts located across the width and along the length of the fuel tube.

Each BWR fuel basket has a capacity of 87 fuel assemblies in an aligned configuration. Square tubes are assembled in an array where the tubes function as independent fuel positions and as sidewalls for the adjacent fuel positions in what is called a developed cell array. Consequently, the 87 fuel positions are developed using only 45 tubes. The array is surrounded by weldments that serve both as sidewalls for some perimeter fuel positions and as the structural load path from the array to the TSC shell wall. Each BWR basket fuel tube has a nominal 5.86-in square opening. Each developed cell fuel position has a nominal 5.77-in square opening.

#### **1.3.1.3 Concrete Cask**

The concrete cask is the storage overpack for the TSC and it is designed to hold both lengths of TSCs. The concrete cask provides structural support, shielding, protection from environmental conditions, and natural convection cooling of the TSC during long-term storage. The principal dimensions and materials of fabrication of the concrete cask are shown in Table 1.3-1.

The concrete cask is a reinforced concrete structure with a structural steel inner liner and base. The reinforced concrete wall and steel liner provide the neutron and gamma radiation shielding for the stored spent fuel. Inner and outer reinforcing steel (rebar) assemblies are encased within the concrete. The reinforced concrete wall provides the structural strength to protect the TSC and its contents in natural phenomena events such as tornado wind loading and wind-driven missiles and during nonmechanistic tip-over events (refer to Figure 1.3-3). The concrete surfaces remain accessible for inspection and maintenance over the life of the cask, so that any necessary restoration actions may be taken to maintain shielding and structural conditions.

The concrete cask provides an annular air passage to allow the natural circulation of air around the TSC to remove the decay heat from the contents. The lower air inlets and upper air outlets are steel-lined penetrations in the concrete cask body. Each air inlet/outlet is covered with a screen. The weldment baffle directs the air upward and around the pedestal that supports the TSC. Decay heat is transferred from the fuel assemblies to the TSC wall by conduction, convection, and radiation. Heat is removed by convection and radiation from the TSC shell to the air flowing upward through the annular air passage and to the concrete cask inner liner, respectively. Heat radiated to the liner can be transferred to the air annulus and by conduction through the concrete cask wall. The heated air in the annulus exhausts through the air outlets. The passive cooling system is designed to maintain the peak fuel cladding temperature below acceptable limits during long-term storage [10]. The concrete cask thermal design also maintains the bulk concrete temperature and surface temperatures below the American Concrete Institute (ACI) limits under normal operating conditions. The inner liner of the concrete cask incorporates standoffs that provide lateral support to the TSC in side impact accident events.

A carbon steel and concrete lid is bolted to the top of the concrete cask. The lid reduces skyshine radiation and provides a cover to protect the TSC from the environment and postulated tornado missiles.

Fabrication of the concrete cask requires no unique or unusual forming, concrete placement, or reinforcement operations. The concrete portion of the cask is constructed by placing concrete between a reusable, exterior form and the steel liner. Reinforcing bars are used near the inner and outer concrete surfaces to provide structural integrity. The structural steel liner and base are shop fabricated. Refer to Table 1.3-4 for the fabrication specifications for the concrete cask.

Daily visual inspection of the air inlet and outlet screens for blockage assures that airflow through the cask meets licensed requirements. A description of the visual inspection is included in the Technical Specifications, Chapter 13. As an alternative to daily visual inspections, the loaded concrete cask in storage may include the capability to measure air temperature at the four outlets. Each air outlet may be equipped with a remote temperature detector mounted in the outlet air plenum. The air temperature-monitoring system, designed to provide verification of heat dissipation capabilities, can be designed for remote or local read-out capabilities at the option of the licensee. The temperature-monitoring system can be installed on all or some of the concrete casks at the Independent Spent Fuel Storage Installation (ISFSI) facility.

#### **1.3.1.4      Transfer Cask**

The transfer cask is designed, fabricated, and tested to meet the requirements of ANSI N14.6 [11] as a special lifting device. The transfer cask provides biological shielding and structural



protection for a loaded TSC, and is used to lift and move the TSC between workstations. The transfer cask is also used to shield the vertical transfer of a TSC into a concrete cask or a transport cask.

The transfer cask design incorporates three retaining blocks, pin-locked in place, to prevent a loaded TSC from being inadvertently lifted through its top opening. The transfer cask has retractable bottom shield doors. During TSC loading and handling operations, the shield doors are closed and secured. After placement of the transfer cask on the concrete cask, the doors are retracted using hydraulic cylinders and a hydraulic supply. The TSC is then lowered into a concrete cask for storage. Refer to Figure 1.3-1 for the general arrangement of the transfer cask, TSC, and concrete cask during loading and Table 1.3-1 for the principal dimensions and materials of fabrication of the transfer cask.

Sixteen penetrations, eight at the top and eight at the bottom, are available to provide a water supply to the transfer cask annulus. Penetrations not used for water supply or draining are capped. The transfer cask annulus is isolated using inflatable seals located between the transfer cask inner shell and the TSC near the upper and lower ends of the transfer cask.

During TSC closure, clean or demineralized spent fuel pool water may be circulated through these penetrations into the annulus region to minimize component temperatures and improve canister preparation time limits. The auxiliary annulus circulating water cooling system can be utilized through completion of TSC activities. The annulus circulating water cooling system is turned off prior to movement of the transfer cask for TSC transfer operations into the concrete cask.

A similar process of clean or demineralized spent fuel pool water flow into the annulus is used during in-pool fuel loading to minimize the potential for contamination of the TSC exterior surfaces.

The transfer cask penetrations can also be used for the introduction of auxiliary forced air or gas to cool the exterior of the TSC. Alternately, if auxiliary cooling is required to lower fuel cladding or TSC component temperatures, the loaded TSC may be returned to the spent fuel pool or shelf for cooling.

### **1.3.2 Operational Features**

In storage, MAGNASTOR does not require any active operational systems. The principal MAGNASTOR operational activities are loading, welding, and preparing the TSC for storage and transferring the TSC to the concrete cask. The transfer cask is designed to meet the requirements of these operations. The transfer cask holds the TSC during fuel loading

operations, provides biological shielding during TSC closure and preparation, and positions the TSC for transfer into the concrete cask. The lid design of the TSC assures structural integrity, while reducing the time and dose involved in TSC closure.

The detailed generic step-by-step operating procedures for the loading and transferring of MAGNASTOR are presented in Chapter 9. The following is a list of the major loading activities. This list assumes that the empty TSC is installed in the transfer cask.

- Fill the TSC with water or borated water if required.
- Lift the transfer cask over the pool and start the flow of water to the transfer cask annulus and lower the cask to the bottom of the pool.
- Load the selected spent fuel assemblies into the TSC.
- Install the closure lid.
- Remove the transfer cask from the pool and place it in the cask preparation workstation.
- Decontaminate the transfer cask.
- Lower the TSC water level and weld the closure lid to the TSC shell. Examine the weld.
- Hydrostatically test the TSC.
- Install and weld the closure ring. Examine the weld.
- Drain the remaining pool water from the TSC.
- Dry the TSC cavity. Verify cavity dryness.
- Establish a helium backfill.
- Install and weld the inner vent and drain port covers. Examine the welds.
- Helium leak test the inner vent and drain port covers.
- Install and weld the outer vent and drain port covers. Examine the welds.
- Install the TSC lifting system.
- Install the adapter plate on the concrete cask.
- Lift and place the transfer cask on the transfer adapter.
- Attach the TSC lifting system to the crane hook and raise the TSC off of the shield doors.
- Open the shield doors.
- Lower the TSC into the concrete cask (see Figure 1.3-1).
- Remove the transfer cask, transfer adapter, and TSC lifting systems.
- Install the lid on the concrete cask.
- Move the loaded concrete cask to the storage pad.
- Move the concrete cask to its designated location on the storage pad.

The TSC unloading and spent fuel removal from the TSC are essentially the reverse of these steps, except that weld removal and cooldown of the contents is required. This typical sequence of operations, and individual steps, may be modified by the approved site procedure to accommodate specific site requirements, as long as the requirements of the Technical Specifications and the CoC are met.

Figure 1.3-1 Major Component Configuration for Loading the Concrete Cask

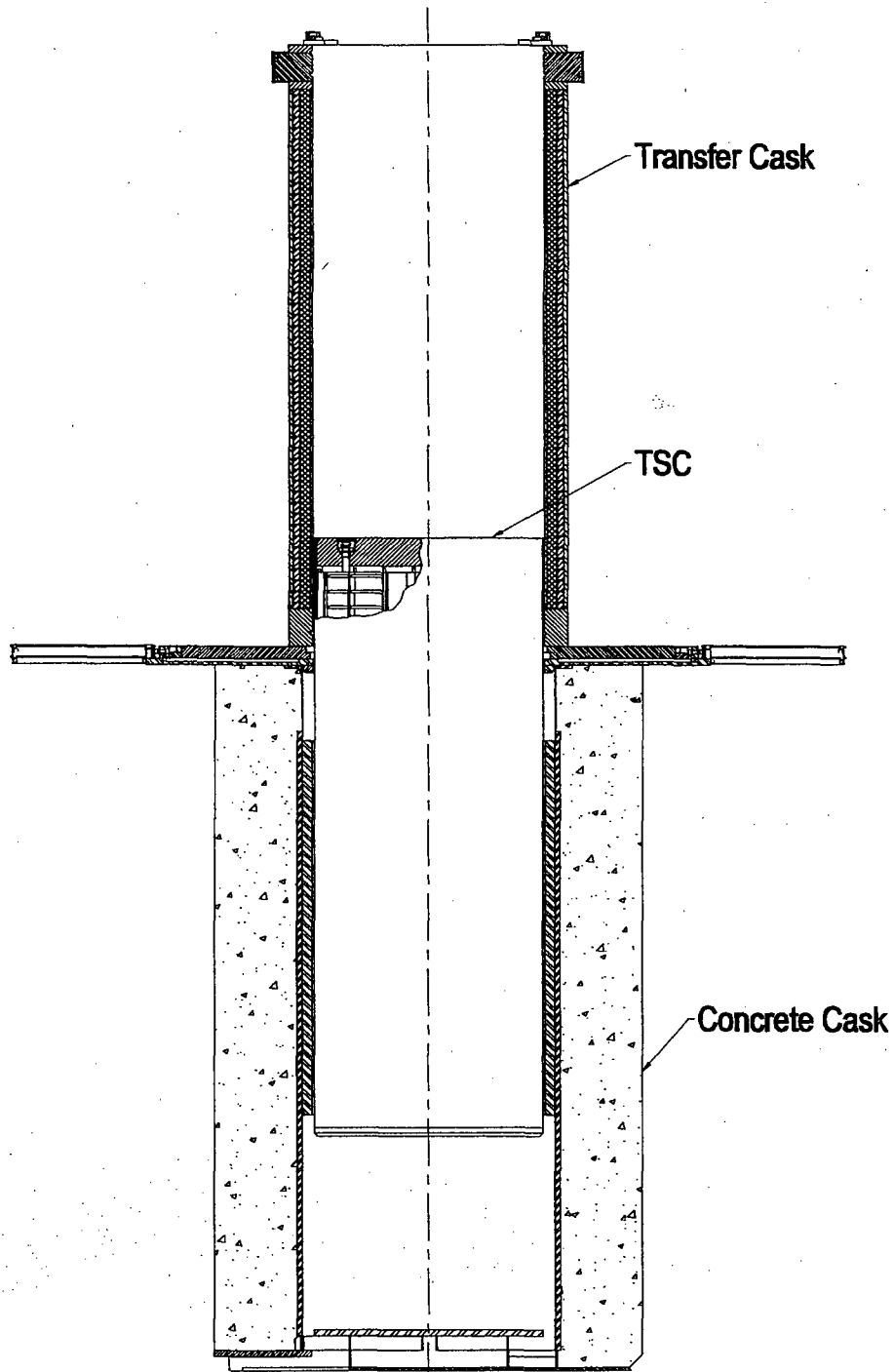


Figure 1.3-2 TSC and Basket

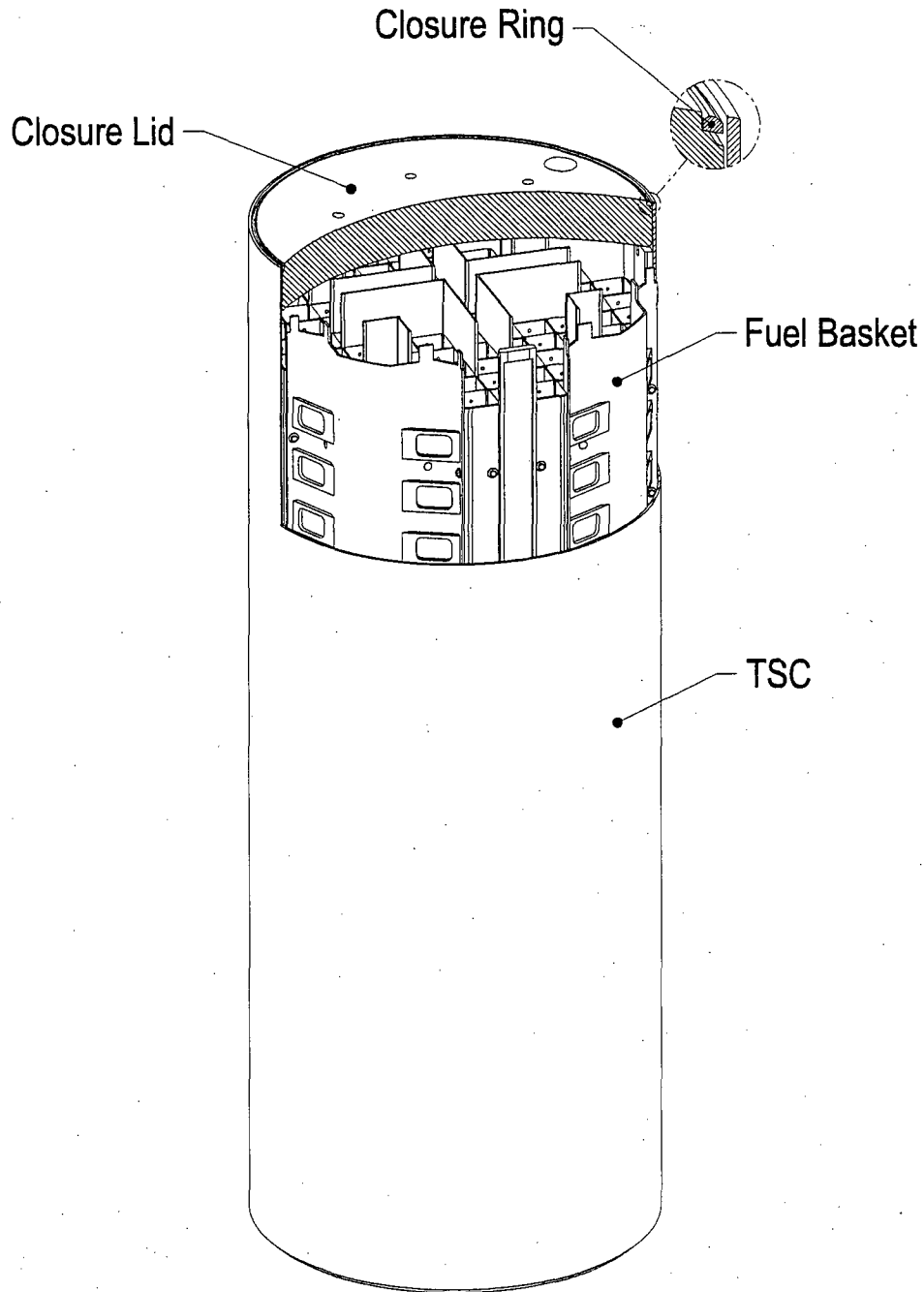


Figure 1.3-3 Concrete Cask

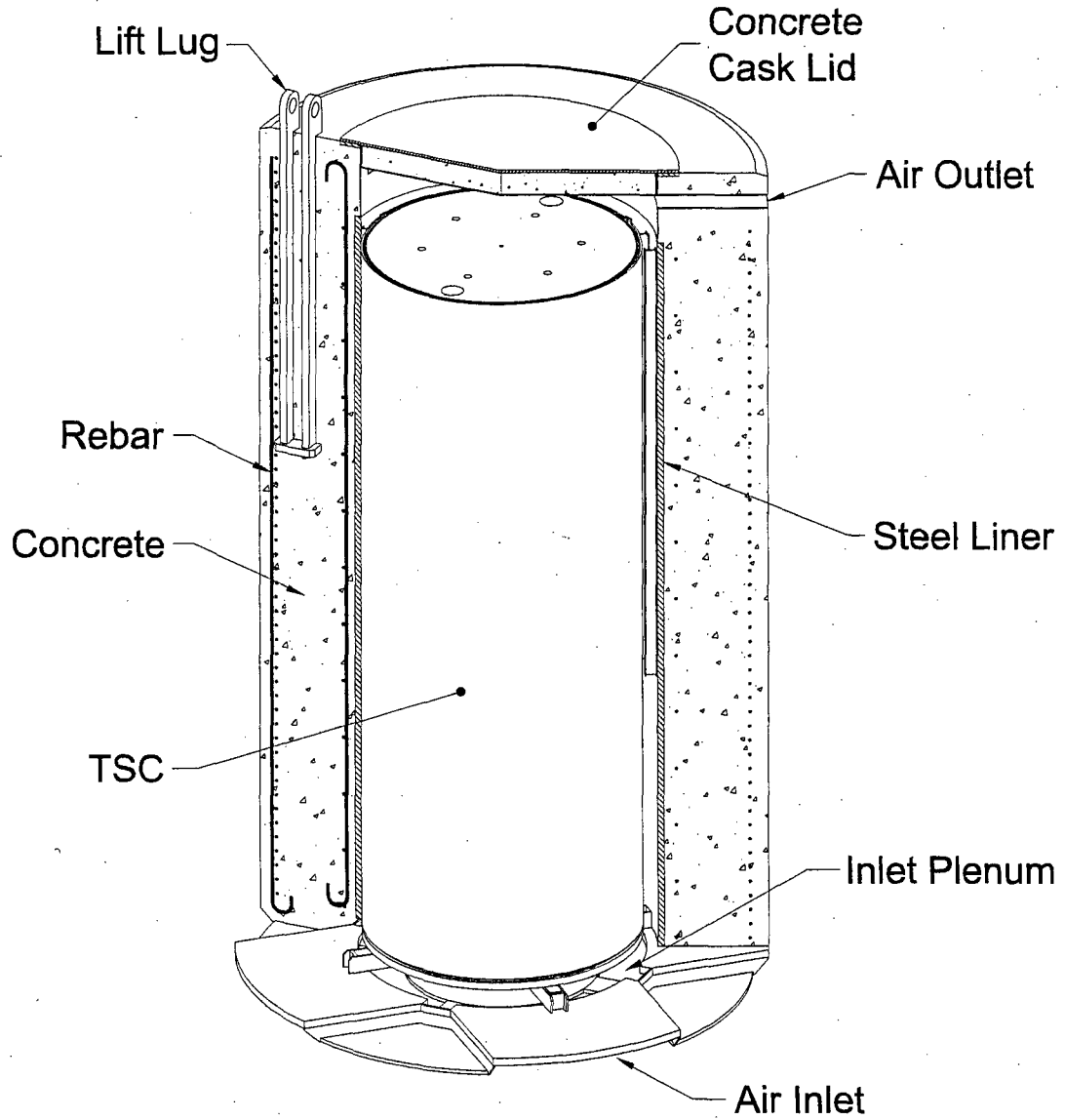


Table 1.3-1 Design Characteristics

|                  | Design Characteristic      | Nominal Value (in) <sup>a</sup>        | Material                                |  |
|------------------|----------------------------|--|---|--|
| TSC              | Shell                      | 0.5 × 72 dia.                          | Stainless Steel                         |  |
|                  | Bottom                     | 2.75                                   | Stainless Steel                         |  |
|                  | Closure Lid                | 9                                      | Stainless Steel                         |  |
|                  | Closure Ring               | 0.75 square                            | Stainless Steel                         |  |
|                  | Length                     |  |   |  |
|                  | Group 1 & 3                | 184.8                                  |   |  |
|                  | Group 2 & 4                | 191.8                                  |   |  |
| Fuel Basket      | PWR Fuel Tube Wall         | 0.31                                   | Carbon Steel                            |  |
|                  | BWR Fuel Tube Wall         | 0.25                                   | Carbon Steel                            |  |
|                  | Neutron Absorber           | 0.125 (PWR), 0.1 (BWR)                 | Metallic Composite/Matrix               |  |
|                  | Neutron Absorber Retainer  | 0.015                                  | Stainless Steel                         |  |
|                  | Support Plates & Gussets   | 0.5 to 0.75                            | Carbon Steel                            |  |
|                  | Support Bars (PWR)         | 0.875                                  | Carbon Steel                            |  |
|                  | Support Plate (BWR)        | 0.75                                   | Carbon Steel                            |  |
|                  | Length                     |  |   |  |
|                  |                            | Group 1 & 3                            | 172.5                                   |  |
|                  |                            | Group 2 & 4                            | 179.5                                   |  |
|                  |                            | Assembly dia.                          | 70.76                                   |  |
|                  |                            | # of Fuel Tubes/Fuel Loading Positions |   |  |
|                  |                            | PWR                                    | 21/37                                   |  |
|                  | BWR                        | 45/87                                  |   |  |
| Transfer Cask    | Outer Shell                | 1.25 × 88 dia.                         | Low Alloy Steel                         |  |
|                  | Inner Shell                | 0.75 × 74.5 dia.                       | Low Alloy Steel                         |  |
|                  | Retaining Block            | 8 × 8.75 × 1.50                        | Stainless Steel                         |  |
|                  | Trunnions                  | 9.5 dia.                               | Low Alloy Steel                         |  |
|                  | Bottom Forging             | 12 × 88 dia.                           | Low Alloy Steel                         |  |
|                  | Top Forging                | 14 × 88 dia.                           | Low Alloy Steel                         |  |
|                  | Shield Doors               | 5.0                                    | Low Alloy Steel                         |  |
|                  | Door Rails                 | 5.25 × 7.5 × 52.0                      | Low Alloy Steel                         |  |
|                  | Gamma Shield               | 3.2                                    | Lead                                    |  |
|                  | Neutron Shield             | 2.25                                   | NS-4-FR, Solid Synthetic Polymer        |  |
| Transfer Adapter | Base Plate                 | 2.0                                    | Carbon Steel                            |  |
|                  | Guide Ring                 | 2.5 × 79 dia.                          | Carbon Steel                            |  |
| Concrete Cask    | <b>Weldment Structures</b> |  |   |  |
|                  | Liner                      | 1.75 × 83 dia                          | Carbon Steel                            |  |
|                  | Top Flange                 | 1 × 91 dia.                            | Carbon Steel                            |  |
|                  | Standoffs (Channels)       | 3 × 7.5 (s-beam)                       | Carbon Steel                            |  |
|                  | Pedestal Plate             | 2 × 72 dia.                            | Carbon Steel                            |  |
|                  | Bottom Weldment            | 1 × 128 in                             | Carbon Steel                            |  |
|                  | Inlet Top                  | 2 × 136 dia.                           | Carbon Steel                            |  |
|                  | <b>Concrete Cask</b>       |  |   |  |
|                  | Concrete Shell             | 26.5 × 136 dia.                        | Type II Portland Cement                 |  |
|                  | Lid                        | 6.75 × 88 dia.                         | Carbon Steel                            |  |
|                  | Rebar                      | various lengths                        | Type II Portland Cement<br>Carbon Steel |  |

<sup>a</sup> Thickness unless otherwise indicated.

Table 1.3-2 Physical Design Parameters of the TSC and Fuel Baskets

| Component                       | Characteristic                              | Parameter                   | Nominal Value |
|---------------------------------|---|-----------------------------|---------------|
| TSC                             | Canister Weldment                           | Shell Outside Diameter (in) | 72            |
|                                 |   | Shell Thickness (in)        | 0.5           |
|                                 |   | Bottom Thickness (in)       | 2.75          |
|                                 | Length                                      | Group 1 & 3 (in)            | 184.8         |
|                                 |   | Group 2 & 4 (in)            | 191.8         |
| Capacity (# of fuel assemblies) | PWR   | 37                          |               |
|                                 | BWR   | 87                          |               |
| Fuel Basket                     | Length (in)                                 | Group 1 & 3 (in)            | 172.5         |
|                                 |   | Group 2 & 4 (in)            | 179.5         |
|                                 | Diameter                                    | Assembly Diameter (in)      | 70.76         |
|                                 | Number of Fuel Tubes/Fuel Loading Positions | PWR                         | 21/37         |
| BWR                             |   | 45/87                       |               |



**Table 1.3-3 TSC Fabrication Specification Summary**

**Materials**

- All materials shall be governed by the referenced drawings and meet the applicable ASME Code sections.

**Welding**

- Welds shall be in accordance with the referenced drawings.
- Filler metals shall be appropriate ASME Code materials.
- Welders and welding operators shall be qualified in accordance with ASME Code Section IX [12].
- Welding procedures shall be written and qualified in accordance with ASME Code Section IX.
- Personnel performing weld examinations shall be qualified in accordance with the NAC International Quality Assurance Program and SNT-TC-1A [13].
- Weld inspection and examination requirements and acceptance criteria are specified in Chapter 10.

**Fabrication**

- Cutting, welding, and forming shall be in accordance with ASME Code, Section III, NB-4000 [8] unless otherwise specified. Code stamping is not required.
- Surfaces shall be cleaned to a surface cleanliness classification C, or better, as defined in ANSI N45.2.1 [14], Section 2.
- Fabrication tolerances shall meet the requirements of the referenced drawings after fabrication.

**Packaging**

- Packaging and shipping shall be in accordance with ANSI N45.2.2 [15].

**Quality Assurance**

- The TSC shall be fabricated under a quality assurance program that meets 10 CFR 72, Subpart G, and 10 CFR 71, Subpart H.

**Table 1.3-4 Concrete Cask Fabrication Specification Summary**

**Materials**

- Concrete mix shall be in accordance with the requirements of ACI 318 and ASTM C94 [16].
- Type II Portland Cement, ASTM C150 [17].
- Fine aggregate ASTM C33 [18] or C637 [19].
- Coarse aggregate ASTM C33.
- Admixtures
  - Water Reducing and Superplasticizing ASTM C494 [20].
  - Pozzolanic Admixture (loss on ignition 6% or less) ASTM C618 [21].
- Compressive strength 4000 psi minimum at 28 days.
- Specified air entrainment per ACI 318.
- All steel components shall be of the material as specified in the referenced drawings.

**Construction**

- A minimum of two samples for each concrete cask shall be taken in accordance with ASTM C172 [22] and ASTM C31 [23] for the purpose of obtaining concrete slump, density, air entrainment, and 28-day compressive strength values. The two samples shall not be taken from the same batch or truck load.
- Test specimens shall be tested in accordance with ASTM C39 [24].
- Formwork shall be in accordance with ACI 318.
- All sidewall formwork shall remain in place in accordance with the requirements of ACI 318.
- Grade, type, and details of all reinforcing steel shall be in accordance with the referenced drawings.
- Embedded items shall conform to ACI 318 and the referenced drawings.
- The placement of concrete shall be in accordance with ACI 318.
- Surface finish shall be in accordance with ACI 318.
- Welding and inspection requirements and acceptance criteria are specified in Chapter 10.

**Quality Assurance**

- The concrete cask shall be constructed under a quality assurance program that meets 10 CFR 72, Subpart G.

#### 1.4 MAGNASTOR Contents

MAGNASTOR is designed to store up to 37 PWR fuel assemblies or up to 87 BWR fuel assemblies in a pressurized helium atmosphere. PWR fuel assemblies may be stored with inserted burnable poison rod assemblies, thimble plugs or control element assemblies. Stainless steel rod inserts for guide tube dashpots may also be inserted. BWR fuel assemblies may be stored with or without channels. Assemblies may contain solid filler rods or burnable absorber rods replacing fuel rods in the assembly lattice. Steel filler rods must be unirradiated. The design content conditions are specified in the CoC for MAGNASTOR. Unenriched fuel assemblies are not evaluated and are not included as allowable contents. Assemblies may contain unenriched axial end blankets.

### 1.5 Identification of Agents and Contractors

The prime contractor for the MAGNASTOR design is NAC. All design, analysis, licensing, and procurement activities are performed by NAC in accordance with its approved Quality Assurance Program, as described in Chapter 14. Fabrication of the steel components will be by qualified vendors. A qualified concrete contractor will perform construction of the concrete cask. All vendors and contractors will be selected and their performance monitored in accordance with the NAC Quality Assurance Program. All MAGNASTOR fabrication and assembly activities will be performed in accordance with quality assurance programs that meet the requirements of 10 CFR 72, Subpart G.

NAC as a contractor, or the licensee, may perform construction of the ISFSI and MAGNASTOR loading operations on site in accordance with the NAC or licensee quality assurance program, as appropriate. The licensee will perform decommissioning of the ISFSI in accordance with the licensee quality assurance program.

NAC was founded as a private corporation in 1968, with the primary focus of tracking, inspecting, handling, storing, and transporting spent nuclear fuel. NAC is a wholly owned subsidiary of USEC, Inc., since completion of its acquisition in November 2004. NAC is recognized in the industry as an expert in all aspects of the design, licensing, and operation of spent fuel handling, inspection, storage, and transport equipment, as well as in the management of spent fuel inventories.

Within the past 15 years, NAC has completed fabrication or has under construction the following transportation and/or storage systems.

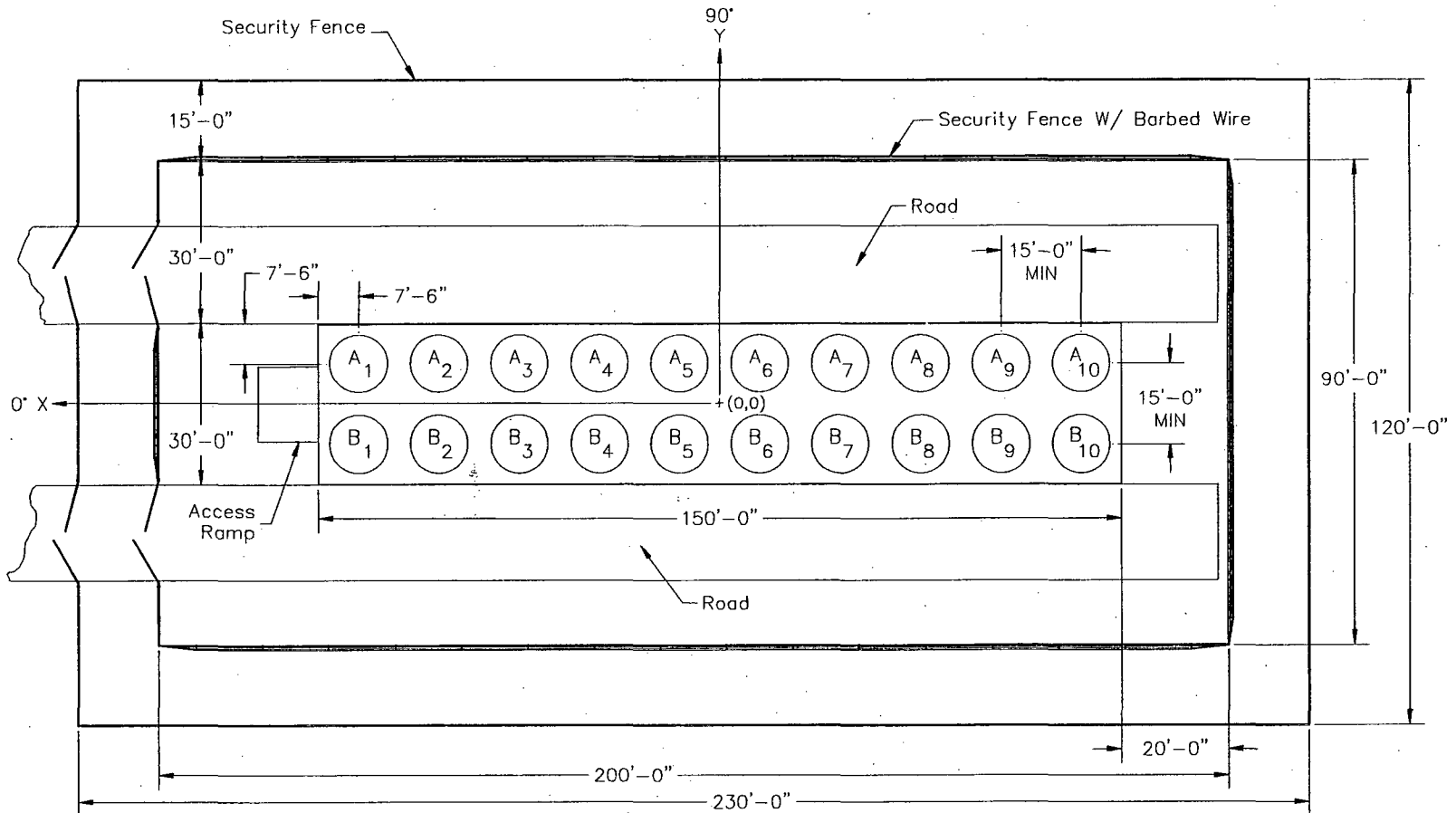
| <b>Part 71<br/>(Transport Casks)</b> | <b>Part 72<br/>(Storage System Casks and Components)</b> |
|--------------------------------------|--|
| 8 NAC-LWT                            | 7 UMS®/MPC transfer casks                                |
| 16 TRUPACT-II                        | 2 NAC-I28 S/T metal casks                                |
| 6 RH-TRU 72B                         | 1 NAC-I26 S/T metal cask                                 |
| 2 NAC-STC                            | > 210 UMS®/MPC TSCs                                      |
|                                      | > 212 UMS®/MPC concrete casks                            |

## 1.6 Generic Concrete Cask Arrays

A typical ISFSI storage pad layout for 20 MAGNASTOR systems is provided in Figure 1.6-1. As shown in this figure, roads parallel the sides of the pad to facilitate transfer of the concrete cask from the transporter to the designated storage position on the pad. Alternately, a ramp or low-profile concrete pad may be used to allow access for a motorized or towed frame for concrete cask transfer and placement. Loaded concrete casks are placed in the vertical orientation on the pad in a linear array. Array sizes could accommodate from 1 to more than 200 casks. Figure 1.6-1 shows the minimum concrete cask spacing and representative site dimensions. Actual spacing and facility dimensions are dependent on the general site layout, access roads, site boundaries, and transfer equipment selection, but must conform to the spacing specified in the Technical Specifications.

The reinforced concrete storage pad is capable of sustaining the transient loads from the cask transporter and the general loads of the stored casks. If necessary, the pad can be constructed in phases to specifically meet utility-required expansions.

Figure 1.6-1 Typical ISFSI Storage Pad Layout



## 1.7 References

1. 10 CFR 72, "Licensing Requirements for the Independent Storage of Spent Nuclear Fuel and High-Level Radioactive Waste and Reactor-Related Greater Than Class C Waste," Code of Federal Regulations, US Nuclear Regulatory Commission, Washington, DC.
2. NUREG-1536, "Standard Review Plan for Dry Cask Storage Systems," US Nuclear Regulatory Commission, Washington, DC, January 1997.
3. 10 CFR 71, "Packaging and Transportation of Radioactive Materials," Code of Federal Regulations, US Nuclear Regulatory Commission, Washington, DC.
4. Regulatory Guide 3.61, "Standard Format and Content for a Topical Safety Analysis Report for a Spent Fuel Dry Concrete Cask," US Nuclear Regulatory Commission, Washington, DC, February 1989.
5. ISG-15, "Materials Evaluation," US Nuclear Regulatory Commission, Washington, DC, Revision 0, January 10, 2001.
6. ANSI/ANS 57.9-1992, "Design Criteria for an Independent Spent Fuel Storage Installation (Dry Type)," American Nuclear Society, La Grange Park, IL, May 1992.
7. ACI 318-95, "Building Code Requirements for Structural Concrete," American Concrete Institute, Farmington Hills, MI.
8. ASME Boiler and Pressure Vessel Code, Section III, Subsection NB, "Class I Components," American Society of Mechanical Engineers, New York, NY, 2001 Edition with 2003 Addenda.
9. ASME Boiler and Pressure Vessel Code, Section III, Subsection NG, "Core Support Structures," American Society of Mechanical Engineers, New York, NY, 2001 Edition with 2003 Addenda.
10. ISG-11, "Cladding Considerations for the Transport and Storage of Spent Fuel," US Nuclear Regulatory Commission, Washington, DC, Revision 3, November 17, 2003.
11. ANSI N14.6-1993, "American National Standard for Radioactive Materials – Special Lifting Devices for Shipping Containers Weighing 10,000 Pounds (4,500 kg) or More," American National Standards Institute, Inc., Washington, DC, June 1993.
12. ASME Boiler and Pressure Vessel Code, Section IX, "Qualification Standards for Welding and Brazing Procedures, Welders, Brazers, and Welding and Brazing Operators," American Society of Mechanical Engineers, New York, NY, 2001 Edition with 2003 Addenda.
13. Recommended Practice No. SNT-TC-1A, "Personnel Qualification and Certification in Nondestructive Testing," The American Society for Nondestructive Testing, Inc., Columbus OH, edition as invoked by the applicable ASME Code.

14. ANSI N45.2.1-1980, "Cleaning of Fluid Systems and Associated Components During Construction Phase of Nuclear Power Plants," American National Standards Institute, Inc., Washington, DC.
15. ANSI N45.2.2-1978, "Packaging, Shipping, Receiving, Storage, and Handling of Items for Nuclear Power Plants," American National Standards Institute, Inc., Washington, DC.
16. ASTM C94<sup>a</sup>, "Standard Specification for Ready-Mixed Concrete," American Society for Testing and Materials, West Conshohocken, PA.
17. ASTM C150<sup>a</sup>, "Standard Specification for Portland Cement," American Society for Testing and Materials, West Conshohocken, PA.
18. ASTM C33<sup>a</sup>, "Standard Specification for Concrete Aggregates," American Society for Testing and Materials, West Conshohocken, PA.
19. ASTM C637<sup>a</sup>, "Specification for Aggregates for Radiation-Shielding Concrete," American Society for Testing and Materials, West Conshohocken, PA.
20. ASTM C494<sup>a</sup>, "Standard Specification for Chemical Admixtures for Concrete," American Society for Testing and Materials, West Conshohocken, PA.
21. ASTM C618<sup>a</sup>, "Specification for Fly Ash and Raw or Calcined Natural Pozzolan for Use as a Mineral Admixture in Portland Cement Concrete," American Society for Testing and Materials, West Conshohocken, PA.
22. ASTM C172<sup>a</sup>, "Standard Practice for Sampling Freshly Mixed Concrete," American Society for Testing and Materials, West Conshohocken, PA.
23. ASTM C31<sup>a</sup>, "Method of Making and Curing Concrete Test Specimens in the Field," American Society for Testing and Materials, West Conshohocken, PA.
24. ASTM C39<sup>a</sup>, "Standard Test Method for Compressive Strength of Cylindrical Concrete Specimens," American Society for Testing and Materials, West Conshohocken, PA.

---

<sup>a</sup> Current edition of testing standards at time of fabrication/construction is to be used.



**1.8**      **License Drawings**

This section presents the list of License Drawings for MAGNASTOR.

| Drawing Number | Title  | Revision No. |
|----------------|--|--------------|
| 71160-551      | Fuel Tube Assembly, MAGNASTOR – 37 PWR                           | 5            |
| 71160-560      | Assembly, Standard Transfer Cask, MAGNASTOR                      | 1            |
| 71160-561      | Structure, Weldment, Concrete Cask, MAGNASTOR                    | 3            |
| 71160-562      | Reinforcing Bar and Concrete Placement, Concrete Cask, MAGNASTOR | 2            |
| 71160-571      | Details, Neutron Absorber, Retainer, MAGNASTOR – 37 PWR          | 4            |
| 71160-572      | Details, Neutron Absorber, Retainer, MAGNASTOR – 87 BWR          | 4            |
| 71160-574      | Basket Support Weldments, MAGNASTOR – 37 PWR                     | 3            |
| 71160-575      | Basket Assembly, MAGNASTOR – 37 PWR                              | 6            |
| 71160-581      | Shell Weldment, Canister, MAGNASTOR                              | 2            |
| 71160-584      | Details, Canister, MAGNASTOR                                     | 2            |
| 71160-585      | TSC Assembly, MAGNASTOR  | 5            |
| 71160-590      | Loaded Concrete Cask, MAGNASTOR                                  | 3            |
| 71160-591      | Fuel Tube Assembly, MAGNASTOR – 87 BWR                           | 5            |
| 71160-598      | Basket Support Weldments, MAGNASTOR – 87 BWR                     | 4            |
| 71160-599      | Basket Assembly, MAGNASTOR – 87 BWR                              | 5            |
| 71160-600      | Basket Assembly, MAGNASTOR – 82 BWR                              | 3            |

R-205078


| REV | CHANGE        |
|-----|---------------|
| 0   | INITIAL ISSUE |
| 1   | ISSUE DEC 74  |
| 2   | ISSUE DEC 74  |
| 3   | ISSUE DEC 74  |
| 4   | ISSUE DEC 74  |
| 5   | ISSUE DEC 74  |

Security Related Information  
 Figure Withheld Under 10 CFR 2.390

| UNLESS OTHERWISE STATED  |  | GROUP | NAME               | DATE          | FUEL TUBE ASSEMBLY,<br>MAGNASTOR - 37 PWR             |
|--|--|-------|--------------------|---------------|---|
| <small>Engineering and Technical Staff<br/>           of the U.S. Atomic Energy Commission<br/>           All drawings herein shall be the property of the U.S. Atomic Energy Commission</small> |  |       | <i>[Signature]</i> | 1/25/76       |   |
|  |  |       | <i>[Signature]</i> | 1/25/76       |   |
|  |  |       | <i>[Signature]</i> | 1/25/76       |   |
|  |  |       | <i>[Signature]</i> | 1/25/76       |   |
| <small>ALL DRAWINGS ARE IN METRIC<br/>           UNLESS OTHERWISE STATED<br/>           NEXT AVAILABLE 71160-575</small>   |  |       | <i>[Signature]</i> | 1/25/76       |   |
| <small>ISSUING OFFICE LICENSE</small>  |  |       | <i>[Signature]</i> | 1/25/76       |   |
|  |  |       |                    | PROJECT 71160 | <small>FIGURE 551</small><br><small>OF 1 OF 2</small> |



Security Related Information  
Figure Withheld Under 10 CFR 2.390

|  |           |
|--|-----------|
|  <b>NAC<br/>INTERNATIONAL</b> |           |
| FUEL TUBE ASSEMBLY,<br>MAGNASTOR - 37 PWR  |           |
| PROJECT 71160  | ISSUE 551 |
| REV 3  |           |
| PAGE 2 OF 2  |           |

R-201938


|     |                 |
|-----|-----------------|
| REV | DATE            |
| 1   | INITIAL ISSUE   |
| 2   | REV. CORR. DATA |

Security Related Information  
Figure Withheld Under 10 CFR 2.390


| UNLESS OTHERWISE STATED<br>"EXHAUSTION AND RELAZIONE DATES"<br>OF ALL ASSESSMENTS |                   |         | NAC<br>INTERNATIONAL                              |
|---|-------------------|---------|---|
| GROUP   | NAME              | DATE    |   |
| GROUP   | R. J. [Signature] | 8/21/04 | ASSEMBLY, STANDARD<br>TRANSFER CASK,<br>MAGNASTOR |
| GROUP   | R. J. [Signature] | 8/21/04 |   |
| GROUP   | [Signature]       | 8/21/04 |   |
| GROUP   | [Signature]       | 8/21/04 |   |
| ALL EXHAUSTION ARE IN PAGES   |                   |         |   |
| EXHAUSTION DATES ARE IN PAGES   |                   |         |   |
| ASSET NUMBER  | N/A               |         | 71160   |
| ISSUE DATE  | LICENSE           |         | 560   |

NAC  
DCRM  
01


Security Related Information  
Figure Withheld Under 10 CFR 2.390

|  |             |
|--|-------------|
|  <b>MAC INTERNATIONAL</b> |             |
| ASSEMBLY, STANDARD<br>TRANSFER CASK,<br>MAGNASTOR  |             |
| PROJECT 71160  | REVISED 560 |
|  | REV 2 OF 1  |

Security Related Information  
Figure Withheld Under 10 CFR 2.390

|  |     |
|--|-----|
|  <b>NAC<br/>INTERNATIONAL</b> |     |
| ASSEMBLY, STANDARD<br>TRANSFER CASK,<br>MAGNASTOR  |     |
| 71160  | 560 |
| 3 of 4   |     |



Security Related Information  
Figure Withheld Under 10 CFR 2.390

|  |         |
|--|---------|
|  <b>NAC<br/>INTERNATIONAL</b> |         |
| ASSEMBLY, STANDARD<br>TRANSFER CASK,<br>MAGNASTOR  |         |
| PROJECT 71160  | REV 560 |
| 1 of 4   |         |

R-203559

| REV | DATE          | DESCRIPTION |
|-----|---------------|-------------|
| 0   | INITIAL ISSUE |             |
| 1   | LINE 1001 DA  |             |
| 2   | LINE 1001 DA  |             |


Security Related Information  
 Figure Withheld Under 10 CFR 2.390

|   |                       |         |   |       |     |
|---|-----------------------|---------|---|-------|-----|
| UNLESS OTHERWISE STATED<br><small>Engineering and Technical Staff<br/>       of this firm shall be<br/>       all those who are employed by us<br/>       and are in a position<br/>       of direct contact.</small> |                       |         |  |       |     |
| GROUP   | NAME                  | DATE    | STRUCTURE, WELDMENT,<br>CONCRETE CASK,<br>MAGNASTOR                                   |       |     |
| OWNER   | <i>R. [Signature]</i> | 8-18-52 |   |       |     |
| DESIGNER  | <i>R. [Signature]</i> | 8-18-52 |   |       |     |
| CONTRACTOR  | <i>[Signature]</i>    | 8-18-52 |   |       |     |
| <small>ALL CONTRACTS ARE IN FORCE<br/>       CONTRACTS SUBJECT TO BE VIEWED BY<br/>       ANY PERSON 71160-562<br/>       DRAWING NO. LICENSE</small>   |                       |         |  | 71160 | 561 |
|   |                       |         | <small>of 1 of 4</small>  |       |     |


NAC  
DCRM  
01




Security Related Information  
Figure Withheld Under 10 CFR 2.390

|  |             |
|--|-------------|
|  <b>NAC<br/>INTERNATIONAL</b> |             |
| STRUCTURE, WELDMENT,<br>CONCRETE CASK,<br>MAGNASTOR  |             |
| PROJECT 71160  | REVISED 561 |
|  | OF 2 OF 4   |

Security Related Information  
Figure Withheld Under 10 CFR 2.390

|  |             |
|--|-------------|
|  <b>NAC<br/>INTERNATIONAL</b> |             |
| STRUCTURE, WELDMENT,<br>CONCRETE CASK,<br>MAGNASTOR  |             |
| PROJECT 71160  | REVISED 561 |
|  | REVISED 3 4 |

Security Related Information  
Figure Withheld Under 10 CFR 2.390

|  |             |
|--|-------------|
|  <b>NAC<br/>INTERNATIONAL</b> |             |
| STRUCTURE, WELDMENT,<br>CONCRETE CASK,<br>MAGNASTOR  |             |
| PROJECT 71160  | DRAWING 561 |
|  | REV 3       |

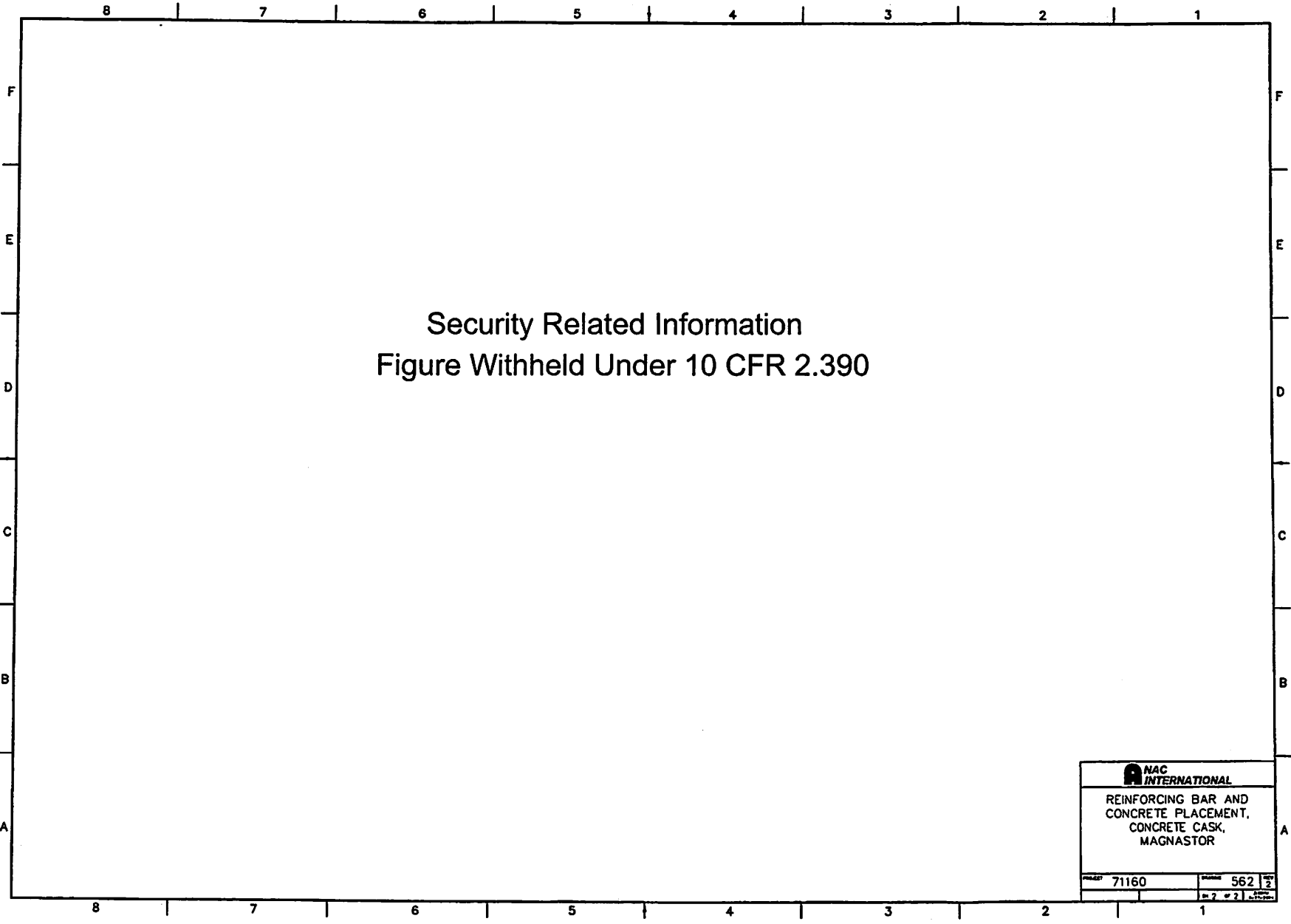
R-201971

| REV | DATE | DESCRIPTION   |
|-----|------|---------------|
| 0   |      | INITIAL ISSUE |
| 1   |      | ENG. CHG. 01  |
| 2   |      | ENG. CHG. 1A  |

Security Related Information  
 Figure Withheld Under 10 CFR 2.390

NAC  
DCRM  
01

| UNLESS OTHERWISE SPECIFIED |                         |         | NAC INTERNATIONAL  |     |
|----------------------------|-------------------------|---------|--|-----|
| GROUP                      | NAME                    | DATE    | REINFORCING BAR AND CONCRETE PLACEMENT, CONCRETE CASK, MAGNASTOR |     |
|                            | <i>[Signature]</i>      | 8/22/04 |  |     |
|                            | <i>[Signature]</i>      | 8/22/04 |  |     |
|                            | <i>[Signature]</i>      | 8/22/04 |  |     |
|                            | <i>[Signature]</i>      | 8/22/04 |  |     |
|                            | A. R. L. P. H.          | 8/22/04 | 71160  | 562 |
|                            | B. F. R. A. H. E. R. S. | 8/22/04 |  |     |



Security Related Information  
 Figure Withheld Under 10 CFR 2.390

|   |             |
|---|-------------|
| <b>NAC<br/>INTERNATIONAL</b>  |             |
| REINFORCING BAR AND<br>CONCRETE PLACEMENT,<br>CONCRETE CASK,<br>MAGNASTOR |             |
| PROJECT 71160   | DRAWING 562 |
|   | 2           |

R-206963

| REV | DATE | DESCRIPTION   |
|-----|------|---------------|
| 0   |      | INITIAL ISSUE |
| 1   |      | REVISION      |
| 2   |      | REVISION      |
| 3   |      | REVISION      |

Security Related Information  
 Figure Withheld Under 10 CFR 2.390

|  |  |  |       |                         |         |   |
|--|--|--|-------|-------------------------|---------|---|
| UNLESS OTHERWISE STATED<br><small>INCORPORATED AND REVISIONS SHALL<br/>     BE FOR THE ORIGINAL</small>                          |  |  | GROUP | NAME                    | DATE    | DETAILS,<br>NEUTRON ABSORBER, RETAINER,<br>MAGNASTOR - 37 PWR |
| ALL DIMENSIONS UNLESS OTHERWISE STATED<br><small>ARE TO BE<br/>     DIMENSIONS AS SHOWN UNLESS<br/>     OTHERWISE NOTED.</small> |  |  | GROUP | <i>Allen Lammann</i>    | 6/09/00 |   |
|  |  |  | GROUP | <i>Anthony E. Pardo</i> | 6/15/08 |   |
|  |  |  | GROUP | <i>Ken Bisher</i>       | 6/5/08  |   |
|  |  |  | GROUP | <i>Ken Bisher</i>       | 6/5/08  |   |
| ALL DIMENSIONS ARE TO UNLESS<br><small>OTHERWISE NOTED TO BE OTHERWISE NOTED</small>   |  |  | GROUP | <i>Anthony E. Pardo</i> | 6/15/08 | PROJECT 71160   |
| NEXT REVISION: 71160-575   |  |  | GROUP | <i>Al D'Amico</i>       | 6/26/08 | REVISION 571  |
| DRAWING TYPE LICENSE   |  |  | GROUP |                         |         | OF 1 OF 1   |

NAC  
 DCRM  
 01

R-206965

| REV | CHANGE        |
|-----|---------------|
| 0   | INITIAL ISSUE |
| 1   | INC - DER DA  |
| 2   | INC - DER DA  |
| 3   | INC - DER DA  |
| 4   | INC - DER SA  |

Security Related Information  
 Figure Withheld Under 10 CFR 2.390

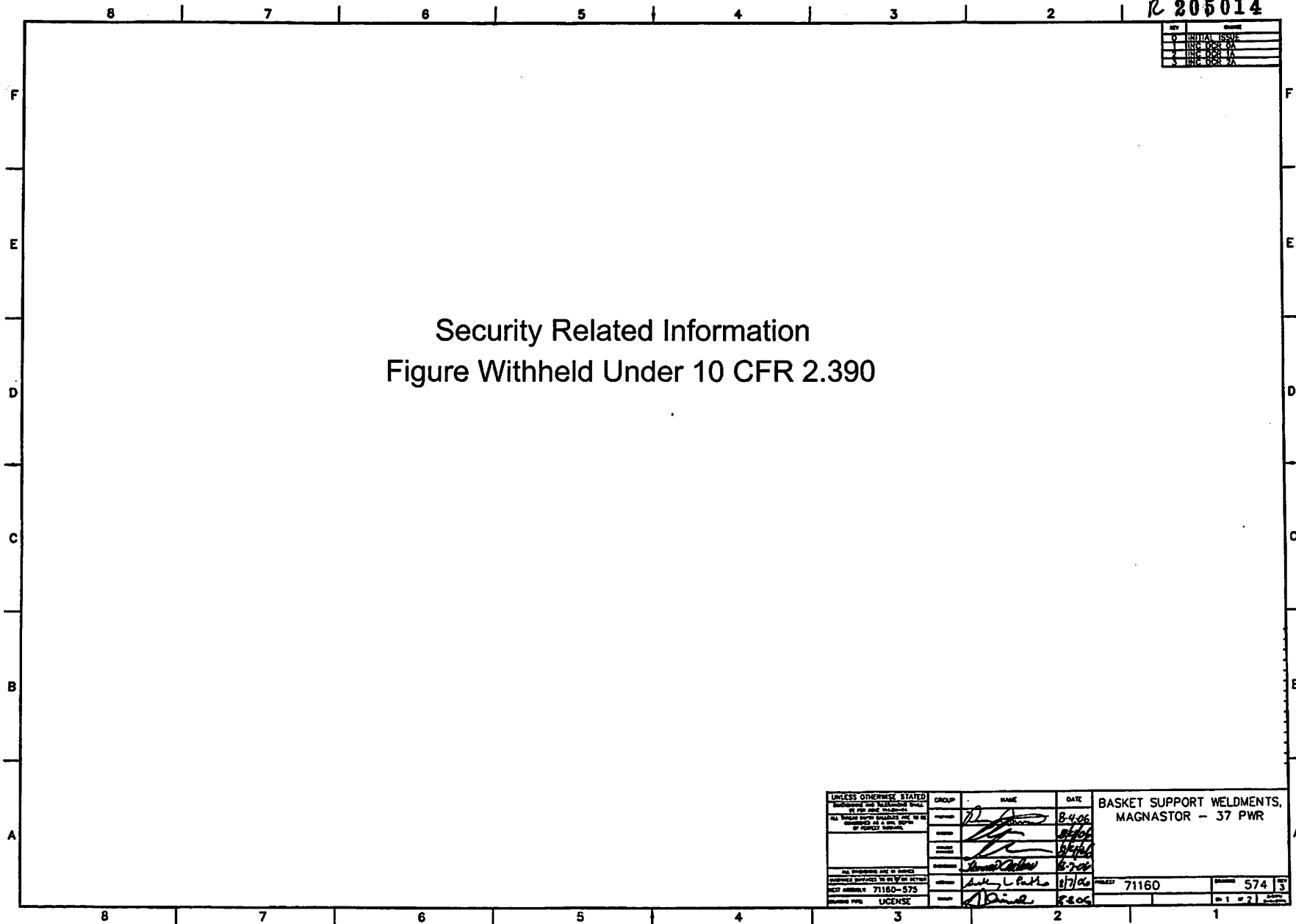
| UNLESS OTHERWISE STATED  |  | GROUP | NAME             | DATE          | DETAILS,<br>NEUTRON ABSORBER, RETAINER,<br>MAGNASTOR - B7 BWR |
|--|--|-------|------------------|---------------|---|
| * Professional and Technical Staff<br>or other staff                                   |  | OWNER | James Aronson    | 6/5/58        |   |
| ALL OTHERS MUST SIGNIFY HOW TO BE<br>CONSIDERED AS A UNIT WITHIN<br>OF PROJECT NUMBER. |  | OWNER | Anthony L. Patis | 6/5/58        |   |
|  |  | OWNER | James Aronson    | 6/5/58        |   |
|  |  | OWNER | Anthony L. Patis | 6/5/58        |   |
| ALL WORKING AND IN WORK  |  | OWNER | James Aronson    | 6/5/58        |   |
| UNLESS OTHERWISE STATED  |  | OWNER | Anthony L. Patis | 6/5/58        |   |
| NFP NUMBER 71160-591   |  | OWNER | James Aronson    | 6/5/58        |   |
| ISSUANCE TYPE LICENSE  |  | OWNER | Anthony L. Patis | 6/5/58        |   |
|  |  |       |                  | PROJECT 71160 | NUMBER 572  |
|  |  |       |                  | REV 4         |   |

NAC  
 DCRM  
 01

R 205014

|   |               |
|---|---------------|
| 0 | INITIAL ISSUE |
| 1 | REISSUE       |
| 2 | REISSUE       |
| 3 | REISSUE       |

Security Related Information  
 Figure Withheld Under 10 CFR 2.390




MAC  
 Dec 01

|  |        |                    |        |   |
|--|--------|--------------------|--------|---|
| UNLESS OTHERWISE STATED<br>Engineering and Technical Staff<br>at the time of work  | GROUP  | NAME               | DATE   | BASKET SUPPORT WELDMENTS,<br>MAGNASTOR - 37 PWR |
| ALL WORKER SIGNATURES ARE TO BE<br>CORRECTED AS A ONE COPY<br>OF PERFECT SIGNATURE | Welder | <i>[Signature]</i> | 8-4-06 |   |
|  | Welder | <i>[Signature]</i> | 8/7/06 |   |
|  | Welder | <i>[Signature]</i> | 8/7/06 |   |
| ALL SIGNATURES ARE TO BE<br>CORRECTED TO BE IN FULL<br>ACTUALITY 71160-573         | Welder | <i>[Signature]</i> | 8/7/06 | PROJECT 71160                                   |
| ISSUED BY LICENSE  | Welder | <i>[Signature]</i> | 8-2-06 | ISSUED 574                                      |



Security Related Information  
Figure Withheld Under 10 CFR 2.390

|  |            |
|--|------------|
|  <b>NAC<br/>INTERNATIONAL</b> |            |
| BASKET SUPPORT WELDMENTS,<br>MAGNASTOR - 37 PWR  |            |
| PROJECT 71160  | NUMBER 574 |
|  | OF 2 OF 2  |

R-205053


| NO. | ISSUE | DATE |
|-----|-------|------|
| 1   | ISSUE | DA   |
| 2   | ISSUE | DA   |
| 3   | ISSUE | DA   |
| 4   | ISSUE | DA   |
| 5   | ISSUE | DA   |
| 6   | ISSUE | DA   |

-Security Related Information  
Figure Withheld Under 10 CFR 2.390


| UNLESS OTHERWISE STATED<br>REGISTRATION FOR LICENSES SHALL<br>BE BY THE ISSUING<br>OFFICE                                    |  |  | GROUP | NAME               | DATE   | BASKET ASSEMBLY,<br>MAGNASTOR - 37 PWR |
|--|--|--|-------|--------------------|--------|--|
| ALL LICENSES MUST BE REISSUED<br>ANNUALLY OR AS OTHERWISE<br>DIRECTED BY THE ISSUING<br>OFFICE                               |  |  |       | <i>[Signature]</i> | 8/4/06 |  |
|  |  |  |       | <i>[Signature]</i> | 8/1/06 |  |
|  |  |  |       | <i>[Signature]</i> | 8/1/06 |  |
|  |  |  |       | <i>[Signature]</i> | 8/1/06 |  |
| ALL OPERATIONS ARE TO BE<br>CONDUCTED IN ACCORDANCE WITH<br>THE REGULATIONS OF THE<br>NRC AND/OR THE STATE OF<br>MISSISSIPPI |  |  |       | <i>[Signature]</i> | 8/1/06 |  |
| NEXT REGISTRATION IS BY THE ISSUING<br>OFFICE  |  |  |       | <i>[Signature]</i> | 8/1/06 |  |
| REGISTRATION NO. 71160-585   |  |  |       | <i>[Signature]</i> | 8/1/06 | ISSUE 575                              |
| ISSUING OFFICE LICENSE   |  |  |       | <i>[Signature]</i> | 8/1/06 | OF 1 OF 3                              |

MAC  
DCRM  
01

Security Related Information  
Figure Withheld Under 10 CFR 2.390

|  |     |
|--|-----|
|  <b>NAC<br/>INTERNATIONAL</b> |     |
| BASKET ASSEMBLY,<br>MAGNASTOR - 37 PWR   |     |
| 71160  | 575 |
|  | 2 3 |

Security Related Information  
Figure Withheld Under 10 CFR 2.390

|  |           |
|--|-----------|
|  <b>NAC<br/>INTERNATIONAL</b> |           |
| BASKET ASSEMBLY,<br>MAGNASTOR - 37 PWR   |           |
| PROJECT 71160  | ISSUE 575 |
| REV 8  |           |
| = 3 of 3   |           |

R-208564


|     |               |
|-----|---------------|
| REV | CHANGE        |
| 0   | INITIAL ISSUE |
| 1   | REV. DES. 1A  |
| 2   | REV. DES. 1A  |

Security Related Information  
 Figure Withheld Under 10 CFR 2.390

| UNLESS OTHERWISE STATED:<br><small>Endorsements and Endorsement Dates<br/>         of this and all weldments</small>           | GROUP   | NAME               | DATE      | SHELL WELDMENT,<br>CANISTER,<br>MAGNASTOR |
|--|---------|--------------------|-----------|---|
| <small>ALL WELDMENT DATA CALLED OUT ARE TO BE<br/>         CONSIDERED AS A PART HEREOF<br/>         OF RECORD DRAWING.</small> | WELDER  | <i>Raymond</i>     | 7-5-05    |   |
|  | WELDER  | <i>R. Wells</i>    | 7-6-05    |   |
|  | WELDER  | <i>[Signature]</i> | 7-27-05   |   |
|  | WELDER  | <i>[Signature]</i> | 9-22-05   |   |
| <small>ALL DIMENSIONS ARE IN INCHES<br/>         UNLESS OTHERWISE SPECIFIED</small>  | WELDER  | <i>[Signature]</i> | 9-25-05   |   |
| <small>NEXT ASSEMBLY 71160-585</small>   | PROJECT | 71160              | SHEET 581 | OF 2                                      |
| <small>ISSUANCE DATE</small>   | LICENSE | <i>Raymond</i>     | 7-29-05   | OF 2                                      |

NAC  
 DCRM  
 01

Security Related Information  
Figure Withheld Under 10 CFR 2.390

|   |     |
|---|-----|
|  |     |
| SHELL WELDMENT,<br>CANISTER,<br>MAGNASTOR   |     |
| 71160   | 581 |
| 2 2   |     |

R-203565

| REV | DATE          |
|-----|---------------|
| 1   | INITIAL ISSUE |
| 2   | REC'D BY DA   |
| 3   | REC'D BY TA   |

Security Related Information  
 Figure Withheld Under 10 CFR 2.390

|  |           |  |       |      |      |                                    |
|--|-----------|--|-------|------|------|------------------------------------|
| UNLESS OTHERWISE STATED  |           |  | GROUP | NAME | DATE | DETAILS,<br>CANISTER,<br>MAGNASTOR |
| REGISTRATION AND INSPECTION BOARD<br>OF THE<br>NRC                             |           |  |       |      |      |                                    |
| ALL TABLES MUST BE COMPLETED AND TO BE<br>CORRECTED AS A MATTER OF<br>COURTESY |           |  |       |      |      |                                    |
| ALL INFORMATION ARE IN WORDS   |           |  |       |      |      |                                    |
| CHANGES INDICATED BY CE OR V OR OTHER  |           |  |       |      |      |                                    |
| NEW SERIALS  | 71160-585 |  |       |      |      | 71160                              |
| ISSUING OFFICE   | LICENSE   |  |       |      |      | 584                                |
|  |           |  |       |      |      | 1                                  |

NAC  
DCRM  
01

R-205016

| REV | CHANGE        |
|-----|---------------|
| 0   | INITIAL ISSUE |
| 1   | INC DEC 1A    |
| 2   | INC DEC 2A    |
| 3   | INC DEC 3A    |
| 4   | INC DEC 4A    |
| 5   | INC DEC 5A    |


Security Related Information  
 Figure Withheld Under 10 CFR 2.390

NAC  
 DCRM  
 01

| UNLESS OTHERWISE STATED<br><small>ENGINEERING AND TECHNICAL STAFF<br/>       OF THE UNIT INDICATED</small>              | GROUP | NAME               | DATE    | TSC ASSEMBLY,<br>MAGNASTOR |
|---|-------|--------------------|---------|----------------------------|
| <small>ALL SIGNS SHOULD BE PLACED AND TO BE<br/>       IDENTIFIED AS A SIGN, COPY<br/>       OF PROJECT NUMBER.</small> |       | <i>[Signature]</i> | 4-25-06 |                            |
|   |       | <i>[Signature]</i> | 4/26/06 |                            |
|   |       | <i>[Signature]</i> | 5-3-06  |                            |
| <small>ALL SIGNATURES ARE IN BLOCK</small>  |       | <i>[Signature]</i> | 5/4/06  |                            |
| <small>IDENTIFIED SIGNATURE TO BE VIEWED BY<br/>       THE PUBLIC UNDER 10 CFR 2.390</small>                            |       | <i>[Signature]</i> | 5-11-06 |                            |
| <small>PROJECT NUMBER</small>   |       |                    |         | 71160                      |
| <small>ISSUE NUMBER</small>   |       |                    |         | 585                        |
| <small>ISSUE DATE</small>   |       |                    |         | 1 of 2                     |




Security Related Information  
Figure Withheld Under 10 CFR 2.390

|  |           |
|--|-----------|
|  <b>NAC<br/>INTERNATIONAL</b> |           |
| TSC ASSEMBLY,<br>MAGNASTOR   |           |
| PROJECT 71160  | REV 585 3 |
|  | 2 2       |




Security Related Information  
Figure Withheld Under 10 CFR 2.390

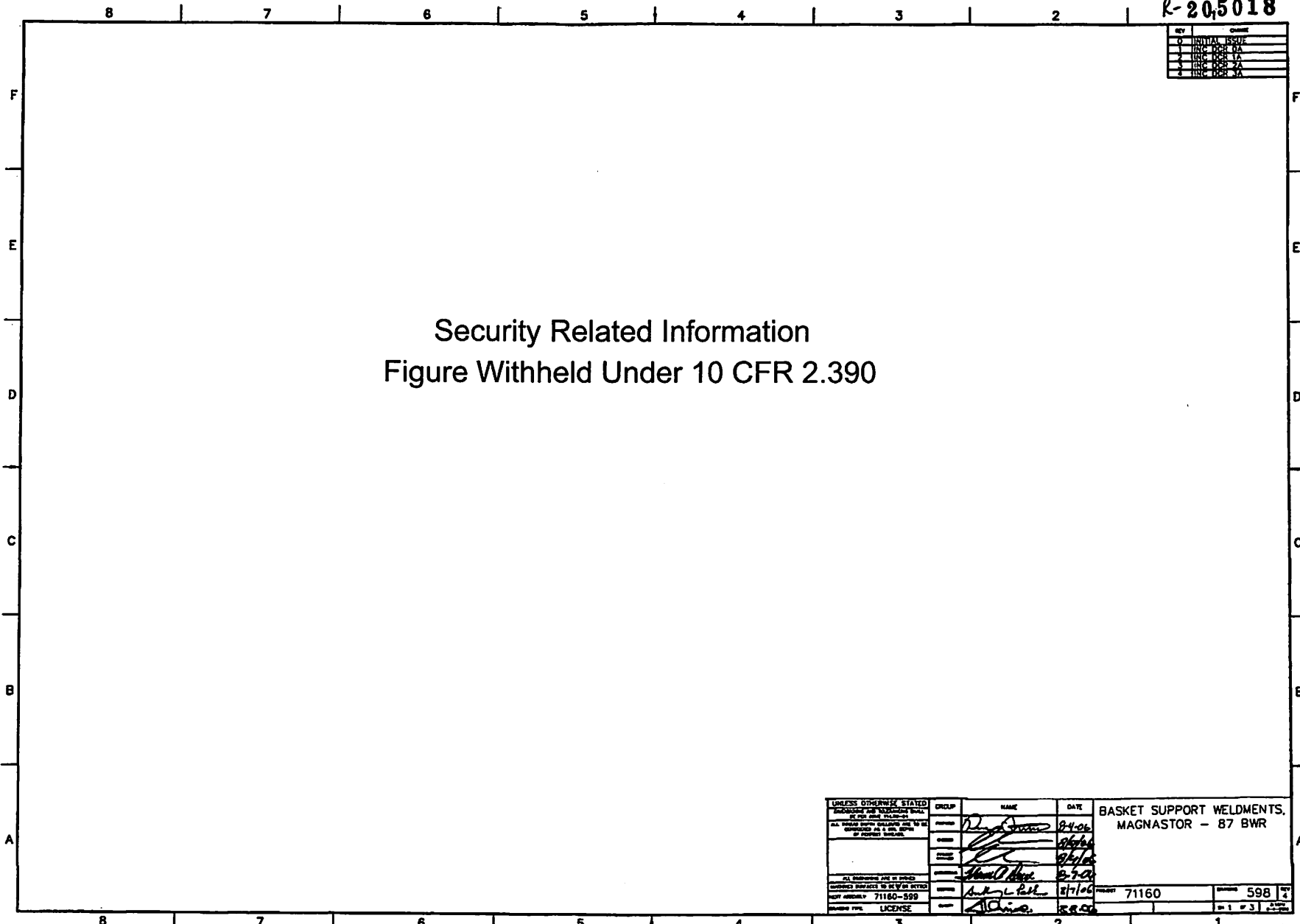
|  |     |
|--|-----|
|  <b>NAC<br/>INTERNATIONAL</b> |     |
| LOADED CONCRETE CASK,<br>MAGNASTOR   |     |
| 71160  | 590 |
|  | 2 2 |



Security Related Information  
Figure Withheld Under 10 CFR 2.390

|   |            |       |
|---|------------|-------|
|  |            |       |
| FUEL TUBE ASSEMBLY,<br>MAGNASTOR - 87 BWR   |            |       |
| PROJECT 71160   | REVISE 591 | REV 5 |
|   | 2 2        |       |

R-20,5018




| REV | CHANGE        |
|-----|---------------|
| 0   | INITIAL ISSUE |
| 1   | INC. DES. VA  |
| 2   | INC. DES. VA  |
| 3   | INC. DES. VA  |
| 4   | INC. DES. VA  |


| UNLESS OTHERWISE STATED   |  |  |  | GROUP | NAME | DATE   | BASKET SUPPORT WELDMENTS,<br>MAGNASTOR - 87 BWR |       |
|---|--|--|--|-------|------|--------|---|-------|
| EXCEPT FOR SIGNATURES SHALL BE FOR THIS PROJECT                         |  |  |  |       |      |        |   |       |
| ALL TRADE SHOWS SHALL BE TO BE COMPLETED AS A PERCENT OF PROJECT BUDGET |  |  |  |       |      | 24-06  |   |       |
|   |  |  |  |       |      | 8/2/06 |   |       |
|   |  |  |  |       |      | 2-3-07 |   |       |
| ALL SIGNATURES MUST BE PRINTED  |  |  |  |       |      |        |   |       |
| EMERGENCY RESPONSE TO NEW OR BETTER                                     |  |  |  |       |      |        |   |       |
| NEW MODEL 71160-599   |  |  |  |       |      | 8/7/06 | 71160   |       |
| ISSUE TYPE LICENSE  |  |  |  |       |      | 8/2/06 |   |       |
|   |  |  |  |       |      |        | 598   | REV 4 |
|   |  |  |  |       |      |        | 1   | 3     |

10  
10  
C  
MIN

Security Related Information  
Figure Withheld Under 10 CFR 2.390

|  |             |
|--|-------------|
|  <b>NAC<br/>INTERNATIONAL</b> |             |
| BASKET SUPPORT WELDMENTS,<br>MAGNASTOR - 87 BWR  |             |
| PROJECT 71160  | DRAWING 598 |
|  | 2 of 3      |

Security Related Information  
Figure Withheld Under 10 CFR 2.390

|  |             |
|--|-------------|
|  <b>NAC<br/>INTERNATIONAL</b> |             |
| BASKET SUPPORT WELDMENTS,<br>MAGNASTOR - 87 BWR  |             |
| PROJECT 71160  | DRAWING 598 |
|  | OF 3 OF 3   |



R-205054

| REV | DATE     | DESCRIPTION |
|-----|----------|-------------|
| 1   | 11/15/00 | ISSUE       |
| 2   | 11/15/00 | ISSUE       |
| 3   | 11/15/00 | ISSUE       |
| 4   | 11/15/00 | ISSUE       |
| 5   | 11/15/00 | ISSUE       |

Security Related Information  
 Figure Withheld Under 10 CFR 2.390

| UNLESS OTHERWISE STATED  |  | GROUP   | NAME   | DATE    |
|--|--|---------|--------|---------|
| INDICATING THE SIGNATURE SHALL BE THE SIGNATURE OF THE SIGNATORY               |  |         |        |         |
| ALL SIGNED DOCUMENTS SHALL BE TO BE CONSIDERED AS A SIGNATURE OF THE SIGNATORY |  |         |        |         |
| ALL SIGNATURES MUST BE SIGNED  |  |         |        |         |
| UNLESS OTHERWISE STATED, THE SIGNATURE SHALL BE THE SIGNATURE OF THE SIGNATORY |  |         |        |         |
| NAC APPROVAL 71160-585   |  |         |        |         |
| Signature Form   |  | LICENSE | Alaine | 1/15/00 |


BASKET ASSEMBLY,  
MAGNASTOR - 87 BWR

71160 599 3


1 = 3

NAC  
DCRM  
01

Security Related Information  
Figure Withheld Under 10 CFR 2.390

|  |               |
|--|---------------|
|  <b>NAC<br/>INTERNATIONAL</b> |               |
| BASKET ASSEMBLY,<br>MAGNASTOR - 87 BWR   |               |
| PROJECT 71160  | ISSUE 599   3 |
|  | 2 of 3        |

Security Related Information  
Figure Withheld Under 10 CFR 2.390

|  |         |
|--|---------|
|  <b>NAC<br/>INTERNATIONAL</b> |         |
| BASKET ASSEMBLY,<br>MAGNASTOR - 87 BWR   |         |
| PROJECT 71160  | REV 599 |
|  | 3       |
|  | 3       |

R-205055


| REV | DATE          |
|-----|---------------|
| 1   | INITIAL ISSUE |
| 2   | REV. 08-04    |
| 3   | REV. 08-04    |

Security Related Information  
 Figure Withheld Under 10 CFR 2.390


| UNLESS OTHERWISE STATED                 | GROUP        | NAME               | DATE    | BASKET ASSEMBLY,<br>MAGNASTOR - 82 BWR |        |
|---|--------------|--------------------|---------|--|--------|
| UNLESS OTHERWISE STATED                 | OWNER        | <i>[Signature]</i> | 8/4/00  | PROJECT                                | 71160  |
| ALL INITIAL SERVICE CONTRACTS ARE TO BE | OPERATOR     | <i>[Signature]</i> | 8/5/00  | ISSUE                                  | 600    |
| NUMBERED AS A SET WITH                  | MAINTENANCE  | <i>[Signature]</i> | 8/15/00 | REVISED                                | 3      |
| OF PROJECT RECORDS.                     | INSPECTION   | <i>[Signature]</i> | 8/15/00 | BY                                     | 1 of 3 |
| ALL DIMENSIONS ARE IN INCHES            | CONSTRUCTION | <i>[Signature]</i> | 8/15/00 |  |        |
| DIMENSIONS SHOWN TO BE IN FEET          | PERMIT       | <i>[Signature]</i> | 8/15/00 |  |        |
| NOT DRAWN TO SCALE                      | APPROVED     | <i>[Signature]</i> | 8/15/00 |  |        |
| PROJECT NO. 71160-505                   | LICENSE      | <i>[Signature]</i> | 8/15/00 |  |        |
| DRAWING NO. 71160-505                   |              |                    |         |  |        |

NAC  
DCRM  
01


Security Related Information  
Figure Withheld Under 10 CFR 2.390

|  |           |
|--|-----------|
|  <b>MAC<br/>INTERNATIONAL</b> |           |
| BASKET ASSEMBLY,<br>MAGNASTOR - 82 BWR   |           |
| PROJECT 71160  | REV 600   |
|  | of 2 of 3 |


Security Related Information  
Figure Withheld Under 10 CFR 2.390

|  |     |
|--|-----|
|  <b>NAC<br/>INTERNATIONAL</b> |     |
| BASKET ASSEMBLY,<br>MAGNASTOR - 82 BWR   |     |
| 71160  | 600 |
| = 3 * 5  |     |

Security Related Information  
Figure Withheld Under 10 CFR 2.390

|  |             |
|--|-------------|
|  <b>NAC<br/>INTERNATIONAL</b> |             |
| BASKET ASSEMBLY,<br>MAGNASTOR - 82 BWR   |             |
| 71160  | 600   3     |
|  | Dr. 4. 0. 5 |

Security Related Information  
Figure Withheld Under 10 CFR 2.390

|  |              |
|--|--------------|
|  <b>NAC<br/>INTERNATIONAL</b> |              |
| BASKET ASSEMBLY,<br>MAGNASTOR - 82 BWR   |              |
| PROJECT 71160  | ISSUES 600 3 |
|  | 5 5          |



## Chapter 2 Principal Design Criteria

### Table of Contents

|        |   |       |
|--------|---|-------|
| 2      | PRINCIPAL DESIGN CRITERIA .....   | 2-1   |
| 2.1    | MAGNASTOR System Design Criteria .....                                  | 2.1-1 |
| 2.2    | Spent Fuel To Be Stored .....   | 2.2-1 |
| 2.2.1  | PWR Fuel Evaluation .....   | 2.2-1 |
| 2.2.2  | BWR Fuel Evaluation .....   | 2.2-2 |
| 2.3    | Design Criteria for Environmental Conditions and Natural Phenomena..... | 2.3-1 |
| 2.3.1  | Tornado Missiles and Wind Loadings .....                                | 2.3-1 |
| 2.3.2  | Water Level (Flood) Design.....   | 2.3-2 |
| 2.3.3  | Seismic Design.....   | 2.3-3 |
| 2.3.4  | Snow and Ice Loadings .....   | 2.3-4 |
| 2.3.5  | Combined Load Criteria.....   | 2.3-4 |
| 2.3.6  | Environmental Temperatures.....   | 2.3-6 |
| 2.4    | Safety Protection Systems.....  | 2.4-1 |
| 2.4.1  | General .....   | 2.4-1 |
| 2.4.2  | Confinement Barriers and Systems .....                                  | 2.4-2 |
| 2.4.3  | Concrete Cask Cooling .....   | 2.4-3 |
| 2.4.4  | Protection by Equipment.....  | 2.4-3 |
| 2.4.5  | Protection by Instrumentation .....                                     | 2.4-3 |
| 2.4.6  | Nuclear Criticality Safety.....   | 2.4-3 |
| 2.4.7  | Radiological Protection.....  | 2.4-5 |
| 2.4.8  | Fire Protection.....  | 2.4-6 |
| 2.4.9  | Explosion Protection.....   | 2.4-6 |
| 2.4.10 | Auxiliary Structures .....  | 2.4-6 |
| 2.5    | Decommissioning Considerations .....                                    | 2.5-1 |
| 2.6    | References.....   | 2.6-1 |

### List of Figures

|              |   |       |
|--------------|---|-------|
| Figure 2.2-1 | PWR Fuel Preferential Loading Zones ..... | 2.2-4 |
| Figure 2.2-2 | 82-Assembly-BWR Basket Pattern.....       | 2.2-5 |

### List of Tables

|             |  |       |
|-------------|--|-------|
| Table 2.1-1 | MAGNASTOR System Design Criteria .....                         | 2.1-2 |
| Table 2.1-2 | ASME Code Alternatives for MAGNASTOR Components .....          | 2.1-3 |
| Table 2.2-1 | PWR Fuel Assembly Characteristics .....                        | 2.2-6 |
| Table 2.2-2 | BWR Fuel Assembly Characteristics.....                         | 2.2-7 |
| Table 2.3-1 | Load Combinations for the Concrete Cask.....                   | 2.3-7 |
| Table 2.3-2 | Load Combinations for the TSC .....                            | 2.3-7 |
| Table 2.3-3 | Structural Design Criteria for Components Used in the TSC..... | 2.3-8 |
| Table 2.4-1 | Safety Classification of MAGNASTOR Components.....             | 2.4-7 |

## 2 PRINCIPAL DESIGN CRITERIA

MAGNASTOR<sup>®</sup> is a canister-based spent fuel dry storage cask system designed in accordance with the requirements of 10 CFR 72 [10], Subpart L, Approval of Spent Fuel Storage Casks. It is designed to store a variety of undamaged PWR and BWR spent fuel assemblies. This chapter presents the principal design criteria for the MAGNASTOR components.

## 2.1 MAGNASTOR System Design Criteria

The design of MAGNASTOR ensures that the stored spent fuel is maintained subcritical in an inert environment, within allowable temperature limits, and is retrievable. The acceptance testing and maintenance program specified in Chapter 10 ensures that the system is, and remains, suitable for the intended purpose. The MAGNASTOR design criteria appear in Table 2.1-1.

Approved alternatives to the ASME Code for the design procurement, fabrication, inspection, and testing of MAGNASTOR TSCs and spent fuel baskets are listed in Table 2.1-2.

Proposed alternatives to ASME Code, Section III, 2001 Edition with Addenda through 2003, including alternatives listed in Table 2.1-2, may be used when authorized by the Director of the Office of Nuclear Material Safety and Safeguards or designee. The request for such alternatives should demonstrate the following.

- The proposed alternatives would provide an acceptable level of quality and safety, or compliance with the specified requirements of ASME Code, Section III, Subsections NB and NG, 2001 Edition with Addenda through 2003, would result in hardship or unusual difficulty without a compensating increase in the level of quality and safety.
- Requests for alternatives shall be submitted in accordance with 10 CFR 72.

Table 2.1-1 MAGNASTOR System Design Criteria

| Parameter                                | Criteria  |
|--|---|
| Design Life                              | 50 years  |
| Design Code – Confinement                |   |
| TSC                                      | ASME Code, Section III, Subsection NB [1] for confinement boundary                          |
| TSC Cavity Atmosphere                    | Helium  |
| Gas Pressure                             | 7.0 atmospheres gauge (103 psig)  |
| Design Code - Nonconfinement             |   |
| Fuel Basket                              | ASME Code, Section III, Subsection NG [2] and NUREG/CR-6322 [3]                             |
| Concrete Cask                            | ACI-349 [4], ACI-318 [5]  |
| Transfer Cask                            | ANSI N14.6 [6], NUREG-0612 [15]   |
| Thermal                                  |   |
| Maximum Fuel Cladding Temperature        | 752°F (400°C) for Normal and Transfer [7]<br>1058°F (570°C) for Off-Normal and Accident [8] |
| Ambient Temperature                      |   |
| Normal (average annual ambient)          | 76°F  |
| Off-Normal (extreme cold; extreme hot)   | -40°F; 106°F  |
| Accident                                 | 133°F   |
| Concrete Temperature                     |   |
| Normal Conditions                        | ≤150°F (bulk) [4]; ≤ 200°F (local) [9]  |
| Off-Normal/Accident Conditions           | ≤ 350°F local/ surface [4]  |
| Radiation Protection/Shielding           |   |
| Owner-Controlled Area Boundary Dose [10] |   |
| Normal/Off-Normal Conditions             | 25 mrem (Annual Whole Body) [10]  |
| Accident Whole Body Dose                 | 5 rem (Whole Body) [10]   |

**Table 2.1-2 ASME Code Alternatives for MAGNASTOR Components**

| <b>Component</b>                 | <b>Reference ASME Code Section/Article</b>                                       | <b>Code Requirement</b>  | <b>Exception, Justification and Compensatory Measures</b>  |
|----------------------------------|--|--|--|
| TSC and Fuel Basket              | NCA-1000, NCA-2000, NCA-3000, NCA-4000, NCA-5000, NCA-8000, NB-1110, and NG-1110 | Requirements for Code stamping of NB components and preparation of Code Design Specifications, Design Reports, Overpressure Protection Report (TSC only), and Data Reports, and Quality Assurance requirements in accordance with Code requirements. | Code stamping is not required for the TSC or fuel baskets. Code Design Specifications, Design Reports, Overpressure Protection Report, and Data Reports are not required. The TSC and Fuel Basket are designed, procured, fabricated, inspected and tested in accordance with a QA Program meeting 10 CFR 72, Subpart G. Authorized Nuclear Inspection Agency Services are not required. |
| TSC Pressure-Retaining Materials | NB-2000  | Pressure-retaining material to be provided by ASME-approved Material Organization.   | Materials will be supplied with Certified Material Test Reports by NAC approved suppliers.   |
| TSC Closure Lid-to-Shell Weld    | NB-4243  | Full penetration welds required for Category C joints.   | The closure lid-to-shell weld is not a full penetration weld. The design and analysis of the closure lid weld utilizes a 0.8 stress reduction factor in accordance with ISG-15 [23].   |
| Port Cover-to-Closure Lid Weld   | NB-5230  | Radiographic (RT) examination required.  | Final surface liquid penetrant examination to be performed per ASME Code Section V, Article 6. PT acceptance criteria is to be in accordance with NB-5350.   |
| TSC Closure Lid-to-Shell Weld    | NB-5230  | Radiographic (RT) examination required.  | In accordance with ISG-15, the TSC closure lid-to-shell weld is to be inspected by progressive surface liquid penetrant (PT) examination of the root, midplane and final surface layers. The progressive PT examination of the weld will be performed in accordance with ASME Code, Section V, Article 6, and acceptance criteria per NB-5350.   |

Table 2.1-2 ASME Code Alternatives for MAGNASTOR Components

| Component   | Reference ASME Code Section/Article | Code Requirement  | Exception, Justification and Compensatory Measures   |
|---|-------------------------------------|---|--|
| TSC Closure Ring-to-TSC Shell & TSC Closure Ring-to-Closure Lid | NB-5230                             | Radiographic (RT) examination required.   | Final surface liquid penetrant examination to be performed per ASME Code Section V, Article 6. PT acceptance criteria is to be in accordance with NB-5350.   |
| TSC   | NB-6111                             | All completed pressure retaining systems shall be pressure tested.  | Following closure lid to TSC shell welding, each TSC shall be hydrostatically pressure tested to 125% of MNOP. No observable pressure drop or water leakage from the closure lid to TSC shell weld is allowed. Since the shell welds of the TSC cannot be checked for leakage during this pressure test, as required by the Code, the shop leakage test to $10^{-7}$ ref cc/sec (as described in Section 10.1.3) provides reasonable assurance as to its leak tightness. |
| TSC   | NB-7000                             | Pressure vessels shall be protected from the consequences of pressure conditions exceeding design pressure. | No overpressure protection is provided. The function of the TSC is to confine radioactive contents without release under normal conditions, or off-normal and accident events of storage. The TSC is designed to withstand the maximum internal pressure considering 100% fuel rod failure and maximum accident condition temperatures.  |
| TSC   | NB-8000                             | States requirements for nameplates, stamping and reports per NCA-8000.                                      | The TSC is marked and identified to ensure proper identification of the contents. Code stamping is not required.   |
| TSC Basket Assembly Structural Materials                        | NG-2000                             | Core support structural materials are to be provided by an ASME approved Material Organization.             | Fuel basket structural materials with Certified Material Test Reports to be supplied by NAC approved suppliers.  |

**Table 2.1-2 ASME Code Alternatives for MAGNASTOR Components**

| <b>Component</b>                          | <b>Reference ASME Code Section/Article</b> | <b>Code Requirement</b>   | <b>Exception, Justification and Compensatory Measures</b>   |
|---|--|---|---|
| TSC Basket Assembly Structural Components | NG-8000                                    | Requirements for nameplates, stamping and reports per NCA-8000. | The TSC basket structural assembly is marked and identified to ensure component traceability in accordance with NAC's QA Program. |



## 2.2 Spent Fuel To Be Stored

MAGNASTOR is designed to safely store up to 37 PWR or up to 87 BWR spent fuel assemblies, contained within a TSC. The fuel assemblies are assigned to two groups of PWR and two groups of BWR fuel assemblies on the basis of fuel assembly length. Refer to Chapter 1 for the fuel assembly length groupings. For TSC spent fuel content loads less than a full basket, empty fuel positions shall include an empty fuel cell insert.

Undamaged PWR and BWR fuel assemblies having parameters as shown in Table 2.2-1 and Table 2.2-2, respectively, may be stored in MAGNASTOR.

The minimum initial enrichment limits are shown in Table 2.2-1 and Table 2.2-2 for PWR and BWR fuel, respectively, and exclude the loading of fuel assemblies enriched to less than 1.3 wt%  $^{235}\text{U}$ , including unenriched fuel assemblies. Fuel assemblies with unenriched axial end-blankets may be loaded into MAGNASTOR.

### 2.2.1 PWR Fuel Evaluation

MAGNASTOR evaluations are based on bounding PWR fuel assembly parameters that maximize the source terms for the shielding evaluations, the reactivity for criticality evaluations, the decay heat load for the thermal evaluations, and the fuel weight for the structural evaluations. These bounding parameters are selected from the various spent fuel assemblies that are candidates for storage in MAGNASTOR. The bounding fuel assembly values are established based primarily on how the principal parameters are combined, and on the loading conditions (or restrictions) established for a group of fuel assemblies based on its parameters. Each TSC may contain up to 37 undamaged PWR fuel assemblies.

The limiting parameters of the PWR fuel assemblies authorized for loading in MAGNASTOR are shown in Table 2.2-1. The maximum initial enrichments listed are based on a minimum soluble boron concentration of 2,500 ppm in the spent fuel pool water. Lower soluble boron concentrations are allowed in the spent fuel pool water for fuel assemblies with lower maximum enrichments. The maximum initial enrichment authorized represents the peak fuel rod enrichment for variably enriched PWR fuel assemblies. The PWR fuel assembly characteristics are summarized by fuel assembly type in Table 6.4.3-1. Table 2.2-1 assembly physical information is limited to the criticality analysis input of fuel mass, array configuration, and number of fuel rods. These analysis values are key inputs to the shielding and criticality evaluations in Chapters 5 and 6. Lattice parameters dictating system reactivity are detailed in Chapter 6. Enrichment limits are set for each fuel type to produce reactivities at the upper

subcritical limit (USL). The maximum TSC decay heat load for the storage of PWR fuel assemblies is 35.5 kW. Uniform and preferential loading patterns are allowed in the PWR basket. The uniform loading pattern permits assemblies with a maximum heat load of 0.96 kW/assembly. The preferential loading pattern permits peak heat loads of 1.20 kW, as indicated in the zone description in Figure 2.2-1. The bounding thermal evaluations are based on the Westinghouse 17×17 fuel assembly. The minimum cool times are determined based on the maximum decay heat load of the contents. The fuel assemblies and source terms that produce the maximum storage and transfer cask dose rates are summarized in Table 5.1.3-3. A bounding weight of 1,680 pounds, as shown in Table 2.2-1, based on a B&W 15×15 fuel assembly with control components inserted, has been structurally evaluated in each location of the PWR fuel basket.

As noted in Table 2.2-1, the evaluation of PWR fuel assemblies includes thimble plugs (flow mixers), burnable poison rod assemblies (BPRAs), control element assemblies (CEAs), and/or solid filler rods. Empty fuel rod positions are filled with a solid filler rod or a solid neutron absorber rod that displaces a volume not less than that of the original fuel rod.

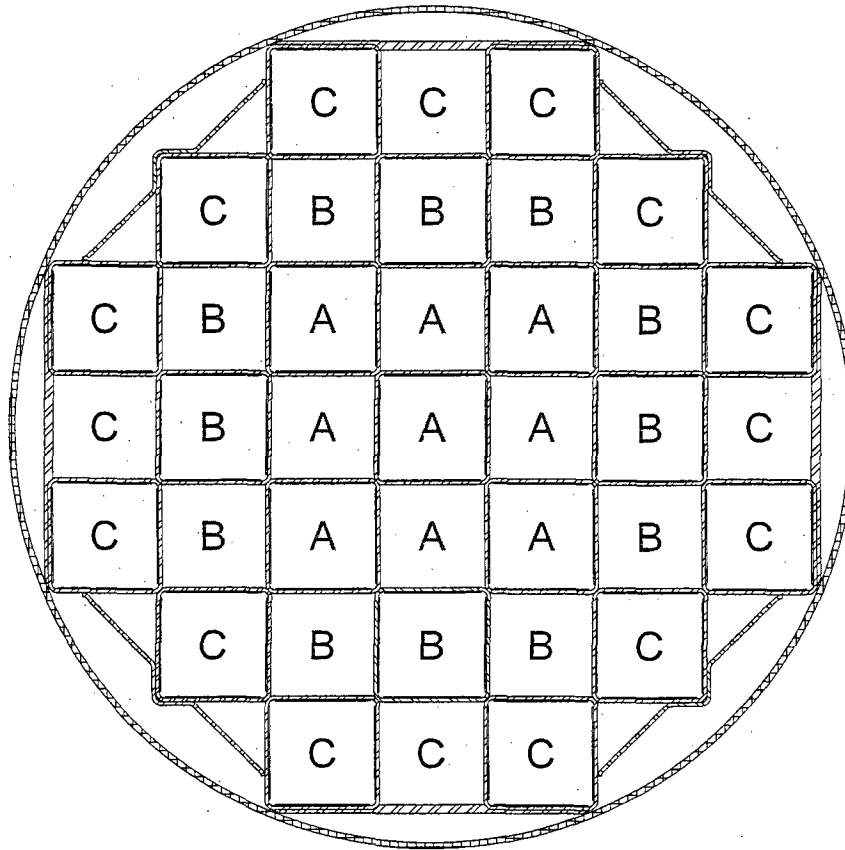
## **2.2.2 BWR Fuel Evaluation**

MAGNASTOR evaluations are based on bounding BWR fuel assembly parameters that maximize the source terms for the shielding evaluations, the reactivity for the criticality evaluations, the decay heat load for the thermal evaluations, and the fuel weight for the structural evaluations. These bounding parameters are selected from the various spent fuel assemblies that are candidates for storage in MAGNASTOR. The bounding fuel assembly values are established based primarily on how the principal parameters are combined, and on the loading conditions or restrictions established for a group of fuel assemblies based on its parameters. Each TSC may contain up to 87 undamaged BWR fuel assemblies. To increase allowed assembly enrichments over those determined for the 87-assembly basket configuration, an optional 82-assembly loading pattern may be used. The required fuel assembly locations in the 82-assembly pattern are shown in Figure 2.2-2.

The limiting parameters of the BWR fuel assemblies authorized for loading in MAGNASTOR are shown in Table 2.2-2. The maximum initial enrichment represents the peak planar-average enrichment. The BWR fuel assembly characteristics are summarized by fuel type in Table 6.4.3-2. Table 2.2-2 assembly physical information is limited to the critical analysis input of fuel mass, array configuration, and number of fuel rods. These analysis values are key inputs to the shielding and criticality evaluations in Chapters 5 and 6. Lattice parameters dictating system

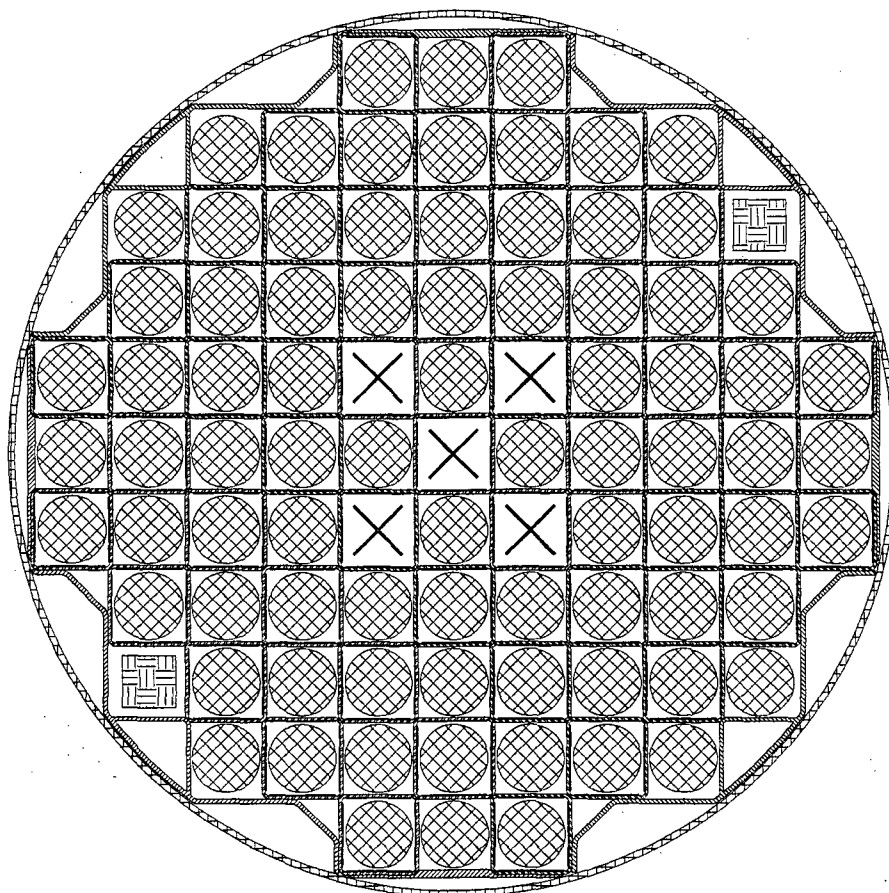
reactivity are detailed in Chapter 6. Enrichment limits are set for each fuel type to produce reactivities at the USL. The maximum decay heat load per TSC for the storage of BWR fuel assemblies is 33.0 kW (average of 0.379 kW/assembly). Only uniform loading is permitted for BWR fuel assemblies. The bounding thermal evaluations are based on the GE 10×10 fuel assembly. The minimum cooling times are determined based on the maximum decay heat load of the contents. The fuel assemblies and source terms that produce the maximum storage and transfer cask dose rates are summarized in Table 5.1.3-3. A bounding weight of 704 pounds, as shown in Table 2.2-2, is based on the maximum weight of GE 7×7 and 8×8 assemblies with channels; this weight has been structurally evaluated in each storage location of the BWR basket. As noted in Table 2.2-2, the evaluation of BWR fuel envelopes unchanneled assemblies and assemblies with channels up to 120 mils thick. Empty fuel rod positions are filled with a solid filler rod or a solid neutron absorber rod that displaces a volume not less than that of the original fuel rod.

Figure 2.2-1 PWR Fuel Preferential Loading Zones



| Zone Description | Designator | Heat Load (W/assy) | # Assemblies |
|------------------|------------|--------------------|--------------|
| Inner Ring       | A          | 922                | 9            |
| Middle Ring      | B          | 1,200              | 12           |
| Outer Ring       | C          | 800                | 16           |

Figure 2.2-2 82-Assembly-BWR Basket Pattern



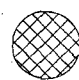


-  = Fuel Assembly Locations
-  = Vent/Drain Port Locations
-  = Designated Nonfuel Locations

Table 2.2-1 PWR Fuel Assembly Characteristics

| Characteristic   | Fuel Class |        |        |         |        |                    |
|--|------------|--------|--------|---------|--------|--------------------|
|  | 14x14      | 14x14  | 15x15  | 15x15   | 16x16  | 17x17              |
| Base Fuel Type <sup>a</sup>                              | CE, SPC    | W, SPC | W, SPC | BW, FCF | CE     | BW, SPC,<br>W, FCF |
| Max Initial Enrichment (wt% <sup>235</sup> U)            | 5.0        | 5.0    | 5.0    | 5.0     | 5.0    | 5.0                |
| Min Initial Enrichment (wt% <sup>235</sup> U)            | 1.3        | 1.3    | 1.3    | 1.3     | 1.3    | 1.3                |
| Number of Fuel Rods                                      | 176        | 179    | 204    | 208     | 236    | 264                |
| Max Assembly Average Burnup (MWd/MTU)                    | 60,000     | 60,000 | 60,000 | 60,000  | 60,000 | 60,000             |
| Peak Average Rod Burnup (MWd/MTU)                        | 62,500     | 62,500 | 62,500 | 62,500  | 62,500 | 62,500             |
| Min Cool Time (years)                                    | 4          | 4      | 4      | 4       | 4      | 4                  |
| Max Weight (lb) per Storage Location                     | 1,680      | 1,680  | 1,680  | 1,680   | 1,680  | 1,680              |
| Max Decay Heat (Watts) per Preferential Storage Location | 1,200      | 1,200  | 1,200  | 1,200   | 1,200  | 1,200              |

- Fuel cladding is a zirconium-based alloy.
- All reported enrichment values are nominal preirradiation fabrication values.
- Weight includes the weight of nonfuel-bearing components.
- Assemblies may contain a flow mixer (thimble plug), a burnable poison rod assembly, a control element assembly, and/or solid stainless steel or zirconium-based alloy filler rods.
- Maximum initial enrichment is based on a minimum soluble boron concentration in the spent fuel pool water. Required soluble boron content is fuel type and enrichment specific. Minimum soluble boron content varies between 1,500 and 2,500 ppm. Maximum initial enrichment represents the peak fuel rod enrichment for variably-enriched fuel assemblies.
- Spacers may be used to axially position fuel assemblies to facilitate handling.
- Maximum uniform heat load is 959 watts per storage location.

<sup>a</sup> Indicates assembly and/or nuclear steam supply system (NSSS) vendor/type referenced for fuel input data. Fuel acceptability for loading is not restricted to the indicated vendor provided that the fuel assembly meets the limits listed in Table 6.4.3-1. Table 6.2.1-1 contains vendor information by fuel rod array. Abbreviations are as follows: Westinghouse (W), Combustion Engineering (CE), Siemens Power Corporation (SPC), Babcock and Wilcox (BW), and Framatome Cogema Fuels (FCF).

Table 2.2-2 BWR Fuel Assembly Characteristics

| Characteristic                                | Fuel Class |                 |                 |                   |
|---|------------|-----------------|-----------------|-------------------|
|   | 7×7        | 8×8             | 9×9             | 10×10             |
| Base Fuel Type <sup>a</sup>                   | SPC, GE    | SPC, GE         | SPC, GE         | SPC, GE, ABB      |
| Max Initial Enrichment (wt% <sup>235</sup> U) | 4.5        | 4.5             | 4.5             | 4.5               |
| Number of Fuel Rods                           | 48         | 59              | 72              | 91 <sup>c</sup>   |
|   | 49         | 60              | 74 <sup>c</sup> | 92 <sup>c</sup>   |
|   |            | 61              | 76              | 96 <sup>c,d</sup> |
|   |            | 62              | 79              | 100 <sup>d</sup>  |
|   |            | 63              | 80              |                   |
|   |            | 64 <sup>b</sup> |                 |                   |
| Max Assembly Average Burnup (MWd/MTU)         | 60,000     | 60,000          | 60,000          | 60,000            |
| Peak Average Rod Burnup (MWd/MTU)             | 62,500     | 62,500          | 62,500          | 62,500            |
| Min Cool Time (years)                         | 4          | 4               | 4               | 4                 |
| Min Average Enrichment (wt% <sup>235</sup> U) | 1.3        | 1.3             | 1.3             | 1.3               |
| Max Weight (lb) per Storage Location          | 704        | 704             | 704             | 704               |
| Max Decay Heat (Watts) per Storage Location   | 379        | 379             | 379             | 379               |

- Each BWR fuel assembly may have a zirconium-based alloy channel up to 120 mil thick.
- Assembly weight includes the weight of the channel.
- Maximum initial enrichment is the peak planar-average enrichment.
- Water rods may occupy more than one fuel lattice location. Fuel assembly to contain nominal number of water rods for the specific assembly design.
- All enrichment values are nominal preirradiation fabrication values.
- Spacers may be used to axially position fuel assemblies to facilitate handling.

<sup>a</sup> Indicates assembly vendor/type referenced for fuel input data. Fuel acceptability for loading is not restricted to the indicated vendor/type provided that the fuel assembly meets the limits listed in Table 6.4.3-2. Table 6.2.1-2 contains vendor information by fuel rod array. Abbreviations are as follows: General Electric/Global Nuclear Fuels (GE), Exxon/Advanced Nuclear Fuels/Siemens Power Corporation (SPC).

<sup>b</sup> May be composed of four subchannel clusters.

<sup>c</sup> Assemblies may contain partial-length fuel rods.

<sup>d</sup> Composed of four subchannel clusters.

### 2.3 Design Criteria for Environmental Conditions and Natural Phenomena

This section presents the design criteria for site environmental conditions and natural phenomena applied in the design basis analyses of MAGNASTOR. Analyses to demonstrate that the design basis system meets the design criteria defined in this section are presented in the appropriate chapters.

The use of MAGNASTOR at a specific site requires that the site either meet the design criteria of this section or be separately evaluated against the site-specific conditions to ensure the acceptable performance of the system.

#### 2.3.1 Tornado Missiles and Wind Loadings

The concrete casks are typically placed outdoors on an unsheltered reinforced concrete storage pad at an ISFSI site. This storage condition exposes the casks to tornado and wind loading.

##### 2.3.1.1 Applicable Design Parameters

The design basis tornado and wind loading is defined based on Regulatory Guide 1.76 [11], Region 1, and NUREG-0800 [12]. The tornado and wind loading criteria are as follows.

| <b>Tornado and Wind Condition</b> | <b>Limit</b> |
|-----------------------------------|--------------|
| Rotational Wind Speed, mph        | 290          |
| Translational Wind Speed, mph     | 70           |
| Maximum Wind Speed, mph           | 360          |
| Radius of Maximum Wind Speed, ft  | 150          |
| Pressure Drop, psi                | 3.0          |
| Rate of Pressure Drop, psi/sec    | 2.0          |

##### 2.3.1.2 Determination of Forces on Structures

Tornado wind forces on the concrete cask are calculated by multiplying the dynamic wind pressure by the frontal area of the cask normal to the wind direction. Wind forces are applied to the cask in the wind direction. No streamlining is assumed. The cask is demonstrated to remain stable under design basis tornado wind loading in conjunction with impact from a high-energy tornado missile.



### 2.3.1.3 Tornado Missiles

The design basis tornado missile impacts are defined in Paragraph 4, Subsection III, Section 3.5.1.4 of NUREG-0800 [12]. The design basis tornado is considered to generate three types of missiles that impact the cask at normal incidence.

|   |  |
|---|--|
| Massive Missile –<br>(deformable w/high kinetic energy) | Weight = 4,000 lb<br>Frontal Area = 20 sq ft |
| Penetration Missile –<br>(rigid hardened steel)         | Weight = 280 lb<br>Diameter = 8.0 in         |
| Protective Barrier Missile –<br>(solid steel sphere)    | Weight = 0.15 lb<br>Diameter = 1.0 in        |

Each missile is assumed to impact the concrete cask at a velocity of 126 miles per hour, horizontal to the ground, which is 35% of the maximum wind speed of 360 miles per hour. For missile impacts in the vertical direction, the assumed missile velocity is  $(0.7)(126) = 88.2$  miles per hour.

The analysis of the loaded concrete cask for missile impacts applies the laws of conservation of momentum and conservation of energy to determine the rigid body response of the concrete cask. Each missile impact is evaluated, and all missiles are assumed to impact in a manner that produces the maximum damage to the cask.

### 2.3.2 Water Level (Flood) Design

The loaded concrete cask may be exposed to a flood during storage on an unsheltered concrete storage pad at an ISFSI site. The source and magnitude of the probable maximum flood depend on specific site characteristics.

#### 2.3.2.1 Flood Elevations

The concrete cask design basis is a maximum floodwater depth of 50 feet above the base of the cask and a floodwater velocity of 15 ft per second. Under design basis flood conditions, the cask does not move or tip on the storage pad and the confinement function is maintained.

#### 2.3.2.2 Phenomena Considered in Design Load Calculations

The occurrence of flooding at an ISFSI site is dependent upon the specific site location and the surrounding natural and man-made geographical features. Some possible sources of a flood at an ISFSI site are: overflow from a river or stream due to unusually heavy rain, snow-melt runoff, or a dam or major water supply line break caused by a seismic event (earthquake); high tides

produced by a hurricane; and a tsunami (tidal wave) caused by an underwater earthquake or volcanic eruption.

Flooding at an ISFSI site is highly improbable because of the extensive environmental impact studies that are performed during the selection of a site for a nuclear facility.

### **2.3.2.3 Flood Force Application**

The evaluation of the concrete cask for a flood condition determines a maximum permissible floodwater current velocity and a maximum permissible floodwater depth. The criteria employed in the determination of the maximum permissible values are that a cask tip-over will not occur, and that the TSC material yield strength is not exceeded.

The force of the floodwater current on the concrete cask is calculated as a function of the velocity, which is a factor comprised of the dynamic water pressure, the frontal area of the cask that is normal to the direction of the current, and a drag coefficient dependent on the Reynold's number. The maximum permissible force of the floodwater current is determined such that the overturning moment on the cask will be less than that required to tip the cask over.

During a flood condition, the force of the floodwater exerts a hydrostatic pressure on the canister shell. This pressure is based on the design basis flood: floodwater depth of 50 ft and floodwater velocity of 15 ft per second. Therefore, the force exerted on the canister shell is 22 psi. The analysis of the canister shell will demonstrate that there is no containment malfunction or impairment of the ability to retrieve fuel from the canister.

### **2.3.2.4 Flood Protection**

The inherent strength of the reinforced concrete cask provides a substantial margin of safety against any permanent deformation of the cask for a credible flood event at an ISFSI site.

Therefore, no special flood protection measures for the cask are necessary. For the design basis flood, the allowable stresses in the TSC are not exceeded.

### **2.3.3 Seismic Design**

An ISFSI site may be subject to seismic events (earthquakes) during its lifetime. The seismic response spectra experienced by the concrete cask depends upon the geographical location of the specific site and the distance from the epicenter of the earthquake. The possible significant effect of a beyond-design-basis seismic event on the concrete cask would be a tip-over; however, the loaded concrete cask does not tip over during the design-basis seismic event. Although it is a nonmechanistic event, the loaded concrete cask design basis includes consideration of the consequences of a hypothetical cask tip-over event.

The TSC is analyzed for loads induced by the application of a 0.37g seismic acceleration to the concrete cask at the top surface of the ISFSI pad.

#### **2.3.4 Snow and Ice Loadings**

The criterion for determining design snow loads is based on ANSI/ASCE 7-93 [13], Section 7.0. Flat roof snow loads apply and the design basis snow and ice load are calculated from the following formula.

$$\begin{aligned} p_f &= 0.7C_eC_tIp_g \\ &= 100.8 \text{ psf} \end{aligned}$$

where:

$p_f$  = flat roof snow load (psf)

$C_e$  = exposure factor = 1.0

$C_t$  = thermal factor = 1.2

$I$  = importance factor = 1.2

$p_g$  = ground snow load, (psf) = 100

The numerical values of  $C_e$ ,  $C_t$ ,  $I$ , and  $p_g$  are obtained from Tables 1, 18, 19, and 20 and Figure 7, respectively, of ANSI/ASCE 7-93.

The exposure factor,  $C_e$ , accounts for wind effects. The exposure factor of the concrete cask is assumed to be Category C, which is defined to be "locations in which snow removal by wind cannot be relied on to reduce roof loads because of terrain, higher structures, or several trees nearby." The thermal factor,  $C_t$ , accounts for the importance of buildings and structures in relation to public health and safety. The concrete cask is conservatively classified as a Category III building or other structure. Ground snow loads for the contiguous United States are given in Figures 5, 6, and 7 of ANSI/ASCE 7-93. A worst-case value of 100 lb per square ft is assumed.

The design basis snow and ice load is bounded by the weight of the loaded transfer cask on the top of the concrete cask shell and by the tornado missile loading on the concrete cask lid. The snow load is considered in the load combinations evaluations of the concrete cask.

#### **2.3.5 Combined Load Criteria**

Each normal condition and off-normal and accident event has a combination of load cases that defines the total combined loading for that condition/event. The individual load cases considered include thermal, seismic, external and internal pressure, missile impacts, drops, snow and ice.

loads, and/or flood water forces. The load conditions to be evaluated for storage casks are identified in 10 CFR 72 [10] and ANSI/ANS-57.9 [14].

#### **2.3.5.1 Load Combinations and Design Strength - Concrete Cask**

Refer to Table 2.3-1 for the load combinations for the concrete cask. The live loads are considered to vary from 0% to 100% to ensure that the worst-case condition is evaluated. In each case, use of 100% of the live load produces the maximum load condition. The steel liner of the concrete cask is a stay-in-place form that also provides radiation shielding. The concrete cask is designed to the requirements of ACI 349 [4].

In calculating the design strength of concrete in the concrete cask body, nominal strength values are multiplied by a strength reduction factor in accordance with Section 9.3 of ACI 349.

#### **2.3.5.2 Load Combinations and Design Strength – TSC and Fuel Basket**

The TSC is designed in accordance with the ASME Code, Section III, Subsection NB [1]. The basket is designed in accordance with the ASME Code, Section III, Subsection NG [2]. Structural buckling of the basket is evaluated in accordance with NUREG/CR-6322 [3].

Refer to Table 2.3-2 for the load combinations for all normal conditions and off-normal or accident events and the corresponding ASME service levels. Levels A and D service limits represent normal conditions and accident events, respectively. Levels B and C service limits are used for off-normal events. The analysis criteria of the ASME Code, Section III, Subsection NB are employed. Stress intensities produced by pressure, temperature, and mechanical loads are combined before comparison to the ASME Code allowable criteria. For components used in the TSC, refer to the allowable criteria in Table 2.3-3.

The load combinations considered for the fuel basket for normal conditions and off-normal or accident events are the same as those identified for the TSC in Table 2.3-2, except that there are no internal pressure loads. The analysis criteria of the ASME Code, Section III, Subsection NG are employed. For the fuel basket components, refer to the allowable criteria in Table 2.3-3.

#### **2.3.5.3 Design Strength - Transfer Cask**

The transfer cask is a special lifting device. It is designed, fabricated, and load tested to meet the requirements of ANSI N14.6 [6] for the handling of vertical loads defined in NUREG 0612 [15]. The design criteria are as follows.

- The combined shear stress or maximum tensile stress during the lift (with 10% dynamic load factor) shall be  $\leq S_v/6$  and  $S_u/10$ .

- For off-normal (Level C) conditions, membrane stresses shall be less than  $1.2S_m$  and membrane plus bending stresses shall be the lesser of  $1.8S_m$  and  $1.5S_y$ .
- The ferritic steel material used for the load-bearing members of the transfer cask shall satisfy the material toughness requirements of ANSI N14.6, paragraph 4.2.6.

Refer to Chapter 10 for information on load testing of the transfer cask.

### 2.3.6 Environmental Temperatures

A temperature of 76°F is defined as the design base normal operations temperature for MAGNASTOR in storage. This temperature conservatively bounds the maximum average annual temperature in the 48 contiguous United States, specifically, Miami, FL, at 75.6°F [16] and meets the normal condition thermal boundary defined in NUREG-1536 [25]. Use of this design base establishes a bounding condition for existing and potential ISFSI sites in the United States. Refer to Chapter 4 for the evaluation of this environmental condition along with the thermal analysis models. Refer to Chapter 3 for the thermal stress evaluation for the normal operating conditions. Normal temperature fluctuations are bounded by the severe ambient temperature cases that are evaluated as off-normal and accident events.

Off-normal, severe environmental events are defined as -40°F with no solar loads and 106°F with solar loads. An extreme environmental condition of 133°F with maximum solar loads is evaluated as an accident case to show compliance with the maximum heat load case required by ANSI/ANS-57.9. Thermal performance is also evaluated assuming both the half blockage of the concrete cask air inlets and the complete blockage of the air inlets.

The design basis temperatures used in the concrete cask analysis follow. Solar insolation is as specified in 10 CFR 71.71 [17] and Regulatory Guide 7.8 [18].

| Condition                | Ambient Temperature | Solar Insolation |
|--------------------------|---------------------|------------------|
| Normal                   | 76°F                | yes              |
| Off-Normal - Severe Heat | 106°F               | yes              |
| Off-Normal - Severe Cold | -40°F               | no               |
| Accident - Extreme Heat  | 133°F               | yes              |

Table 2.3-1 Load Combinations for the Concrete Cask

| Load Combination | Condition               | Dead  | Live   | Wind   | Thermal             | Seismic         | Tornado/ Missile | Drop/ Impact | Flood |
|------------------|-------------------------|-------|--------|--------|---------------------|-----------------|------------------|--------------|-------|
| 1                | Normal                  | 1.4D  | 1.7L   |        |                     |                 |                  |              |       |
| 2                | Normal                  | 1.05D | 1.275L |        | 1.275T <sub>o</sub> |                 |                  |              |       |
| 3                | Normal                  | 1.05D | 1.275L | 1.275W | 1.275T <sub>o</sub> |                 |                  |              |       |
| 4                | Off-Normal and Accident | D     | L      |        | T <sub>a</sub>      |                 |                  |              |       |
| 5                | Accident                | D     | L      |        | T <sub>o</sub>      | E <sub>ss</sub> |                  |              |       |
| 6                | Accident                | D     | L      |        | T <sub>o</sub>      |                 |                  | A            |       |
| 7                | Accident                | D     | L      |        | T <sub>o</sub>      |                 |                  |              | F     |
| 8                | Accident                | D     | L      |        | T <sub>o</sub>      |                 | W <sub>t</sub>   |              |       |

Load Combinations are from ANSI/ANS-57.9 [14] and ACI 349 [4]. Where:

- D = Dead Load
- L = Live Load
- W = Wind
- T<sub>o</sub> = Normal Temperature
- F = Flood
- T<sub>a</sub> = Off-Normal or Accident Temperature
- E<sub>ss</sub> = Design Basis Earthquake
- W<sub>t</sub> = Tornado/Tornado Missile
- A = Drop/Impact

Table 2.3-2 Load Combinations for the TSC

| LOAD                                 |  | NORMAL |   |   | OFF-NORMAL |   |   |   |   | ACCIDENT |   |   |   |   |   |
|--------------------------------------|--|--------|---|---|------------|---|---|---|---|----------|---|---|---|---|---|
| ASME Service Level Load Combinations |  | A      |   |   | B          |   | C |   |   | D        |   |   |   |   |   |
|                                      |  | 1      | 2 | 3 | 1          | 2 | 3 | 4 | 5 | 1        | 2 | 3 | 4 | 5 | 6 |
| Dead Weight                          | TSC w/ fuel                                  | X      | X | X | X          | X | X | X | X | X        | X | X | X | X | X |
| Thermal                              | Inside concrete cask: 76°F ambient           | X      |   | X |            |   |   | X |   | X        | X | X | X | X |   |
|                                      | Inside transfer cask: 76°F ambient           |        | X |   | X          |   | X |   |   |          |   |   |   |   | X |
|                                      | Inside concrete cask: -40°F or 106°F ambient |        |   |   |            | X |   |   | X |          |   |   |   |   |   |
| Internal Pressure                    | Normal                                       | X      | X | X |            |   | X | X | X | X        | X | X | X |   |   |
|                                      | Off-Normal                                   |        |   |   | X          | X |   |   |   |          |   |   |   |   |   |
|                                      | Accident (fire)                              |        |   |   |            |   |   |   |   |          |   |   |   | X | X |
| Handling Load                        | Normal (1.1g)                                |        | X | X | X          |   |   |   |   |          |   |   |   |   |   |
|                                      | Off-Normal                                   |        |   |   |            |   | X | X | X |          |   |   |   |   |   |
| Drop/Impact                          | 24-in drop, < 60g                            |        |   |   |            |   |   |   |   | X        |   |   |   |   |   |
| Seismic                              | Tip-over and complete burial                 |        |   |   |            |   |   |   |   |          | X |   |   |   |   |
| Flood                                | 50-ft water head                             |        |   |   |            |   |   |   |   |          |   | X |   |   |   |
| Tornado                              | Pressure drop of 3.0 psi                     |        |   |   |            |   |   |   |   |          |   |   | X |   |   |

Table 2.3-3 Structural Design Criteria for Components Used in the TSC

| Component  | Criteria   |
|--|--|
| 1. Normal Operations: Service Level A<br>TSC: ASME Section III, Subsection NB [1]<br>Basket: ASME Section III, Subsection NG [2]                                       | $P_m \leq S_m$<br>$P_L + P_b \leq 1.5 S_m$<br>$P_L + P_b + Q \leq 3S_m$<br>$P_s < 0.6 S_m$   |
| 2. Off-Normal Operations: Service Level B<br>TSC: ASME Section III, Subsection NB  | $P_m < 1.1 S_m$<br>$P_L + P_b < 1.65 S_m$<br>$P_s < 0.6 S_m$   |
| 3. Off-Normal Operations: Service Level C<br>TSC: ASME Section III, Subsection NB<br>Basket: ASME Section III, Subsection NG   | Subsection NB Criteria:<br>$P_m < 1.2 S_m$ or $S_y$ (whichever is greater)<br>$P_L + P_b < 1.8 S_m$ or $1.5 S_y$ (whichever is lesser)<br>$P_s < 0.6 S_m$<br>Subsection NG Criteria:<br>$P_m < 1.5 S_m$<br>$P_L + P_b < 2.25 S_m$<br>$P_s < 0.6 S_m$ |
| 4. Accident Conditions, Service Level D<br>TSC: ASME Section III, Subsection NB<br><br>Basket: ASME Section III, Appendix F<br>Basket: ASME Section III, Subsection NG | $P_m \leq 0.4 S_m$ or $0.7 S_u$ (whichever is lesser)<br>$P_L + P_b \leq 3.6 S_m$ or $1.0 S_u$ (whichever is lesser)<br>$P_s < 0.42 S_u$<br>Plastic Analysis (Basket):<br>$P_m \leq 0.7 S_u$<br>$P_{int} \leq 0.9 S_u$<br>$P_s < 0.42 S_u$           |
| 5. Basket Structural Buckling  | NUREG/CR-6322 [3]  |

Symbols:

$S_m$  = material design stress intensity  
 $S_u$  = material ultimate strength  
 $S_y$  = material yield strength

$P_L$  = primary local membrane stress  
 $P_m$  = primary general membrane stress  
 $P_b$  = primary bending stress  
 $P_{int}$  = primary stress intensity  
 $P_s$  = average primary shear across a section loaded in pure shear

## 2.4 Safety Protection Systems

MAGNASTOR relies upon passive systems to ensure the protection of public health and safety, except in the case of fire or explosion. As previously discussed, fire and explosion events are effectively precluded by site administrative controls that prevent the introduction of flammable and explosive materials. The use of passive systems provides protection from mechanical or equipment failure.

### 2.4.1 General

MAGNASTOR is designed for safe, long-term storage of spent fuel. The system will withstand all of the evaluated normal conditions and off-normal and postulated accident events without release of radioactive material or excessive radiation exposure to workers or the general public. The major design considerations to assure safe, long-term fuel storage and retrievability for ultimate disposal by the Department of Energy in accordance with the requirements of 10 CFR 72 and ISG-2 [24] are as follows.

- Continued radioactive material confinement in postulated accidents.
- Thick steel and concrete biological shield.
- Passive systems that ensure reliability.
- Pressurized inert helium atmosphere to provide corrosion protection for fuel cladding and enhanced heat transfer for the stored fuel.

Retrievability is defined as: "maintaining spent fuel in substantially the same physical condition as it was when originally loaded into the storage cask, which enables any future transportation, unloading and ultimate disposal activities to be performed using the same general type of equipment and procedures as were used for the initial loading."

Each major component of the system is classified with respect to its function and corresponding potential effect on public safety. In accordance with Regulatory Guide 7.10 [19], each major system component is assigned a safety classification (see Table 2.4-1). The safety classification is based on review of the component's function and the assessment of the consequences of its failure following the guidelines of NUREG/CR-6407 [20]. The safety classification categories are defined in the following list.

Category A - Components critical to safe operations whose failure or malfunction could directly result in conditions adverse to safe operations, integrity of spent fuel, or public health and safety.

Category B - Components with major impact on safe operations whose failure or malfunction could indirectly result in conditions adverse to safe operations, integrity of spent fuel, or public health and safety.



Category C - Components whose failure would not significantly reduce the packaging effectiveness and would not likely result in conditions adverse to safe operations, integrity of spent fuel, or public health and safety.

As discussed in the following sections, the MAGNASTOR design incorporates features addressing the design considerations described previously to assure safe operation during loading, handling, and storage of spent nuclear fuel.

#### **2.4.2 Confinement Barriers and Systems**

The radioactive materials that MAGNASTOR must confine during storage originate from the stored fuel assemblies and residual contamination inside the TSC. The system is designed to safely confine this radioactive material under all storage conditions.

The stainless steel TSC is assembled and closed by welding. All of the field-installed welds are liquid penetrant examined as detailed in Chapter 10 and on the License Drawings. The longitudinal and girth shop welds of the TSC shell are full penetration welds that are radiographically and liquid penetrant examined during fabrication. The TSC bottom-plate-to-shell shop weld joint is ultrasonically and liquid penetrant examined during fabrication.

The TSC vessel provides a leaktight boundary precluding the release of solid, volatile, and gaseous radioactive material. There are no evaluated normal conditions or off-normal or accident events that result in damage to the TSC producing a breach in the confinement boundary.

Neither normal conditions of operation or off-normal events preclude retrieval of the TSC for transport and ultimate disposal. The TSC is designed to withstand accident conditions, including a 24-inch end drop in the concrete cask and a tip-over of the concrete cask, without precluding the subsequent removal of the fuel (i.e., the fuel tubes do not deform such that they bind the fuel assemblies).

Operator radiation exposure during handling and closure of the TSC is minimized by the following.

- Minimizing the number of operations required to complete the TSC loading and sealing process.
- Placing the closure lid on the TSC while the transfer cask and TSC are under water in the fuel pool.
- Using temporary shielding, including a weld shield plate as the mounting component of the weld machine.
- Using retaining blocks on the transfer cask to ensure that the TSC is not raised out of the transfer cask.

### **2.4.3 Concrete Cask Cooling**

The loaded concrete cask is passively cooled. Ambient air enters at the bottom of the concrete cask through four air inlets and heated air exits through the four air outlets at the top of the cask due to natural convection heat transfer. Radiant heat transfer also occurs from the TSC to the concrete cask liner. Consequently, the liner also heats the convective airflow. This natural circulation of air inside the concrete cask, in conjunction with radiation from the TSC surface, maintains the fuel cladding and concrete cask component temperatures below their design limits. Conduction does not play a substantial role in heat removal from the TSC surface. Refer to Chapter 4 for details on the concrete cask thermal analyses.

### **2.4.4 Protection by Equipment**

There is no important-to-safety equipment required for the safe storage operation of MAGNASTOR. The important-to-safety equipment employed in the handling of MAGNASTOR is the lifting yoke used to lift the transfer cask. The lifting yoke is designed, fabricated, and tested in accordance with ANSI N14.6 as a special lifting device as defined in NUREG-0612. The lifting yoke is proof load tested to 300% of its design load when fabricated. Following the load test, the bolted connections are disassembled, and the components are inspected for deformation. Permanent deformation of components is not acceptable. Engagement pins are examined by dye penetrant examination. The transfer cask and lifting yoke are inspected for visible defects prior to each use. Transfer cask annual maintenance requirements are defined in Chapter 10.

### **2.4.5 Protection by Instrumentation**

No instrumentation is required for the safe storage operations of MAGNASTOR.

A remote temperature-monitoring system may be used to measure the outlet air temperature of the concrete casks in long-term storage. The outlet temperature can be monitored daily as a check of the continuing thermal performance of the concrete cask. Alternately, a daily visual inspection for blockage of the air inlet and air outlet screens of all concrete casks may be performed. Following any natural phenomena event, such as an earthquake or tornado, the concrete casks shall be inspected for damage and air inlet and air outlet blockage.

### **2.4.6 Nuclear Criticality Safety**

MAGNASTOR design includes features to ensure that nuclear criticality safety is maintained (i.e., the cask remains subcritical under normal conditions and off-normal and accident events).

The design of the TSC and fuel basket is such that, under all conditions, the highest neutron multiplication factor ( $k_{\text{eff}}$ ) is less than 0.95.

#### **2.4.6.1 Control Methods for Prevention of Criticality**

The principal design criterion is that  $k_{\text{eff}}$  remain less than 0.95 for all conditions. Criticality control for PWR spent fuel is achieved using neutron absorber material fixed in the basket and by maintaining a minimum boron concentration in the TSC during fuel loading. The fixed neutron absorber attracts thermal neutrons that are moderated in the water surrounding the fuel. Fast, high-energy neutrons escape the system. The minimum effective loading for neutron absorber sheets is 0.036 and 0.027 g  $^{10}\text{B}/\text{cm}^2$  for PWR and BWR fuel baskets, respectively. The required minimum boron loading in a neutron absorber sheet is determined based on the assumed boron effectiveness used in the criticality analysis, i.e., 75% for Boral (registered trademark of AAR Advanced Structures) and 90% for borated aluminum alloys and for borated metal matrix composites (MMCs). Neutron absorber sheets are mechanically attached to the fuel tube structure to ensure that the neutron absorber remains in place during the design basis normal conditions and off-normal and accident events.

The basket designs ensure that there is sufficient absorption of moderated neutrons by the neutron absorber (and by boron in the cavity water in some cases) to maintain criticality control in the basket ( $k_{\text{eff}} < 0.95$ ). See Chapter 6 for the detailed criticality analyses.

#### **2.4.6.2 Error Contingency Criteria**

The standards and regulations of criticality safety require that  $k_{\text{eff}}$ , including uncertainties, be less than 0.95. The bias and 95/95 uncertainty are applied to the calculation using an upper subcritical limit (USL) approach [22]. The  $k_{\text{eff}} + 2\sigma$  value must be less than the USL. Based on MCNP critical benchmarks, the USL as a function of fission neutron lethargy (eV) is shown as:

$$\text{USL} = 0.9364 + 8.4409 \times 10^{-3} \times x$$

where:

$x$  = energy of average neutron lethargy causing fission

#### **2.4.6.3 Verification Analyses**

The MCNP criticality analysis code is benchmarked through a series of calculations based on critical experiments. These experiments span a range of fuel enrichments, fuel rod pitches, poison sheet characteristics, shielding materials, and geometries that are typical of light water

reactor fuel in a cask. To achieve accurate results, three-dimensional models, as close to the actual experiment as possible, are used to evaluate the experiments.

#### **2.4.7 Radiological Protection**

MAGNASTOR is designed to minimize operator radiological exposure in keeping with the As Low As Reasonably Achievable (ALARA) philosophy.

##### **2.4.7.1 Access Control**

Access to MAGNASTOR at an ISFSI site will be controlled by a fence with lockable truck and personnel access gates to meet the requirements of 10 CFR 72, 10 CFR 73, and 10 CFR 20 [21]. Access to the storage area, and its designation as to the level of radiation protection required, will be established by site procedures by the licensee.

##### **2.4.7.2 Shielding**

MAGNASTOR is designed to limit the dose rates in accordance with 10 CFR 72.104 and 72.106, which set whole body dose limits for an individual located beyond the controlled area at  $\leq 25$  mrem per year (whole body) during normal operations and  $\leq 5$  rem (5,000 mrem) from any design basis accident. Burnup profile shape should be considered during ALARA and site boundary planning by the system licensee, as it may affect system dose rate profiles.

##### **2.4.7.3 Ventilation Off-Gas**

MAGNASTOR is passively cooled by radiation and natural convection heat transfer at the outer surface of the concrete cask and in the TSC-concrete cask annulus. In the TSC-concrete cask annulus, air enters the air inlets, flows up between the TSC and concrete cask liner in the annulus, and exits the air outlets. If the exterior surface of the TSC is excessively contaminated, the possibility exists that contamination could be carried aloft by the airflow. Therefore, during fuel loading, the spent fuel pool water is minimized in the transfer cask/TSC annulus by supplying the annulus with clean or demineralized spent fuel pool water. Water is supplied into the annulus while the transfer cask is submerged. The use of the annulus system minimizes the potential for contamination of the exterior surfaces of the TSC.

After the transfer cask is removed from the pool, removable contamination levels on the TSC exterior are determined. If TSC decontamination is required, clean water can be used to flush the annulus. To facilitate decontamination, the TSC exterior surfaces are smooth.

MAGNASTOR has no radioactive releases during normal conditions or off-normal or accident events of storage. Hence, there are no off-gas system requirements for MAGNASTOR.

#### **2.4.7.4 Radiological Alarm Systems**

No radiological alarms are required on MAGNASTOR. Typically, total radiation exposure due to the ISFSI installation is monitored by the use of the licensee's boundary dose monitoring program.

#### **2.4.8 Fire Protection**

A major ISFSI fire is not considered credible, since there is very little material near the concrete casks that could contribute to a fire. The concrete cask is largely impervious to incidental thermal events. Administrative controls will be established by the licensee to ensure that the presence of combustibles at the ISFSI is minimized. A hypothetical 1,475°F fire occurring at the base of the cask for eight minutes is evaluated as an accident condition.

#### **2.4.9 Explosion Protection**

MAGNASTOR is analyzed to ensure its proper function under an over-pressure event. The TSC is protected from direct over-pressure conditions by the concrete cask. For the same reasons as for the fire condition, a severe explosion on an ISFSI site is not considered credible. The evaluated 20 psig over-pressure condition is considered to bound any explosive over-pressure resulting from an industrial explosion at the boundary of the owner-controlled area.

#### **2.4.10 Auxiliary Structures**

The loading, welding, drying, transfer, and transport of MAGNASTOR require the use of auxiliary equipment as described in Chapter 9. External transfer of a TSC may require the use of a structure, referred to as a "TSC Handling and Transfer Facility." The TSC Handling and Transfer Facility is a specially designed and engineered structure independent of the 10 CFR 50 facilities at the site.

The design of the TSC Handling and Transfer Facility would meet the requirements for MAGNASTOR described in the Design Features presented in Appendix A of the Technical Specifications, in addition to those requirements established by the licensee.

The design, analysis, fabrication, operation, and maintenance of the TSC Handling and Transfer Facility would be performed in accordance with the quality assurance program requirements of the licensee. The components of the TSC Handling and Transfer Facility would be classified as Important-to-Safety or Not-Important-to-Safety in accordance with the guidelines of NUREG-6407.

Table 2.4-1 Safety Classification of MAGNASTOR Components

| Component Description  | Reference Drawings   | Safety Function                               | Safety Classification |
|--|--|---|-----------------------|
| TSC Assembly<br>Shell and Base Plate<br>Closure Lid<br>Closure Ring<br>Port Covers   | 71160-581<br>71160-584<br>71160-584<br>71160-585   | Structural and Confinement                    | A                     |
| Fuel Basket Assembly<br>Basket Support Weldments<br>Fuel Tube Assemblies<br>Neutron Absorbers                                  | 71160-551<br>71160-571<br>71160-572<br>71160-574<br>71160-575<br>71160-591<br>71160-598<br>71160-599 | Criticality, Structural and Thermal           | A                     |
| Transfer Cask Assembly<br>Trunnions<br>Inner and Outer Shells<br>Shield Doors and Rails<br>Lead Gamma Shield<br>Neutron Shield | 71160-560  | Structural, Shielding and Operations          | B                     |
| Adapter Plate Assembly<br>Base Plate<br>Door Rails<br>Hydraulic Operating System<br>Side Shields                               | None   | Operations and Shielding                      | NQ                    |
| Concrete Cask Assembly<br>Structural Weldments and Base Plate<br>Lid Weldment<br>Lifting Lugs<br>Reinforcing Bars<br>Concrete  | 71160-561<br>71160-562<br>71160-590  | Structural, Shielding, Operations and Thermal | B                     |

## 2.5 Decommissioning Considerations

The principal components of MAGNASTOR are the concrete cask and the TSC. Refer to Chapter 15 for information on decommissioning MAGNASTOR.

Decommissioning of MAGNASTOR involves removing the TSC by offsite transport and disassembling the concrete cask. It is expected that the concrete will be broken up and the steel components segmented to reduce volume. The concrete and carbon steel are not expected to be surface-contaminated and no significant activation is expected.

The TSC is designed and fabricated to ensure its retrievability for use as a component of the waste package for permanent disposal at the Mined Geological Disposal System in accordance with the guidance of ISG-2 [24] and the requirements of 10 CFR 72. Consequently, decommissioning may not be required. If necessary, the TSC could be decommissioned following unloading by decontaminating the inside and segmenting the shell and closure plates. Since the neutron flux rate from the stored fuel is low, only minimal activation of the TSC is expected. The resulting stainless steel could be disposed of, or recycled, in accordance with the appropriate regulatory requirements.

The storage pad, fence, and supporting utility fixtures are not expected to require decontamination as a result of use of MAGNASTOR. Consequently, these items may be reused or disposed of as locally generated clean waste.

## 2.6 References

1. ASME Boiler and Pressure Vessel Code, Section III, Subsection NB, "Class 1 Components," American Society of Mechanical Engineers, New York, NY, 2001 Edition with 2003 Addenda.
2. ASME Boiler and Pressure Vessel Code, Section III, Subsection NG, "Core Support Structures," American Society of Mechanical Engineers, New York, NY, 2001 Edition with 2003 Addenda.
3. NUREG/CR-6322, "Buckling Analysis of Spent Fuel Basket," US Nuclear Regulatory Commission, Washington, DC, May 1995.
4. "Code Requirements for Nuclear Safety Related Concrete Structures (ACI 349-85) and Commentary (ACI 349R)," American Concrete Institute, Farmington Hills, MI.
5. "Building Code Requirements for Structural Concrete (ACI 318) and Commentary (ACI 318R)," American Concrete Institute, Farmington Hills, MI.
6. ANSI N14.6-1993, "American National Standard for Radioactive Materials - Special Lifting Devices for Shipping Containers Weighing 10,000 Pounds (4,500 kg) or More," American National Standards Institute, Inc., Washington, DC, June 1993.
7. ISG-11, "Cladding Considerations for the Transport and Storage of Spent Fuel," US Nuclear Regulatory Commission, Washington, DC, Revision 3, November 17, 2003.
8. PNL-4835, "Technical Basis for Storage of Zircaloy-Clad Spent Fuel in Inert Gases," Johnson, A.B., and Gilbert, E.R., Pacific Northwest Laboratory, Richland, WA, September, 1983.
9. NUREG-1567, "Standard Review Plan for Spent Fuel Dry Storage Facilities," US Nuclear Regulatory Commission, Washington, DC, March 2000.
10. 10 CFR 72, Code of Federal Regulations, "Licensing Requirements for the Independent Storage of Spent Nuclear Fuel, High-Level Radioactive Waste and Reactor-Related Greater Than Class C Waste," US Government, Washington, DC.
11. Regulatory Guide 1.76, "Design Basis Tornado for Nuclear Power Plants," US Nuclear Regulatory Commission, Washington, DC, April 1974.
12. NUREG-0800, "Standard Review Plan," US Nuclear Regulatory Commission, Washington, DC, April 1996.
13. ANSI/ASCE 7-93 (formerly ANSI A58.1), "Minimum Design Loads for Buildings and Other Structures," American Society of Civil Engineers, New York, NY, May 1994.
14. ANSI/ANS-57.9-1992, "Design Criteria for an Independent Spent Fuel Storage Installation (Dry Type)," American Nuclear Society, La Grange Park, IL, May 1992.



15. NUREG-0612, "Control of Heavy Loads at Nuclear Power Plants," US Nuclear Regulatory Commission, Washington, DC, July 1980.
16. ASHRAE Handbook, "Fundamentals," American Society of Heating, Refrigeration, and Air Conditioning Engineers, Atlanta, GA, 1993.
17. 10 CFR 71, "Packaging and Transportation of Radioactive Materials," Code of Federal Regulations, US Government, Washington, DC.
18. Regulatory Guide 7.8, "Load Combinations for the Structural Analysis of Shipping Casks for Radioactive Material," US Nuclear Regulatory Commission, Washington, DC, March 1989.
19. Regulatory Guide 7.10, "Establishing Quality Assurance Programs for Packaging Used in the Transport of Radioactive Material," US Nuclear Regulatory Commission, Washington, DC, March 2005.
20. NUREG/CR-6407, "Classification of Transportation Packaging and Dry Spent Fuel Storage System Components According to Importance to Safety," US Nuclear Regulatory Commission, Washington, DC, February 1996.
21. 10 CFR 20, "Standards for Protection Against Radiation," Code of Federal Regulations, US Government, Washington, DC.
22. NUREG/CR-6361, "Criticality Benchmark Guide for Light-Water-Reactor Fuel in Transportation and Storage Packages," US Nuclear Regulatory Commission, Washington, DC, December 1997.
23. ISG-15, "Materials Evaluation," US Nuclear Regulatory Commission, Washington, DC, Revision 0, January 10, 2001.
24. ISG-2, "Fuel Retrievability," US Nuclear Regulatory Commission, Washington, DC, October 1998.
25. NUREG-1536, "Standard Review Plan for Dry Cask Storage Systems," US Nuclear Regulatory Commission, Washington, DC, January 1997.

## Chapter 3 Structural Evaluation

### Table of Contents

|        |  |          |
|--------|--|----------|
| 3      | STRUCTURAL EVALUATION.....                                     | 3-1      |
| 3.1    | MAGNASTOR Structural Design.....                               | 3.1-1    |
| 3.1.1  | Major Components.....  | 3.1-1    |
| 3.1.2  | Discussion of MAGNASTOR.....                                   | 3.1-3    |
| 3.1.3  | Design Criteria Summary.....                                   | 3.1-5    |
| 3.2    | Weights and Centers of Gravity.....                            | 3.2-1    |
| 3.2.1  | Calculated Maximum Weights and Centers of Gravity.....         | 3.2-1    |
| 3.3    | Materials.....   | 3.3-1    |
| 3.4    | General Standards for Casks.....                               | 3.4-1    |
| 3.4.1  | Chemical and Galvanic Reactions.....                           | 3.4-1    |
| 3.4.2  | Positive Closure.....  | 3.4-1    |
| 3.4.3  | Lifting Devices.....   | 3.4-2    |
| 3.5    | Normal Operating Conditions.....                               | 3.5-1    |
| 3.5.1  | TSC Evaluation for Normal Operating Conditions.....            | 3.5-1    |
| 3.5.2  | Fuel Basket Evaluation for Normal Operating Conditions.....    | 3.5-7    |
| 3.5.3  | Concrete Cask Evaluations for Normal Operating Conditions..... | 3.5-24   |
| 3.6    | Off-Normal Operating Events.....                               | 3.6-1    |
| 3.6.1  | TSC Evaluations for Off-Normal Operating Events.....           | 3.6-1    |
| 3.6.2  | Fuel Basket Evaluation for Off-Normal Operating Events.....    | 3.6-4    |
| 3.6.3  | Concrete Cask Evaluation for Off-Normal Operating Events.....  | 3.6-12   |
| 3.7    | Storage Accident Events.....                                   | 3.7-1    |
| 3.7.1  | TSC Evaluations for Storage Accident Conditions.....           | 3.7-1    |
| 3.7.2  | Fuel Baskets Evaluation for Storage Accident Events.....       | 3.7-6    |
| 3.7.3  | Concrete Cask Evaluation for Storage Accident Events.....      | 3.7-46   |
| 3.8    | Fuel Rods.....   | 3.8-1    |
| 3.8.1  | PWR Fuel Rod Buckling Evaluation.....                          | 3.8-1    |
| 3.8.2  | BWR Fuel Rod Buckling Evaluation.....                          | 3.8-6    |
| 3.8.3  | Thermal Evaluation of Fuel Rods.....                           | 3.8-7    |
| 3.8.4  | Side Drop Evaluation.....                                      | 3.8-8    |
| 3.9    | References.....  | 3.9-1    |
| 3.10   | Structural Evaluation Detail.....                              | 3.10-1   |
| 3.10.1 | PWR Fuel Basket Finite Element Models.....                     | 3.10.1-1 |
| 3.10.2 | BWR Fuel Basket Finite Element Models.....                     | 3.10.2-1 |

Table of Contents (cont'd)

|        |   |          |
|--------|---|----------|
| 3.10.3 | TSC Finite Element Model.....   | 3.10.3-1 |
| 3.10.4 | Concrete Cask Finite Element Models.....  | 3.10.4-1 |
| 3.10.5 | Transfer Cask Finite Element Model .....  | 3.10.5-1 |
| 3.10.6 | Basket Stability Evaluation for Concrete Cask Tip-Over Accident<br>Condition.....           | 3.10.6-1 |
| 3.10.7 | Fuel Tube Plastic Analysis for Concrete Cask Tip-Over Accident<br>Condition.....            | 3.10.7-1 |
| 3.10.8 | Basket Pin-Slot Connection Evaluation for Concrete Cask Tip-Over<br>Accident Condition..... | 3.10.8-1 |
| 3.10.9 | TSC-Basket Finite Element Models.....   | 3.10.9-1 |

List of Figures

|                  |  |           |
|------------------|--|-----------|
| Figure 3.1.1-1   | Principal Components of MAGNASTOR .....  | 3.1-2     |
| Figure 3.4.3-1   | Top Ring Section Cuts .....  | 3.4-25    |
| Figure 3.7.2-1   | PWR Basket Fuel Tube Displacement for Tip-Over Accident.....                                   | 3.7-39    |
| Figure 3.7.2-2   | BWR Basket Fuel Tube Displacement for Tip-Over Accident .....                                  | 3.7-40    |
| Figure 3.7.2-3   | PWR Neutron Absorber and Retainer Finite Element Model .....                                   | 3.7-41    |
| Figure 3.7.3-1   | Acceleration Time History of the Upper-Bound Weight TSC – 24-<br>Inch Concrete Cask Drop.....  | 3.7-65    |
| Figure 3.7.3-2   | Acceleration Time History of the Lower-Bound Weight TSC – 24-<br>Inch Concrete Cask Drop.....  | 3.7-66    |
| Figure 3.7.3-3   | Acceleration Time History for Concrete Cask Tip-Over Condition -<br>Standard Pad .....         | 3.7-67    |
| Figure 3.7.3-4   | Acceleration Time History of Oversized Pad .....   | 3.7-68    |
| Figure 3.8.1-1   | Overall Model Plot for a Typical PWR Fuel Assembly .....                                       | 3.8-4     |
| Figure 3.8.1-2   | Detailed View of the PWR 14×14 Fuel Assembly .....   | 3.8-5     |
| Figure 3.8.4-1   | ANSYS Model for the PWR Fuel Rod High Burnup Condition.....                                    | 3.8-10    |
| Figure 3.10.1-1  | Expanded View of PWR Basket.....   | 3.10.1-8  |
| Figure 3.10.1-2  | Bolted Attachment Details.....   | 3.10.1-9  |
| Figure 3.10.1-3  | Free-Body Diagram of PWR Basket Fuel Tube Detail.....  | 3.10.1-10 |
| Figure 3.10.1-4  | Free-Body Diagram of Basket Support Structure .....  | 3.10.1-11 |
| Figure 3.10.1-5  | PWR Basket Periodic Model – 0° Basket Orientation .....  | 3.10.1-12 |
| Figure 3.10.1-6  | PWR Basket Periodic Model – 45° Basket Orientation .....                                       | 3.10.1-13 |
| Figure 3.10.1-7  | Thermal Stress Evaluation Model.....   | 3.10.1-14 |
| Figure 3.10.1-8  | PWR Basket Plastic Model - 0° Basket Orientation.....  | 3.10.1-15 |
| Figure 3.10.1-9  | PWR Basket Plastic Model - 45° Basket Orientation.....   | 3.10.1-16 |
| Figure 3.10.1-10 | Typical PWR Fuel Tube Pin Finite Element Model Details.....                                    | 3.10.1-17 |
| Figure 3.10.1-11 | PWR Basket Model Boundary Conditions for a Transverse Loading –<br>0° Basket Orientation.....  | 3.10.1-18 |
| Figure 3.10.1-12 | PWR Basket Model Boundary Conditions for a Transverse Loading –<br>45° Basket Orientation..... | 3.10.1-19 |
| Figure 3.10.1-13 | PWR Fuel Tube Array – 0° Basket Orientation.....   | 3.10.1-20 |
| Figure 3.10.1-14 | PWR Fuel Tube Section Cuts – 0° Basket Orientation .....                                       | 3.10.1-21 |
| Figure 3.10.1-15 | PWR Fuel Tube Array – 45° Basket Orientation.....  | 3.10.1-22 |
| Figure 3.10.1-16 | PWR Fuel Tube Section Cuts – 45° Basket Orientation .....                                      | 3.10.1-23 |
| Figure 3.10.1-17 | PWR Corner Support Weldment Section Cuts – 0° Basket Orientation                               | 3.10.1-24 |
| Figure 3.10.1-18 | PWR Corner Support Weldment Section Cuts – 45° Basket<br>Orientation .....                     | 3.10.1-25 |
| Figure 3.10.1-19 | PWR Side Support Weldment Section Cuts – 0° Basket Orientation ...                             | 3.10.1-26 |
| Figure 3.10.1-20 | PWR Side Support Weldment Section Cuts – 45° Basket Orientation .                              | 3.10.1-27 |
| Figure 3.10.2-1  | Expanded View of BWR Basket.....   | 3.10.2-8  |
| Figure 3.10.2-2  | Bolted Attachment Details.....   | 3.10.2-9  |
| Figure 3.10.2-3  | Free-Body Diagram of BWR Basket Fuel Tube Detail .....   | 3.10.2-10 |

## List of Figures (cont'd)

|                  |  |           |
|------------------|--|-----------|
| Figure 3.10.2-4  | Free-Body Diagram of Basket Support Structure .....  | 3.10.2-11 |
| Figure 3.10.2-5  | BWR Basket Periodic Model – 0° Basket Orientation .....  | 3.10.2-12 |
| Figure 3.10.2-6  | BWR Basket Periodic Model – 45° Basket Orientation .....   | 3.10.2-13 |
| Figure 3.10.2-7  | Thermal Stress Evaluation Model.....   | 3.10.2-14 |
| Figure 3.10.2-8  | BWR Basket Plastic Model - 0° Basket Orientation .....   | 3.10.2-15 |
| Figure 3.10.2-9  | BWR Basket Plastic Model - 45° Basket Orientation .....  | 3.10.2-16 |
| Figure 3.10.2-10 | Typical BWR Fuel Tube Pin Finite Element Model Details .....   | 3.10.2-17 |
| Figure 3.10.2-11 | BWR Basket Model Boundary Conditions for a Transverse Loading –<br>0° Basket Orientation.....          | 3.10.2-18 |
| Figure 3.10.2-12 | BWR Basket Model Boundary Conditions for a Transverse Loading –<br>45° Basket Orientation.....         | 3.10.2-19 |
| Figure 3.10.2-13 | BWR Fuel Tube Array – 0° Basket Orientation .....  | 3.10.2-20 |
| Figure 3.10.2-14 | BWR Fuel Tube Section Cuts – 0° Basket Orientation.....  | 3.10.2-21 |
| Figure 3.10.2-15 | BWR Fuel Tube Array – 45° Basket Orientation .....   | 3.10.2-22 |
| Figure 3.10.2-16 | BWR Fuel Tube Section Cuts – 45° Basket Orientation.....   | 3.10.2-23 |
| Figure 3.10.2-17 | BWR Corner Support Weldment Section Cuts – 0° Basket<br>Orientation .....                              | 3.10.2-24 |
| Figure 3.10.2-18 | BWR Corner Support Weldment Section Cuts – 45° Basket<br>Orientation .....                             | 3.10.2-25 |
| Figure 3.10.2-19 | BWR Side Support Weldment Section Cuts – 0° Basket Orientation...                                      | 3.10.2-26 |
| Figure 3.10.2-20 | BWR Side Support Weldment Section Cuts – 45° Basket Orientation.                                       | 3.10.2-27 |
| Figure 3.10.3-1  | MAGNASTOR TSC Finite Element Model.....  | 3.10.3-5  |
| Figure 3.10.3-2  | Identification of Sections for Evaluating Linearized Stresses in TSC ...                               | 3.10.3-6  |
| Figure 3.10.4-1  | Concrete Cask Pedestal Finite Element Model for Lift Evaluation.....                                   | 3.10.4-8  |
| Figure 3.10.4-2  | Concrete Cask Finite Element Model for Thermal Stress Evaluation....                                   | 3.10.4-9  |
| Figure 3.10.4-3  | Concrete Cask Model – Elements for Rebar.....  | 3.10.4-10 |
| Figure 3.10.4-4  | Concrete Cask Model Boundary Conditions .....  | 3.10.4-11 |
| Figure 3.10.4-5  | Concrete Cask Pedestal Finite Element Model for 24-inch Drop<br>Evaluation .....                       | 3.10.4-12 |
| Figure 3.10.4-6  | Stress-Strain Curve for A36 Carbon Steel.....  | 3.10.4-13 |
| Figure 3.10.4-7  | Finite Element Models for Tip-Over Evaluation.....   | 3.10.4-14 |
| Figure 3.10.5-1  | Finite Element Model for the Transfer Cask .....   | 3.10.5-2  |
| Figure 3.10.6-1  | Basket Pin-Tube Slot Connections at Fuel Tube Corners .....  | 3.10.6-10 |
| Figure 3.10.6-2  | PWR Basket Finite Element Model for Concrete Cask Tip-Over<br>Accident – 0° Basket Orientation.....    | 3.10.6-11 |
| Figure 3.10.6-3  | PWR Basket Finite Element Model for Concrete Cask Tip-Over<br>Accident – 18° Basket Orientation.....   | 3.10.6-12 |
| Figure 3.10.6-4  | PWR Basket Finite Element Model for Concrete Cask Tip-Over<br>Accident – 22.5° Basket Orientation..... | 3.10.6-13 |
| Figure 3.10.6-5  | PWR Basket Finite Element Model for Concrete Cask Tip-Over<br>Accident – 27° Basket Orientation.....   | 3.10.6-14 |

List of Figures (cont'd)

Figure 3.10.6-6 PWR Basket Finite Element Model for Concrete Cask Tip-Over  
Accident – 34° Basket Orientation..... 3.10.6-15

Figure 3.10.6-7 PWR Basket Finite Element Model for Concrete Cask Tip-Over  
Accident – 43° Basket Orientation..... 3.10.6-16

Figure 3.10.6-8 BWR Basket Finite Element Model for Concrete Cask Tip-Over  
Accident – 0° Basket Orientation..... 3.10.6-17

Figure 3.10.6-9 BWR Basket Finite Element Model for Concrete Cask Tip-Over  
Accident – 22.5° Basket Orientation ..... 3.10.6-18

Figure 3.10.6-10 BWR Basket Finite Element Model for Concrete Cask Tip-Over  
Accident – 45° Basket Orientation..... 3.10.6-19

Figure 3.10.6-11 PWR Basket Finite Element Model – Boss Connection for Corner and  
Side Support Weldment..... 3.10.6-20

Figure 3.10.6-12 BWR Basket Finite Element Model – Boss Connection for Corner  
Support Weldment..... 3.10.6-21

Figure 3.10.6-13 BWR Basket Finite Element Model – Boss Connection for Side  
Support Weldment..... 3.10.6-22

Figure 3.10.6-14 Acceleration Time History for Basket Stability Evaluation ..... 3.10.6-23

Figure 3.10.6-15 Typical Response of PWR Basket Fuel Tubes Pin-Slot Connections ... 3.10.6-24

Figure 3.10.6-16 Typical Response of BWR Basket Fuel Tubes Pin-Slot Connections... 3.10.6-25

Figure 3.10.6-17 Typical Gap Measurement at Fuel Tube Corners ..... 3.10.6-26

Figure 3.10.6-18 Time History of Maximum Gap Change at Fuel Tube Corner – PWR  
Basket 0° and 18° Orientation ..... 3.10.6-27

Figure 3.10.6-19 Time History of Maximum Gap Change at Fuel Tube Corner – PWR  
Basket 22.5° and 27° Orientation ..... 3.10.6-28

Figure 3.10.6-20 Time History of Maximum Gap Change at Fuel Tube Corner –  
PWR Basket 34° and 43° Orientation..... 3.10.6-29

Figure 3.10.6-21 Time History of Maximum Gap Change at Fuel Tube Corner –  
BWR Basket 0° and 22.5° Orientation ..... 3.10.6-30

Figure 3.10.6-22 Time History of Maximum Gap Change at Fuel Tube Corner – BWR  
Basket 45° Orientation..... 3.10.6-31

Figure 3.10.6-23 Typical Time History of Gap at Boss for BWR Support Weldments.... 3.10.6-32

Figure 3.10.7-1 Typical Finite Element Model for the Basket Fuel Tube Displacement.. 3.10.7-2

Figure 3.10.8-1 BWR Basket Finite Element Model – Location of Pin-Slot  
Connection with Refined Mesh ..... 3.10.8-3

Figure 3.10.8-2 BWR Basket Finite Element Model – Pin-Slot Connection with  
Refined Mesh..... 3.10.8-4

Figure 3.10.8-3 PWR Basket Finite Element Model – Location of Pin-Slot  
Connection with Refined Mesh ..... 3.10.8-5

Figure 3.10.8-4 PWR Basket Finite Element Model – Pin-Slot Connection with  
Refined Mesh..... 3.10.8-6

Figure 3.10.8-5 BWR Basket Pin-Slot Connection Plastic Strain – Cask Tip-over  
Condition ..... 3.10.8-7

**List of Figures (cont'd)**

|                 |  |          |
|-----------------|--|----------|
| Figure 3.10.8-6 | PWR Basket Pin-Slot Connection Plastic Strain .....  | 3.10.8-8 |
| Figure 3.10.9-1 | PWR Canister-Basket Finite Element Model for Concrete Cask<br>Tip-Over Accident – 45° Basket Orientation .....                     | 3.10.9-3 |
| Figure 3.10.9-2 | PWR Canister-Basket Finite Element Model for Concrete Cask<br>Tip-Over Accident – Basket Elements - 45° Basket Orientation .....   | 3.10.9-4 |
| Figure 3.10.9-3 | PWR Canister-Basket Finite Element Model for Concrete Cask<br>Tip-Over Accident – Basket Elements – 22.5° Basket Orientation ..... | 3.10.9-5 |
| Figure 3.10.9-4 | BWR Canister-Basket Finite Element Model for Concrete Cask<br>Tip-Over Accident – 45° Basket Orientation .....                     | 3.10.9-6 |
| Figure 3.10.9-5 | BWR Canister-Basket Finite Element Model for Concrete Cask<br>Tip-Over Accident – Basket Elements – 22.5° Basket Orientation ..... | 3.10.9-7 |
| Figure 3.10.9-6 | PWR Canister Shell Lateral Displacement Contour – 45° Basket<br>Orientation .....  | 3.10.9-8 |
| Figure 3.10.9-7 | BWR Canister Shell Lateral Displacement Contour – 45° Basket<br>Orientation .....  | 3.10.9-9 |

### List of Tables

|                |  |           |
|----------------|--|-----------|
| Table 3.2.1-1  | MAGNASTOR Storage Weight and Center of Gravity Summary .....                                   | 3.2-2     |
| Table 3.4.3-1  | Stress Intensity for Trunnions and Top Ring .....  | 3.4-26    |
| Table 3.4.3-2  | Stress Intensity for Transfer Cask Shells and Bottom Ring.....                                 | 3.4-26    |
| Table 3.5.1-1  | TSC Thermal Stress, Q .....  | 3.5-6     |
| Table 3.5.1-2  | TSC Normal Conditions, $P_m$ Stresses .....  | 3.5-6     |
| Table 3.5.1-3  | TSC Normal Conditions, $P_m + P_b$ Stresses .....  | 3.5-6     |
| Table 3.5.1-4  | TSC Normal Conditions, $P + Q$ Stresses .....  | 3.5-6     |
| Table 3.5.3-1  | Concrete Cask Vertical Stress Summary – Outer Surface, psi .....                               | 3.5-27    |
| Table 3.5.3-2  | Concrete Cask Vertical Stress Summary – Inner Surface, psi .....                               | 3.5-27    |
| Table 3.5.3-3  | Concrete Cask Circumferential Stress Summary – Inner Surface, psi.....                         | 3.5-27    |
| Table 3.6.1-1  | TSC Off-Normal Events, $P_m$ Stresses.....   | 3.6-3     |
| Table 3.6.1-2  | TSC Off-Normal Events, $P_m + P_b$ Stresses .....  | 3.6-3     |
| Table 3.6.1-3  | TSC Off-Normal Events, $P + Q$ Stresses .....  | 3.6-3     |
| Table 3.7.1-1  | TSC Accident Events, $P_m$ Stresses.....   | 3.7-5     |
| Table 3.7.1-2  | TSC Accident Events, $P_m + P_b$ Stresses.....   | 3.7-5     |
| Table 3.7.2-1  | PWR Fuel Tube Stress Intensity – Concrete Cask Tip-over Accident .....                         | 3.7-42    |
| Table 3.7.2-2  | PWR Corner Weldment Mounting Plate Stress Intensity – Concrete<br>Cask Tip-over Accident ..... | 3.7-43    |
| Table 3.7.2-3  | PWR Corner Support Bar Stress Intensity – Concrete Cask Tip-over<br>Accident.....              | 3.7-43    |
| Table 3.7.2-4  | PWR Side Weldment Stress Intensity – Concrete Cask Tip-over<br>Accident.....                   | 3.7-43    |
| Table 3.7.2-5  | BWR Fuel Tube Stress Intensity – Concrete Cask Tip-over Accident.....                          | 3.7-44    |
| Table 3.7.2-6  | BWR Corner Weldment Mounting Plate Stress Intensity – Concrete<br>Cask Tip-over Accident ..... | 3.7-44    |
| Table 3.7.2-7  | BWR Corner Support Plate Stress Intensity – Concrete Cask Tip-over<br>Accident.....            | 3.7-44    |
| Table 3.7.2-8  | BWR Side Weldment Stress Intensity – Concrete Cask Tip-over<br>Accident.....                   | 3.7-45    |
| Table 3.7.3-1  | Concrete Cask Vertical Stress Summary – Inner Surface, psi .....                               | 3.7-69    |
| Table 3.7.3-2  | Concrete Cask Circumferential Stress Summary – Inner Surface, psi.....                         | 3.7-69    |
| Table 3.7.3-3  | Basket Modal Frequency for Concrete Cask Tip-over .....  | 3.7-70    |
| Table 3.7.3-4  | DLF and Amplified Accelerations for Concrete Cask Tip-over.....                                | 3.7-70    |
| Table 3.10.3-1 | TSC Normal Pressure plus Handling, $P_m$ , ksi.....  | 3.10.3-7  |
| Table 3.10.3-2 | TSC Normal Pressure plus Handling, $P_m + P_b$ , ksi .....                                     | 3.10.3-8  |
| Table 3.10.3-3 | TSC Normal Pressure plus Handling, $P + Q$ , ksi.....  | 3.10.3-9  |
| Table 3.10.3-4 | TSC Normal Pressure, $P_m$ , ksi .....   | 3.10.3-10 |
| Table 3.10.3-5 | TSC Normal Pressure, $P_m + P_b$ , ksi.....  | 3.10.3-11 |
| Table 3.10.3-6 | TSC Thermal Stresses, Q, ksi .....   | 3.10.3-12 |
| Table 3.10.3-7 | TSC Off-Normal Pressure plus Handling, $P_m$ , ksi.....  | 3.10.3-13 |
| Table 3.10.3-8 | TSC Off-Normal Pressure plus Handling, $P_m + P_b$ , ksi.....                                  | 3.10.3-14 |



List of Tables (cont'd)

|                 |   |           |
|-----------------|---|-----------|
| Table 3.10.3-9  | TSC Off-Normal Pressure plus Handling, $P + Q$ , ksi.....   | 3.10.3-15 |
| Table 3.10.3-10 | TSC Normal Pressure plus Off-Normal Handling, $P_m$ , ksi.....  | 3.10.3-16 |
| Table 3.10.3-11 | TSC Normal Pressure plus Off-Normal Handling, $P_m + P_b$ , ksi.....  | 3.10.3-17 |
| Table 3.10.3-12 | TSC Normal Pressure plus 24-inch Drop, $P_m$ , ksi.....   | 3.10.3-18 |
| Table 3.10.3-13 | TSC Normal Pressure plus 24-inch Drop, $P_m + P_b$ , ksi.....   | 3.10.3-19 |
| Table 3.10.3-14 | TSC Accident Pressure plus Dead Weight, $P_m$ , ksi.....  | 3.10.3-20 |
| Table 3.10.3-15 | TSC Accident Pressure plus Dead Weight, $P_m + P_b$ , ksi.....  | 3.10.3-21 |
| Table 3.10.3-16 | TSC Tip-Over plus Normal Pressure, $P_m$ , ksi.....   | 3.10.3-22 |
| Table 3.10.3-17 | TSC Tip-Over plus Normal Pressure, $P_m + P_b$ , ksi.....   | 3.10.3-23 |
| Table 3.10.6-1  | Load Cases Evaluated for PWR Fuel Basket Stability.....   | 3.10.6-33 |
| Table 3.10.6-2  | Load Cases Evaluated for BWR Fuel Basket Stability.....   | 3.10.6-34 |
| Table 3.10.6-3  | Summary of Maximum Gap Changes at Pin-Slot Connections for<br>PWR Basket.....   | 3.10.6-35 |
| Table 3.10.6-4  | Summary of Maximum Gap Changes at Pin-Slot Connections for<br>BWR Basket.....   | 3.10.6-36 |
| Table 3.10.9-1  | Canister Shell Displacements Used as Boundary Conditions for the<br>LS-DYNA Models for PWR Basket Stability Evaluation..... | 3.10.9-10 |
| Table 3.10.9-2  | Canister Shell Displacements Used as Boundary Conditions for the<br>LS-DYNA Models for BWR Basket Stability Evaluation..... | 3.10.9-11 |

### 3 STRUCTURAL EVALUATION

This chapter describes the design and analysis of the principal structural components of MAGNASTOR®. It demonstrates that MAGNASTOR meets the structural requirements for confinement of contents, criticality control, heat dissipation, radiological shielding, and contents retrievability required by 10 CFR 72 [1] for the design basis normal conditions, and off-normal and accident events.

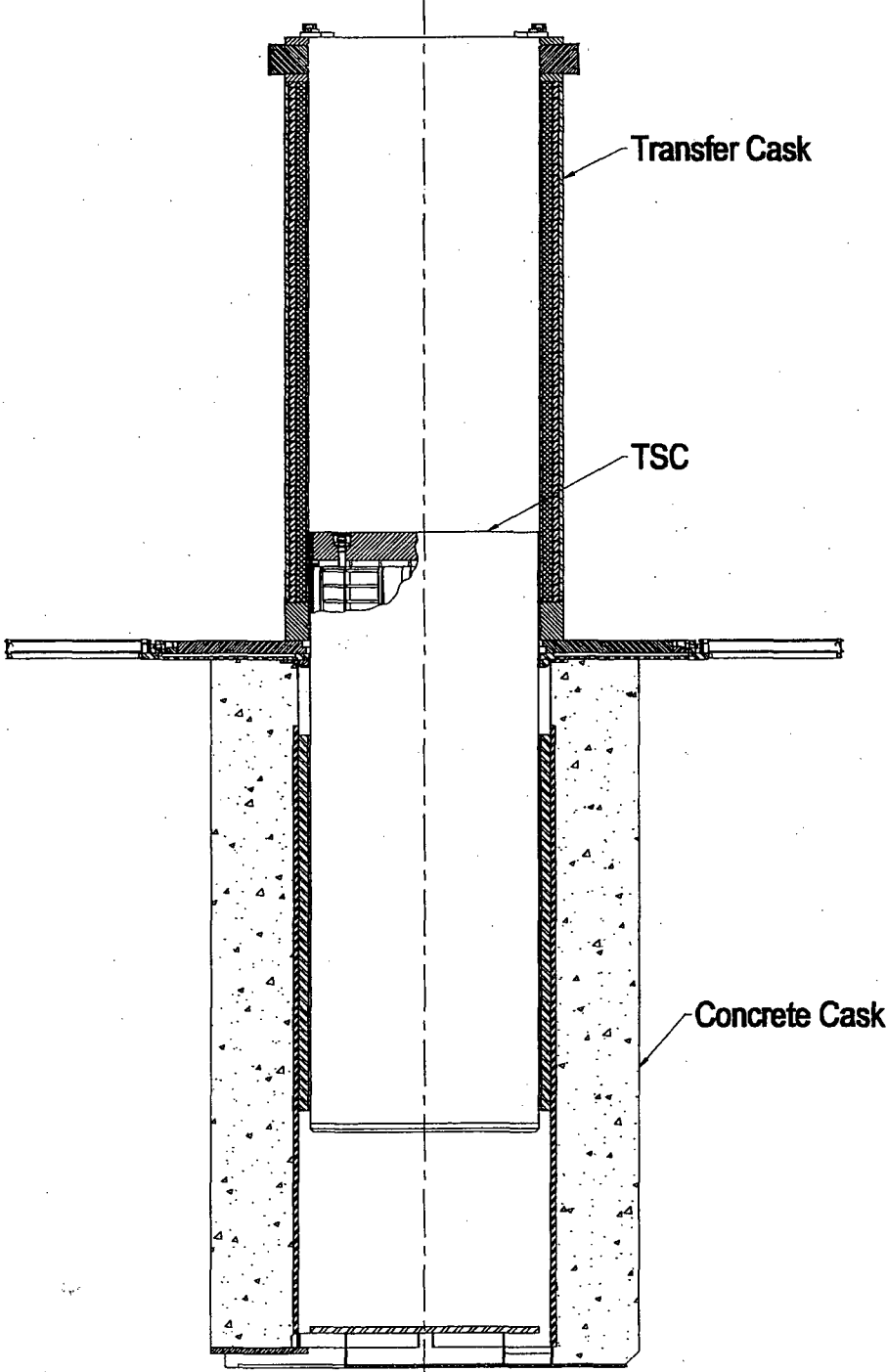
### 3.1 MAGNASTOR Structural Design

#### 3.1.1 Major Components

The three principal components of MAGNASTOR are the concrete cask, the TSC, and the transfer cask (refer to Figure 3.1.1-1). The following table shows the principal structural components of the three major MAGNASTOR components.

| Concrete Cask             | TSC                               | Transfer Cask                |
|---------------------------|-----------------------------------|------------------------------|
| Reinforced concrete shell | Closure lid and closure ring      | Trunnions                    |
| Liner weldment            | Shell                             | Inner and outer steel shells |
| Bottom weldment           | Bottom plate                      | Shield doors                 |
| Lid assembly              | Fuel basket assembly (PWR or BWR) | Door support rails           |
|                           |                                   | Lead and NS-4-FR shielding   |

Figure 3.1.1-1 Principal Components of MAGNASTOR



### 3.1.2 Discussion of MAGNASTOR

MAGNASTOR has four basic configurations to accommodate all PWR and BWR fuel assemblies. The type (PWR or BWR) and overall length of the fuel assembly determine the basic storage configuration, or group. The allocation of a fuel design to the MAGNASTOR grouping is shown in Table 1.3-2. The TSC is designed in two different lengths to accommodate the four groupings of PWR (2) and BWR (2) fuel assemblies. The concrete cask and transfer cask are one length that accommodates the two TSC lengths. The bounding weights and center of gravity of a loaded concrete cask are presented in Table 3.2.1-1.

The evaluations presented in this chapter are based on the bounding, or limiting, configuration of the components for the condition being evaluated. In most cases, the bounding condition evaluates the heaviest configuration, with either a total weight or bounding weight used as specified in the analysis. Factors of safety greater than ten are generally stated in the analyses as "Large." Numerical values are shown for factors of safety that are less than ten.

#### Concrete Cask

The concrete cask is a reinforced concrete cylinder with an outside diameter of 136 inches and an overall height of approximately 225 inches. The internal cavity of the concrete cask is lined by a 1.75-inch thick carbon steel shell with an inside diameter of 79.5 inches. There are 24 standoffs ( $3 \times 7\frac{1}{2}$  S-Beam) welded to the inner diameter of the liner. The overall cavity opening in the concrete cask is 73.5 inches. The liner thickness is designed primarily on radiation shielding requirements, but is also related to the need to establish a practical limit for the diameter of the concrete shell. The concrete shell, constructed using Type II Portland Cement, has a nominal density of 145 lb/ft<sup>3</sup> and a compressive strength of 4,000 psi at ambient temperature. Vertical hook bars and horizontal hoop bars form the inner and outer rebar assemblies.

A ventilation airflow path is formed by inlets at the bottom of the concrete cask, the annular space between the concrete cask inner shell and the TSC, and outlets in the concrete cask lid assembly. The passive ventilation system operates by natural convection as cool air enters the bottom inlets, is heated by the TSC, and exits from the outlets. Both the air inlets and air outlets are formed with carbon steel in the concrete cask body.

The lid assembly is composed of carbon steel and concrete and forms the concrete cask closure. The lid assembly is 6.75-inches thick and 88 inches in diameter.

## TSC

The TSC consists of a cylindrical shell closed at its top end by a closure lid. The bottom of the TSC is a 2.75-inch thick stainless steel plate that is welded to the TSC shell. The TSC forms the confinement boundary for the PWR or BWR spent fuel that is contained in the fuel basket assembly. The TSC is designed to accommodate both PWR and BWR classes of spent fuel assemblies. The TSC is fabricated from dual-certified SA240 Type 304/304L stainless steel. SA182 Type 304 stainless steel may be substituted for the SA240 Type 304 stainless steel used in the closure lid assembly provided that the SA182 material yield and ultimate strengths are equal to, or greater than, those of the SA240 material. The TSC shell is a 0.5-inch thick plate formed into a 72-inch outer diameter cylinder. The TSC closure lid consists of a 9-inch thick stainless steel plate. The closure lid is welded to the TSC shell to seal the TSC with a partial penetration groove weld. Prior to welding, the closure lid assembly is supported by four lift lugs attached to the inside diameter of the TSC at equally spaced angular intervals. A closure ring is welded to the closure lid and canister shell and redundant port covers are welded to the closure lid at both the vent and the drain ports to provide the redundant sealed closure of the TSC. Handling of the TSC is accomplished by the use of six hoist rings threaded into the closure lid, providing redundancy for heavy lifts.

The fuel basket assembly is provided in two configurations – one for up to 37 PWR fuel assemblies and one for up to 87 BWR fuel assemblies. The baskets are manufactured from SA537 Class 1 Carbon Steel. For both the PWR basket and BWR basket, the basic components are the same. The baskets are assembled from three major components – fuel tube assemblies, corner support weldments, and side support weldments. The fuel tube assemblies are equipped with neutron absorbers and stainless steel covers on up to four interior surfaces of the fuel tubes. The geometric integrity of the fuel tube array (21 fuel tubes – PWR, 45 fuel tubes – BWR) is maintained by the corner and side support weldments, which are bolted to the fuel tube array. The nominal inner dimension of the PWR fuel tubes is 8.86-inches square. The nominal inner dimension of the BWR fuel tubes is 5.86-inches square.

## Transfer Cask

The transfer cask, with its lifting yoke, is primarily a shielded lifting device used to handle the TSC. It provides biological shielding for a loaded TSC. The transfer cask is used for the vertical transfer of the TSC between workstations and the concrete cask, or transport cask. The shielding of the cask incorporates a multiwall (steel/lead/NS-4-FR/steel) design. The transfer cask is provided in one configuration capable of handling both the PWR and BWR configurations. The transfer cask can handle a loaded TSC weighing up to 118,000 pounds. The transfer cask is a

heavy lifting device that is designed, fabricated, and load-tested to the requirements of ANSI-N14.6 [2] and NUREG-0612 [3]. The transfer cask design incorporates three retainer assemblies attached to the top of the transfer cask to prevent a loaded TSC from being inadvertently lifted through the top of the transfer cask. The transfer cask has retractable bottom shield doors. During loading operations, the doors are closed and secured by bolts/pins so they cannot inadvertently open. During unloading, the doors are retracted using hydraulic cylinders to allow the TSC to be lowered into the concrete cask or transport cask.

### **Component Evaluation**

The following components are evaluated in this chapter.

- TSC lifting devices
- TSC shell, bottom plate, and closure lid
- Fuel basket assembly
- Transfer cask trunnions, shells, retainer assemblies, shield doors, and support rails
- Concrete cask body
- Concrete cask steel components (reinforcement, inner shell, lid assembly, bottom weldment, etc.)

Other MAGNASTOR components shown on the license drawings in Chapter 1 are included as loads in these component evaluations.

The structural evaluations in this chapter demonstrate that MAGNASTOR components meet their respective structural design criteria and are capable of safely storing the design basis PWR or BWR spent fuel assemblies.

#### **3.1.3 Design Criteria Summary**

MAGNASTOR structural design criteria are described in Chapter 2. Load combinations for normal, off-normal, and accident loads are evaluated in accordance with ANSI/ANS-57.9 [4] and ACI 349 [5]. The TSC is evaluated in accordance with ASME Code, Section III, Subsection NB for Class 1 components [6]. The basket is evaluated in accordance with ASME Code, Section III Subsection NG [7] and ASME Code, Section III, Appendix F [8]. The buckling evaluation of the fuel basket is performed in accordance with NUREG/CR-6322 [9]. The transfer cask and lifting yoke are lifting devices that are designed to NUREG-0612 [3] and ANSI N14.6 [2].

## 3.2 Weights and Centers of Gravity

### 3.2.1 Calculated Maximum Weights and Centers of Gravity

The maximum calculated weights and centers of gravity (CGs) for MAGNASTOR PWR and BWR configurations are presented in Table 3.2.1-1. The weights and CGs presented in this section are calculated based on nominal design dimensions.



Table 3.2.1-1 MAGNASTOR Storage Weight and Center of Gravity Summary

| Description  | PWR         |         | BWR         |         |
|--|-------------|---------|-------------|---------|
|  | Weight (lb) | CG (in) | Weight (lb) | CG (in) |
| Fuel (rod insert weight included for PWR fuel)   | 62,500      | -       | 61,500      | -       |
| Basket   | 20,000      | -       | 22,000      | -       |
| TSC w/o Lid  | 9,500       | -       | 9,500       | -       |
| Closure Lid  | 10,500      | -       | 10,500      | -       |
| Water in TSC   | 17,000      | -       | 16,000      | -       |
| Transfer Cask (does not include lifting yoke or transfer adapter)                              | 108,500     | -       | 108,500     | -       |
| Concrete Cask (does not include Lid)   | 214,000     | -       | 214,000     | -       |
| Lifting Yoke (not included in transfer cask weight)  | 3,000       | -       | 3,000       | -       |
| Concrete Cask Lid  | 5,000       | -       | 5,000       | -       |
| Loaded TSC (TSC, lid, basket, and fuel)  | 101,500     | 96      | 102,500     | 98      |
| Storage Cask Loaded (concrete cask, TSC, basket, fuel, concrete cask lid)                      | 320,000     | 103     | 321,000     | 104     |
| Transfer Cask, TSC, Basket, Lifting Yoke - Empty   | 141,000     | -       | 143,000     | -       |
| Under Hook Wet Weight (Transfer Cask, TSC, Basket, Lifting Yoke, Closure Lid, Fuel, and Water) | 229,500     | -       | 229,500     | -       |
| Under Hook Dry Weight (Transfer Cask, TSC, Basket, Transfer Yoke, Closure Lid, Fuel)           | 212,000     | -       | 213,000     | -       |

- Weights and CGs are maximum calculated values based on nominal component dimensions.
- All weights rounded to the nearest 500 pounds. Component weights are rounded individually, so total assembly weights may not equal the sum of the component weights.
- CG is measured from the bottom of each component.
- Average concrete density is considered to be 148 pcf for conservative weight calculation.
- Transfer cask lifting yoke weight for specific sites may vary from listed weight. The site-specific yoke weight should be used for site-specific applications.
- Concrete cask weight bounds alternate segmented body.

**3.3**      **Materials**

Refer to Chapter 8 for the information on Materials.

### **3.4 General Standards for Casks**

MAGNASTOR is designed for safe, long-term storage of spent fuel. The system will withstand all of the evaluated normal conditions, and off-normal and postulated accident events without release of radioactive material or excessive radiation exposure to workers or to the general public.

#### **3.4.1 Chemical and Galvanic Reactions**

The materials used in the fabrication and operation of MAGNASTOR are evaluated in Section 8.10.

#### **3.4.2 Positive Closure**

A stainless steel closure lid closes the top end of the TSC. Prior to being welded to the TSC shell, the closure lid is supported by lugs welded on the inside surface of the TSC shell at an elevation that allows for thermal expansion of the canister and fuel basket without contact with the closure lid. The lugs also serve as the handling points for the empty TSC shipping/receiving and placement in the transfer cask. The closure lid includes locations for installing load-tested hoist rings or lifting points that are used to lift and lower the loaded TSC after the closure lid is welded to the TSC shell. The closure lid and its weld to the TSC shell can support the weight of the TSC with a load factor of six on material yield strength and ten on material ultimate strength (ANSI N14.6/NUREG-0612). The TSC has a single 0.5-inch J-groove weld attaching the closure lid to the TSC shell. A closure ring, which provides the double weld redundant sealing of the confinement boundary, is installed in the TSC-to-closure lid groove and welded to both the closure lid and the TSC shell. Two port penetrations through the closure lid are used for water removal/TSC drying/helium backfill. Both have single welded, redundant port covers over them to provide the double weld confinement boundary. The port cover welds and the closure ring welds are field welds, and the final weld surfaces are liquid penetrant (PT) examined. The TSC closure lid weld is a field weld and the root, midplane, and final weld surfaces are liquid penetrant (PT) examined. The critical flaw evaluation defines the progressive inspection requirements for the closure lid weld and considers the following criteria.

- Weld is a partial penetration groove weld with an effective throat of 0.5 inch
- Weld filler material is E308L
- Weld process is Gas Tungsten Arc Welding (GTAW)
- Inner diameter of the TSC is 71.0 inches

### 3.4.3 Lifting Devices

To provide more efficient handling of MAGNASTOR, different methods of lifting are designed for each of the components. The transfer cask, the TSC, and the concrete cask, are handled using trunnions, hoist rings, and lift lugs, respectively.

The design of the MAGNASTOR addresses the concerns identified in NRC Bulletin 96-02, "Movement of Heavy Loads Over Spent Fuel, Over Fuel in the Reactor Core, or Over Safety-Related Equipment" (April 11, 1996) listed as follows.

- The MAGNASTOR lifting and handling components satisfy the requirements of NUREG-0612 and ANSI N14.6 for safety factors on redundant and nonredundant load paths as described in this chapter.
- Transfer cask lifting in the spent fuel pool or cask loading pit, or transfer cask lifting and movement above the spent fuel pool operating floor will be addressed on a plant-specific basis.

#### 3.4.3.1 Concrete Cask Lift

The concrete cask is lifted by means of embedded lug assemblies located in the top of the concrete cask body or by air pads beneath the cask. It is noted that movement of the concrete cask with air pads uses four load modules, one placed in each cask inlet, developing a minimum lift interface area of 5,760 in<sup>2</sup>, (48 in × 30 in × 4) and bearing stress less than 60 psi (322,000/5,760) at the lift module to cask interface. Use of air pads to move the concrete cask produces insignificant stress in the cask body; therefore, further evaluation of the cask movement is focused on the use of a vertical lift transporter. The concrete cask lift is analyzed in accordance with ANSI N14.6 and ACI 349. The concrete cask lid assembly is evaluated for lift conditions related to installation on the concrete cask body.

#### Lift Lug

A weight of 322,000 lb is conservatively used for the evaluation of the lift lugs, which bounds the maximum weight of a loaded concrete cask. Assuming a 10% dynamic load factor, the design load (P) on each lug is as follows.

$$P = \frac{322,000 \times 1.1}{4} = 88,550 \text{ lb}$$

The lugs are evaluated for adequate strength using this bounding load. The bearing stresses and loads for lug failure involving bearing, shear-tear-out, or hoop tension are determined using an allowable load coefficient (K). Actual lug failures may involve more than one failure mode, but such interaction effects are accounted for in the values of K [10].

The allowable ultimate bearing load ( $P_{bruL}$ ) for lug failure in bearing, shear-tear-out, or hoop tension is determined to be as follows.

$$P_{bruL} = 445.8 \text{ kip}$$

where the lug materials are:

$$F_{tu} = 80.0 \text{ ksi} \text{ ----- Ultimate strength, A537 CL2, at } 100^{\circ}\text{F}$$

$$F_{ty} = 60.0 \text{ ksi} \text{ ----- Yield strength, A537 CL2, at } 100^{\circ}\text{F}$$

The allowable yield bearing load ( $P_{bryL}$ ) is calculated as follows.

$$P_{bryL} = 341.9 \text{ kip}$$

Using the criteria of minimum factors of safety of 5 on ultimate strength and 3 on yield strength, the factors of safety (FS) for the lugs are shown as follows.

Ultimate Bearing:

$$FS = \frac{P_{bruL}}{P} = \frac{445.8}{88.55} = 5.03 > 5$$

Yield Bearing:

$$FS = \frac{P_{bryL}}{P} = \frac{341.9}{88.55} = 3.86 > 3$$

The tensile stress ( $\sigma$ ) in the net cross-sectional area of the lug is calculated to be as follows.

$$\sigma = \frac{P}{A} = \frac{88.55}{7.08} = 12.5 \text{ ksi}$$

The factors of safety (FS) are listed as follows.

Ultimate:

$$FS = \frac{80.0}{12.5} = 6.4 > 5$$

Yield:

$$FS = \frac{60.0}{12.5} = 4.8 > 3$$

### **Lift Anchor**

From the previous lug analysis, the maximum load on each embedment plate is 88.55 kip. The ultimate strength ( $\sigma$ ) in the plate is calculated as follows.

$$\sigma = \frac{P}{A} = \frac{88.55}{15.2} = 5.8 \text{ ksi}$$

The factors of safety (FS) are as follows.

Ultimate Tensile:

$$FS = \frac{80.0}{5.8} = 13.8 > 5$$

Yield Tensile:

$$FS = \frac{53.0}{5.8} = 9.1 > 3$$

Where the embedment plate material strengths are listed as follows.

$$F_{tu} = 80.0 \text{ ksi} \text{ ----- Ultimate strength, A537 CL2, at } 200^{\circ}\text{F}$$

$$F_{ty} = 53.0 \text{ ksi} \text{ ----- Yield strength, A537 CL2, at } 200^{\circ}\text{F}$$

### Concrete Anchor

The concrete shear area is conservatively assumed to be the perimeter of the bottom plate of the lift anchor. The shear cone in the concrete is conservatively ignored, and the minimum strength of concrete is used for the material temperature of 300°F. The required anchor depth, D, is determined to be as follows.

$$D = \frac{W}{\phi 2P \sqrt{f'_c}} = \frac{177,100}{0.85 \times 2 \times 39.6 \times \sqrt{3,800}} = 42.7 \text{ inch} \quad [5]$$

where:

$$W = 2 \times 88.55 \text{ kip} = 177,100 \text{ lb} \text{ ----- Anchor load}$$

$$\phi = 0.85 \text{ ----- Shear factor}$$

$$f'_c = 3,800 \text{ psi} \text{ ----- Concrete strength at } 300^{\circ}\text{F}$$

$$P = 39.6 \text{ inch} \text{ ----- Perimeter of bottom plate}$$

Excluding the bottom anchor plate, the length of the anchor is 65.5 inches; therefore, the factor of safety (FS) is as follows.

$$FS = \frac{65.5}{42.7} = 1.53$$

**Lift Pin**

The lift pin allowable ultimate shear load ( $P_{usp}$ ) for the symmetrical joint is the double shear strength of the pin.

$$P_{usp} = 1.571D_p^2F_{sup} = 678.6 \text{ kip} \quad [10]$$

where:

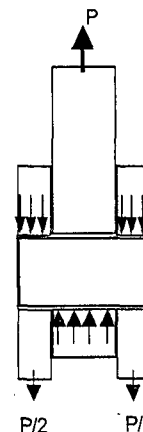
$$D_p = 4.0 \text{ inch} \text{ ----- Pin diameter}$$

$$F_{sup} = 0.6S_m = 0.6 \times 45.0 \text{ ksi} = 27 \text{ ksi}$$

$$S_m = 45.0 \text{ ksi} \text{ ----- 17-4PH stainless steel, at } 200^\circ\text{F}$$

The load on the pin is twice the lift lug load ( $P$ ); therefore, the factor of safety (FS) for the pin is as follows.

$$FS = \frac{P_{usp}}{2 \times P} = \frac{678.6}{2 \times 88.55} = 3.83 > 3.0$$



**Lift Lug Bolt**

The eight bolts that attach each set of the lift lugs to the embedded anchor are in tension. The tensile load is the combination of axial loads and the prying action of the lug fitting. The load per bolt ( $P_t$ ) is as follows.

$$P_t = \frac{W_1}{8} = \frac{177.1}{8} = 22.1 \text{ kip}$$

where:

$$W_1 = 2 \times 88.55 = 177.1 \text{ kip} \text{ ----- Anchor load}$$

The tensile load ( $Q$ ) on the bolt due to prying is calculated to be 2.4 kip [11].

The total load on the bolt ( $T$ ) is as follows.

$$T = P_t + Q = 22.1 + 2.4 = 24.5 \text{ kip}$$

The allowable bolt tensile load is as follows.

$$T_{all} = \frac{\pi D^2 F_y}{4} = \frac{\pi \times 1.25^2 \times 144.0}{4} = 176.7 \text{ kip}$$

where:

$$F_y = 144.0 \text{ ksi} \text{ ----- Yield strength, SB637 Grade N07718 nickel alloy steel, at } 200^\circ\text{F}$$

The factor of safety (FS) is as follows.

$$FS = \frac{176.7}{24.5} = 7.2$$

The bolts are threaded into the top plate of the lift anchor. The plate material is A537 Class 2 carbon steel. The bolt material is SB637 Grade N07718 nickel alloy steel. Bolt threads are 1-1/4-7 UNC 2A. For mating internal and external threads of materials having equal tensile strength, the length of engagement ( $L_e$ ) is calculated as shown in the following.

$$L_e = \frac{2A_t}{3.1416(K_{n\max}) \left[ \frac{1}{2} + 0.57735(n)(E_{s\min} - K_{n\max}) \right]} = 0.90 \text{ inch [12]}$$

where:

$$A_t = \pi \left( \frac{E_{s\min}}{2} - \frac{0.16238}{n} \right)^2 = 0.952 \text{ inch}^2 \text{ -- Tensile area of 1-1/4-7 UNC 2A}$$

Since the bolt and plate materials are different, the required length of engagement (Q) is calculated to be as follows.

$$Q = L_e J = 0.9 \times 1.59 = 1.43$$

where:

$$J = \frac{A_s \times S_{u \text{ bolt}}}{A_n \times S_{u \text{ plate}}} = 1.59 > 1.0$$

$$S_{u \text{ bolt}} = 177.6 \text{ ksi} \text{ ----- Ultimate strength, SB-637 Grade N07718 nickel alloy steel, at } 200^\circ\text{F}$$

$$S_{u \text{ plate}} = 80.0 \text{ ksi} \text{ ----- Ultimate strength, A-537 Class 2 carbon steel, at } 200^\circ\text{F}$$

The bolt thread length is 2.0 inches; therefore, the factor of safety (FS) is as follows.

$$FS = \frac{2.0}{1.43} = 1.40$$



### Concrete Cask Lid Assembly Lift

The lid assembly of the concrete cask is lifted using three ¾-10 UNC 2A threaded bolts with a ¾-inch thread engagement in the A36 carbon steel lid. A weight of 5,000 lb is conservatively used for the evaluation of the cask lid assembly lift, which bounds the maximum weight of the lid assembly. The load per bolt (P), including dynamic load factor of 10%, is as follows.

$$P = \frac{5,000 \times 1.1}{3} = 1,834 \text{ lb}$$

The required length of engagement is calculated to be as shown in the following.

$$L_e = \frac{2A_t}{3.1416(K_{n_{\max}}) \left[ \frac{1}{2} + 0.57735(n)(E_{s_{\min}} - K_{n_{\max}}) \right]} = 0.54 \text{ inch [12]}$$

The factor of safety (FS) is as follows.

$$FS = \frac{0.75}{0.54} = 1.39$$

### Pedestal Structural Evaluation

This section presents the structural evaluation of the pedestal during a concrete cask top-end lift. The ANSYS finite element model, presented in Section 3.10.4, is used to evaluate the concrete cask pedestal. The critical loading is during the concrete cask lift operations using the concrete cask lift anchors mounted on top of the concrete cask body.

#### Component Stresses

From the finite element model, the maximum stresses in the pedestal stand occur in the support rails. The critical section is the unsupported region between the pedestal stand and the inlet top. The maximum membrane stress is 16.7 ksi. The maximum membrane plus bending stress is 25.3 ksi. The factors of safety (FS) are shown as follows.

Membrane

$$FS = \frac{S_m}{\sigma_m} = \frac{19.3}{16.7} = 1.16$$

Membrane plus bending

$$FS = \frac{1.5S_m}{\sigma_{m+b}} = \frac{28.95}{25.3} = 1.14$$

where:

$$S_m = 19.3 \text{ ksi} \text{ ----- Design stress intensity, A-36 carbon steel, at } 300^\circ\text{F}$$

### Pedestal Welds

The pedestal is a welded assembly. The structural welds in the pedestal are evaluated using an allowable stress of  $0.6S_m$ . The weld forces ( $F_x$ ,  $F_y$ , and  $F_z$ ) are obtained from the pedestal finite element analysis results. The total weld load ( $F_w$ ) is obtained by using the square root of the sum of the squares method of the weld forces.

### Support Rail to Inlet Top Weld

The support rails are welded to the inlet top with a  $\frac{5}{8}$ -inch fillet weld. The stress in the weld ( $\sigma$ ) is as follows.

$$\sigma = \frac{F_w}{A} = 9.1 \text{ ksi}$$

where:

$$\begin{aligned} F_w &= 36,077 \text{ lb} \text{ ----- Total weld load} \\ F_x &= 3,248 \text{ lb} \text{ ----- Weld force, X-direction} \\ F_y &= 32,351 \text{ lb} \text{ ----- Weld force, Y-direction} \\ F_z &= -15,633 \text{ lb} \text{ ----- Weld force, Z-direction} \\ A &= 3.95 \text{ inch}^2 \text{ ----- Area} \\ l_w &= 8.95 \text{ inches} \text{ ----- Weld length} \\ t_w &= \frac{5}{8}\text{-inch} \text{ ----- Weld size} \end{aligned}$$

The factor of Safety (FS) is as follows.

$$FS = \frac{0.6S_m}{\sigma} = 1.27$$

where:

$$S_m = 19.3 \text{ ksi} \text{ ----- Design stress intensity, A-36 carbon steel, } 300^\circ\text{F}$$

### Inlet Top to Inlet Side Weld

The inlet top is welded to the inlet side with a  $\frac{1}{8}$ -inch fillet weld plus a  $\frac{1}{4}$ -inch groove weld. The stress in the weld is as follows.

$$\sigma = \frac{F_w}{A} = \frac{34,099}{8.03} = 4.2 \text{ ksi}$$

where:

$$\begin{aligned}
 F_w &= 34,099 \text{ lb} \text{----- Total weld load} \\
 F_x &= 10,437 \text{ lb} \text{----- Weld force, X-direction} \\
 F_y &= -32,351 \text{ lb} \text{----- Weld force, Y-direction} \\
 F_z &= -2,685 \text{ lb} \text{----- Weld force, Z-direction} \\
 A &= l_w \times t_w = 8.03 \text{ inch}^2 \text{----- Area} \\
 l_w &= 30.9 \text{ inches} \text{----- Weld length} \\
 t_w &= ((0.125 + 0.25) \times .707) = 0.26 \text{ inch} \text{---- Weld size}
 \end{aligned}$$

The factor of Safety (FS) is as follows.

$$FS = \frac{0.6S_m}{\sigma} = \frac{0.6 \times 19.3}{4.2} = 2.76$$

where:

$$S_m = 19.3 \text{ ksi} \text{----- Design stress intensity, A-36 carbon steel, at } 300^\circ\text{F}$$

Inlet Side to Base Plate Weld

The critical section of the inlet side to base plate weld is the 8.25-inch segment at the inner end of the inlet. The weld is a ¼-inch groove weld. The stress in the weld is as follows.

$$\sigma = \frac{F_w}{A} = 9.9 \text{ ksi}$$

where:

$$\begin{aligned}
 F_w &= \sqrt{F_x^2 + F_y^2 + F_z^2} = 20,484 \text{ lb} \\
 F_x &= 270 \text{ lb} \text{----- Weld force, X-direction} \\
 F_y &= 20,459 \text{ lb} \text{----- Weld force, Y-direction} \\
 F_z &= -971 \text{ lb} \text{----- Weld force, Z-direction} \\
 A &= l_w \times t_w = 2.06 \text{ inch}^2 \\
 l_w &= 8.25 \text{ inches} \text{----- Weld length} \\
 t_w &= 0.25 \text{ inch} \text{----- Weld size}
 \end{aligned}$$

The factor of safety (FS) is as follows.

$$FS = \frac{0.6S_m}{\sigma} = \frac{0.6 \times 19.3}{9.9} = 1.17$$

where:

$$S_m = 19.3 \text{ ksi} \text{ ----- Design stress intensity, A-36 carbon steel, at } 300^\circ\text{F}$$

Support Rail Gusset to Support Rail Weld

The rail gusset weld is a 5/8-inch fillet weld. The stress in the weld is as follows.

$$\sigma = \frac{F_w}{A} = 2.5 \text{ ksi}$$

where:

$$F_w = \sqrt{F_x^2 + F_y^2 + F_z^2} = 4,915 \text{ lb}$$

$$F_x = 2,224 \text{ lb} \text{ ----- Weld force, X-direction}$$

$$F_y = -1,636 \text{ lb} \text{ ----- Weld force, Y-direction}$$

$$F_z = -4,066 \text{ lb} \text{ ----- Weld force, Z-direction}$$

$$A = l_w \times (t_w \times 0.707) = 1.97 \text{ inch}^2$$

$$l_w = 4.45 \text{ inches} \text{ ----- Weld length}$$

$$t_w = 5/8\text{-inch} \text{ ----- Weld size}$$

The factor of safety (FS) is as follows.

$$FS = \frac{0.6S_m}{\sigma} = 4.63$$

where:

$$S_m = 19.3 \text{ ksi} \text{ ----- Design stress intensity, A-36 carbon steel, at } 300^\circ\text{F}$$

Nelson Studs

During a top-end concrete cask lift, the Nelson studs transmit the weight of a loaded TSC to the concrete cask. The liner is not directly attached to the pedestal. The ability of the Nelson studs to transfer load to the concrete cask is based upon the compressive strength of the concrete.

Using ACI 349-85 [5], the maximum pullout strength of the concrete is defined by the equation

$$P_d = 4 \times \phi \times \sqrt{f'_c} \times A_{cd}$$

where:

$$\phi = 0.85 \text{ ----- Strength reduction factor}$$

$$f'_c = 3,800 \text{ psi} \text{ ----- Concrete compression strength, } 300^\circ\text{F}$$
$$A_{cd} = \text{Projected cone area of Nelson stud less head area}$$

The projected area of a single Nelson stud is calculated by creating a cone that projects 45° from the head of the Nelson stud and omits the projected area of the Nelson stud head.

For a 0.75-inch diameter, 6.0-inch long Nelson stud, the projected area is as follows.

$$A_{cd} = \pi(l_e(l_e + d_h)) = 116.6 \text{ inch}^2$$

where:

$$l_e = 5.5 \text{ inches} \text{ ----- Bolt length}$$
$$d_h = 1.25 \text{ inches} \text{ ----- Head diameter}$$

For a single Nelson stud, the allowable concrete pullout strength is as follows.

$$P_d = 4 \times 0.85 \times \sqrt{3800} \times 116.6 = 24,438 \text{ lb}$$

The maximum load on a Nelson stud is 17,145 lb; therefore, the factor of safety (FS) is as follows.

$$FS = \frac{P_d}{F} = \frac{24,438}{17,145} = 1.43$$

The geometry of the four Nelson studs on the inlet top plate is such that the projected cones intersect each other. The combined projected area ( $A_{cd}$ ) is 332 inches<sup>2</sup>. The total load on the four Nelson studs is 18,817 pounds. The allowable concrete pullout strength ( $P_{cd}$ ) is as follows.

$$P_{cd} = 4 \times 0.85 \times \sqrt{3800} \times 332.0 = 69,584 \text{ lb}$$

The factor of safety (FS) is as follows.

$$FS = \frac{P_{cd}}{F} = \frac{69,584}{18,817} = 3.70$$

The maximum stress in a Nelson stud is as follows.

$$\sigma = \frac{F}{A_s} = 39.0 \text{ ksi}$$

where:

$$A_s = \frac{\pi}{4} D^2 = 0.44 \text{ inch}^2$$

The factor of safety (FS) is as follows.

$$FS = \frac{S_u}{\sigma} = \frac{58.0}{39.0} = 1.49$$

where:

$$S_u = 58.0 \text{ ksi} \text{ ----- Ultimate strength, A-36 carbon steel, at } 300^\circ\text{F}$$

**3.4.3.2 TSC Lift**

The adequacy of the TSC lifting components is demonstrated by evaluating the hoist rings, the TSC closure lid, and the weld that joins the closure lid to the TSC shell against the criteria in NUREG-0612 [3] and ANSI N14.6 [2]. The lifting configuration for the TSC consists of six hoist rings threaded into the closure lid assembly at equally spaced angular intervals. The hoist rings are analyzed as a redundant system with two three-legged lifting slings. For redundant lifting systems, ANSI N14.6 requires that load-bearing members be capable of lifting three times the load without exceeding the yield strength of the material and five times the load without exceeding the ultimate strength of the material. The closure lid is evaluated for lift conditions as a redundant system that demonstrates a factor of safety greater than three based on yield strength and a factor of safety greater than five based on ultimate strength. The TSC lift analysis is based on a load of 120,000 lb, which bounds the weight of the heaviest loaded TSC configuration. A dynamic load factor of 10% is considered in the analysis.

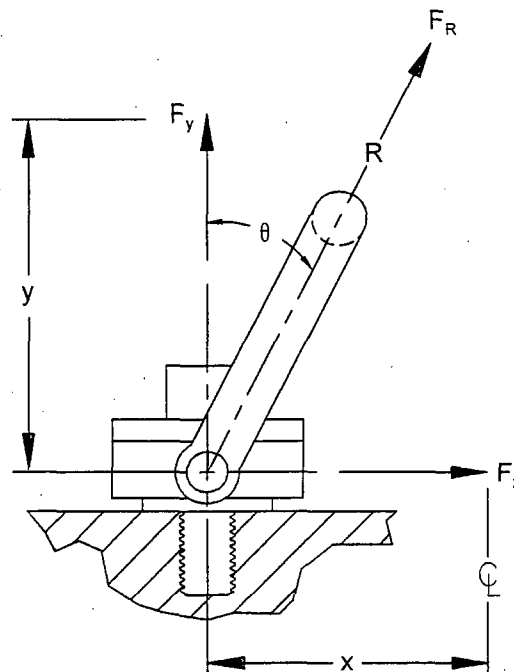
**Hoist Ring and Sling Evaluation**

The TSC lift configuration is shown in the accompanying sketch.

The vertical component force on the hoist ring, assuming a 10% dynamic load factor, is as follows.

$$F_y = \frac{120,000 \text{ lb} \times 1.1}{3 \text{ lift points}} = 44,000 \text{ lb}$$

As shown in the sketch, x is the distance from the TSC centerline to the hoist ring centerline (20.5 inch); F<sub>x</sub> is the horizontal component of force on the hoist ring; R is the sling length; F<sub>R</sub> is the maximum allowable force on the hoist ring; and the angle θ is the angle from vertical to the sling.



The hoist rings are rated at 50,000 lb with a safety factor of five on ultimate strength. Calculating the maximum angle ( $\theta$ ) that will limit  $F_R$  to 50,000 pounds is as follows.

$$\theta = \cos^{-1}\left(\frac{F_y}{F_R}\right) = \cos^{-1}\left(\frac{44,000}{50,000}\right) = 28.4^\circ$$

The minimum sling length,  $R$ , is as follows.

$$R = \frac{x}{\sin \theta} = \frac{20.5}{\sin 28.4} = 43.1 \text{ inches}$$

A 50-inch sling places the lift hook about 44 inches above the top of the TSC ( $y = R \cos \theta = 50 \cos 28.4^\circ = 44$  inches).

### **Bolt Shear**

From the Machinery's Handbook [12], the shear stress ( $\tau$ ) in the hoist ring hole threads (2½-4-UNC) in the closure lid is calculated as follows.

$$\tau = \frac{F_y}{A_n} = \frac{44,000 \text{ lb}}{12.148 \text{ in}^2} = 3,622 \text{ psi}$$

where:

$$A_n = 12.148 \text{ inch}^2 \text{----- Shear area of the closure lid assembly threads based on a length of engagement of 2.0 inches.}$$

The TSC closure lid is constructed of SA240, Type 304 stainless steel. Using shear allowables of  $0.6 S_y$  and  $0.5 S_u$  at a temperature of 300°F, the shear stress factors of safety are as follows.

Yield:

$$FS_y = \frac{0.6 \times 22,400 \text{ psi}}{3,622 \text{ psi}} = 3.7 > 3$$

Ultimate:

$$FS_u = \frac{0.5 \times 66,200 \text{ psi}}{3,622 \text{ psi}} = 9.1 > 5$$

The criteria of NUREG-0612 and ANSI N14.6 for redundant systems are met and the minimum thread engagement length of 2.0 inches is adequate.

The weight of the heaviest loaded transfer cask is less than 230,000 pounds. Three times the bounding weight of the loaded TSC is  $(3 \times 120,000)$  360,000 lb, which is greater than the weight of the heaviest transfer cask plus the weight of the loaded TSC (108,500 + 102,500 lb).

Consequently, the preceding analysis bounds the inadvertent lift of the transfer cask during the handling of the TSC.

### **TSC Lift Evaluation**

The structural adequacy of the TSC closure lid assembly and weld is evaluated using a finite element model described in Section 3.10.3. During a TSC lift, the acceleration due to gravity, with a dynamic load factor of 10%, is applied to the fully loaded TSC in the vertical direction. The maximum stress intensity experienced by the various TSC components during a three-point lift is as follows.

| <b>Component Description</b>       | <b>Stress Intensity (psi)</b> |
|------------------------------------|-------------------------------|
| TSC Shell (below Closure Lid Weld) | 1,516                         |
| Closure Lid Weld                   | 1,481                         |

The TSC shell and closure lid are constructed of SA240, Type 304 stainless steel. The yield strength is 18,000 psi and the ultimate strength is 63,400 psi. These are conservatively evaluated at a temperature of 650°F. The strength of the weld joint is taken as the same as the strength of the base material. Thus, when compared to the yield and ultimate strengths, the maximum nodal stress intensity of 1,516 psi produces the following factors of safety for a three-point lift.

Yield:

$$FS_y = \frac{\text{yield strength}}{\text{maximum stress intensity}} = \frac{18,000 \text{ psi}}{1,516 \text{ psi}} = 12 > 3$$

Ultimate:

$$FS_u = \frac{\text{ultimate strength}}{\text{maximum stress intensity}} = \frac{63,400 \text{ psi}}{1,516 \text{ psi}} = 42 > 5$$

The criteria of NUREG-0612 and ANSI N14.6 for redundant systems are met. Thus, the TSC shell and closure lid are adequate.



### 3.4.3.3 Transfer Cask Lift

The MAGNASTOR transfer cask is analyzed for loads associated with the heavy lift requirements specified in ANSI N14.6 [2] and NUREG-0612 [3]. All load path components of the cask are evaluated for structural adequacy. The transfer cask is analyzed for loads associated with the vertical lift of the transfer cask. The transfer cask is not designed for redundant lifting; therefore, factors of safety of six on material yield strength and ten on material ultimate strength are required for the lifting trunnions.

The analysis of the fully loaded transfer cask consists of a finite element analysis using the ANSYS program to calculate the stress in the transfer cask forgings, shells, and the trunnion region for the operational vertical lift condition. Details of the ANSYS finite element model are presented in Section 3.10.5. The structural evaluations of the rail, the shield door, and the rail welds are performed using standard engineering equations. The design weight of the transfer cask is 230,000 pounds. A bounding weight of the transfer cask of 240,000 lb is considered in the evaluation. A conservative load of 264,000 lb ( $240,000 \times 1.1$  dynamic load factor) is used in the finite element analysis.

### Transfer Cask Body

Table 3.4.3-1 provides the summaries of the stress intensities for the seven cross-sectional locations of the trunnion and top ring. Table 3.4.3-2 provides the stress summaries for the inner and outer shells and bottom ring. The maximum primary membrane stress intensity,  $P_m$ , and the maximum primary membrane plus bending stress intensity,  $P_m + P_b$ , is compared with the allowable stress criteria.

The cross-section of the trunnion is circular. Two cross-sectional areas are examined as shown in Figure 3.4.3-1. The maximum bending stress occurs at the cross-section ( $x = 43.9$  inches) at the intersection of the trunnions with the outer diameter of the top forging ring. The maximum stress occurs at the trunnion surface. The maximum stress in the trunnion is 3.8 ksi. Comparing the stress to the material (A350 Grade LF 2) allowable yield and ultimate strength, the factors of safety are 8.1 ( $>6$ ) for material yield strength and 18.5 ( $>10$ ) for material ultimate strength.

For the top ring, the five cross-sectional areas selected for stress examination are shown in Figure 3.4.3-1. The maximum bending plus membrane stress occurs at the radial cross-section (topring-A1) above the trunnion. The bending stress through this cross-sectional area is 4.9 ksi.

Comparing the stress to the material (A516 Gr 70) allowable yield and ultimate strength, the

factors of safety are 6.6 ( $>6$ ) and 14.2 ( $>10$ ) for yield and ultimate material strengths, respectively.

For the inner shell, the maximum stress intensity occurs at the location of " $\theta = 10^\circ$ ,  $z = -7.0$  inches", which is outside the intersection just below the trunnion. The maximum bending plus membrane stress through the shell is 2.3 ksi. Comparing the stress to the material (A588) allowable yield and ultimate strengths, the factors of safety are 18.6 ( $>6$ ) and 30.2 ( $>10$ ), respectively.

For the outer shell, the maximum stress intensity occurs at the location of " $\theta = 10^\circ$ ,  $z = -7.0$  inches", which is outside the intersection just below the trunnion. The maximum bending plus membrane stress in the shell thickness is 3.5 ksi. Comparing the stress to the material (A588) allowable yield and ultimate strengths, the factors of safety are 12.3 ( $>6$ ) and 20 ( $>10$ ), respectively.

For the bottom ring the maximum stress intensity occurs at the nodal location of " $\theta = 90^\circ$ ,  $z = -173.5$  inches", which is just below the inner and outer shells. The maximum membrane plus bending stress in the ring thickness is 0.7 ksi. Comparing this stress to the material (A588) allowable yield and ultimate strengths, the factors of safety are 58 ( $>6$ ) and 94 ( $>10$ ) for yield and ultimate strength, respectively.

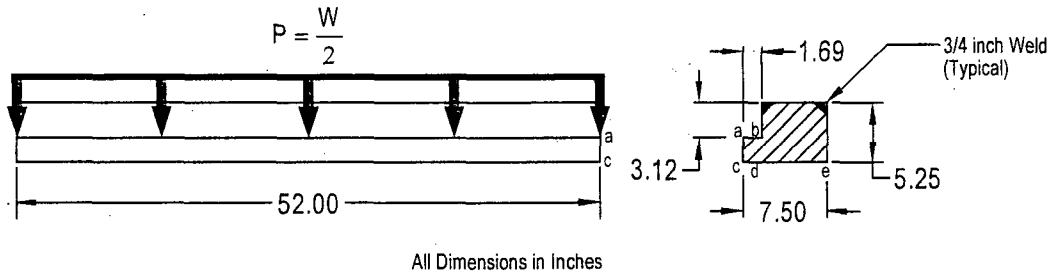
### **Transfer Cask Shield Door Rails and Welds**

This section demonstrates the adequacy of the transfer cask shield doors, door rails, and welds in accordance with NUREG-0612 and ANSI N14.6, which require safety factors of six and ten on material yield strength and ultimate strength, respectively, for nonredundant lift systems. The transfer cask shield doors and door rails are designed to retain and support the maximum loaded TSC weight of 118,000 lb, which includes the weight of basket, fuel, and water. The shield doors are 5-inch thick plates that slide on the door rails. The rails are 7.50-inches wide  $\times$  52-inches long and are welded to the bottom ring of the transfer cask. The doors and the rails are constructed of A-588 and SA-350 Grade LF 2 low alloy steel, respectively.

A weight of 143,000 lb ( $>118,000 \times 1.1$ ) is conservatively used for the evaluation of the rails. This weight bounds the weight of the heaviest loaded TSC, the weight of the water in the TSC, and the weight of the shield doors and rails. The 10% dynamic load factor is included to ensure that the evaluation bounds all normal operating conditions. Allowable stress for the component materials are taken at 400°F, which bounds the maximum temperature at the bottom of the transfer cask under normal conditions.

**Stress Evaluation for Door Rail**

Each rail is assumed to carry one-half of the load.



The shear stress ( $\tau$ ) in each door rail bottom plate (section b-d) due to the applied load is as follows.

$$\tau = \frac{P}{A} = \frac{143.0/2}{110.8} = 0.65 \text{ ksi}$$

where:

$$A = (5.25 - 3.12) \times 52 = 110.8 \text{ inch}^2 \text{----- Shear area}$$

The bending stress ( $\sigma_b$ ) in each rail bottom section b-d due to the applied load, P, is as follows.

$$\sigma_b = \frac{6M}{Lt_{a-c}^2} = 3.1 \text{ ksi}$$

where:

- $M = P \times L_{a-b} = 120.8 \text{ inch-kip}$
- $L_{a-b} = 1.69 \text{ inches}$  ----- Applied load moment arm
- $L = 52 \text{ inches}$  ----- Length of the rail
- $t_{a-c} = 2.13 \text{ inches}$  ----- Thickness of the rail

The maximum stress ( $\sigma$ ) intensity in the bottom section of the rail is as follows.

$$\sigma = \sqrt{(\sigma_b)^2 + 4\tau^2} = 3.4 \text{ ksi}$$

The factor of safety (FS) based on the material yield strength is as follows.

$$FS = \frac{S_y}{\sigma} = \frac{30.8 \text{ ksi}}{3.4 \text{ ksi}} = 9.1 > 6$$

where:

$$S_y = 30.8 \text{ ksi} \text{----- Yield strength for A350 Grade LF 2, at } 400^\circ\text{F}$$

The factor of safety (FS) based on the material ultimate strength is as follows.

$$FS = \frac{S_u}{\sigma} = \frac{70 \text{ ksi}}{3.4 \text{ ksi}} = 20.6 > 10$$

where:

$$S_u = 70.0 \text{ ksi} \text{ ----- Ultimate strength A-350 Grade LF 2, at } 400^\circ\text{F}$$

Stress Evaluation for the Shield Doors

The shield doors are 5-inches thick at the center and step down to 2.94-inches thick at the edges, where they rest on the rails. The stepped edges of the two door leaves are designed to interlock at the center. Therefore, the doors are analyzed as single simply supported plates. The engagement length of the door with the rail is 52 inches. The shear stress ( $\tau$ ) at the edge of the shield door where the door contacts the rail is as follows.

$$\tau = \frac{P}{A_s} = 0.94 \text{ ksi}$$

where:

$$A_s = t_d \times L = 152.9 \text{ inch}^2 \text{ ----- Total shear area}$$

$$t_d = 5.0 - 2.06 = 2.94 \text{ inches ----- Thickness of the door at edge}$$

$$L = 52 \text{ inches ----- Length of door and rail engagement}$$

The maximum bending stress ( $\sigma_b$ ) at the center of the doors is as follows.

$$\sigma_b = \frac{Mc}{I} = 4.0 \text{ ksi}$$

where:

$$M = \frac{WL}{8} = 1.36 \times 10^6 \text{ inch-lb}$$

$$W = 143,000 \text{ lb ----- Total weight}$$

$$c = \frac{h}{2} = 2.5 \text{ inches ----- Distance to surface}$$

$$I = \frac{bh^3}{12} = 855 \text{ inch}^4 \text{ ----- Cross-sectional moment of inertia}$$

$$L = 76 \text{ inches ----- Span length}$$

The maximum stress intensity ( $\sigma$ ) in the door is as follows.

$$\sigma = \sqrt{(\sigma_b)^2 + 4\tau^2} = 4.1 \text{ ksi}$$

The factor of safety (FS) based on the yield strength is as follows.

$$FS = \frac{S_y}{\sigma} = \frac{43 \text{ ksi}}{4.1 \text{ ksi}} = 10.5 > 6$$

where:

$$S_y = 43 \text{ ksi} \text{----- Yield strength for A-588, at } 400^\circ\text{F}$$

The factor of safety (FS) based on the ultimate strength is as follows.

$$FS = \frac{S_u}{\sigma} = \frac{70 \text{ ksi}}{4.1 \text{ ksi}} = 17.1 > 10$$

where:

$$S_u = 70.0 \text{ ksi} \text{----- Ultimate strength for A-588, at } 400^\circ\text{F}$$

### Door Rail Weld Evaluation

The door rails are attached to the bottom forging of the transfer cask by 0.75-inch partial penetration bevel groove welds that extend the full length of the inside and outside of each rail. The loaded TSC weight is conservatively assumed to act at a point on the inside edge of the rail. Since the base metal is the limiting strength of the welded section, the ultimate strength on the inner weld is evaluated. Summing moments about the edge of outer weld are as follows.

$$\Sigma M = 0 = P \times L_{c-e} - F_w \times \left( L_{d-e} - \frac{L_w}{2} \right) \Rightarrow F_w = 91 \text{ kip}$$

where:

$$P = \frac{W}{2} = 71.5 \text{ kip} \text{----- Load on a single rail}$$

$$L_w = 0.75 \text{ inch} \text{----- Weld length}$$

$$L_{d-e} = 7.5 - 1.69 = 5.81 \text{----- Distance from edge of inner weld to edge of outer weld}$$

$$L_{c-e} = 7.5 \text{ inches} \text{----- Width of the rail}$$

The maximum stress ( $\sigma$ ) in the base metal attached by the inner weld is as follows.

$$\sigma = \frac{F_w}{A_w} = 2.3 \text{ ksi}$$

where:

$$A_w = 0.75 \times 52 = 39 \text{ inch}^2 \text{ ----- Area on the base metal supporting inner weld}$$

The factor of safety (FS) based on the yield strength is as follows.

$$FS = \frac{43 \text{ ksi}}{2.3 \text{ ksi}} = 18.7 > 6$$

The factor of safety (FS) based on the ultimate strength is as follows.

$$FS = \frac{70 \text{ ksi}}{2.3 \text{ ksi}} = 30.4 > 10$$

### Trunnion Bearing Stress Evaluation

During a vertical lifting load case, the transfer cask is being lifted by the trunnions.

The load on each trunnion is 132 kips ( $240 \times 1.1/2$ ). The minimum trunnion bearing engagement depth is 7.5-inches, but only 50% of this is used in the evaluation. The diameter of the trunnion is 9 inches. The bearing stress on the trunnion ( $\sigma_b$ ) is as follows.

$$\sigma_{\text{brg}} = \frac{W_{\text{VL}}}{A_{\text{brg}}} = \frac{132}{33.75} = 3.92 \text{ ksi}$$

The factor of safety (FS) is as follows.

$$FS = \frac{S_y}{\sigma} = \frac{30.8}{3.92} = 7.85$$

where:

$$S_y = 30.8 \text{ ksi ----- Yield strength, SA-350 LF2, at } 400^\circ\text{F}$$

### Inadvertent Lift of Transfer Cask by TSC

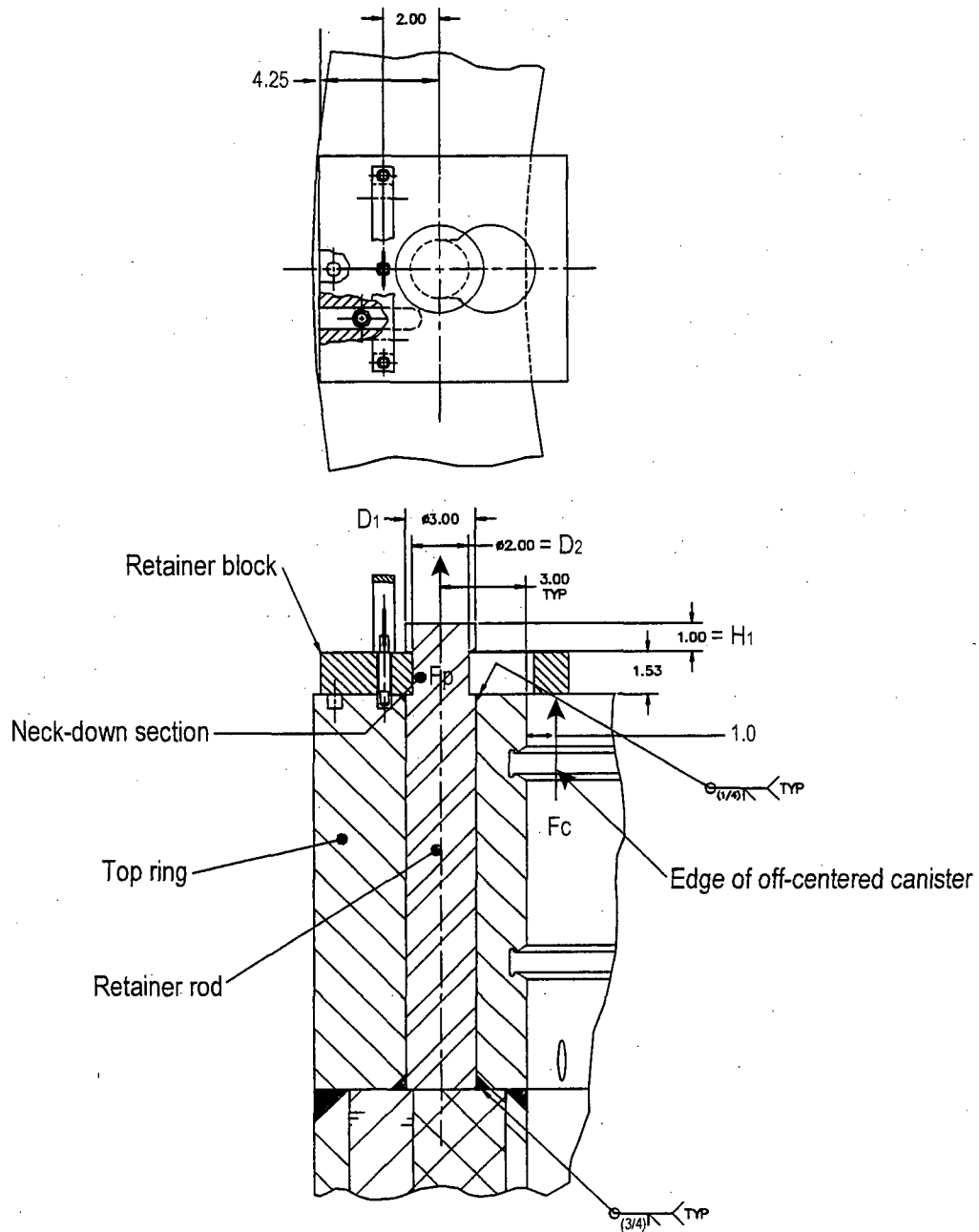
The inadvertent lift of the transfer cask by the TSC is considered an off-normal event. The stresses associated with this condition are required to satisfy allowable stress limits for ASME Boiler and Pressure Vessel Code, Service Level C condition. The temperature of the cask at the top is assumed to be 300°F.

In the event the transfer cask is lifted by the TSC during handling operations, instead of by the transfer cask trunnions, the weight of the transfer cask is supported by the three retaining blocks mounted on top of the transfer cask top ring. In this case, the retaining blocks must have

sufficient strength to support the weight of the transfer cask. The three retaining blocks on the top-forging ring are spaced 120° apart.

**Retainer Rod Evaluation**

During an inadvertent lift of the transfer cask, the retainer rod is subjected to a tensile load,  $F_p$ , due to the prying action of the retaining block. The top view and the side view of the retaining block are shown in the following sketches.



A conservative weight of 110,000 lb is used for this evaluation. This weight bounds the maximum weight of the transfer cask. The dynamic load factor, DLF, is 1.1. The maximum uplifting force applied by the TSC to the retainer block,  $F_c$ , is 110 kip  $(1.1)/3 = 40.3$  kip. When the TSC is off-center, the maximum distance between the TSC outer edge and the inner edge of the transfer cask is one inch. The prying force applied to the retainer rod ( $F_p$ ) is as follows.

$$F_p = \frac{40.3 \times (1 + 3 + 4.25)}{4.25} = 78.2 \text{ kip}$$

**Effective Stress Areas of Retainer Rod**

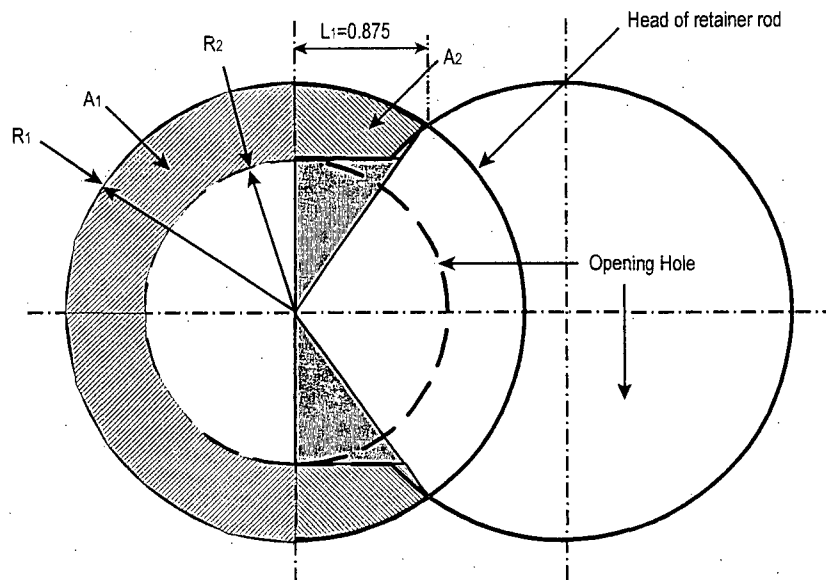
Referring to the previous sketch, the cross-sectional areas for the retainer rod evaluation are as follows.

$$A_t = \frac{\pi}{4} D_2^2 = 3.14 \text{ inch}^2 \text{----- Tensile area (neck down area)}$$

$$A_{ws} = \pi D_1 H_w = 7.07 \text{ inch}^2 \text{----- Weld shear area}$$

$$A_{sh} = \pi D_2 H_1 = 6.28 \text{ inch}^2 \text{----- Head shear area (through head thickness)}$$

The bearing area in the retainer rod just above the neck-down area is the hatched area as shown in the following sketch.



The total bearing area ( $A_{brg}$ ) is as follows.

$$A_{brg} = 2(A_1 + A_2) = 2(0.982 + 0.342) = 2.648 \text{ inch}^2$$

Retainer Rod Load Capacity:

The load capabilities of the retainer rod are calculated in the following.



$F_{\text{tensile}} = (A_t)(S_M) = (3.14)(26.9) = 84.4 \text{ kip}$  ----- Load capability at D2  
 $F_{\text{ws}} = (A_{\text{ws}})(S_S) = (7.07)(13.4) = 94.7 \text{ kip}$  ----- Shear capability of weld  
 $F_{\text{brg}} = (A_{\text{brg}})(S_{\text{brg}}) = (2.648)(33.6) = 88.9 \text{ kip}$  ----- Bearing capability of rod head  
 $F_{\text{sh}} = (A_{\text{sh}})(S_S) = (6.28)(13.4) = 84.2 \text{ kip}$  ----- Shear capability under rod head

where:

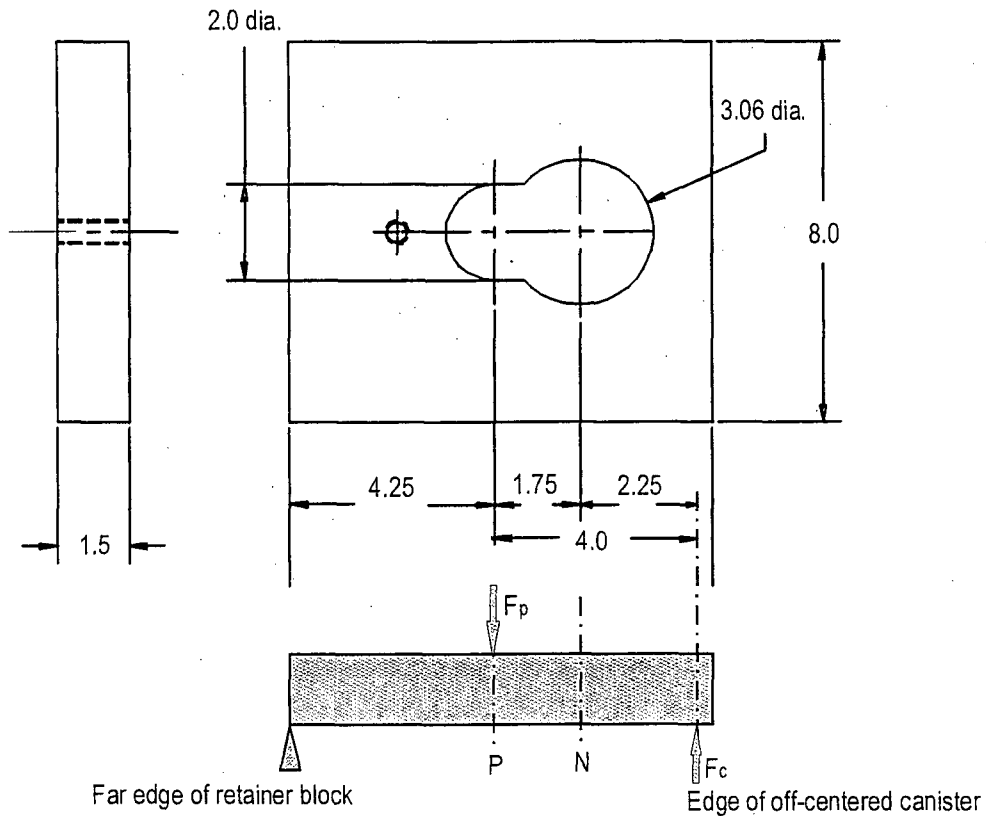
$S_M = 1.2 S_m = 1.2 (22.4) = 26.9 \text{ ksi}$   
 $S_S = 0.6 S_m = 0.6 (22.4) = 13.4 \text{ ksi}$   
 $S_{\text{brg}} = S_y = 33.6 \text{ ksi}$   
 $S_y = 33.6 \text{ ksi}$  ----- Yield strength, SA-516 Grade 70 at 300°F  
 $S_m = 22.4 \text{ ksi}$  ----- Design stress intensity, SA-516 Grade 70 at 300°F

The minimum factor of safety (FS) is as follows.

$$FS = \frac{F_{\text{sh}}}{F_p} = \frac{84.2}{78.2} = 1.08$$

**Retainer Block Evaluation**

The retainer block and the force-loading diagram are shown in the following sketch.



Point P is where the headed retainer rod is loaded under prying force  $F_p$ . The maximum bending stress ( $\sigma_b$ ) in the retainer block is as follows.

$$\sigma_b = \frac{Mc}{I} = 71.6 \text{ ksi}$$

where:

$$M = F_c(4) = 161.2 \text{ kip-inch}$$

$$F_c = 40.3 \text{ kip}$$

$$I = \frac{bh^3}{12} = 1.688 \text{ inch}^4$$

$$C = 0.75 \text{ inch}$$

The factor of safety (FS) is as follows.

$$FS = \frac{1.8S_m}{\sigma_b} = 1.13$$

where:

$$S_m = 45.0 \text{ ksi} \text{ ----- Yield strength, 17-4 PH at 300°F}$$

Figure 3.4.3-1 Top Ring Section Cuts

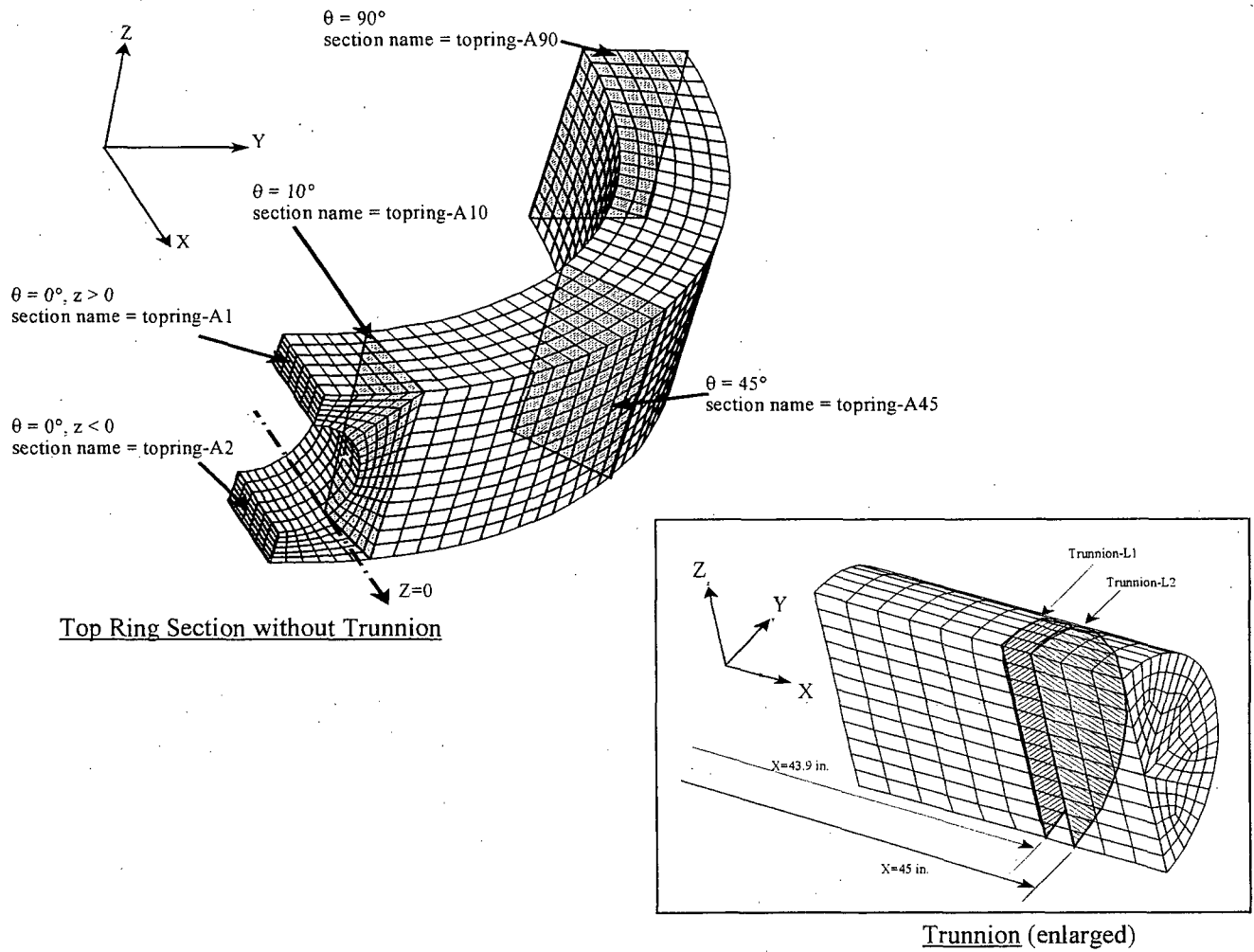


**Table 3.4.3-1 Stress Intensity for Trunnions and Top Ring**

| Location <sup>a</sup> | Position <sup>a</sup> | P <sub>m</sub> <sup>b</sup><br>ksi | P <sub>b</sub> <sup>b</sup><br>ksi | P <sub>m</sub> +P <sub>b</sub> <sup>b</sup><br>ksi | Material | S <sub>yield</sub><br>ksi | S <sub>ultimate</sub><br>ksi | FS <sub>Yield</sub> | FS <sub>Ultimate</sub> |
|-----------------------|-----------------------|------------------------------------|------------------------------------|--|----------|---------------------------|------------------------------|---------------------|------------------------|
| Trunnion-L1           | x = 43.9 inch         | 0.04                               | 3.75                               | 3.79   | SA350    | 30.8                      | 70.0                         | 8.1                 | Large                  |
| Trunnion-L2           | x = 45 inch           | 0.00                               | 2.05                               | 2.05   | SA350    | 30.8                      | 70.0                         | Large               | Large                  |
| TopRing-A1            | θ = 0°, z > 0         | 2.37                               | 2.57                               | 4.93   | SA516    | 32.5                      | 70.0                         | 6.6                 | Large                  |
| TopRing-A2            | θ = 0°, z < 0         | 0.33                               | 1.29                               | 1.63   | SA516    | 32.5                      | 70.0                         | Large               | Large                  |
| TopRing-A10           | θ = 10°               | 0.07                               | 1.02                               | 1.09   | SA516    | 32.5                      | 70.0                         | Large               | Large                  |
| TopRing-A45           | θ = 45°               | 0.11                               | 0.84                               | 0.95   | SA516    | 32.5                      | 70.0                         | Large               | Large                  |
| TopRing-A90           | θ = 90°               | 0.11                               | 0.75                               | 0.86   | SA516    | 32.5                      | 70.0                         | Large               | Large                  |

**Table 3.4.3-2 Stress Intensity for Transfer Cask Shells and Bottom Ring**

| Location <sup>c</sup> | Position <sup>c</sup> | P <sub>m</sub> +P <sub>b</sub> <sup>d</sup><br>ksi | Material | S <sub>yield</sub><br>ksi | S <sub>ultimate</sub><br>ksi | FS <sub>Yield</sub> | FS <sub>Ultimate</sub> |
|-----------------------|-----------------------|--|----------|---------------------------|------------------------------|---------------------|------------------------|
| Inner Shell           | θ = 10°, z = -7 inch  | 2.32   | A588     | 43.0                      | 70.0                         | Large               | Large                  |
| Outer Shell           | θ = 10°, z = -7 inch  | 3.50   | A588     | 43.0                      | 70.0                         | Large               | Large                  |
| Bottom Ring           | θ = 90°, z = -173.5   | 0.74   | A588     | 43.0                      | 70.0                         | Large               | Large                  |

<sup>a</sup> The locations and positions are defined in Figure 3.4.3-1.

<sup>b</sup> P<sub>m</sub> = primary membrane stress intensity; P<sub>b</sub> = primary bending stress intensity; P<sub>m</sub> + P<sub>b</sub> = primary membrane + bending stress intensity.

<sup>c</sup> The locations and positions correspond to the axis shown in Figure 3.10.5-1, Section 3.10.5.

<sup>d</sup> P<sub>m</sub> + P<sub>b</sub> = primary membrane + bending stress intensity.

### **3.5 Normal Operating Conditions**

This section presents the analyses of the major structural components of MAGNASTOR for normal conditions of storage. The TSC, fuel baskets, and concrete cask are evaluated using finite element models and classical hand calculations.

#### **3.5.1 TSC Evaluation for Normal Operating Conditions**

For normal conditions of storage, the TSC is evaluated using ASME Code, Section III, Subsection NB 'Service Level A' allowable stresses. For detailed analysis results for normal conditions, see Table 3.10.3-1 through Table 3.10.3-6.

##### **3.5.1.1 TSC Thermal Stress Analysis**

The thermal stresses in the TSC during normal conditions of storage are evaluated using a finite element model described in Section 3.10.3. The thermal gradient applied to the TSC model bounds all conditions of storage; therefore, the results presented are conservative. The resulting maximum (secondary) thermal stresses in the TSC are shown in Table 3.5.1-1. The locations of the stress sections are shown in Figure 3.10.3-2 in Section 3.10.3.

##### **3.5.1.2 TSC Dead Load**

The TSC is analyzed for a dead load using the finite element model described in Section 3.10.3. The normal handling plus normal pressure conditions presented in Section 3.5.1.5 bound the resulting maximum TSC dead load stresses; therefore, results for the dead load analysis are not presented separately.

##### **3.5.1.3 TSC Maximum Internal Pressure**

The TSC is analyzed for a maximum internal pressure load using the finite element model described in Section 3.10.3. A maximum internal pressure of 110 psig is applied as a surface load to the elements along the internal surface of the TSC shell, bottom plate, and closure lid. This pressure bounds the maximum calculated pressure for PWR and BWR fuel under normal conditions.

The resulting maximum internal pressure load stresses for the TSC are summarized in Table 3.5.1-2 and Table 3.5.1-3 for primary membrane and primary membrane plus primary bending

stress categories, respectively. The locations for the stress sections are shown in Figure 3.10.3-2 in Section 3.10.3.

**3.5.1.4 TSC Handling Loads**

The TSC is analyzed for handling loads using the finite element model described in Section 3.10.3. Normal handling is simulated by constraining the model at nodes on the closure lid simulating three lift points. A 1.1g acceleration load, which corresponds to the dead weight with a 10% dynamic load factor, is applied to the model in the axial direction. Pressure is applied to the TSC bottom plate to simulate the weight of the basket and fuel with an acceleration of 1.1g.

The resulting maximum stresses in the TSC due to handling loads are bounded by the maximum stresses for the normal handling loads plus normal pressure condition presented in Section 3.5.1.5; therefore, the stress results for the handling condition are not presented separately.

The lift lugs are evaluated for dead weight using classical methods. The TSC lift lugs are welded to the inner surface of the TSC shell to accommodate handling of the empty TSC and to support the closure lid prior to completion of the weld to the shell. The total weight, W, imposed on the lift lugs conservatively considers the weight of the closure lid and supplemental support equipment. A 10% load factor is also applied to ensure all normal operating loads are bounded. The stresses evaluated for the lift lugs are bearing stress and shear stress through the weld. The bearing stress is as follows.

$$\sigma_{\text{bearing}} = \frac{W}{4A} = \frac{22,550 \text{ lb}}{21.6 \text{ in}^2} = 1,044 \text{ psi}$$

where:

$$W = (10,500 \text{ lb} + 10,000 \text{ lb}) \times 1.1 = 22,550 \text{ lb}$$
$$A = 5.4 \text{ inch}^2 \text{ ----- Area of lifting lug}$$

Using a conservative temperature of 650°F, the factor of safety (FS) is as follows.

$$FS = \frac{1.0 S_y}{\sigma_{\text{bearing}}} = \frac{19,400 \text{ psi}}{1,044 \text{ psi}} = \text{Large}$$

where:

$$S_y = 19,400 \text{ psi} \text{ ----- Yield strength of SA-240, Type 304 stainless steel}$$

The attachment weld for the lift lugs is a 1/8-inch double-bevel weld. The shear stress ( $\tau_w$ ) is as follows.

$$\tau_w = \frac{W}{4A_{eff}} = \frac{22,550 \text{ lb}}{5.40 \text{ in}^2} = 4,176 \text{ psi}$$

where:

$$A_{eff} = L_{eff} \times t_{eff} = 1.35 \text{ inch}^2 \text{----- Area of lifting lug weld}$$

$$L_{eff} = 5.4 \times 2 = 10.8 \text{ inches----- Length of lifting lug weld}$$

$$t_{eff} = 0.125 \text{ inch ----- Thickness of lifting lug weld}$$

Conservatively using the temperature of 650°F and material allowables of the base metal, the factor of safety (FS) is as follows.

$$FS = \frac{S_{allow}}{\tau_w} = \frac{0.6 S_m}{\tau_w} = \frac{9,720 \text{ psi}}{4,176 \text{ psi}} = 2.3$$

where:

$$S_{allow} = 0.6 S_m \text{----- Weld allowable}$$

$$S_m = 16,200 \text{ psi ----- Design stress intensity of SA-240, Type 304 stainless steel}$$

### 3.5.1.5 TSC Load Combinations

The TSC is structurally analyzed for combined thermal, dead, maximum internal pressure, and handling loads using the finite element model described in Section 3.10.3.

The resulting maximum stresses in the TSC for combined loads are summarized in Table 3.5.1-2, Table 3.5.1-3, and Table 3.5.1-4 for primary membrane, primary membrane plus primary bending, and primary plus secondary stresses, respectively. The sectional stresses at 15 locations are evaluated for each angular division of the model. The locations for the stress sections are shown in Figure 3.10.3-2, Section 3.10.3.

As shown in Table 3.5.1-2 through Table 3.5.1-4, the TSC maintains factors of safety greater than one for the combined load conditions. The minimum factor of safety of 1.23 occurs at Section 3 for the  $P_m+P_b$  stresses.

### 3.5.1.6 TSC Fatigue Evaluation

The purpose of this section is to evaluate whether an analysis for cyclic service is required for the TSC. For the TSC, the requirements for cyclic operation are presented in ASME Code, Section III, Subsection NB, Article NB-3222.4 [6]. The criteria for determining whether cyclic loading analysis is required are comprised of six conditions, which, if met, preclude the requirement for further analysis.

1. Atmospheric to Service Pressure Cycle
2. Normal Service Pressure Fluctuation
3. Temperature Difference — Startup and Shutdown
4. Temperature Difference — Normal and Off-Normal Service
5. Temperature Difference — Dissimilar Materials
6. Mechanical Loads

The evaluation of these conditions is as follows.

#### Condition 1 — Atmospheric to Service Pressure Cycle

This condition is not applicable. The ASME Code defines a cycle as an excursion from atmospheric pressure to service pressure and back to atmospheric pressure. Once sealed, the TSC remains closed throughout its operational life, and no atmospheric to service pressure cycles occur.

#### Condition 2 — Normal Service Pressure Fluctuation

This condition is not applicable. The condition establishes a maximum pressure fluctuation as a function of the number of significant pressure fluctuation cycles specified for the component, the design pressure, and the allowable stress intensity of the component material. Operation of the TSC is not cyclic, and no significant cyclic pressure fluctuations are anticipated.

#### Condition 3 — Temperature Difference — Startup and Shutdown

This condition is not applicable. MAGNASTOR is a passive, long-term storage system that does not experience cyclic startups and shutdowns.

#### Condition 4 — Temperature Difference — Normal and Off-Normal Service

The ASME Code specifies that temperature excursions are not significant if the change in  $\Delta T$  between two adjacent points does not experience a cyclic change of more than the quantity:

$$\Delta T = \frac{S_a}{2E\alpha} = 57^\circ\text{F}$$



where:

for Type 304 stainless steel,

$S_a = 28,200$  psi ----- Value obtained from the fatigue curve for  
service cycles  $< 10^6$

$E = 25.1 \times 10^6$  psi ----- Modulus of elasticity at 650 °F

$\alpha = 9.9 \times 10^{-6}$  inch/inch-°F ----- Coefficient of thermal expansion at 650°F

Because of the large thermal mass of the TSC and the concrete cask and the relatively constant heat load produced by the TSC's contents, cyclic changes in  $\Delta T$  greater than 57°F will not occur.

### **Condition 5 — Temperature Difference — Dissimilar Materials**

The TSC and its internal components contain several materials. However, the design of all components considers thermal expansion, thus precluding the development of unanalyzed thermal stress concentrations.

### **Condition 6 — Mechanical Loads**

This condition does not apply. Cyclic mechanical loads are not applied to the concrete cask and TSC during storage conditions. Therefore, no further cyclic loading evaluation is required.

The criteria of ASME Code, Section III, Subsections NB, Articles NB-3222.4 and NG-3222.4 are met; therefore, fatigue analysis is not required.

**Table 3.5.1-1 TSC Thermal Stress, Q**

| Load Case | Service Level | Section <sup>a</sup> | Component Stresses (ksi) <sup>b</sup> |                |                |                 |                 |                 | S <sub>int</sub> |
|-----------|---------------|----------------------|---------------------------------------|----------------|----------------|-----------------|-----------------|-----------------|------------------|
|           |               |                      | S <sub>x</sub>                        | S <sub>y</sub> | S <sub>z</sub> | S <sub>xy</sub> | S <sub>yz</sub> | S <sub>xz</sub> |                  |
| Thermal   | A             | 12                   | -16.87                                | -14.95         | -4.20          | -0.50           | -1.60           | -0.10           | 13.05            |

**Table 3.5.1-2 TSC Normal Conditions, P<sub>m</sub> Stresses**

| Load Case           | Service Level | Section <sup>a</sup> | Component Stresses (ksi) <sup>b</sup> |                |                |                 |                 |                 | S <sub>int</sub> | S <sub>allow</sub> | FS   |
|---------------------|---------------|----------------------|---------------------------------------|----------------|----------------|-----------------|-----------------|-----------------|------------------|--------------------|------|
|                     |               |                      | S <sub>x</sub>                        | S <sub>y</sub> | S <sub>z</sub> | S <sub>xy</sub> | S <sub>yz</sub> | S <sub>xz</sub> |                  |                    |      |
| Pressure            | A             | 3                    | -0.50                                 | -6.93          | 3.91           | 0.13            | 0.02            | 0.85            | 11.01            | N/A                | N/A  |
| Pressure + Handling | A             | 3                    | -0.58                                 | -9.49          | 4.83           | -0.19           | -0.03           | 1.01            | 14.51            | 20.00              | 1.38 |

**Table 3.5.1-3 TSC Normal Conditions, P<sub>m</sub> + P<sub>b</sub> Stresses**

| Load Case           | Service Level | Section <sup>a</sup> | Component Stresses (ksi) <sup>b</sup> |                |                |                 |                 |                 | S <sub>int</sub> | S <sub>allow</sub> | FS   |
|---------------------|---------------|----------------------|---------------------------------------|----------------|----------------|-----------------|-----------------|-----------------|------------------|--------------------|------|
|                     |               |                      | S <sub>x</sub>                        | S <sub>y</sub> | S <sub>z</sub> | S <sub>xy</sub> | S <sub>yz</sub> | S <sub>xz</sub> |                  |                    |      |
| Pressure            | A             | 2                    | 2.37                                  | -11.47         | -16.71         | 0.00            | 0.00            | -0.99           | 19.19            | N/A                | N/A  |
| Pressure + Handling | A             | 3                    | -0.25                                 | -4.94          | 19.45          | -0.08           | -0.04           | 1.27            | 24.48            | 30.00              | 1.23 |

**Table 3.5.1-4 TSC Normal Conditions, P + Q Stresses**

| Load Case                     | Service Level | Section <sup>a</sup> | Component Stresses (ksi) <sup>b</sup> |                |                |                 |                 |                 | S <sub>int</sub> | S <sub>allow</sub> | FS   |
|-------------------------------|---------------|----------------------|---------------------------------------|----------------|----------------|-----------------|-----------------|-----------------|------------------|--------------------|------|
|                               |               |                      | S <sub>x</sub>                        | S <sub>y</sub> | S <sub>z</sub> | S <sub>xy</sub> | S <sub>yz</sub> | S <sub>xz</sub> |                  |                    |      |
| Pressure + Handling + Thermal | A             | 12                   | -41.04                                | -37.90         | -8.45          | -1.25           | -0.15           | -1.51           | 33.17            | 60.00              | 1.81 |

<sup>a</sup> See Figure 3.10.3-2 for section locations.

<sup>b</sup> The x, y, z components of stress are to be interpreted radial, circumferential, and axial directions, respectively.

**3.5.2 Fuel Basket Evaluation for Normal Operating Conditions**

**3.5.2.1 PWR Fuel Basket**

This section evaluates the MAGNASTOR PWR fuel basket for normal operating conditions. Factors of safety for the PWR fuel basket are calculated based on the criteria for Service Level 'A' limits from ASME Code, Section III, Subsection NG [7].

**Normal Handling Evaluation**

The PWR fuel basket is analyzed using classical hand calculations for a 1.1g inertia loading in the basket axial direction to account for the dead load and the handling load. During normal conditions, the PWR fuel assemblies do not apply loads to the basket; they rest on the TSC bottom. Using a bounding basket weight of 22,500 lb, the maximum stress in the fuel tube is calculated. There are 21 fuel tubes in the PWR fuel basket. Conservatively assuming the entire basket weight is carried through the fuel tubes, the stress in the tube ( $\sigma_{\text{tube}}$ ) is as follows.

$$\sigma_{\text{tube}} = \frac{P_{\text{tube}}}{A} = \frac{1178}{11.4} = 0.1 \text{ ksi}$$

where:

$$P_{\text{tube}} = \frac{W \times a}{n} = 1,178 \text{ lb} \text{ ----- Load per tube}$$

$$W = 22,500 \text{ lb} \text{ ----- Bounding basket weight}$$

$$a = 1.1g \text{ ----- Inertia g-load}$$

$$n = 21 \text{ ----- Number of fuel tubes}$$

$$A = 11.4 \text{ inch}^2 \text{ ----- Tube cross-sectional area}$$

The factor of safety (FS) is as follows.

$$FS = \frac{S_m}{\sigma_{\text{tube}}} = \frac{21.4}{0.1} = \text{Large}$$

where:

$$S_m = 21.4 \text{ ksi} \text{ ----- Design stress intensity, SA-537 Class 1, at } 700^\circ\text{F}$$

The weight of the fuel tubes,  $P_t$ , is supported on connector pins. Referring to Figure 3.10.1-13, the interior tubes (Tube #4) are supported by four connector pins; the side fuel tubes (Tube #1) are supported by two connector pins and the side and corner weldments; and the corner fuel tubes

(Tube #3) are supported by three connector pins. The bearing area is the intersection of the connector pin assembly and the fuel tubes. The following sketch shows the cross-sectional area of adjacent fuel tubes that are loaded by the connector pin assembly supporting the basket. The diameter of the connector pin assembly is 0.75 inch. The bearing stress on the fuel tube ( $\sigma_{brg}$ ) is as follows.

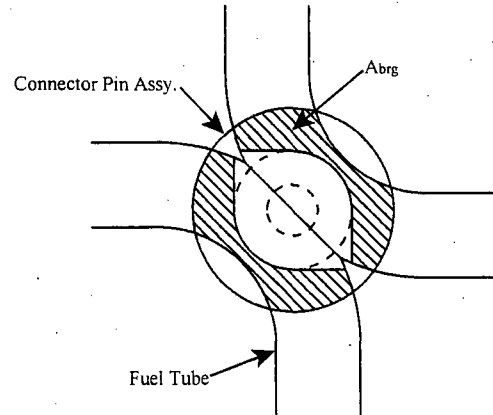
$$\sigma_{brg} = \frac{1.1 \times P_{pin}}{A_{brg}} = \frac{1.1 \times 394}{0.21} = 2.1 \text{ ksi}$$

where:

$$A_{brg} = 0.21 \text{ inch}^2$$

$$P_{pin} = \frac{1}{3}P_t + \frac{1}{4}P_t = 394 \text{ lb}$$

$$P_t = 675 \text{ lb}$$



The factor of safety (FS) for bearing is as follows.

$$FS = \frac{S_y}{\sigma_{brg}} = \frac{32.3}{2.1} = \text{Large}$$

where:

$$S_y = 32.3 \text{ ksi} \text{ ----- Yield strength, SA-537 Class 1, at } 700^\circ\text{F}$$

The bearing stress ( $\sigma_{brg}$ ) in the connector pin at the TSC bottom plate, conservatively using  $P_{tube}$ , as previously determined is as follows.

$$\sigma_{brg} = \frac{P_{tube}}{A_{brg}} = \frac{1178}{0.41} = 2.9 \text{ ksi}$$

where:

$$A_{brg} = \frac{\pi}{4}(D_o^2 - D_i^2) = \frac{\pi}{4}(0.75^2 - 0.19^2) = 0.41 \text{ inch}^2$$

The factor of safety (FS) for bearing is as follows.

$$FS = \frac{S_y}{\sigma_{brg}} = \frac{20.7}{2.9} = 7.1$$

where:

$$S_y = 20.7 \text{ ksi} \text{ ----- Yield strength, SA-240 Type 304, at } 400^\circ\text{F}$$

The buckling evaluation of the connector pin is performed for the governing condition of the 24-inch concrete cask end-drop accident, as shown in Section 3.7.2.1. The accident condition buckling is bounding due to the 60g axial inertia loading.

The weight of the side and corner weldments is carried through to the TSC bottom plate by supports at the bottom of the basket. The bounding dimensions for the supports of the weldments are 5.0 inches in length and 0.3125-inch thickness (corner weldment). The maximum weight of one weldment is 800 lb (bounding side weldment). The weldment supports one-quarter of the weight of two fuel tubes (675 lb per tube, bounding). The bearing stress ( $\sigma_{brg}$ ) is as follows.

$$\sigma_{brg} = \frac{1.1 \times W_{sup}}{A_{sup}} = \frac{1.1 \times 1138}{1.56} = 0.8 \text{ ksi}$$

where:

$$W_{sup} = 800 + 2 \times (0.25 \times 675) = 1138 \text{ lb}$$

$$A_{sup} = 5.0 \times 0.3125 = 1.56 \text{ inch}^2$$

The factor of safety (FS) for bearing is as follows.

$$FS = \frac{S_y}{\sigma_{brg}} = \frac{32.3}{0.8} = \text{Large}$$

where:

$$S_y = 32.3 \text{ ksi} \text{ ----- Yield strength, SA-537 Class 1, } 700^\circ\text{F}$$

The side and corner weldments are attached to the fuel tube array with bolts. The maximum torque on the 5/8-inch bolt is 50.0 inch-lb (40 inch-lb  $\pm$  10 inch-lb). The preload on the bolt (P) is as follows.

$$P = \frac{T}{0.2D} = \frac{50}{0.2 \times 0.625} = 400 \text{ lb} \quad [12]$$

where:

$$T = 50 \text{ inch-lb} \text{ ----- Maximum bolt torque}$$

$$D = 0.625 \text{ inch} \text{ ----- Bolt diameter}$$

A bounding bolt load of 1,500 lb is used for the bolt evaluation. The bolt thread is a 5/8-11 UNC and the length of engagement is 0.50 inch. From Machinery's Handbook [12], the tensile stress ( $\sigma_t$ ) in the bolt is as follows.

$$\sigma_t = \frac{P}{A_t} = \frac{1,500}{0.23} = 6.5 \text{ ksi}$$

where:

$$A_t = 0.7854 \left( D - \frac{0.9743}{n} \right)^2 = 0.23 \text{ inch}^2$$

$$D = 0.625 \text{ inch}$$

$$n = 11$$

The factor of safety (FS), based on ASME Code, Section III, Subsection NB, Article NB-3230, is as follows.

$$FS = \frac{2(S_{mbm})}{\sigma_t} = \frac{2 \times 21.2}{6.5} = 6.5$$

where:

$$S_{mbm} = 21.2 \text{ ksi} \text{ ----- Design stress intensity for SA 193, Gr B6 at } 700^\circ\text{F}$$

The shear stress ( $\tau_{bolt}$ ) in the bolt thread is as follows.

$$\tau_{bolt} = \frac{P}{A_s} = \frac{1,500}{0.499} = 3.0 \text{ ksi}$$

where:

$$A_s = 3.1416nL_c K_{n \max} \left[ \frac{1}{2n} + 0.57735(E_{s \min} - K_{n \max}) \right] = 0.499 \text{ inch}^2$$

The factor of safety (FS) is as follows.

$$FS = \frac{0.6S_m}{\tau_{bolt}} = \frac{0.6 \times 23.3}{3.0} = 4.66$$

where:

$$S_m = 23.3 \text{ ksi} \text{ ----- Design stress intensity, SA-193 Grade B6 at } 700^\circ\text{F}$$

The shear stress in the boss thread ( $\tau_{\text{boss}}$ ) is as follows.

$$\tau_{\text{boss}} = \frac{P}{A_n} = \frac{1,500}{0.713} = 2.1 \text{ ksi}$$

where:

$$A_n = 3.1416nL_e D_{s \text{ min}} \left[ \frac{1}{2n} + 0.57735(D_{s \text{ min}} - E_{n \text{ max}}) \right] = 0.713 \text{ inch}^2$$

The factor of safety (FS) is as follows.

$$\text{FS} = \frac{0.6S_m}{\tau_{\text{bolt}}} = \frac{0.6 \times 19.2}{2.1} = 5.4$$

where:

$$S_m = 19.2 \text{ ksi} \text{ ----- Design stress intensity, SA-695 Type B, Gr } 40, \text{ at } 700^\circ\text{F}$$

The boss is welded into the fuel tube with a 1/4-inch groove weld. The shear stress in the boss weld ( $\tau_{\text{weld}}$ ), is as follows.

$$\tau_{\text{weld}} = \frac{P}{A_w} = \frac{1,500}{0.98} = 1.5 \text{ ksi}$$

where:

$$\begin{aligned} P &= 1,500 \text{ lb} \\ A_w &= \pi D t_{\text{weld}} = \pi \times 1.25 \times 0.25 = 0.98 \text{ inch} \\ D &= 1.25 \text{ inches} \text{ ----- Boss diameter} \end{aligned}$$

Using the lesser allowable,  $S_m$ , of SA537 Class 1 or SA695 Type B, Gr 40, the factor of safety (FS) is as follows.

$$\text{FS} = \frac{w_f \times 0.6S_m}{\tau_{\text{weld}}} = 2.7$$

where:

$$wf = 0.35 \text{ ----- Weld quality factor visual inspection (ASME Code Section III, NG, Article NG-3352)}$$

$$S_m = 19.2 \text{ ksi ----- Design stress intensity, SA-695 Type B, Gr 40, at } 700^\circ\text{F}$$

The washers under the bolts are subjected to a bending load due to the bolt preload. Using Roark's [13], Table 24-1a, the maximum stress in the washer is calculated. The maximum stress ( $\sigma$ ) in the washer is as follows.

$$\sigma = \frac{6M_t}{t^2} = \frac{6 \times 180}{0.3125^2} = 11.1 \text{ ksi}$$

where:

$$a = \frac{1.50}{2} = 0.75 \text{ inch ----- Radius of the cut out in support weldments}$$

$$b = \frac{0.75}{2} = 0.375 \text{ inch ----- Inner radius of the washer}$$

$$r_o = 0.55 \text{ inch ----- Average radius of bolt head}$$

$$t = 5/16 \text{ inch ----- Thickness of washer}$$

$$E = 27.0 \times 10^6 \text{ psi ----- Modulus of elasticity (SA-240 Type 304)}$$

$$\nu = 0.3 \text{ ----- Poisson's ratio}$$

$$w = \frac{P}{\pi \times 2r_o} = \frac{1,500}{\pi \times 2 \times 0.55} = 434 \text{ lb/in}$$

$$G = \frac{E}{2(1+\nu)} = \frac{27.0 \times 10^6}{2(1+0.3)} = 10.38 \times 10^6 \text{ psi}$$

$$D = \frac{Et^3}{12(1-\nu^2)} = \frac{27.0 \times 10^6 (0.3125^3)}{12(1-0.3^2)} = 75,460 \text{ inch-lb}$$

$$M_t = 180 \text{ inch-lb ----- Calculated using formulas in Roark's [13]}$$

The factor of safety (FS) is as follows.

$$FS = \frac{1.5S_m}{\sigma} = \frac{1.5 \times 16.0}{11.1} = 2.16$$

where:

$$S_m = 16.0 \text{ ksi ----- Design stress intensity, SA-240 Type 304, at } 700^\circ\text{F}$$



The evaluation of the neutron absorber for normal handling conditions is bounded by the evaluation for the 24-inch concrete cask end-drop accident (60g) as shown in Section 3.7.2.1. Therefore, no evaluation for normal handling is presented in this section.

**Thermal Stress Evaluation**

The thermal stresses for the PWR fuel basket are calculated using a three-dimensional quarter-symmetry ANSYS finite element model (Section 3.10.1.2). The model represents the top or bottom 47 inches of the basket and calculates the stresses in the basket based upon bounding thermal gradients in basket axial and radial directions. The thermal stresses are combined with the maximum stresses for the normal handling condition. Factors of safety are calculated based on Service Level ‘A’ limits from ASME Code, Section III, Subsection NG [7]. The maximum handling stress in the basket is 0.1 ksi. The following presents the combined normal handling plus thermal stress (P+Q) for the PWR basket.

| Component         | S <sub>therm</sub> , ksi | S <sub>total</sub> , ksi | S <sub>allow</sub> , ksi | FS   |
|-------------------|--------------------------|--------------------------|--------------------------|------|
| Fuel Tube         | 48.1                     | 48.2                     | 62.7                     | 1.30 |
| Support Weldments | 17.4                     | 17.5                     | 62.7                     | 3.58 |

The total stress is the sum of the component thermal stress and the normal handling stress. The allowable stress is 3S<sub>m</sub> (3 × 20.9 = 62.7 ksi for SA537 Class 1 at 755°F). Note that 755°F is conservatively used to envelope all normal, off-normal and transfer conditions.

The axial average temperature at the center of the basket is 521°F. The axial average temperature at the outer radius of the basket is 454°F. The relative thermal expansion of the basket in the axial direction between the center and outer edge of the basket is as follows.

$$\Delta x = \Delta x_{inner} - \Delta x_{outer} = 0.57 - 0.48 = 0.09 \text{ inch}$$

where:

$$\Delta x_{inner} = \Delta T \times L \times \alpha_1 = (521 - 70)(173.5)(7.33 \times 10^{-6}) = 0.57 \text{ inch}$$

$$\Delta x_{outer} = \Delta T \times L \times \alpha_2 = (454 - 70)(173.5)(7.21 \times 10^{-6}) = 0.48 \text{ inch}$$

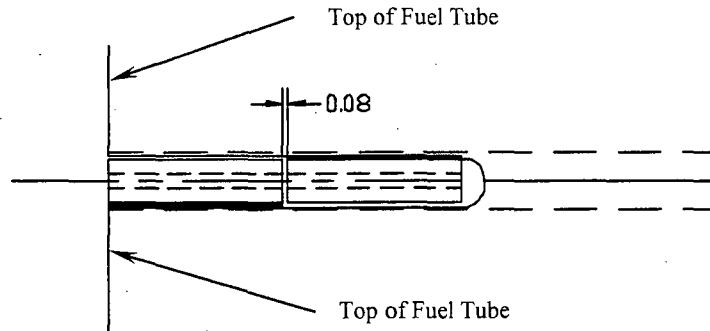
$$L = 173.5 \text{ inches} \text{----- Fuel tube length}$$

$$\alpha_1 = 7.33 \times 10^{-6} \text{ inch/inch/}^\circ\text{F} \text{----- Coefficient of thermal expansion, SA537 CL1, at 521}^\circ\text{F}$$

$$\alpha_2 = 7.21 \times 10^{-6} \text{ inch/inch/}^\circ\text{F} \text{----- Coefficient of thermal expansion, SA537 CL1, at 454}^\circ\text{F}$$

Connector pins at the top and bottom of the basket are used to maintain the geometry of the fuel tube array during manufacturing. A pin is inserted into the connector pin to maintain geometry between adjacent fuel tubes. Adjacent fuel tube connector pins have a 0.08-inch gap between the connector pins; see the following sketch. There are a minimum of two connector pin assemblies

in the radial direction of the PWR basket. Therefore, the relative thermal expansion between the adjacent tubes is approximately 0.05 inch (0.09/2), which is less than the pin gap of 0.08 inch. No axial thermal stresses are produced by the axial expansion of the basket.



The maximum shear load calculated by ANSYS in the basket attachment bosses is 3.5 kip due to the radial thermal expansion of the basket. The shear stress in the boss ( $\tau_{\text{boss}}$ ) is as follows.

$$\tau_{\text{boss}} = \frac{P}{A} = \frac{3.5}{0.92} = 3.8 \text{ ksi}$$

where:

$$A = \frac{\pi}{4}(D_o^2 - D_i^2) = 0.92 \text{ inch}^2$$

$$D_o = 1.25 \text{ inches}$$

$$D_i = 0.63 \text{ inch}$$

The factor of safety (FS) is as follows.

$$FS = \frac{0.6S_m}{\tau_{\text{boss}}} = \frac{0.6 \times 19.2}{3.8} = 3.03$$

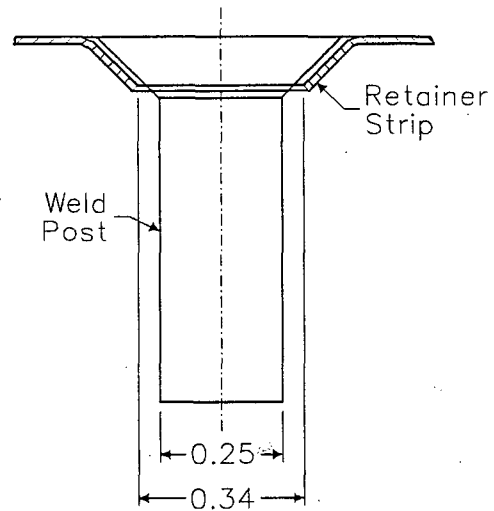
where:

$$S_m = 19.2 \text{ ksi} \text{ ----- Design stress intensity SA-695 Type B, Gr 40 at } 700^\circ\text{F}$$

Based on the analysis results from the thermal stress model, the thermal expansion of the basket does not result in additional tensile load in the attachment bolts. Therefore, no additional bolt analysis for thermal loads is required.

**Neutron Absorber Retainer Thermal Stress Evaluation**

The attachment of the retainer strip and neutron absorber to the fuel tube using weld posts allows each component to move independently during thermal growth. In the case of the stainless steel retainer strip, the expansion of the neutron shield material, which is composed primarily of aluminum, and the carbon steel fuel tube tends to tighten the joint created by the weld post. Thermal stresses may develop between the weld posts because the carbon steel fuel tube expands at a different rate than the retainer strip.



The equation used to calculate the difference in expansion between carbon and stainless steel,  $\Delta$ , is as follows.

$$\Delta = (\alpha_{ss} \times \Delta T \times L) - (\alpha_{cs} \times \Delta T \times L) \quad (1)$$

The standard formula to calculate the deflection of a beam or plate is as follows.

$$\Delta = \frac{PL}{AE} = \frac{\sigma L}{E} \quad (2)$$

Substituting equation (1) into equation (2) and solving the retainer strip thermal stress,  $\sigma$ , is as follows.

$$\sigma = \frac{E\Delta}{L} = E(\alpha_{ss} - \alpha_{cs})(\Delta T) = 38.4 \text{ ksi} \quad (3)$$

where:

- $\alpha_{ss} = 10.0 \times 10^{-6} \text{ inch/inch/}^\circ\text{F}$  ----- Coefficient of thermal expansion, SA-240 Type 304, at 755°F
- $\alpha_{cs} = 7.7 \times 10^{-6} \text{ inch/inch/}^\circ\text{F}$  ----- Coefficient of thermal expansion, SA-537 Class 1, at 755°F
- $\Delta T = 755^\circ\text{F} - 70^\circ\text{F} = 630^\circ\text{F}$  ----- Difference between maximum PWR temperature and ambient conditions
- $T_{\text{max}} = 755^\circ\text{F}$  ----- Bounding basket temperature
- $E = 24.4 \times 10^6 \text{ psi}$  ----- Modulus of elasticity, SA-240 Type 304, at 755°F

The factor of safety (FS) is as follows.

$$FS = \frac{3S_m}{\sigma} = \frac{46.5}{38.4} = 1.21$$

where:

$$S_m = 15.5 \text{ psi} \text{ ----- Design stress intensity, SA-240 Type 304, at } 755^\circ\text{F}$$

**3.5.2.2 BWR Fuel Basket**

This section evaluates the MAGNASTOR BWR basket for normal operating conditions. Factors of safety for the BWR basket are calculated based on the criteria for Service Level ‘A’ limits from ASME Code, Section III, Subsection NG [7].

**Normal Handling Evaluation**

The BWR basket is analyzed using classical hand calculations for a 1.1g inertia loading in the basket axial direction to account for the dead load and the handling load. During normal conditions, the BWR fuel assemblies do not apply loads to the basket; they rest on the TSC bottom. Using a bounding weight of 24,000 lb, the maximum stress in the fuel tube is calculated. There are 45 fuel tubes in the BWR basket. Conservatively assuming the entire basket weight is carried through the fuel tubes, the stress in the tube ( $\sigma_{\text{tube}}$ ) is as follows.

$$\sigma_{\text{tube}} = \frac{P_{\text{tube}}}{A} = \frac{587}{6.1} = 0.1 \text{ ksi}$$

where:

$$P_{\text{tube}} = \frac{W \times a}{n} = 587 \text{ lb} \text{ ----- Load per tube}$$

$W = 24,000 \text{ lb}$  ----- Bounding basket weight  
 $a = 1.1g$  ----- Inertia g-load  
 $n = 45$  ----- Number of fuel tubes  
 $A = 6.1 \text{ inch}^2$  ----- Tube cross-sectional area

The factor of safety (FS) is as follows.

$$FS = \frac{S_m}{\sigma_{\text{tube}}} = \frac{21.4}{0.1} = \text{Large}$$

where:

$$S_m = 21.4 \text{ ksi} \text{ ----- Design stress intensity, SA-537 Class 1, at } 700^\circ\text{F}$$

The weight of the fuel tubes,  $P_t$ , is supported on connector pins. For tube locations presented in Figure 3.10.2-13, the interior tubes (Tube #4) are supported by four connector pins; the side fuel tubes (Tube #1) are supported by two connector pins and the side and corner weldments; and the corner fuel tubes (Tube #5) are supported by three connector pins. The bearing area is the intersection of the connector pin assembly and the fuel tubes. The following sketch shows the cross-sectional area of adjacent figure tubes that is loaded by the connector pin assembly. The diameter of the connector pin assembly is 1.0 inch. The bearing stress on the fuel tube ( $\sigma_{brg}$ ) is as follows.

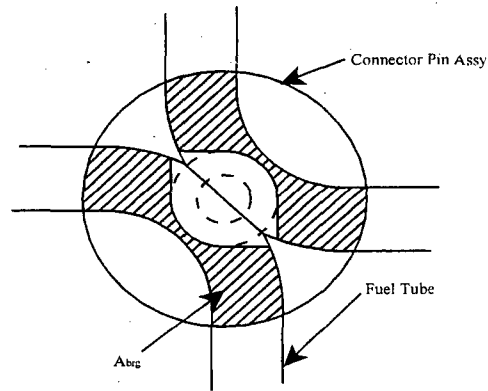
$$\sigma_{brg} = \frac{1.1 \times P_{pin}}{A_{brg}} = \frac{1.1 \times 233}{0.34} = 0.8 \text{ ksi}$$

where:

$$A_{brg} = 0.34 \text{ inch}^2$$

$$P_{pin} = \frac{1}{3}P_t + \frac{1}{4}P_t = 233 \text{ lb}$$

$$P_t = 400 \text{ lb}$$



The factor of safety (FS) for bearing is as follows.

$$FS = \frac{S_y}{\sigma_{brg}} = \frac{32.3}{0.8} = \text{Large}$$

where:

$$S_y = 32.3 \text{ ksi} \text{ ----- Yield strength, SA-537 Class 1, at } 700^\circ\text{F}$$

The bearing stress ( $\sigma_{brg}$ ) in the connector pin at the TSC bottom plate, conservatively using  $P_{tube}$  as previously determined, is as follows.

$$\sigma_{brg} = \frac{P_{tube}}{A_{brg}} = \frac{587}{0.75} = 0.8 \text{ ksi}$$

where:

$$A_{brg} = \frac{\pi}{4}(D_o^2 - D_i^2) = \frac{\pi}{4}(1.0^2 - 0.19^2) = 0.75 \text{ inch}^2$$

The factor of safety (FS) for bearing is as follows.

$$FS = \frac{S_y}{\sigma_{brg}} = \frac{24.7}{0.8} = \text{Large}$$

where:

$$S_y = 24.7 \text{ ksi} \text{ ----- Yield strength, SA-240 Type 304, at } 700^\circ\text{F}$$

The buckling evaluation of the connector pin is performed for the governing condition of the 24-inch concrete cask end-drop accident, as prescribed in Section 3.7.2.2. The accident event buckling evaluation is bounding due to the 60g axial inertia loading.

The weight of the side and corner weldments is carried through to the TSC bottom plate by supports at the bottom of the basket. The corner weldment is bounding for the top and bottom supports. The dimensions for the corner support weldment are 8.0 inches in length and 0.375-inch thickness. The bounding weight of the corner weldment is 1,100 pounds. The corner weldment also supports one-quarter of the weight of four fuel tubes (400 lb per tube, bounding). The bearing stress ( $\sigma_{brg}$ ) is as follows.

$$\sigma_{brg} = \frac{W_{sup}}{A_{sup}} = \frac{1650}{3.0} = 0.6 \text{ ksi}$$

where:

$$W_{sup} = 1.1 \times (1,100 + 4 \times (0.25 \times 400)) = 1650 \text{ lb}$$
$$A_{sup} = 8.0 \times 0.375 = 3.0 \text{ inch}^2$$

The factor of safety (FS) for bearing is as follows.

$$FS = \frac{S_y}{\sigma_{brg}} = \frac{32.3}{0.6} = \text{Large}$$

where:

$$S_y = 32.3 \text{ ksi} \text{ ----- Yield strength, SA-537 Class 1, } 700^\circ\text{F}$$

The side and corner weldments are attached to the fuel tube array with bolts. The maximum torque on the 5/8-inch bolt is 50 inch-lb (40 ±10 inch-lb). The preload on the bolt (P) is as follows.

$$P = \frac{T}{0.2D} = \frac{50}{0.2 \times 0.625} = 400 \text{ lb} \quad [12]$$

where:

$$T = 50 \text{ inch-lb} \text{----- Maximum bolt torque}$$

$$D = 0.625 \text{ inch} \text{----- Bolt diameter}$$

The bolt thread is a 5/8-11 UNC and the minimum length of engagement is 0.38 inch. A bolt load of 1,000 lb is conservatively used for the evaluation. From Machinery's Handbook [12], the tensile strength ( $\sigma_t$ ) in the bolt is as follows.

$$\sigma_t = \frac{P}{A_t} = \frac{1,000}{0.23} = 4.3 \text{ ksi}$$

where:

$$A_t = 0.7854 \left( D - \frac{0.9743}{n} \right)^2 = 0.23 \text{ inch}^2$$

$$D = 0.625 \text{ inch}$$

$$n = 11$$

The factor of safety (FS) is as follows.

$$FS = \frac{2(S_{mBM})}{\sigma_t} = \frac{2 \times 21.2}{4.3} = 9.8$$

where:

$$S_{mBM} = 21.2 \text{ ksi} \text{----- Design stress intensity for SA-193, Gr B6, at } 700^\circ\text{F}$$

The shear stress in the bolt thread ( $\tau_{bolt}$ ) is as follows.

$$\tau_{bolt} = \frac{P}{A_s} = \frac{1,000}{0.379} = 2.6 \text{ ksi}$$

where:

$$A_s = 3.1416nL_eK_{n,max} \left[ \frac{1}{2n} + 0.57735(E_{s,min} - K_{n,max}) \right] = 0.379 \text{ inch}^2$$

$$n = 11$$

The factor of safety (FS) is as follows.

$$FS = \frac{0.6S_m}{\tau_{bolt}} = \frac{0.6 \times 23.3}{2.6} = 5.37$$

where:

$$S_m = 23.3 \text{ ksi} \text{ ----- Design stress intensity, SA-193 Grade B6, at } 700^\circ\text{F}$$

The shear stress in the boss thread ( $\tau_{\text{boss}}$ ) is as follows.

$$\tau_{\text{boss}} = \frac{P}{A_n} = \frac{1,000}{0.542} = 1.8 \text{ ksi}$$

where:

$$A_n = 3.1416nL_eD_{s \text{ min}} \left[ \frac{1}{2n} + 0.57735(D_{s \text{ min}} - E_{n \text{ max}}) \right] = 0.542 \text{ inch}^2$$

$$L_e = 0.38 \text{ inch}$$

$$E_{n \text{ max}} = 0.5732$$

$$D_{s \text{ min}} = 0.6113$$

$$n = 11$$

The factor of safety (FS) is as follows.

$$FS = \frac{0.6S_m}{\tau_{\text{bolt}}} = \frac{0.6 \times 19.2}{1.8} = 6.4$$

where:

$$S_m = 19.2 \text{ ksi} \text{ ----- Design stress intensity, SA-695, Type B, Gr 40, at } 700^\circ\text{F}$$

The boss is welded into the fuel tube with a 3/16-inch groove weld. The shear stress in the boss weld ( $\tau_{\text{weld}}$ ) is as follows.

$$\tau_{\text{weld}} = \frac{P}{A_w} = \frac{1,000}{0.59} = 1.7 \text{ ksi}$$

where:

$$P = 1000 \text{ lb}$$

$$A_w = \pi D t_{\text{weld}} = \pi \times 1.00 \times 0.1875 = 0.59 \text{ inch}$$

$$D = 1.00 \text{ inch} \text{ ----- Smallest boss diameter}$$

Using the lesser allowable,  $S_m$ , of SA-537 Class 1 or SA-695 Type B, Gr 40, the factor of safety (FS) is as follows.



$$FS = \frac{0.35 \times 0.6 S_m}{\tau_{\text{weld}}} = 2.37$$

where:

$$S_m = 19.2 \text{ ksi} \text{ ----- Design stress intensity, SA-695 Type B Grade 40, at } 700^\circ\text{F}$$

The washers under the bolts are subjected to a bending load due to the torque of the bolts. The inner and outer radius of the washer is 0.75 inch and 1.50 inches, respectively. The washer is evaluated using the maximum bolt load (1,000 lb) and minimum washer thickness (3/16 inch). The maximum bending moment in the washer is calculated to be 34.2 inch-lb. The maximum stress ( $\sigma$ ) in the washer is as follows.

$$\sigma = \frac{6M_t}{t^2} = \frac{6 \times 0.034}{0.1875^2} = 5.8 \text{ ksi}$$

where:

$$t = 3/16 \text{ inch} \text{ ----- Thickness of washer}$$

$$M_t = 0.034 \text{ inch-kip}$$

The factor of safety (FS) is as follows.

$$FS = \frac{1.5 S_m}{\sigma} = \frac{1.5 \times 16.0}{5.8} = 4.14$$

where:

$$S_m = 16.0 \text{ ksi} \text{ ----- Design stress intensity, SA-240 Type 304, at } 700^\circ\text{F}$$

The evaluation of the neutron absorber for normal handling conditions is bounded by the evaluation for the 24-inch concrete cask end-drop accident (60g) as shown in Section 3.7.2.2. Therefore, no evaluation for normal handling is presented in this section.

### **Thermal Stress Evaluation**

The thermal stresses for the BWR fuel basket are calculated using a three-dimensional quarter-symmetry ANSYS finite element model (Section 3.10.2.2). The model represents the top or bottom 43 inches of the basket and calculates the stresses in the basket based upon bounding thermal gradients in basket axial and radial directions. The thermal stresses are combined with

the maximum stresses for the normal handling condition. Factors of safety are calculated based on Service Level 'A' limits from ASME Code, Section III, Subsection NG [7]. The maximum handling stress in the basket is 0.1 ksi. The following presents the combined normal handling plus thermal stress (P+Q) for the BWR fuel basket.

| Component         | S <sub>therm</sub> , ksi | S <sub>total</sub> , ksi | S <sub>allow</sub> , ksi | FS   |
|-------------------|--------------------------|--------------------------|--------------------------|------|
| Fuel Tube         | 28.5                     | 28.6                     | 63.6                     | 2.22 |
| Support Weldments | 8.5                      | 8.6                      | 63.6                     | 7.40 |

The total stress is the sum of the component thermal stress and the normal condition stress. The allowable stress is 3Sm (3 × 21.2 = 63.6 ksi for SA-537 Class 1 steel at 720°F). Note that 720°F is conservatively used to bound all normal, off-normal and transfer conditions.

The average temperature at the center of the basket is 509°F. The average temperature at the outer radius of the basket is 437°F. The relative thermal expansion of the basket in the axial direction between the center and outer edge of the basket is as follows.

$$\Delta x = \Delta x_{inner} - \Delta x_{outer} = 0.53 - 0.44 = 0.09 \text{ inch}$$

where:

$$\Delta x_{inner} = \Delta T \times L \times \alpha_1 = (509 - 70)(166.5)(7.31 \times 10^{-6}) = 0.53 \text{ inch}$$

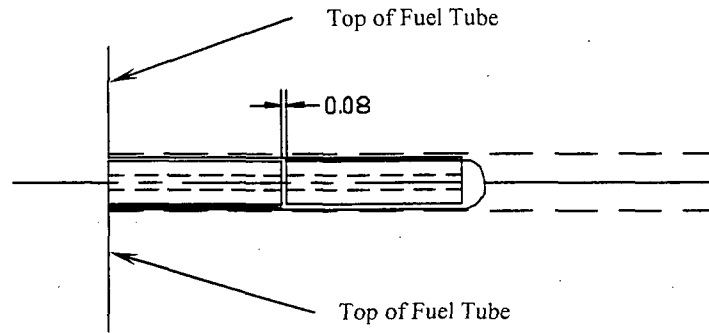
$$\Delta x_{outer} = \Delta T \times L \times \alpha_2 = (437 - 70)(166.5)(7.17 \times 10^{-6}) = 0.44 \text{ inch}$$

$$L = 166.5 \text{ inch} \text{ ----- Fuel tube length}$$

$$\alpha_1 = 7.31 \times 10^{-6} \text{ inch/inch/}^\circ\text{F} \text{ ----- Coefficient of thermal expansion, SA537 CL1, at } 509^\circ\text{F}$$

$$\alpha_2 = 7.17 \times 10^{-6} \text{ inch/inch/}^\circ\text{F} \text{ ----- Coefficient of thermal expansion, SA537 CL1, at } 437^\circ\text{F}$$

Connector pins at the top and bottom of the basket are used to maintain the geometry of the fuel tube array. A pin is inserted into the connector pin to maintain geometry between adjacent fuel tubes. Adjacent fuel tube connector pins have a 0.08-inch gap between the connector pins; see the following sketch. There are a minimum of three connector pin assemblies in the radial direction of the BWR basket. Therefore, the relative thermal expansion between the adjacent tubes is approximately 0.03 inch (0.09/3), which is less than the pin gap of 0.08 inch. No axial thermal stresses are produced by the axial expansion of the basket.



The maximum shear load calculated by ANSYS in the basket attachment bosses is 4.2 kip due to the radial thermal expansion of the basket. The shear stress in the boss ( $\tau_{boss}$ ) is as follows.

$$\tau_{boss} = \frac{P}{A} = \frac{4.2}{0.47} = 8.9 \text{ ksi}$$

where:

$$A = \frac{\pi}{4}(D_o^2 - D_i^2) = 0.47 \text{ inch}^2$$

$$D_o = 1.00 \text{ inch}$$

$$D_i = 0.63 \text{ inch}$$

The factor of safety (FS) is as follows.

$$FS = \frac{0.6S_m}{\tau_{boss}} = \frac{0.6 \times 19.2}{8.9} = 1.29$$

where:

$$S_m = 19.2 \text{ ksi} \text{ ----- Design stress intensity, SA-695 Type B, Gr 40, at } 700^\circ\text{F}$$

The thermal expansion of the basket does not add significant additional tensile loads to the bolts; therefore, no additional bold analysis for thermal loads is required.

### Neutron Absorber Retainer Thermal Stress Evaluation

The stainless steel retainer strips are fastened to the carbon steel fuel tube using fixed weld posts spaced along the length of the tube. Because of the dissimilar material properties, differential thermal expansion of the components results in thermal stresses in some of the components. Since the stress due to differential thermal expansion is not a function of length, the evaluation

provided in Section 3.5.2.1 for retainer for the PWR is applicable to that for the BWR. No further analysis is required.

**3.5.3 Concrete Cask Evaluations for Normal Operating Conditions**

The structural evaluation of the concrete cask for normal conditions considers the combination of thermal stresses, dead and live loads, and wind loads (see Chapter 2 for load combinations). The analysis results are presented in Section 3.5.3.3. The conservative stress due to wind loads is obtained from Section 3.7.3.2.

**3.5.3.1 Concrete Cask Thermal Stresses**

Using the finite element model presented in Section 3.10.4, a structural evaluation of the concrete cask for normal conditions thermal loads was performed. The analysis conservatively considered a bounding temperature profile corresponding to the off-normal thermal event (106°F ambient).

The following summarizes the critical thermal stresses for normal conditions.

| Component             | Stress (ksi) |
|-----------------------|--------------|
| Circumferential Rebar | 15.6         |
| Vertical Rebar        | 19.1         |
| Concrete, Compression | 1.0          |
| Concrete, Tension     | 0.1          |

**3.5.3.2 Dead and Live Loads**

**Dead Loads**

The concrete cask dead load consists primarily of the weight of the concrete. Assuming all dead loads are reacted by the lower concrete surface only, stress levels can be determined. Under these conditions, the only stress component is the vertical axial compression stress. The maximum stress ( $\sigma_{cask}$ ) at the base of the concrete cask in the concrete is as follows.

$$\sigma_{cask} = \frac{W_{cask}}{A} = \frac{210,000}{9,119} = 23.0 \text{ psi}$$

where:

$W_{cask} = 210,000 \text{ lb}$  ----- Bounding weight for empty concrete cask  
 $D_o = 136.0 \text{ inch}$

$$D_i = 82.98 \text{ inch}$$

$$A = \pi (D_o^2 - D_i^2) / 4 = 9,119 \text{ inch}^2$$

The concrete bearing strength ( $f_b$ ) is much larger than the applied load.

$$f_b = \phi(0.85f'_cA) = 0.85(0.85 \times 3800 \times 9119) = 25.0 \times 10^6 \text{ lb} > 210,000 \text{ lb}$$

where:

$$f'_c = 3,800 \text{ psi} \text{ ----- Compressive strength, concrete, at } 300^\circ\text{F}$$

**Live Loads**

The live load calculation considers the loaded transfer cask positioned on top of the concrete cask for transfer of the TSC for development of the peak live load bounding condition. Assuming live loads are reacted by concrete sections (no credit taken for steel liner), stress levels are conservatively determined. Under these conditions, the only stress component is the vertical axial compression stress ( $\sigma_{\text{concrete cask}}$ ).

$$\sigma_{\text{concrete cask}} = \frac{W_{\text{TFR}}}{A} = \frac{230,000}{9,119} = 25.2 \text{ psi}$$

where:

$$W_{\text{TFR}} = 230,000 \text{ lb} \text{ ----- Loaded transfer cask}$$

$$D_o = 136.0 \text{ inch}$$

$$D_i = 82.98 \text{ inch}$$

$$A = \pi (D_o^2 - D_i^2) / 4 = 9,119 \text{ inch}^2$$

**3.5.3.3 Concrete Cask Combined Stresses**

The load combinations described in Chapter 2 are used to evaluate the concrete cask for normal conditions of storage (Load Conditions 1, 2, and 3). Concrete cask stresses are summarized in Table 3.5.3-1, Table 3.5.3-2, and Table 3.5.3-3 for the various loading conditions on the concrete cask.

The allowable compressive stress for concrete ( $S_{\text{con}}$ ) is as follows.

$$S_{\text{con}} = \phi f'_c = 2,660 \text{ psi}$$

where:

$$\phi = 0.7 \text{ ----- Strength reduction factor [5]}$$

$$f'_c = 3,800 \text{ psi} \text{ ----- Compressive strength of concrete at } 300^\circ\text{F}$$

The concrete ultimate strength allowable is 8% to 15% of the compressive stress [14]; therefore, the allowable ultimate strength ( $S_{tc}$ ) is as follows.

$$S_{tc} = 0.08 \times S_{con} = 0.08 \times 2660 = 213 \text{ psi or } 0.21 \text{ ksi}$$

The maximum concrete compressive stress is 1,332 psi (see Table 3.5.3-2); therefore, the minimum factor of safety (FS) for normal conditions is as follows.

$$FS = \frac{2,660}{1,332} = 2.00$$

From Section 3.5.3.1, the maximum concrete ultimate strength due to thermal load is 0.1 ksi. Multiplying the stress by a 1.275 factor for normal conditions thermal stresses (see Chapter 2), the factor of safety (FS) for concrete ultimate strengths is as follows.

$$FS = \frac{S_{tc}}{S_t \times 1.275} = \frac{0.21}{0.1 \times 1.275} = 1.62$$

The allowable stress for rebar ( $S_{rebar}$ ) is as follows.

$$S_{rebar} = \phi F_r = 54.0 \text{ ksi}$$

where:

$$\phi = 0.9 \text{----- Strength reduction factor [5]}$$

$$F_r = 60.0 \text{ ksi ----- Yield strength, rebar}$$

From Section 3.5.3.1, the maximum rebar stress due to thermal load is 19.1 ksi. The stresses due to other loadings are negligible for normal conditions. Compressive loads are carried by the concrete. Multiplying the stress by a 1.275 factor for normal conditions thermal stresses (see Chapter 2), the factor of safety (FS) for the rebar is as follows.

$$FS = \frac{S_{rebar}}{S_t \times 1.275} = \frac{54.0}{19.1 \times 1.275} = 2.21$$

**Table 3.5.3-1 Concrete Cask Vertical Stress Summary – Outer Surface, psi**

| Condition | Dead | Live | Wind | Thermal | Seismic | Flood | Tornado | Total |
|-----------|------|------|------|---------|---------|-------|---------|-------|
| 1         | -32  | -43  | 0    | 0       | 0       | 0     | 0       | -75   |
| 2         | -24  | -32  | 0    | 0       | 0       | 0     | 0       | -56   |
| 3         | -24  | -32  | -24  | 0       | 0       | 0     | 0       | -80   |

**Table 3.5.3-2 Concrete Cask Vertical Stress Summary – Inner Surface, psi**

| Condition | Dead | Live | Wind | Thermal | Seismic | Flood | Tornado | Total |
|-----------|------|------|------|---------|---------|-------|---------|-------|
| 1         | -32  | -43  | 0    | 0       | 0       | 0     | 0       | -75   |
| 2         | -24  | -32  | 0    | -1261   | 0       | 0     | 0       | -1317 |
| 3         | -24  | -32  | -15  | -1261   | 0       | 0     | 0       | -1332 |

**Table 3.5.3-3 Concrete Cask Circumferential Stress Summary – Inner Surface, psi**

| Condition | Dead | Live | Wind | Thermal | Seismic | Flood | Tornado | Total |
|-----------|------|------|------|---------|---------|-------|---------|-------|
| 1         | 0    | 0    | 0    | 0       | 0       | 0     | 0       | 0     |
| 2         | 0    | 0    | 0    | -566    | 0       | 0     | 0       | -566  |
| 3         | 0    | 0    | 0    | -566    | 0       | 0     | 0       | -566  |

### **3.6 Off-Normal Operating Events**

This section presents the analyses of the major structural components of MAGNASTOR for off-normal events of storage. MAGNASTOR is evaluated using finite element models and classical hand calculations for the fuel baskets and TSC. Off-normal environmental events are defined as -40°F with no solar load, 106°F with solar load, and half-blockage of the concrete cask air inlets.

#### **3.6.1 TSC Evaluations for Off-Normal Operating Events**

##### **3.6.1.1 Thermal Stresses for Off-Normal Events**

The thermal stresses of the TSC are calculated using the ANSYS finite element model described in Section 3.10.3. As discussed in Section 3.5.1.1, the temperature gradient applied to the TSC bounds the temperature gradient for all conditions of storage. Therefore, the maximum thermal stresses for the off-normal severe ambient temperature event are bounded by those presented in Table 3.5.1-1.

##### **3.6.1.2 Off-Normal TSC Load Analyses**

Based on the load combinations specified in Table 2.3-2, the following two off-normal load events are evaluated.

- Off-normal internal pressure + normal handling + thermal (ASME Code, Level B)
- Normal internal pressure + off-normal handling (ASME Code, Level C)

For detailed analyses results for off-normal conditions, see Table 3.10.3-7 through Table 3.10.3-11.

##### **Off-Normal Internal Pressure with Normal Handling**

The TSC is analyzed for off-normal pressurization and normal handling loads using the finite element model described in Section 3.10.3. Applying a 1.1g acceleration load in the axial direction to a loaded TSC simulates normal handling. To represent the off-normal pressure, an internal pressure of 130 psig is applied to all internal surfaces. A bounding temperature profile is considered for the thermal stress calculation, as discussed in Section 3.10.3.

The resulting maximum stresses in the TSC for Service Level 'B' off-normal loads are summarized in Table 3.6.1-1 for primary membrane, Table 3.6.1-2 for primary membrane plus primary bending, and Table 3.6.1-3 for primary plus secondary stress categories. The minimum

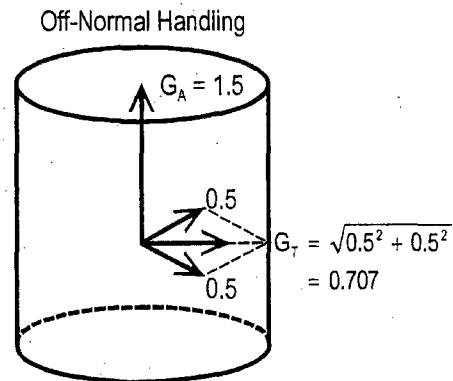


factor of safety of 1.18 ( $P_m + P_b$ ) occurs at Section 3. The locations for the stress sections are shown in Section 3.10.3.

### Off-Normal Handling with Normal Internal Pressure

An evaluation is performed for the off-normal handling loads on the TSC during the installation of the TSC in the concrete cask, removal of the TSC from the concrete cask, and removal from the transfer cask. The TSC is handled vertically in both the concrete and transfer casks.

The TSC is analyzed for handling loads using the finite element model described in Section 3.10.3. The off-normal TSC handling loads are defined as 0.5g applied in all directions (i.e., in the global x, y, and z directions) in addition to a 1g lifting load applied in the finite element model. The resulting off-normal handling accelerations are 0.707g in the lateral direction and 1.5g (0.5g + 1.0g) in the vertical direction. To represent the normal pressure, an internal pressure of 110 psig is applied to all internal surfaces.



The resulting maximum stresses in the TSC for Service Level 'C' off-normal loads are summarized in Table 3.6.1-1 for primary membrane, Table 3.6.1-2 for primary membrane plus primary bending, and Table 3.6.1-3 for primary plus secondary stress categories. The minimum factor of safety of 1.27 ( $P_m + P_b$ ) occurs at Section 3. The locations for the stress sections are shown in Section 3.10.3.

Table 3.6.1-1 TSC Off-Normal Events,  $P_m$  Stresses

| Load Case                             | Service Level | Section <sup>a</sup> | Component Stresses (ksi) <sup>b</sup> |        |       |          |          |          | $S_{int}$ | $S_{allow}$ | FS   |
|---------------------------------------|---------------|----------------------|---------------------------------------|--------|-------|----------|----------|----------|-----------|-------------|------|
|                                       |               |                      | $S_x$                                 | $S_y$  | $S_z$ | $S_{xy}$ | $S_{yz}$ | $S_{xz}$ |           |             |      |
| Off-Normal Pressure + Normal Handling | B             | 3                    | -0.67                                 | -10.75 | 5.54  | -0.21    | -0.03    | 1.16     | 16.51     | 22.00       | 1.33 |
| Normal Pressure + Off-Normal Handling | C             | 3                    | -0.62                                 | -10.75 | 5.15  | -0.25    | -0.02    | 1.07     | 16.10     | 24.50       | 1.52 |

Table 3.6.1-2 TSC Off-Normal Events,  $P_m + P_b$  Stresses

| Load Case                             | Service Level | Section <sup>a</sup> | Component Stresses (ksi) <sup>b</sup> |       |       |          |          |          | $S_{int}$ | $S_{allow}$ | FS   |
|---------------------------------------|---------------|----------------------|---------------------------------------|-------|-------|----------|----------|----------|-----------|-------------|------|
|                                       |               |                      | $S_x$                                 | $S_y$ | $S_z$ | $S_{xy}$ | $S_{yz}$ | $S_{xz}$ |           |             |      |
| Off-Normal Pressure + Handling        | B             | 3                    | -0.28                                 | -5.53 | 22.31 | 0.00     | 0.00     | 1.47     | 27.94     | 33.00       | 1.18 |
| Normal Pressure + Off-Normal Handling | C             | 3                    | -0.23                                 | -6.17 | 21.24 | -0.14    | 0.05     | 1.35     | 27.49     | 34.80       | 1.27 |

Table 3.6.1-3 TSC Off-Normal Events,  $P + Q$  Stresses

| Load Case                                       | Service Level | Section <sup>a</sup> | Component Stresses (ksi) <sup>b</sup> |        |       |          |          |          | $S_{int}$ | $S_{allow}$ | FS   |
|---|---------------|----------------------|---------------------------------------|--------|-------|----------|----------|----------|-----------|-------------|------|
|   |               |                      | $S_x$                                 | $S_y$  | $S_z$ | $S_{xy}$ | $S_{yz}$ | $S_{xz}$ |           |             |      |
| Off-Normal Pressure + Normal Handling + Thermal | B             | 12                   | -44.54                                | -41.22 | -9.07 | -1.36    | 0.06     | -1.71    | 36.12     | 60.00       | 1.66 |

<sup>a</sup> See Figure 3.10.3-2 for section cut locations.

<sup>b</sup> The x, y, z components of stress are to be interpreted radial, circumferential and axial directions, respectively.

**3.6.2 Fuel Basket Evaluation for Off-Normal Operating Events**

**3.6.2.1 PWR Fuel Basket**

This section evaluates the MAGNASTOR PWR basket for off-normal events using both classical hand calculations and finite element analysis methods. Factors of safety for the PWR basket are calculated based on the criteria for Service Level 'C' limits from ASME Code, Section III, Subsection NG [7].

The inertia loading for off-normal handling events is a 1.5g vertical acceleration and a 0.707g (0.5g in each transverse direction) transverse acceleration. The basket stresses due to the transverse loading are calculated using the three-dimensional periodic finite element models described in Section 3.10.1. Both half-symmetry models for the 0° and 45° basket orientations are used. Using a bounding weight of 22,500 pounds for the PWR basket, the maximum stress in the fuel tube in the axial direction is calculated. Conservatively assuming the entire basket weight is carried through the fuel tubes, the stress in the tube due to the axial acceleration is as follows.

$$\sigma_{\text{tube}} = \frac{P_{\text{tube}}}{A} = \frac{1607}{11.4} = 0.14 \text{ ksi}$$

where:

$$P_{\text{tube}} = \frac{W \times a}{n} = \frac{22500 \times 1.5}{21} = 1,607 \text{ lb}$$

W = 22,500 lb ----- Bounding basket weight

n = 21 ----- Number of fuel tubes

a = 1.5g ----- Inertia g-load

A = 11.4 inch<sup>2</sup> ----- Tube cross-sectional area

The maximum primary membrane and primary membrane plus bending due to transverse loading ( $S_{\text{tran}}$ ) from the finite element analysis results are shown in the following table. See Figure 3.10.1-13 through Figure 3.10.1-20 for locations of critical sections where the stresses are reported. The combined maximum stress intensity ( $S_{\text{tot}}$ ) is conservatively obtained by adding the maximum stresses due to axial load ( $\sigma_{\text{tube}}$ ) to the maximum stresses due to transverse load ( $S_{\text{tran}}$ ). The combined stresses and factors of safety are presented in the following table. The allowable stresses for the off-normal events (Level C) are  $1.5S_m$  for membrane stresses and  $2.25S_m$  for membrane plus bending stresses. A bounding temperature of 755°F is conservatively used.

| Component                      | $S_{tran}$ , ksi | $S_{tot}$ , ksi | $S_{allow}$ , ksi | FS    |
|--------------------------------|------------------|-----------------|-------------------|-------|
| Fuel Tube, $P_m$               | 5.8              | 5.9             | 31.4              | 5.32  |
| Fuel Tube, $P_m + P_b$         | 18.9             | 19.0            | 47.0              | 2.47  |
| Support Weldments, $P_m$       | 0.4              | 0.5             | 31.4              | Large |
| Support Weldments, $P_m + P_b$ | 5.6              | 5.7             | 47.0              | 8.25  |

The weight of the fuel tubes is supported on connector pins. Referring to Figure 3.10.1-13, the interior tubes (Tube #4, typical) are supported by four connector pins; the side fuel tubes (Tube #1, typical) are supported by two connector pins and the side and corner weldments; and the corner fuel tubes (Tube #3, typical) are supported by three connector pins. The bearing stress on the fuel tube ( $\sigma_{brg}$ ) is as follows.

$$\sigma_{brg} = \frac{1.5 \times P_{pin}}{A_{brg}} = \frac{1.5 \times 394}{0.21} = 2.8 \text{ ksi}$$

where:

$$A_{brg} = 0.21 \text{ inch}^2 \text{ ----- Bearing area}$$

$$P_{pin} = \frac{1}{3}P_t + \frac{1}{4}P_t = 394 \text{ lb} \text{ ----- Combined loading on one support pin}$$

$$P_t = 675 \text{ lb} \text{ ----- Tube weight}$$

The factor of safety (FS) for bearing is as follows.

$$FS = \frac{S_y}{\sigma_{brg}} = \frac{32.3}{2.8} = \text{Large}$$

where:

$$S_y = 32.3 \text{ ksi} \text{ ----- Yield strength, SA-537 Class 1, at } 700^\circ\text{F}$$

The bearing stress ( $\sigma_{brg}$ ) in the connector pin at the TSC bottom plate, conservatively using  $P_{tube}$  as previously determined, is as follows.

$$\sigma_{brg} = \frac{P_{tube}}{A_{brg}} = \frac{1607}{0.41} = 3.9 \text{ ksi}$$

where:

$$A_{brg} = \frac{\pi}{4}(D_o^2 - D_i^2) = \frac{\pi}{4}(0.75^2 - 0.19^2) = 0.41 \text{ inch}^2$$

$$D_o = 0.75 \text{ inch}$$

$$D_i = 0.19 \text{ inch}$$

The factor of safety (FS) for bearing is as follows.

$$FS = \frac{S_y}{\sigma_{brg}} = \frac{24.7}{3.9} = 6.3$$

where:

$$S_y = 24.7 \text{ ksi} \text{ ----- Yield strength, SA-240 Type 304, at } 700^\circ\text{F}$$

The weight of the side and corner weldments is carried through to the TSC bottom plate by supports at the bottom of the basket. The bounding dimensions for the supports of the weldments are 5.0 inches in length and 0.3125-inch thickness (corner weldment). The maximum weight of one weldment is 800 lb (bounding, side weldment). The weldment supports one-quarter of the weight of two fuel tubes (675 lb per tube, bounding). The bearing stress is as follows.

$$\sigma_{brg} = \frac{1.5 \times W_{sup}}{A_{sup}} = 1.1 \text{ ksi}$$

where:

$$W_{sup} = 800 + 2 \times (0.25 \times 675) = 1138 \text{ lb}$$

$$A_{sup} = 5.0 \times 0.3125 = 1.56 \text{ inch}^2$$

The factor of safety (FS) for bearing is as follows.

$$FS = \frac{S_y}{\sigma_{brg}} = \frac{32.3}{1.1} = \text{Large}$$

where:

$$S_y = 32.3 \text{ ksi} \text{ ----- Yield strength, SA-537 Class 1, at } 700^\circ\text{F}$$

The buckling evaluation of the connector pin is performed in Section 3.7.2.1. The accident condition buckling evaluation is bounding due to the conservative 60g axial inertia loading.

The maximum tensile load in the attachment bolts for the off-normal condition is 770 pounds. The bolts have been evaluated for the bounding load of 1,500 lb for the normal condition in Section 3.5.2.1. The maximum shear load on a boss for the off-normal condition is 842 pounds. The bosses were evaluated with a bounding shear load of 3,500 lb for the normal condition. Therefore, no further analysis is required for the bolts and bosses for off-normal conditions.

The analysis presented in Section 3.7.2.1 bounds the off-normal analysis of the neutron absorber and retainer strip; therefore, no additional analysis is required.

### 3.6.2.2 BWR Fuel Basket

The analysis of the BWR basket for off-normal events uses both classical hand calculations and finite element analysis methods. The ANSYS finite element model and boundary conditions are presented in Section 3.10.2 for the 0° and 45° basket orientations. Factors of safety for the BWR basket are calculated based on the criteria for Service Level 'C' limits from ASME Code, Section III, Subsection NG [7]. The inertia loading for off-normal events is a 1.5g vertical acceleration and a 0.707g (0.5g in each transverse direction) transverse acceleration

For off-normal events of storage, a 1.5g acceleration (a) is applied to the basket in the axial direction. Using a bounding weight of 24,000 lb for the BWR basket, the maximum stress in the fuel tube in the axial direction is calculated. Conservatively assuming the entire basket weight is carried through the fuel tubes, the stress in the tube due to the axial acceleration is as follows.

$$\sigma_{\text{tube}} = \frac{P_{\text{tube}}}{A} = \frac{800}{6.1} = 0.13 \text{ ksi}$$

where:

$$P_{\text{tube}} = \frac{W \times a}{n} = \frac{24,000 \times 1.5}{45} = 800 \text{ lb}$$

W = 24,000 lb ----- Bounding basket weight

N = 45 ----- Number of fuel tubes

a = 1.5g ----- Inertia g-load

A = 6.1 inch<sup>2</sup> ----- Tube cross-sectional area

The maximum primary membrane and primary membrane plus bending stresses due to transverse loading ( $S_{\text{tran}}$ ) from the finite element analysis results are as follows. See Figure 3.10.2-14 through Figure 3.10.2-20 for locations of critical sections where stresses are reported. The combined maximum stress intensity ( $S_{\text{tot}}$ ) is conservatively obtained by adding the maximum stresses due to axial load ( $\sigma_{\text{tube}}$ ) to the maximum stresses due to transverse load ( $S_{\text{tran}}$ ). The combined stresses and factors of safety are presented in the following table. The allowable stresses for the off-normal events (Level C) are  $1.5S_m$  for membrane stresses and  $2.25S_m$  for membrane plus bending stresses.

| Component  | S <sub>tran</sub> , ksi | S <sub>tot</sub> , ksi | S <sub>allow</sub> , ksi | FS    |
|--|-------------------------|------------------------|--------------------------|-------|
| Fuel Tube, P <sub>m</sub>                          | 11.8                    | 11.9                   | 32.10                    | 2.70  |
| Fuel Tube, P <sub>m</sub> + P <sub>b</sub>         | 32.9                    | 33.0                   | 48.15                    | 1.46  |
| Support Weldments, P <sub>m</sub>                  | 0.5                     | 0.6                    | 32.10                    | Large |
| Support Weldments, P <sub>m</sub> + P <sub>b</sub> | 5.3                     | 5.4                    | 48.15                    | 8.92  |

The weight of the fuel tubes is supported on connector pins. Referring to Figure 3.10.2-13, the interior tubes (Tube #4, typical) are supported by four connector pins; the side fuel tubes (Tube #1, typical) are supported by two connector pins and the side and corner weldments; and the corner fuel tubes (Tube #5, typical) are supported by three connector pins. The bearing stress ( $\sigma_{brg}$ ) on the fuel tube is as follows.

$$\sigma_{brg} = \frac{1.5 \times P_{pin}}{A_{brg}} = \frac{1.5 \times 233}{0.34} = 1.0 \text{ ksi}$$

where:

$$A_{brg} = 0.34 \text{ inch}^2 \text{----- Bearing area}$$

$$P_{pin} = \frac{1}{3}P_t + \frac{1}{4}P_t = 233 \text{ lb----- Combined loading on one pin}$$

$$P_t = 400 \text{ lb ----- Fuel tube weight}$$

The factor of safety (FS) for bearing is as follows.

$$FS = \frac{S_y}{\sigma_{brg}} = \frac{32.3}{1.0} = \text{Large}$$

where:

$$S_y = 32.3 \text{ ksi ----- Yield strength, SA-537 Class 1, at } 700^\circ\text{F}$$

The bearing stress ( $\sigma_{brg}$ ) in the connector pin at the TSC bottom plate, conservatively using P<sub>tube</sub> as previously determined, is as shown.

$$\sigma_{brg} = \frac{P_{tube}}{A_{brg}} = \frac{800}{0.75} = 1.1 \text{ ksi}$$

where:

$$A_{brg} = \frac{\pi}{4}(D_o^2 - D_i^2) = \frac{\pi}{4}(1.0^2 - 0.19^2) = 0.75 \text{ inch}^2$$

$$D_o = 1.00 \text{ inch}$$

$$D_i = 0.19 \text{ inch}$$

The factor of safety (FS) for bearing is as follows.

$$FS = \frac{S_y}{\sigma_{brg}} = \frac{24.7}{1.1} = \text{Large}$$

where:

$$S_y = 24.7 \text{ ksi} \text{ ----- Yield strength, SA-240 Type 304, at } 700^\circ\text{F}$$

The weight of the side and corner weldments is carried through to the TSC bottom plate by supports at the bottom of the basket. The corner weldment is bounding for the top and bottom supports. The dimensions for the corner support weldment are 8.0 inches in length and 0.375-inch thickness. The bounding weight of the corner weldment is 1,100 pounds. The corner weldment also supports one-quarter of the weight of four fuel tubes (conservatively 400 lb per tube). The bearing stress is as follows.

$$\sigma_{brg} = \frac{W_{sup}}{A_{sup}} = 0.8 \text{ ksi}$$

where:

$$W_{sup} = 1.5 \times (1,100 + 4 \times (0.25 \times 400)) = 2,250 \text{ lb}$$

$$A_{sup} = 8.0 \times 0.375 = 3.0 \text{ inch}^2$$

The factor of safety (FS) for bearing is as follows.

$$FS = \frac{S_y}{\sigma_{brg}} = \frac{32.3}{0.8} = \text{Large}$$

where:

$$S_y = 32.3 \text{ ksi} \text{ ----- Yield strength, SA-537 Class 1, at } 700^\circ\text{F}$$

The maximum bolt load due to off-normal load is 1,241 pounds. Combined with a bolt preload of 400 lb, the maximum bolt load is 1,641 pounds. A bolt load of 1,700 lb is used for the evaluation. From Machinery's Handbook [12], the tensile strength ( $\sigma_t$ ) in the bolt is as follows.

$$\sigma_t = \frac{P}{A_t} = \frac{1,700}{0.23} = 7.4 \text{ ksi}$$



where:

$$A_t = 0.7854 \left( D - \frac{0.9743}{n} \right)^2 = 0.23 \text{ inch}^2$$

$$D = 0.625 \text{ inch}$$
$$n = 11$$

The factor of safety (FS) is as follows.

$$FS = \frac{S_m}{\sigma_t} = \frac{23.3}{7.4} = 3.15$$

where:

$$S_m = 23.3 \text{ ksi} \text{ ----- Design stress intensity for SA-193, Gr B6, at } 700^\circ\text{F}$$

The shear stress in the bolt thread ( $\tau_{\text{bolt}}$ ) is as follows.

$$\tau_{\text{bolt}} = \frac{P}{A_s} = \frac{1,700}{0.379} = 4.5 \text{ ksi}$$

where:

$$A_s = 3.1416nL_eK_{n \text{ max}} \left[ \frac{1}{2n} + 0.57735(E_{s \text{ min}} - K_{n \text{ max}}) \right] = 0.379 \text{ inch}^2$$

$$n = 11$$

The factor of safety (FS) is as follows.

$$FS = \frac{0.6S_y}{\tau_{\text{bolt}}} = \frac{0.6 \times 70.0}{4.5} = 9.3$$

where:

$$S_y = 70.0 \text{ ksi} \text{ ----- Yield strength, SA-193 Grade B6, at } 700^\circ\text{F}$$

The shear stress in the boss thread ( $\tau_{\text{boss}}$ ) is as follows.

$$\tau_{\text{boss}} = \frac{P}{A_n} = \frac{1,700}{0.542} = 3.1 \text{ ksi}$$

where:

$$A_n = 3.1416nL_e D_{s\min} \left[ \frac{1}{2n} + 0.57735(D_{s\min} - E_{n\max}) \right] = 0.542 \text{ inch}^2$$

$$L_e = 0.38 \text{ inch}$$

$$E_{n\max} = 0.5732$$

$$D_{s\min} = 0.6113$$

$$n = 11$$

The factor of safety (FS) is as follows.

$$FS = \frac{0.6S_y}{\tau_{\text{bolt}}} = \frac{0.6 \times 28.6}{3.1} = 5.54$$

where:

$$S_y = 28.6 \text{ ksi} \text{ ----- Yield strength, SA-695, Type B, Gr 40, at } 700^\circ\text{F}$$

The boss is welded into the fuel tube with a 3/16-inch groove weld. The shear stress in the boss weld ( $\tau_{\text{weld}}$ ) is as follows.

$$\tau_{\text{weld}} = \frac{P}{A_w} = \frac{1,700}{0.59} = 2.9 \text{ ksi}$$

where:

$$P = 1,700 \text{ lb}$$

$$A_w = \pi D t_{\text{weld}} = \pi \times 1.00 \times 0.1875 = 0.4959 \text{ inch}$$

$$D = 1.00 \text{ inch} \text{ ----- Smallest boss diameter}$$

Using the lesser allowable,  $S_m$ , of SA-537 Class 1 or SA-695 Type B, Gr 40, the factor of safety (FS) is as follows.

$$FS = \frac{0.35 \times 0.9S_m}{\tau_{\text{weld}}} = 2.10$$

where:

$$S_m = 19.2 \text{ ksi} \text{ ----- Design Stress Intensity, SA-695 Type B Grade 40, at } 700^\circ\text{F}$$

The washers under the bolts are subjected to a bending load due to the torque of the bolts. Using the maximum bolt load (1,700 lb) and the minimum washer thickness (3/16 inch), the maximum

bending moment in the washer is calculated to be 58.1 inch-lb. The maximum stress ( $\sigma$ ) in the washer is as follows.

$$\sigma = \frac{6M_t}{t^2} = \frac{6 \times 0.058}{0.1875^2} = 9.9 \text{ ksi}$$

where:

$$t = 3/16 \text{ inch} \text{----- Thickness of washer}$$

$$M_t = 0.058 \text{ inch-kip}$$

The factor of safety (FS) is as follows.

$$FS = \frac{2.25S_m}{\sigma} = 3.64$$

where:

$$S_m = 16.0 \text{ ksi} \text{----- Design stress intensity, SA-240 Type 304, at } 700^\circ\text{F}$$

The buckling evaluation of the connector pin is performed in Section 3.7.2.2. The accident condition buckling evaluation is bounding due to the 60g axial inertia loading.

The maximum shear load on a boss for the off-normal condition is 821 pounds. The bosses were evaluated with a bounding shear load of 4,200 lb for the normal condition in Section 3.5.2.2.

Therefore, no further analysis is required for the bosses for off-normal conditions.

The analysis presented in Section 3.7.2.2 bounds the off-normal analysis of the neutron absorber and retainer strip; therefore, no additional analysis is required.

### **3.6.3 Concrete Cask Evaluation for Off-Normal Operating Events**

Section 3.5.3.1 presents the thermal stress evaluation for normal conditions for the concrete cask. The analysis used the 106°F ambient condition thermal gradient, which is the off-normal event; therefore, the analysis is conservative. The analysis bounds both the normal and off-normal events; therefore, no thermal stress evaluation is presented in this section. All analyses of the concrete cask are bounded by the analyses presented in the normal and accident sections.

### 3.7 Storage Accident Events

This section presents the analyses of the structural components of MAGNASTOR for storage accident events. MAGNASTOR is evaluated using finite element models and classical hand calculations for the TSC, fuel baskets, and concrete cask.

#### 3.7.1 TSC Evaluations for Storage Accident Conditions

The TSC is analyzed for an accident pressurization of 250 psig, a 24-inch end drop of the concrete cask, and the hypothetical concrete cask tip-over accident. For detailed analyses results for accident conditions, see Table 3.10.3-12 through Table 3.10.3-17.

##### 3.7.1.1 Accident Pressurization

Accident pressurization is a hypothetical event that assumes the failure of all of the fuel rods contained within the TSC. No postulated storage condition is expected to lead to the rupture of all fuel rods. The TSC is analyzed for accident pressurization and dead weight loads using the finite element model and conditions described in Section 3.10.3. Dead weight is simulated by applying a 1.0g acceleration load in the axial direction in conjunction with pressure being applied to the TSC bottom plate to simulate the weight of the basket and fuel. To represent the accident pressure, an internal pressure of 250 psig is applied to all inner surfaces of the TSC. The canister bottom plate, which is resting on the pedestal plate, is conservatively subjected to the 250 psig pressure and the dead weight of the fuel and basket.

The resulting TSC stresses for the accident pressurization condition are summarized in Table 3.7.1-1 and Table 3.7.1-2 for primary membrane and primary membrane plus primary bending stress categories, respectively. The minimum factor of safety of 1.59 occurs at Section 3 for the  $P_m+P_b$  stresses. The locations for the stress sections are shown in Section 3.10.3.

Results of analysis of this event demonstrate that the TSC is not significantly affected by the increase in internal pressure that results from the hypothetical rupture of all PWR or BWR fuel rods in the TSC.

##### 3.7.1.2 Concrete Cask 24-inch End-Drop

This section addresses the TSC stresses and potential TSC shell buckling associated with the postulated 24-inch end-drop accident of the concrete cask. The evaluation of the TSC during the

end impact is performed using an inertial load of 60g. This inertial load conservatively bounds the maximum calculated acceleration including dynamic load factor (DLF).

**3.7.1.2.1 TSC End Impact Stress Evaluation**

The TSC is analyzed for the concrete cask 24-inch drop accident condition using the finite element model described in Section 3.10.3. The 24-inch drop is simulated by applying a 60g acceleration load in the axial direction, with pressure applied to the TSC bottom plate to simulate the inertial load of the basket and fuel. To represent the normal pressure, an internal pressure of 110 psig is applied to all inner surfaces of the TSC. The canister bottom plate, which is resting on the pedestal plate, is conservatively subjected to the pressure due to the 60g inertia of the basket and fuel, as well as the 110 psig internal pressure.

The resulting maximum stresses in the TSC for the 24-inch drop accident events are summarized in Table 3.7.1-1 and Table 3.7.1-2 for primary membrane, and primary membrane plus primary bending stress categories, respectively. The minimum factor of safety of 3.71 occurs at section 4 (lower TSC shell) for the  $P_m$  stresses. The locations for the stress sections are shown in Section 3.10.3.

**3.7.1.2.2 TSC Buckling Evaluation**

During the 24-inch bottom-end drop of the concrete cask, the 60g inertial load conservatively applied to the closure lid assembly generates longitudinal compressive stresses in the TSC shell. The critical buckling stress ( $S_{CR}$ ) in the TSC shell based on the TSC geometry and material properties is as follows.

$$S_{CR} = E \frac{0.605 - 10^{-7} m^2}{m(1 + 0.004\phi)} = 34.5 \text{ ksi} \quad [15]$$

where:

- $E = 25.8 \times 10^3 \text{ ksi}$  ----- Modulus of elasticity of SA-240, Type 304, at 500°F
- $\phi = \frac{E}{S_y} = 1,330$  ----- Inverse strain parameter
- $S_y = 19.4 \text{ ksi}$  ----- Yield strength of SA-240, Type 304, at 500°F
- $m = \frac{r_m}{t} = 71.5$  ----- Mean radius to thickness ratio
- $r_m = 35.75 \text{ inch}$  ----- Mean radius TSC shell
- $t = 0.5 \text{ inch}$  ----- Thickness of TSC shell

The results from the 24-inch end-drop analysis are screened for the maximum longitudinal compressive stress. The maximum longitudinal compressive stress,  $S_z$ , of 9.3 ksi occurs at the intersection of the TSC shell and bottom plate (see Section 3.10.3). The factor of safety (FS) is as follows.

$$FS = \frac{S_{CR}}{S_z} = \frac{34.5 \text{ ksi}}{9.3 \text{ ksi}} = 3.7$$

Therefore, buckling of the TSC does not occur.

### 3.7.1.3 Concrete Cask Tip-Over

The TSC is analyzed for the concrete cask tip-over using the finite element model described in Section 3.10.3. A tapered inertial load (40g at top of TSC closure lid and 1g at the base of the concrete cask) is considered as a side impact load on the TSC. The 40g inertial load is conservatively used in the evaluation to bound the calculated maximum g-load for the TSC during the concrete cask tip-over event including the dynamic load factor (Section 3.7.3.7).

The resulting maximum stresses in the TSC for tip-over conditions are summarized in Table 3.7.1-1 and Table 3.7.1-2 for primary membrane and primary membrane plus primary bending stress categories, respectively. The minimum factor of safety is 1.20 at Section 11 for the  $P_m$  stresses and 1.08 at Section 5 for the  $P_m+P_b$  stresses. The factor of safety,  $P_m+P_b$ , for the structural lid closure weld, Section 11, is 1.39. The locations for the stress sections are shown in Section 3.10.3. Note that the maximum stresses occur at the section cut at the 0-degree location.

### 3.7.1.4 Flood

This evaluation considers design basis flood conditions of a 50-foot depth of water having a velocity of 15 feet per second. The hydrostatic pressure ( $P_h$ ) exerted on the TSC during a 50-foot flood event is as follows.

$$P_h = \rho \times h = \left(62.4 \frac{\text{lb}}{\text{ft}^3}\right) \left(\frac{1 \text{ ft}^3}{1728 \text{ in}^2}\right) \times (50 \text{ ft}) \left(\frac{12 \text{ in}}{1 \text{ ft}}\right) = 22 \text{ psi}$$

where:

$$\begin{aligned} \rho &= 62.4 \text{ lb/ft}^3 \text{ ----- Density of water} \\ h &= 50 \text{ ft ----- Immersion depth} \end{aligned}$$

During normal conditions, the TSC is evaluated for an internal pressure of 110 psig. Because the pressure differential is reduced during flood conditions ( $110 - 22 = 88$  psig), stresses in the TSC shell are reduced. Therefore, the hydrostatic pressure exerted by the 50-foot depth of water actually reduces the stress in the TSC. MAGNASTOR is, therefore, not adversely affected by the design basis flood.

### **3.7.1.5 Tornado and Tornado-Driven Missiles**

The postulated tornado wind loading and tornado missile impacts are not capable of overturning the concrete cask, or penetrating the boundary established by the concrete cask. Consequently, there is no effect on the TSC. Stresses resulting from the decreased external pressure due to a tornado are bounded by the stresses due to the accident internal pressure condition evaluated in Section 3.7.1.1.

Table 3.7.1-1 TSC Accident Events,  $P_m$  Stresses

| Load Case                      | Service Level | Section <sup>b</sup> | Component Stresses <sup>a</sup> (ksi) |        |        |          |          |          | $S_{int}$ | $S_{allow}$ | FS   |
|--------------------------------|---------------|----------------------|---------------------------------------|--------|--------|----------|----------|----------|-----------|-------------|------|
|                                |               |                      | $S_x$                                 | $S_y$  | $S_z$  | $S_{xy}$ | $S_{yz}$ | $S_{xz}$ |           |             |      |
| Accident Pressure              | D             | 3                    | -1.13                                 | -15.79 | 8.74   | 0.29     | 0.06     | 1.93     | 24.90     | 47.15       | 1.89 |
| Normal Pressure + 24-inch Drop | D             | 4                    | -0.03                                 | 7.81   | -4.26  | 0.00     | 0.00     | 0.00     | 12.07     | 44.80       | 3.71 |
| Normal Pressure + Tip-Over     | D             | 11                   | -23.89                                | -17.09 | -19.05 | 10.77    | -1.77    | -8.92    | 29.05     | 34.72       | 1.20 |

Table 3.7.1-2 TSC Accident Events,  $P_m + P_b$  Stresses

| Load Case                      | Service Level | Section <sup>b</sup> | Component Stresses <sup>a</sup> (ksi) |       |       |          |          |          | $S_{int}$ | $S_{allow}$ | FS   |
|--------------------------------|---------------|----------------------|---------------------------------------|-------|-------|----------|----------|----------|-----------|-------------|------|
|                                |               |                      | $S_x$                                 | $S_y$ | $S_z$ | $S_{xy}$ | $S_{yz}$ | $S_{xz}$ |           |             |      |
| Accident Pressure              | D             | 3                    | -0.46                                 | -7.35 | 35.72 | 0.09     | 0.07     | 2.43     | 43.24     | 68.60       | 1.59 |
| Normal Pressure + 24-inch Drop | D             | 12                   | 17.98                                 | 18.23 | 1.64  | 0.67     | 0.76     | -0.94    | 17.24     | 68.60       | 3.98 |
| Normal Pressure + Tip-Over     | D             | 5                    | 0.68                                  | 59.72 | 41.78 | 0.02     | 0.81     | 0.28     | 59.06     | 63.75       | 1.08 |

<sup>a</sup> The x, y, z components of stress are to be interpreted radial, circumferential and axial directions, respectively.

<sup>b</sup> See Figure 3.10.3-2 for section cut locations.



**3.7.2 Fuel Baskets Evaluation for Storage Accident Events**

**3.7.2.1 PWR Basket**

**3.7.2.1.1 24-inch Concrete Cask End Drop**

For the 24-inch concrete cask drop, a 60g acceleration (a) is conservatively applied to the PWR basket in the axial direction. The basket is evaluated using classical hand calculations. Using a bounding weight of 22,500 lb for the PWR basket, the maximum stress in the fuel tube is calculated. Factors of safety for the PWR basket are calculated based on the criteria for Service Level 'D' limits from ASME Code, Section III, Subsection NG [7] and Appendix F [8]. Conservatively assuming the entire basket weight is carried through the fuel tubes, the stress in the tube is as follows.

$$\sigma_{\text{tube}} = \frac{P_{\text{tube}}}{A} = \frac{64286}{11.4} = 5.6 \text{ ksi}$$

where:

$$P_{\text{tube}} = \frac{W \times a}{n} = \frac{22,500 \times 60}{21} = 64,286 \text{ lb}$$

- W = 22,500 lb ----- Bounding basket weight
- n = 21 ----- Number of fuel tubes
- A = 11.4 inch<sup>2</sup> ----- Tube cross-sectional area

The factor of safety (FS) is as follows.

$$FS = \frac{0.7 \times S_u}{\sigma_{\text{tube}}} = \frac{0.7 \times 68.4}{5.6} = 8.6$$

where:

- S<sub>u</sub> = 68.4 ksi ----- Ultimate strength, SA-537 Class 1, at 700°F

The weight of the fuel tubes is supported by connector pins. Referring to Figure 3.10.1-13, the interior tubes (Tube #4, typical) are supported by four connector pins; the side fuel tubes (Tube #1, typical) are supported by two connector pins and the side and corner weldments; and three connector pins support the corner fuel tubes (Tube #3, typical). The load is transferred by shear through the connector pin welds (four welds on two connector pins, which attaches them to the fuel tube at bottom of basket) and by axial compression through the area of the end of the fuel tube in contact with the connector pin assembly, which rests on the bottom canister plate.

The load capability ( $P_{\text{joint}}$ ) of the weld and the common area is determined by the sum of the loads, which each load path can sustain. A conservative evaluation is performed in which the stresses are evaluated against allowables associated with an elastic evaluation, as opposed to the plastic evaluation permitted in Appendix F [8].

$$P_{\text{joint}} = A_m(0.7S_u) + A_w(wf \times 0.42S_u) = 25.3 \text{ kips}$$

where:

$$\begin{aligned} A_m &= 0.21 \text{ inch}^2 \text{----- Common area for compression} \\ A_w &= 4(l_w t_w) = 1.52 \text{ inch}^2 \text{----- Weld area for shear} \\ l_w &= 2.0 \text{ inch} \text{----- Connector pin length} \\ t_w &= 3/16 \text{ inch} \text{----- Weld size} \\ wf &= 0.35 \text{----- Weld quality factor visual inspection} \\ &\quad \text{(ASME Code Section III, Subsection NG;} \\ &\quad \text{Article NG-3352)} \\ S_u &= 68.4 \text{ ksi} \text{----- Ultimate strength, SA-537 Class 1, at 700°F} \end{aligned}$$

The load in the tube joint ( $P$ ) is as follows.

$$P = 60 \times P_{\text{pin}} = 60 \times 394 = 23.6 \text{ ksi}$$

where:

$$\begin{aligned} P_{\text{pin}} &= \frac{1}{3}P_t + \frac{1}{4}P_t = 394 \text{ lb} \\ P_t &= 675 \text{ lb} \text{----- Tube weight} \end{aligned}$$

The factor of safety (FS) is as follows.

$$FS = \frac{P_{\text{joint}}}{P} = \frac{25.3}{23.6} = 1.07$$

The weight of the side and corner weldments is carried through to the TSC base plate by supports at the bottom of the weldments. The bounding dimensions for the supports of the weldments are 5.0 inches in length and 0.3125-inch thickness (corner weldment). The maximum weight of one weldment is 800 lb (bounding, side weldment). The weldment supports one-quarter of the weight of two fuel tubes (675 lb per tube, bounding). The membrane stress ( $\sigma_m$ ) is as follows.

$$\sigma_m = \frac{60 \times W_{\text{sup}}}{A_{\text{sup}}} = \frac{60 \times 1,138}{1.56} = 43.8 \text{ ksi}$$

where:

$$W_{sup} = 800 + 2 \times (0.25 \times 675) = 1138 \text{ lb}$$
$$A_{sup} = 5.0 \times 0.3125 = 1.56 \text{ inch}^2$$

The factor of safety (FS) is as follows.

$$FS = \frac{0.7S_u}{\sigma_m} = \frac{0.7 \times 68.4}{43.8} = 1.09$$

where:

$$S_u = 68.4 \text{ ksi} \text{ ----- Ultimate strength, SA-537 Class 1, at } 700^\circ\text{F}$$

The 32-basket connector pins support the PWR basket during a 60g bottom-end drop accident. The bounding temperature at the bottom of the basket is 500°F. The pins are subjected to compressive loads; therefore, a buckling evaluation of the pins is presented. The load on one connector pin ( $P_{pin}$ ) is as follows.

$$P_{pin} = \frac{W \times 60}{n} = \frac{22500 \times 60}{32} = 42.2 \text{ kips}$$

where:

$$W = 22,500 \text{ lb} \text{ ----- Bounding basket weight}$$
$$n = 32 \text{ ----- Number of pins}$$

Using the Euler buckling theory, the critical buckling load ( $P_{cr}$ ) is as follows.

$$P_{cr} = \frac{\pi^2 EI}{(KL)^2} = \frac{\pi^2 \times (25.8 \times 10^6) \times 0.015}{(2 \times 3.0)^2} = 106.0 \text{ kip [9]}$$

where:

$$A_{pin} = 0.44 \text{ inch}^2$$
$$D = 0.75 \text{ inch} \text{ ----- Pin diameter}$$
$$L = 3.0 \text{ inch} \text{ ----- Pin length}$$
$$I = \frac{\pi r^4}{4} = 0.015 \text{ inch}^4$$
$$K = 2.0 \text{ ----- Buckling constant, clamped-free}$$
$$E = 25.8 \times 10^6 \text{ psi} \text{ ----- SA-240 Type 304, at } 500^\circ\text{F}$$

The factor of safety (FS) for buckling of the connector pins is as follows.

$$FS = \frac{P_{cr}}{P_{pin}} = \frac{106.0 \text{ kip}}{42.2 \text{ kip}} = 2.51$$

### PWR Neutron Absorber Evaluation

During the end impact condition, the PWR neutron absorber and the weld post are subject to shearing force in the longitudinal direction of the neutron absorber. The neutron absorber is considered to be supported by two weld posts located at the bottom end of the neutron absorber. The evaluation is conservatively performed for an acceleration of 60g at a bounding temperature of 350°F. The inertia load applied to the neutron absorber ( $F_{na}$ ) at each weld post during the end impact is as follows.

$$F_{na} = L \times W \times t \times \rho \times a / 2 = 525 \text{ lb}$$

where:

|                              |       |  |
|------------------------------|-------|--|
| $\rho = 0.1 \text{ lb/in}^3$ | ----- | Bounding density of the neutron absorber |
| $a = 60g$                    | ----- | End drop acceleration                    |
| $t = 0.125 \text{ in}$       | ----- | Thickness of neutron absorber            |
| $L = 173 \text{ in}$         | ----- | Length of neutron absorber               |
| $W = 8.1 \text{ in}$         | ----- | Width of neutron absorber                |

The shearing capacity of the neutron absorber is as follows.

$$F_{\text{shear}_{na}} = A_s \times \Phi_a = 0.44 \times 2260 = 994 \text{ lb}$$

where:

|   |       |   |
|---|-------|---|
| $A_s = L_{NA} \times 1.414 \times 2 \times t = 0.44 \text{ in}^2$ | ----- | Shear area at both sides of each weld-post<br>(at the 45° shear planes) |
| $L_{NA} = 1.25 \text{ in}$  | ----- | Min. edge distance of the neutron absorber                              |
| $\Phi_a = 0.42 S_u = 2.26 \text{ ksi}$                            | ----- | Allowable shear stress  |
| $S_u = 5.38 \text{ ksi}$  | ----- | Tensile strength of neutron absorber at<br>350°F                        |

The factor of safety (FS) is as follows.

$$FS = F_{\text{shear}_{na}} / F_{na} = 994 / 525 = 1.89$$

The strength of the weld posts is significantly higher than that of the neutron absorber. Therefore, no evaluation is required for the weld posts for the concrete cask 24-inch end-drop condition.

### **3.7.2.1.2 Concrete Cask Tip-Over**

The analysis results for the PWR basket subjected to a hypothetical concrete cask tip-over accident are presented in this section. Factors of safety for the PWR basket are calculated based on the criteria for Service Level 'D' limits from ASME Code, Section III, Subsection NG [7] and Appendix F [8].

### **PWR Fuel Tube Evaluation**

The PWR basket fuel tubes are analyzed for a tip-over accident using the three dimensional periodic plastic finite element models described in Section 3.10.1. The fuel tube is conservatively evaluated for 35g side impact load.

Equivalent plastic stresses are calculated for the PWR fuel tubes for the bounding basket orientations of 0° and 45° (see Figure 3.10.1-13 and Figure 3.10.1-15 for tube IDs). The maximum primary membrane and primary membrane plus bending stress intensity for each fuel tube are reported in Table 3.7.2-1. Note that for plastic analysis, ANSYS reports stresses in the elastic region as the yield strength (35.4 ksi, at 500°F) for the stress-strain curve.

The ANSYS plastic finite element model follows the material stress-strain curve and allows for nonlinear behavior above the yield strength point. The stress allowables for plastic analysis are based on ASME Code, Section III, Appendix F [8]. The allowable primary membrane stress intensity is  $0.7S_u$ . The allowable primary membrane plus bending stress intensity is  $0.9S_u$ . The minimum factors of safety for the PWR fuel tubes are 1.16 for primary membrane stresses (45° basket orientation) and 1.40 for primary membrane plus bending stresses (0° basket orientation). The critical stress locations occur in the fuel tube corners.

The PWR fuel tubes are constructed by welding two tube halves together using a full-penetration weld for the length of the fuel tube. A surface MT weld examination per ASME Code, Section III, Subsection NG, Article NG-5232 is used when structural qualification of the weld joint is performed with a 0.65 weld quality factor (wf), per Table NG-3352-1. From the plastic analysis of the PWR basket, the maximum membrane and membrane plus bending stress intensity at a tube weld is 8.4 ksi and 25.7 ksi, respectively. It is noted that the weld quality factor for the PWR tube is different than the weld quality factor used in the evaluation of the BWR tube weld to limit weld inspection to surface MT. The factors of safety (FS) for the weld are as follows. A bounding temperature of 720°F is conservatively used.

Membrane:

$$FS = \frac{0.7S_u \times wf}{\sigma} = 3.69$$

Membrane plus bending:

$$FS = \frac{0.9S_u \times wf}{\sigma} = 1.55$$

where:

$$S_u = 68.1 \text{ ksi} \text{ ----- Ultimate strength, SA-537 Class 1, at } 720^\circ\text{F}$$

The pins between adjacent tubes are subjected to shear load. From the finite element models, the maximum shear load (P) in the pin is 13,218 lb and 3,474 lb for 0° and 45° basket orientations, respectively. The shear load is determined by summing the nodal forces at the contact region between the pin and tube slot. Using a bounding load (P) of 15,000 lb, the shear stress in the pin is

$$\tau_{\text{pin}} = \frac{P}{Dl_{\text{pin}}} = 21.0 \text{ ksi}$$

where:

$$D = 0.44 \text{ inch} \text{ ----- Pin diameter}$$

$$l_{\text{pin}} = 3.25/2 = 1.625 \text{ inch} \text{ ----- Length of pin in the model}$$

The factor of safety (FS) is as follows.

$$FS = \frac{0.42S_u}{\tau_{\text{pin}}} = 1.38$$

where:

$$S_u = 68.9 \text{ ksi} \text{ ----- Ultimate strength, SA-695 Type B Gr 40, at } 720^\circ\text{F}$$

The bearing stress ( $\sigma_{\text{brg}}$ ) on the pin is evaluated using the bounding load of 15,000 lb. The bearing area is determined based on a 30° contact arc between the pin and the fuel tube slot.

$$\sigma_{\text{brg}} = \frac{P}{LS} = 83.9 \text{ ksi}$$

where:

$$P = 15,000 \text{ lb} \text{ Maximum load on pin}$$

- L=1.625 inch----- Length of pin in ANSYS model
- $S = \pi D \frac{30}{360} = 0.11$  in ----- Bearing arc length
- D=0.44 inch ----- Pin diameter

Per ASME Appendix F-1336, the allowable bearing stress is  $2.1S_u$ . The factor of safety (FS) is as follows.

$$FS = \frac{2.1S_u}{\sigma_{brg}} = 1.72$$

where:

$$S_u = 68.9 \text{ ksi}----- \text{Ultimate strength, SA-695 Type B Gr 40, at } 720^\circ\text{F}$$

### **PWR Neutron Absorber and Retainer**

The PWR neutron absorber and retainer are conservatively evaluated for a 60g side-impact load and for the concrete cask tip-over event. The retainer strip consists of 304 stainless steel and is restrained by an array of posts welded to the inside surface of the fuel tube. Two rows of posts are separated four inches apart and a spacing of ten inches exists between the posts along the axial direction of the fuel tube.

The pitches of the slotted holes in the neutron absorber are the same as the holes in the retainer strip through which the weld posts are connected to the fuel tube. The slotted holes are used to prevent interference during differential thermal expansion between the neutron absorber and the fuel tube. The head of the weld posts supporting the retainer strip are engaged in the recessed conical pockets of the retainer.

As shown in Figure 3.7.2-3, a quarter-symmetry finite element model is generated to represent one-half of the ten-inch periodic section for the PWR design. The model is comprised of the retainer strip with the conical slot, the neutron absorber, and the weld post. Inelastic properties are employed for the stainless steel retainer strip and the neutron absorber at 700°F to adequately represent the stiffness at the maximum temperature condition. Note that the peak fuel tube temperature is less than 720°F and occurs in a localized region. The difference in material properties between 700°F and 720°F is not significant and has no effect on the conclusion of the analysis, which uses a very conservative acceleration time history for the impact loading. The model for the neutron absorber plate is comprised of three layers of materials. The two outer layers employ the inelastic properties of aluminum 1100 series cladding at 700°F. The center layer represents the neutron absorber material, which is assigned a yield strength of 10 psi and an

elastic modulus of elasticity of 1,000 psi. The low yield strength for the core material allows the neutron absorber core to provide only a minimal contribution of stiffness to the neutron absorber plate. The weld post was modeled as being rigid to maximize deformation of the conical-shaped section of the retainer by the weld post. Symmetry conditions were imposed along the planes of symmetry, which are present on all four sides of the model. The parts are modeled independently and the automatic contact surface option in LS-DYNA was used between the parts to transfer load between the neutron absorber, the retainer and the weld post. The evaluation of the side impact was performed using LS-DYNA and the impact was simulated by imposing the acceleration time history whose maximum acceleration was 60g. This conservatively envelops the maximum tip-over acceleration of 35g.

Since the function of the retainer is to maintain the neutron absorber in its position, the criteria for the retainer is to limit the motion of the neutron absorber during and after the impact. This is confirmed by considering the permanent strain and the permanent displacement of the retainer. The strain of 3.3%, which is minimal, is local to the conical-shaped hole. Since inelastic strains are not recovered, this indicates that maximum inelastic strain during the impact is also limited to 3.3 percent. Such a minimal strain level indicates that the conical pocket retains its configuration for the weld post to restrain the retainer. The final maximum displacement of the retainer strip at the axial midpoint between the weld posts is computed to be 0.06 inch, which is consistent with the minimal plastic strain in the retainer. This also confirms that the retainer remains engaged with the weld post during and after the impact.

The maximum stress intensity in the stainless steel retainer strip is determined to be 35.8 ksi, which is also local to conical-shaped hole at the weld post. The allowable stress for accident condition is  $0.9S_u$  per ASME Section III Appendix F. The ultimate strength ( $S_u$ ) of Type 304 stainless steel at 720°F is 63.1 ksi.

The factor of safety (FS) is as follows.

$$FS = \frac{0.9 \times 63.1}{35.8} = 1.59$$

The peak force on the weld post determined from the analysis is 74 pounds. The shear area governs the capacity of the weld. The depth of the weld ( $h$ ) is 0.13 inch. The diameter of the weld post ( $D$ ) is 0.25 inch. The governing stress is the shear stress in the base material. The allowable shear stress for the accident condition is  $0.42S_u$ . The ultimate strength ( $S_u$ ) of the base material (SA240, Type 304) at 720°F is 63,100 psi. The weld capacity,  $F_{cap}$ , is calculated as shown in the following.

$$\begin{aligned} F_{cap} &= 0.42 \times n \times S_u \times h \times BD \\ &= 0.42 \times 0.3 \times 63,100 \times 0.13 \times (3.1416 \times 0.25) \\ &= 812 \text{ lb} \end{aligned}$$



where:

$n = 0.3$  ----- The design factor per ASME Code, Section III, Subsection NG, Table NG-3352-1 for the intermittent plug weld employing a surface visual examination method per NG-5260.

The factor of safety (FS) is as follows.

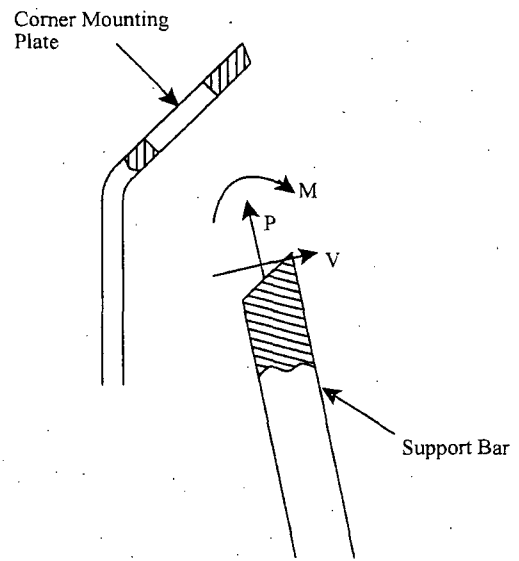
$$FS = \frac{812}{74} = \text{Large}$$

**PWR Corner Support Weldment Evaluation**

The PWR basket corner support weldment is analyzed for the tip-over accident using the three-dimensional plastic finite element model and boundary conditions described in Section 3.10.1. The corner support weldment is comprised of two major components: the mounting plate (vertical plate) and the side support bars, which are located on five-inch centers.

The analysis results for the corner support weldment are presented in Table 3.7.2-2 and Table 3.7.2-3. The maximum primary membrane plus bending stress intensity is conservatively compared to the primary membrane stress allowable of  $0.7 S_u$  per ASME Code Section III Appendix F. The minimum factor of safety for the corner weldment mounting plates is 1.34. The minimum factor of safety for the corner weldment support bars is 2.28.

The support bar is a continuous bar that is bent at the ridge gusset. The support bars are welded to the corner mounting plate where cutouts in the corner mounting plate accept the end of the bars. The bars are welded to the wall on the backside with a minimum 5/16-inch groove weld on the sides of the bars using the visual inspection criteria per ASME Code, Section III, Subsection NG, Article NG-5260. A weld quality factor of 0.35 is applied based on visual inspection of the weld per ASME Code, Section III, Subsection NG, Article NG-3352.



The welded joint between the support bar and corner mounting plate is capable of carrying bending, axial, and shear loads. The maximum weld loads occur in the 0° basket orientation. The bending moment (M), axial load (P), and shear load (V) are 1, 726 in-lb, 3,643 lb, and 122 lb, respectively. The weld stress intensity ( $\sigma_{weld}$ ) is as follows.

$$\sigma_{\text{weld}} = \sqrt{\left(\frac{M}{S_w} + \frac{P}{A_w}\right)^2 + 4\left(\frac{V}{A_w}\right)^2} = 13.9 \text{ ksi}$$

where:

$$S_w = 0.875 \times 0.3125 \times 0.875 = 0.239 \text{ in}^3$$

$$A_w = 0.875 \times 2 \times 0.3125 = 0.547 \text{ in}^2$$

The factor of safety (FS) for the weld is as follows.

$$FS = \frac{0.35(S_u)}{\sigma_{\text{weld}}} = 1.72$$

where:

$$S_u = 68.4 \text{ ksi} \text{ ----- Ultimate strength, SA-537 Class 1, at } 700^\circ\text{F}$$

The ridge gusset is welded to the corner mounting plate with 1/8-inch flair bevel welds on both sides of the plate. The weld uses the visual inspection criteria per ASME Code, Section III, Subsection NG, Article NG-5260 and quality factor of 0.35, as defined previously. From the finite element analysis, the governing weld loads consist of a bending moment of 132 in-lb and a shear force of 115 pounds. The stress in the weld ( $\sigma_{\text{weld}}$ ) is as follows.

$$\sigma_{\text{weld}} = \sqrt{\left(\frac{0.132}{0.5}\right)^2 + 4\left(\frac{0.115}{1.0}\right)^2} = 0.4 \text{ ksi}$$

where:

$$S_w = t_{\text{plate}} \times t_{\text{weld}} \times l_{\text{weld}} = 0.5 \text{ in}^3$$

$$A_{\text{wg}} = t_{\text{weld}} \times l_{\text{weld}} = 0.125 \times 8.0 = 1.0 \text{ in}^2$$

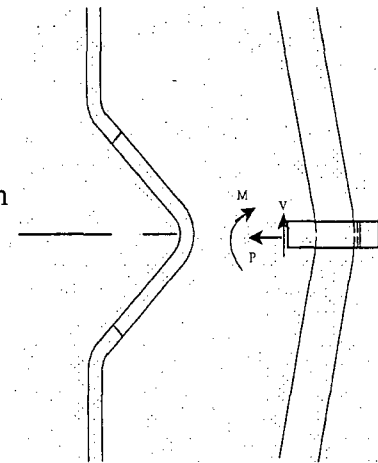
$$t_{\text{weld}} = \frac{1}{8}\text{-inch}$$

$$t_{\text{plate}} = 0.5 \text{ inch}$$

$$l_{\text{weld}} = 8.0 \text{ inch}$$

The factor of safety (FS) in the weld is as follows.

$$FS = \frac{0.35 \times S_u}{\sigma_{\text{weld}}} = \text{Large}$$



where:

$$S_u = 68.4 \text{ ksi} \text{ ----- Ultimate strength, SA-537 Class 1, at } 700^\circ\text{F}$$

### PWR Side Support Weldment Evaluation

The PWR basket side support weldment is analyzed for the tip-over accident using the three-dimensional periodic plastic finite element model and boundary conditions described in Section 3.10.1. The analysis results for the side support weldment are presented in Table 3.7.2-4. Conservatively, the maximum primary membrane plus bending stress intensity is compared to the primary membrane stress allowable,  $0.7S_u$ . The minimum factor of safety for the side support weldment is 1.35.

### PWR Side and Corner Weldment / Fuel Tube Attachment Evaluation

The corner and side support weldments are the primary structure that maintains the geometry of the fuel tube array during a hypothetical tip-over accident. The support weldments are bolted to the fuel tubes at 16 circumferential locations. The boss and bolt connection is designed so that the bolts are only loaded in tension, including preload. Otherwise, the support weldments apply a bearing load on the fuel tube array. From the finite element results of the  $0^\circ$  and  $45^\circ$  basket orientations, the maximum bolt tensile load is 3,888 pounds. Combined with the bolt preload of 400 pounds, the maximum bolt load is 4,288 pounds. A bounding load of 5,000 pounds is conservatively used for evaluation.

The tensile stress in the bolt is as follows.

$$\sigma_t = \frac{P}{A_t} = \frac{5.0}{0.23} = 21.7 \text{ ksi}$$

where:

$$A_t = 0.7854 \left( D - \frac{0.9743}{n} \right)^2 = 0.23 \text{ inch}^2$$

$$D = 0.625 \text{ inch}$$

$$n = 11$$

The factor of safety (FS) is as follows.

$$FS = \frac{S_y}{\sigma_t} = \frac{70.0}{21.7} = 3.23$$

where:

$$S_y = 70.0 \text{ ksi} \text{ ----- Yield strength for SA 193, Gr B6 at } 700^\circ\text{F}$$

The shear stress ( $\tau_{\text{bolt}}$ ) in the bolt thread is as follows.

$$\tau_{\text{bolt}} = \frac{P}{A_s} = \frac{5.0}{0.499} = 10.0 \text{ ksi}$$

where:

$$A_s = 3.1416nL_e K_{n \max} \left[ \frac{1}{2n} + 0.57735(E_{s \min} - K_{n \max}) \right] = 0.499 \text{ inch}^2$$

The factor of safety (FS) is as follows.

$$FS = \frac{0.42S_u}{\tau_{\text{bolt}}} = \frac{0.42 \times 90.6}{10.0} = 3.81$$

where:

$$S_u = 90.6 \text{ ksi} \text{ ----- Ultimate strength, SA-193 Grade B6 at } 700^\circ\text{F}$$

The shear stress in the boss thread ( $\tau_{\text{boss}}$ ) is as follows.

$$\tau_{\text{boss}} = \frac{P}{A_n} = \frac{5.0}{0.713} = 7.0 \text{ ksi}$$

where:

$$A_n = 3.1416nL_e D_{s \min} \left[ \frac{1}{2n} + 0.57735(D_{s \min} - E_{n \max}) \right] = 0.713 \text{ inch}^2$$

The factor of safety (FS) is as follows.

$$FS = \frac{0.42S_u}{\tau_{\text{boss}}} = \frac{0.42 \times 70.0}{7.0} = 4.2$$

where:

$$S_u = 70.0 \text{ ksi} \text{ ----- Ultimate strength, SA-695 Type B, Gr 40, at } 700^\circ\text{F}$$

The boss is welded into the fuel tube with a 1/4-inch groove weld. The weld uses the visual inspection criteria per ASME Code, Section III, Subsection NG, Article NG-5260 and a quality factor of 0.35. The shear stress in the boss weld ( $\tau_{weld}$ ), is as follows.

$$\tau_{weld} = \frac{P}{A_w} = \frac{5.0}{0.98} = 5.1 \text{ ksi}$$

where:

- P = 5.0 kips
- $A_w = \pi D t_{weld} = \pi \times 1.25 \times 0.25 = 0.98 \text{ inch}$
- D = 1.25 inches ----- Boss diameter

The factor of safety (FS) is

$$FS = \frac{0.35 \times 0.42 S_u}{\tau_{weld}} = \frac{0.35 \times 0.42 \times 68.4}{5.1} = 1.97$$

where:

- $S_u = 68.4 \text{ ksi}$  ----- Ultimate strength, SA-537 Class 1, at 700°F

The washers under the bolts are subjected to a bending load due to the bolt preload. Using Roark's [13], Table 24-1a, the maximum stress in the washer is calculated. The maximum stress ( $\sigma$ ) in the washer is as follows.

For the corner and side support weldment, the maximum load, including pre-load, on the washer is 5,000 lb, 0° basket orientation.

$$\sigma = \frac{6M_t}{t^2} = \frac{6 \times 0.599}{0.3125^2} = 36.8 \text{ ksi}$$

where:

- $a = \frac{1.50}{2} = 0.75 \text{ inch}$  ----- Radius of the cutout in support weldments
- $b = \frac{0.75}{2} = 0.375 \text{ inch}$  ----- Inner radius of the washer
- $r_o = 0.55 \text{ inch}$  ----- Average radius of bolt head
- t = 5/16 inch ----- Thickness of washer - thinnest
- E =  $27.0 \times 10^6 \text{ psi}$  ----- Modulus of elasticity (SA-240 Type 304)
- v = 0.3 ----- Poisson's ratio

$$w = \frac{P}{\pi \times 2r_o} = \frac{5,000}{\pi \times 2 \times 0.55} = 1,447 \text{ lb/in}$$

$$G = \frac{E}{2(1+\nu)} = \frac{27.0 \times 10^6}{2(1+0.3)} = 10.38 \times 10^6 \text{ psi}$$

$$D = \frac{Et^3}{12(1-\nu^2)} = \frac{27.0 \times 10^6 (0.3125^3)}{12(1-0.3^2)} = 75,460 \text{ inch-lb}$$

$$M_t = 0.599 \text{ inch-kip} \text{ ----- Calculated using formulas in Roark's}$$

The factor of safety (FS) is as follows.

$$FS = \frac{S_u}{\sigma} = \frac{63.2}{36.8} = 1.72$$

where:

$$S_u = 63.2 \text{ ksi} \text{ ----- Ultimate strength, SA-240 Type 304, at } 700^\circ\text{F}$$

The bosses transfer shear loads between the support weldments and fuel tube array. The maximum shear load on a boss is 4.1 kip, 45° basket orientation. The outer diameter of the boss is 1.25 inches and the inner diameter is 0.625 inch. The corresponding cross-sectional area (A) is 0.92 in<sup>2</sup>. The shear stress on the boss is as follows.

$$\tau_{\text{boss}} = \frac{P}{A} = \frac{4.1}{0.92} = 4.5 \text{ ksi}$$

The factor of safety (FS) is as follows.

$$FS = \frac{0.42S_u}{\tau_{\text{boss}}} = \frac{0.42 \times 70.0}{4.5} = 6.53$$

where:

$$S_u = 70.0 \text{ ksi} \text{ ----- Ultimate strength, SA-695, Type B, Gr 40, at } 700^\circ\text{F}$$

Loads between the fuel tube array and the corner and side weldments are reacted out in shear and bearing in the support weldments. Bearing stresses are not considered for accident events. Due to the geometry of the basket, the cutout in the corner support weldments has an edge distance less than two times the diameter of the cutout. The shear stress in the corner weldment mounting plate is as follows.

$$\tau = \frac{P}{A_{\text{shear}}} = \frac{4.1}{1.14} = 3.6 \text{ ksi}$$

where:

$$A_{\text{shear}} = 2 \left[ \frac{L_{\text{ed}}}{\sin 45^\circ} t_{\text{plate}} \right] = 1.14 \text{ inch}^2$$

$$L_{\text{ed}} = 1.30 \text{ inch} \text{----- Boss cutout edge distance in corner weldment}$$

$$t_{\text{plate}} = 0.31 \text{ inch} \text{----- Mounting plate thickness}$$

The factor of safety (FS) is as follows.

$$FS = \frac{0.42 S_u}{\tau} = \frac{0.42 \times 68.4}{3.6} = 7.98$$

where:

$$S_u = 68.4 \text{ ksi} \text{----- Ultimate strength, SA-537 Class 1, at } 700^\circ\text{F}$$

### **PWR Fuel Basket Buckling Evaluation**

For the hypothetical concrete cask tip-over accident, a buckling evaluation of the basket tube side wall is performed per NUREG/CR-6322 [9] is also performed. Based on the finite element analysis results, the governing buckling load of a fuel tube side wall (Axial Compression=25.3 kips, Bending Moment=5.3 inch-kip) occurs at Tube 12 (see Figure 3.10.1-13) for the 0° basket orientation. The factor of safety is calculated based on the interaction Equations 31 and 32 in NUREG/CR-6322. These two equations adopt the “Limit Analysis Design” approach for structural members subjected to stresses beyond the yield limit of the material. Methodology and equations for the buckling evaluation are summarized as follows.

Symbols and Units:

P = Applied axial compressive loads, kips

M = Applied bending moment, kips-inch

P<sub>a</sub> = Allowable axial compressive load, kips

P<sub>cr</sub> = Critical axial compression load, kips

P<sub>e</sub> = Euler buckling loads, kips

P<sub>y</sub> = Average yield load, equal to profile area times specified yield strength, kips

C<sub>c</sub> = Column slenderness ratio separating elastic and inelastic buckling

C<sub>m</sub> = Coefficient applied to bending term in interaction equation

M<sub>m</sub> = Critical moment that can be resisted in the absence of axial load, kip-inch

$M_p$  = Plastic moment, kip-inch.

$F_a$  = Axial compressive stress permitted in the absence of bending moment, ksi

$F_e$  = Euler stress for a prismatic member divided by factor of safety, ksi

$K$  = Ratio of effective column length to actual unsupported length

$l$  = Unsupported length of member, inch

$r$  = Radius of gyration, inch

$S_y$  = Yield strength, ksi

$A$  = Cross sectional area of member, inch<sup>2</sup>

$Z_x$  = Plastic section modulus, inch<sup>3</sup>

$\lambda$  = Allowable reduction factor, dimensionless.

From NUREG/CR-6322, the following interaction equations (Eqn. 31 and 32) are used for the evaluation of accident events.

$$\frac{P}{P_{cr}} + \frac{C_m M}{M_m \left[ 1 - \frac{P}{P_e} \right]} \leq 1.0$$

$$\frac{P}{P_y} + \frac{M}{1.18M_p} \leq 1.0$$

where:

$$P_{cr} = 1.7 \times A \times F_a$$

$$F_a = \frac{P_a}{A} \quad \text{for} \quad P_a = P_y \left[ \frac{1 - \frac{\lambda^2}{4}}{1.11 + 0.5\lambda + 0.17\lambda^2 - 0.28\lambda^3} \right]$$

and

$$\lambda = \frac{1}{\pi} \left( \frac{Kl}{r} \right) \sqrt{\frac{S_y}{E}}$$

$$F_e = \frac{\pi^2 E}{1.30 \left( \frac{kl}{r} \right)^2}$$

$$P_e = 1.92 \times A \times F_e$$

$$P_y = S_y \times A$$



$$C_m = 0.85 \text{ for members with joint translation (sideways)}$$

$$M_p = S_y \times Z_x$$

$$M_m = M_p \left( 1.07 - \frac{\left(\frac{1}{r}\right) \sqrt{S_y}}{3160} \right) \leq M_p$$

From NUREG/CR-6322, the factors of safety are calculated using the following equations.

$$P_1 = \frac{P}{P_{cr}}$$

$$M_1 = \frac{C_m M}{\left(1 - \frac{P}{P_e}\right) M_m}$$

$$P_2 = \frac{P}{P_y}$$

$$M_2 = \frac{M}{1.18} M_p$$

$$FS_1 = \frac{1}{P_1 + M_1}$$

$$FS_2 = \frac{1}{P_2 + M_2}$$

For the PWR basket fuel tube the following parameters are used in the buckling evaluation.

- t = 0.31 inch ----- Tube thickness
- b = 10.00 inch ----- Model length
- l = 8.20 inch ----- Sidewall length
- K = 0.80 ----- Effective length factor
- E = 27.3 × 10<sup>6</sup> psi ----- Modulus of elasticity, SA-537 Class 1, at 700°F
- S<sub>y</sub> = 35.4 ksi ----- Yield strength, SA-537 Class 1, at 700°F

For P = 25.3 kip and M = 5.3 inch-kip (Tube 12, 0° basket orientation):

$$P_1 = \frac{P}{P_{cr}} = 0.24$$

$$M_1 = \frac{C_m M}{\left(1 - \frac{P}{P_e}\right) M_m} = 0.65$$

$$P_2 = \frac{P}{P_y} = 0.23$$

$$M_2 = \frac{M}{1.18} M_p = 0.52$$

The factors of safety are listed as follows.

$$FS_1 = \frac{1}{P_1 + M_1} = \frac{1}{0.24 + 0.65} = 1.12$$

$$FS_2 = \frac{1}{P_2 + M_2} = \frac{1}{0.23 + 0.52} = 1.34$$

### **PWR Basket Displacement**

The nominal dimension of the fuel tube opening for the PWR basket is 8.86 in × 8.86 in for the manufactured fuel tubes and 8.76 in × 8.76 in for the developed fuel slot formed by 4 adjacent fuel tubes. The maximum width of a PWR fuel assembly is 8.54 inches. Based on the quasi-static analysis results using the three-dimensional periodic plastic models for the cask tip-over accident, the minimum clearance between the fuel assembly and the fuel tube is 0.25 inch for the manufactured tubes and 0.13 inch for the developed tubes during the 35-g side impact loading. As presented in Section 3.10.7, a three-dimensional half-symmetry model for a PWR fuel tube is constructed using the LS-DYNA program to calculate the maximum displacement of a fuel tube as function of time due the side impact load for cask tip-over accident. The LS-DYNA analysis considers a displacement loading based on the maximum diagonal displacements of the fuel tubes during the impact (see Figure 3.7.2-1) obtained from the finite element analysis results using the three-dimensional periodic plastic model. The permanent displacement in the tube diagonal direction, after the impact, is calculated to be 0.008 inch, which is less than the fabrication tolerance of the fuel tubes and, therefore, not significant.

**3.7.2.2 BWR Fuel Basket**

**3.7.2.2.1 24-inch Concrete Cask End-Drop**

For the 24-inch concrete cask drop, a 60g acceleration (a) is conservatively applied to the BWR basket in the axial direction. The basket is evaluated using classical hand calculations. Factors of safety for the BWR basket are calculated based on the criteria for Service Level 'D' limits from ASME Code, Section III Subsection NG [7] and Appendix F [8]. Using a bounding weight of 24,000 pounds for the BWR basket, the maximum stress in the fuel tube is calculated. Conservatively assuming the entire basket weight is carried through the fuel tubes, the stress in the tube is as follows.

$$\sigma_{\text{tube}} = \frac{P_{\text{tube}}}{A} \approx 5.3 \text{ ksi}$$

where:

$$P_{\text{tube}} = \frac{W \times 60}{n} = \frac{24,000 \times 60}{45} = 32,000 \text{ lb}$$

W = 24,000 lb ----- Bounding basket weight

n = 45 ----- Number of fuel tubes

A = 6.1 inch<sup>2</sup> ----- Tube cross-sectional area

The factor of safety (FS) is as follows.

$$FS = \frac{0.7 \times S_u}{\sigma_{\text{tube}}} = \frac{0.7 \times 68.4}{5.3} = 9.03$$

where:

S<sub>u</sub> = 68.4 ksi ----- Ultimate strength, SA-537 Class 1, at 700°F

The weight of the fuel tubes is supported on connector pins. Referring to Figure 3.10.2-13, the interior tubes (Tube #4, typical) are supported by four connector pins; the side fuel tubes (Tube #1, typical) are supported by two connector pins and the side and corner weldments; and the corner fuel tubes (Tube #5, typical) are supported by three connector pins. The stress (σ) on the fuel tube is as follows.

$$\sigma = \frac{60 \times P_{\text{pin}}}{A_m} = \frac{60 \times 233}{0.34} = 41.1 \text{ ksi}$$

where:

$$A_m = 0.34 \text{ inch}^2 \text{----- Common area}$$

$$P_{pin} = \frac{1}{3}P_t + \frac{1}{4}P_t = 233 \text{ lb}$$

$$P_t = 400 \text{ lb ----- Tube weight}$$

The factor of safety (FS) is as follows.

$$FS = \frac{0.7 \times S_u}{\sigma_{brg}} = \frac{0.7 \times 68.4}{41.1} = 1.17$$

where:

$$S_u = 68.4 \text{ ksi ----- Ultimate strength, SA-537 Class 1, at } 700^\circ\text{F}$$

The weight of the side and corner weldments is carried through to the TSC base plate by supports at the bottom of the weldments. The corner weldment is bounding for the supports. The dimensions for the corner support weldment are 8.0 inches in length and 0.375-inch thickness. The bounding weight of the corner weldment is 1,100 pounds. The corner weldment also supports one-quarter of the weight of four fuel tubes (400 lb per tube, bounding). The membrane stress ( $\sigma_m$ ) is as follows.

$$\sigma_m = \frac{W_{sup}}{A_{sup}} = \frac{90,000}{3.0} = 30.0 \text{ ksi}$$

where:

$$W_{sup} = 60 \times (1,100 + 4 \times (0.25 \times 400)) = 90,000 \text{ lb}$$

$$A_{sup} = 8.0 \times 0.375 = 3.0 \text{ inch}^2$$

The factor of safety (FS) is as follows.

$$FS = \frac{0.7S_u}{\sigma_m} = \frac{0.7 \times 68.4}{30.0} = 1.60$$

where:

$$S_u = 68.4 \text{ ksi ----- Ultimate strength, SA-537 Class 1, at } 700^\circ\text{F}$$

The 76 basket connector pins support the BWR basket during a 60g bottom-end drop accident. The bounding temperature at the bottom of the basket is 500°F. The pins are subjected to

compressive loads; therefore, a buckling evaluation of the pins is presented as follows. The load on one connector pin ( $P_{pin}$ ) is as follows.

$$P_{pin} = \frac{W \times 60}{n} = \frac{24,000 \times 60}{76} = 18.9 \text{ kips}$$

where:

$$W = 24,000 \text{ lb} \text{----- Bounding basket weight}$$

$$n = 76 \text{----- Number of pins}$$

Using the Euler buckling theory, the critical buckling load ( $P_{cr}$ )

$$P_{cr} = \frac{\pi^2 EI}{(KL)^2} = \frac{\pi^2 \times (25.8 \times 10^6) \times 0.049}{(2 \times 3.0)^2} = 346.6 \text{ kip} \quad [9]$$

where:

$$A_{pin} = \frac{\pi}{4} D^2 = 0.78 \text{ inch}^2$$

$$D = 1.0 \text{ inch} \text{----- Pin Diameter}$$

$$L = 3.0 \text{ inches} \text{----- Pin Length}$$

$$I = \frac{\pi r^4}{4} = 0.049 \text{ inch}^4$$

$$K = 2.0 \text{----- Buckling constant, clamped-free}$$

$$E = 25.8 \times 10^6 \text{ psi} \text{----- Modulus of elasticity of SA-240 Type 304, at } 500^\circ\text{F}$$

The factor of safety (FS) for buckling of the hinge pins is as follows.

$$FS = \frac{P_{cr}}{P_{pin}} = \frac{346.6}{18.9} = \text{Large}$$

**BWR Neutron Absorber Evaluation**

During the end impact condition, the BWR neutron absorber and the weld post are subject to shearing force in the longitudinal direction of the neutron absorber. The neutron absorber is considered to be supported by two weld posts located at the bottom end of the neutron absorber.

The evaluation is conservatively performed for an acceleration of 60g at a bounding temperature of 350°F. The inertia load applied to the neutron absorber ( $F_{na}$ ) at each weld post during the end impact is as follows.

$$F_{na} = L \times W \times t \times \rho \times a / 2 = 272 \text{ lb}$$

where:

- $\rho = 0.1 \text{ lb/in}^3$  ----- Bounding density of the neutron absorber
- $a = 60\text{g}$ ----- End drop acceleration
- $t = 0.1 \text{ in}$  ----- Thickness of neutron absorber
- $L = 165 \text{ in}$ ----- Length of neutron absorber
- $W = 5.5 \text{ in}$  ----- Width of neutron absorber

The shearing capacity of the neutron absorber is as follows.

$$F_{\text{shear\_na}} = A_s \times \Phi_a = 0.15 \times 2260 = 339 \text{ lb}$$

where:

- $A_s = L_{\text{NA}} \times 1.414 \times 2 \times t = 0.15 \text{ in}^2$ ----- Shear area at both sides of each weld-post  
(at the 45° shear planes)
- $L_{\text{NA}} = 0.53 \text{ in}$ ----- Min. edge distance of the neutron absorber
- $\Phi_a = 0.42 S_u = 2.26 \text{ ksi}$ ----- Allowable shear stress
- $S_u = 5.38 \text{ ksi}$ ----- Tensile strength of neutron absorber at  
350°F

The factor of safety (FS) is as follows.

$$FS = F_{\text{shear\_na}} / F_{\text{na}} = 339 / 272 = 1.25$$

The strength of the weld posts is significantly higher than that of the neutron absorber. Therefore, no evaluation is required for the weld posts for the concrete cask 24-inch end-drop evaluation.

### 3.7.2.2.2 Concrete Cask Tip-over

The analysis results for the BWR basket subjected to a hypothetical concrete cask tip-over accident are presented in this section. Each basket component is evaluated in the following sections. Factors of safety for the BWR basket are calculated based on the criteria for Service Level 'D' limits from ASME Code, Section III, Subsection NG [7] and Appendix F [8].

#### BWR Fuel Tube Evaluation

The BWR basket fuel tubes are analyzed for a tip-over accident using the three-dimensional periodic plastic finite element models described in Section 3.10.2. The fuel tube is conservatively evaluated for a 35g side impact load.

Equivalent plastic stresses are calculated for the BWR fuel tubes for the 0° and 45° basket orientations (see Figure 3.10.2-13 and Figure 3.10.2-15 for tube IDs). The maximum primary

membrane and primary membrane plus bending stress intensity for each fuel tube are reported in Table 3.7.2-5. Note that for a plastic analysis, ANSYS reports stresses in the elastic region as the yield strength (35.4 ksi at 500°F).

The ANSYS plastic finite element model employs the material stress-strain curve and accounts for the inelastic behavior of the material. The stress allowables for plastic analysis are based on ASME Code, Section III, Appendix F [8]. The allowable primary membrane stress is  $0.7S_u$ . The allowable primary membrane plus bending stress intensity is  $0.9S_u$ . The minimum factors of safety for the fuel tubes are 1.12 (45° basket orientation) for membrane stresses and 1.17 (0° basket orientation) for primary membrane plus bending stresses. The critical stress locations occur in the fuel tube corners.

The fuel tubes are constructed by welding two tube halves together using a full penetration weld the length of the fuel tube. A root and final MT weld examination per ASME Code, Section III, Subsection NG-5232 is used when structural qualification of the weld joint is performed with a 0.75 weld quality factor (wf), per Table NG-3352-1. From the plastic analysis of the BWR basket, the maximum membrane and membrane plus bending stress intensity at the tube weld is 11.5 ksi and 35.4 ksi, respectively. The factors of safety (FS) for the weld are as follows.

Membrane:

$$FS = \frac{0.7S_u \times wf}{\sigma} = \frac{0.7 \times 68.4 \times 0.75}{11.5} = 3.12$$

Membrane plus bending:

$$FS = \frac{0.9S_u \times wf}{\sigma} = \frac{0.9 \times 68.4 \times 0.75}{35.4} = 1.30$$

where:

$$S_u = 68.4 \text{ ksi} \text{ ----- Ultimate strength, SA-537 Class 1, at } 700^\circ\text{F}$$

The pins react shear loads between adjacent tubes. From the finite element models, the maximum shear load (P) in the pin is 11,216 lb for the 0° basket orientation and 10,306 lb for the 45° basket orientation. The shear load is calculated by summing the nodal forces of the nodes in the pin slot on the tube adjacent to the tube to which the pin is welded. The forces are calculated in a localized coordinate system aligned with the corner flat on the fuel tube. Using a bounding load (P) of 15,000 lb, the shear stress in the pin is

$$\tau_{pin} = \frac{P}{D l_{pin}} = 26.3 \text{ ksi}$$

where:

$$D = 0.38 \text{ inch} \text{----- Pin diameter}$$
$$l_{\text{pin}} = 1.5 \text{ inch} \text{----- Half length of pin}$$

The factor of safety (FS) is as follows.

$$FS = \frac{0.42S_u}{\tau_{\text{pin}}} = 1.12$$

where:

$$S_u = 70.0 \text{ ksi} \text{----- Ultimate strength, SA-695 Type B Gr 40, at } 700^\circ\text{F}$$

The bearing stress ( $\sigma_{\text{brg}}$ ) on the pin is evaluated using the bounding load of 15,000 lb. The bearing area is determined based on a 30° contact arc between the pin and the fuel tube slot.

$$\sigma_{\text{brg}} = \frac{P}{LS} = 100.7 \text{ ksi}$$

where:

$$P = 15,000 \text{ lb} \text{----- Maximum load on pin}$$
$$L = 1.5 \text{ inch} \text{----- Length of pin in ANSYS model}$$
$$S = \pi D \frac{30}{360} = 0.10 \text{ in} \text{----- Bearing arc length}$$
$$D = 0.38 \text{ inch} \text{----- Pin diameter}$$

Per ASME Appendix F-1336, the allowable bearing stress is  $2.1S_u$ . The factor of safety (FS) is as follows.

$$FS = \frac{2.1S_u}{\sigma_{\text{brg}}} = 1.47$$

where:

$$S_u = 70.0 \text{ ksi} \text{----- Ultimate strength, SA-695 Type B Gr 40, at } 700^\circ\text{F}$$

### **BWR Neutron Absorber and Retainer**

The BWR neutron absorber and retainer are conservatively evaluated for a 60g side-impact load and for the concrete cask tip-over event. The retainer strip assembly consists of 304 stainless steel and is restrained by an array of posts welded to the inside surface of the fuel tube. Two



rows of post are separated 3.6 inches apart, and a spacing of 12 inches exists between the posts along the axial direction of the fuel tube.

The neutron absorber is supported by the retainer strip at the inside surface of the fuel tube. The pitches of the slotted holes in the neutron absorber are the same as the holes in the retainer strip through which the weld posts are connected to the fuel tube. The slotted holes are used to prevent interference during differential thermal expansion between the neutron absorber and the fuel tube. The head of the weld posts supporting the retainer strip are engaged in the recessed conical pockets of the retainer.

The finite element model for the BWR neutron absorber and retainer is similar to the model shown in Figure 3.7.2-3, with the exception of the spacing of the posts in the lateral direction and the axial direction. This resulted in minimal change to the finite element mesh used for the PWR model. Boundary conditions applied in the PWR model shown in Figure 3.7.2-3 were also applied to the BWR model. LS-DYNA was used to determine the dynamic response to a 60g loading, which was also used for the PWR design.

The results of the transient evaluations show that the maximum strain in the retainer for the BWR fuel is 2.5%, which is minimal, and is local to the conical-shaped hole. Since inelastic strains are not recovered, this indicates that maximum inelastic strain during the impact is also limited to 2.5 percent. Such a minimal strain level indicates that the conical pocket retains its configuration for the weld post to restrain the retainer. The final displacement of the retainer strip at the midpoint between the weld posts is computed to be 0.07 inch, which is consistent with the minimal plastic strain in the retainer. This also confirms that the retainer remains engaged with the weld post during and after the impact.

The peak force on the weld post determined from the analysis is 50 pounds. The shear area governs the capacity of the weld. The depth of the weld ( $h$ ) is 0.13 inch. The diameter of the weld post ( $D$ ) is 0.25 inch. The governing stress is the shear stress in the base material. The allowable shear stress for the accident condition is  $0.42S_u$ . The ultimate strength ( $S_u$ ) of the base material (SA240, Type 304) is 63,200 psi. The weld capacity,  $F_{cap}$ , is calculated as shown in the following.

$$\begin{aligned} F_{cap} &= 0.42 \times n \times S_u \times h \times BD \\ &= 0.42 \times 0.3 \times 63,200 \times 0.13 \times (3.1416 \times 0.25) \\ &= 813 \text{ lb} \end{aligned}$$

where:

$$n = 0.3 \text{ ----- The design factor per ASME Code, Section III, Subsection NG, Table NG-3352-1 for the intermittent plug weld employing a surface visual examination method per NG-5260.}$$

The factor of safety (FS) is as follows.

$$FS = \frac{813}{50} = 16$$

**BWR Corner Support Weldment Evaluation**

The BWR basket corner support weldment is analyzed for the tip-over accident using the three-dimensional periodic plastic finite element model and boundary conditions described in Section 3.10.2. The corner support weldment is comprised of two major components: the mounting plate, which is the vertical plate, and the side support plate, which are located on ten-inch centers.

The analysis results for the corner support weldment mounting plate are presented in Table 3.7.2-6 and Table 3.7.2-7. The maximum primary membrane plus bending stress intensity is compared to the primary membrane stress allowable. The minimum factor of safety for the corner support weldment is 1.34.

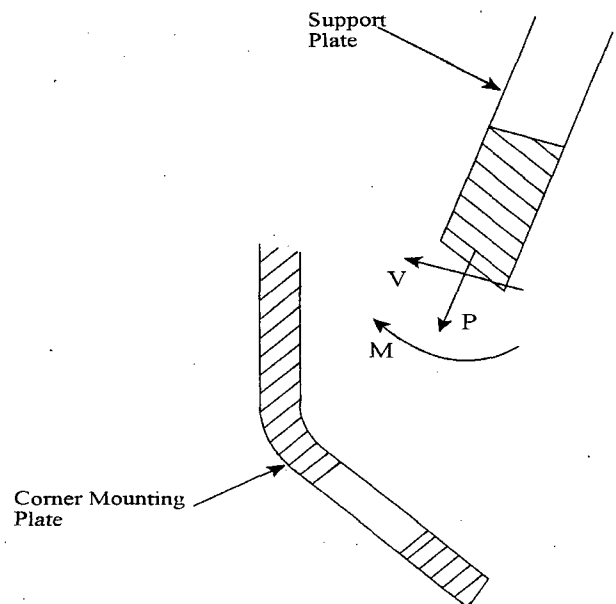
The center support plates are welded to the corner mounting plates with full-penetration welds. The welds have an inspection criteria per ASME Code, Section III, Subsection NG-5233, and a weld quality factor of 0.65. The maximum primary membrane plus bending stress intensity in the weld is 29.9 ksi. The factor of safety (FS) for the weld is as follows.

$$FS = \frac{0.65(S_u)}{\sigma_{weld}} = \frac{0.65 \times 68.4}{29.9} = 1.49$$

where:

$$S_u = 68.4 \text{ ksi, ---SA-537 Class 1, at } 700^\circ\text{F}$$

The support plate is welded to the corner mounting plate. The plate is welded to the wall cutout with two 5/16-inch groove welds on the sides of the plate using the visual inspection criteria per ASME Code, Section III, Subsection NG-5260, and a weld



quality factor of 0.35. The maximum loads in the plate weld consist of a bending moment of 9,838 in-lb, an axial force of 14,308 lb and a shear force of 1,993 lb. The weld stress intensity is

$$\sigma_{\text{weld}} = \sqrt{(S_b)^2 + 4\tau^2} = 11.3 \text{ ksi}$$

where:

$$S_b = \frac{9.8}{1.35} + \frac{14.3}{3.62} = 11.2 \text{ ksi}$$

$$\tau = \frac{2.0}{3.62} = 0.6 \text{ ksi}$$

$$S_w = h \times t_p \times t_w = 1.35 \text{ in}^2$$

$$A = 2 \times h \times t_w = 2 \times 5.8 \times 0.3125 = 3.62 \text{ in}^2$$

$$h = 5.8 \text{ inch} \text{----- Height of plate}$$

$$t_w = 5/16 \text{ inch} \text{----- Weld size}$$

$$t_p = 0.75 \text{ inch} \text{----- Plate thickness}$$

The factor of safety (FS) for the weld is as follows.

$$FS = \frac{0.35(S_u)}{\sigma_{\text{weld}}} = \frac{0.35 \times 68.4}{11.3} = 2.12$$

where:

$$S_u = 68.4 \text{ ksi} \text{----- Tensile strength, SA-537 Class 1, at 700°F}$$

### **BWR Side Support Weldment Evaluation**

The BWR basket side support weldment is analyzed for the tip-over accident using the three-dimensional periodic finite element model and boundary conditions described in Section 3.10.2. The analysis results for the side support weldment are presented in Table 3.7.2-8. The maximum primary membrane plus bending stress intensity is conservatively compared to the primary membrane stress allowable. The minimum factor of safety for the side support weldment is 1.34.

### **BWR Side and Corner Weldment / Fuel Tube Attachment Evaluation**

The corner and side support weldments are the primary structure that maintains the geometry of the fuel tube array during a hypothetical tip-over accident. The support weldments are bolted to the fuel tubes at 12 circumferential locations. The boss and bolt connection is designed so that the bolts are only loaded in tension, including preload. Otherwise, the support weldments apply a bearing load on the fuel tube array.

During a hypothetical concrete cask tip-over accident, the maximum tensile load on a bolt is 4,641 lb (0° basket model). Combining this load with the bolt preload (400 lb), the tensile load (P) on the bolt is 5,041 pounds.

The bolt thread is a 5/8-11 UNC and the length of engagement is a minimum of 0.38 inch. The bolt material is SA-193 Grade B6 stainless steel. From Machinery's Handbook [12], the ultimate stress in the bolt ( $\sigma_t$ ) is as follows.

$$\sigma_t = \frac{P}{A_t} = \frac{5.04}{0.23} = 21.9 \text{ ksi}$$

where:

$$A_t = 0.7854 \left( D - \frac{0.9743}{n} \right)^2 = 0.23 \text{ inch}^2 \quad [12]$$

$$D = 0.625 \text{ inch}$$

$$n = 11$$

The factor of safety (FS) is as follows.

$$FS = \frac{S_y}{\sigma_t} = 3.20$$

where:

$$S_y = 70.0 \text{ ksi} \text{ ----- Yield strength for SA 193, Gr B6, at } 700^\circ\text{F}$$

The shear stress in the bolt thread ( $\tau_{\text{bolt}}$ ) is as follows.

$$\tau_{\text{bolt}} = \frac{P}{A_s} = \frac{5.04}{0.370} = 13.3 \text{ ksi}$$

where:

$$A_s = 3.1416nL_e K_{n \max} \left[ \frac{1}{2n} + 0.57735(E_{s \min} - K_{n \max}) \right] = 0.379 \text{ inch}^2 \quad [12]$$

$$L_e = 0.38 \text{ inch}$$

$$K_{n \max} = 0.546$$

$$E_{s \min} = 0.5589$$

$$n = 11$$

The factor of safety (FS) is as follows.

$$FS = \frac{0.42S_u}{\tau_{\text{bolt}}} = 2.86$$

where:

$$S_u = 90.6 \text{ ksi} \text{ ----- Ultimate strength for SA 193, Gr B6, at } 700^\circ\text{F}$$

The shear stress in the boss thread ( $\tau_{\text{boss}}$ ) is as follows.

$$\tau_{\text{boss}} = \frac{P}{A_n} = \frac{5.04}{0.541} = 9.3 \text{ ksi}$$

where:

$$A_n = 3.1416nL_e D_{s \text{ min}} \left[ \frac{1}{2n} + 0.57735(D_{s \text{ min}} - E_{n \text{ max}}) \right] = 0.541 \text{ inch}^2 [12]$$

$$L_e = 0.38 \text{ inch}$$

$$E_{n \text{ max}} = 0.5732$$

$$D_{s \text{ min}} = 0.6113$$

$$n = 11$$

The factor of safety (FS) is as follows.

$$FS = \frac{0.42S_u}{\tau_{\text{bolt}}} = 3.16$$

where:

$$S_u = 70.0 \text{ ksi} \text{ ----- Ultimate strength, SA-695 Type B, Gr 40, at } 700^\circ\text{F}$$

The boss is welded into the fuel tube with a 3/16-inch groove weld. The weld uses the visual inspection criteria per ASME Code, Section III, Subsection NG, Article NG-5260 and a quality factor of 0.35. The weld is evaluated using a bounding bolt load (P) of 5.04 kips. For the corner weldment, the shear stress in the boss weld ( $\tau_{\text{weld}}$ ) is as follows.

$$\tau_{\text{weld}} = \frac{P}{A_w} = \frac{5.04}{0.81} = 6.2 \text{ ksi}$$

where:

$$A_w = \pi D t_{\text{weld}} = \pi \times 1.38 \times 0.1875 = 0.81 \text{ in}^2$$

$$D = 1.38 \text{ inch} \text{ ----- Boss Diameter}$$

For the side weldment, the shear stress in the boss weld ( $\tau_{\text{weld}}$ ) is as follows.

$$\tau_{\text{weld}} = \frac{P}{A_w} = \frac{5.04}{0.59} = 8.5 \text{ ksi}$$

where:

$$A_w = \pi D t_{\text{weld}} = \pi \times 1.00 \times 0.1875 = 0.59 \text{ in}^2$$

$$D = 1.00 \text{ inch} \text{----- Boss Diameter}$$

Using the lesser of SA-537 Class 1 and SA-695 Type B, Gr 40  $S_u$  allowable, the minimum factor of safety (FS) is as follows.

$$FS = \frac{0.35 \times 0.42 S_u}{\tau_{\text{weld}}} = 1.18$$

where:

$$S_u = 68.4 \text{ ksi} \text{----- Ultimate strength, SA-537 Class 1, at } 700^\circ\text{F}$$

The washers under the bolts are subjected to a bending load due to the preload. Using a bounding bolt load (5,100 lb) and a minimum washer thickness (3/16 inch), the maximum bending moment ( $M_t$ ) in the washer is calculated to be 167 in-lb.

The stress in the washer is as follows.

$$\sigma = \frac{6M_t}{t^2} = \frac{6 \times 0.167}{0.1875^2} = 27.8 \text{ ksi}$$

where:

$$t = 3/16 \text{ inch} \text{----- Thickness of washer}$$

The factor of safety (FS) is as follows.

$$FS = \frac{S_u}{\sigma} = \frac{63.2}{27.8} = 2.27$$

where:

$$S_u = 63.2 \text{ ksi} \text{----- Ultimate Strength, SA-240 Type 304, at } 700^\circ\text{F}$$

The maximum shear load in the bosses for side support weldment attachment ( $P_1$ ) is 2.07 kip ( $0^\circ$  basket orientation). The maximum shear load in the corner support weldment ( $P_2$ ) is 5.95 kip.

For the side weldment boss, the shear stress in the boss ( $\tau_{\text{boss}}$ ) is as follows.

$$\tau_{\text{boss}} = \frac{P_1}{A} = \frac{2.07}{0.47} = 4.4 \text{ ksi}$$

where:

$$A = \frac{\pi}{4}(D_o^2 - D_i^2) = 0.47 \text{ inch}^2$$
$$D_o = 1.00 \text{ inch}$$
$$D_i = 0.63 \text{ inch}$$

The factor of safety (FS) is as follows.

$$FS = \frac{0.42S_u}{\tau_{boss}} = 6.68$$

where:

$$S_u = 70.0 \text{ ksi} \text{ ----- Ultimate strength, SA-695 Type B, Gr 40, at } 700^\circ\text{F}$$

For the corner weldment boss, the shear stress in the boss ( $\tau_{boss}$ ) is as follows.

$$\tau_{boss} = \frac{P_2}{A} = \frac{5.95}{1.17} = 5.09 \text{ ksi}$$

where:

$$A = \frac{\pi}{4}(D_o^2 - D_i^2) = 1.17 \text{ inch}^2$$
$$D_o = 1.375 \text{ inch}$$
$$D_i = 0.63 \text{ inch}$$

The factor of safety (FS) is as follows.

$$FS = \frac{0.42S_u}{\tau_{boss}} = 5.78$$

where:

$$S_u = 70.0 \text{ ksi} \text{ ----- Ultimate strength, SA-695 Type B, Gr 40, at } 700^\circ\text{F}$$

Loads between the fuel tube array and the corner and side weldments are reacted out in shear and bearing in the support weldments. Bearing stresses are not considered for accident events. Due to the geometry of the basket, the cutout in the corner support weldments has an edge distance less than two times the diameter of the cutout. The shear stress in the corner weldment mounting plate is as follows.

$$\tau = \frac{P_2}{A_{\text{shear}}} = \frac{5.95}{1.14} = 5.2 \text{ ksi}$$

where:

$$A_{\text{shear}} = 2 \left[ \frac{L_{\text{ed}}}{\sin 45^\circ} t_{\text{plate}} \right] = 1.14 \text{ inch}^2$$

$L_{\text{ed}} = 1.30 \text{ inch}$  ----- Boss edge distance

$t_{\text{plate}} = 0.31 \text{ inch}$  ----- Mounting plate thickness

The factor of safety (FS) is as follows.

$$FS = \frac{0.42S_u}{\tau} = 5.52$$

where:

$S_u = 68.4 \text{ ksi}$  ----- Ultimate strength, SA-537 Class 1, at 700°F

### **BWR Basket Buckling Evaluation**

The buckling evaluation of the BWR basket is an evaluation of a side of the fuel tube per NUREG/CR-6322 [9]. Using the plastic finite element model, the critical buckling of a fuel tube occurs in the 0° basket orientation (Tube 24, Figure 3.10.2-13). The applied loads on a side of the fuel tube are 15.9 kip axial compression and 4.2 inch-kip bending moment.

The factor of safety is calculated based on the interaction Equations 31 and 32 in NUREG/CR-6322. These two equations adopt the “Limit Analysis Design” approach for structural members subjected to stresses beyond the yield limit of the material. Methodology and equations for the buckling evaluation are the same as those presented in Section 3.7.2.1.2 for the PWR basket.

For the BWR basket fuel tube, the following parameters are used in the buckling evaluation.

$t = 0.25 \text{ inch}$  ----- Tube thickness

$b = 10.00 \text{ inches}$  ----- Unit thickness

$l = 5.34 \text{ inches}$  ----- Sidewall length

$K = 0.80$  ----- Effective length factor

$E = 27.3 \times 10^6 \text{ psi}$  ----- SA-537 Class 1, at 700°F

$S_y = 35.4 \text{ ksi}$  ----- Yield strength, SA-537 Class 1, at 700°F

For  $P = 15.9 \text{ kip}$  and  $M = 4.2 \text{ inch-kip}$  (Tube 24, 0° basket orientation)

$$P_1 = \frac{P}{P_{\text{cr}}} = 0.17$$



$$M_1 = \frac{C_m M}{\left(1 - \frac{P}{P_e}\right) M_m} = 0.73$$

$$P_2 = \frac{P}{P_y} = 0.18$$

$$M_2 = \frac{M}{1.18} M_p = 0.64$$

The factors of safety are as follows.

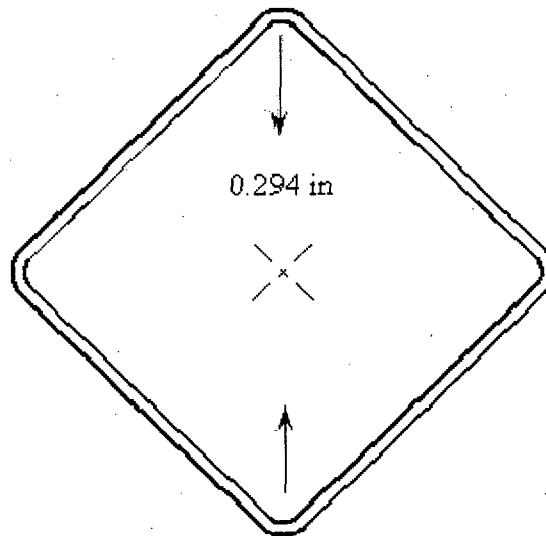
$$FS_1 = \frac{1}{P_1 + M_1} = 1.11$$

$$FS_2 = \frac{1}{P_2 + M_2} = 1.22$$

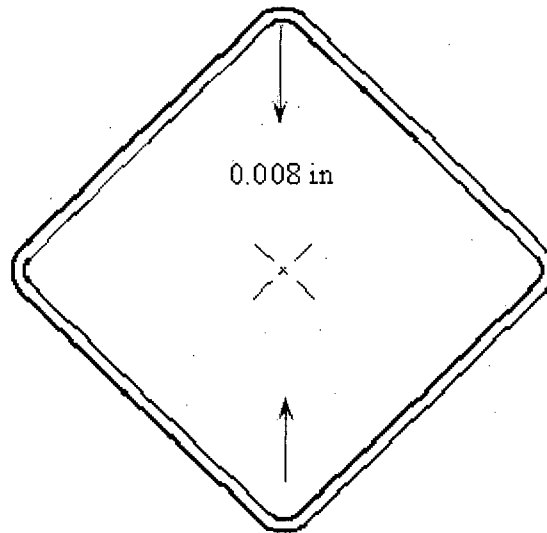
### **BWR Basket Displacement**

The nominal dimensions of the fuel tube opening for the BWR basket is 5.86 in × 5.86 in for the manufactured fuel tubes and 5.77 in × 5.77 in for the developed fuel slot formed by four adjacent fuel tubes. The maximum width of a BWR fuel assembly is 5.52 inches. Based on the quasi-static analysis results using the three-dimensional periodic plastic models for the cask tip-over accident, the minimum clearance between the fuel assembly and the fuel tube is 0.28 inch for the manufactured tubes and 0.16 inch for the developed tubes during the 35-g side impact loading. As presented in Section 3.10.7, a three-dimensional half-symmetry model for a BWR fuel tube is constructed using the LS-DYNA program to calculate the maximum displacement of the fuel tube as function of time due to the side impact loading for the cask tip-over accident. The LS-DYNA analysis consider a displacement loading based on the maximum diagonal displacement of the fuel tubes during the impact (see Figure 3.7.2-2) from the LS-DYNA analysis presented in Section 3.10.6. The permanent displacement in the tube diagonal direction, after the impact, is calculated to be 0.004 inch, which is less than the minimum clearance between the fuel assembly and the tube.

Figure 3.7.2-1 PWR Basket Fuel Tube Displacement for Tip-Over Accident

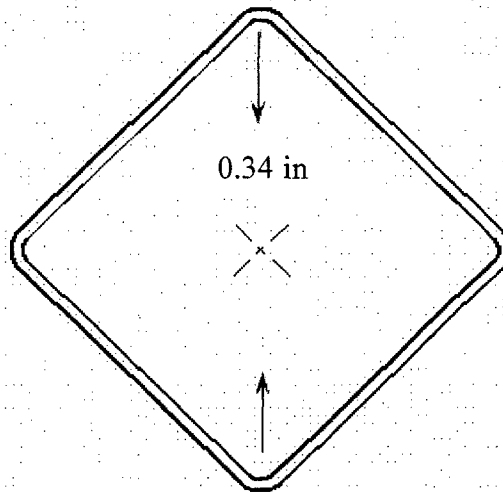


Maximum Diagonal Displacement During Impact

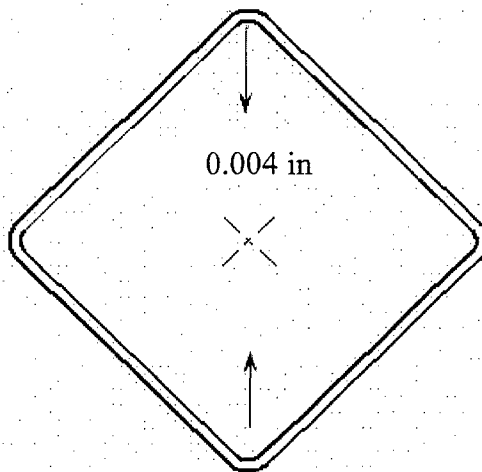


Maximum Diagonal Displacement After Impact

Figure 3.7.2-2 BWR Basket Fuel Tube Displacement for Tip-Over Accident



Maximum Diagonal Displacement During Impact



Maximum Diagonal Displacement After Impact

Figure 3.7.2-3 PWR Neutron Absorber and Retainer Finite Element Model

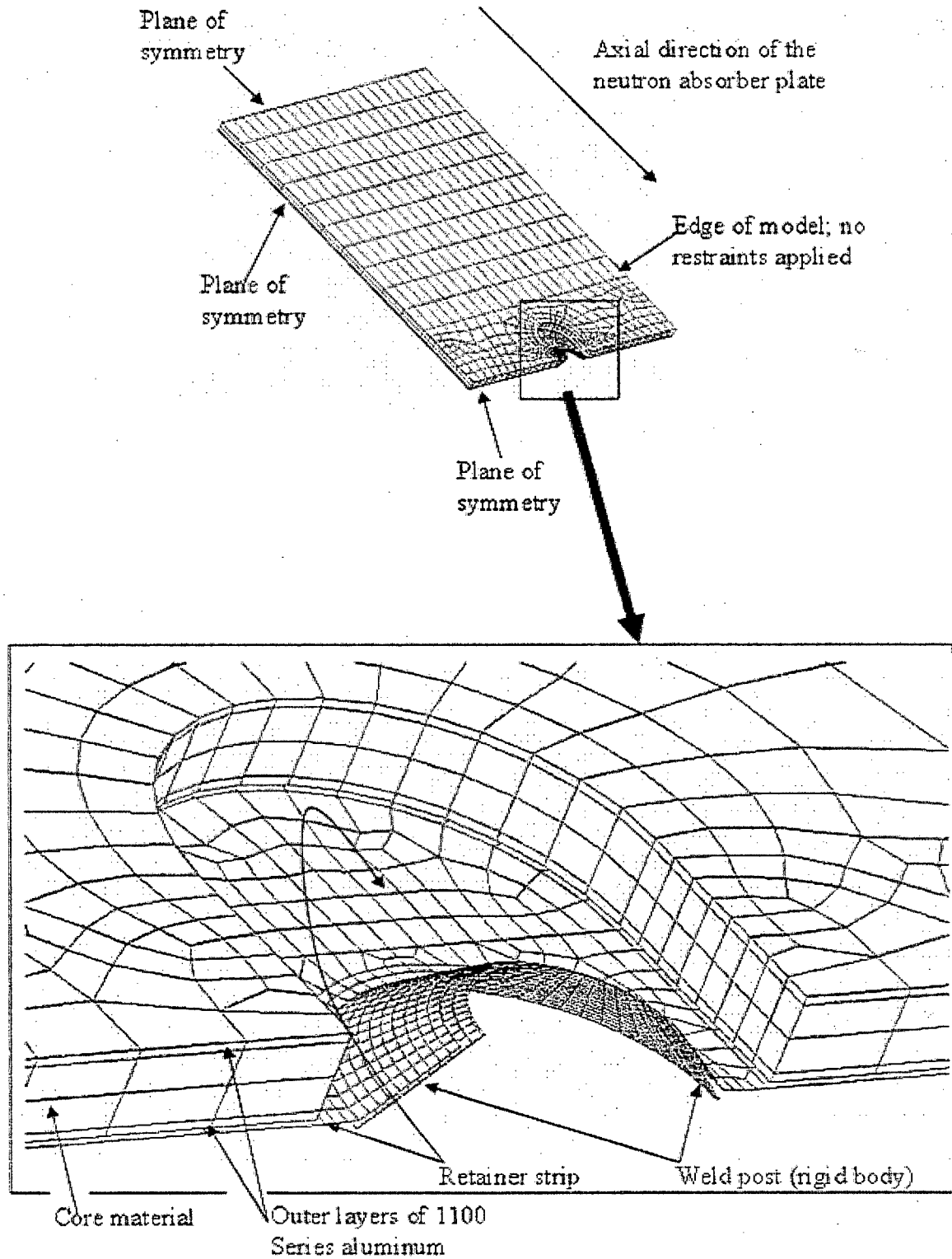


Table 3.7.2-1 PWR Fuel Tube Stress Intensity – Concrete Cask Tip-over Accident

| Tube <sup>a</sup> | Basket (deg) | P <sub>m</sub> (ksi) |                    |      | Tube <sup>a</sup> | Basket (deg) | P <sub>m</sub> + P <sub>b</sub> (ksi) |                    |      |
|-------------------|--------------|----------------------|--------------------|------|-------------------|--------------|---------------------------------------|--------------------|------|
|                   |              | S                    | S <sub>allow</sub> | FS   |                   |              | S                                     | S <sub>allow</sub> | FS   |
| 3                 | 45           | 41.2                 | 47.67              | 1.16 | 11                | 0            | 43.8                                  | 61.29              | 1.40 |
| 7                 | 45           | 41.1                 | 47.67              | 1.16 | 10                | 0            | 43.5                                  | 61.29              | 1.41 |
| 10                | 45           | 41.1                 | 47.67              | 1.16 | 6                 | 0            | 43.0                                  | 61.29              | 1.43 |
| 6                 | 45           | 41.1                 | 47.67              | 1.16 | 7                 | 0            | 42.8                                  | 61.29              | 1.43 |
| 9                 | 45           | 41.0                 | 47.67              | 1.16 | 8                 | 0            | 41.9                                  | 61.29              | 1.46 |
| 11                | 0            | 41.0                 | 47.67              | 1.16 | 12                | 45           | 38.7                                  | 61.29              | 1.58 |
| 8                 | 0            | 40.9                 | 47.67              | 1.17 | 9                 | 0            | 38.2                                  | 61.29              | 1.60 |
| 4                 | 45           | 40.9                 | 47.67              | 1.17 | 12                | 0            | 38.0                                  | 61.29              | 1.61 |
| 12                | 0            | 40.9                 | 47.67              | 1.17 | 6                 | 45           | 37.3                                  | 61.29              | 1.64 |
| 11                | 45           | 40.9                 | 47.67              | 1.17 | 10                | 45           | 37.9                                  | 61.29              | 1.62 |

<sup>a</sup> See Figure 3.10.1-13 and Figure 3.10.1-15 for tube locations for 0° and 45° basket orientations, respectively.

**Table 3.7.2-2 PWR Corner Weldment Mounting Plate Stress Intensity – Concrete Cask Tip-over Accident**

| Basket | S (ksi)           | S <sub>allow</sub> (ksi) | FS   |
|--------|-------------------|--------------------------|------|
| 0°     | 35.4 <sup>a</sup> | 47.88                    | 1.35 |
| 45°    | 35.8 <sup>b</sup> | 47.88                    | 1.34 |

**Table 3.7.2-3 PWR Corner Support Bar Stress Intensity – Concrete Cask Tip-over Accident**

| Basket | S (ksi)           | S <sub>allow</sub> (ksi) | FS   |
|--------|-------------------|--------------------------|------|
| 0°     | 21.0 <sup>c</sup> | 47.88                    | 2.28 |
| 45°    | 17.2 <sup>d</sup> | 47.88                    | 2.78 |

**Table 3.7.2-4 PWR Side Weldment Stress Intensity – Concrete Cask Tip-over Accident**

| Basket | S (ksi)           | S <sub>allow</sub> (ksi) | FS   |
|--------|-------------------|--------------------------|------|
| 0°     | 35.4 <sup>e</sup> | 47.88                    | 1.35 |
| 45°    | 35.4 <sup>f</sup> | 47.88                    | 1.35 |

- <sup>a</sup> Maximum stress occurs at location 18 of Figure 3.10.1-17.
- <sup>b</sup> Maximum stress occurs at location 25 of Figure 3.10.1-18.
- <sup>c</sup> Maximum stress occurs at location 24 of Figure 3.10.1-17.
- <sup>d</sup> Maximum stress occurs at location 20 of Figure 3.10.1-18.
- <sup>e</sup> Maximum stress occurs at location 12 of Figure 3.10.1-19.
- <sup>f</sup> Maximum stress occurs at location 14 of Figure 3.10.1-20.

**Table 3.7.2-5 BWR Fuel Tube Stress Intensity – Concrete Cask  
Tip-over Accident**

| Tube <sup>a</sup> | Basket (deg) | P <sub>m</sub> (ksi) |                    |      | Tube | Basket (deg) | P <sub>m</sub> + P <sub>b</sub> (ksi) |                    |      |
|-------------------|--------------|----------------------|--------------------|------|------|--------------|---------------------------------------|--------------------|------|
|                   |              | S                    | S <sub>allow</sub> | FS   |      |              | S                                     | S <sub>allow</sub> | FS   |
| 8                 | 45           | 42.8                 | 47.88              | 1.12 | 21   | 0            | 52.5                                  | 61.56              | 1.17 |
| 18                | 45           | 42.0                 | 47.88              | 1.14 | 25   | 0            | 47.7                                  | 61.56              | 1.29 |
| 13                | 45           | 41.7                 | 47.88              | 1.15 | 8    | 45           | 47.1                                  | 61.56              | 1.31 |
| 23                | 45           | 41.2                 | 47.88              | 1.16 | 23   | 0            | 42.2                                  | 61.56              | 1.46 |
| 12                | 45           | 41.2                 | 47.88              | 1.16 | 20   | 0            | 42.2                                  | 61.56              | 1.46 |
| 5                 | 45           | 41.2                 | 47.88              | 1.16 | 18   | 45           | 41.9                                  | 61.56              | 1.47 |
| 21                | 0            | 41.1                 | 47.88              | 1.16 | 23   | 45           | 41.6                                  | 61.56              | 1.48 |
| 24                | 45           | 41.1                 | 47.88              | 1.16 | 15   | 0            | 41.6                                  | 61.56              | 1.48 |
| 23                | 0            | 41.0                 | 47.88              | 1.17 | 24   | 0            | 41.6                                  | 61.56              | 1.48 |
| 25                | 0            | 41.0                 | 47.88              | 1.17 | 19   | 0            | 41.2                                  | 61.56              | 1.49 |

**Table 3.7.2-6 BWR Corner Weldment Mounting Plate Stress Intensity – Concrete Cask  
Tip-over Accident**

| Basket | S (ksi)           | S <sub>allow</sub> (ksi) | FS   |
|--------|-------------------|--------------------------|------|
| 0°     | 35.6 <sup>b</sup> | 47.88                    | 1.34 |
| 45°    | 35.7 <sup>c</sup> | 47.88                    | 1.34 |

**Table 3.7.2-7 BWR Corner Support Plate Stress Intensity – Concrete Cask Tip-over  
Accident**

| Basket | S (ksi)           | S <sub>allow</sub> (ksi) | FS   |
|--------|-------------------|--------------------------|------|
| 0°     | 35.7 <sup>d</sup> | 47.88                    | 1.34 |
| 45°    | 35.5 <sup>e</sup> | 47.88                    | 1.35 |

- <sup>a</sup> See Figure 3.10.2-13 and Figure 3.10.2-15 for tube locations for 0° and 45° basket orientations, respectively.
- <sup>b</sup> Maximum stress occurs at location 36 of Figure 3.10.2-17
- <sup>c</sup> Maximum stress occurs at location 36 of Figure 3.10.2-18.
- <sup>d</sup> Maximum stress occurs at the plate cut-out near location 36 of Figure 3.10.2-17.
- <sup>e</sup> Maximum stress occurs at the plate cut-out near location 28 of Figure 3.10.2-18.

**Table 3.7.2-8 BWR Side Weldment Stress Intensity – Concrete Cask Tip-over Accident**

| Basket | S (ksi)           | S <sub>allow</sub> (ksi) | FS   |
|--------|-------------------|--------------------------|------|
| 0°     | 35.5 <sup>a</sup> | 47.88                    | 1.35 |
| 45°    | 35.8 <sup>b</sup> | 47.88                    | 1.34 |

<sup>a</sup> Maximum stress occurs at location 8 of Figure 3.10.2-19.

<sup>b</sup> Maximum stress occurs at location 6 of Figure 3.10.2-20.



**3.7.3 Concrete Cask Evaluation for Storage Accident Events**

Structural evaluation of the concrete is performed for accident events, including the extreme temperature events (133°F ambient), tornado and tornado-driven missiles, flood, earthquake, concrete cask 24-inch drop and the tip-over accident.

**3.7.3.1 Concrete Cask Thermal Stresses**

Using the finite element model presented in Section 3.10.4, a structural evaluation of the concrete cask for accident thermal loads was performed. The analysis considered a temperature profile corresponding to the accident thermal condition (133°F ambient). The following summarizes the critical thermal stresses for accident events.

| Component             | Stress (ksi) |
|-----------------------|--------------|
| Circumferential Rebar | 16.6         |
| Vertical Rebar        | 20.2         |
| Concrete, Compression | 1.0          |
| Concrete, Tension     | 0.1          |

**3.7.3.2 Tornado and Tornado-Driven Missiles**

This section evaluates the strength and stability of the concrete cask for a maximum tornado wind loading and for the impacts of tornado-driven missiles. It also demonstrates that the concrete cask remains stable in tornado wind loading in conjunction with an impact from a high-energy tornado missile.

Concrete cask stability analysis for the maximum tornado wind loading is based on NUREG-0800, Section 3.3.1, "Wind Loadings," and Section 3.3.2, "Tornado Loadings," [16]. Loads due to tornado-driven missiles are based on NUREG-0800, Section 3.5.1.4, "Missiles Generated by Natural Phenomena."

The concrete cask stability in a maximum tornado wind is evaluated based on the design wind pressure calculated in accordance with ANSI/ASCE 7-93, [17] and using classical free body stability analysis methods.

Local damage to the concrete shell is assessed using a formula developed in NSS 5-940.1 [18]. This formula predicts the depth of missile penetration and minimum concrete thickness requirements to prevent scabbing of the concrete.

The local shear strength of the concrete shell is evaluated on the basis of ACI 349-85, Section 11.11.2.1 [5], without considering the reinforcing steel and the steel liner. The concrete shell shear capacity is also evaluated for missile loading using ACI 349-85, Section 11.7.

**Tornado Wind Loading**

The tornado wind velocity is transformed into an effective pressure applied to the concrete cask using procedures in ANSI/ASCE 7-93, "Building Code Requirements for Minimum Design Loads in Buildings and Other Structures" [17]. The maximum pressure (q) is determined from the maximum tornado wind velocity as follows:

$$q = (0.00256)(K \times I \times V)^2 \text{ lb/ft}^2 = (0.00256)(360)^2 \times 180 = 331.8 \text{ psf}$$

where:

- V = 360 mph ----- Maximum tornado wind speed
- K = 1.0 ----- Terrain effect
- I = 1.0 ----- Importance factor

Considering that the concrete cask is small with respect to the tornado radius, the velocity pressure is assumed uniform over the projected area of the concrete cask. Because the concrete cask is vented, the tornado-induced pressure drop is equalized from inside to outside and has no effect on the concrete cask structure. The total wind loading (F<sub>w</sub>) on the projected area of the concrete cask is computed as follows.

$$F_w = q \times G \times C_f \times A_p = 36,003 \text{ lb} \approx 36,100 \text{ lb}$$

where:

- q = 331.8 lb/ft<sup>2</sup> ----- Maximum pressure
- C<sub>f</sub> = 0.51 ----- Force coefficient (ASCE 7-93)
- A = H × D<sub>o</sub> = 30,637 inch<sup>2</sup> = 212.7 ft<sup>2</sup> ----- Projected area
- H = 225.27 inch ----- Concrete cask height
- D<sub>o</sub> = 136.0 inch ----- Concrete cask outer diameter
- G = 1.0 ----- Gust factor

The wind overturning moment (M<sub>w</sub>) is as follows.

$$M_w = F_w \times \frac{H}{2} = 4,066,123 \text{ inch-lb} = 3.38 \times 10^5 \text{ ft-lb}$$

The stability moment (M<sub>s</sub>) of the concrete cask (with the TSC, basket and no fuel load) about the edge of the base is as follows.

$$M_s = W_{cc} \times \frac{D_o}{2} = 14.72 \times 10^6 \text{ inch-lb} = 1.23 \times 10^6 \text{ ft-lb}$$

where:

- D<sub>o</sub> = 128.0 inch ----- Concrete cask base plate diameter

$W_{cc} = 230,000 \text{ lb}$  ----- Minimum concrete cask loaded weight.  
Conservatively defined as the concrete cask empty weight for evaluation of external loads.

ASCE 7-93 requires that the overturning moment due to wind load shall not exceed two-thirds of the dead load stabilizing moment unless the structure is anchored. Therefore, the factor of safety (FS) against overturning is as follows.

$$FS = \frac{0.67M_s}{M_w} = 2.44$$

The stresses in the concrete due to the tornado wind load are conservatively calculated. The concrete cask is considered to be fixed at its base. The stresses in the concrete are as follows.

$$\sigma_{outer} = \frac{M_{max} c_{outer}}{I} = 19.1 \text{ psi (tension or compression)}$$

$$\sigma_{inner} = \frac{M_{max} c_{inner}}{I} = 11.7 \text{ psi (tension or compression)}$$

where:

$$D_o = 136.0 \text{ inches}$$

$$D_i = 82.98 \text{ inches}$$

$$H = 225.27 \text{ inches}$$

$$A = \frac{\pi(D_o^2 - D_i^2)}{4} = 9,119 \text{ inch}^2$$

$$I = \frac{\pi(D_o^4 - D_i^4)}{64} = 14.47 \times 10^6 \text{ inch}^4$$

$$M_{max} = \frac{F_w \times H}{2} = 4.07 \times 10^6 \text{ lb-inch}$$

$$c_{outer} = 136.0/2 = 68.0 \text{ inches}$$

$$c_{inner} = 82.98/2 = 41.49 \text{ inches}$$

### **Tornado Missiles**

The concrete cask is designed to withstand the effects of impacts associated with postulated tornado-driven missiles identified in NUREG-0800 [16], Section 3.5.1.4.III.4, Spectrum I missiles. These missiles are listed as follows.

- A massive high kinetic-energy missile (4,000 lb automobile, with a frontal area of 20 square feet that deforms on impact).
- A 280 lb, 8.0-inch-diameter armor piercing artillery shell.

- A 1.0-inch-diameter solid steel sphere.

All of these missiles are assumed to impact in a manner that produces the maximum damage at a velocity of 126 mph (35% of the maximum tornado wind speed of 360 mph). The concrete cask is evaluated for impact effects associated with each of the previously listed missiles.

The concrete cask has no openings except for the four air outlets at the top and four air inlets at the bottom. The outlets are configured such that a one-inch diameter solid steel missile cannot directly enter the concrete cask interior. Additionally, the basket is protected by the TSC closure lid. The TSC is protected from small missiles entering the inlets by the pedestal plate; therefore, a detailed analysis of the impact of a one-inch diameter steel missile is not required.

**Concrete Shell Local Damage (Penetration Missile)**

Local damage to the concrete cask body is assessed by using the methodology presented by NSS 5-940.1 [18]. This method predicts the depth of penetration and minimum concrete thickness requirements to prevent scabbing. Penetration depths calculated by using this formula have been shown to provide reasonable correlation with test results. The penetration depth is as follows.

$$x = \left[ 4KNW(d^{-0.8} \left( \frac{V}{1000} \right)^{1.8} \right]^{0.5} = 5.82 \text{ inch}$$

where:

- d = 8.0 inch ----- Missile diameter
- K = 180/(f<sub>c</sub>')<sup>1/2</sup> = 2.92 ----- Coeff. depending on concrete strength
- N = 1.14 ----- Shape factor for sharp nosed missiles
- W = 280 lb ----- Missile weight
- V = 126 mph = 185 ft/sec ----- Missile velocity
- f<sub>c</sub>' = 3,800 psi ----- Concrete compressive strength at conservative 300°F

The minimum concrete shell thickness to prevent scabbing is three times the penetration depth (17.46 inch). The thickness of the concrete shell is 26.51 inches. The factor of safety (FS) is as follows.

$$FS = \frac{26.51}{17.46} = 1.52$$

Note that the steel liner and rebar of the concrete cask is conservatively ignored in the previously listed evaluation.

**Closure Plate Local Damage (Penetration Missile)**

The concrete cask is closed with a 6.75-inch deep lid assembly. The top plate is 3/4-inch carbon steel with a carbon steel clad disk of concrete 5.75-inches deep. In this evaluation, only the steel plate is considered to withstand the impact of the 280-lb armor-piercing missile, impacting at 126 mph. The perforation thickness (T) of the closure steel plate is calculated by using the methodology presented in BC-TOP-9A [19].

$$T = \frac{\left( \frac{m_m V_s^2}{2} \right)^{2/3}}{672D} = 0.52 \text{ inch}$$

where:

- $m_m = 280 \text{ lb}/32.174 \text{ ft/sec}^2$  ----- 8.70 slugs (lb-sec<sup>2</sup>/ft) missile mass
- $V_s = 185 \text{ ft/sec}$  ----- Missile velocity
- $D = 8 \text{ inch}$ ----- Missile diameter

The report recommends that the plate thickness be 25% greater than the calculated perforation thickness (T) to prevent perforation. The recommended plate thickness is as follows.

$$T = 1.25 \times 0.52 = 0.65 \text{ inch}$$

The factor of safety (FS) is as follows.

$$FS = \frac{0.75}{0.65} = 1.15$$

**High-Energy Missile Impact Damage Prediction**

The concrete cask is a freestanding structure. Therefore, the principal consideration in overall damage response is the potential for overturning the concrete cask as a result of the high-energy missile impact. From the principle of conservation of momentum, the impulse of the force from the missile impact on the concrete cask must equal the change in angular momentum of the concrete cask. Also, the impulse force due to the impact of the missile must equal the change in linear momentum of the missile. These relationships may be expressed as follows:

Change in momentum of the missile, during the deformation phase

$$\int_{t_1}^{t_2} (F)(dt) = m_m (v_2 - v_1)$$

where:

- F ----- Impact impulse force on missile

|   |       |   |
|---|-------|---|
| $m_m = 4,000 \text{ lb/g} = 124 \text{ slugs}/12 = 10.4 \text{ (lb sec}^2 \text{ /inch)}$ | ----- | Missile mass                            |
| $t_1$   | ----- | Time at missile impact                  |
| $t_2$   | ----- | Time at conclusion of deformation phase |
| $v_1 = 126 \text{ mph} = 185 \text{ ft/sec}$  | ----- | Missile velocity at impact              |
| $v_2$   | ----- | Velocity of missile at time $t_2$       |

The change in angular momentum of the concrete cask, about the bottom outside edge/rim, opposite the side of impact is as follows.

$$\int_{t_1}^{t_2} M_c (dt) = \int_{t_1}^{t_2} (H)(F)(dt) = I_m (\omega_1 - \omega_2)$$

Substituting,

$$\int (F)(dt) = m_m (v_2 - v_1) = \frac{I_m (\omega_1 - \omega_2)}{H}$$

where:

|  |       |   |
|--|-------|---|
| $M_c$  | ----- | Moment of the impact force on the concrete cask                                 |
| $I_m$  | ----- | Concrete cask mass moment of inertia, about point of rotation on the bottom rim |
| $\omega_1$   | ----- | Angular velocity at time $t_1$  |
| $\omega_2$   | ----- | Angular velocity at time $t_2$  |
| $m_c = 230,000/32.174 = 7,149 \text{ slugs}/12 = 596 \text{ lb sec}^2 \text{ /inch}$ | ----- | Mass of concrete cask   |
| $I_{mx} = 1/12(m_c)(3r^2 + H^2) = 3.21 \times 10^6 \text{ lb-sec}^2\text{-inch}$     |       |   |
| $I_m = I_{mx} + (m_c)(d_{CG})^2 = 13.9 \times 10^6 \text{ lb-sec}^2\text{-inch}$     |       |   |
| $r = 68.0 \text{ inches}$  | ----- | Concrete cask radius  |
| $H = 225.27 \text{ inches}$  | ----- | Concrete cask height  |
| $d_{CG} = \sqrt{118.0^2 + 64.0^2} = 134.2 \text{ inches}$                            | ----- | Distance from CG to rotation point  |

Based on conservation of momentum, the impulse of the impact force on the missile is equated to the impulse of the force on the concrete cask.

$$m_m(v_2 - v_1) = I_m (\omega_1 - \omega_2)/H$$

at time  $t_1$ ,  $v_1 = 185 \text{ ft/sec}$  and  $\omega_1 = 0 \text{ rad/sec}$   
at time  $t_2$ ,  $v_2 = 0 \text{ ft/sec}$

During the restitution phase, the final velocity of the missile depends upon the coefficient of restitution of the missile, the geometry of the missile and target, the angle of incidence, and on the amount of energy dissipated in deforming the missile and target. On the basis of tests conducted by EPRI, the final velocity ( $v_f$ ) of the missile following the impact is assumed to be zero. This conservatively assumes that all of the missile energy is transferred to the concrete.

cask. Equating the impact force on the missile to the impulse force on the concrete cask yields the following.

$$(10.4)(v_2 - 185(12)) = 13.9 \times 10^6 (0 - \omega_2)/225.27$$

Setting  $v_2 = 0$  and solving for  $\omega_2$

$$\omega_2 = 0.374 \text{ rad/sec}$$

The distance ( $Z$ ) from the point of missile impact to the point of concrete cask rotation is as follows.

$$Z = \sqrt{132.0^2 + 225.27^2} = 261.1 \text{ inch}$$

And the impulse velocity is as follows.

$$v_2 = Z \times \omega_2 = (261.1)(0.374) = 97.7 \text{ inch/sec}$$

The line of missile impact is conservatively assumed normal to the concrete cask. Equating the force on the missile during restitution to the impulse of the force on the concrete cask yields the following.

$$-[m_m(v_f - v_2)] = I_m (\omega_f - \omega_2)/Z$$

$$-[10.4(0 - 97.7)] = 13.9 \times 10^6 (\omega_f - 0.374)/261.1$$

$$\omega_f = 0.393 \text{ rad/sec}$$

where:

$$v_f = 0$$

$$v_2 = 97.7 \text{ inch/sec}$$

$$\omega_2 = 0.374 \text{ rad/sec}$$

Thus, the final energy ( $E_k$ ) of the concrete cask following the impact is as follows.

$$E_k = (I_m)(\omega_f)^2 / (2) = 10.73 \times 10^5 \text{ inch-lb}$$

The change in potential energy ( $E_p$ ) of the concrete cask due to rotating it until its center of gravity is above the point of rotation is calculated. The height of the center of gravity has increased by the distance,  $h_{PE} = d_{cg} - h_{cg}$ .

$$E_p = (W_{cc})(h_{PE})$$

$$E_p = 230,000 \text{ lb} \times 16.2 \text{ inch}$$

$$E_p = 3.73 \times 10^6 \text{ inch-lb}$$

The massive high kinetic-energy tornado-driven missile imparts less kinetic energy to the concrete cask than the change in potential energy of the concrete cask to reach the tip-over point. Therefore, concrete cask overturning from missile impact will not occur. The factor of safety (FS) against overturning is as follows.

$$FS = \frac{3.73 \times 10^6}{10.73 \times 10^5} = 3.48$$

### **Combined Tornado Wind and Missile Loading (High-Energy Missile)**

The concrete cask rotation due to the heavy missile impact is as follows.

$$h_{KE} = \frac{E_k}{W_{cc}} = \frac{10.73 \times 10^5}{230,000} = 4.67 \text{ inch}$$

The rotation after impact is as follows.

$$\theta = \alpha - \beta = 28.4 - 23.9 = 4.5^\circ$$

where:

$$\cos \beta = \frac{h_{cg} + h_{KE}}{d_{cg}} = \frac{118.0 + 4.67}{134.2} = 0.9141$$

$$\beta = 23.9^\circ$$

$$\cos \alpha = \frac{h_{cg}}{d_{cg}} = \frac{118.0}{134.2} = 0.8793$$

$$\alpha = 28.4^\circ$$

$$e = d_{cg} \sin \beta = 134.2 \times \sin(23.9^\circ) = 54.4 \text{ inch}$$

The available gravity restoration moment after missile impact is as follows.

$$M_{rst} = W_{cc}e = 230,000 \times 54.4 = 12.5 \times 10^6 \text{ inch-lb} = 1.04 \times 10^6 \text{ ft-lb}$$

The tornado wind moment is  $3.38 \times 10^5$  ft-lb; therefore, the factor of safety (FS) is as follows.

$$FS = \frac{0.67(1.04 \times 10^6)}{3.38 \times 10^5} = 2.06$$

Therefore, the concrete cask will not overturn due to the combined effect of tornado wind loading and high-energy missile impact.



**Local Shear Strength Capacity of Concrete Shell (High-Energy Missile)**

This section evaluates the punching shear strength of the concrete shell when impacted by a high-energy missile. The high-energy missile is equivalent to a 20-ft<sup>2</sup> cross-sectional area object moving at 185 ft/sec, weighing 4,000 lb, having proportions of 2 horizontal to 1 vertical. The missile is assumed to impact flush with the top of the concrete shell. The concrete area required to resist the high-energy missile impact is as follows.

$$A = 2b \times b = 2(9.64)^2 = 185.9 \text{ inch}^2 = 1.3 \text{ ft}^2 < 20 \text{ ft}^2$$

where:

Setting the factored shear force,  $V_u$ , equal to the force of the high kinetic-energy missile,  $F_u$ , the leg dimension,  $b$ , of the equivalent impacting area is as follows.

$$V_u = F_u \Rightarrow \phi V_c = F_u \Rightarrow \phi 4\sqrt{f'_c} b_o d = F_u \Rightarrow \phi 4\sqrt{f'_c} (4b + 53)d \Rightarrow b = 9.64 \text{ inch}$$

and

$$V_c = \left( 2 + \frac{4}{\beta_c} \right) \sqrt{f'_c} (b_o d) = 4\sqrt{f'_c} (b_o d) \text{ ----- Concrete punching shear strength capacity}$$

[5, Eq. 11-36]

$$\beta_c = 2/1 = 2 \text{ ----- Ratio of long side to short side}$$

$$d = 26.51 \text{ inch ----- Concrete thickness}$$

$$f'_c = 3,800 \text{ psi ----- Concrete strength, 300°F}$$

$$b_o = (2b + 26.51) + 2(b + 13.26) = 4b + 53 \text{ Perimeter of punching shear area at approximately } d/2 \text{ from the missile contact area}$$

$$\phi = 0.85 \text{ ----- Strength reduction factor [5]}$$

$$F_u = LF \times F = 508.8 \text{ kip ----- Force of high kinetic energy missile with load factor [19]}$$

$$F = 0.625(v)(W_m) = 462.5 \text{ kip ----- Force of high-energy missile [19]}$$

$$v = 185 \text{ ft/sec ----- Velocity of the missile}$$

$$W_m = 4,000 \text{ lb ----- Weight of high-energy missile}$$

$$LF = 1.1 \text{ ----- 10% load factor}$$

Therefore, the concrete shell alone has sufficient capacity to resist the high-energy missile impact force.

**3.7.3.3 Flood**

This section will verify the stability of the concrete cask against overturning during a design basis flood accident, and ensure that the design is adequate to withstand stresses induced by the flood.

Overturning of the concrete cask due to the drag force of the flood water flow is resisted by the weight of the loaded cask. Assuming a full submersion and steady-state flow conditions, the drag force ( $F_D$ ) on the concrete cask is calculated using classical fluid mechanics for turbulent flow conditions. The resultant drag force acts horizontally through the CG of the cask. The effective weight of the concrete cask acts vertically downward through the CG. The tendency of the concrete cask to overturn is determined by comparing the moment of the drag force about a point on the bottom edge of the concrete cask to the moment of effective concrete cask weight about the same point.

The effective weight of the fully submerged concrete cask is the actual weight minus the buoyancy force due to the displaced water. The bounding condition for buoyancy occurs for the concrete cask configuration with the greatest volume to weight ratio. Thus, for conservatism, the concrete cask is assumed to be empty.

The capacity of the concrete cask to react to the stresses induced by the flood water flow drag forces is evaluated using the methodology described in ACI 349-85 [5]. For conservatism, only the concrete shell is considered.

Assuming a hollow cylinder, the volume of the concrete cask ( $V_{cc}$ ) is as follows.

$$V_{cc} = \frac{\pi}{4}(D_o^2 - D_i^2)h = \frac{\pi}{4}(136.0^2 - 79.48^2)225.27 = 2,154,777 \text{ inch}^3$$

where:

$D_o$  = 136.0 inches ----- Concrete cask outer diameter

$D_i$  = 79.48 inches ----- Concrete cask inner diameter

$h$  = 225.27 inches ----- Concrete cask height

The buoyancy force ( $F_b$ ) is equal to the weight of water ( $62.4 \text{ lb/ft}^3$ ) displaced by the fully submerged concrete cask.

$$F_b = \frac{V_{cc}}{12^3} W_{h20} = \frac{2,154,777}{12^3} 62.4 \approx 77,800 \text{ lb}$$

Assuming complete submersion and steady-state flow for a rigid cylinder, the drag force ( $F_{D15}$ ) of the water on the concrete cask is as follows.

$$F_{D15} = C_D \rho V^2 \left( \frac{A}{2} \right) = 0.7 \times 1.94 \times 15.0^2 \left( \frac{212.7}{2} \right) \approx 32,500 \text{ lb} \quad [20]$$

where:

$C_D = 0.7$  ----- Drag coefficient [20]  
 $\rho = 1.94 \text{ slugs/ft}^3$  ----- Density of water  
 $V = 15 \text{ ft/sec}$  ----- Flow velocity  
 $A = H \times D_o = 30,637 \text{ inch}^2 = 212.7 \text{ ft}^2$  ----- Projected area  
 $H = 225.27 \text{ inches}$  ----- Concrete cask height  
 $D_o = 136.0 \text{ inches}$  ----- Concrete cask outer diameter

The force ( $F_D$ ) required to overturn the concrete cask is determined by summing the moments of the drag force and the submerged concrete cask about a point on the bottom of the concrete cask. Assuming an empty concrete cask, the minimum required overturning force is as follows.

$$F_D = \frac{(W_{cc} - F_b) D_r}{h} = \frac{(200,000 - 77,800) 128}{225.27} = 69,435 \text{ lb}$$

where:

$W_{cc} = 200,000 \text{ lb}$  ----- Conservatively defined minimum empty concrete cask weight  
 $D_r = 128.0 \text{ inches}$  ----- Concrete cask base diameter  
 $h = 225.27 \text{ inches}$  ----- Concrete cask height

The water velocity ( $V$ ) required to overturn the concrete cask is as follows.

$$V = \sqrt{\frac{2F_D}{C_D \rho A}} = \sqrt{\frac{2 \times 69,435}{0.7 \times 1.94 \times 212.7}} = 21.9 \text{ ft/sec}$$

Therefore, the factor of safety (FS) is as follows.

$$FS = \frac{21.9}{15.0} = 1.46$$

The stresses in the concrete due to the drag force ( $F_D$ ) are conservatively calculated by considering the concrete cask to be fixed.

$$\sigma_{v \text{ outer}} = M / S_{\text{outer}} = 17.2 \text{ psi (tension or compression)}$$

$$\sigma_{v \text{ inner}} = M / S_{\text{inner}} = 10.5 \text{ psi (tension or compression)}$$

where:

$$D_o = 136.0 \text{ inches}$$

$$\begin{aligned}
 D_i &= 82.98 \text{ inches} \\
 h &= 225.27 \text{ inches} \\
 A &= \pi (D_o^2 - D_i^2) / 4 = 9,119 \text{ inch}^2 \\
 I &= \pi (D_o^4 - D_i^4) / 64 = 14.47 \times 10^6 \text{ inch}^4 \\
 S_{\text{outer}} &= 2I/D_o = 212,794 \text{ inch}^3 \\
 S_{\text{inner}} &= 2I/(D_i) = 348,759 \text{ inch}^3 \\
 w &= F_{D15}/h = 144.3 \text{ lb/inch} \\
 M &= w (h)^2 / 2 = 3.66 \times 10^6 \text{ inch-lb}
 \end{aligned}$$

### 3.7.3.4 Earthquake

The maximum horizontal acceleration at the surface of the concrete storage pad due to an earthquake is evaluated. Per 10 CFR 72.102 [1], the required minimum earthquake ground acceleration is 0.25g. This evaluation will show that MAGNASTOR is stable during a 0.37g earthquake horizontal acceleration (including a 1.1 factor of safety). The vertical acceleration is defined as two-thirds of the horizontal acceleration in accordance with ASCE 4-86 [21].

This calculation determines the effects of ground accelerations (components  $a_x$ ,  $a_y$  and  $a_z$ ) on the concrete cask for tip-over. The peak ground acceleration is associated with a safe shutdown earthquake. For this evaluation, the maximum overturning moment is compared to the restoring moment required to keep the concrete cask in a stable upright position (i.e., a concrete cask will not tip over due to the earthquake). The maximum ground accelerations and overturning/restoring forces and moment are calculated for both empty and fully loaded concrete cask configurations.

In the event of earthquake, there exists a base shear force or overturning force due to the horizontal ground acceleration, and a restoring force due to the net force of vertical ground acceleration and gravity. This ground motion tends to rotate the concrete cask about its bottom corner at the point of rotation (at the chamfer). The horizontal moment arm is from the center of gravity (CG) toward the outer radius of the concrete cask. The vertical moment arm is from the CG to the bottom of the concrete cask. If the overturning moment is greater than the restoring moment, the concrete cask may tip over. Using the geometry of the concrete cask design, the maximum horizontal and vertical ground accelerations that the concrete cask can safely withstand without becoming unstable are identified.

The two orthogonal horizontal acceleration components ( $a_x$  and  $a_z$ ) are combined for maximum horizontal acceleration magnitude. The result is applied simultaneously with the vertical component to statically evaluate the overturning force and moment. Upward ground acceleration reduces the vertical force that restores the cask to its undisturbed vertical position. Based upon the requirements presented in NUREG-0800 [16], the static analysis method is considered

applicable if the natural frequency of the structure is greater than 33 cps. The natural frequency of the MAGNASTOR concrete cask is 138.3 Hz. During the design basis earthquake event, a factor of safety of 1.1 against tip-over of the concrete cask must be maintained.

**Tip-Over Evaluation**

To maintain the concrete cask in equilibrium, the restoring moment,  $M_R$ , must be greater than, or equal to, the overturning moment,  $M_o$ . The combination of horizontal and vertical acceleration components is based on the 100-40-40 approach of ASCE 4-86 [21], which considers that when the maximum response from one component occurs, the responses from the other two components are 40% of the maximum. The vertical component of acceleration can be obtained by scaling the corresponding ordinates of the horizontal components by two-thirds. The vertical component is conservatively considered to be the same as the horizontal component.

Let:

- $a_x = a_z = a$  ----- Horizontal acceleration components
- $a_y = a$  ----- Vertical acceleration component
- $G_h$  ----- Vector sum of two horizontal acceleration components
- $G_v$  ----- Vertical acceleration component

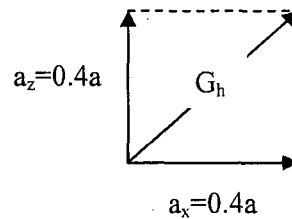
Two cases are analyzed:

Case 1) The vertical acceleration,  $a_y$ , is at its peak:

$(a_y = 1.0a, a_x = 0.4a, \text{ and } a_z = 0.4a)$

$G_h = \sqrt{a_x^2 + a_z^2} = \sqrt{(0.4a)^2 + (0.4a)^2} = 0.566a$

$G_v = 1.0a_y = 1.0a$

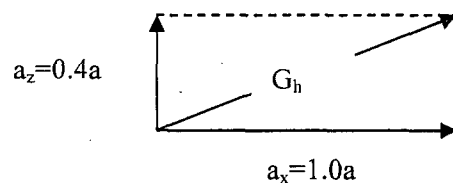


Case 2) One horizontal acceleration,  $a_x$ , is at its peak:

$(a_y = 0.4 \times a, a_x = a, \text{ and } a_z = 0.4a)$

$G_h = \sqrt{a_x^2 + a_z^2} = \sqrt{(1.0a)^2 + (0.4a)^2} = 1.077a$

$G_v = 0.4a_y = 0.4a$



For the cask to resist overturning, the restoring moment ( $M_R$ ) about the point of rotation must be greater than the overturning moment ( $M_o$ ).

$$M_R \geq M_O, \text{ or } F_r b \geq F_o d \Rightarrow (W \times 1 - W \times G_v) \times b \geq (W \times G_h) \times d$$

- d ----- Vertical distance measured from the base of the concrete cask to the center of gravity
- b ----- Horizontal distance measured from the point of rotation to the C.G.
- W ----- Weight of the concrete cask
- F<sub>o</sub> ----- Overturning force
- F<sub>r</sub> ----- Restoring force

Substituting for G<sub>y</sub> and G<sub>x</sub> gives:

Case 1

$$(1 - a) \frac{b}{d} \geq 0.566a$$

$$a \leq \frac{\frac{b}{d}}{0.566 + \frac{b}{d}}$$

Case 2

$$(1 - 0.4a) \frac{b}{d} \geq 1.077a$$

$$a \leq \frac{\frac{b}{d}}{1.077 + 0.4 \frac{b}{d}}$$

**Empty concrete cask:**

Case 1

$$a \leq \frac{\frac{64.0}{116.0}}{0.566 + \frac{64.0}{116.0}} = 0.49$$

Case 2

$$a \leq \frac{\frac{64.0}{116.0}}{1.077 + 0.4 \frac{64.0}{116.0}} = 0.43$$

where:

b = 64.0 inch  
 d = 116.0 inch

**Loaded concrete cask:**

Case 1

$$a \leq \frac{\frac{63.77}{118.0}}{0.566 + \frac{63.77}{118.0}} = 0.488$$

Case 2

$$a \leq \frac{\frac{63.77}{118.0}}{1.077 + 0.4 \frac{63.77}{118.0}} = 0.41$$

where:

d = 118.0 inch  
 b = 64.0 - x = 64.0 - 0.23 = 63.77 inches

$$e = \frac{73.44 - 72.0}{2} = 0.72 \text{ inch} \text{----- TSC CG shift}$$

$$x = \frac{W_{\text{can}} e}{W_{\text{CC}}} = \frac{103,000 \times 0.72}{322,000} = 0.23 \text{ inch -- Loaded concrete cask CG shift}$$

The minimum acceleration is 0.41g. A factor of safety of 1.1 is required for an earthquake evaluation; therefore, the maximum allowable horizontal acceleration ( $a_{\text{max}}$ ) at the top of the concrete pad that will preclude a cask tip-over is as follows.

$$a_{\text{max}} = \frac{0.41}{1.1} = 0.37g$$

### Concrete Cask Stress

To demonstrate the ability of the concrete cask to withstand earthquake loading conditions, the fully loaded cask is conservatively evaluated for seismic loads of 0.5g in the horizontal and 0.5g in the vertical direction. These accelerations reflect a more rigorous seismic loading and, therefore, bound the design basis earthquake. No credit is taken for the concrete cask steel liner. The maximum compressive stresses at the concrete shell outer and inner surfaces are conservatively calculated by considering the cask as a cantilever beam with its bottom end fixed. The maximum compressive stresses are as follows.

$$\sigma_{v \text{ outer}} = \frac{M}{S_{\text{outer}}} + \frac{(1 + a_y)W_{\text{CC}}}{A} = 138 \text{ psi}$$

$$\sigma_{v \text{ inner}} = \frac{M}{S_{\text{inner}}} + \frac{(1 + a_y)W_{\text{CC}}}{A} = 105 \text{ psi}$$

where

$$\begin{aligned} a_x &= 0.50g \text{----- Horizontal direction} \\ a_y &= 0.50g \text{----- Vertical direction} \\ W_{\text{CC}} &= 322,000 \text{ lb ----- Bounding weight of concrete cask} \\ D_o &= 136.0 \text{ inches} \\ D_i &= 82.98 \text{ inches} \\ A &= \pi (D_o^2 - D_i^2) / 4 = 9,119 \text{ inch}^2 \\ I &= \pi (D_o^4 - D_i^4) / 64 = 14.47 \times 10^6 \text{ inch}^4 \\ S_{\text{outer}} &= 2I/D_o = 212,794 \text{ inch}^3 \\ S_{\text{inner}} &= 2I/(D_i) = 348,759 \text{ inch}^3 \\ w &= (a_x \times W_{\text{CC}}) / 225.27 = 715 \text{ lb-inch} \\ M &= (w \times 225.27^2) / 2 = 1.81 \times 10^7 \text{ lb-inch} \end{aligned}$$

### 3.7.3.5 Concrete Cask Combined Stresses

The load combinations described in Table 2.3-1 are used to evaluate the concrete cask for accident events of storage. Concrete stresses are summarized in Table 3.7.3-1 and Table 3.7.3-2 for the loading combination Nos. 4, 5, 7, and 8. Loading combination No. 6 corresponds to drop accidents, 24-inch end drop and tip-over, which are evaluated in Section 3.7.3.6 and Section 3.7.3.7, respectively.

As shown in Table 3.7.3-1, the maximum concrete compressive stress is 1,201 psi; therefore, the minimum compressive factor of safety (FS) for accident events is as follows.

$$FS = \frac{S_{con}}{S_c} = \frac{2,660}{1,201} = 2.21$$

where:

$$S_{con} = \phi F_c = 0.7 \times 3,800 = 2,660 \text{ psi} \text{----- Concrete compressive allowable}$$

From Section 3.7.3.1, the maximum concrete ultimate strength due to thermal load is 0.1 ksi. The factor of safety (FS) for concrete ultimate strengths is as follows.

$$FS = \frac{S_{tc}}{S_t} = \frac{0.21}{0.1} = 2.10$$

where:

$$S_{tc} = 0.08 \times S_{con} = 0.08 \times 2660 = 213 \text{ psi or } 0.21 \text{ ksi} \text{..... Concrete ultimate strength}$$

From Section 3.7.3.1, the maximum rebar stress ( $S_{rb}$ ) is due to thermal load is 20.2 ksi. The factor of safety (FS) for the rebar is as follows.

$$FS = \frac{S_{rebar}}{S_{rb}} = \frac{54.0}{20.2} = 2.67$$

where:

$$S_{rebar} = \phi F_r = 0.9 \times 60.0 = 54.0 \text{ ksi} \text{----- Rebar stress allowable}$$

### 3.7.3.6 Concrete Cask 24-inch Drop

#### Evaluation of the Concrete Cask

During the 24-inch bottom-end drop of the concrete cask, the cylindrical portion of the concrete is in contact with the steel bottom plate that is a part of the base weldment. The plate is assumed



to be part of an infinitely rigid storage pad. No credit is taken for the crush properties of the storage pad or the underlying soil layer. Therefore, energy absorbed by the crushing of the cylindrical concrete region of the concrete cask equals the product of the compressive strength of the concrete, the crush depth of the concrete, and the projected area of the concrete cylinder. Crushing of the concrete continues until the energy absorbed equals the potential energy of the cask at the initial drop height. The TSC is not rigidly attached to the concrete cask, so it is not considered to contribute to the concrete crushing. The energy balance equation is as follows.

$$w(h + \delta) = P_o A\delta$$

where:

- h = 24.0 inches ----- Drop height
- δ ----- The crush depth of the concrete cask
- P<sub>o</sub> = 3,800 psi ----- Compressive strength of the concrete, 300°F
- A = π(R<sub>2</sub><sup>2</sup> - R<sub>1</sub><sup>2</sup>) = 9,119 inch<sup>2</sup> ----- Area of the concrete shield wall
- R<sub>1</sub> = 41.49 inches ----- Inside radius of the concrete
- R<sub>2</sub> = 68 inches ----- Outside radius of the concrete
- w = 185,000 lb ----- Bounding weight of concrete, rebar, and lid assembly

It is assumed that the maximum force that can be exerted on the concrete cask is the compressive strength of the concrete multiplied by the area of the concrete being crushed. The concrete cask's steel shell will not experience any significant damage during a 24-inch drop. Therefore, its functionality will not be impaired due to the drop.

The crush distance computed from the energy balance equation is as follows.

$$\delta = \frac{hw}{P_o A - w} = \frac{(24)(185,000)}{(3800)(9,119) - (185,000)} = 0.13 \text{ inch}$$

**Pedestal Crush Evaluation**

Upon a bottom-end impact of the concrete cask, the TSC produces a force on the pedestal (base weldment) located near the bottom of the cask. The ring above the air inlets is expected to yield. To determine the resulting acceleration of the TSC and deformation of the pedestal, a LS-DYNA analysis is used. As described in Section 3.10.4.3, a quarter-symmetry finite element model of the pedestal is used for this evaluation. To ensure that maximum deformations and accelerations are determined, two analyses are performed. One analysis, which uses the upper-bound weight of 105 kips, envelops the maximum deformation of the pedestal. The second analysis employs the lower-bound weight of 60 kips to account for maximum acceleration.

The maximum accelerations of the TSC during the 24-inch bottom-end impact are calculated to be 14.5g and 25.2g for the upper-bound weight TSC and lower-bound weight TSC, respectively.

The resulting acceleration time histories of the TSC, which correspond to a filter frequency of 200 Hz, are shown in Figure 3.7.3-1 for the analysis using the upper-bound weight model and Figure 3.7.3-2 for the lower-bound weight model. The dynamic load factor (DLF) for the TSC is calculated to be 1.35 for the upper-bound weight TSC and 0.95 (consider 1.0) for the lower-bound weight TSC, based on the response of one-degree systems subjected to a triangular load pulse [22]. Therefore, the accelerations for the upper-bound weight and lower-bound weight TSC are 19.6g and 25.2g, respectively.

The maximum strain in the pedestal is 15.4%. Since the ultimate strain of A36 steel is greater than 25%, the pedestal is not subject to failure. The maximum vertical displacement of the air inlet is calculated to be 1.46 inches for the upper-bound and lower-bound weight TSC. The original opening is 4.4 inches. Since the maximum displacement is 1.46 inches, the minimum air inlet opening is 2.9 inches (4.4 – 1.46), which is approximately 66% of the original air inlet opening. This condition is bounded by the consequences of the loss of one-half of the air inlets off-normal event.

#### **3.7.3.7 Concrete Cask Tip-Over**

Tip-over of the concrete cask is a nonmechanistic, hypothetical accident condition that presents a bounding case for evaluation. Existing postulated design basis accidents do not result in the tip-over of the concrete cask. Functionally, the concrete cask does not suffer significant adverse consequences due to this event. The concrete cask, TSC, and basket maintain design basis shielding, geometry control of contents, and contents confinement performance requirements.

For a tip-over event to occur, the center of gravity of the concrete cask and loaded TSC must be displaced beyond its outer radius, i.e., the point of rotation. When the center of gravity passes beyond the point of rotation, the potential energy of the cask and TSC is converted to kinetic energy as the cask and TSC rotate toward a horizontal orientation on the ISFSI pad. The subsequent motion of the cask is governed by the structural characteristics of the cask, the ISFSI pad and the underlying soil.

The MAGNASTOR concrete cask tip-over analyses are performed using LS-DYNA. LS-DYNA is an explicit finite element program for the nonlinear dynamic analysis of structures in three dimensions. Details of the finite element model are presented in Section 3.10.4.

Two geometries are considered in this evaluation. The pad width of 30 ft in the models corresponds to the typical width of a concrete storage pad. One model considers a pad length of 30 ft, while the second model referred to as the “oversized pad,” employs a length of 60 feet. The second model allows the effect of the pad length used in the analysis to be assessed.

The acceleration time histories for the TSC and basket for the standard and oversized pad cases are shown in Figure 3.7.3-3 and Figure 3.7.3-4. A cut-off frequency of 200 Hz is applied to filter the analysis results and measure the peak accelerations. The following is a summary of the peak accelerations.

| Location               | Position from Base of Concrete Cask (in) | Acceleration Standard Pad (g) | Acceleration Oversized Pad (g) |
|------------------------|--|-------------------------------|--------------------------------|
| Top of basket          | 177.7                                    | 26.4                          | 26.6                           |
| Top of TSC closure lid | 197.6                                    | 29.5                          | 29.6                           |

Using two-dimensional models of the PWR and BWR basket (similar to the models described in Sections 3.10.1 and 3.10.2, meshing density modified for modal analysis), the modal frequencies for the basket are calculated. Table 3.7.3-3 summarized the frequencies for the first mode shape for the PWR and BWR baskets in the 0° and 45° basket orientations. The dynamic load factors are determined using the response of one-degree systems subjected to a triangular load pulse [22]. The dynamic load factors and the maximum accelerations at the top of the TSC and top of the basket are summarized in

Table 3.7.3-4. As the table and figures show, maximum accelerations are less than the specified design value of 40g. The acceleration results indicate that even with a 100% increase in the pad length, the resulting change in the maximum accelerations is less than 1 percent. This demonstrates that the effect of the pad size employed in the analysis has an insignificant effect on the maximum accelerations.

**Figure 3.7.3-1 Acceleration Time History of the Upper-Bound Weight TSC –  
24-Inch Concrete Cask Drop**

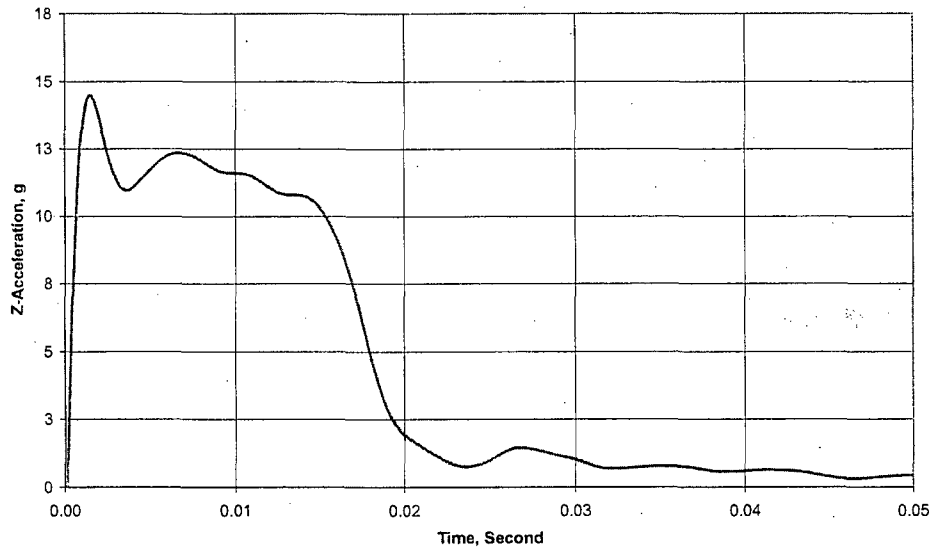


Figure 3.7.3-2 Acceleration Time History of the Lower-Bound Weight TSC –  
24-Inch Concrete Cask Drop

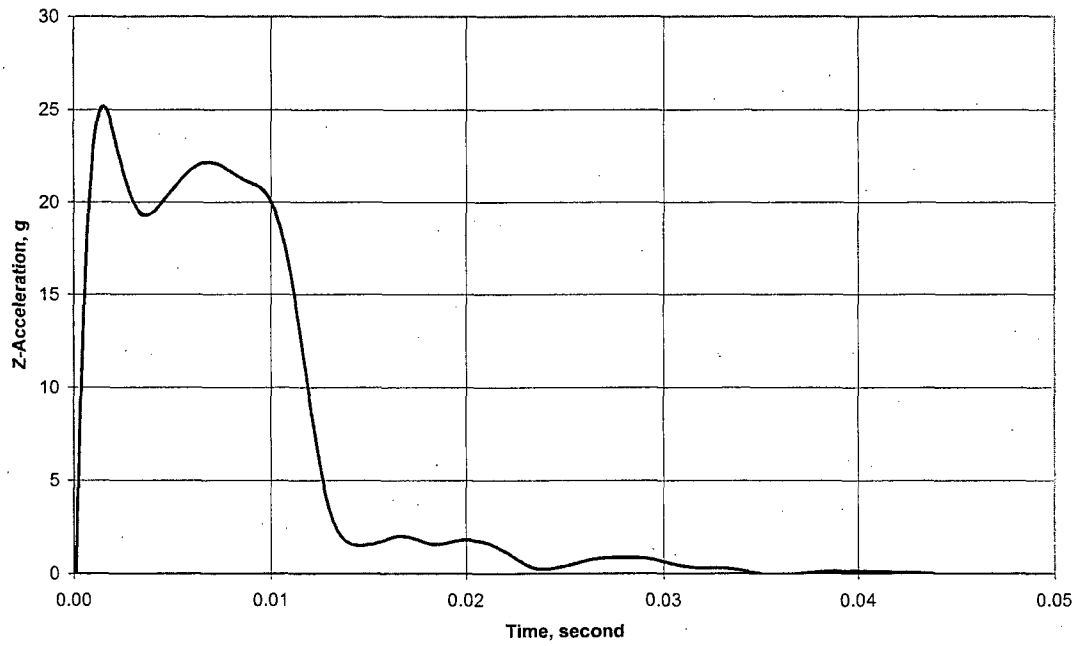


Figure 3.7.3-3 Acceleration Time History for Concrete Cask Tip-Over Condition - Standard Pad

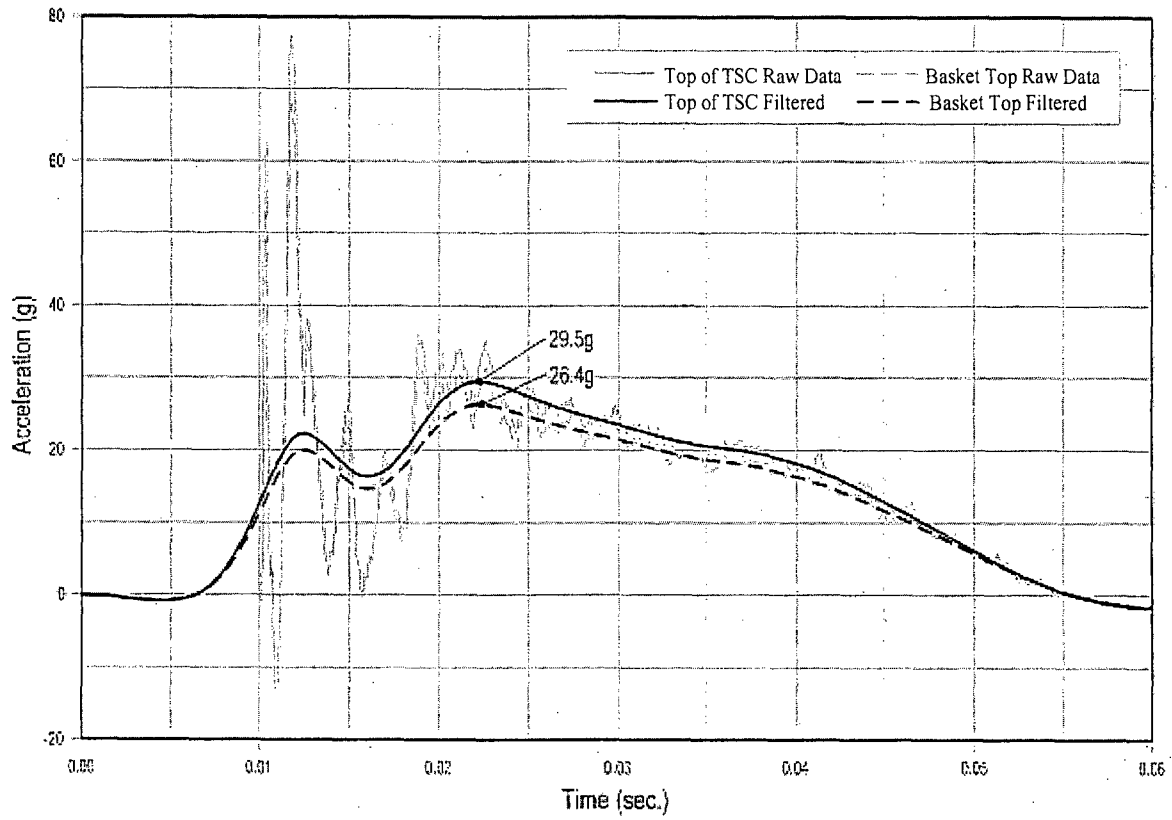
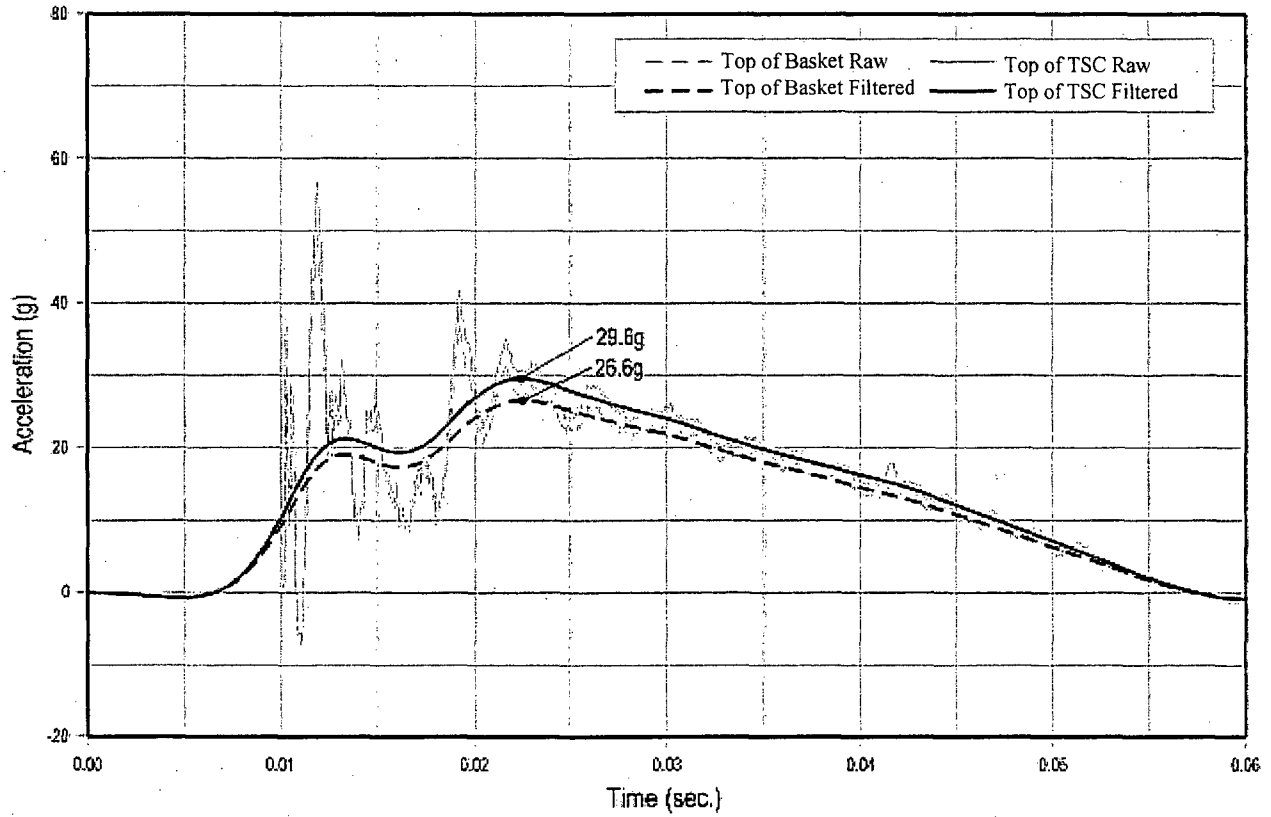


Figure 3.7.3-4 Acceleration Time History of Oversized Pad



**Table 3.7.3-1 Concrete Cask Vertical Stress Summary – Inner Surface, psi**

| Condition | Dead | Live | Wind | Thermal | Seismic | Flood | Tornado | Total |
|-----------|------|------|------|---------|---------|-------|---------|-------|
| 4         | -23  | -25  | 0    | -1048   | 0       | 0     | 0       | -1096 |
| 5         | -23  | -25  | 0    | -989    | -105    | 0     | 0       | -1201 |
| 7         | -23  | -25  | 0    | -989    | 0       | -11   | 0       | -1107 |
| 8         | -23  | -25  | 0    | -989    | 0       | 0     | -12     | -1108 |

**Table 3.7.3-2 Concrete Cask Circumferential Stress Summary – Inner Surface, psi**

| Condition | Dead | Live | Wind | Thermal | Seismic | Flood | Tornado | Total |
|-----------|------|------|------|---------|---------|-------|---------|-------|
| 4         | 0    | 0    | 0    | -217    | 0       | 0     | 0       | -217  |
| 5         | 0    | 0    | 0    | -211    | 0       | 0     | 0       | -211  |
| 7         | 0    | 0    | 0    | -211    | 0       | 0     | 0       | -211  |
| 8         | 0    | 0    | 0    | -211    | 0       | 0     | 0       | -211  |



**Table 3.7.3-3 Basket Modal Frequency for Concrete Cask Tip-over**

| Fuel Type and Basket Angle | Frequency (F), Hz |
|----------------------------|-------------------|
| PWR-0°                     | 269               |
| PWR-45°                    | 33                |
| BWR-0°                     | 140               |
| BWR-45°                    | 39                |

**Table 3.7.3-4 DLF and Amplified Accelerations for Concrete Cask Tip-over**

| Fuel Type and Basket Angle | Top of TSC Lid       |     |                           | Top of Fuel Basket   |      |                           |
|----------------------------|----------------------|-----|---------------------------|----------------------|------|---------------------------|
|                            | Base Acceleration, g | DLF | Amplified Acceleration, g | Base Acceleration, g | DLF  | Amplified Acceleration, g |
| PWR-0°                     | 29.6                 | 1.0 | 29.6                      | 26.6                 | 1.01 | 26.9                      |
| PWR-45°                    | 29.6                 | 1.0 | 29.6                      | 26.6                 | 1.21 | 32.2                      |
| BWR-0°                     | 29.6                 | 1.0 | 29.6                      | 26.6                 | 1.02 | 27.1                      |
| BWR-45°                    | 29.6                 | 1.0 | 29.6                      | 26.6                 | 1.07 | 28.5                      |

### 3.8 Fuel Rods

This section presents an evaluation of the PWR and BWR fuel rods for the storage conditions of the MAGNASTOR system.

#### 3.8.1 PWR Fuel Rod Buckling Evaluation

This section presents the buckling evaluation for MAGNASTOR high burnup PWR fuel (burnup greater than 45,000 MWD/MTU) having cladding oxide layers that are 80 and 120 microns thick. A reduced cladding thickness is assumed due to the cladding oxide layer. These analyses show that the maximum stresses in the high burnup PWR fuel remain below the yield strength in the design basis accident events and confirm that the fuel rods will return to their original configuration. A 24-inch end drop orientation of the concrete cask subjects the fuel rods to axial loading. The 24-inch drop evaluation employs two acceleration time histories. The 24-inch concrete cask end drop described in Section 3.10.4.3 resulted in the acceleration time history shown in Figure 3.7.3-2. The maximum acceleration for the time history shown in Figure 3.7.3-2 is 25.3g's (the strong segment of the pulse lasts for 0.015 second). A bounding triangular-shaped time history with a maximum acceleration of 45g's for a duration of 0.02 second is also used.

In the end drop orientation, the fuel rods are laterally restrained by the grids and come into contact with the fuel assembly base. The only vertical constraint for the fuel rod is the base of the assembly. As opposed to employing a straight fuel assembly in the evaluation with all the grids present, the fuel assembly is considered to be bowed, and a fuel assembly grid may be missing and still meet the acceptable configuration for undamaged fuel. The evaluation of the PWR fuel rods is based on the following representative samples.

| Fuel Assembly | Cladding Diameter (in) | Cladding Thickness (in) | Fuel Rod Pitch (in) | Gap Between Fuel Assembly and Fuel Tube Wall (in) |
|---------------|------------------------|-------------------------|---------------------|---|
| We 17×17      | 0.360                  | 0.021                   | 0.496               | 0.564   |
| We 15×15      | 0.417                  | 0.024                   | 0.563               | 0.561   |
| We 14×14      | 0.400                  | 0.022                   | 0.556               | 1.232   |
| CE16×16       | 0.382                  | 0.025                   | 0.506               | 0.888   |
| CE14×14       | 0.440                  | 0.031                   | 0.580               | 0.880   |
| BW17×17       | 0.377                  | 0.022                   | 0.502               | 0.451   |
| BW15×15       | 0.414                  | 0.022                   | 0.568               | 0.494   |

Review of the design basis fuel inventory indicates that the largest gap between the enveloping of the fuel rods of a straight fuel assembly and the basket fuel tube inner wall could be 1.23 inches, corresponding to a 14×14 rod array having a minimum rod pitch of 0.556 inch and a minimum rod diameter of 0.40 inch inside a maximum basket fuel cell with an inside dimension of 8.86 inches. In this evaluation, an assembly with an initial bow of 0.55 inch is permitted to displace an additional 0.68 inch to the full gap displacement of 1.23 inches. A PWR 17×17 fuel assembly with a bow of 0.55 inch (less than the gap of 0.564 inch, as shown in the preceding table) can still fit into a MAGNASTOR basket fuel tube. To implement a bow of 0.55 inch into the fuel assembly, the half-symmetry ANSYS model corresponding to a row of fuel rods (Figure 3.8.1-1) is used. The clad is modeled with shell elements (Figure 3.8.1-2). Each grid is modeled using brick elements to maintain the spacing between the fuel rods at the grid (Figure 3.8.1-2). The fuel tube is modeled using brick elements to restrict the lateral motion of the fuel assembly. Each of the fuel rods in the ANSYS model is simply supported at each end. A static force is applied to the ANSYS model at the grid nearest the axial center to develop a 0.55-inch lateral displacement. The purpose of the ANSYS model and solution is to provide the coordinates of the fuel clad for the LS-DYNA model. This is accomplished by obtaining a static solution with the ANSYS model, and then using the option to update the coordinates of the nodes based on the displacements from the solution.

Five LS-DYNA models are considered for the 24-inch cask end drop conditions. All models incorporate a bow of 0.55 inch. These cases envelop the range of the cross-sectional moments for the PWR fuel rods and the grid spacing at the bottom of the fuel assembly as summarized in the following table. Case 5 is used to confirm that the acceleration associated with the 24-inch end drop of the MAGNASTOR System provides bounding stresses.

| <b>Case</b> | <b>Fuel Assembly</b> | <b>Lowest Grid Spacing (inch)</b> | <b>Acceleration Definition</b> |
|-------------|----------------------|-----------------------------------|--------------------------------|
| 1           | 14×14                | 60*                               | 45g                            |
| 2           | 14×14                | 33                                | 45g                            |
| 3           | 17×17                | 60*                               | 45g                            |
| 4           | 17×17                | 33                                | 45g                            |
| 5           | 17×17                | 60*                               | 25.3g                          |

\* The 60-inch spacing corresponds to the fuel rod configuration with two missing grids at the bottom of the fuel assembly.

In all cases, the thickness of the clad was reduced by 120 microns (0.0047 inch). Cases 1 through 4 require a separate ANSYS model and LS-DYNA model to represent unique coordinates or boundary conditions (geometry of Case 5 is the same as for Case 3). The LS-DYNA model employs the same nodes and elements as the ANSYS model (with the incorporation of the 0.55-inch bow). Elastic properties are used in the ANSYS model and the bilinear properties are employed in the LS-DYNA model. An initial downward velocity of 136 in/sec (corresponding to a 24-inch end drop for the storage condition) is assigned to all nodes in the model. The deceleration time history is applied to the nodes of the brick elements representing the fuel tube. The side walls of the fuel tube are restrained in the lateral direction to maximize the effect of the fuel rods impacting the fuel tube side wall.

The LS-DYNA analyses for Cases 1 through 4 were performed for the duration of 0.08 second to capture the response of the fuel after the 0.02 second loading duration. Post-processing each analysis result identifies the maximum shear stress occurring at the shell surface. The maximum shear stress result from LS-DYNA is factored by two to determine the maximum stress intensity.

The following table contains the maximum stress intensity for the five cases.

**Maximum Stress Intensity for the Five LS-DYNA Analyses**

| Case | Maximum Stress Intensity (ksi) | Factor of Safety Against Yield Strength |
|------|--------------------------------|---|
| 1    | 25.4                           | 3.08                                    |
| 2    | 21.8                           | 3.59                                    |
| 3    | 41.9                           | 1.86                                    |
| 4    | 34.7                           | 2.25                                    |
| 5    | 22.0                           | 3.54                                    |

The case using the 60-inch spacing in conjunction with the minimal cross-section (Case 3) is identified as the bounding case. All stresses were shown to be less than the yield strength.

The results confirm that high burnup PWR fuel with a maximum distance of 60 inches from the bottom to the first grid will remain structurally adequate for the storage design basis cask end drop load conditions.

Figure 3.8.1-1 Overall Model Plot for a Typical PWR Fuel Assembly

Overall Plot of PWR Model

Model without the  
Fuel Clad

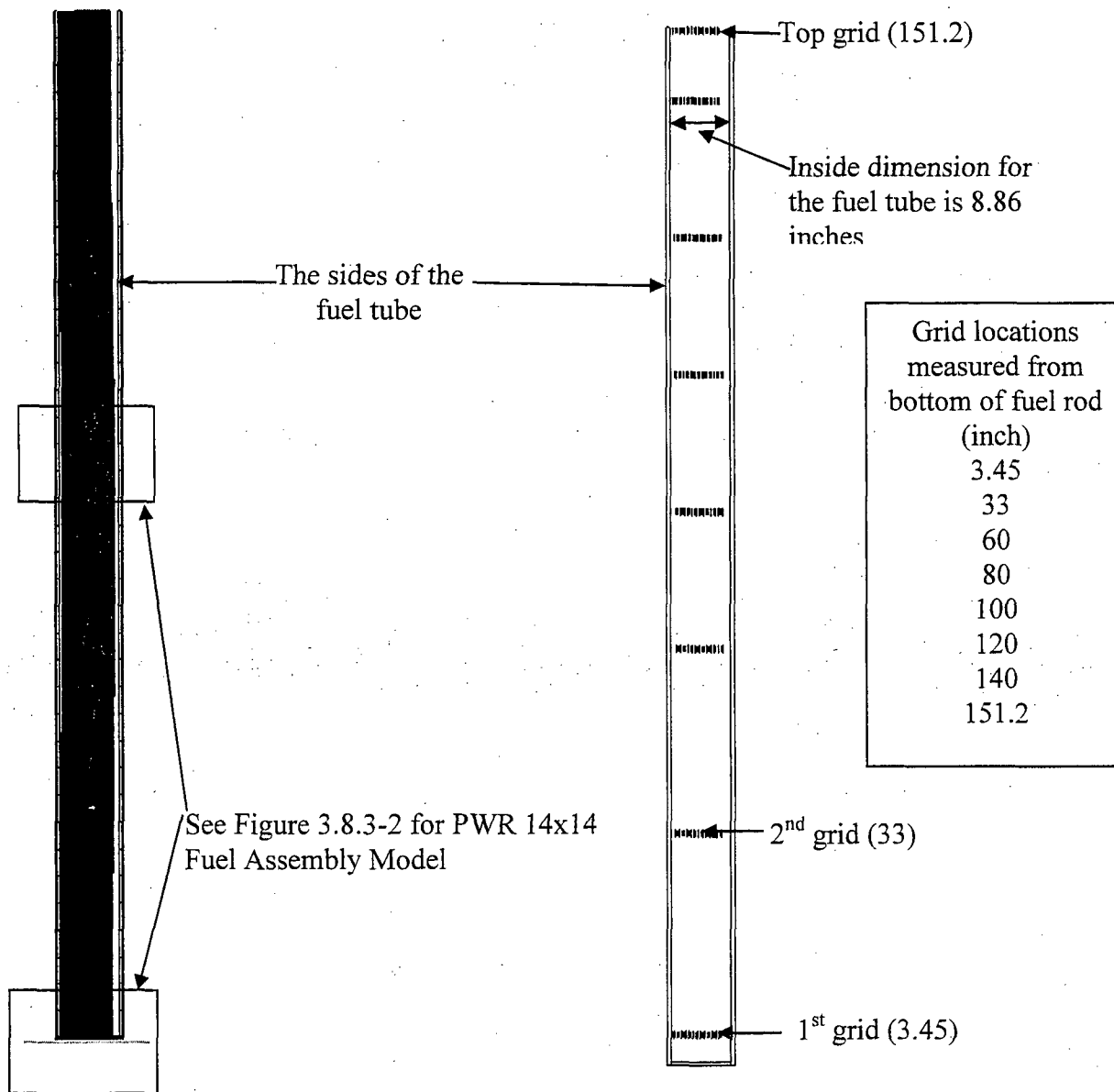
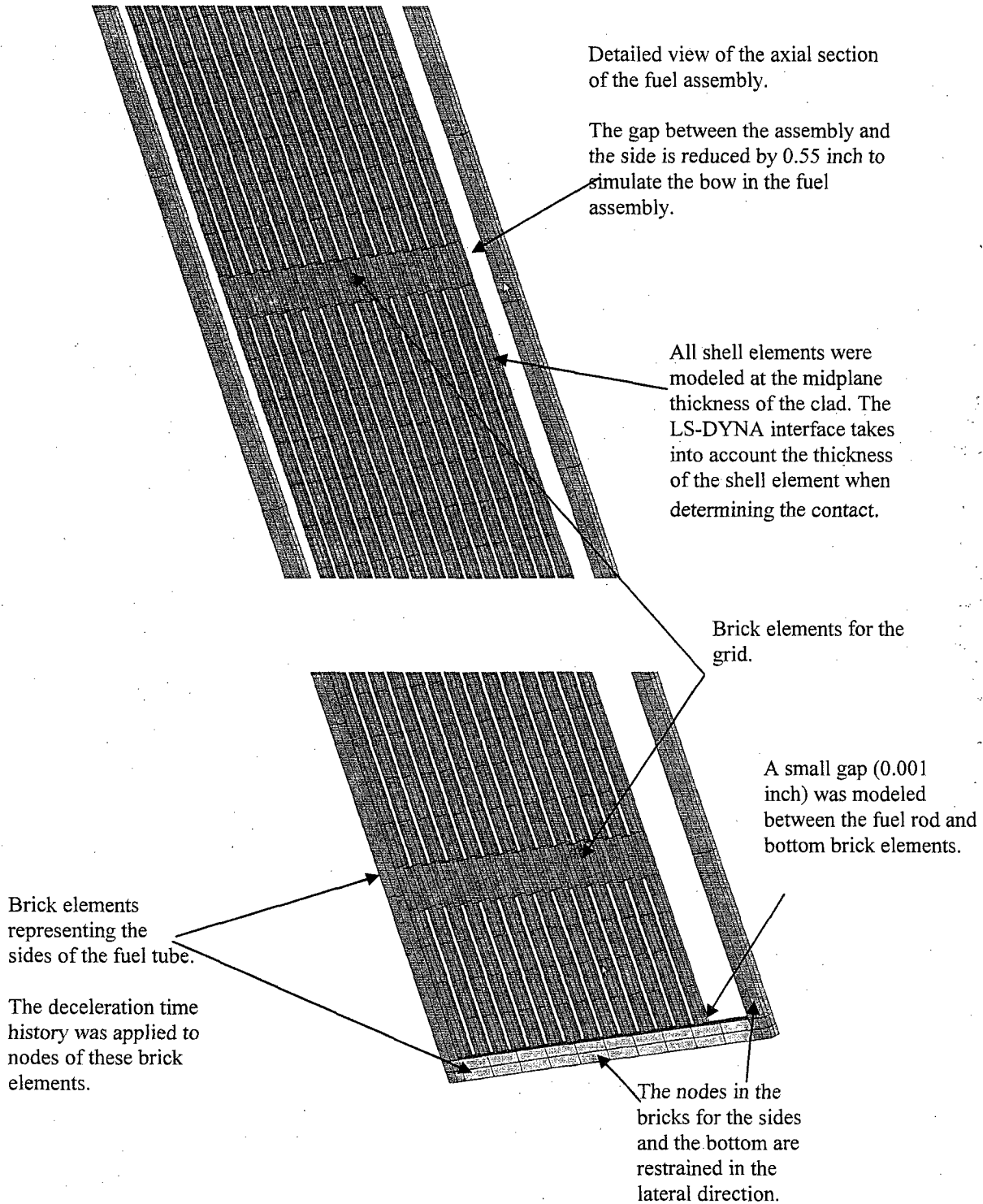


Figure 3.8.1-2 Detailed View of the PWR 14×14 Fuel Assembly



**3.8.2 BWR Fuel Rod Buckling Evaluation**

The evaluation of the BWR fuel rod is based on the following representative samples of BWR fuel rods.

| Fuel Assembly | Cladding Diameter (in) | Cladding Thickness (in) |
|---------------|------------------------|-------------------------|
| GE 7x7        | 0.563                  | 0.032                   |
| GE 8x8-2      | 0.483                  | 0.032                   |
| GE 8x8-4      | 0.484                  | 0.032                   |
| GE 9x9-2      | 0.441                  | 0.028                   |
| GE 10x10-2    | 0.378                  | 0.024                   |

The location of the lateral constraints in the BWR fuel are: 0.00 in, 22.88 in, 43.03 in, 63.18 in, 83.33 in, 103.48 in, 122.3 in, 143.78 in, and 163.42 inches.

For the PWR fuel rod (with all grids and with the 120-micron thickness reduction), the largest ratio of unsupported length (L) to radius of gyration of the cladding cross-section (r) is:

$$L/r = \frac{33}{0.5 \times \sqrt{((0.360 - 2 \times 0.0047)/2)^2 + (0.318/2)^2}} = 279$$

The ratio (L/r) for a BWR fuel rod (with the 125-micron thickness reduction for the high burnup fuel) is:

$$L/r = \frac{22.88}{0.5 \times \sqrt{((0.378 - 2 \times 0.0049)/2)^2 + (0.330/2)^2}} = 185$$

The analysis presented in Section 3.8.1 is bounding for both PWR and BWR fuel rods because the "L/r" for the PWR fuel rod is larger than the "L/r" for the BWR fuel rod. Therefore, no further evaluation of the BWR fuel rod is required.

### 3.8.3 Thermal Evaluation of Fuel Rods

MAGNASTOR limits normal storage condition fuel cladding temperatures to be  $\leq 400^{\circ}\text{C}$  ( $752^{\circ}\text{F}$ ) in accordance with ISG-11, Rev 3. Zirconium alloy or stainless steel cladding degradation is not expected to occur below this temperature in an inert gas environment.

The fuel cladding temperature limit for short-term off-normal and accident events is  $570^{\circ}\text{C}$  ( $1,058^{\circ}\text{F}$ ). Refer to Chapter 4, which demonstrates that the maximum fuel cladding temperatures are well below the temperature limits for all design conditions of storage.



**3.8.4 Side Drop Evaluation**

The basket side drop configuration is evaluated using a uniformly applied 60g's along the length of the basket. This significantly bounds the accelerations developed in the concrete cask tip-over accident in which the accelerations vary from near-zero value at the point of rotation to a maximum acceleration reported in Section 3.7.3.7 of 26.6g's at the top of the basket. The analyzed bounding fuel rod length of 60.0 inches envelops all fuel types and includes the condition with a missing support grid in the fuel assembly. During a side drop, the maximum deflection of a fuel rod is based on the fuel rod spacing of the fuel assembly. Assuming a 17x17 array (fuel assembly with the maximum number of rods), the maximum fuel rod deflection, including the 120-micron oxide layer, is:

$$(17-1) \times (0.496-0.36+2 \times 120 \times 10^{-6} \times 39.37) = 2.33 \text{ in.}$$

The side drop loading is evaluated for three fuel rods, which corresponds to the limits of the stress modulus Z (ratio of the cross-sectional moment of inertia to the maximum radius to relate the maximum fiber stress (S) to the bending moment (M),  $S=M/Z$ ) and the maximum span, as shown in the following table.

| Case    | Rod Diameter (inches) | Clad Thickness (inches) | Z (in <sup>3</sup> ) (10 <sup>-3</sup> ) | Span (inches) |
|---------|-----------------------|-------------------------|--|---------------|
| CE14x14 | 0.440                 | 0.031                   | 3.18                                     | 16.8          |
| WE15x15 | 0.417                 | 0.024                   | 2.20                                     | 26.2          |
| WE17x17 | 0.360                 | 0.0205                  | 1.33                                     | 20.6          |

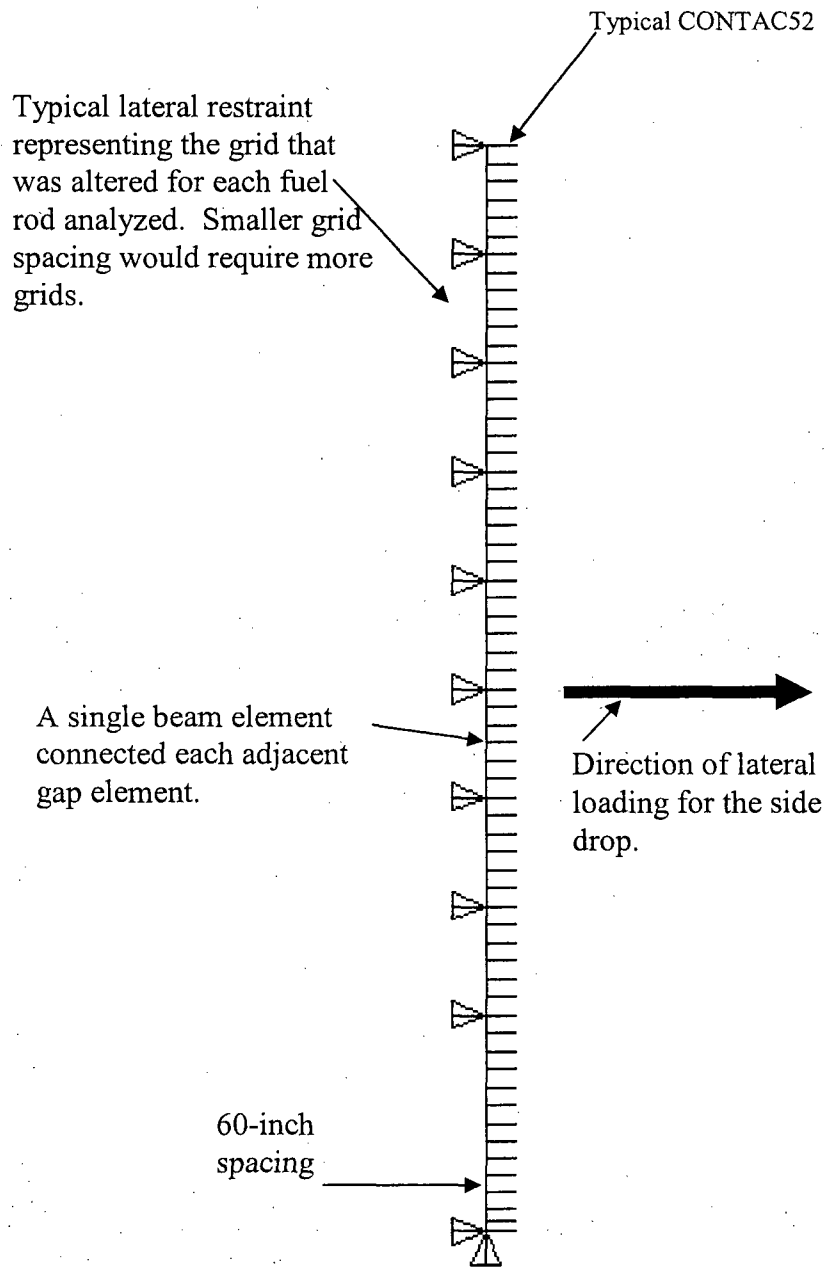
ANSYS is used to perform a static analysis with a lateral loading of 60g. The model is shown in Figure 3.8.4-1. The fuel rod is modeled with beam elements, and the properties for the fuel clad take into account the reduction of the outer radius by 0.0047 inch (120 microns). The density of the beam element material was based on the zircaloy clad (0.237 lb/in<sup>3</sup>) and the pellet density (0.396 lb/in<sup>3</sup>). The lateral constraints show the location of the grids used in the model, and the distance from the end of the fuel rod to the first support is 60 inches. The analyses confirm that the rod lateral displacement is 2.33 inches, which results in the fuel rod being supported with the 60-inch distance between adjacent grids. Therefore, the location of the unsupported span along the fuel rod is not significant. The spacing for the adjacent grids is shown in the preceding table. To represent the maximum gap of 2.33 inches, which the fuel rod can displace in the side drop, CONTAC52s were modeled at each node. The gap for each CONTAC52 was set to 2.33 inches

to limit the lateral displacement of the fuel rod to 2.33 inches. The gap stiffness for each CONTAC52 was defined to be  $10^6$  lb/in, which simulates the resistance of the basket to the lateral motion of the fuel rod. The lateral flexural stiffness of the fuel rod is considered to be insignificant compared to the stiffness of the basket. The effect of this stiffness, whether larger or smaller, would not influence the maximum stress. The maximum stress in the fuel rods is shown in the following table, and the allowable stress is the material yield strength at 752°F (69.6 ksi).

| Case    | Maximum Stress (ksi) | Margin of Safety Against Yield Strength |
|---------|----------------------|---|
| CE14×14 | 37.1                 | +0.88                                   |
| WE15×15 | 48.1                 | +0.45                                   |
| WE17×17 | 46.3                 | +0.50                                   |

This confirms that the PWR fuel rod subject to high burnup will remain intact for a 60g side drop condition, which bounds the tip-over accident condition.

Figure 3.8.4-1 ANSYS Model for the PWR Fuel Rod High Burnup Condition



### 3.9 References

1. 10 CFR 72, Code of Federal Regulations, "Licensing Requirements for the Independent Storage of Spent Fuel, High Level Radioactive Waste and Reactor-Related Greater than Class C Waste," US Nuclear Regulatory Commission, Washington, DC.
2. American National Standard for Radioactive Materials N14.6-1993, "Special Lifting Devices for Shipping Containers Weighing 10,000 Pounds (4500 kg) or More," American National Standard Institute, Inc., Washington, DC, 1993.
3. NUREG-0612, "Control of Heavy Loads at Nuclear Power Plants," U. S. Nuclear Regulatory Commission, Washington, D.C., 1980.
4. ANSI/ANS-57.9-1992, American National Standard Design Criteria for an Independent Spent Fuel Storage Installation (Dry Type), American Nuclear Society, La Grange Park, IL, May 1992.
5. "Code Requirements for Nuclear Safety Related Concrete Structures (ACI 349-85) and Commentary (ACI 349R)," American Concrete Institute, Farmington Hills, MI.
6. ASME Boiler and Pressure Vessel Code, Section III, Subsection NB, "Class 1 Components," American Society of Mechanical Engineers, New York, NY, 2001 Edition with 2003 Addenda.
7. ASME Boiler and Pressure Vessel Code, Section III Subsection NG, "Core Support Structures", American Society of Mechanical Engineers, New York, NY, 2001, with 2003 Addenda.
8. ASME Boiler and Pressure Vessel Code, Appendix F, "Rules for Evaluation of Service Loadings with Level D Service Limits," The American Society of Mechanical Engineers, New York, NY, 2001, with 2003 Addenda.
9. NUREG/CR-6322, "Buckling Analysis of Spent Fuel Basket," Lawrence Livermore National Laboratory, Livermore, CA, 1995.
10. AFFDL-TR-69-42, "Stress Analysis Manual", Air Force Flight Dynamics Laboratory, Dayton, Ohio, 1969.
11. "Steel Structures Design and Behavior," C.G. Salmon and J.E. Johnson, Harper and Row Publishers, New York, NY, Second Edition, 1980.
12. "Machinery's Handbook," Industrial Press, New York, NY, 25th Edition, 1996.
13. "Roark's Formulas for Stress & Strain," Warren C. Young, McGraw Hill, New York, NY, Sixth Edition, 1989.
14. "Reinforced Concrete Design," Kenneth Leet, McGraw-Hill, New York, NY, Second Edition, 1991.

15. "Practical Stress Analysis in Engineering Design," Alexander Blake, Marcel Dekker, Inc., New York, NY, Second Edition, 1990.
16. NUREG-0800, "Standard Review Plan," U.S. Nuclear Regulatory Commission Draft, Washington, DC, June 1987.
17. ASCE 7-93, "Minimum Design Loads for Buildings and Other Structures," American Society of Civil Engineers, New York, NY, March 12, 1994.
18. NSS 5-940.1, "A Review of Procedures for the Analysis and Design of Concrete Structures to Resist Missile Impact Effects," Nuclear and Systems Sciences Group, Holmes & Narver, Inc., Anaheim, CA, September 1975.
19. BC-TOP-9A, Revision 2, Topical Report, "Design of Structures for Missile Impact," Bechtel Power Corporation, San Francisco, CA, September 1974.
20. "Engineering Fluid Mechanics," J. A. Roberson and C. T. Crowe, Houghton Mifflin Co., Boston, MA, 1975.
21. ASCE 4-86, "Seismic Analysis of Safety-Related Nuclear Structures and Commentary on Standard for Seismic Analysis of Safety-Related Nuclear Structures," American Society of Civil Engineers, New York, NY, 1986.
22. "Structural Dynamics," John M. Biggs, McGraw-Hill, New York, NY, 1964.
23. ISG-15, Revision 0, "Materials Evaluation," US Nuclear Regulatory Commission, Washington, DC, January 10, 2001.
24. "Dynamics of Structures," R. W. Clough and Joseph Penzien, 2nd Edition, McGraw-Hill, Inc., New York, NY, 1993.
25. Nuclear Power Plant Engineering, J. H. Rust, Georgia Institute of Technology, 1979.
26. ISG-12, Revision 1, "Buckling of Irradiated Fuel under Bottom End Drop Conditions," US Nuclear Regulatory Commission, Washington, DC, January 15, 2001.
27. "Mechanical Properties for Irradiated Zircaloy," K. J. Geelhood and C. E. Beyer, Pacific Northwest National Laboratory, Richland, WA.
28. NUREG/CR-5009, "Assessment of the Use of Extended Burnup Fuel in Light Water Power Reactors," Battelle Pacific Northwest Labs, Richland, Washington, February 1998.
29. ANSI N45.2.15 - 1981, "Hoisting, Rigging and Transporting of Items for Nuclear Power Plants.

**3.10      Structural Evaluation Detail**

This section contains evaluation detail not found in the preceding sections.

### 3.10.1 PWR Fuel Basket Finite Element Models

#### 3.10.1.1 Load Path Description

This section describes the load paths and interactions between basket components during storage conditions. The MAGNASTOR PWR fuel basket is designed to accommodate 37 PWR fuel assemblies. For the normal conditions of storage, the weight of the fuel assemblies is directly supported by the bottom plate of the TSC. The basket is subjected to its self-weight only. For the off-normal and accident events associated with loadings in the transverse direction of the basket (e.g., off-normal handling load, concrete cask tip-over accident), the weight of the fuel assemblies is supported by the 21 fuel tubes, side support weldments, and corner support weldments. Referring to Figure 3.10.1-1, load transfer between the fuel tubes, '1', is through contact at the tube corners. This contact consists of two types: the connector pins and the region between pins where the tube sections are in contact. The connector pin slot connections at 20-inch center-to-center distance prevent the fuel tubes from sliding past each other. The shear load transmitted across the pins is reacted out in bearing in the fuel tube pin slots. The tube region between pins transmits bearing directly between fuel tubes. Shear loads between the tube corners can be transmitted by friction; however, friction is not considered in the finite element analyses of the basket. The detailed interaction between fuel tube corners, as well as a free-body diagram of a tube section, is shown in Figure 3.10.1-3. As the figure shows, the pin welded to one tube fits into the slots cut into the adjoining tube.

Connector pin assemblies are installed as redundant supports at the top and bottom of the fuel basket. The connector pin assemblies join adjacent fuel tubes to ensure each tube is properly aligned during the assembly process. The connector pin assembly provides an end weldment effect that allows for handling of the assembled basket outside of the TSC without special fixtures. The bottom connector pins also provide a standoff between the TSC bottom plate and basket tubes, and transmit bearing loads from the basket to the TSC bottom plate.

The corner and side support weldments provide rigidity to the basket. The weldments are attached to the fuel tube array by means of bolted boss connections. Bosses welded to the fuel tubes are slotted into the weldments. Connection is made with the use of a washer and bolt combination. Figure 3.10.1-1 and Figure 3.10.1-2 show the boss connection details, '2'. To ensure the connection is in tension, the bosses are designed not to penetrate completely through the weldment wall. Therefore, once installed and preloaded, the bolts are always in tension. Shear loads are reacted out by the interaction of the bosses, boss welds, and the support

weldments, '3'. When the support weldments are in compression, bearing loads are transferred through the support weldment to the fuel tube array, '4' (Figure 3.10.1-2). Figure 3.10.1-4 shows a free-body diagram of the fuel tube interaction with the support structure.

**3.10.1.2 Finite Element Model Descriptions**

This section describes the finite element models used in the PWR basket structural evaluation. The following describes the finite element models and the applicable ASME Code section.

| Finite Element Model      | Analysis Usage   | Loading Condition | ASME Code Section |
|---------------------------|--|-------------------|-------------------|
| 3D Periodic Model         | Off-normal TSC handling conditions (loads in basket in transverse direction) | Level C           | III-NG            |
| 3D Thermal Stress Model   | Thermal stress evaluation  | Level A           | III-NG            |
| 3D Periodic Plastic Model | Concrete cask tip-over accident evaluation                                   | Level D           | III-NG, App. F    |

**3.10.1.2.1 PWR Basket Three-Dimensional Periodic Models**

Two three-dimensional periodic half-symmetry models of the PWR basket are used to calculate the stresses in the basket due to the transverse loading during the off-normal TSC handling conditions. These models correspond to the critical basket orientations, 0° and 45°, as shown in Figure 3.10.1-5 and Figure 3.10.1-6. The fuel tube support pins and slot joints are spaced on 20.0-inch centers. Therefore, the periodic model extends from the axial center of a fuel tube support pin to the midpoint of the fuel tube between the pins (10.0-inch segment). The end effect of the basket on pinned connections is ignored.

The finite element models are constructed using ANSYS SOLID45, SHELL63, and BEAM4 elements. Fuel tube assemblies, pins, and side support weldments are modeled using SOLID45 elements. Corner weldment plates are modeled using SHELL63 elements. BEAM4 elements are used to model the support bars on the corner support weldments. The interaction between fuel tubes, corner support assemblies, and side support assemblies are modeled with CONTAC52 gap elements. These gap elements allow the transfer of loads between the basket structural components. The fuel tube/pin interaction is also modeled with the CONTAC52 elements at the gap between the pin and the tube slot. BEAM4 elements with minimal properties (Area = 0.001 in<sup>2</sup>) are defined at pin-to-slot weld locations between the fuel tubes and pins to assist in obtaining convergence of the ANSYS solution. CONTAC52 gap elements are used to simulate the total gap between the PWR basket and the transfer cask. The effect of the TSC shell is conservatively not included in the model.



The corner support and side support weldment assemblies are bolted to the fuel tube array at eight locations in the half-symmetry basket models. The bolt/boss joints are modeled using LINK10 (tension only) elements for the bolts and COMBIN40 elements for the boss. The COMBIN40 elements represent the shear restraint generated by the bosses welded to the fuel tubes.

Loads and boundary conditions are discussed in Section 3.10.1.3. The weight of the neutron absorbers and the retainers, which are not included in the finite element model, are considered by adjusting the density of the carbon steel for the fuel tube sides.

#### **3.10.1.2.2 PWR Basket Three-Dimensional Thermal Stress Model**

The structural evaluation for thermal stresses is performed using a three-dimensional quarter-symmetry finite element model, as shown in Figure 3.10.1-7. The model represents the top or bottom 47 inches of the PWR basket to evaluate the bounding axial and radial thermal gradients considering the end restraint of the basket due to the connector pin assemblies. This model includes the connector pin assemblies at the end of the fuel tubes and two intermediate pin and bolt locations. The connector pin assemblies at the end of the basket are modeled with nodal constraints in the basket transverse directions at the interface of two adjacent connector pins. The modeling methodology of the model is the same as that of the three-dimensional periodic model as discussed in Section 3.10.1.2.1.

#### **3.10.1.2.3 PWR Basket Three-Dimensional Periodic Plastic Model**

The evaluation of the PWR basket of the cask tip-over event is performed using two three-dimensional plastic periodic models, as shown in Figure 3.10.1-8 and Figure 3.10.1-9 for 0° and 45° basket orientations, respectively. The models are similar to the three-dimensional periodic models used for the off-normal handling evaluations presented in Section 3.10.1.2.1. In this model, the SHELL43 elements are used for the corner weldment mounting plates instead of SHELL63 elements. SHELL43 elements are also used for the corner weldment support bars instead of BEAM4 elements. The CONTAC52 elements are used to model the interface between basket components except that CONTA173 and TARGE170 elements are used to model the interaction of the pins and fuel tube slots, as shown in Figure 3.10.1-10. CONTAC52 elements are also used to simulate the gap between the PWR basket and the canister shell in the vertical concrete cask. The bolt/boss joints are modeled the same as in the three-dimensional period model using LINK10 and COMBIN40 elements. Bilinear elastic-plastic material properties are used for all basket components in the model.

Loads and boundary conditions are discussed in Section 3.10.1.3. The weight of the neutron absorbers and the retainers, which are not included in the finite element model, are considered by adjusting the density of the carbon steel for the fuel tube sides.

### **3.10.1.3 Finite Element Model Boundary Conditions**

#### **3.10.1.3.1 Off-Normal Handling Boundary Conditions**

For off-normal handling events, the three-dimensional periodic models described in Section 3.10.1.2.1 are used to calculate the stresses due to loading in the transverse direction of the basket. The gap between the basket and the transfer cask is 0.62 inch (0.12-inch basket-TSC and 0.50-inch TSC-cask). To represent the loads from the fuel assemblies, a bounding pressure load of 1.2 psi is applied to the fuel tubes.

The boundary conditions for 0° and 45° basket orientations are shown in Figure 3.10.1-11 and Figure 3.10.1-12, respectively. For off-normal events, an inertia load of 0.707g (resultant of 0.5g loading in the two transverse directions) is applied in the transverse direction of the basket. Applied pressure loads for fuel assemblies are also multiplied by 0.707g.

The 0° and 45° basket orientations are critical for the PWR basket for loading in the transverse direction. The 0° basket orientation maximizes the stresses in the fuel tube sidewalls and the 45° basket orientation maximizes the bending stresses in the tube corners. Intermediate basket orientations are bounded by the 0° and 45° orientations. Therefore, the basket evaluation is performed using two half-symmetry models for the 0° and 45° basket orientations, respectively. Symmetry boundary conditions are applied at the plane of symmetry. Symmetry boundary conditions are also applied to both ends of the finite element model to represent a periodic section of the basket. CONTAC52 elements are used at the periphery of the basket to represent the interface of the basket and the canister shell inside the transfer cask. Outer nodes of the CONTAC52 elements are fixed. For off-normal events, material properties at 100°F are conservatively used (using the modulus of elasticity for carbon steel at lower temperature results in slightly higher stress results.)

#### **3.10.1.3.2 Thermal Stress Analysis Boundary Conditions**

The three-dimensional quarter-symmetry model described in Section 3.10.1.2.1 is used to calculate the thermal stress due to the thermal expansion. As shown in the following table, a total of five cases of temperature boundary conditions are defined that envelop the maximum temperature gradients ( $\Delta T$ ) in the axial and radial directions of the basket for all conditions of storage and transfer. Prior to performing the thermal stress analysis, the steady-state temperature

distribution in the model is determined by a thermal conduction analysis. The SOLID45, SHELL43 and BEAM4 structural elements were converted to SOLID70, SHELL57 and LINK33 thermal elements, respectively, for the thermal conduction solution.

**Thermal Boundary Temperatures – PWR Basket (°F)**

| C           |     | Axial end of basket | D            |     |
|-------------|-----|---------------------|--------------|-----|
| Center Line |     | 47"                 | Outer Radius |     |
| A           |     |                     |              | B   |
| Case        | A   | B                   | C            | D   |
| 1           | 600 | 440                 | 360          | 300 |
| 2           | 680 | 500                 | 580          | 440 |
| 3           | 640 | 520                 | 700          | 590 |
| 4           | 430 | 380                 | 210          | 260 |
| 5           | 700 | 500                 | 550          | 400 |

Symmetry boundary conditions are applied at the planes of symmetry. In the basket axial direction, the model is restrained at one end.

**3.10.1.3.3 Concrete Cask Tip-Over Accident Boundary Conditions**

The concrete cask tip-over is evaluated as a side impact for the basket. During the concrete cask tip-over event, acceleration varies from 1g at the bottom of the concrete cask to a maximum acceleration at the top of the TSC. The three-dimensional plastic model is used for the evaluation of the basket (Section 3.10.1.2.3). A bounding acceleration of 35g is applied to the basket models in the transverse direction. The 35g acceleration bounds the maximum acceleration in the basket, including the dynamic load factor for the concrete cask tip-over accident.

Pressure loads are applied to the PWR basket models to represent the fuel assembly weight with a 35g acceleration.

For the tip-over accident (loading in the transverse direction), the 0° and 45° basket orientations are critical for the PWR basket as discussed in Section 3.10.1.2.3. Therefore, the basket is evaluated using models corresponding to the 0° and 45° basket orientations. Symmetry boundary conditions are applied at the plane of symmetry. Symmetry boundary conditions are also applied to both ends of the three-dimensional periodic finite element model. CONTAC52 elements are used to represent the interface of the basket and the canister shell inside the concrete cask. The location of the outer nodes of the gap elements at the basket periphery incorporates the canister shell displacements during the concrete cask tip-over accident. The canister shell displacement at approximately mid-height (100 inches from canister bottom) of the canister shell is used. This is conservative since the g-load at this location is significantly lower than the bounding g-load

used in the basket analysis (35g). The boundary conditions for these models are shown in Figure 3.10.1-11 and Figure 3.10.1-12. For accident conditions, material properties at 100°F are conservatively used.

#### **3.10.1.4 Post-Processing Finite Element Analysis Results**

##### **3.10.1.4.1 Maximum Stresses for Off-Normal Handling Condition**

The post-processing of the finite element analysis results from the periodic model for the off-normal event is performed by taking section cuts at various locations in the model.

The fuel tube section cuts are divided into two regions. Region 1 is the region between the pin supports. For the periodic model, this region is defined from the base of the model (mid-distance between pins) to the base of the pin. Region 2 is the pin region. This region starts at the base of the pin and extends to the top of the finite element model (mid-plane of pin). For both regions, the region just above and below the pin cutout ( $\pm 0.25$  inch) is omitted from the section cuts to eliminate stress concentrations in the model. The membrane stresses are calculated by taking a section cut at the center of the tube thickness. The membrane plus bending stress is calculated by taking the maximum of the stresses calculated at the inner or outer surface of the fuel tube. Refer to Figure 3.10.1-13 through Figure 3.10.1-16 for the tube identification and the locations of the section cuts.

The maximum stresses for the corner support weldments are calculated by taking section cuts along the length of the weldment (ten inches for the periodic model). Since the corner weldment is modeled using SHELL63 elements, the membrane stresses are calculated at the mid plane of the element and the membrane plus bending stresses are calculated using the maximum stresses of either the inner or outer surface of the element. Refer to Figure 3.10.1-17 and Figure 3.10.1-18 for the locations of the section cuts.

The maximum stresses for the side weldments are calculated taking section cuts along the length of the weldment (ten inches for the periodic model). The membrane stresses are calculated by taking a section cut at the mid-thickness of the weldment. The membrane plus bending stress is calculated by taking the maximum of the stresses calculated at the inner or outer surface of the weldment. Refer to Figure 3.10.1-19 and Figure 3.10.1-20 for the locations of the section cuts.

The bolt tensile loads are obtained from the LINK10 element results. The boss shear loads are extracted from the COMBIN40 element results.

#### **3.10.1.4.2 Maximum Thermal Stresses**

The post-processing of the finite element analysis results for the thermal stress evaluation is performed by extracting the maximum nodal stress intensities from the model. The maximum nodal stress is obtained for two separate regions: (1) fuel tubes and (2) corner and side support weldments. The bolt tensile loads are extracted from the LINK10 elements, and the boss shear loads are extracted from the COMBIN40 elements.

#### **3.10.1.4.3 Maximum Stresses for Concrete Cask Tip-Over Accident**

The post-processing of finite element analysis results for the basket tip-over accident using the three-dimensional plastic model is performed by extracting stresses in the basket for the 0° and 45° basket orientations.

For the fuel tube stresses, the primary membrane stresses are calculated by extracting the maximum nodal stress at the mid-thickness of the tube wall. Based on the differences in stress criterion summarized from the plastic finite element results [i.e.,  $(\sigma + 3\tau)^{1/2}$ ] and the ASME Code, Section III stress criterion [i.e.,  $(\sigma + 4\tau)^{1/2}$ ], calculated membrane stress results are conservatively increased by a factor of  $(4/3)^{1/2}$ . The primary membrane plus bending stresses are evaluated by extracting the maximum stress intensity results of each fuel tube.

The stresses for the corner and side support weldments are calculated using the three-dimensional plastic models. The maximum primary membrane plus bending stress intensity for the corner and side weldments are extracted from the model. The maximum primary membrane plus bending stress intensity is compared to the membrane allowable to obtain a conservative bounding factor of safety.

Figure 3.10.1-1 Expanded View of PWR Basket

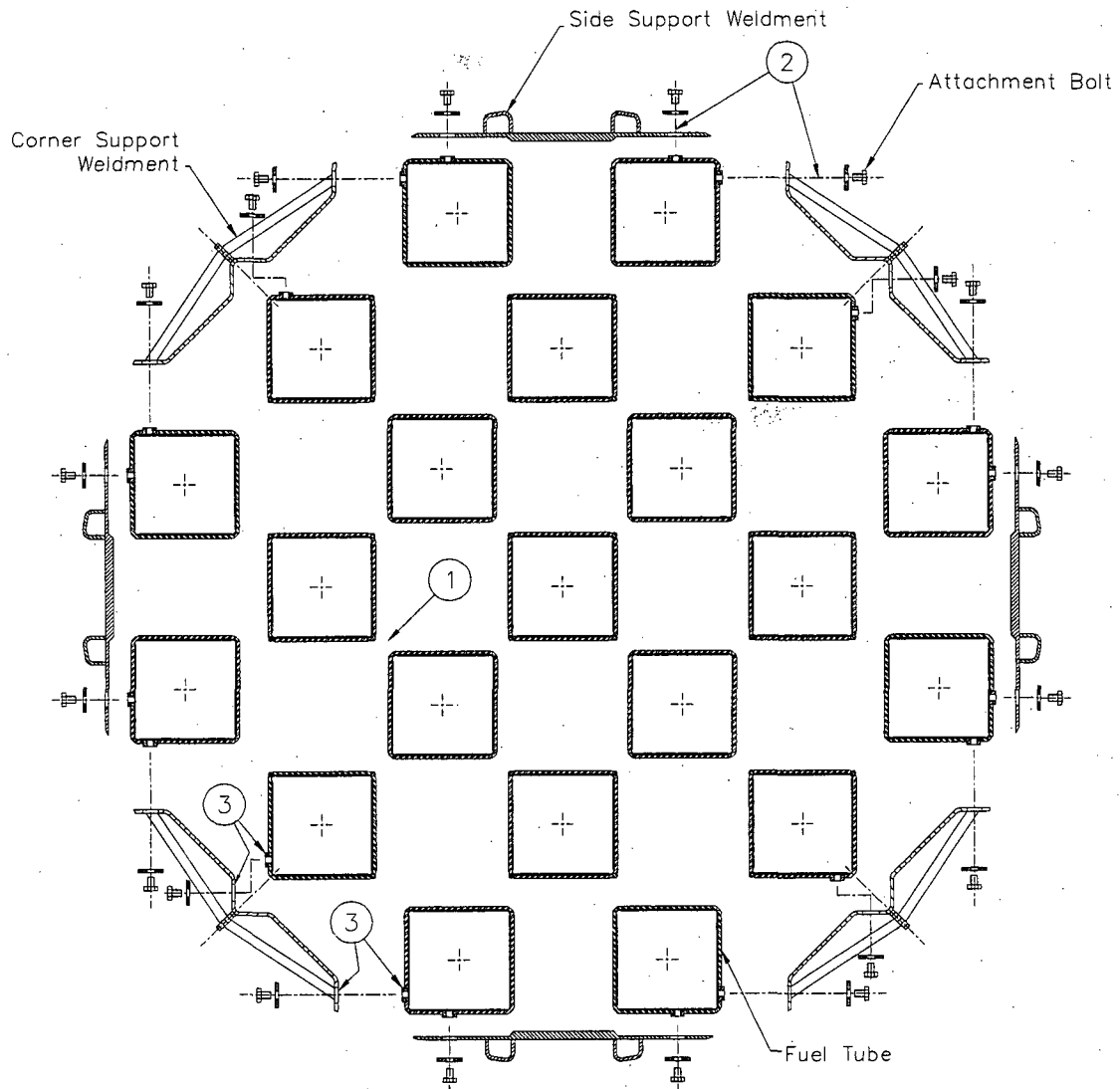


Figure 3.10.1-2 Bolted Attachment Details

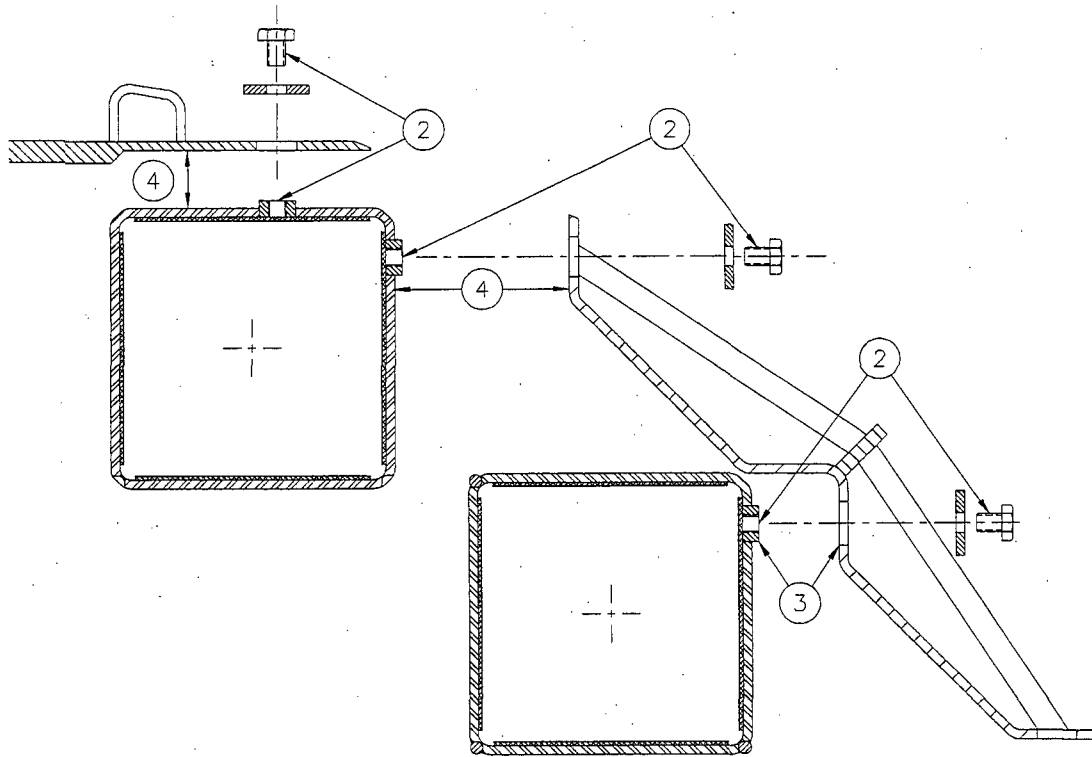
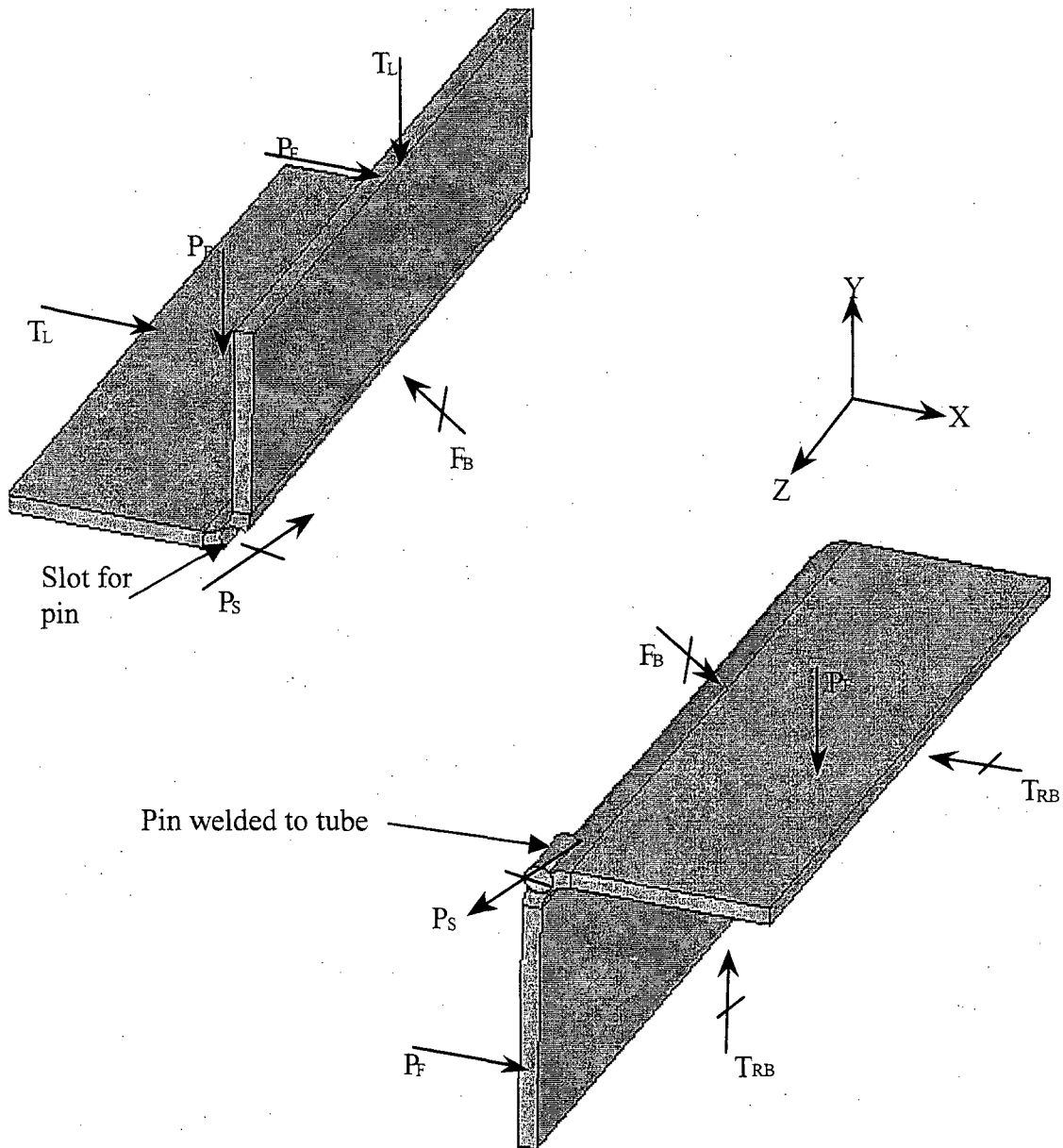


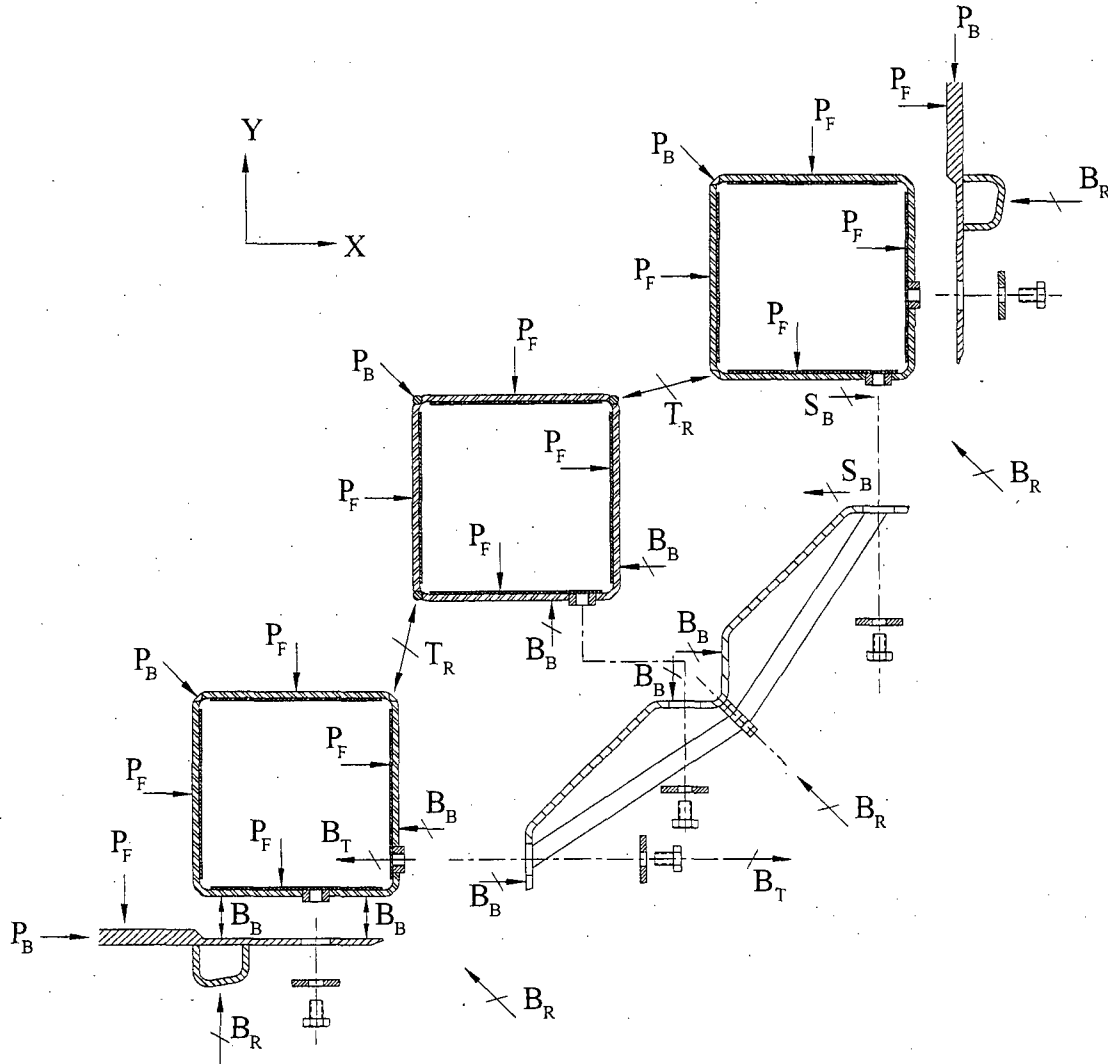
Figure 3.10.1-3 Free-Body Diagram of PWR Basket Fuel Tube Detail



- $T_L$  Loads from adjacent tube or fuel assembly
- $P_F$  Local load due to fuel assembly
- $T_{RB}$  Reaction loads in tubes for equilibrium at symmetry planes of tubes
- $P_S$  Shear Reaction thru pin joint (in the XY plane)
- $F_B$  Bearing Reaction across tube flat



Figure 3.10.1-4 Free-Body Diagram of Basket Support Structure



- $P_B$  Loads due to adjacent basket structure
- $P_F$  Local load due to fuel assembly
- $B_R$  Basket reaction with TSC shell locations
- $B_T$  Tensile load at bolt and tube boss (typical)
- $B_B$  Bearing reaction between tube sidewall and support structure (typical)
- $S_B$  Shear reaction between support structure and tube boss (typical)
- $T_R$  Reactions between tubes detailed in Figure 3.10.1-3

Figure 3.10.1-5 PWR Basket Periodic Model – 0° Basket Orientation

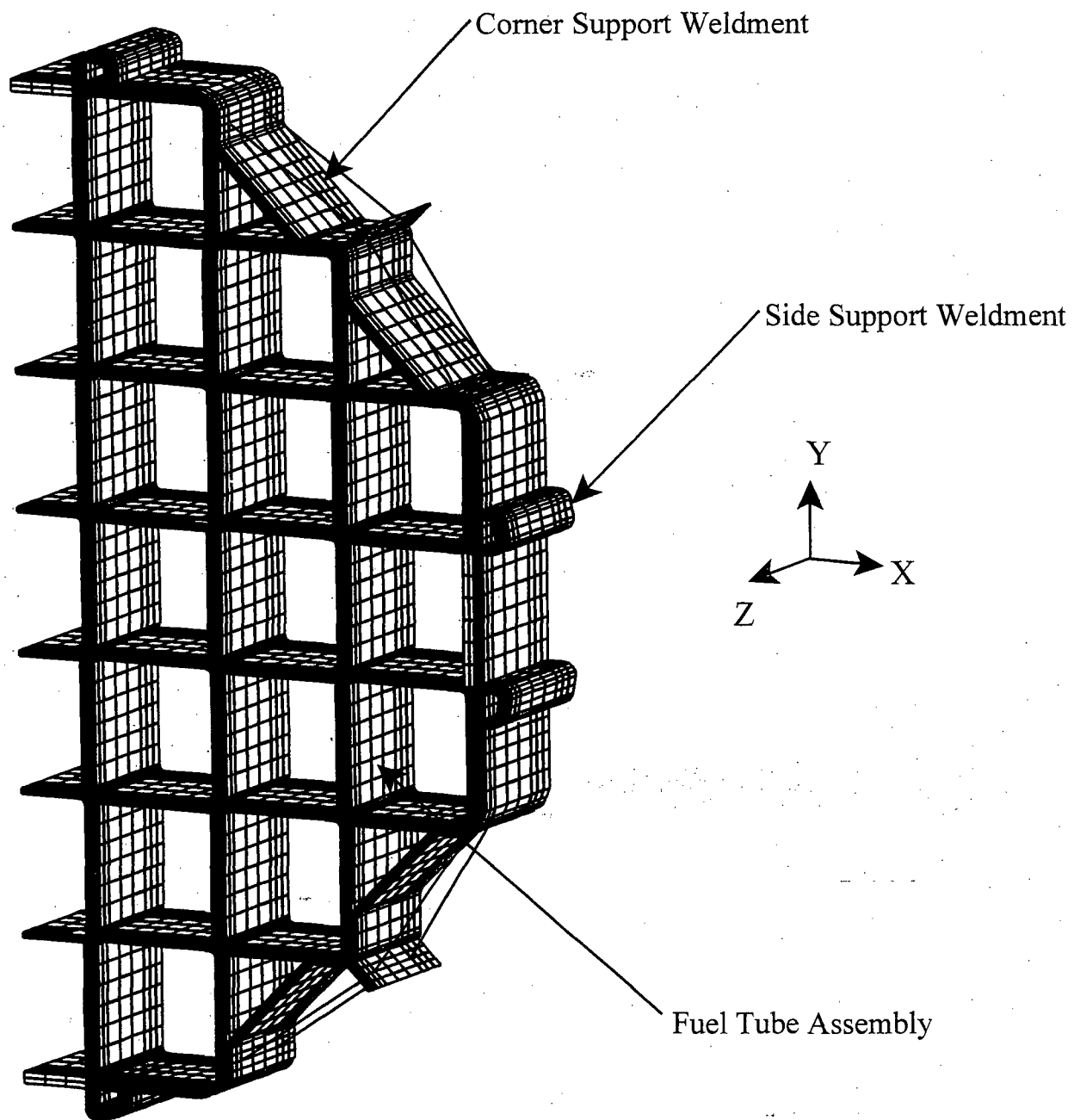


Figure 3.10.1-6 PWR Basket Periodic Model – 45° Basket Orientation

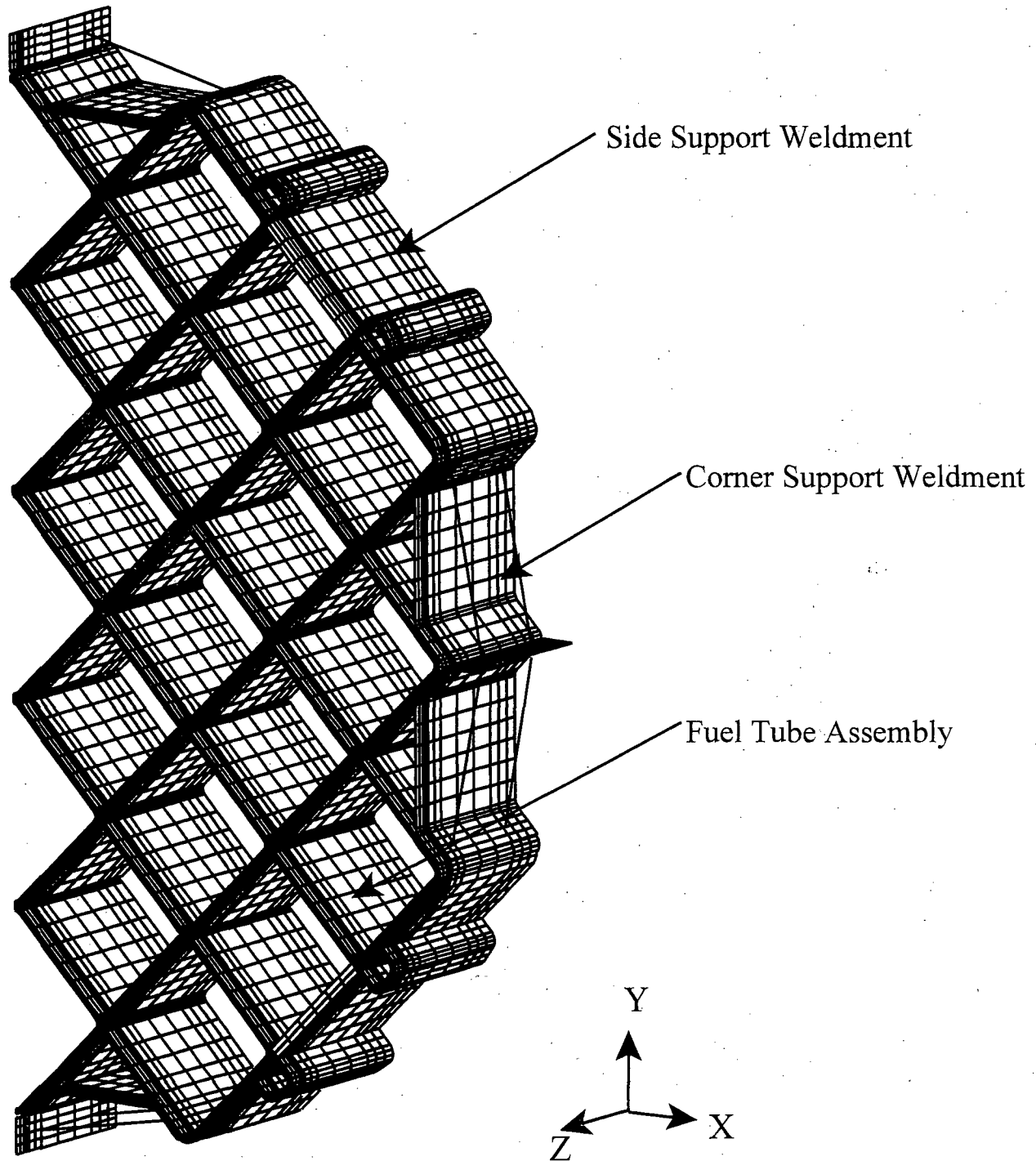


Figure 3.10.1-7 Thermal Stress Evaluation Model

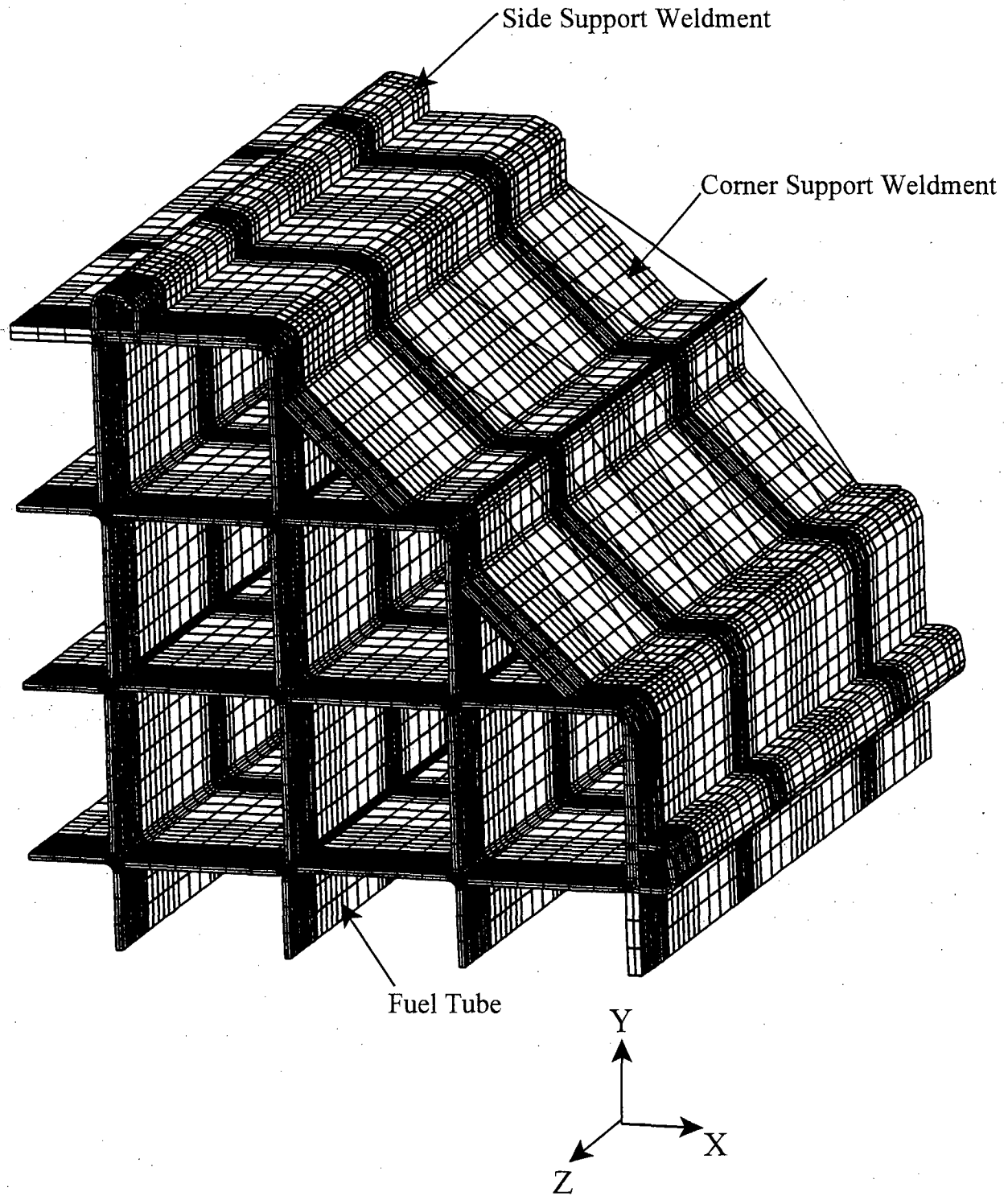


Figure 3.10.1-8 PWR Basket Plastic Model - 0° Basket Orientation

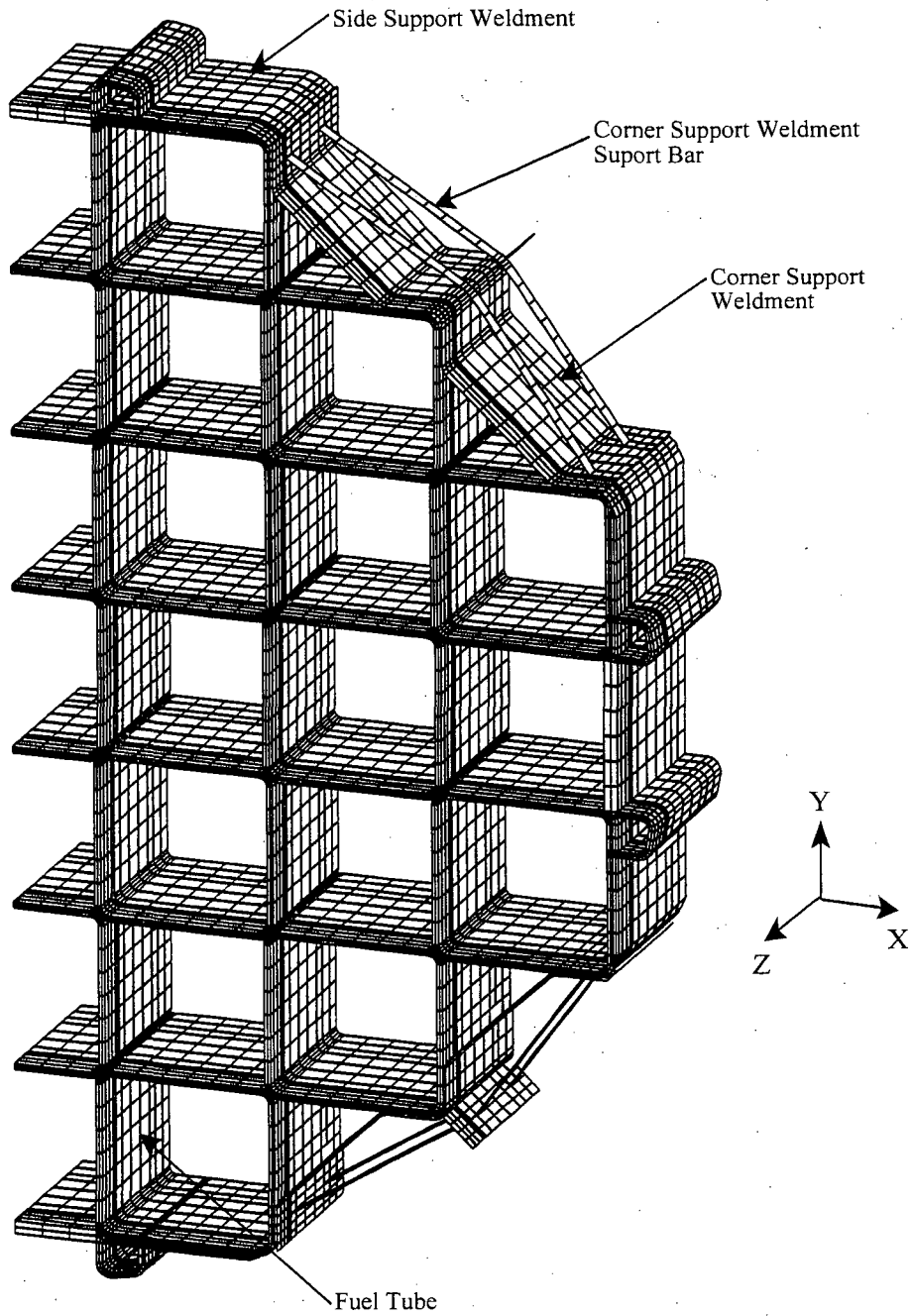


Figure 3.10.1-9 PWR Basket Plastic Model - 45° Basket Orientation

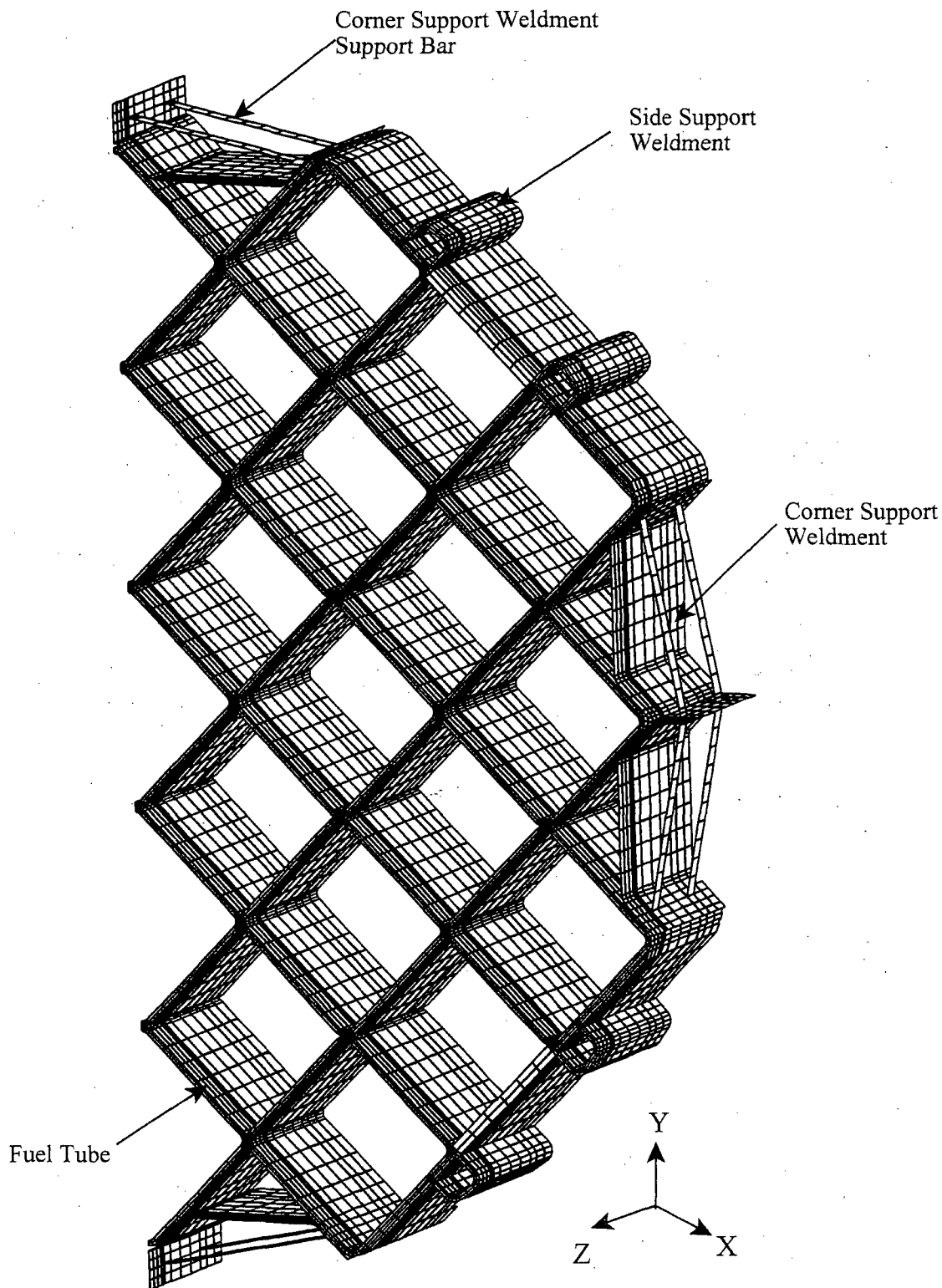


Figure 3.10.1-10 Typical PWR Fuel Tube Pin Finite Element Model Details

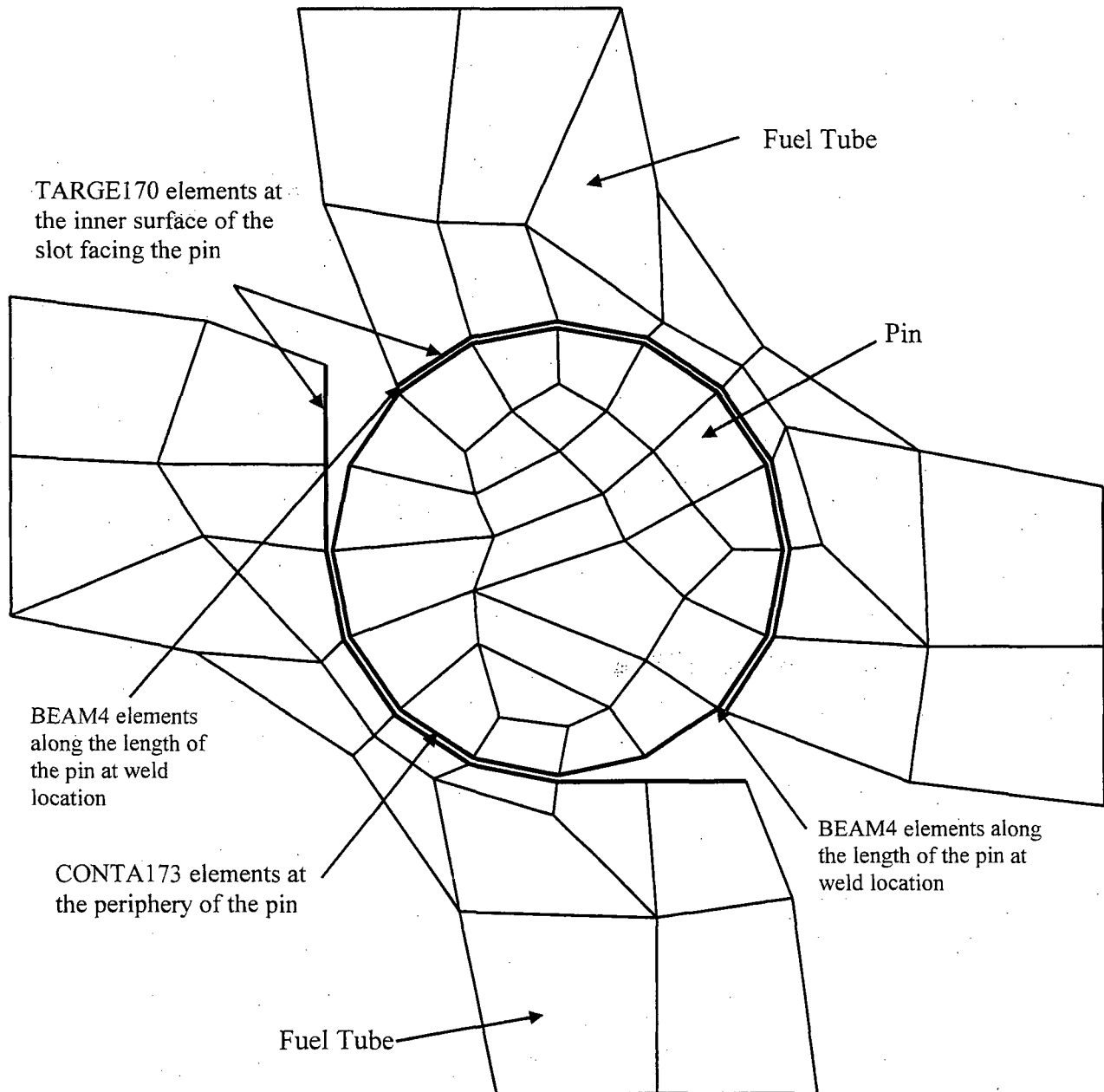


Figure 3.10.1-11 PWR Basket Model Boundary Conditions for a Transverse Loading –  
0° Basket Orientation

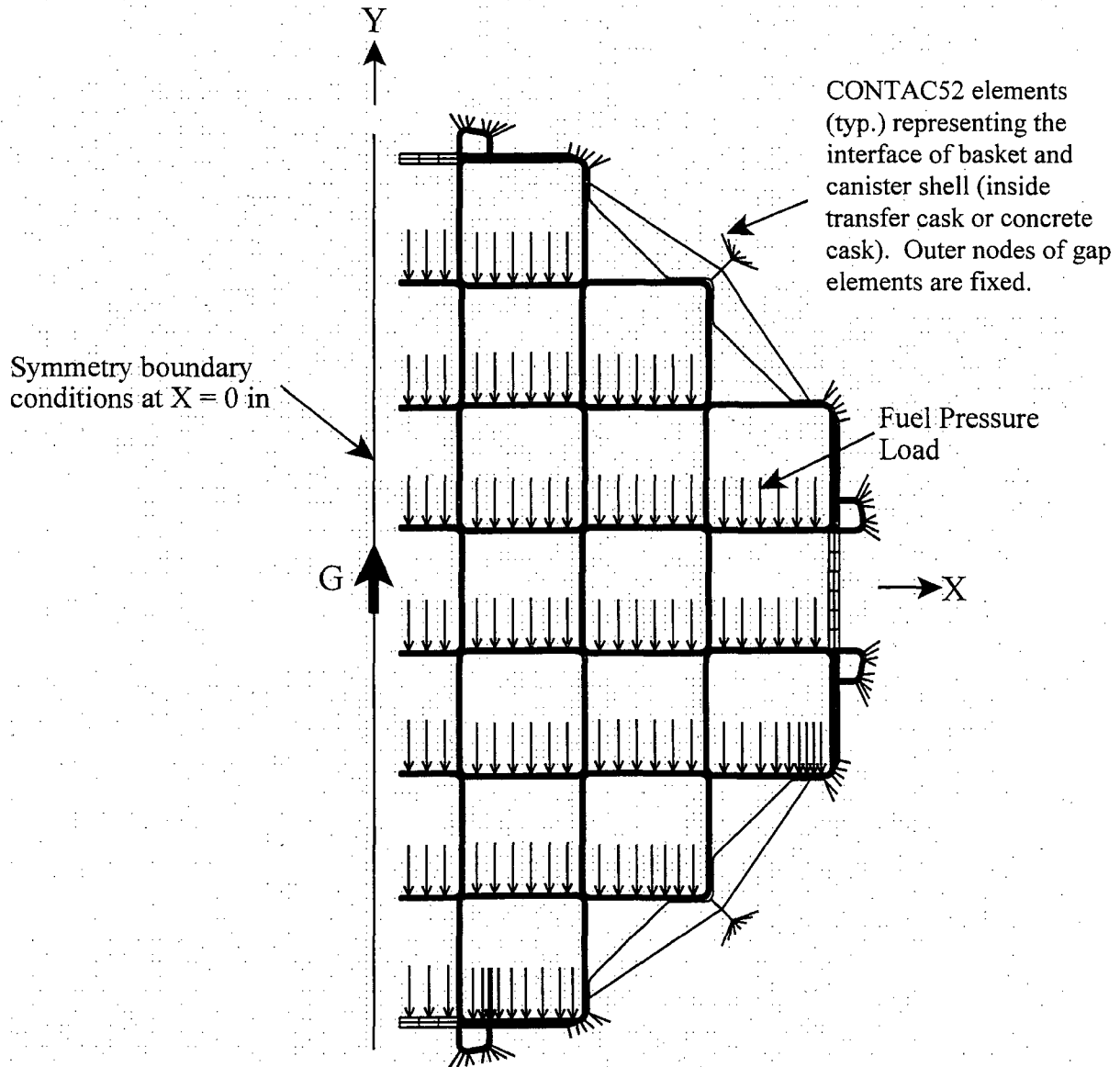




Figure 3.10.1-12 PWR Basket Model Boundary Conditions for a Transverse Loading –  
45° Basket Orientation

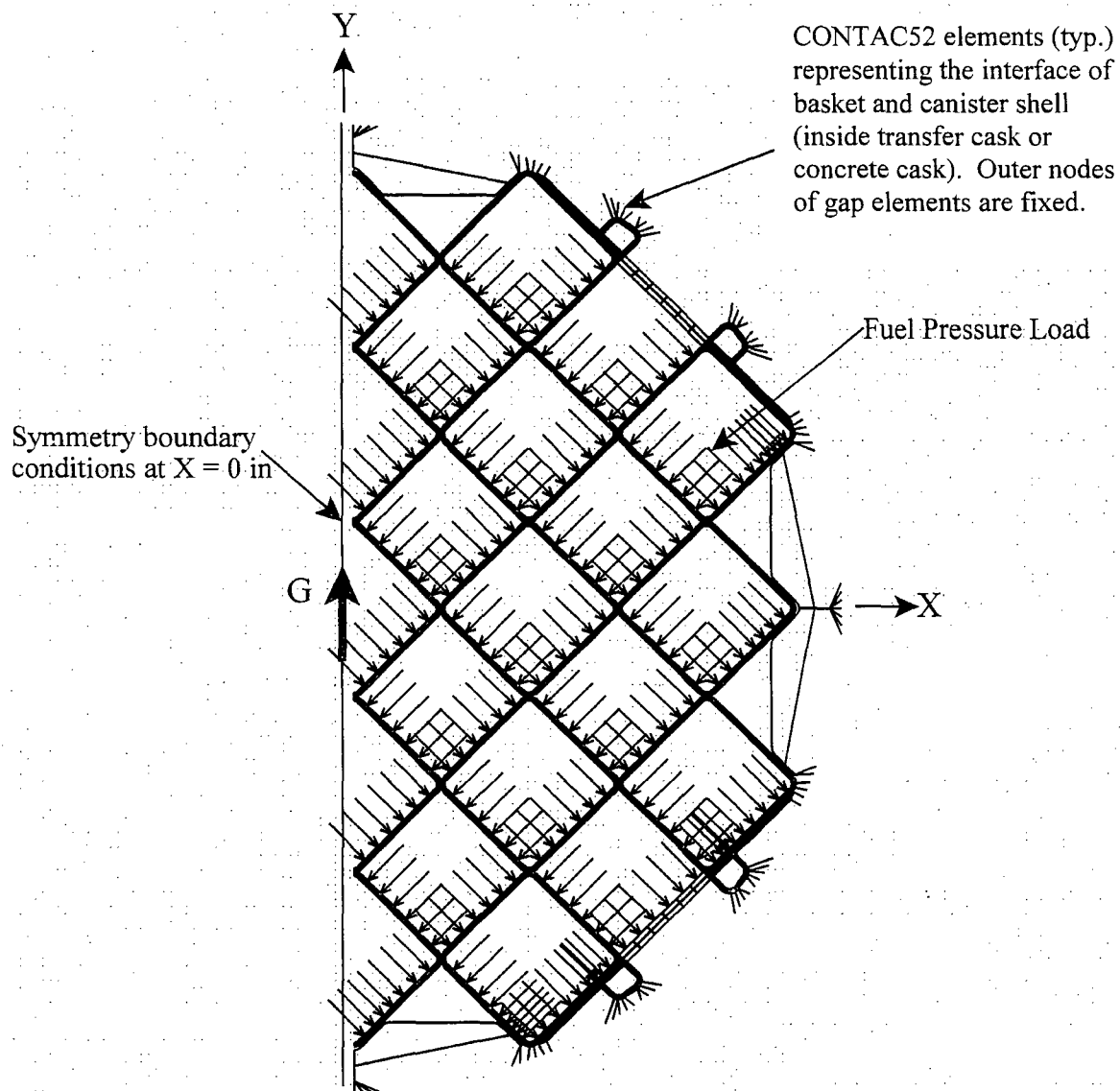


Figure 3.10.1-13 PWR Fuel Tube Array – 0° Basket Orientation

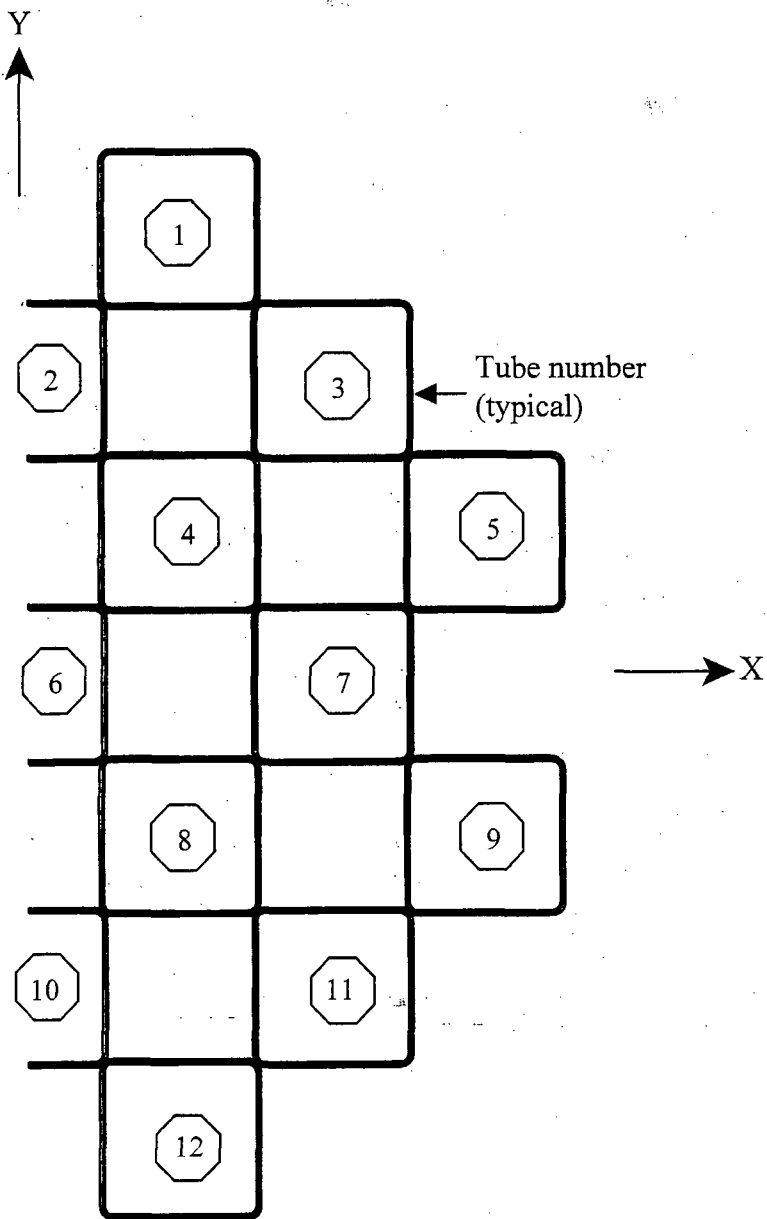


Figure 3.10.1-14 PWR Fuel Tube Section Cuts – 0° Basket Orientation

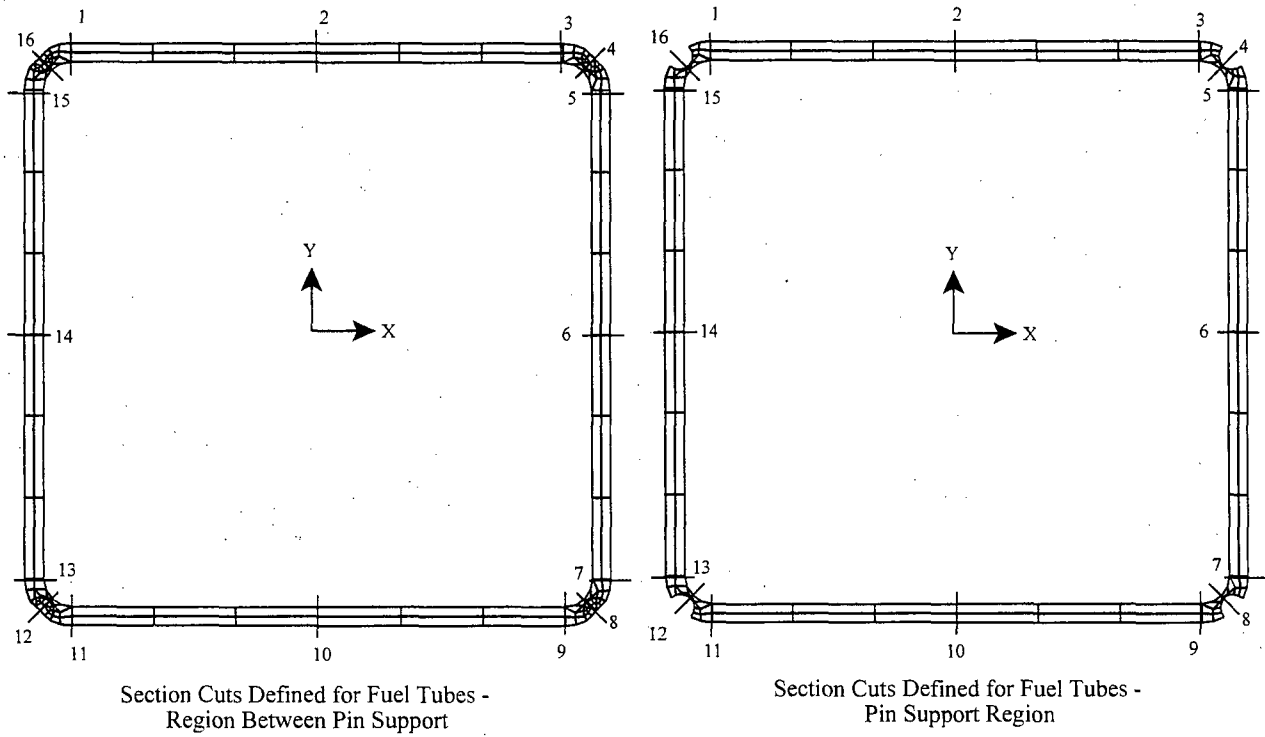


Figure 3.10.1-15 PWR Fuel Tube Array – 45° Basket Orientation

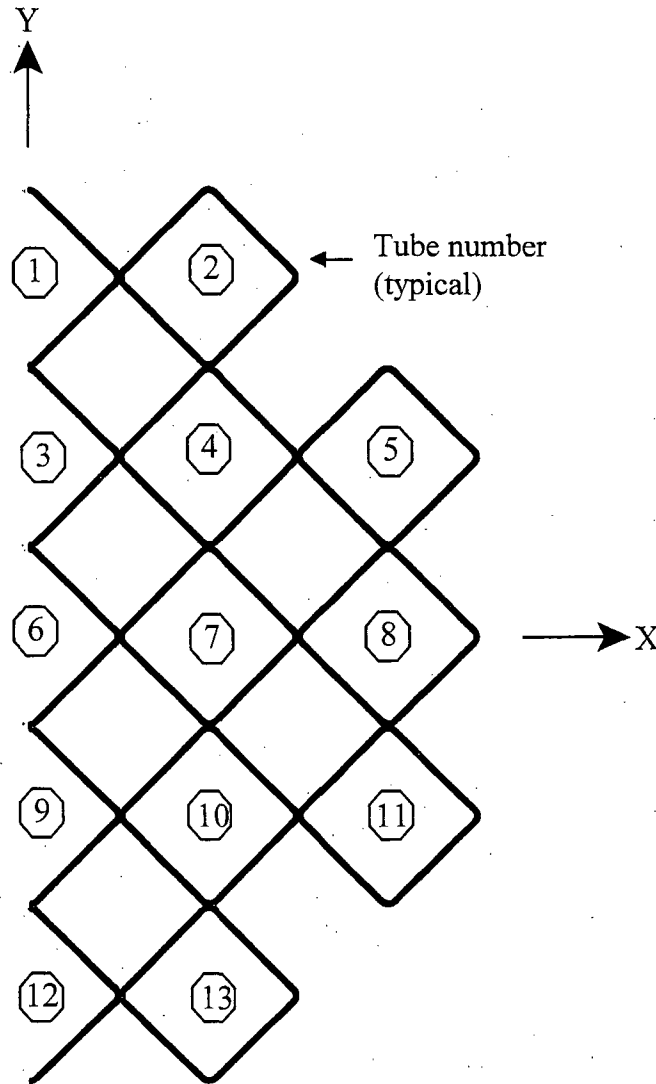
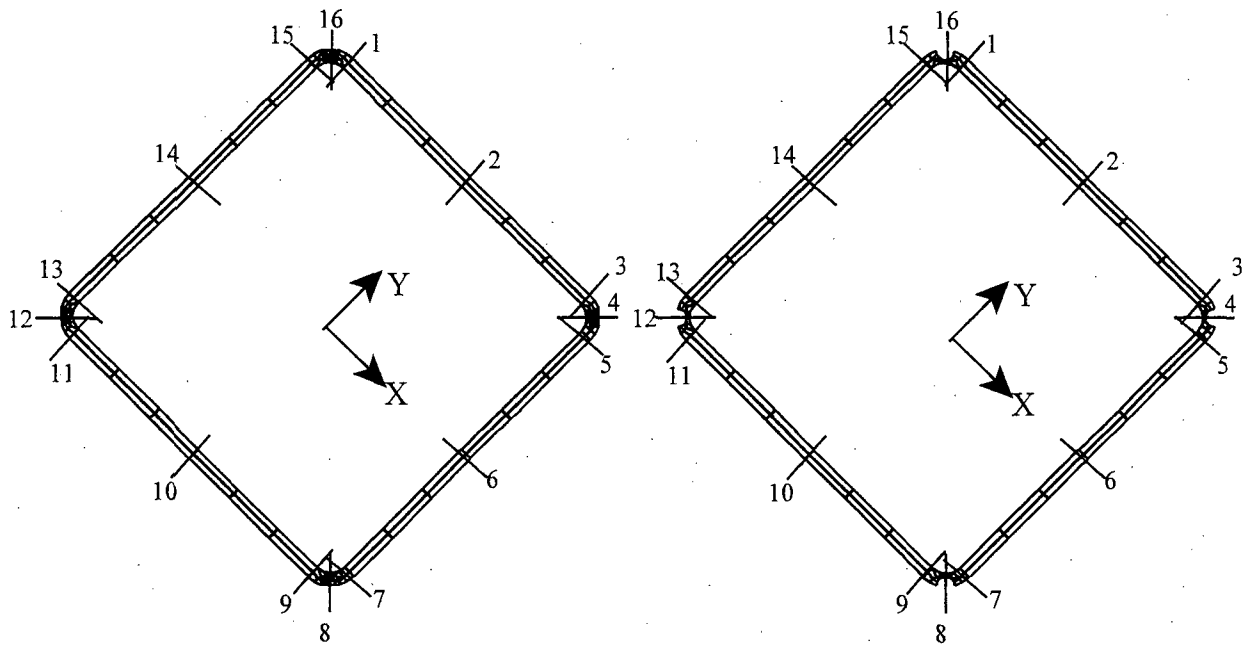


Figure 3.10.1-16 PWR Fuel Tube Section Cuts – 45° Basket Orientation



Section Cuts Defined for Fuel Tubes -  
Region Between Pin Support

Section Cuts Defined for Fuel Tubes -  
Pin Support Region

Figure 3.10.1-17 PWR Corner Support Weldment Section Cuts – 0° Basket Orientation

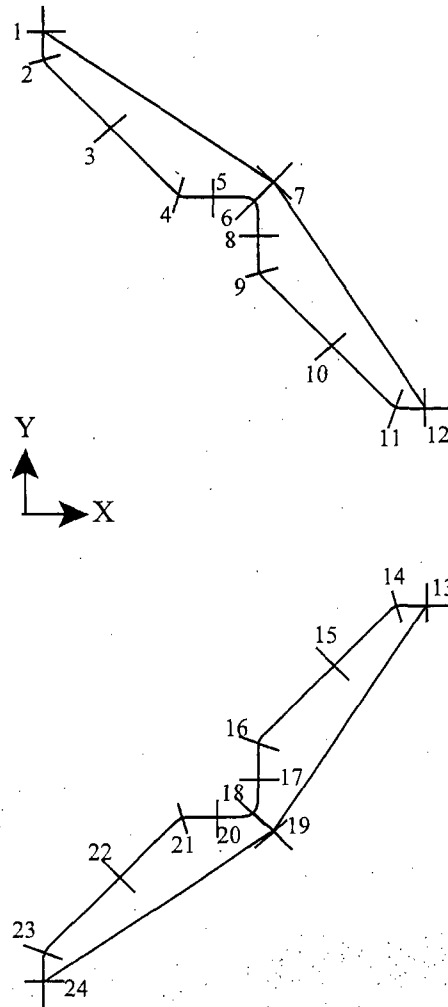


Figure 3.10.1-18 PWR Corner Support Weldment Section Cuts – 45° Basket Orientation

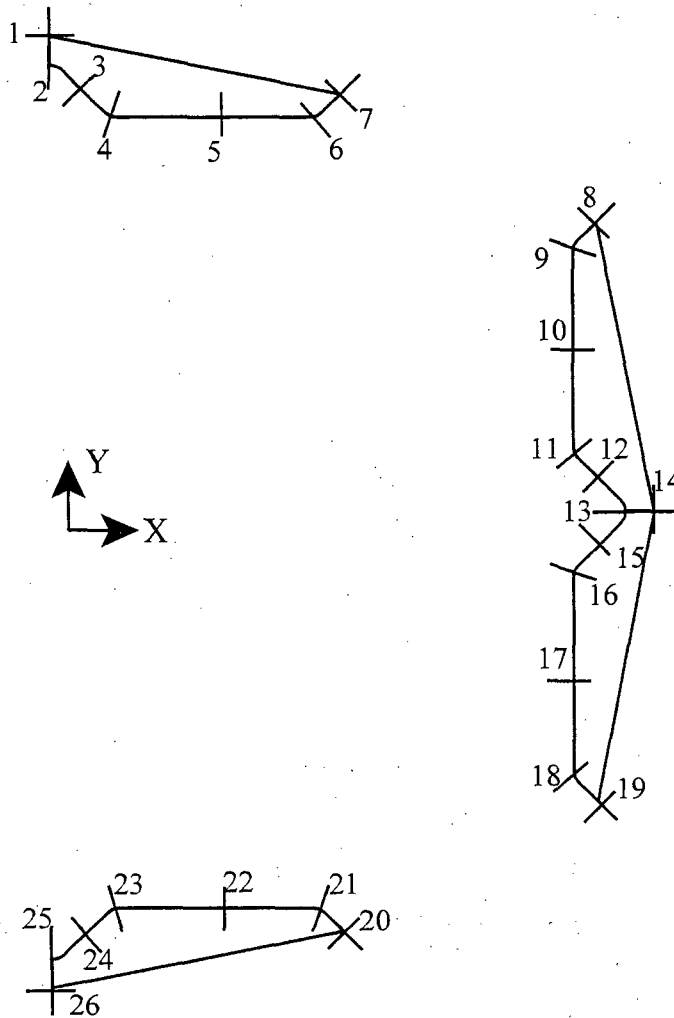


Figure 3.10.1-19 PWR Side Support Weldment Section Cuts – 0° Basket Orientation

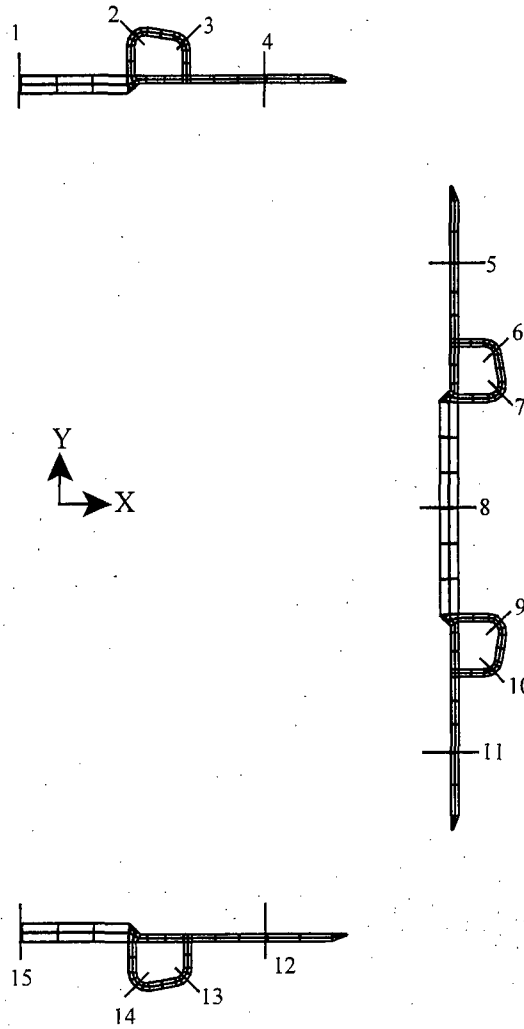
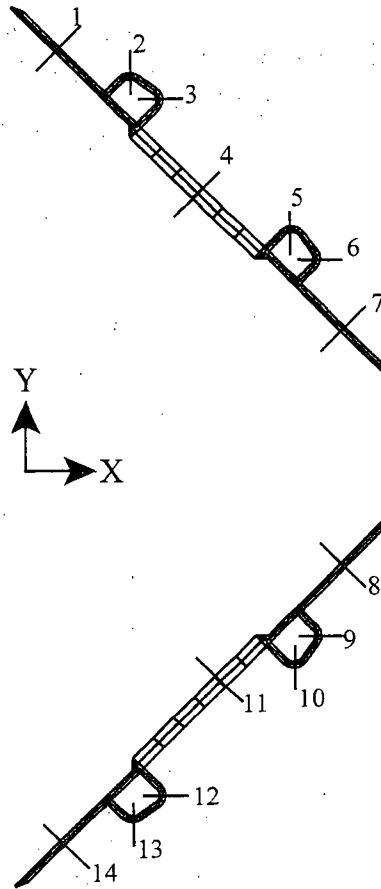




Figure 3.10.1-20 PWR Side Support Weldment Section Cuts – 45° Basket Orientation



### 3.10.2 BWR Fuel Basket Finite Element Models

#### 3.10.2.1 Load Path Description

This section explains the load paths in the basket that ensure the structural integrity of the BWR MAGNASTOR during all conditions of storage. The MAGNASTOR BWR fuel basket is designed to accommodate 87 BWR fuel assemblies. For normal conditions of storage, the weight of the fuel assemblies is directly supported by the bottom plate of the TSC. The basket is subjected to its self-weight only. For the off-normal and accident conditions associated with loadings in the transverse direction of the basket (e.g. off-normal handling load, concrete cask tip-over accident), the weight of the fuel assemblies is supported by the 45 fuel tubes, side support weldments, and the corner support weldments. Referring to Figure 3.10.2-1, load transfer between the fuel tubes, '1', is through bearing contact at the corners. The bearing contact consists of two load paths: the connector pins transmit load directly between each fuel tube; and where the tubes are in contact, bearing loads are transmitted. The shear load transmitted across the pins is reacted out in bearing in the pin slots. The detailed interaction between fuel tube corners is shown in Figure 3.10.2-2 and Figure 3.10.2-3. As the figures show, the pins welded to one tube mate to the slots cut into the adjoining tube. Figure 3.10.2-3 shows a free-body diagram of the fuel tube pin joint. Frictional forces are not considered in the finite element analysis of the basket.

At the top and bottom of the fuel basket, connector pin assemblies are used to add additional support to the basket. The end basket configurations do not affect the periodic model analysis of the basket because the connector pin assemblies do not transmit loads in the lateral direction. The connector pin assemblies are installed as a redundant support for the basket system to maintain the structural configuration of the basket. The bottom connector pin assemblies also provide a standoff between the TSC bottom plate and basket tubes, and transmit bearing loads from the basket to the TSC bottom plate.

The corner and side support weldments provide rigidity to the basket. The weldments are attached to the fuel tube array by means of bolted boss connections. Bosses welded to the fuel tubes are slotted in to the weldments. Connection is made with the use of a washer and bolt combination. Referring to Figure 3.10.2-1 and Figure 3.10.2-2, the bolted joints, '2', are designed to transmit tensile loads. Therefore, once installed and preloaded the bolts are always in tension. Shear loads are reacted out by interaction of the bosses, boss welds, and the support weldments, '3'. If the support weldments are bearing on the fuel tube array, the load is

transferred through the bearing contact, '4', of the support weldments and fuel tube array (Figure 3.10.2-2). Figure 3.10.2-4 shows a free-body diagram of the fuel tube interaction with the basket support structure.

**3.10.2.2 Finite Element Model Descriptions**

This section describes the finite element models used in the BWR basket structural evaluation. The following table describes the finite element models and the applicable ASME Code section.

| Finite Element Model      | Analysis Usage   | Loading Condition | ASME Code Section |
|---------------------------|--|-------------------|-------------------|
| 3D Periodic Model         | Off-normal TSC handling conditions (loads in basket in transverse direction) | Level C           | III-NG            |
| 3D Thermal Stress Model   | Thermal stress evaluation  | Level A           | III-NG            |
| 3D Periodic Plastic Model | Concrete cask tip-over accident evaluation                                   | Level D           | III-NG, App. F    |

**3.10.2.2.1 BWR Basket Three-Dimensional Periodic Model**

Two three-dimensional periodic half-symmetry models of the BWR basket are used to calculate the stresses in the basket due to transverse loading during the off-normal TSC handling conditions. These models correspond to the critical basket orientations, 0° and 45°, as shown in Figure 3.10.2-5 and Figure 3.10.2-6. The fuel tube support pins are spaced on 20.0-inch centers; therefore, the periodic model extends from the axial center of a tube pin to the mid-point of the spacing between the pins, a 10.0-inch segment.

The finite element models are constructed using SOLID45, SHELL63, and BEAM4 elements. The fuel tube assemblies, pins, and side support weldments are modeled using SOLID45 elements. The weight of the poison plates is included in the finite element model by adjusting the density of the carbon steel for the fuel tube sides. The corner support weldment is modeled using SHELL63 elements for the vertical wall and support plates. Similar to the three-dimensional periodic model for PWR basket, the interaction between fuel tubes, corner support assemblies, and side support assemblies are modeled with CONTAC52 gap elements. These gap elements allow the transfer of loads between the basket structural components. The fuel tube/pin interaction is also modeled with the CONTAC52 elements at the gap between the pin and the tube slot. For the basket structural evaluation, the TSC is not modeled. CONTAC52 gap elements are used to model the total gap between the BWR basket and the transfer cask.

The corner support and side support assemblies are bolted to the fuel tube array at eight locations in the half-symmetry basket model. The bolt/boss joints are modeled using LINK10 tension only

elements for the bolts and COMBIN40 elements for the boss. The COMBIN40 elements represent the shear restraint generated by the bosses welded to the fuel tubes.

Loads and boundary conditions are discussed in Section 3.10.2.3. The weight of the neutron absorbers and the retainers, which are not included in the finite element model, are considered by adjusting the density of the carbon steel for the fuel tube sides.

#### **3.10.2.2.2 BWR Basket Three-Dimensional Thermal Stress Model**

The structural evaluation for thermal stresses is performed using a three-dimensional quarter-symmetry finite element modeled, as shown in Figure 3.10.2-7. The three-dimensional model represents the top or bottom 43 inches of the BWR basket to evaluate the bounding axial and radial thermal gradients considering the end restraint of the basket due to the connector pin assemblies. This model includes the connector pin assemblies at the end of the fuel tubes and two intermediate pin and bolt locations. The connector pin assemblies at the end of the basket are modeled with nodal constraints in the basket transverse directions at the interface of two adjacent connector pins. The modeling methodology of the model is the same as that of the three-dimensional periodic model as discussed in Section 3.10.2.2.1.

#### **3.10.2.2.3 BWR Basket Three-Dimensional Periodic Plastic Model**

The evaluation of the BWR basket for the cask tip-over event is performed using two three-dimensional plastic periodic models, as shown in Figure 3.10.2-8 and Figure 3.10.2-9. The models are similar to the periodic model presented in Section 3.10.2.2.1. SHELL43 elements are used for the corner support weldment. Other modeling details are identical to those described in Section 3.10.1.2.3 for the three-dimensional periodic plastic model for the PWR basket. A typical model detail for the pin-slot connections is shown in Figure 3.10.2-10.

Loads and boundary conditions are discussed in Section 3.10.2.3. The weight of the neutron absorbers and the retainers, which are not included in the finite element model, are considered by adjusting the density of the carbon steel for the fuel tube sides.

#### **3.10.2.3 Finite Element Model Boundary Conditions**

##### **3.10.2.3.1 Off-Normal Handling Boundary Conditions**

The three-dimensional periodic models as described in Section 3.10.2.2.1 are used to calculate the stresses due to loading in the transverse direction of the basket for off-normal handling conditions. The gap between the basket and the transfer cask is 0.62 inch (0.12-inch basket-TSC and 0.50-inch TSC-cask). To represent the loads from the fuel assemblies, a bounding pressure load is applied to the fuel tubes.

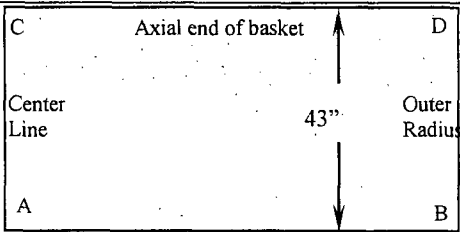
The boundary conditions are the models for 0° and 45° basket orientations, as shown in Figure 3.10.2-11 and Figure 3.10.2-12, respectively. For off-normal events, an inertia load of 0.707g (resultant of 0.5g acceleration applied in the two transverse directions) is applied in the transverse direction of the basket. Applied pressure loads for fuel assemblies are also multiplied by 0.707g.

The 0° and 45° basket orientations are governing for the BWR basket for loading in the transverse direction. The 0° basket orientation maximizes the stresses in the fuel tube sidewalls and the 45° basket orientation maximizes the bending stresses in the tube corners. Intermediate basket orientations are bounded by the 0° and 45° orientations. Therefore, the basket evaluation is performed using two half-symmetry models for the 0° and 45° basket orientations, respectively. Symmetry boundary conditions are applied at the plane of symmetry. Symmetry boundary conditions are also applied to both ends of the finite element model to represent a periodic section of the basket. CONTACT52 elements are used to represent the interface of the basket and the canister shell inside the transfer cask. Outer nodes of gap elements are fixed. For off-normal events, material properties at 100°F are conservatively used (using the modulus of elasticity for carbon steel at lower temperature results in slightly higher stress results.)

#### **3.10.2.3.2 Thermal Stress Boundary Conditions**

The three-dimensional model described in Section 3.10.2.2.2 is used to calculate the thermal stress due to the thermal expansion. As shown in the following table, a total of five cases of temperature boundary conditions are defined that envelop the maximum temperature gradients ( $\Delta T$ ) in the axial and radial directions of the basket for all conditions of storage and transfer. It is noted that these temperature have the same values that have been used for the PWR basket thermal expansion stress analyses. These BWR basket temperatures are conservative for calculation of thermal expansion stresses in the BWR basket, as the PWR heat load is 2.5 kW greater than the BWR heat load. The thermal stress analysis is performed based on the temperature distribution in the model determined by thermal conduction analyses using these boundary temperatures.

Thermal Boundary Temperatures – BWR Basket (°F)

|  |     | Case | A   | B   | C   | D   |
|---|-----|------|-----|-----|-----|-----|
|   |     | 1    | 600 | 440 | 360 | 300 |
| 2   | 680 | 500  | 580 | 440 |     |     |
| 3   | 640 | 520  | 700 | 590 |     |     |
| 4   | 430 | 380  | 210 | 260 |     |     |
| 5   | 700 | 500  | 550 | 400 |     |     |

Symmetry boundary conditions are applied at the planes of symmetry. In the basket axial direction, the model is restrained at one end.

### 3.10.2.3.3 Concrete Cask Tip-Over Accident Boundary Conditions

The concrete cask tip-over is evaluated as a side impact for the basket. During the concrete cask tip-over event, the acceleration varies from 1g at the bottom of the concrete cask to a maximum acceleration at the top of the TSC. The three-dimensional plastic model is used for the evaluation of the BWR basket (see Section 3.10.2.2.3). A bounding acceleration of 35g is applied to the BWR models. The 35g acceleration bounds the maximum acceleration in the basket, including dynamic load factor, for the concrete cask tip-over accident.

Pressure loads are applied to the BWR basket models to represent the fuel assembly weight with a 35g acceleration.

For the tip-over accident (loading in the transverse direction), the 0° and 45° basket orientations are governing for the BWR basket as discussed in Section 3.10.2.3.1. Therefore, the basket is evaluated using models corresponding to the 0° and 45° basket orientations. Symmetry boundary conditions are applied at the plane of symmetry. Symmetry boundary conditions are also applied to both ends of the three-dimensional periodic finite element model. CONTAC52 elements are used to represent the interface of the basket and the canister shell inside the concrete cask. The location of the outer nodes of the gap elements at the basket periphery incorporates the canister shell displacements during the concrete cask tip-over accident. The boundary conditions are shown in Figure 3.10.2-11 and Figure 3.10.2-12 for the tip-over basket evaluation. For accident conditions, material properties at 100°F are conservatively used.

### **3.10.2.4 Post-Processing Finite Element Analysis Results**

#### **3.10.2.4.1 Maximum Stresses for Off-Normal Handling Condition**

The post-processing of the finite element analysis results from the periodic model for the off-normal handling event is performed by taking section cuts at various locations in the model.

The fuel tube section cuts are divided into two regions. Region 1 is the region between the pin supports. For the periodic model, this region is defined from the base of the model (mid-distance between pins) to the base of the pin. Region 2 is the pin region. This region starts at the base of the pin and extends to the top of the finite element model (mid-plane of pin). For both regions, the region just above and below the pin cutout ( $\pm 0.25$  inch) is omitted from the section cuts to eliminate local stress concentrations in the model. The membrane stresses are calculated by taking a section cut at the center of the tube thickness. The membrane plus bending stress is calculated by taking the maximum of the stresses calculated at the inner or outer surface of the fuel tube. Refer to Figure 3.10.2-13 through Figure 3.10.2-16 for tube identification and the locations of the section cuts.

The maximum stresses for the corner support weldments are calculated by taking section cuts along the length of the weldment (ten inches for the periodic model). Since the corner weldment is modeled using SHELL63 elements; the membrane stresses are calculated at the mid-plane of the element, and the membrane plus bending stresses are calculated using the maximum stresses of either the inner or outer surface of the element. Refer to Figure 3.10.2-17 and Figure 3.10.2-18 for the locations of the section cuts.

The maximum stresses for the side weldments are calculated taking section cuts along the length of the weldment (ten inches for the periodic model). The membrane stresses are calculated by taking a section cut at the mid-thickness of the weldment. The membrane plus bending stress is calculated by taking the maximum of the stresses calculated at the inner or outer surface of the weldment. Refer to Figure 3.10.2-19 and Figure 3.10.2-20 for the locations of the section cuts. The bolt tensile loads are obtained from the LINK10 element results. The boss shear loads are extracted from the COMBIN40 element results.

#### **3.10.2.4.2 Maximum Thermal Stresses**

The post-processing of the finite element analysis results for thermal stress evaluation is performed by extracting the maximum nodal stress intensities from the model. The maximum stress is obtained for two separate regions: (1) fuel tubes and (2) corner and side support weldments. The bolt tensile loads are extracted from the LINK10 elements, and the boss shear loads are extracted from the COMBIN40 elements.

#### 3.10.2.4.3 Maximum Stresses for Concrete Cask Tip-over Accident

The post-processing of finite element analysis results for the basket tip-over accident using the three-dimensional plastic model is performed by extracting stresses in the basket for the 0° and 45° basket orientations.

For the fuel tube stresses, the primary membrane stresses are calculated by extracting the maximum nodal stress at the mid-thickness of the tube wall. Based on the differences in stress criterion summarized from the plastic finite element results [i.e.,  $(\sigma + 3 \tau)^{1/2}$ ] and the ASME Code, Section III stress criterion [i.e.,  $(\sigma + 4 \tau)^{1/2}$ ], calculated membrane stress results are conservatively increased by a factor of  $(4/3)^{1/2}$ . The primary membrane plus bending stresses are evaluated by extracting the maximum stress intensity results of each fuel tube.

The stresses for the corner and side support weldments are calculated using the three-dimensional plastic models. The maximum primary membrane plus bending stress intensity for the corner and side weldments are extracted from the model. The maximum primary membrane plus bending stress intensity is compared to the membrane allowable to obtain a conservative bounding factor of safety.



Figure 3.10.2-1 Expanded View of BWR Basket

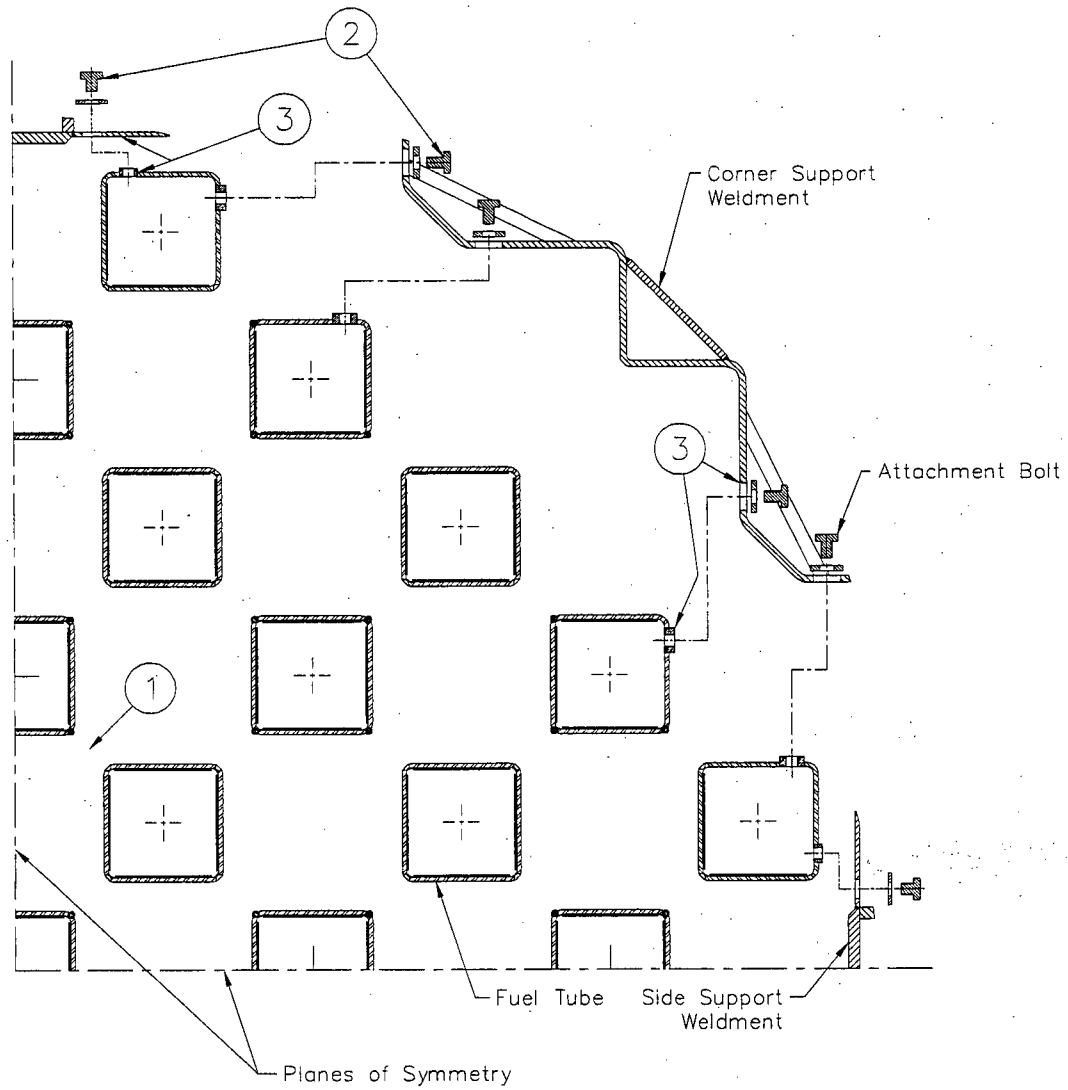


Figure 3.10.2-2 Bolted Attachment Details

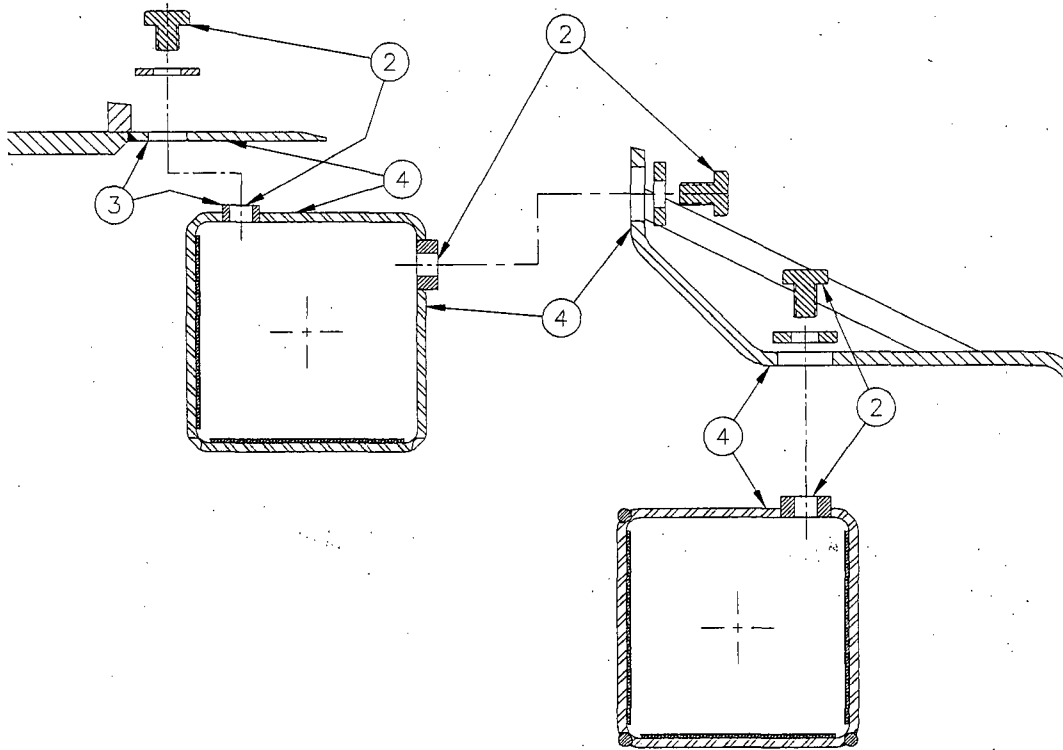
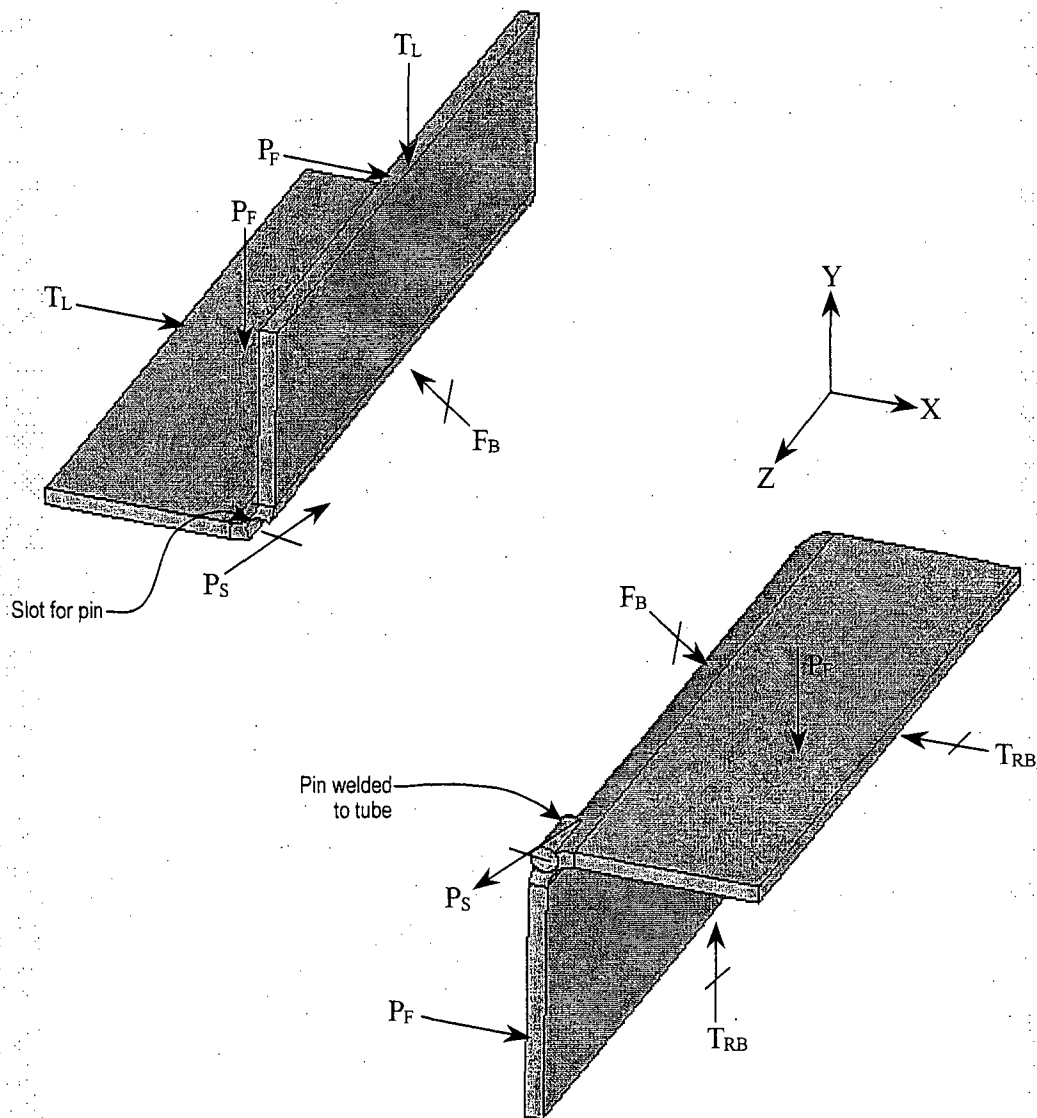
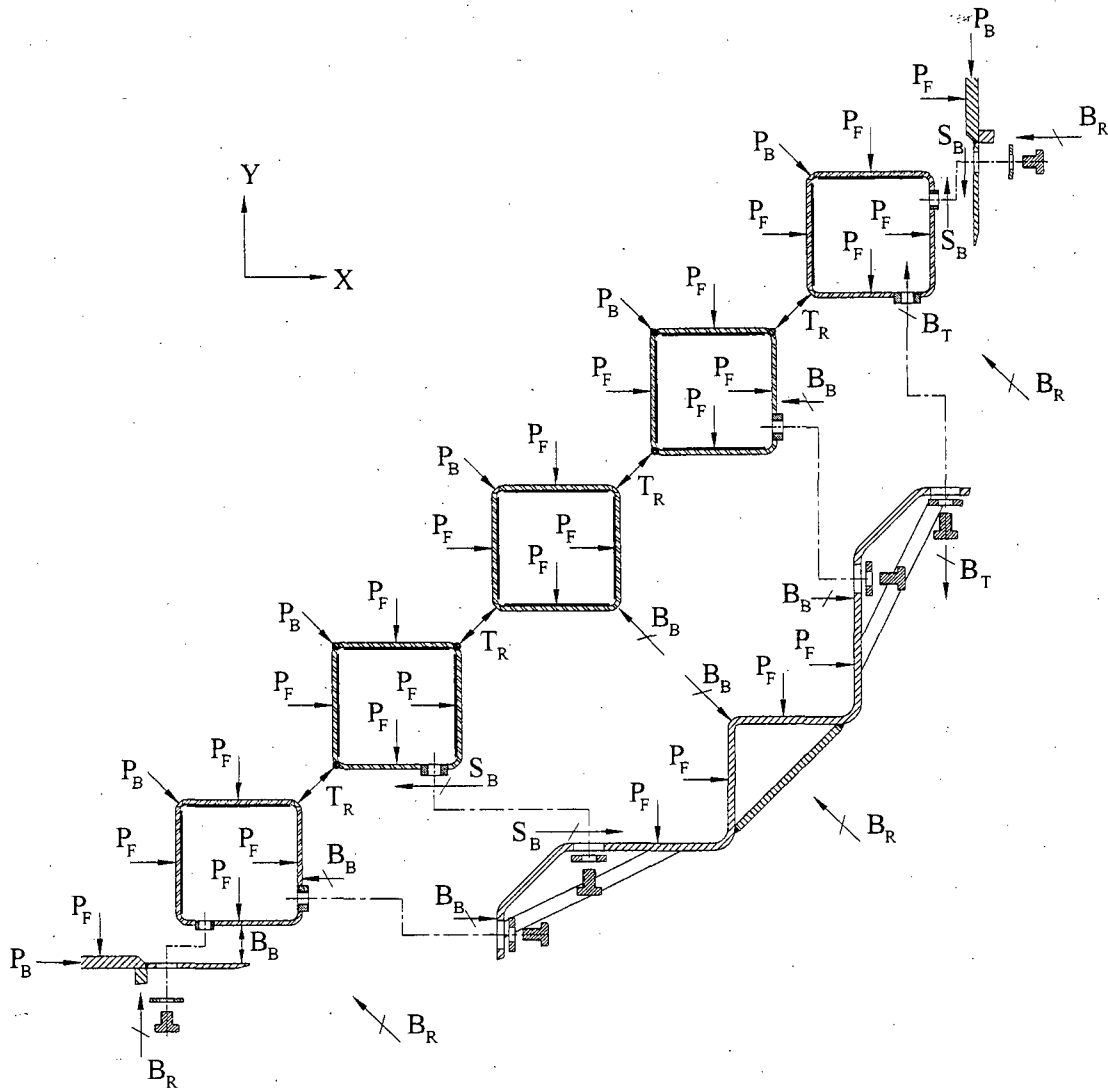


Figure 3.10.2-3 Free-Body Diagram of BWR Basket Fuel Tube Detail



- $T_L$  Loads from adjacent tube or fuel assembly
- $P_F$  Local load due to fuel assembly
- $T_{RB}$  Reaction loads in tubes for equilibrium at symmetry planes of tubes
- $P_S$  Shear Reaction thru pin joint (in the X-Y plane)
- $F_B$  Bearing Reaction across tube flat

Figure 3.10.2-4 Free-Body Diagram of Basket Support Structure



- $P_B$  Loads due to adjacent basket structure
- $P_F$  Local load due to fuel assembly
- $B_R$  Basket reaction with TSC shell locations
- $B_T$  Tensile load at bolt and tube boss (typical)
- $B_B$  Bearing reaction between tube sidewall and support structure (typical)
- $S_B$  Shear reaction between support structure and tube boss (typical)
- $T_R$  Reactions between tubes detailed in Figure 3.10.2-3

Figure 3.10.2-5 BWR Basket Periodic Model – 0° Basket Orientation

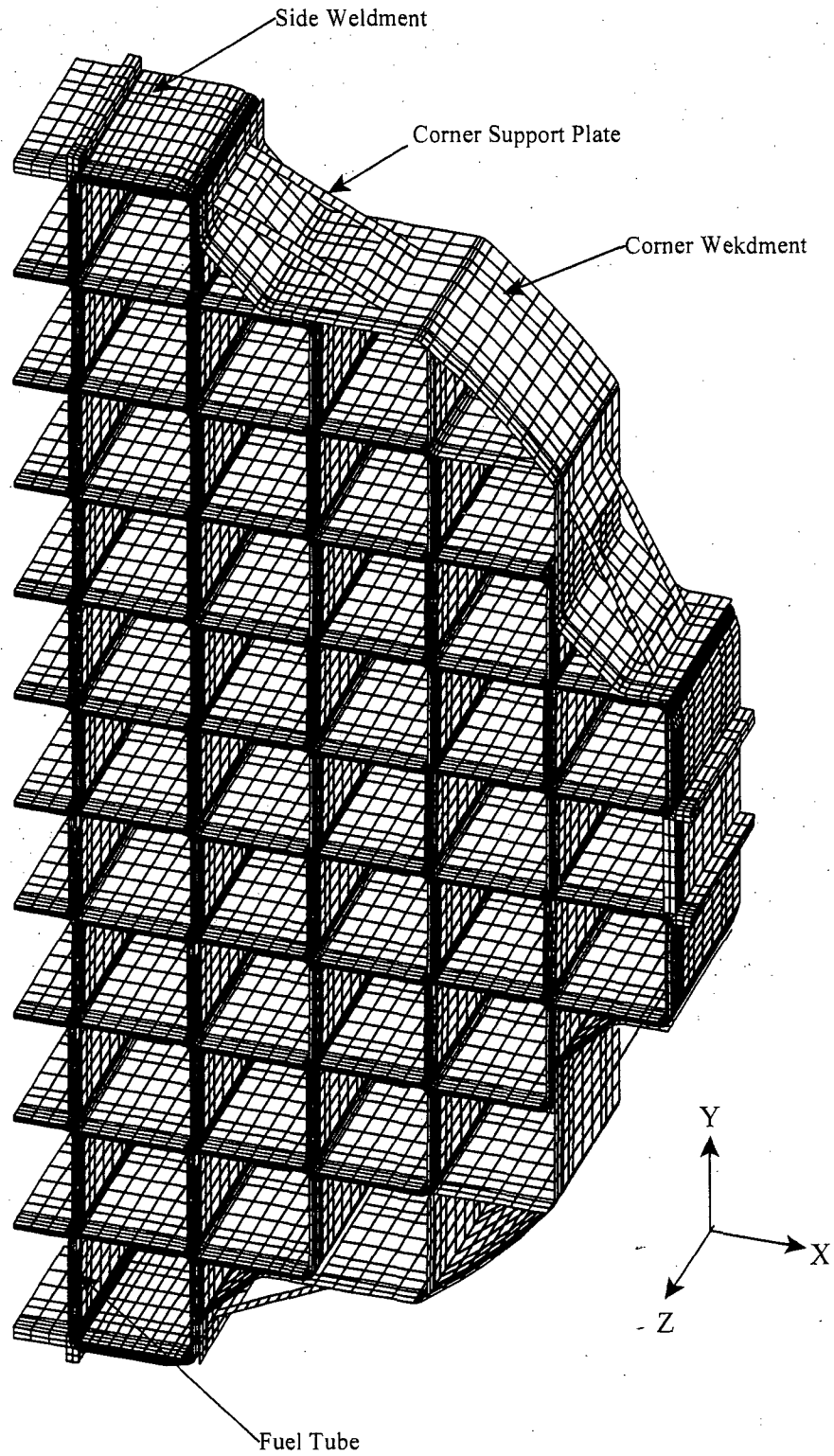


Figure 3.10.2-6 BWR Basket Periodic Model – 45° Basket Orientation

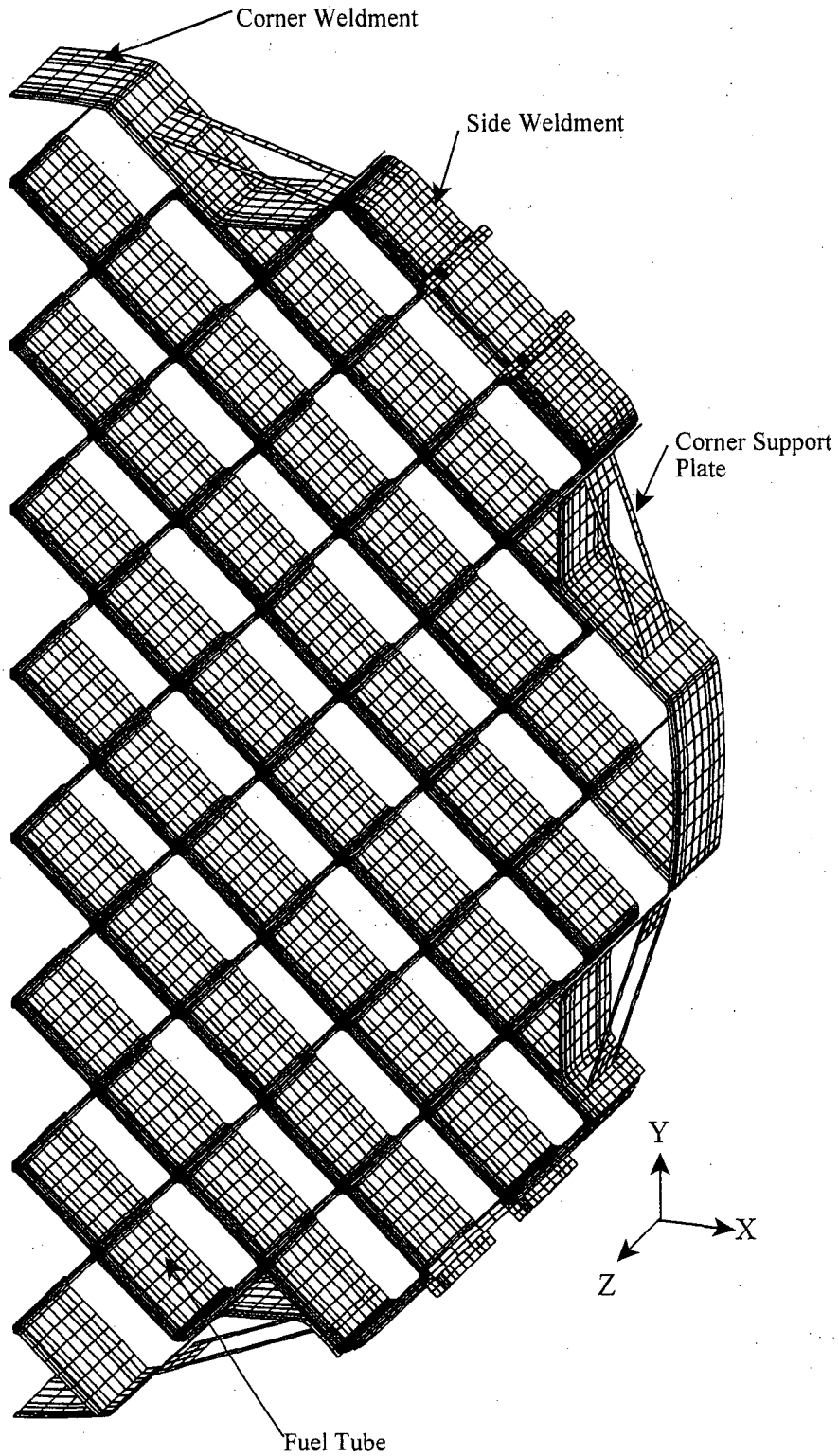


Figure 3.10.2-7 Thermal Stress Evaluation Model

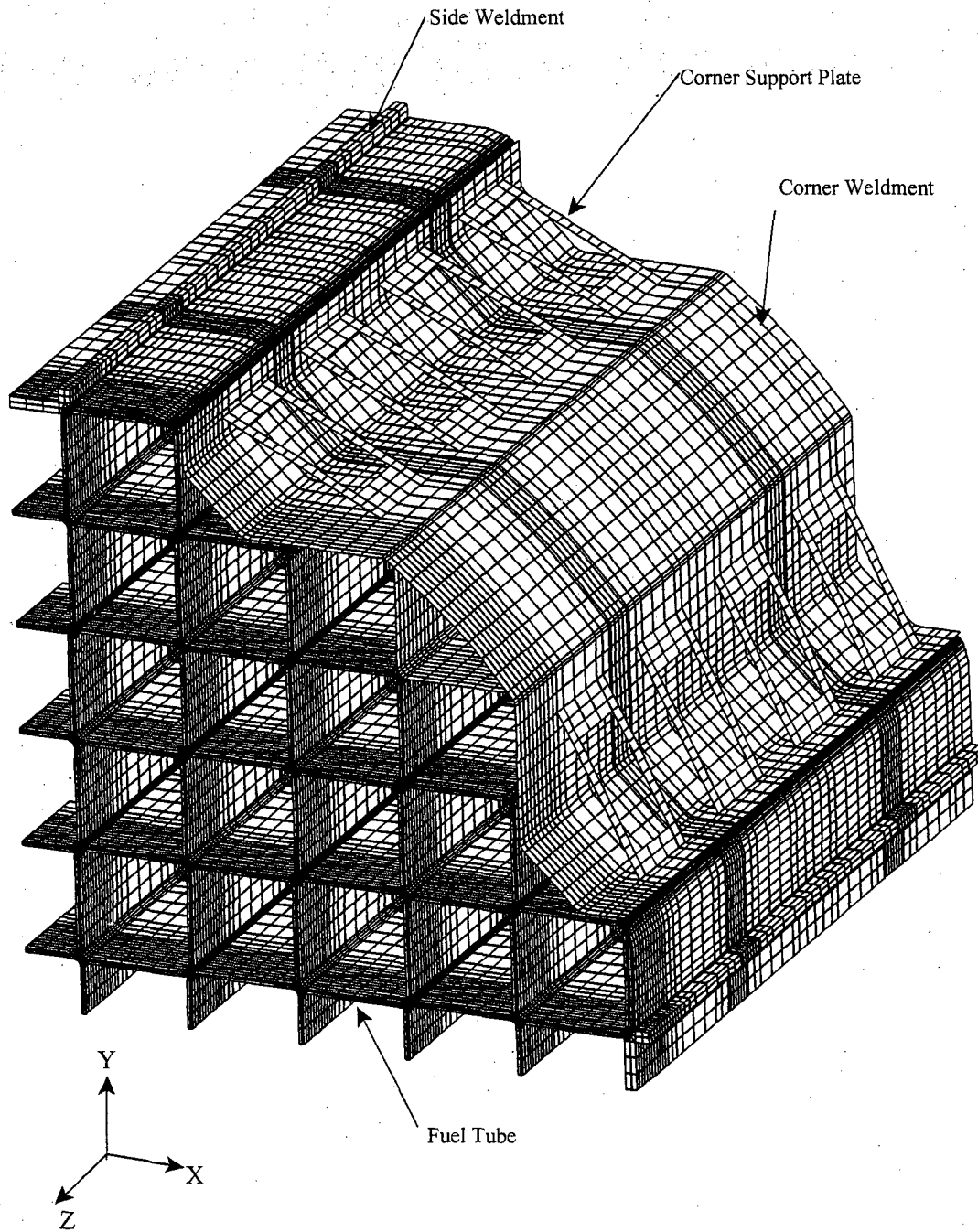


Figure 3.10.2-8 BWR Basket Plastic Model - 0° Basket Orientation

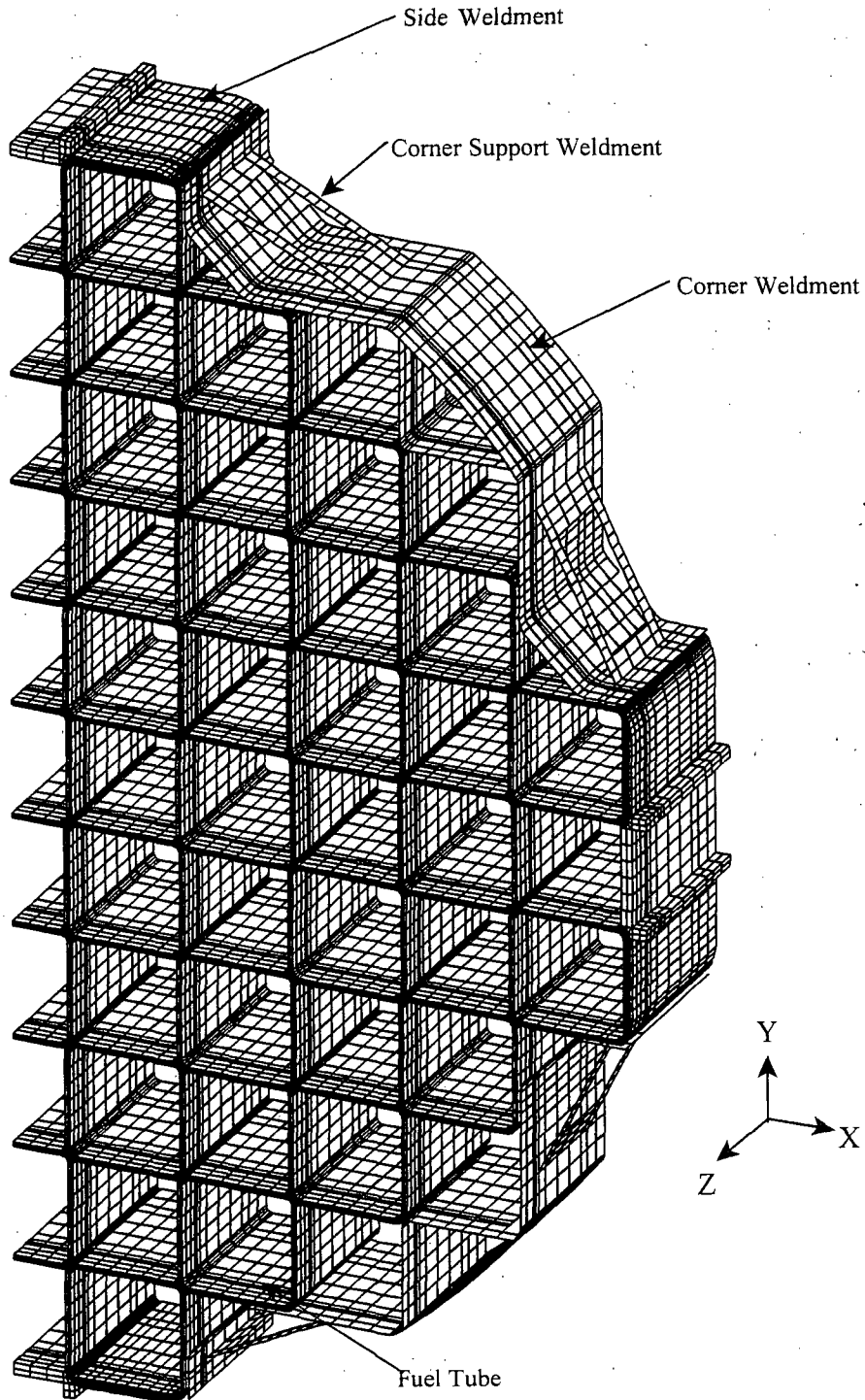




Figure 3.10.2-9 BWR Basket Plastic Model - 45° Basket Orientation

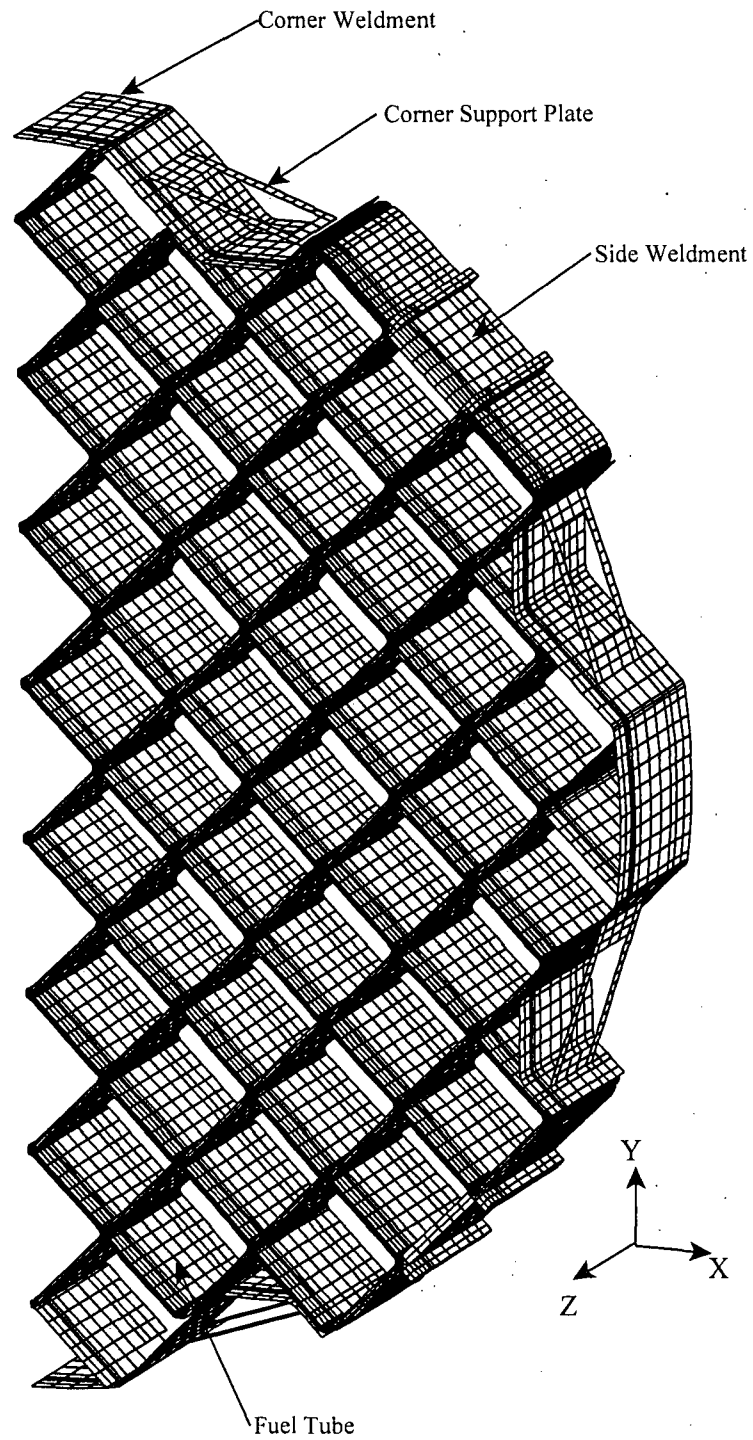


Figure 3.10.2-10 Typical BWR Fuel Tube Pin Finite Element Model Details

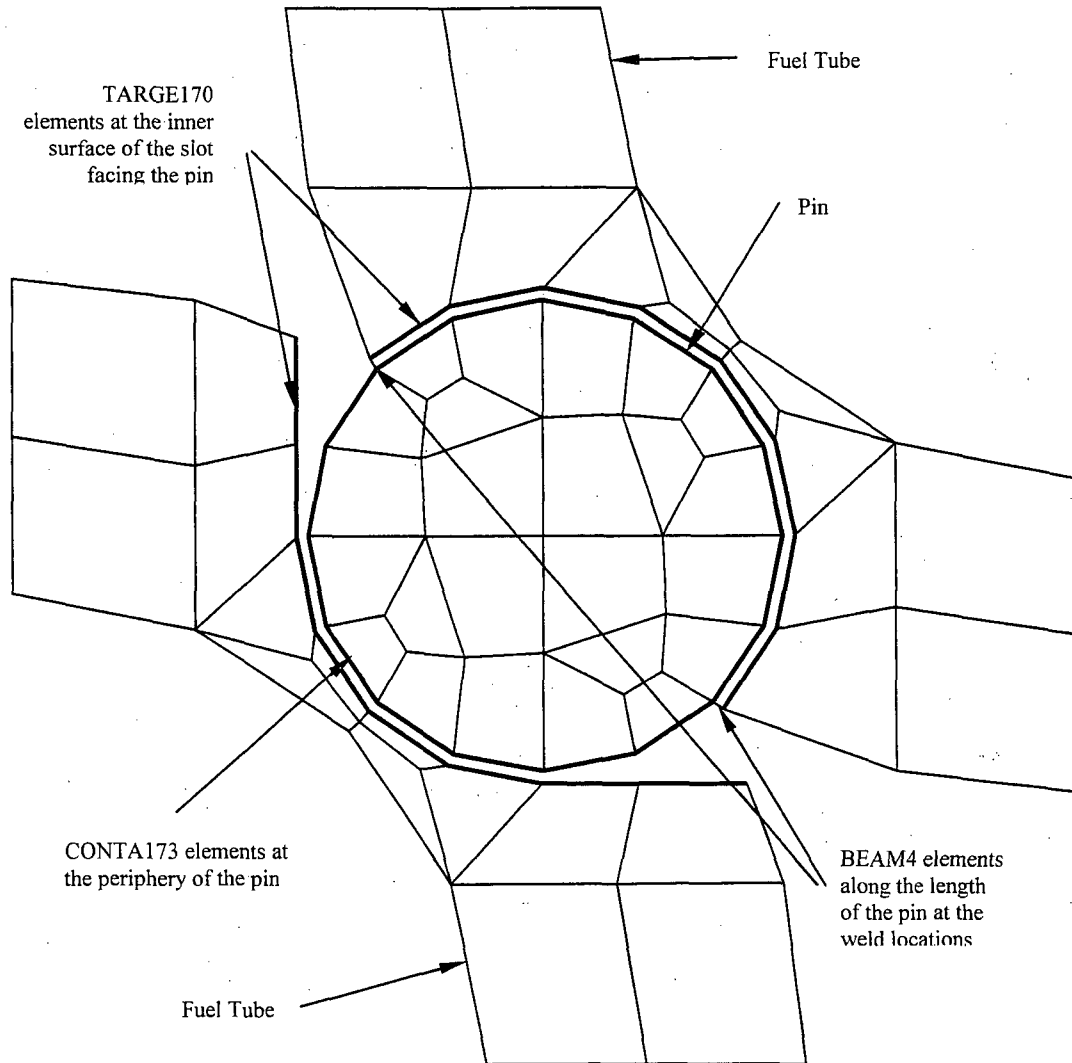


Figure 3.10.2-11 BWR Basket Model Boundary Conditions for a Transverse Loading -  
0° Basket Orientation

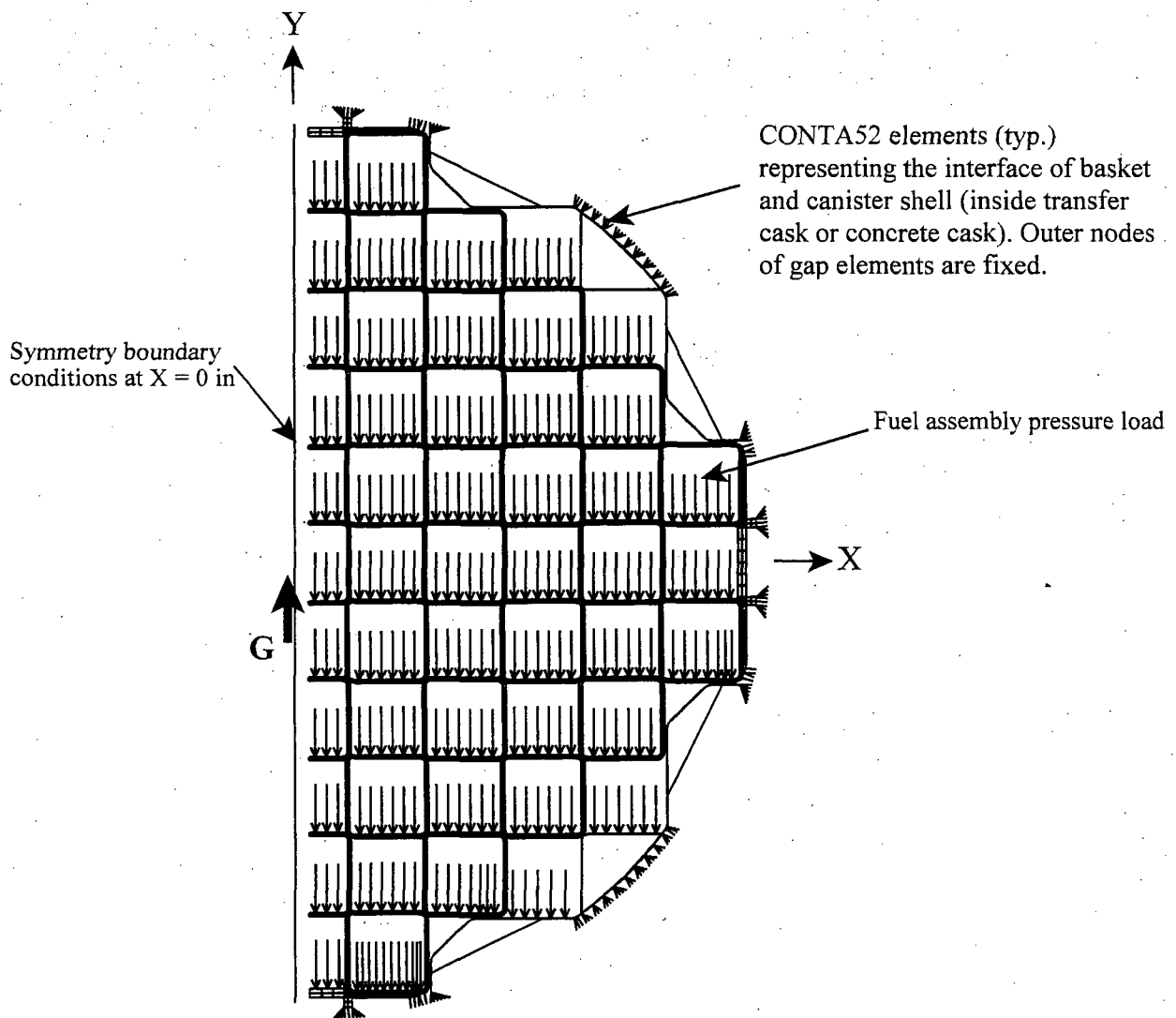


Figure 3.10.2-12 BWR Basket Model Boundary Conditions for a Transverse Loading – 45° Basket Orientation

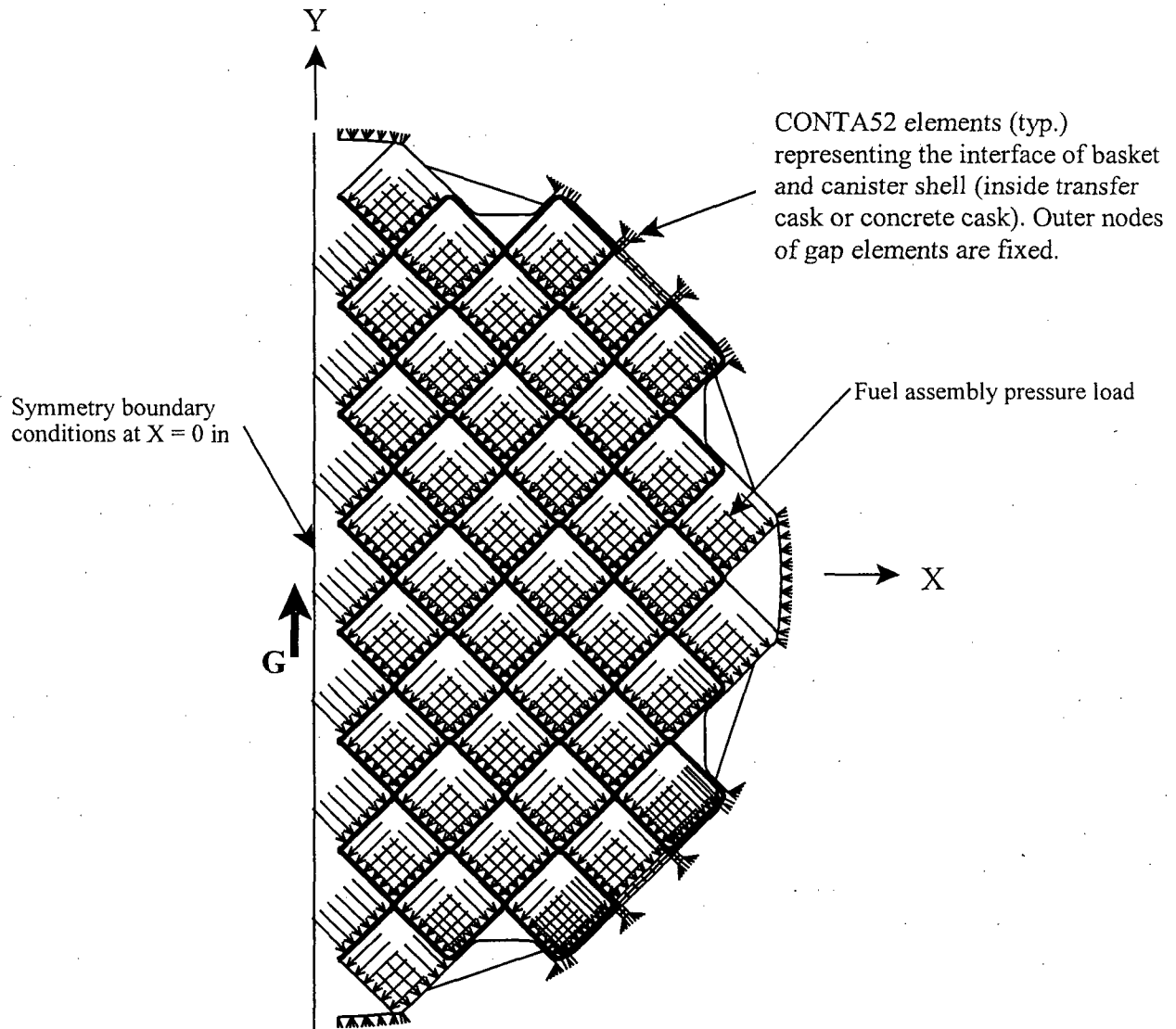


Figure 3.10.2-13 BWR Fuel Tube Array – 0° Basket Orientation

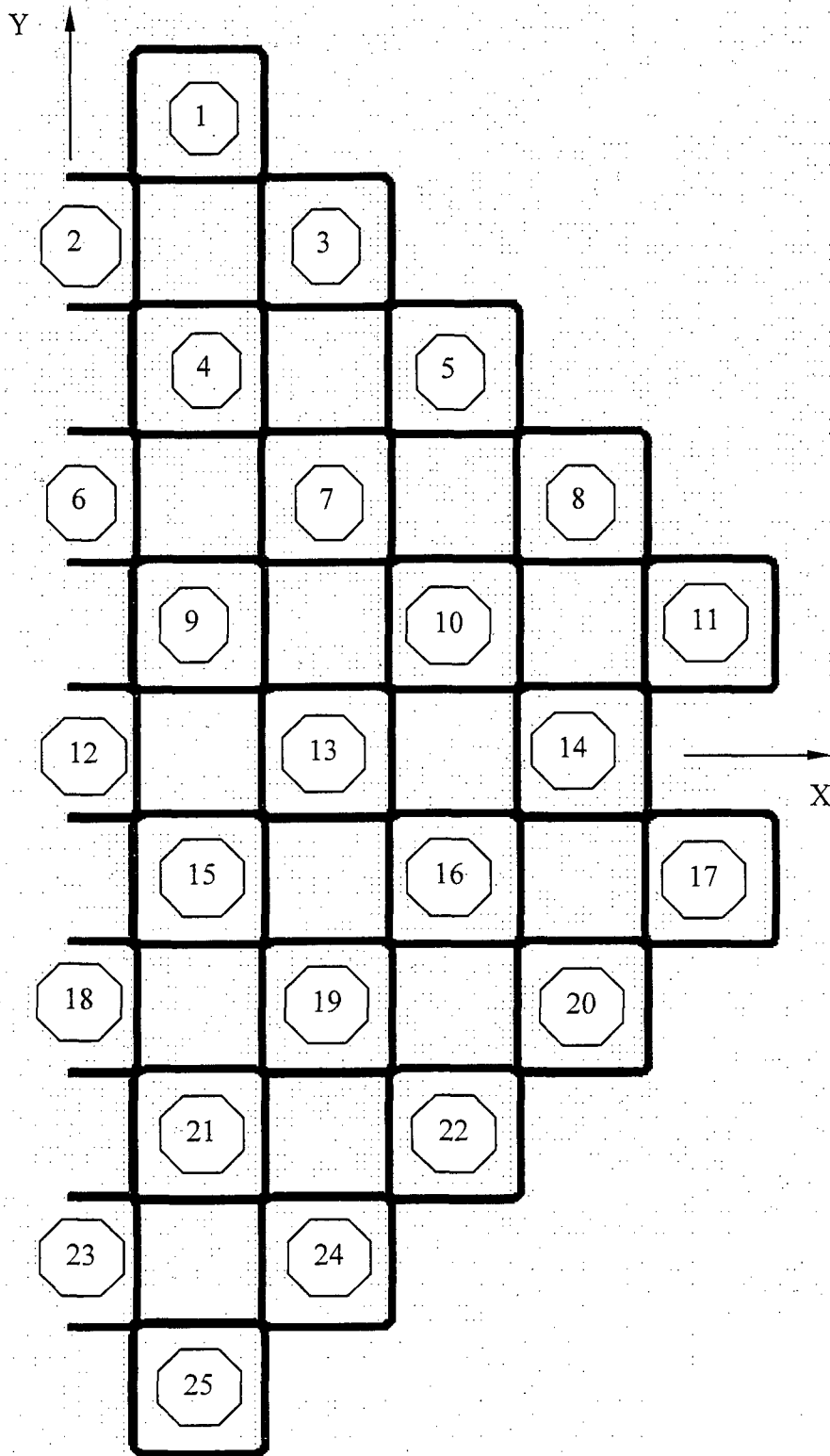


Figure 3.10.2-14 BWR Fuel Tube Section Cuts – 0° Basket Orientation

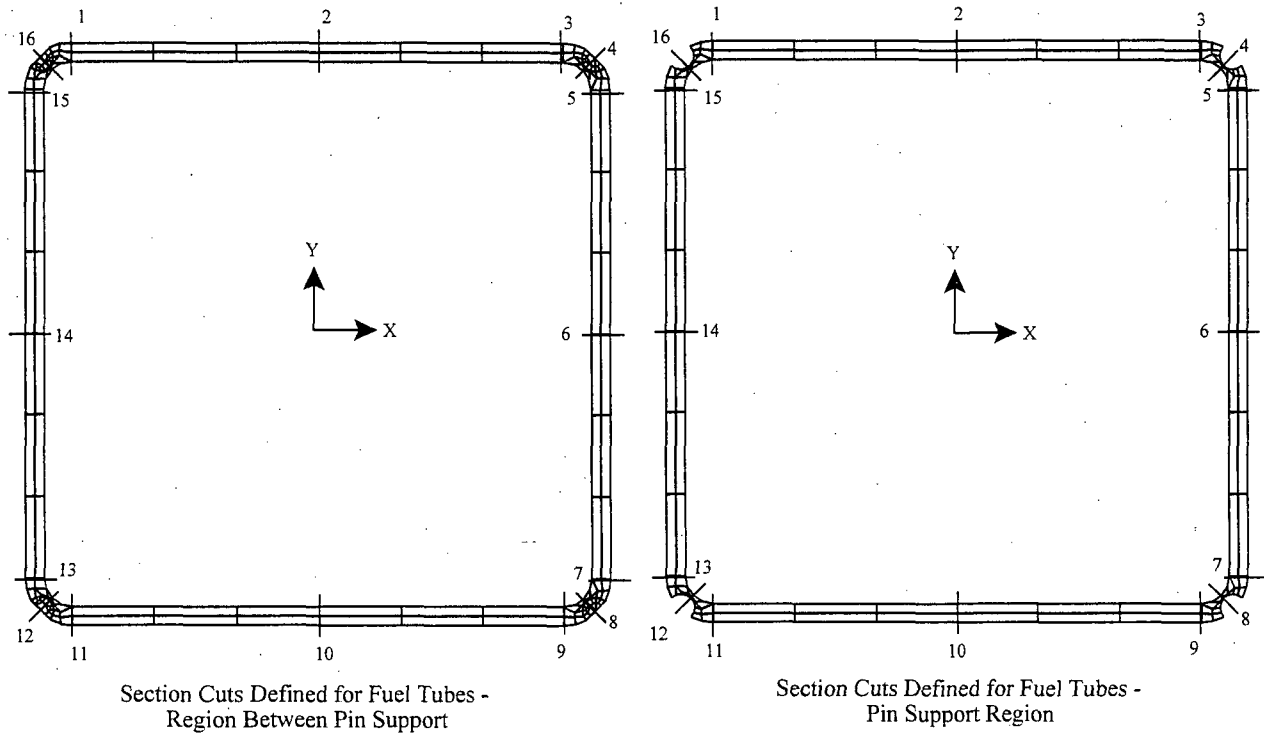


Figure 3.10.2-15 BWR Fuel Tube Array – 45° Basket Orientation

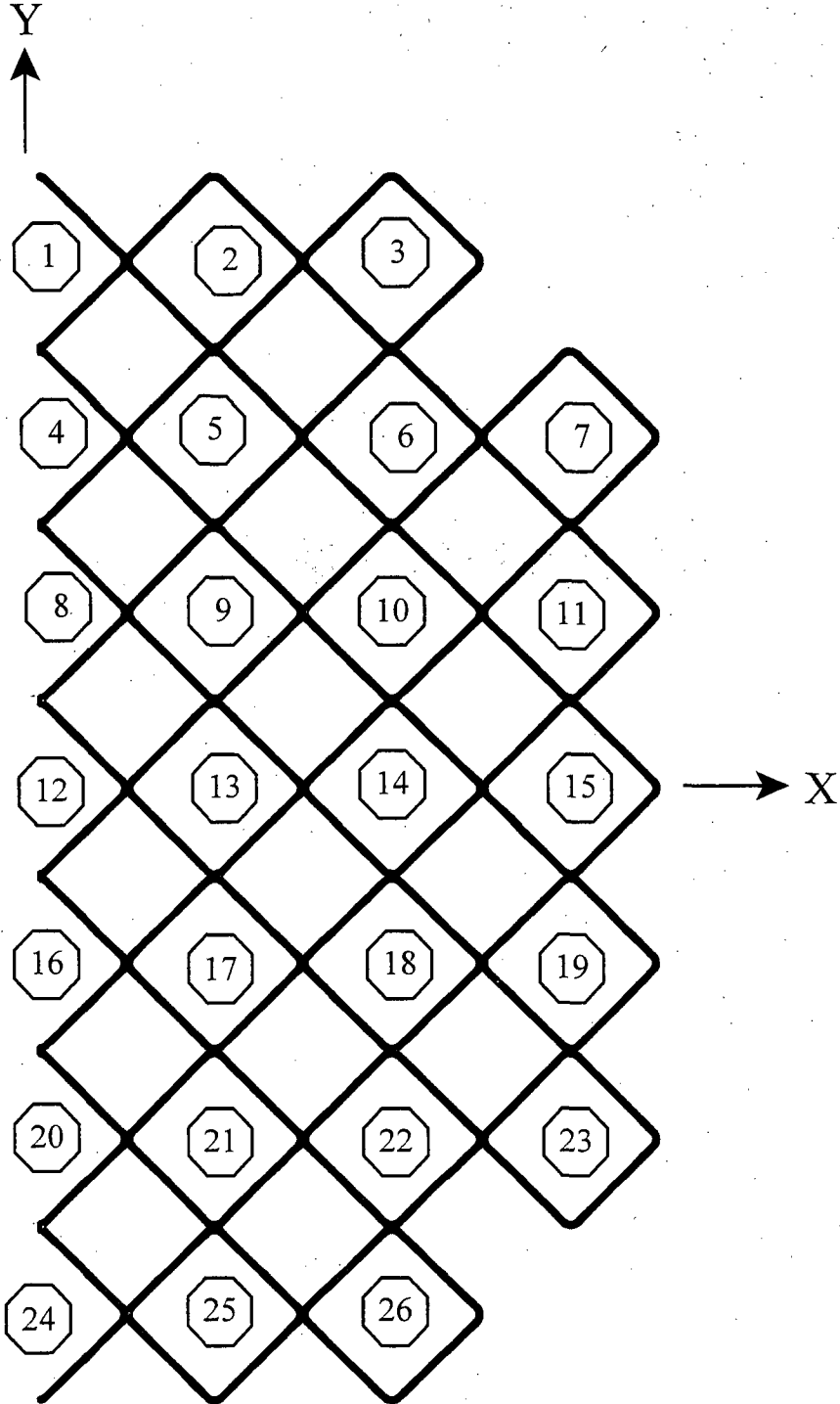
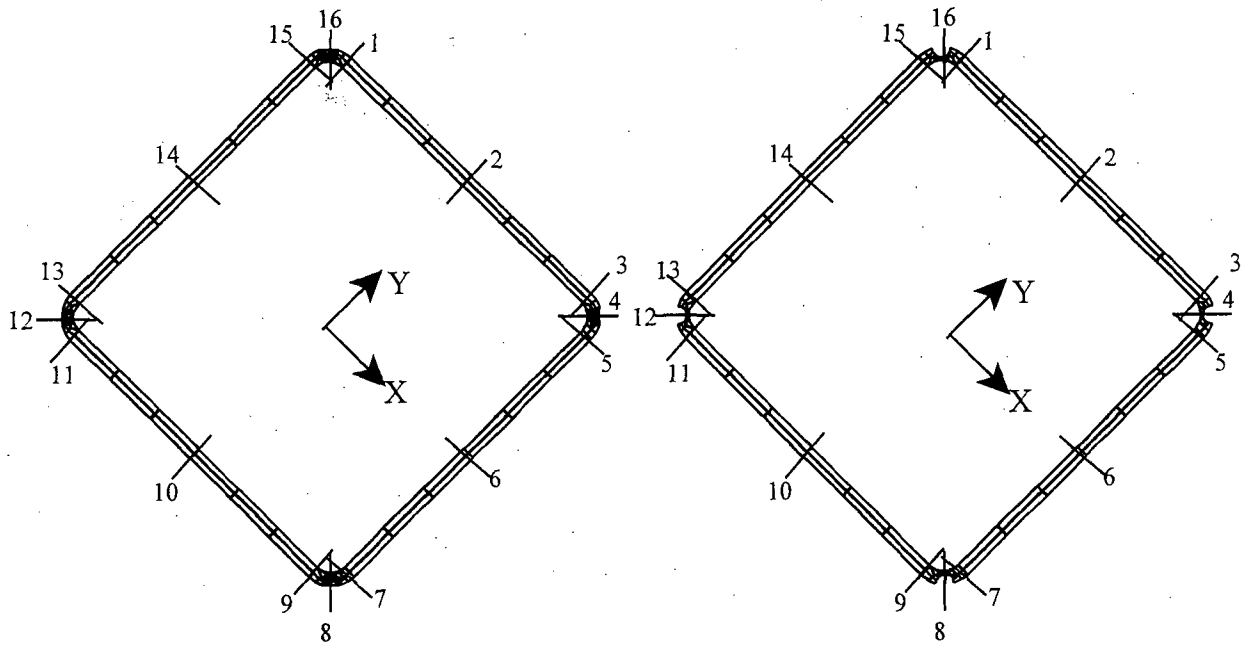


Figure 3.10.2-16 BWR Fuel Tube Section Cuts – 45° Basket Orientation



Section Cuts Defined for Fuel Tubes -  
Region Between Pin Support

Section Cuts Defined for Fuel Tubes -  
Pin Support Region



Figure 3.10.2-17 BWR Corner Support Weldment Section Cuts – 0° Basket Orientation

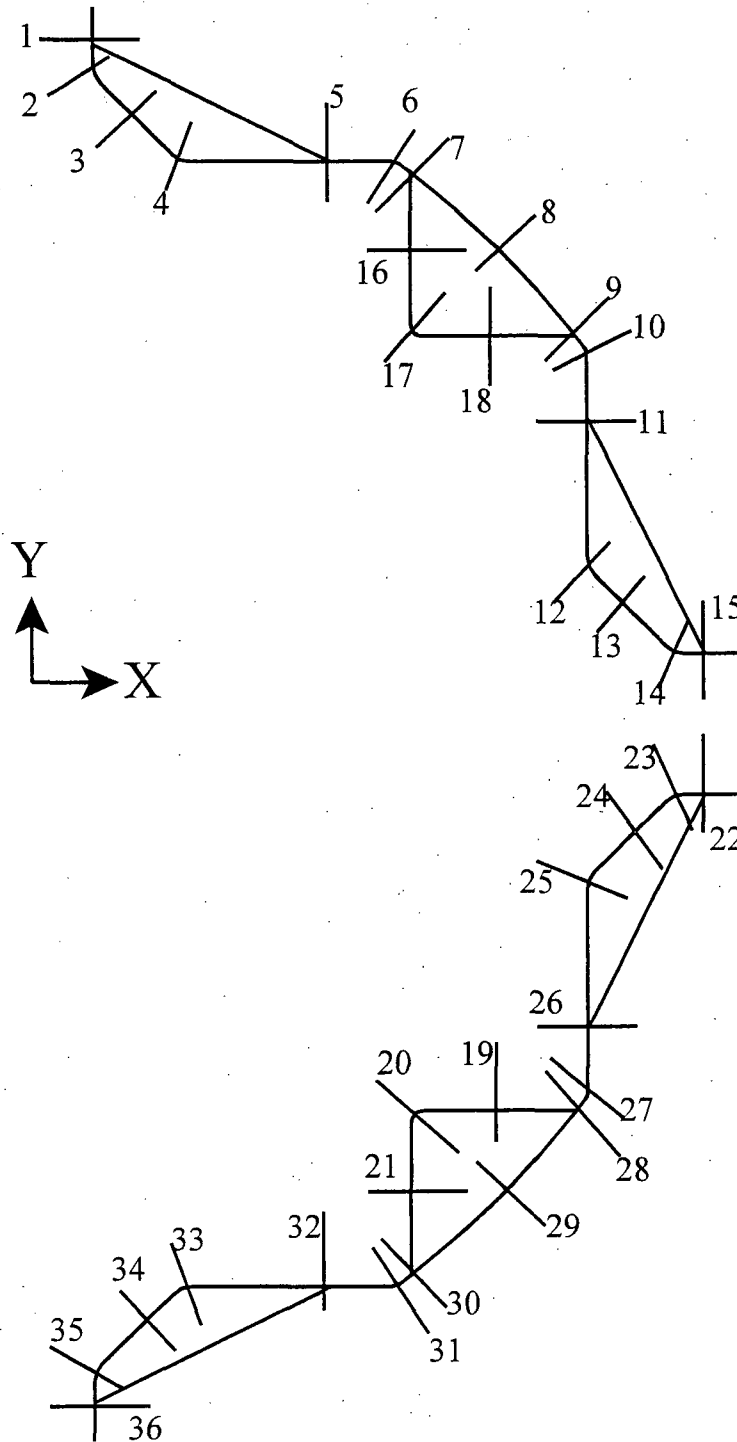


Figure 3.10.2-18 BWR Corner Support Weldment Section Cuts – 45° Basket Orientation

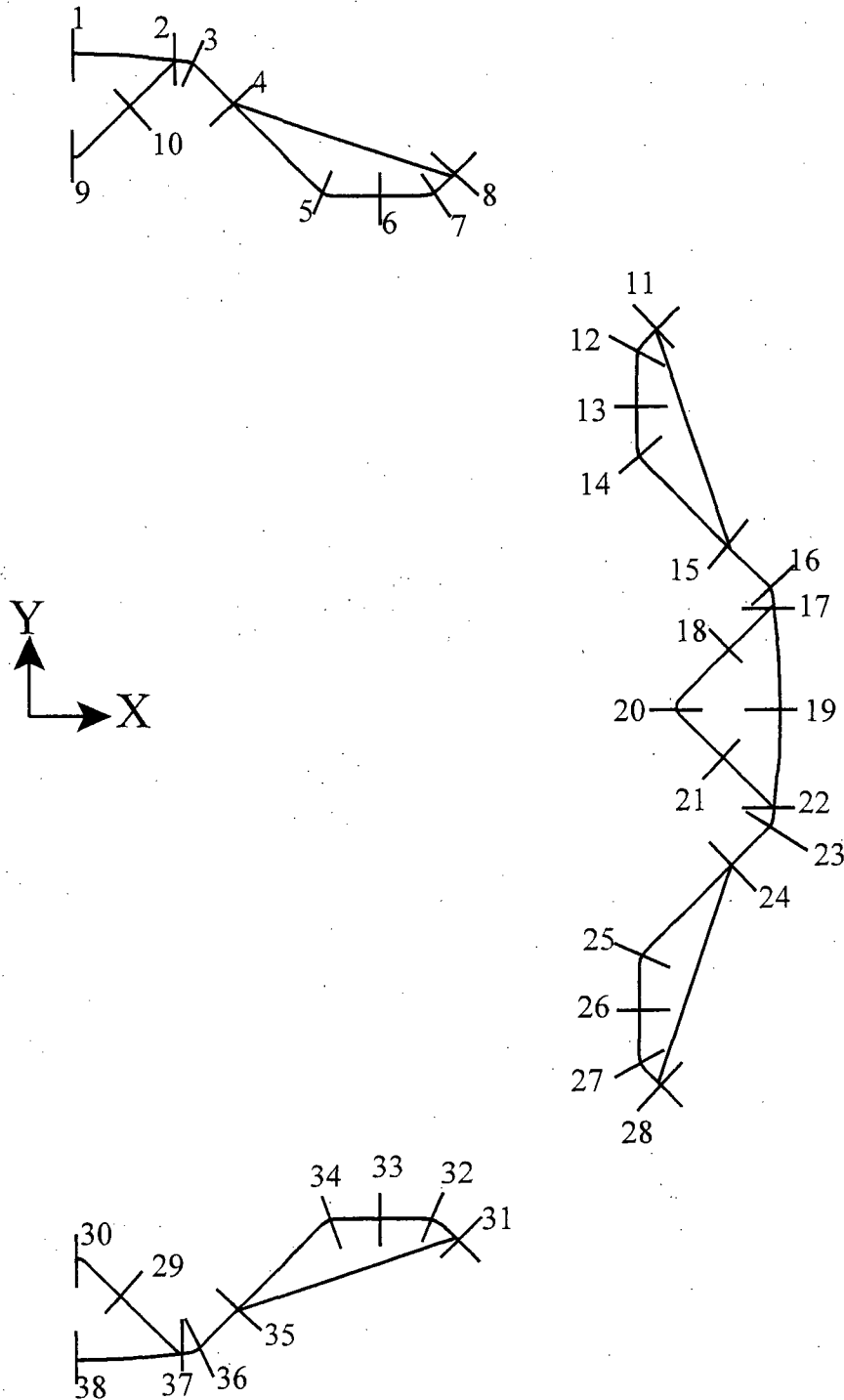


Figure 3.10.2-19 BWR Side Support Weldment Section Cuts – 0° Basket Orientation

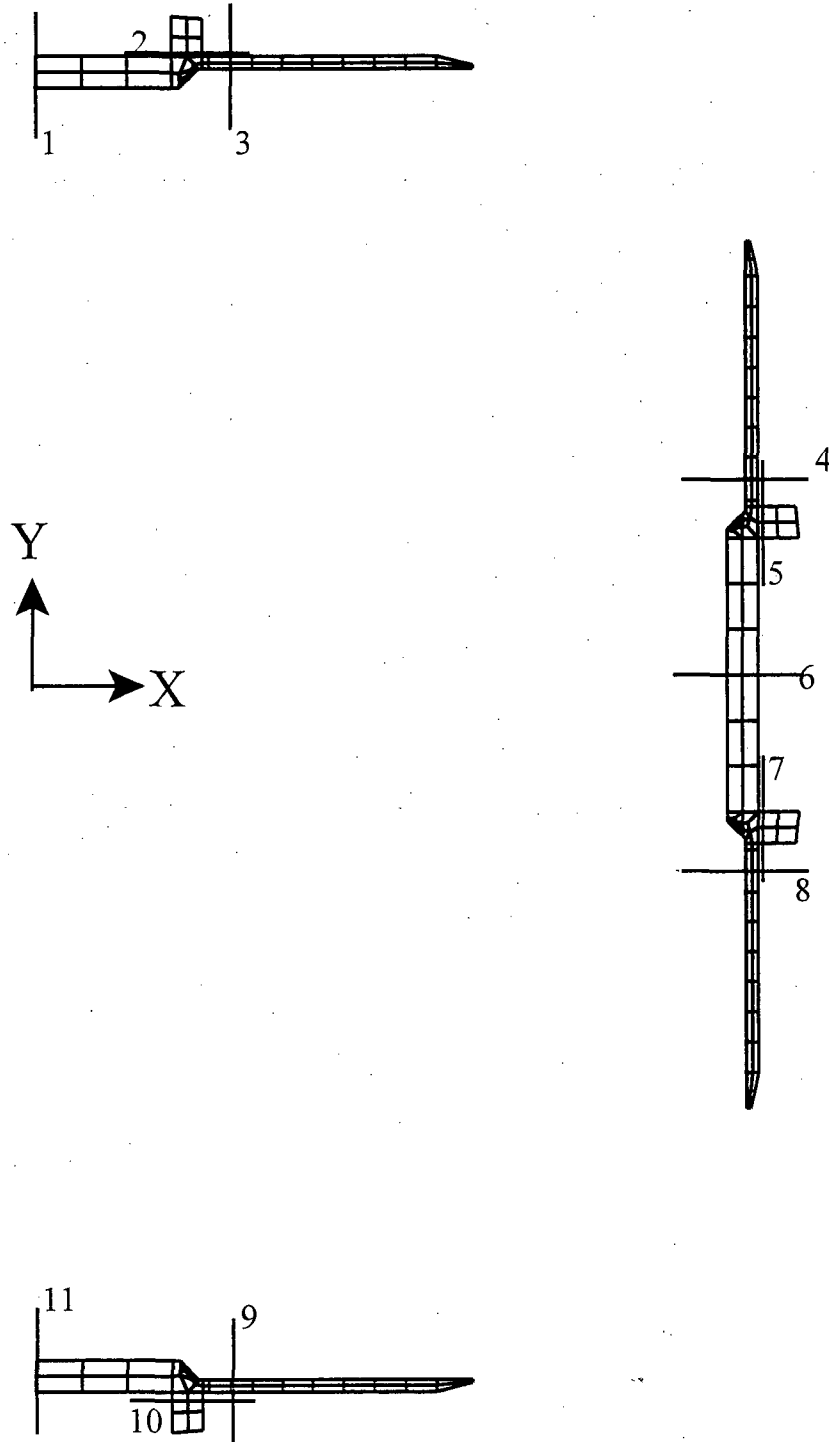
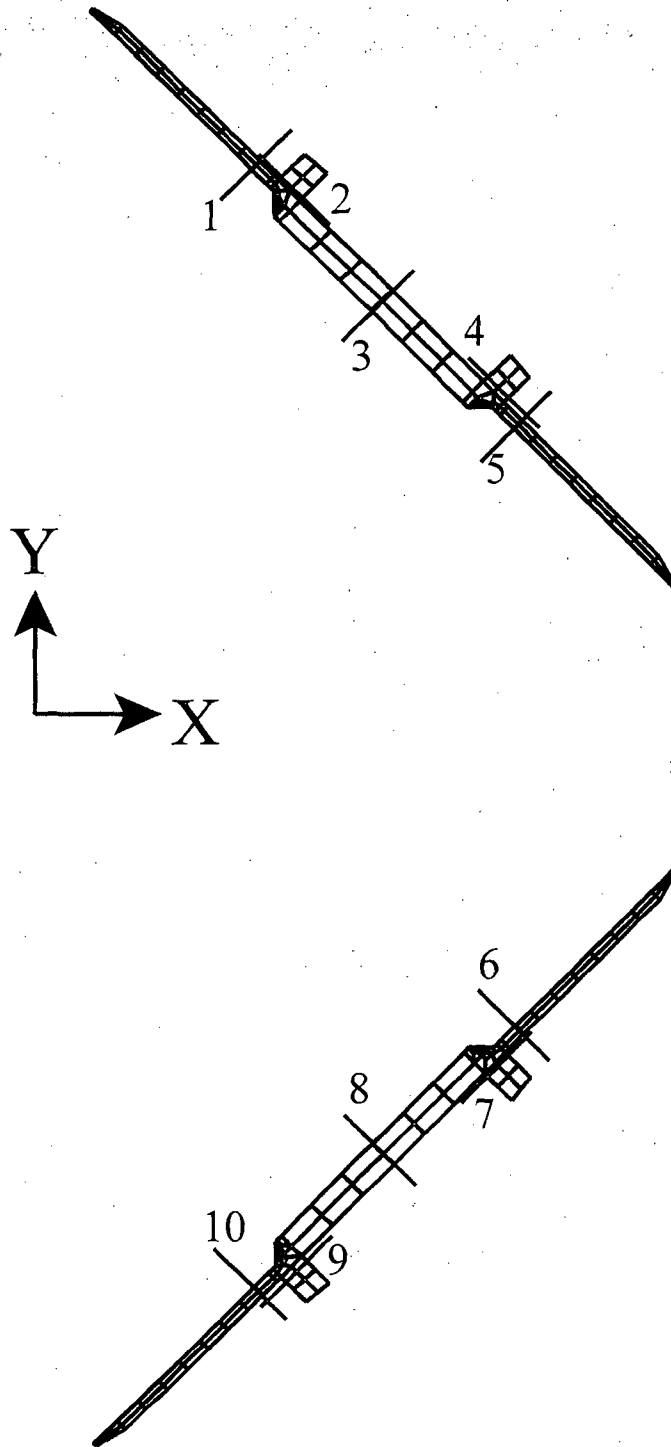


Figure 3.10.2-20 BWR Side Support Weldment Section Cuts – 45° Basket Orientation



### 3.10.3 TSC Finite Element Model

This section presents details on the TSC finite element model used in the structural evaluation of the TSC for lift, normal conditions and off-normal or accident events of storage.

#### TSC Finite Element Model Description

The three-dimensional finite element model of the TSC is constructed using ANSYS SOLID45 elements. By taking advantage of the symmetry of the TSC, the model represents one-half (180° section) of the TSC, including the TSC shell, bottom plate, and closure lid. The finite element model of the TSC is shown in Figure 3.10.3-1. ANSYS CONTAC52 elements are used to model the interaction between the closure lid and the TSC shell. Gap elements are also used to simulate the interaction with the concrete cask inner liner standoffs or transfer cask inner shell during a side impact and pedestal during an end impact. The size of the CONTAC52 gaps is determined from nominal dimensions of contacting components. Due to the relatively large gaps resulting from the nominal geometry, these gaps remain open during all loadings considered. All gap elements are assigned a stiffness of  $1 \times 10^8$  lb/in.

This model represents a “bounding” combination of geometry and loading that envelops the MAGNASTOR PWR and BWR TSCs. Specifically, the longest TSC is modeled in conjunction with a conservative fuel and basket combination. By using the longest TSC with the conservative content weight, bending stresses are maximized at the junction of the shell and lid. Thus, the analysis yields conservative results relative to the expected performance of the actual TSC configurations.

#### Boundary Conditions for TSC Lift

The lifting configuration for the TSC consists of six hoist rings bolted to the closure lid at equally spaced angular intervals. To simulate the lifting of the TSC, nodes representing the hoist rings on the closure lid are constrained in the Y-direction. For heavy lift evaluation, only three of the hoist rings are considered. Due to the symmetry of the model, only the nodes at 60° and 180° are constrained. Symmetry boundary conditions are applied at the plane of symmetry of the model. Pressure representing the weight of the fuel and basket is applied to the TSC bottom. A 1.1g inertia load is applied in the axial direction.

**Boundary Conditions for Normal Conditions and Off-normal or Accident Events**

**Model Constraints**

The model is constrained in the global Z-direction for all nodes in the plane of symmetry. Other constraints for different loading conditions are summarized below. The directions of the coordinate system are shown in Figure 3.10.3-1.

**Model Constraint Summary**

| Condition                     | Constraint                                    |
|-------------------------------|---|
| Dead Weight                   | Y-direction at TSC bottom                     |
| Normal Handling               | Y-direction – lift points in TSC lid          |
| Off-normal Handling - axial   | Y-direction – lift points in TSC lid          |
| Off-normal Handling – lateral | Gap elements at TSC shell in radial direction |
| 24-inch drop                  | Y-direction at TSC bottom                     |
| Tip-over                      | Gap elements at TSC shell in radial direction |

**Inertial Load**

Inertial loads resulting from the weight of the TSC and contents are considered by applying an appropriate deceleration factor (g-load). Inertial loads are summarized below.

**Inertial Load Summary**

| Condition           | Inertial Load  |
|---------------------|--|
| Dead Weight         | 1g – axial   |
| Normal Handling     | 1.1g – axial   |
| Off-normal Handling | 1.5g – axial, 0.707g – lateral   |
| 24-inch drop        | 60g – axial  |
| Tip-over            | Tapered 40g – lateral (40g at top of TSC closure lid, 1g at base of concrete cask) |

**Pressure Load – Internal Pressure**

A uniform pressure is applied to all internal surfaces of the TSC. The TSC pressures used for the normal condition (110 psig), off-normal (130 psig) and accident events (250 psig) bound all pressure conditions.

**Pressure Load – Dead Load, Handling, and 24-inch Drop**

For the dead load, handling, and 24-inch drop analyses, the inertial load produced by the contents weight is considered to be uniformly distributed on the inner surface of TSC bottom plate. Based on the contents weight of 90,000 lb and the TSC inside radius of 35.5 inches, the pressure corresponding to the contents weight is as follows.

$$p = \frac{90,000}{\pi(35.5^2)} = 22.7 \text{ psi}$$

The pressure load is multiplied by appropriate inertia loading (1g, 1.1g and 60g for dead load, handling, and 24-inch drop, respectively).

#### Pressure Load—Off-Normal Handling

For the off-normal handling analysis, the inertial load produced by the contents weight is considered to be uniformly distributed on the inner surface of TSC bottom plate multiplied by 1.5g for the axial component of off-normal handling. For the lateral component of the off-normal handling, the content weight is represented as an equivalent static pressure, with 0.707g, applied on the interior surface of the TSC shell. The pressure is uniformly applied to the canister shell along the TSC cavity length, and is applied in the circumferential direction as a cosine distribution over a 21° arc from the impact centerline in the half-symmetry model.

#### Pressure Load—Tip-Over

The inertial load produced by the 90,000 lb (45,000 lb for the half-symmetry model) content weight is represented as an equivalent static pressure applied on the interior surface of the TSC shell. The pressure is uniformly tapered along the cavity length based on a tapered inertia load of 40g at the top of the canister closure lid and 1g at the base of the concrete cask, and is applied in the circumferential direction as a cosine distribution over a 21° arc from the impact centerline.

#### Temperatures for Thermal Stress Analysis

The finite element thermal stress analysis is performed with TSC temperatures that envelop the TSC temperature gradients for normal (76°F ambient temperature) and off-normal storage (106°F and -40°F ambient temperatures), and transfer conditions for all TSC configurations. Prior to performing the thermal stress analysis, the steady-state temperature distribution is determined using bounding temperature data from the storage and transfer thermal analyses. This is accomplished by converting the SOLID45 structural elements of the TSC model to SOLID70 thermal elements to perform a thermal conduction analysis. Nodal temperatures are applied at key locations for the thermal analysis: top-center of the closure lid, top-outer diameter of the closure lid, bottom-center of the closure lid assembly, bottom-center of the bottom plate, bottom-outer diameter of the bottom plate, and the TSC shell where the maximum temperature occurs.

The temperature distribution used in the structural analyses envelops the temperature gradients experienced by all PWR and BWR TSC configurations under storage and transfer conditions.

The temperatures at the key locations are listed below. Temperatures locations (A through F) are defined in Figure 3.10.3-2. The temperatures for all nodes in the TSC model are obtained by the solution of the steady-state thermal conduction analysis.

|  |   |       |
|--|---|-------|
| Top-center of the closure lid (C)                | = | 510°F |
| Top-outer diameter of the closure lid (F)        | = | 430°F |
| Bottom-center of the closure lid (B)             | = | 570°F |
| Bottom-center of the bottom plate (A)            | = | 350°F |
| Bottom-outer diameter of the bottom plate (D)    | = | 240°F |
| Canister shell at 166 inches from TSC bottom (E) | = | 510°F |

### **Post-Processing**

The stress evaluation for the TSC is performed in accordance with the ASME Code, Section III, Subsection NB, by comparing the linearized sectional stresses against allowable stresses. The sectional stresses at 15 locations of the TSC model are obtained for each 3° angular division of the model. The locations for the stress sections are shown in Figure 3.10.3-2. The allowable stresses for normal conditions and off-normal or accident events are taken from Subsection NB.

Bounding temperatures that envelop the maximum temperatures experienced by TSC components during storage and transfer conditions are used to determine allowable stress values. Temperatures used at each stress section are given in Figure 3.10.3-2. Allowable stress values at temperatures are determined based on mechanical properties for SA-240 Type 304 stainless steel. All stress components are reported in the global cylindrical coordinate system (X = Radial, Y = Circumferential, Z = Axial). Additionally, in accordance with ISG 15, Revision 0, an 0.8 weld reduction factor is applied to the allowable stresses for the closure lid weld (Section 11 of Figure 3.10.3-2).

### **TSC Analysis Result Details**

Table 3.10.3-1 through Table 3.10.3-17 present detailed analyses results for the TSC for normal conditions and off-normal and accident events of storage. Refer to Figure 3.10.3-2 for section cut locations.



Figure 3.10.3-1 MAGNASTOR TSC Finite Element Model

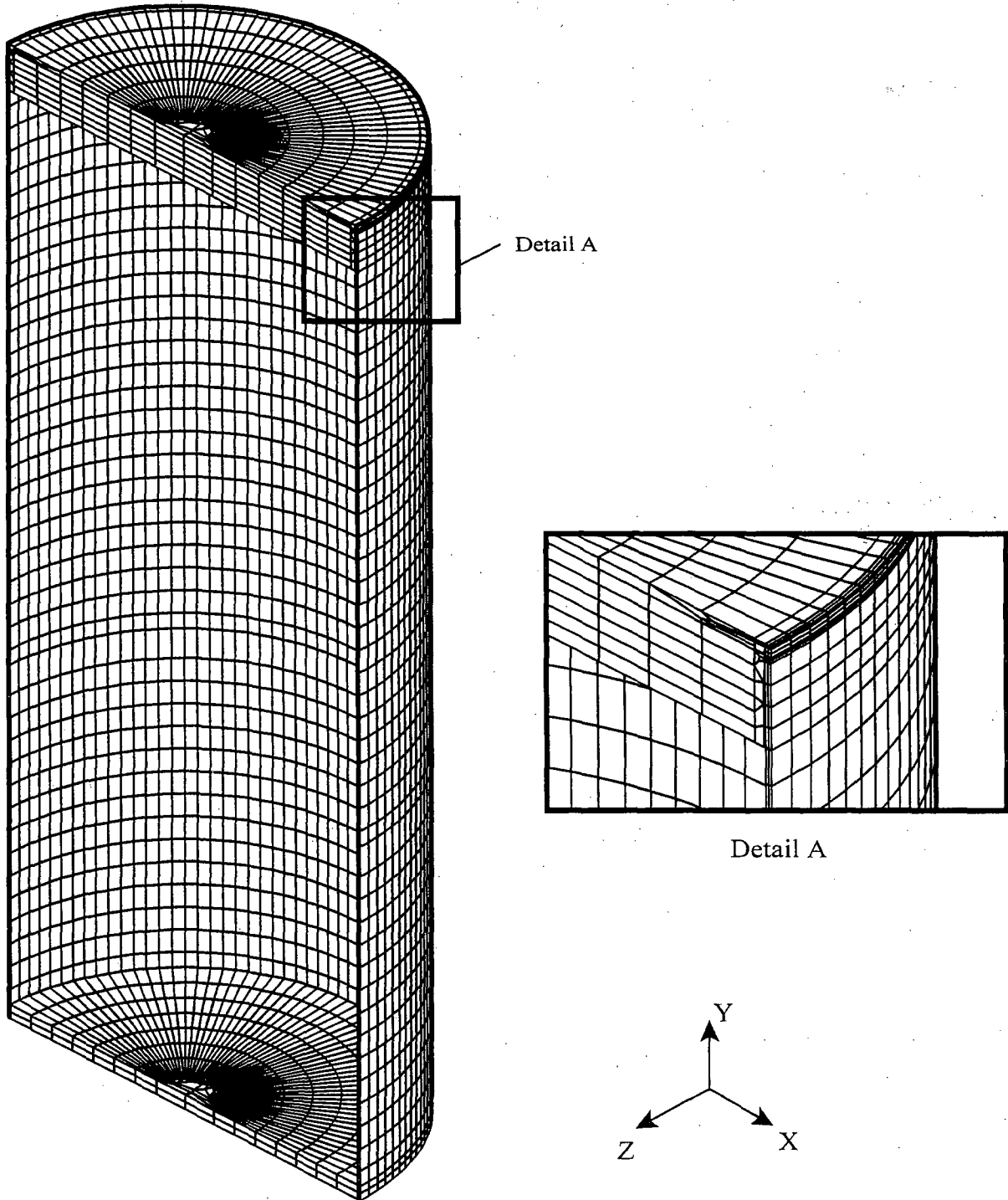
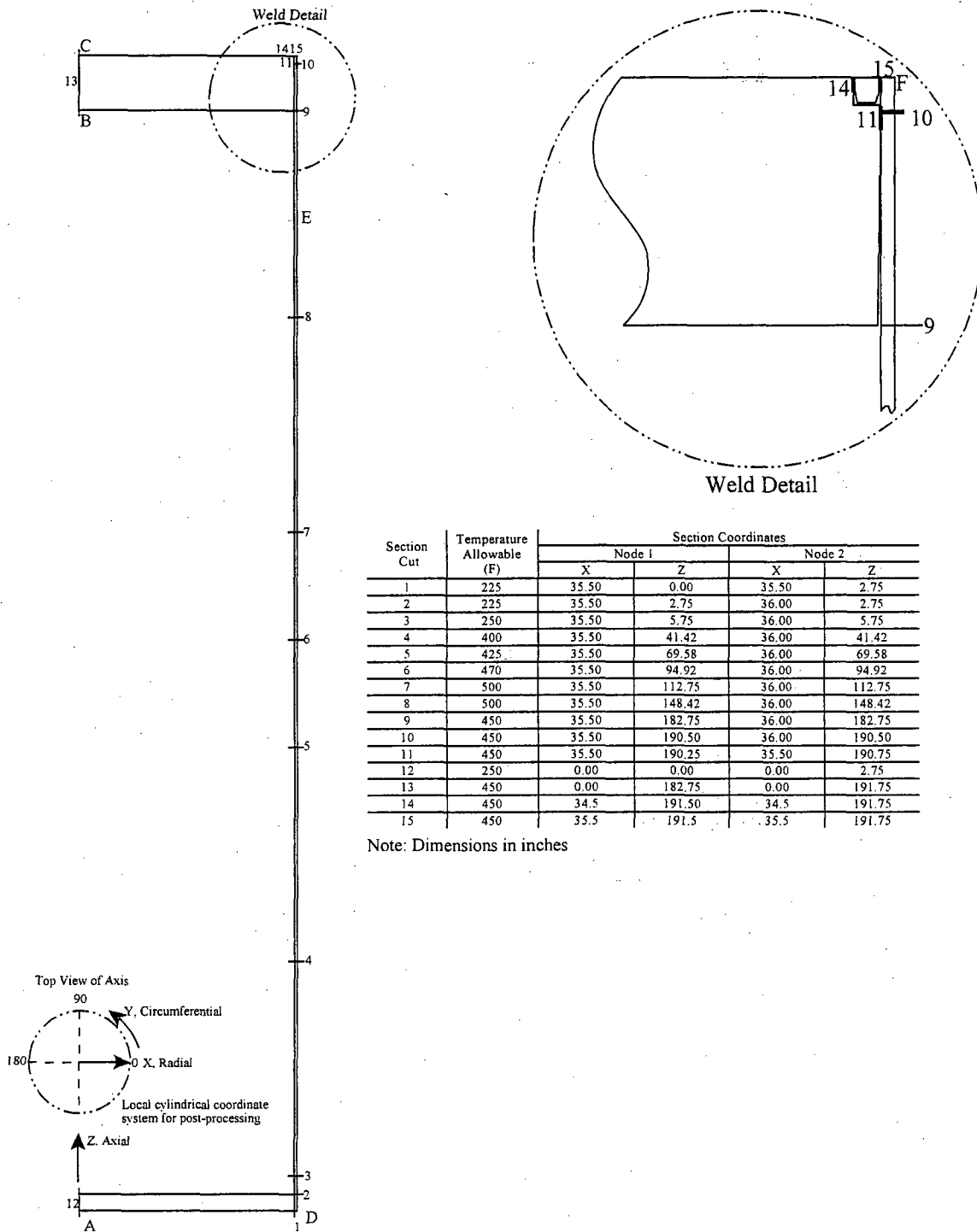


Figure 3.10.3-2 Identification of Sections for Evaluating Linearized Stresses in TSC



| Section Cut | Temperature Allowable (F) | Section Coordinates |        |        |        |
|-------------|---------------------------|---------------------|--------|--------|--------|
|             |                           | Node 1              |        | Node 2 |        |
|             |                           | X                   | Z      | X      | Z      |
| 1           | 225                       | 35.50               | 0.00   | 35.50  | 2.75   |
| 2           | 225                       | 35.50               | 2.75   | 36.00  | 2.75   |
| 3           | 250                       | 35.50               | 5.75   | 36.00  | 5.75   |
| 4           | 400                       | 35.50               | 41.42  | 36.00  | 41.42  |
| 5           | 425                       | 35.50               | 69.58  | 36.00  | 69.58  |
| 6           | 470                       | 35.50               | 94.92  | 36.00  | 94.92  |
| 7           | 500                       | 35.50               | 112.75 | 36.00  | 112.75 |
| 8           | 500                       | 35.50               | 148.42 | 36.00  | 148.42 |
| 9           | 450                       | 35.50               | 182.75 | 36.00  | 182.75 |
| 10          | 450                       | 35.50               | 190.50 | 36.00  | 190.50 |
| 11          | 450                       | 35.50               | 190.25 | 35.50  | 190.75 |
| 12          | 250                       | 0.00                | 0.00   | 0.00   | 2.75   |
| 13          | 450                       | 0.00                | 182.75 | 0.00   | 191.75 |
| 14          | 450                       | 34.5                | 191.50 | 34.5   | 191.75 |
| 15          | 450                       | 35.5                | 191.5  | 35.5   | 191.75 |

Note: Dimensions in inches

Table 3.10.3-1 TSC Normal Pressure plus Handling,  $P_m$ , ksi

| Section <sup>a</sup> | Component Stresses |       |       |          |          |          | $S_{int}$ | $S_{allow}$        | FS    |
|----------------------|--------------------|-------|-------|----------|----------|----------|-----------|--------------------|-------|
|                      | $S_x$              | $S_y$ | $S_z$ | $S_{xy}$ | $S_{yz}$ | $S_{xz}$ |           |                    |       |
| 1                    | -0.12              | 1.60  | 4.36  | -0.04    | 0.05     | -0.18    | 4.50      | 20.00              | 4.44  |
| 2                    | 0.92               | -9.06 | -1.29 | -0.22    | 0.01     | -0.66    | 10.17     | 20.00              | 1.97  |
| 3                    | -0.58              | -9.49 | 4.83  | -0.19    | -0.03    | 1.01     | 14.51     | 20.00              | 1.38  |
| 4                    | -0.02              | 7.81  | 4.78  | -0.21    | 0.00     | 0.00     | 7.84      | 18.70              | 2.39  |
| 5                    | -0.04              | 7.81  | 4.78  | -0.20    | 0.00     | 0.00     | 7.86      | 18.40              | 2.34  |
| 6                    | -0.04              | 7.81  | 4.77  | -0.21    | 0.00     | 0.00     | 7.86      | 17.86              | 2.27  |
| 7                    | -0.05              | 7.81  | 4.76  | -0.21    | 0.00     | 0.00     | 7.86      | 17.50              | 2.23  |
| 8                    | -0.05              | 7.80  | 4.74  | -0.21    | 0.00     | 0.00     | 7.86      | 17.50              | 2.23  |
| 9                    | -0.07              | 7.70  | 4.72  | -0.20    | 0.00     | 0.03     | 7.78      | 18.10              | 2.33  |
| 10                   | -0.35              | 1.26  | 1.08  | 0.00     | 0.00     | 0.07     | 1.62      | 18.10              | large |
| 11                   | -0.09              | 1.15  | 0.38  | -0.01    | 0.00     | -0.85    | 1.89      | 14.48 <sup>b</sup> | 7.66  |
| 12                   | 0.25               | 0.29  | -0.65 | 0.00     | 1.26     | -1.41    | 3.90      | 20.00              | 5.13  |
| 13                   | 0.03               | 0.03  | -0.06 | 0.00     | -0.05    | 0.05     | 0.17      | 18.10              | large |
| 14                   | 0.49               | 1.59  | -0.04 | 0.02     | -0.05    | -0.13    | 1.67      | 18.10              | large |
| 15                   | 0.18               | 1.51  | 0.08  | 0.00     | 0.00     | -0.10    | 1.50      | 18.10              | large |

<sup>a</sup> See Figure 3.10.3-2 for section locations.

<sup>b</sup> Allowable stress includes a reduction factor of 0.8 for the closure lid weld.

Table 3.10.3-2 TSC Normal Pressure plus Handling,  $P_m + P_b$ , ksi

| Section <sup>a</sup> | Component Stresses |        |                    |          |          |          | $S_{int}$ | $S_{allow}$        | FS    |
|----------------------|--------------------|--------|--------------------|----------|----------|----------|-----------|--------------------|-------|
|                      | $S_x$              | $S_y$  | $S_z$              | $S_{xy}$ | $S_{yz}$ | $S_{xz}$ |           |                    |       |
| 1                    | -0.96              | -5.82  | 11.51              | -0.09    | -0.02    | -0.25    | 17.33     | 30.00              | 1.73  |
| 2                    | 2.84               | -14.16 | -1.29 <sup>b</sup> | 0.00     | 0.00     | -1.19    | 17.32     | 30.00              | 1.73  |
| 3                    | -0.25              | -4.94  | 19.45              | -0.08    | -0.04    | 1.27     | 24.48     | 30.00              | 1.23  |
| 4                    | -0.05              | 7.92   | 4.82               | -0.21    | 0.00     | 0.01     | 7.98      | 28.05              | 3.52  |
| 5                    | -0.06              | 7.94   | 4.81               | -0.21    | 0.00     | -0.02    | 8.02      | 27.60              | 3.44  |
| 6                    | -0.07              | 7.95   | 4.81               | -0.21    | 0.00     | 0.00     | 8.03      | 26.79              | 3.34  |
| 7                    | -0.07              | 7.96   | 4.80               | -0.21    | 0.00     | 0.00     | 8.04      | 26.25              | 3.26  |
| 8                    | -0.08              | 7.94   | 4.78               | -0.21    | 0.00     | 0.00     | 8.03      | 26.25              | 3.27  |
| 9                    | -0.05              | 8.12   | 6.32               | -0.21    | 0.00     | 0.01     | 8.18      | 27.15              | 3.32  |
| 10                   | -0.78              | 1.13   | 1.11               | 0.00     | 0.00     | 0.89     | 2.60      | 27.15              | large |
| 11                   | -0.14              | 1.54   | 2.05               | 0.00     | 0.00     | -1.18    | 3.23      | 21.72 <sup>c</sup> | 6.72  |
| 12                   | 24.66              | 23.52  | 2.96               | 0.75     | 1.07     | -1.42    | 22.26     | 30.00              | 1.35  |
| 13                   | 2.87               | 2.85   | 0.04               | 0.00     | -0.06    | 0.04     | 2.82      | 27.15              | 9.63  |
| 14                   | 0.61               | 1.66   | -0.07              | 0.04     | -0.09    | -0.12    | 1.77      | 27.15              | large |
| 15                   | -0.59              | 1.25   | -0.15              | 0.00     | 0.05     | 0.06     | 1.85      | 27.15              | large |

<sup>a</sup> See Figure 3.10.3-2 for section locations.

<sup>b</sup> Localized bending stresses are secondary and are excluded from evaluation.

<sup>c</sup> Allowable stress includes a reduction factor of 0.8 for the closure lid weld.

Table 3.10.3-3 TSC Normal Pressure plus Handling, P + Q, ksi

| Section <sup>a</sup> | Component Stresses |                |                |                 |                 |                 | S <sub>int</sub> | S <sub>allow</sub> | FS    |
|----------------------|--------------------|----------------|----------------|-----------------|-----------------|-----------------|------------------|--------------------|-------|
|                      | S <sub>x</sub>     | S <sub>y</sub> | S <sub>z</sub> | S <sub>xy</sub> | S <sub>yz</sub> | S <sub>xz</sub> |                  |                    |       |
| 1                    | 0.68               | 12.71          | -2.73          | -0.02           | -0.01           | -0.05           | 15.44            | 60.00              | 3.89  |
| 2                    | 2.82               | -11.18         | -19.61         | 0.00            | 0.00            | -1.19           | 22.56            | 60.00              | 2.66  |
| 3                    | -0.29              | -3.60          | 19.95          | 0.00            | 0.04            | 1.22            | 23.63            | 60.00              | 2.54  |
| 4                    | -0.06              | 8.18           | 4.84           | -0.21           | 0.01            | 0.01            | 8.25             | 56.10              | 6.80  |
| 5                    | -0.07              | 8.29           | 4.84           | -0.21           | 0.00            | -0.02           | 8.37             | 55.20              | 6.59  |
| 6                    | -0.08              | 8.33           | 4.82           | -0.21           | 0.00            | 0.00            | 8.42             | 53.58              | 6.36  |
| 7                    | -0.08              | 8.37           | 4.84           | -0.22           | 0.00            | 0.00            | 8.46             | 52.50              | 6.21  |
| 8                    | -0.08              | 8.30           | 4.84           | -0.21           | 0.00            | 0.00            | 8.39             | 52.50              | 6.26  |
| 9                    | -0.07              | 7.92           | 6.29           | 0.00            | 0.00            | 0.00            | 7.99             | 54.30              | 6.80  |
| 10                   | -0.89              | 2.51           | 0.39           | 0.00            | -0.01           | 1.13            | 4.06             | 54.30              | large |
| 11                   | -0.24              | 2.34           | -1.52          | 0.04            | 0.01            | -0.55           | 4.06             | 43.44 <sup>b</sup> | large |
| 12                   | -41.04             | -37.90         | -8.45          | -1.25           | -0.15           | -1.51           | 33.17            | 60.00              | 1.81  |
| 13                   | -13.65             | -12.13         | -3.78          | -0.26           | 0.64            | 0.28            | 9.99             | 54.30              | 5.44  |
| 14                   | 0.06               | 3.03           | -0.40          | 0.00            | 0.00            | -0.10           | 3.45             | 54.30              | large |
| 15                   | -1.13              | 3.57           | -0.13          | 0.09            | -0.01           | -0.02           | 4.70             | 54.30              | large |

<sup>a</sup> See Figure 3.10.3-2 for section locations.

<sup>b</sup> Allowable stress includes a reduction factor of 0.8 for the closure lid weld.

Table 3.10.3-4 TSC Normal Pressure,  $P_m$ , ksi

| Section <sup>a</sup> | Component Stresses |       |       |          |          |          | $S_{int}$ |
|----------------------|--------------------|-------|-------|----------|----------|----------|-----------|
|                      | $S_x$              | $S_y$ | $S_z$ | $S_{xy}$ | $S_{yz}$ | $S_{xz}$ |           |
| 1                    | -0.10              | 1.33  | 3.61  | -0.03    | 0.04     | -0.17    | 3.73      |
| 2                    | 0.79               | -7.22 | -1.16 | 0.18     | -0.01    | -0.55    | 8.17      |
| 3                    | -0.50              | -6.93 | 3.91  | 0.13     | 0.02     | 0.85     | 11.01     |
| 4                    | -0.03              | 7.81  | 3.86  | -0.21    | 0.00     | 0.00     | 7.84      |
| 5                    | -0.04              | 7.81  | 3.85  | -0.21    | 0.00     | 0.00     | 7.86      |
| 6                    | -0.04              | 7.81  | 3.85  | -0.21    | 0.00     | 0.00     | 7.86      |
| 7                    | -0.05              | 7.80  | 3.85  | -0.21    | 0.00     | 0.00     | 7.86      |
| 8                    | -0.05              | 7.80  | 3.85  | -0.21    | 0.00     | 0.00     | 7.86      |
| 9                    | -0.06              | 7.73  | 3.85  | -0.20    | 0.00     | 0.04     | 7.81      |
| 10                   | -0.40              | 0.77  | 0.59  | -0.03    | 0.01     | 0.27     | 1.24      |
| 11                   | -0.11              | 0.95  | 0.83  | -0.03    | -0.01    | -0.60    | 1.53      |
| 12                   | 0.19               | 0.23  | -0.63 | 0.00     | 0.98     | -1.13    | 3.11      |
| 13                   | 0.04               | 0.04  | -0.06 | 0.00     | -0.04    | 0.04     | 0.15      |
| 14                   | 0.31               | 1.06  | -0.09 | -0.02    | 0.00     | -0.07    | 1.16      |
| 15                   | 0.09               | 1.04  | 0.16  | -0.02    | -0.01    | -0.04    | 0.97      |

<sup>a</sup> See Figure 3.10.3-2 for section locations.

Table 3.10.3-5 TSC Normal Pressure,  $P_m + P_b$ , ksi

| Section <sup>a</sup> | Component Stresses |        |        |          |          |          | $S_{int}$ |
|----------------------|--------------------|--------|--------|----------|----------|----------|-----------|
|                      | $S_x$              | $S_y$  | $S_z$  | $S_{xy}$ | $S_{yz}$ | $S_{xz}$ |           |
| 1                    | -0.75              | -4.52  | 9.51   | 0.07     | 0.02     | -0.22    | 14.03     |
| 2                    | 2.37               | -11.47 | -16.71 | 0.00     | 0.00     | -0.99    | 19.19     |
| 3                    | -0.20              | -3.23  | 15.78  | 0.04     | 0.03     | 1.07     | 19.08     |
| 4                    | -0.06              | 7.90   | 3.89   | -0.21    | 0.00     | 0.01     | 7.96      |
| 5                    | -0.07              | 7.90   | 3.87   | -0.21    | 0.00     | -0.02    | 7.98      |
| 6                    | -0.07              | 7.90   | 3.87   | -0.21    | 0.00     | 0.00     | 7.98      |
| 7                    | -0.07              | 7.90   | 3.87   | -0.21    | 0.00     | 0.00     | 7.98      |
| 8                    | -0.08              | 7.89   | 3.87   | -0.21    | 0.00     | 0.00     | 7.98      |
| 9                    | -0.05              | 8.19   | 5.53   | 0.00     | 0.00     | 0.01     | 8.24      |
| 10                   | -0.75              | 0.37   | -0.33  | -0.03    | 0.02     | 1.02     | 2.08      |
| 11                   | 0.07               | 1.40   | 2.30   | -0.04    | -0.01    | -0.90    | 2.87      |
| 12                   | 19.64              | 18.71  | 2.15   | 0.59     | 0.79     | -1.14    | 17.91     |
| 13                   | 2.24               | 2.22   | 0.03   | 0.00     | -0.04    | 0.04     | 2.21      |
| 14                   | 0.43               | 1.14   | -0.08  | -0.02    | 0.02     | -0.05    | 1.22      |
| 15                   | -0.46              | 0.84   | -0.06  | -0.03    | -0.01    | 0.02     | 1.30      |

<sup>a</sup> See Figure 3.10.3-2 for section locations.

Table 3.10.3-6 TSC Thermal Stresses, Q, ksi

| Section <sup>a</sup> | Component Stresses |                |                |                 |                 |                 | S <sub>int</sub> |
|----------------------|--------------------|----------------|----------------|-----------------|-----------------|-----------------|------------------|
|                      | S <sub>x</sub>     | S <sub>y</sub> | S <sub>z</sub> | S <sub>xy</sub> | S <sub>yz</sub> | S <sub>xz</sub> |                  |
| 1                    | -0.05              | 3.72           | 0.05           | 0.00            | 0.00            | 0.04            | 3.79             |
| 2                    | -0.20              | 2.82           | -0.25          | -0.08           | 0.00            | -0.01           | 3.08             |
| 3                    | 0.09               | 1.06           | -0.51          | 0.00            | -0.01           | -0.03           | 1.57             |
| 4                    | 0.00               | -0.27          | -0.15          | 0.01            | 0.00            | 0.00            | 0.27             |
| 5                    | 0.00               | -0.36          | -0.20          | 0.02            | 0.00            | 0.00            | 0.36             |
| 6                    | 0.00               | -0.42          | -0.21          | 0.02            | 0.00            | 0.00            | 0.42             |
| 7                    | 0.00               | -0.43          | -0.23          | 0.02            | 0.00            | 0.00            | 0.43             |
| 8                    | -0.01              | -0.44          | -0.20          | 0.02            | 0.00            | 0.00            | 0.43             |
| 9                    | -0.02              | -0.57          | -0.20          | 0.03            | 0.00            | -0.01           | 0.55             |
| 10                   | -0.12              | 1.37           | -0.74          | 0.00            | -0.01           | 0.24            | 2.20             |
| 11                   | -0.33              | 1.63           | 0.01           | 0.01            | 0.00            | 0.07            | 1.98             |
| 12                   | -16.87             | -14.95         | -4.20          | -0.50           | -1.60           | -0.10           | 13.05            |
| 13                   | -10.85             | -9.35          | -3.62          | -0.26           | 0.69            | 0.22            | 7.38             |
| 14                   | -0.25              | 1.60           | -0.07          | 0.00            | 0.00            | 0.01            | 1.86             |
| 15                   | -0.49              | 2.39           | 0.17           | -0.05           | 0.01            | 0.02            | 2.88             |

<sup>a</sup> See Figure 3.10.3-2 for section locations.



Table 3.10.3-7 TSC Off-Normal Pressure plus Handling,  $P_m$ , ksi

| Section <sup>a</sup> | Component Stresses |        |       |          |          |          | $S_{int}$ | $S_{allow}$        | FS    |
|----------------------|--------------------|--------|-------|----------|----------|----------|-----------|--------------------|-------|
|                      | $S_x$              | $S_y$  | $S_z$ | $S_{xy}$ | $S_{yz}$ | $S_{xz}$ |           |                    |       |
| 1                    | -0.14              | 1.84   | 5.02  | -0.05    | 0.06     | -0.21    | 5.18      | 22.00              | 4.25  |
| 2                    | 1.07               | -10.37 | -1.51 | -0.26    | 0.01     | -0.76    | 11.66     | 22.00              | 1.89  |
| 3                    | -0.67              | -10.75 | 5.54  | -0.21    | -0.03    | 1.16     | 16.51     | 22.00              | 1.33  |
| 4                    | -0.03              | 9.23   | 5.48  | -0.24    | 0.00     | 0.00     | 9.27      | 20.57              | 2.22  |
| 5                    | -0.04              | 9.23   | 5.48  | -0.24    | 0.00     | 0.00     | 9.28      | 20.24              | 2.18  |
| 6                    | -0.05              | 9.23   | 5.47  | -0.24    | 0.00     | 0.00     | 9.29      | 19.65              | 2.11  |
| 7                    | -0.05              | 9.23   | 5.46  | -0.24    | 0.00     | 0.00     | 9.29      | 19.25              | 2.07  |
| 8                    | -0.06              | 9.22   | 5.44  | -0.24    | 0.00     | 0.00     | 9.29      | 19.25              | 2.07  |
| 9                    | -0.08              | 9.11   | 5.42  | -0.24    | 0.00     | 0.04     | 9.20      | 19.91              | 2.16  |
| 10                   | -0.42              | 1.41   | 1.20  | 0.00     | 0.00     | 0.11     | 1.84      | 19.91              | large |
| 11                   | -0.11              | 1.32   | 0.53  | -0.01    | 0.00     | -0.96    | 2.13      | 15.93 <sup>b</sup> | 7.48  |
| 12                   | 0.28               | 0.33   | -0.76 | 0.00     | 1.44     | -1.62    | 4.47      | 22.00              | 4.92  |
| 13                   | 0.04               | 0.04   | -0.07 | 0.00     | -0.06    | 0.06     | 0.20      | 19.91              | large |
| 14                   | 0.54               | 1.79   | -0.06 | 0.02     | -0.05    | -0.14    | 1.88      | 19.91              | large |
| 15                   | 0.20               | 1.70   | 0.11  | 0.00     | 0.00     | -0.11    | 1.67      | 19.91              | large |

<sup>a</sup> See Figure 3.10.3-2 for section locations.

<sup>b</sup> Allowable stress includes a reduction factor of 0.8 for the closure lid weld.

Table 3.10.3-8 TSC Off-Normal Pressure plus Handling,  $P_m + P_b$ , ksi

| Section <sup>a</sup> | Component Stresses |        |                    |          |          |          | $S_{int}$ | $S_{allow}$        | FS    |
|----------------------|--------------------|--------|--------------------|----------|----------|----------|-----------|--------------------|-------|
|                      | $S_x$              | $S_y$  | $S_z$              | $S_{xy}$ | $S_{yz}$ | $S_{xz}$ |           |                    |       |
| 1                    | -1.10              | -6.64  | 13.23              | -0.10    | -0.03    | -0.28    | 19.88     | 33.00              | 1.66  |
| 2                    | 3.27               | -16.24 | -23.02             | 0.00     | 0.00     | -1.37    | 26.44     | 60.00 <sup>b</sup> | 2.27  |
| 2                    | 3.27               | -16.24 | -1.51 <sup>c</sup> | 0.00     | 0.00     | -1.37    | 19.87     | 33.00              | 1.66  |
| 3                    | -0.28              | -5.53  | 22.31              | 0.00     | 0.00     | 1.47     | 27.94     | 33.00              | 1.18  |
| 4                    | -0.06              | 9.36   | 5.52               | -0.25    | 0.00     | 0.01     | 9.43      | 30.86              | 3.27  |
| 5                    | -0.07              | 9.38   | 5.51               | -0.25    | 0.00     | -0.03    | 9.47      | 30.36              | 3.21  |
| 6                    | -0.08              | 9.39   | 5.51               | -0.25    | 0.00     | 0.00     | 9.49      | 29.47              | 3.11  |
| 7                    | -0.09              | 9.39   | 5.50               | -0.25    | 0.00     | 0.00     | 9.49      | 28.88              | 3.04  |
| 8                    | -0.09              | 9.38   | 5.48               | -0.25    | 0.00     | 0.00     | 9.48      | 28.88              | 3.05  |
| 9                    | -0.06              | 9.62   | 7.34               | 0.00     | 0.01     | 0.01     | 9.68      | 29.87              | 3.09  |
| 10                   | -0.92              | 1.19   | 1.05               | 0.00     | 0.00     | 1.08     | 2.92      | 29.87              | large |
| 11                   | -0.13              | 1.79   | 2.47               | 0.00     | 0.00     | -1.35    | 3.75      | 23.89 <sup>d</sup> | 6.37  |
| 12                   | 28.23              | 26.93  | 3.35               | 0.86     | 1.22     | -1.62    | 25.52     | 33.00              | 1.29  |
| 13                   | 3.27               | 3.25   | 0.05               | 0.00     | -0.06    | 0.05     | 3.23      | 29.87              | 9.25  |
| 14                   | 0.68               | 1.87   | -0.09              | 0.04     | -0.09    | -0.13    | 1.99      | 29.87              | large |
| 15                   | -0.67              | 1.41   | -0.16              | 0.00     | 0.05     | 0.07     | 2.09      | 29.87              | large |

<sup>a</sup> See Figure 3.10.3-2 for section locations.

<sup>b</sup> Bending stresses are considered secondary, P+Q stress allowable used.

<sup>c</sup> Localized bending stresses are secondary and are excluded from evaluation.

<sup>d</sup> Allowable stress includes a reduction factor of 0.8 for the closure lid weld.

Table 3.10.3-9 TSC Off-Normal Pressure plus Handling, P + Q, ksi

| Section <sup>a</sup> | Component Stresses |                |                |                 |                 |                 | S <sub>int</sub> | S <sub>allow</sub> | FS    |
|----------------------|--------------------|----------------|----------------|-----------------|-----------------|-----------------|------------------|--------------------|-------|
|                      | S <sub>x</sub>     | S <sub>y</sub> | S <sub>z</sub> | S <sub>xy</sub> | S <sub>yz</sub> | S <sub>xz</sub> |                  |                    |       |
| 1                    | 0.78               | 14.01          | -3.15          | -0.02           | -0.01           | -0.07           | 17.16            | 60.00              | 3.50  |
| 2                    | 3.26               | -13.26         | -22.64         | 0.00            | 0.00            | -1.37           | 26.04            | 60.00              | 2.30  |
| 3                    | -0.32              | -4.19          | 22.81          | 0.00            | 0.04            | 1.41            | 27.09            | 60.00              | 2.21  |
| 4                    | -0.07              | 9.61           | 5.55           | -0.25           | 0.01            | 0.01            | 9.69             | 55.20              | 5.62  |
| 5                    | -0.08              | 9.72           | 5.55           | -0.25           | 0.00            | -0.02           | 9.82             | 53.58              | 5.43  |
| 6                    | -0.09              | 9.77           | 5.53           | -0.25           | 0.00            | 0.00            | 9.87             | 53.58              | 5.43  |
| 7                    | -0.09              | 9.80           | 5.54           | -0.25           | 0.00            | 0.00            | 9.91             | 52.50              | 5.30  |
| 8                    | -0.09              | 9.74           | 5.55           | -0.25           | 0.00            | 0.00            | 9.85             | 52.50              | 5.33  |
| 9                    | -0.08              | 9.41           | 7.30           | 0.00            | -0.01           | 0.00            | 9.49             | 54.30              | 5.72  |
| 10                   | -1.03              | 2.58           | 0.32           | 0.00            | -0.01           | 1.31            | 4.41             | 54.30              | large |
| 11                   | -0.29              | 2.43           | -1.64          | 0.04            | 0.01            | -0.61           | 4.30             | 43.44 <sup>b</sup> | large |
| 12                   | -44.54             | -41.22         | -9.07          | -1.36           | 0.06            | -1.71           | 36.12            | 60.00              | 1.66  |
| 13                   | -14.05             | -12.53         | -3.80          | -0.26           | 0.63            | 0.29            | 10.36            | 54.30              | 5.24  |
| 14                   | 0.43               | 3.48           | -0.16          | 0.04            | -0.09           | -0.13           | 3.66             | 54.30              | large |
| 15                   | -1.21              | 3.72           | -0.14          | 0.10            | -0.01           | -0.01           | 4.94             | 54.30              | large |

<sup>a</sup> See Figure 3.10.3-2 for section locations.

<sup>b</sup> Allowable stress includes a reduction factor of 0.8 for the closure lid weld.

Table 3.10.3-10 TSC Normal Pressure plus Off-Normal Handling,  $P_m$ , ksi

| Section <sup>a</sup> | Component Stresses |        |       |          |          |          | $S_{int}$ | $S_{allow}$        | FS    |
|----------------------|--------------------|--------|-------|----------|----------|----------|-----------|--------------------|-------|
|                      | $S_x$              | $S_y$  | $S_z$ | $S_{xy}$ | $S_{yz}$ | $S_{xz}$ |           |                    |       |
| 1                    | -1.64              | 1.20   | 4.54  | 0.20     | 0.04     | -0.35    | 6.23      | 24.75              | 3.97  |
| 2                    | 1.20               | -10.15 | -1.07 | 0.26     | -0.14    | -0.70    | 11.57     | 24.75              | 2.14  |
| 3                    | -0.60              | -10.57 | 5.42  | 0.01     | -0.10    | 1.06     | 16.17     | 24.50              | 1.52  |
| 4                    | -0.12              | 7.94   | 5.63  | 0.08     | 0.00     | 0.00     | 8.06      | 22.50              | 2.79  |
| 5                    | -0.12              | 7.89   | 5.63  | 0.07     | 0.00     | 0.00     | 8.00      | 22.12              | 2.77  |
| 6                    | -0.12              | 7.88   | 5.59  | 0.06     | 0.00     | 0.00     | 8.00      | 21.45              | 2.68  |
| 7                    | -0.13              | 7.88   | 5.57  | 0.07     | 0.00     | 0.00     | 8.01      | 21.00              | 2.62  |
| 8                    | -0.15              | 7.95   | 5.45  | 0.09     | 0.01     | 0.00     | 8.09      | 21.00              | 2.60  |
| 9                    | -0.08              | 7.91   | 4.90  | 0.03     | -0.08    | 0.03     | 7.98      | 21.75              | 2.73  |
| 10                   | -6.14              | -0.11  | 0.89  | 0.66     | -0.18    | -0.64    | 7.27      | 21.75              | 2.99  |
| 11                   | -4.94              | 0.30   | -0.34 | 0.75     | -0.22    | -1.44    | 6.10      | 17.40 <sup>b</sup> | 2.85  |
| 12                   | 0.24               | 0.32   | -0.65 | 0.00     | 1.37     | -1.51    | 4.18      | 24.50              | 5.86  |
| 13                   | 0.02               | 0.04   | -0.06 | 0.00     | -0.06    | 0.05     | 0.17      | 21.75              | large |
| 14                   | -1.58              | 1.35   | -0.21 | 0.47     | 0.03     | 0.07     | 3.08      | 21.75              | 7.06  |
| 15                   | -3.66              | 0.93   | -0.20 | 0.67     | -0.28    | -0.27    | 4.87      | 21.75              | 4.47  |

<sup>a</sup> See Figure 3.10.3-2 for section locations.

<sup>b</sup> Allowable stress includes a reduction factor of 0.8 for the closure lid weld.

Table 3.10.3-11 TSC Normal Pressure plus Off-Normal Handling,  $P_m + P_b$ , ksi

| Section <sup>a</sup> | Component Stresses |                |                    |                 |                 |                 | S <sub>int</sub> | S <sub>allow</sub> | FS   |
|----------------------|--------------------|----------------|--------------------|-----------------|-----------------|-----------------|------------------|--------------------|------|
|                      | S <sub>x</sub>     | S <sub>y</sub> | S <sub>z</sub>     | S <sub>xy</sub> | S <sub>yz</sub> | S <sub>xz</sub> |                  |                    |      |
| 1                    | -1.04              | -6.70          | 12.44              | 0.35            | 0.10            | -0.29           | 19.17            | 35.40              | 1.85 |
| 2                    | 3.13               | -15.72         | -1.07 <sup>b</sup> | -0.05           | -0.19           | -1.29           | 19.23            | 35.40              | 1.84 |
| 3                    | -0.23              | -6.17          | 21.24              | -0.14           | 0.05            | 1.35            | 27.49            | 34.80              | 1.27 |
| 4                    | -0.14              | 12.81          | 7.14               | -0.35           | 0.02            | 0.01            | 12.96            | 31.10              | 2.40 |
| 5                    | -0.13              | 12.91          | 7.18               | -0.36           | 0.00            | -0.02           | 13.06            | 30.60              | 2.34 |
| 6                    | -0.13              | 12.87          | 7.14               | -0.36           | 0.00            | 0.00            | 13.02            | 29.70              | 2.28 |
| 7                    | -0.14              | 12.92          | 7.13               | -0.36           | 0.00            | 0.00            | 13.07            | 29.10              | 2.23 |
| 8                    | -0.17              | 12.75          | 6.94               | -0.35           | -0.01           | 0.00            | 12.94            | 29.10              | 2.25 |
| 9                    | -0.29              | 9.76           | 4.16               | -0.24           | -0.16           | 0.06            | 10.06            | 30.10              | 2.99 |
| 10                   | -7.43              | -1.04          | 1.17               | 0.59            | -0.18           | 0.21            | 8.68             | 30.10              | 3.47 |
| 11                   | -5.58              | 0.24           | 0.80               | 0.66            | -0.18           | -1.51           | 7.22             | 24.08 <sup>c</sup> | 3.34 |
| 12                   | 26.41              | 25.35          | 3.25               | 0.80            | 1.18            | -1.51           | 23.79            | 34.80              | 1.46 |
| 13                   | 2.95               | 3.19           | 0.05               | 0.00            | -0.06           | 0.03            | 3.14             | 30.10              | 9.59 |
| 14                   | -1.38              | 1.63           | -0.14              | 0.52            | 0.02            | 0.13            | 3.20             | 30.10              | 9.41 |
| 15                   | -3.47              | 1.19           | -0.12              | 0.73            | -0.20           | -0.35           | 4.95             | 30.10              | 6.08 |

<sup>a</sup> See Figure 3.10.3-2 for section locations.

<sup>b</sup> Localized bending stresses are secondary and are excluded from evaluation.

<sup>c</sup> Allowable stress includes a reduction factor of 0.8 for the closure lid weld.

Table 3.10.3-12 TSC Normal Pressure plus 24-inch Drop,  $P_m$ , ksi

| Section <sup>a</sup> | Component Stresses |       |       |          |          |          | $S_{int}$ | $S_{allow}$        | FS    |
|----------------------|--------------------|-------|-------|----------|----------|----------|-----------|--------------------|-------|
|                      | $S_x$              | $S_y$ | $S_z$ | $S_{xy}$ | $S_{yz}$ | $S_{xz}$ |           |                    |       |
| 1                    | -0.11              | 0.79  | 0.27  | -0.02    | 0.07     | 0.37     | 1.14      | 47.58              | large |
| 2                    | 1.34               | -9.26 | -8.42 | 0.24     | -0.02    | -0.99    | 10.71     | 47.58              | 4.44  |
| 3                    | -0.52              | -8.65 | -4.81 | -0.17    | -0.03    | 0.93     | 8.33      | 47.15              | 5.66  |
| 4                    | -0.03              | 7.81  | -4.26 | 0.00     | 0.00     | 0.00     | 12.07     | 44.80              | 3.71  |
| 5                    | -0.04              | 7.80  | -3.77 | -0.20    | 0.00     | 0.00     | 11.58     | 44.10              | 3.81  |
| 6                    | -0.04              | 7.81  | -3.33 | 0.21     | 0.00     | 0.00     | 11.14     | 42.84              | 3.85  |
| 7                    | -0.05              | 7.80  | -3.02 | 0.21     | 0.00     | 0.00     | 10.83     | 42.00              | 3.88  |
| 8                    | -0.05              | 7.80  | -2.40 | 0.21     | 0.00     | 0.00     | 10.21     | 42.00              | 4.11  |
| 9                    | -0.05              | 7.92  | -1.81 | 0.21     | 0.00     | 0.05     | 9.74      | 43.40              | 4.46  |
| 10                   | -0.68              | -1.09 | -2.03 | 0.00     | 0.00     | 1.31     | 2.95      | 43.40              | large |
| 11                   | -0.22              | 0.63  | 3.05  | 0.00     | 0.00     | 0.63     | 3.51      | 34.72 <sup>b</sup> | 9.89  |
| 12                   | 0.46               | 0.38  | -1.22 | -0.01    | 0.98     | -0.95    | 3.19      | 47.15              | large |
| 13                   | 0.04               | 0.04  | -0.05 | 0.00     | 0.02     | -0.02    | 0.10      | 43.40              | large |
| 14                   | -0.61              | -0.65 | -0.26 | 0.00     | 0.00     | 0.12     | 0.44      | 43.40              | large |
| 15                   | -0.67              | -0.56 | 0.15  | 0.01     | -0.02    | 0.14     | 0.87      | 43.40              | large |

<sup>a</sup> See Figure 3.10.3-2 for section locations.

<sup>b</sup> Allowable stress includes a reduction factor of 0.8 for the closure lid weld.

Table 3.10.3-13 TSC Normal Pressure plus 24-inch Drop,  $P_m + P_b$ , ksi

| Section <sup>a</sup> | Component Stresses |        |                    |          |          |          | $S_{int}$ | $S_{allow}$        | FS    |
|----------------------|--------------------|--------|--------------------|----------|----------|----------|-----------|--------------------|-------|
|                      | $S_x$              | $S_y$  | $S_z$              | $S_{xy}$ | $S_{yz}$ | $S_{xz}$ |           |                    |       |
| 1                    | 1.99               | 7.87   | -4.91              | 0.00     | 0.00     | 1.28     | 13.01     | 69.80              | 5.37  |
| 2                    | 3.02               | -14.27 | -8.42 <sup>b</sup> | 0.00     | 0.00     | -1.49    | 17.49     | 69.80              | 3.99  |
| 3                    | -0.84              | -12.49 | -17.20             | 0.00     | -0.01    | 0.71     | 16.42     | 68.60              | 4.18  |
| 4                    | -0.06              | 7.90   | -4.22              | 0.21     | 0.00     | 0.01     | 12.13     | 64.00              | 5.28  |
| 5                    | -0.06              | 7.91   | -3.75              | 0.21     | 0.00     | -0.02    | 11.67     | 63.75              | 5.46  |
| 6                    | -0.07              | 7.91   | -3.30              | 0.21     | 0.00     | 0.00     | 11.22     | 63.30              | 5.64  |
| 7                    | -0.07              | 7.91   | -2.99              | 0.21     | 0.00     | 0.00     | 10.91     | 63.00              | 5.77  |
| 8                    | -0.08              | 7.90   | -2.37              | -0.21    | 0.00     | 0.00     | 10.28     | 63.00              | 6.13  |
| 9                    | -0.08              | 7.36   | -3.87              | 0.19     | 0.00     | 0.06     | 11.24     | 63.50              | 5.65  |
| 10                   | -0.62              | -2.86  | -7.82              | 0.00     | 0.00     | 1.68     | 7.95      | 63.50              | 7.99  |
| 11                   | -1.59              | -0.02  | 2.52               | 0.00     | 0.00     | 0.86     | 4.46      | 50.80 <sup>c</sup> | large |
| 12                   | 17.98              | 18.23  | 1.64               | 0.67     | 0.76     | -0.94    | 17.24     | 68.60              | 3.98  |
| 13                   | 0.92               | 0.92   | -0.09              | 0.00     | 0.02     | -0.02    | 1.01      | 63.50              | large |
| 14                   | -0.83              | -0.80  | -0.46              | 0.00     | 0.00     | 0.17     | 0.51      | 63.50              | large |
| 15                   | -1.65              | -0.97  | -0.29              | 0.01     | -0.02    | 0.33     | 1.52      | 63.50              | large |

<sup>a</sup> See Figure 3.10.3-2 for section locations.

<sup>b</sup> Localized bending stresses are secondary and are excluded from evaluation.

<sup>c</sup> Allowable stress includes a reduction factor of 0.8 for the closure lid weld.

Table 3.10.3-14 TSC Accident Pressure plus Dead Weight,  $P_m$ , ksi

| Section <sup>a</sup> | Component Stresses |        |       |          |          |          | $S_{int}$ | $S_{allow}$        | FS    |
|----------------------|--------------------|--------|-------|----------|----------|----------|-----------|--------------------|-------|
|                      | $S_x$              | $S_y$  | $S_z$ | $S_{xy}$ | $S_{yz}$ | $S_{xz}$ |           |                    |       |
| 1                    | -0.23              | 3.01   | 8.15  | -0.08    | 0.09     | -0.37    | 8.42      | 47.58              | 5.65  |
| 2                    | 1.81               | -16.45 | -2.76 | 0.40     | -0.01    | -1.26    | 18.61     | 47.58              | 2.56  |
| 3                    | -1.13              | -15.79 | 8.74  | 0.29     | 0.06     | 1.93     | 24.90     | 47.15              | 1.89  |
| 4                    | -0.06              | 17.74  | 8.63  | -0.47    | 0.00     | 0.00     | 17.83     | 44.80              | 2.51  |
| 5                    | -0.09              | 17.74  | 8.63  | -0.47    | 0.00     | 0.00     | 17.85     | 44.10              | 2.47  |
| 6                    | -0.10              | 17.74  | 8.63  | -0.47    | 0.00     | 0.00     | 17.86     | 42.84              | 2.40  |
| 7                    | -0.11              | 17.74  | 8.64  | -0.47    | 0.00     | 0.00     | 17.87     | 42.00              | 2.35  |
| 8                    | -0.11              | 17.73  | 8.64  | -0.47    | 0.00     | 0.00     | 17.87     | 42.00              | 2.35  |
| 9                    | -0.15              | 17.58  | 8.66  | -0.46    | 0.00     | 0.08     | 17.75     | 43.40              | 2.45  |
| 10                   | -0.91              | 1.73   | 1.29  | -0.07    | 0.02     | 0.63     | 2.81      | 43.40              | large |
| 11                   | -0.26              | 2.16   | 1.92  | -0.07    | -0.02    | -1.35    | 3.47      | 34.72 <sup>b</sup> | large |
| 12                   | 0.43               | 0.52   | -1.44 | -0.01    | 2.23     | -2.57    | 7.07      | 47.15              | 6.67  |
| 13                   | 0.08               | 0.08   | -0.13 | 0.00     | -0.10    | 0.10     | 0.35      | 43.40              | large |
| 14                   | 0.69               | 2.39   | -0.20 | -0.05    | 0.01     | -0.17    | 2.62      | 43.40              | large |
| 15                   | 0.19               | 2.35   | 0.36  | -0.06    | -0.02    | -0.09    | 2.19      | 43.40              | large |

<sup>a</sup> See Figure 3.10.3-2 for section locations.

<sup>b</sup> Allowable stress includes a reduction factor of 0.8 for the closure lid weld.



Table 3.10.3-15 TSC Accident Pressure plus Dead Weight,  $P_m + P_b$ , ksi

| Section <sup>a</sup> | Component Stresses |                |                    |                 |                 |                 | S <sub>int</sub> | S <sub>allow</sub> | FS    |
|----------------------|--------------------|----------------|--------------------|-----------------|-----------------|-----------------|------------------|--------------------|-------|
|                      | S <sub>x</sub>     | S <sub>y</sub> | S <sub>z</sub>     | S <sub>xy</sub> | S <sub>yz</sub> | S <sub>xz</sub> |                  |                    |       |
| 1                    | -1.74              | -10.29         | 21.53              | 0.15            | 0.04            | -0.50           | 31.84            | 69.80              | 2.19  |
| 2                    | 5.41               | -26.12         | -2.76 <sup>b</sup> | 0.00            | 0.00            | -2.26           | 32.12            | 69.80              | 2.17  |
| 3                    | -0.46              | -7.35          | 35.72              | 0.09            | 0.07            | 2.43            | 43.24            | 68.60              | 1.59  |
| 4                    | -0.13              | 17.95          | 8.70               | -0.47           | 0.00            | 0.02            | 18.10            | 64.00              | 3.54  |
| 5                    | -0.15              | 17.96          | 8.68               | -0.47           | 0.00            | -0.04           | 18.13            | 63.75              | 3.52  |
| 6                    | -0.16              | 17.95          | 8.68               | -0.47           | 0.00            | 0.00            | 18.14            | 63.30              | 3.49  |
| 7                    | -0.17              | 17.95          | 8.68               | -0.47           | 0.00            | 0.00            | 18.15            | 63.00              | 3.47  |
| 8                    | -0.18              | 17.94          | 8.69               | -0.47           | 0.00            | 0.00            | 18.14            | 63.00              | 3.47  |
| 9                    | -0.10              | 18.62          | 12.48              | 0.00            | 0.00            | 0.03            | 18.73            | 63.50              | 3.39  |
| 11                   | 0.17               | 3.19           | 5.25               | -0.08           | -0.03           | -2.02           | 6.49             | 50.80 <sup>c</sup> | 7.83  |
| 10                   | -1.70              | 0.77           | -0.93              | 0.00            | 0.00            | 2.33            | 4.73             | 63.50              | large |
| 12                   | 44.60              | 42.52          | 4.88               | 1.35            | 1.80            | -2.58           | 40.70            | 68.60              | 1.69  |
| 13                   | 5.04               | 5.00           | 0.07               | 0.01            | -0.10           | 0.10            | 4.98             | 63.50              | large |
| 14                   | 0.95               | 2.55           | -0.19              | -0.05           | 0.03            | -0.12           | 2.75             | 63.50              | large |
| 15                   | -1.03              | 1.90           | -0.12              | -0.07           | -0.02           | 0.05            | 2.93             | 63.50              | large |

<sup>a</sup> See Figure 3.10.3-2 for section locations.

<sup>b</sup> Localized bending stresses are secondary and are excluded from evaluation.

<sup>c</sup> Allowable stress includes a reduction factor of 0.8 for the closure lid weld.

Table 3.10.3-16 TSC Tip-Over plus Normal Pressure,  $P_m$ , ksi

| Section <sup>a</sup> | Angle | Component Stresses |        |        |          |          |          | $S_{int}$ | $S_{allow}$        | FS    |
|----------------------|-------|--------------------|--------|--------|----------|----------|----------|-----------|--------------------|-------|
|                      |       | $S_x$              | $S_y$  | $S_z$  | $S_{xy}$ | $S_{yz}$ | $S_{xz}$ |           |                    |       |
| 1                    | 69    | -0.16              | 1.58   | 3.91   | 0.13     | 0.29     | -0.35    | 4.17      | 47.58              | large |
| 2                    | 69    | 1.12               | -8.58  | -2.50  | 0.16     | 0.79     | -0.72    | 9.95      | 47.58              | 4.78  |
| 3                    | 69    | -0.55              | -8.76  | 3.00   | -0.04    | 1.22     | 0.94     | 12.23     | 47.15              | 3.86  |
| 4                    | 27    | -0.03              | 8.93   | 0.26   | 0.01     | 3.26     | 0.00     | 10.84     | 44.80              | 4.13  |
| 5                    | 0     | -4.82              | -12.05 | -10.93 | 12.58    | 0.33     | 1.15     | 26.27     | 44.10              | 2.57  |
| 6                    | 0     | -0.39              | 8.60   | -5.39  | -0.10    | -0.24    | 0.06     | 14.01     | 42.84              | 3.06  |
| 7                    | 0     | -0.32              | 10.05  | -1.64  | -0.02    | -0.15    | 0.00     | 11.69     | 42.00              | 3.59  |
| 8                    | 0     | -0.52              | 8.21   | 1.81   | 0.27     | -0.06    | 0.00     | 8.75      | 42.00              | 4.80  |
| 9                    | 33    | -1.29              | 16.48  | 2.21   | 1.33     | -1.22    | 0.16     | 18.09     | 43.40              | 2.40  |
| 10 <sup>b</sup>      | 6     | -5.49              | 6.78   | -0.91  | -2.40    | -2.01    | -1.82    | 14.33     | 43.40              | 3.03  |
| 11 <sup>c</sup>      | 0-6   | -23.89             | -17.09 | -19.05 | 10.77    | -1.77    | -8.92    | 29.05     | 34.72 <sup>c</sup> | 1.20  |
| 12                   | 0     | 0.18               | 0.23   | -0.56  | 0.00     | 0.87     | -1.04    | 2.82      | 47.15              | large |
| 13                   | 0     | -1.36              | -0.23  | -0.57  | 0.12     | -0.01    | -3.40    | 6.86      | 43.40              | 6.33  |
| 14 <sup>b</sup>      | 6     | 1.90               | -8.88  | 0.00   | 5.20     | 4.00     | -2.09    | 16.65     | 43.40              | 2.61  |
| 15 <sup>b</sup>      | 6     | 0.13               | -6.01  | -2.29  | -0.42    | -0.78    | 0.09     | 6.36      | 43.40              | 6.83  |

<sup>a</sup> See Figure 3.10.3-2 for section locations.

<sup>b</sup> Bearing stress evaluation is not required for accident conditions.

<sup>c</sup> Stresses are determined by averaging the stresses over the impact region. Allowable stress includes a reduction factor of 0.8 for the closure lid weld.

Table 3.10.3-17 TSC Tip-Over plus Normal Pressure,  $P_m+P_b$ , ksi

| Section <sup>a</sup> | Angle | Component Stresses |                |                    |                 |                 |                 | S <sub>int</sub> | S <sub>allow</sub> | FS   |
|----------------------|-------|--------------------|----------------|--------------------|-----------------|-----------------|-----------------|------------------|--------------------|------|
|                      |       | S <sub>x</sub>     | S <sub>y</sub> | S <sub>z</sub>     | S <sub>xy</sub> | S <sub>yz</sub> | S <sub>xz</sub> |                  |                    |      |
| 1                    | 69    | -0.54              | -5.28          | 10.47              | 0.15            | 0.51            | -0.44           | 15.81            | 69.80              | 4.41 |
| 2                    | 66    | 2.77               | -13.66         | -2.50 <sup>b</sup> | 0.07            | 0.78            | -1.17           | 16.74            | 69.80              | 4.17 |
| 3                    | 66    | -0.17              | -4.90          | 16.94              | -0.06           | 1.33            | 1.18            | 22.09            | 68.60              | 3.11 |
| 4                    | 27    | -0.07              | 19.54          | 3.84               | 0.01            | 4.15            | 0.01            | 20.64            | 64.00              | 3.10 |
| 5                    | 60    | 0.68               | 59.72          | 41.78              | 0.02            | 0.81            | 0.28            | 59.06            | 63.75              | 1.08 |
| 6                    | 60    | -0.08              | 20.79          | 11.91              | -0.01           | -0.75           | -0.02           | 20.94            | 63.30              | 3.02 |
| 7                    | 0     | -0.55              | 18.40          | 0.89               | -0.23           | -0.11           | 0.00            | 18.96            | 63.00              | 3.32 |
| 8                    | 0     | -0.87              | 18.35          | 4.84               | 0.01            | -0.02           | 0.00            | 19.22            | 63.00              | 3.28 |
| 9                    | 30    | 5.14               | 55.19          | 39.08              | 0.00            | -1.26           | -1.52           | 50.22            | 63.50              | 1.26 |
| 10 <sup>c</sup>      | 6     | -13.17             | 17.49          | 7.56               | -2.41           | 2.07            | -2.76           | 31.85            | 63.50              | 1.99 |
| 11 <sup>d</sup>      | 0 - 6 | -23.93             | -16.43         | -16.49             | 11.98           | 1.54            | -13.41          | 36.44            | 50.80 <sup>d</sup> | 1.39 |
| 12                   | 0     | 18.01              | 16.62          | 1.95               | 0.55            | 0.71            | -1.04           | 16.40            | 68.60              | 4.18 |
| 13                   | 0     | -4.19              | -2.86          | -1.41              | 0.12            | 0.55            | -3.61           | 7.82             | 63.50              | 8.12 |
| 14 <sup>c</sup>      | 6     | 2.57               | -10.04         | 0.16               | 5.22            | 5.18            | -2.61           | 18.87            | 63.50              | 3.36 |
| 15 <sup>c</sup>      | 6     | 8.66               | -1.44          | 0.34               | -1.10           | 0.55            | -1.76           | 10.79            | 63.50              | 5.88 |

<sup>a</sup> See Figure 3.10.3-2 for section locations.

<sup>b</sup> Localized bending stresses are secondary and are excluded from evaluation.

<sup>c</sup> Bearing stress evaluation is not required for accident conditions.

<sup>d</sup> Stresses are determined by averaging the stresses over the impact region. Allowable stress includes a reduction factor of 0.8 for the closure lid weld.

### 3.10.4 Concrete Cask Finite Element Models

#### 3.10.4.1 Pedestal Finite Element Model for Lift Evaluation

An ANSYS finite element model of the concrete cask pedestal (Figure 3.10.4-1) is used to perform the structural evaluation for the lift condition. The model is constructed using SHELL63, LINK8, and CONTAC52 elements. LINK8 elements are used to model the Nelson studs. The model is a quarter-symmetry model. Symmetry boundary conditions are used on the XZ and YZ planes. The pedestal is a welded structure. CONTAC52 gap elements are used to model regions where components are not welded together (stand to pedestal plate, and support rails to stand). The gap elements do not close during the analysis, which maximizes the bending stresses in the support rails and inlet tops; therefore, the analysis is bounding. During a concrete cask top-end lift, the TSC loads the pedestal plate. A pressure load ( $P_{can}$ ) is used to apply the TSC weight to the pedestal plate.

$$P_{can} = \frac{1.1 \times W_{can}}{A_{ped}} = \frac{1.1 \times 120,000}{4,071} = 32.4 \text{ psi}$$

The load in the pedestal is reacted out by the Nelson studs, which carry the load into the concrete. The tops of the Nelson studs are restrained in all degrees of freedom. An inertia load of 1.1g (Z-direction) is applied to the finite element model for dynamic load factor (DLF). The 1.1g DLF is applied per ANSI/ASME N45.2.15 [29].

#### 3.10.4.2 Concrete Cask Finite Element Model for Thermal Stress Evaluation

A thermal stress evaluation of the concrete cask was performed for normal conditions and off-normal or accident events. A three-dimensional finite element model was created using the ANSYS program. The concrete cask contains 56 periodic radial sections with the 56 vertical rebars. Therefore, the model represents  $6.4^\circ$  ( $1/56^{\text{th}}$ ) of the concrete cask. The model contains only the portion of the concrete cask shell and liner between the top of the lower vents and the lid assembly because the circumferential and vertical rebar are located in this region.

The thermal conduction model is constructed using ANSYS SOLID70 elements for the concrete shell and steel liner. The nodes at the liner/shell interface are coincident and are connected using temperature couples. The model is divided into four sections vertically with 0.1-inch gaps. LINK33 elements are used to connect the four sections to allow for thermal conduction across the gaps. The temperatures vary in the vertical and radial directions. Conservatively, the

temperature profile corresponding to the 106°F (off-normal) ambient condition is used for the normal conditions. The temperature profile for the 133°F ambient condition is used for the accident event. Temperatures are applied to nodes on the inner and outer surfaces of the concrete cask.

The thermal conduction model is modified for the structural evaluation. The SOLID70 elements are replaced with SOLID45 elements. COMBIN14 elements are used between the four vertical sections of the model for the steel liner. CONTAC52 gap elements are used between the liner and concrete shell to permit only compressive loads to be transmitted across the gap. Rebar was modeled into the model using LINK8 elements. LINK8 elements were also modeled across the vertical gaps to represent the vertical rebar; therefore, tensile loads are taken by the rebar. There are 24 vertical rebar on the inner radius and 56 on the outer radius. The properties of the inner vertical rebar are determined by a ratio to represent the  $1/56^{\text{th}}$  model (24/56 ratio). The finite element model is shown in Figure 3.10.4-2 and Figure 3.10.4-3. Boundary conditions are shown in Figure 3.10.4-4.

#### **3.10.4.3 Pedestal Finite Element Model for 24-inch Drop Evaluation**

Subjecting the concrete cask to a bottom end impact, the TSC produces a force on the base weldment located at the bottom of the cask. The ring above the air inlets is expected to yield. To determine the resulting acceleration of the TSC and deformation of the pedestal, a LS-DYNA analysis is used.

A quarter-symmetry model of the base weldment is shown in Figure 3.10.4-5. The model is constructed using 4-node shell elements. Symmetry boundary conditions are applied along the planes of symmetry (X-Z and Y-Z plane). Rigid mass 8-node solid elements located in the TSC bottom plate represent the loaded TSC. Rigid mass 8-node solid elements located above the air inlet duct top represent the weight of the inner liner shell. The impact plane is represented as a rigid plane. To determine the maximum acceleration and deformations, impact analyses are solved using LS-DYNA program.

The weldment support rails, weldment pedestal plate, air inlet ducts, and the cylindrical stand materials are modeled using the piece-wise linear plasticity model in LS-DYNA. The stress-strain curve used for this analysis was obtained from the Atlas of Stress-Strain Curves and is presented in Figure 3.10.4-6. To ensure that maximum deformations and accelerations are determined, two analyses are performed. One analysis, which uses the upper bound weight of 105 kips, envelops the maximum deformation of the pedestal. The second analysis employs the

lower-bound weight of 60 kips to account for maximum acceleration. The details of the model are described as follows.

- All structural components are modeled using shell elements. A layer of solid elements represents the TSC weight.
- The ground base plate of the pedestal is not modeled since the plate is in contact with the impact plane during impact and has no effect on the deformation of the pedestal.
- The gravitational force is aligned with the Z-axis and is acting in the negative Z direction.
- All components of the pedestal are made of ASTM A36 carbon steel.
- The cylindrical shell under the pedestal plate is separated (not welded) from the support rail to allow buckling to occur at a relative lower g-level.
- The loaded TSC is modeled as a rigid body. The density of the TSC is calculated so that the total weight of the TSC model is equal to 105 kips or 60 kips, bounding values for the maximum and minimum TSC loaded weights.
- The concrete cask liner is modeled as a rigid body. The density of the liner is calculated so that the total weight is equal to 16,900 lb, which envelops the weight of the liner shell and the S-shape steel beams attached to the concrete cask liner.
- The column weight of the concrete portion of the concrete cask projected onto the top of an air inlet plate is represented by a uniformly distributed normal pressure acting on the top of the air inlet plate. The weight is only statically applied to the top of the air inlet. Upon impact, since the air inlet is more flexible than the base plate, all of the impact force of the concrete is transmitted to the base plate. The static pressure is always present during the impact.
- The rigid wall is an infinitive rigid plane. The rigid wall featured in LS-DYNA is used to simulate the rigid ground surface on which the concrete cask is supported or dropped.
- The filter frequency used in the LS-DYNA evaluation is determined by performing natural frequency calculations of the various components in the load path of the base weldment. The component with the lowest natural frequency is the cylindrical stand. This calculation results in a natural frequency of 182 Hz. Therefore, a filter frequency of 200 Hz is selected.

### **Material Property**

The pedestal material is A-36 carbon steel. The LS-DYNA material type 24 (Piecewise\_Linear\_Plasticity) is used. The true stress-strain curve of A-36 is shown in Figure 3.10.4-6.

### **Initial Condition**

The body force applied to the TSC and the pedestal assembly is the 1g acceleration representing the ever-present gravitational force. Body force is a vectored input, depending on the angle of

drop. The 1g body force is applied in the  $-Z$  direction. Since the 24-inch drop represents the dynamic force input, the initial velocity,  $V_o$  is computed as shown below.

$$V_o = \sqrt{2gH} = \sqrt{2(386.4)(24)} = 136.1 \text{ inch/sec}$$

where:

$$g = 386.4 \text{ inch/sec}^2$$
$$H = 24.0 \text{ inches ----- Drop height}$$

### **Post-Processing**

To obtain output, a node on the TSC tracks the movements of the TSC as it impacts on the top base plate of the pedestal. Since the TSC is modeled as a rigid body, any node on the TSC is sufficient to track the global movements and deceleration of the TSC. The output database contains a time-series of nodal displacement, velocity, and acceleration. The nodal output file is a text file that the post-processor of LS-DYNA can convert into time-history plots and apply to the plotted graphs signal-conditioning operations such as filtering and rescaling. The acceleration of the TSC is obtained directly from the output file and then filtered to eliminate the ripples. The filtered acceleration (in-inch/sec<sup>2</sup>) is rescaled to units of g (386.4 inch-inch/sec<sup>2</sup>) value.

#### **3.10.4.4 Concrete Cask Finite Element Model for Tip-Over Evaluation**

The concrete cask is designed to hold a TSC during long-term storage conditions and is constructed of a steel liner surrounded by reinforced concrete. The critical locations for measuring accelerations are at the top of the fuel basket and top of the TSC closure lid.

Two half-symmetry finite element models of the concrete cask, concrete pad, and soil subgrade are constructed of solid brick elements using the LS-DYNA program for the cask tip-over evaluation. One model uses a standard sized pad, and the other model uses an oversized pad. The difference between the two models reflects the segments in the concrete pad. The finite element models are shown in Figure 3.10.4-7.

### **Material Properties**

The mechanical properties used in the analyses are described in the following sections. The densities of each part are calculated to account for the total weight of nonstructural components that are not modeled as part of the finite element model.

Concrete:

The concrete is represented as a homogeneous isotropic material. The effect of the reinforcing steel is ignored. The concrete for the cask and the pad are modeled as LS-DYNA material 16 (Mat\_Pseudo\_Tensor), which represents a concrete constitutive model in LS-DYNA. This material model requires an equation-of-state represented in LS-DYNA as EOS\_Tabulated\_Compaction. The LS-DYNA input for the cask concrete is shown below.

$$f'_c = 4,000 \text{ psi} \text{----- Compressive Strength}$$

$$\rho_c = 148 \text{ pcf} = 0.0002217 \text{ lb-sec}^2/\text{in}^4 \text{----- Density}$$

$$\nu_c = 0.22 \text{----- Poisson's Ratio}$$

$$E_c = 33\rho_c^{1.5} \sqrt{f'_c} = 3.758 \times 10^6 \text{ psi} \text{----- Modulus of Elasticity}$$

$$G_c = \frac{E_c}{2(1+\nu_c)} = 1.540 \times 10^6 \text{ psi} \text{----- Shear Modulus}$$

$$K_c = \frac{E_c}{3(1-2\nu_c)} = 2.237 \times 10^6 \text{ psi} \text{----- Bulk Modulus}$$

$$\epsilon_v = \frac{f'_c}{K_c} = 0.001788 \text{----- Volumetric Strain}$$

Using the same formulae presented above, the required input data for the pad concrete is shown below.

| $f'_c$ (psi) | $\rho_c$ (lb/ft <sup>3</sup> ) | $E_c$ (psi)         | $G_c$ (psi)         | $K_c$ (psi)         | $\epsilon_v$ |
|--------------|--------------------------------|---------------------|---------------------|---------------------|--------------|
| 5,000        | 160                            | $4.723 \times 10^6$ | $1.936 \times 10^6$ | $2.811 \times 10^6$ | 0.001779     |

Soil:

An elastic model with the following properties is used to represent the subgrade soil material of the site.

$$\rho = 100 \text{ pcf} \text{----- Density}$$

$$\nu_s = 0.45 \text{----- Poisson's Ratio}$$

$$E = 30,000 \text{ psi} \text{----- Modulus of Elasticity}$$

Steel Inner Liner:

The steel liner is represented by a rigid material model with the following properties.

$$\nu = 0.31 \text{----- Poisson's Ratio}$$

$$E = 29 \times 10^6 \text{ psi} \text{----- Modulus of Elasticity}$$

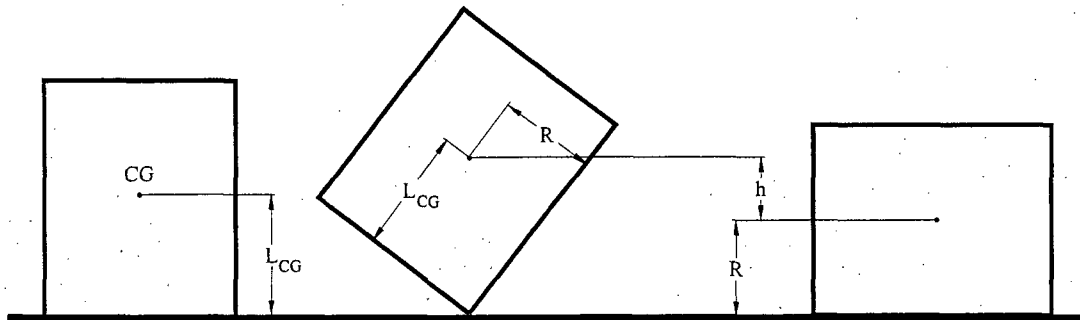
Boundary Conditions

Automatic\_Surface\_To\_Surface contact conditions are employed between the concrete cask and the pad, between the pad and soil, and between the cask steel liner and concrete. Symmetry



boundary conditions are applied to all parts at the plane of symmetry (see Figure 3.10.4-7). The vertical displacements at the bottom of the soil subgrade and horizontal displacements for the three vertical boundaries of the soil are restrained.

Tip-over is simulated by applying an initial angular velocity,  $\omega$ , to the entire concrete cask. The angular velocity value is determined by the conservation of energy about the center of gravity, as the concrete cask rotates from end to corner to side orientations as shown in the figure below.



To ensure accuracy, the LS-DYNA output kinetic energies are compared to actual calculated potential energy. Equating the potential to the kinetic energy during tip-over is as follows.

$$mgh = \frac{I\omega^2}{2}$$

where:

- $\omega = 1.527 \text{ rad/sec}$  ----- Angular velocity for concrete cask
- $m = 785.6 \text{ lb}_m$  ----- Total mass of the concrete cask
- $g = 386.4 \text{ inch/sec}^2$  ----- Acceleration due to gravity
- $h = \sqrt{R^2 + L_{CG}^2} - R$  ----- Height change of the concrete cask mass center
- $I$  ----- Total mass moment of inertia ( $\text{lb-inch}^2$ ) of the concrete cask about the pivot point (automatically calculated by LS-DYNA)
- $R = 68 \text{ inches}$  ----- Outside radius of concrete cask

The potential energy due to the height change of the concrete cask's mass center during tip-over is bounded by the kinetic energy of  $2.0 \times 10^7 \text{ inch-lb}$ .

### Load Cases

Bounding load cases are used to evaluate the loaded concrete cask during tip-over conditions. Two concrete pad and subsoil combinations are considered to bound all possible storage configurations: the standard pad configuration and oversized pad configuration. The standard pad represents typical storage pad properties and boundary conditions. The oversized pad is used as a sensitivity study to determine the effect of increased foundation size on accelerations. The dimensions of the standard concrete pad are 30 ft (length)  $\times$  30 ft (width) with subsoil measuring 35 ft (length)  $\times$  35 ft (width). The dimensions of the oversized concrete pad are 60 ft (length)  $\times$  30 ft (width) with subsoil measuring 70 ft (length)  $\times$  35 ft (width).

With the exception of pad size, the standard and oversized pads use identical parameters and boundary conditions. The mesh density and element aspect ratio of the oversized pad is maintained from the standard model.

Figure 3.10.4-1 Concrete Cask Pedestal Finite Element Model for Lift Evaluation

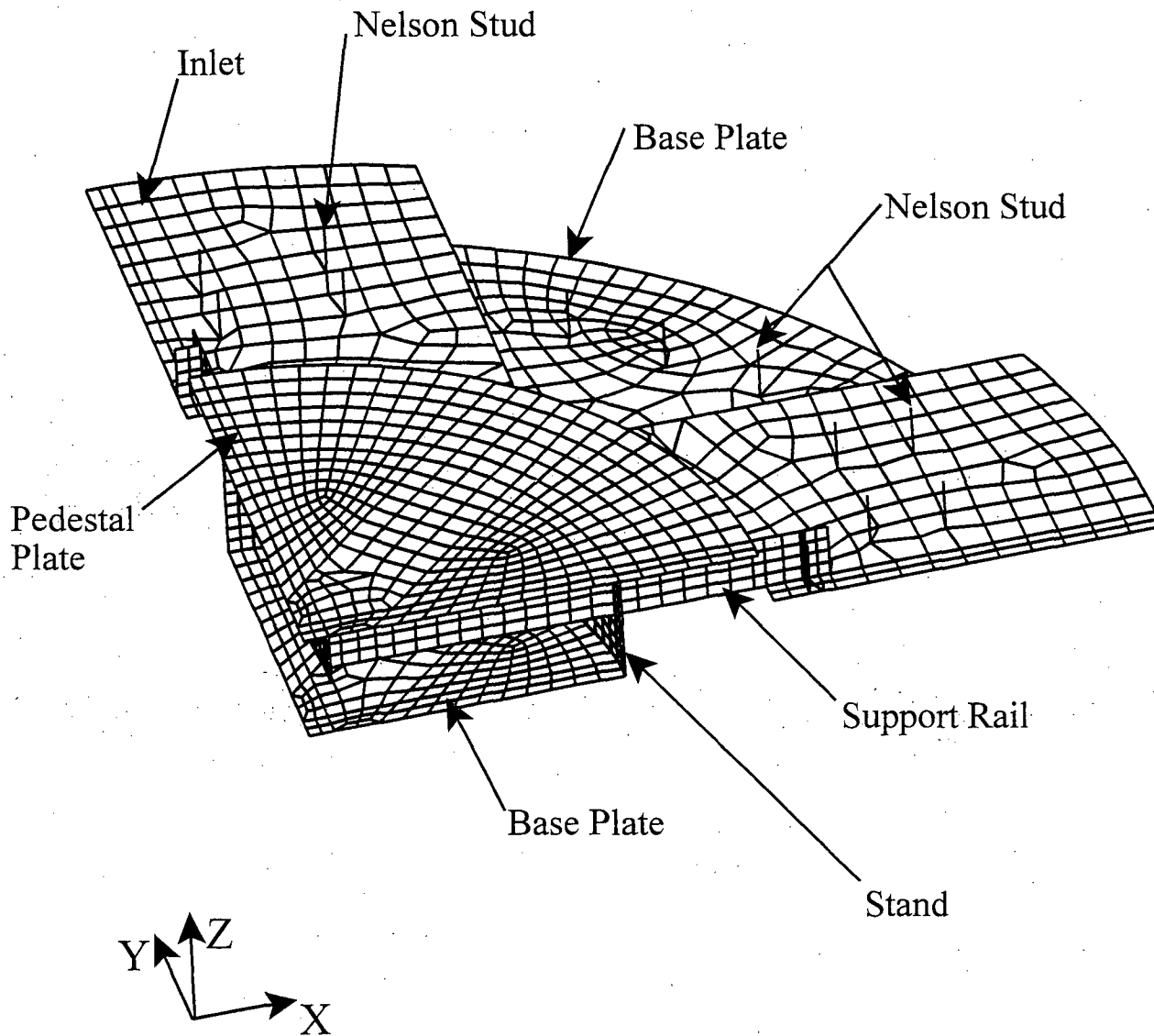


Figure 3.10.4-2 Concrete Cask Finite Element Model for Thermal Stress Evaluation

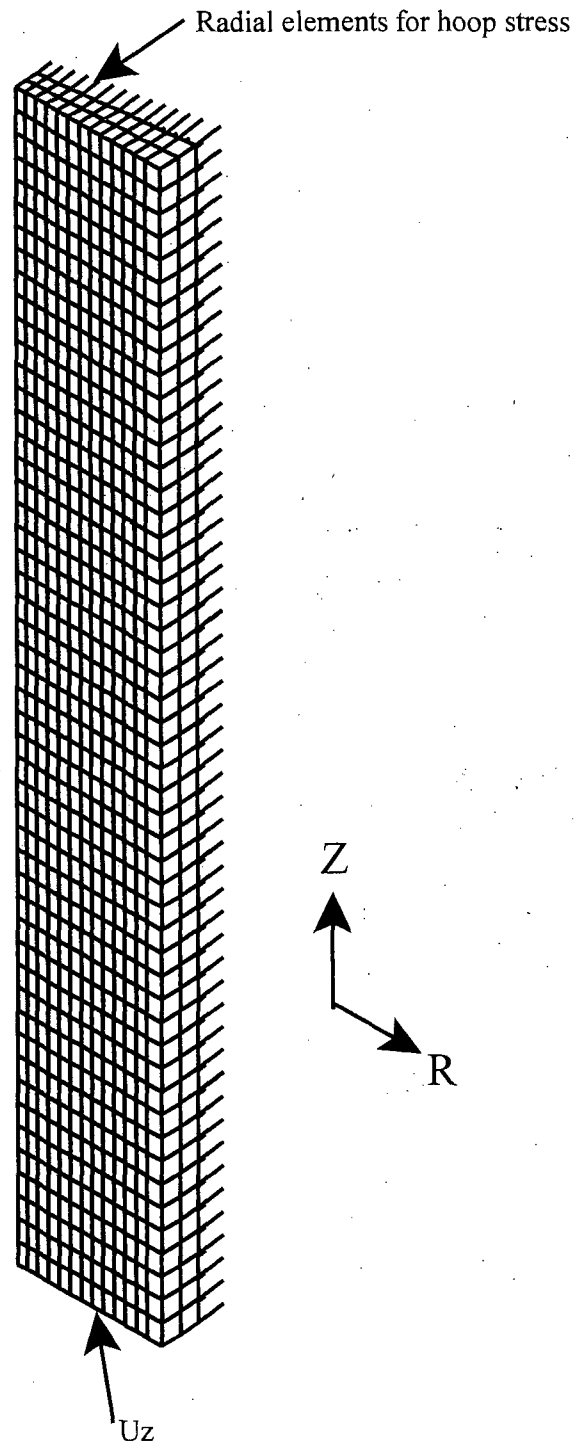


Figure 3.10.4-3 Concrete Cask Model – Elements for Rebar

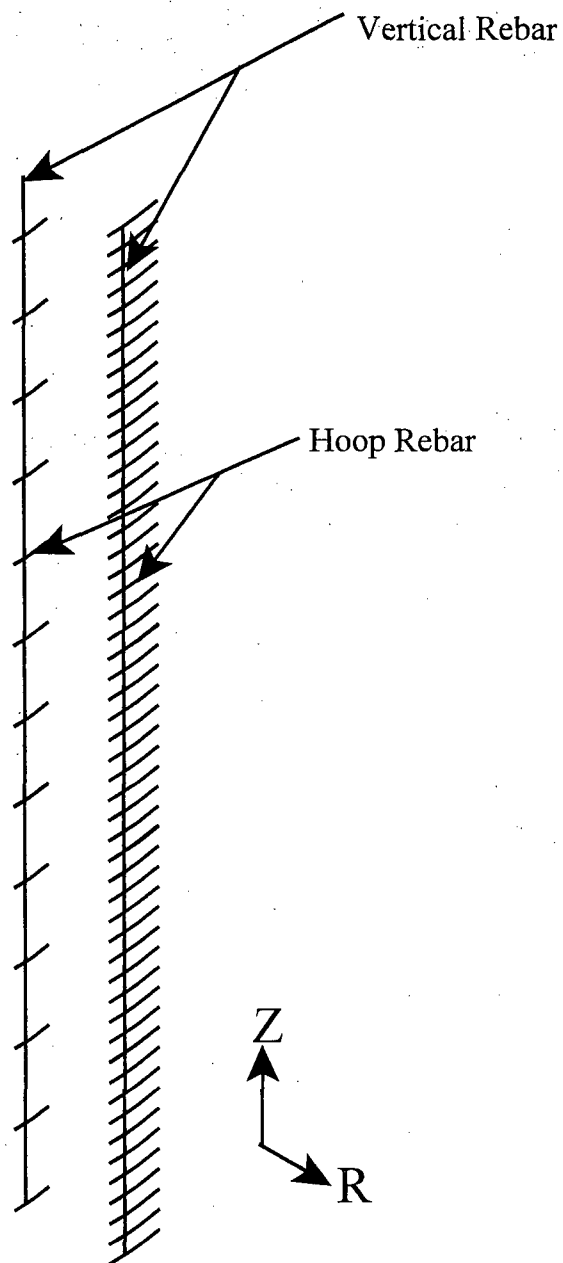


Figure 3.10.4-4 Concrete Cask Model Boundary Conditions

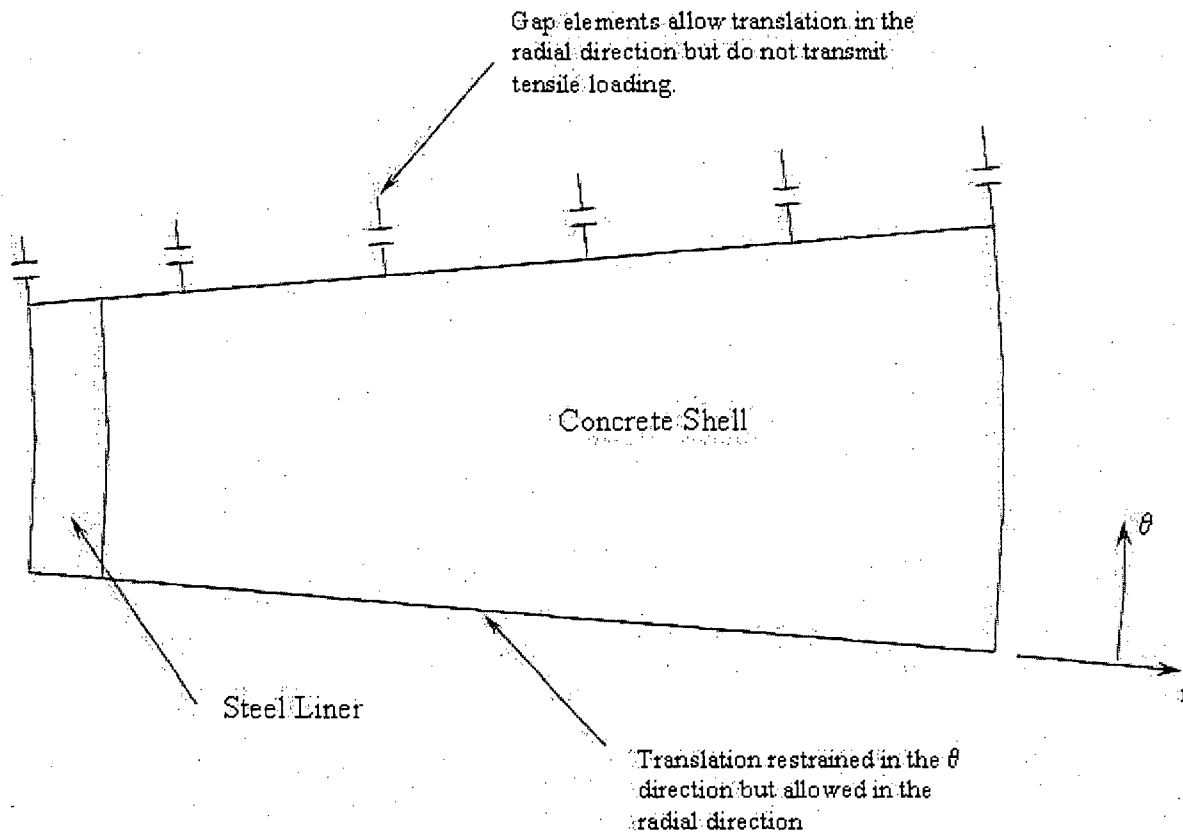


Figure 3.10.4-5 Concrete Cask Pedestal Finite Element Model for 24-inch Drop Evaluation

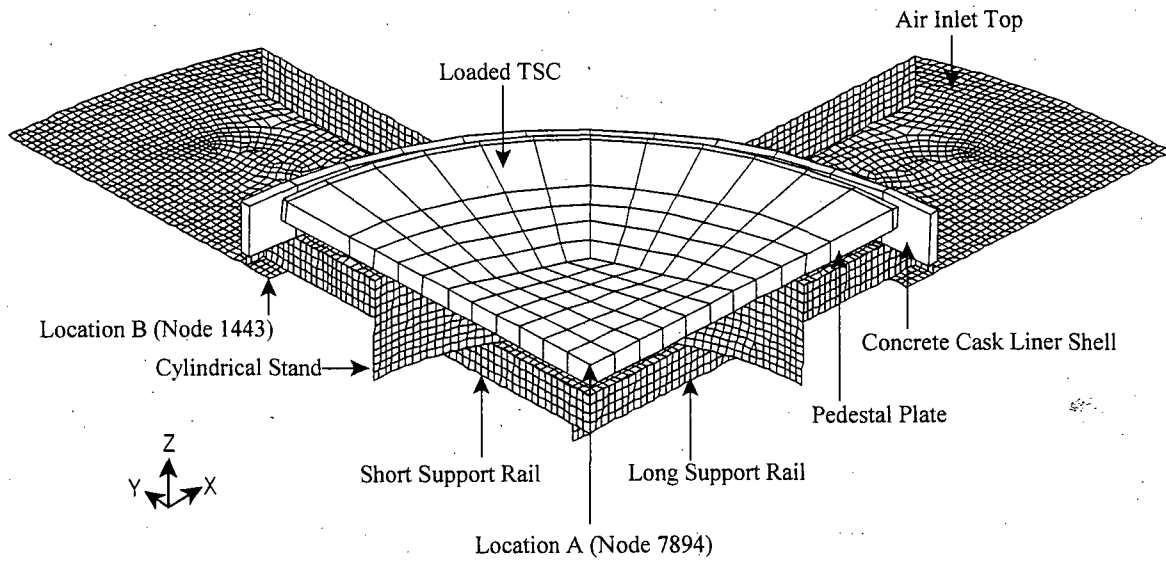


Figure 3.10.4-6 Stress-Strain Curve for A36 Carbon Steel

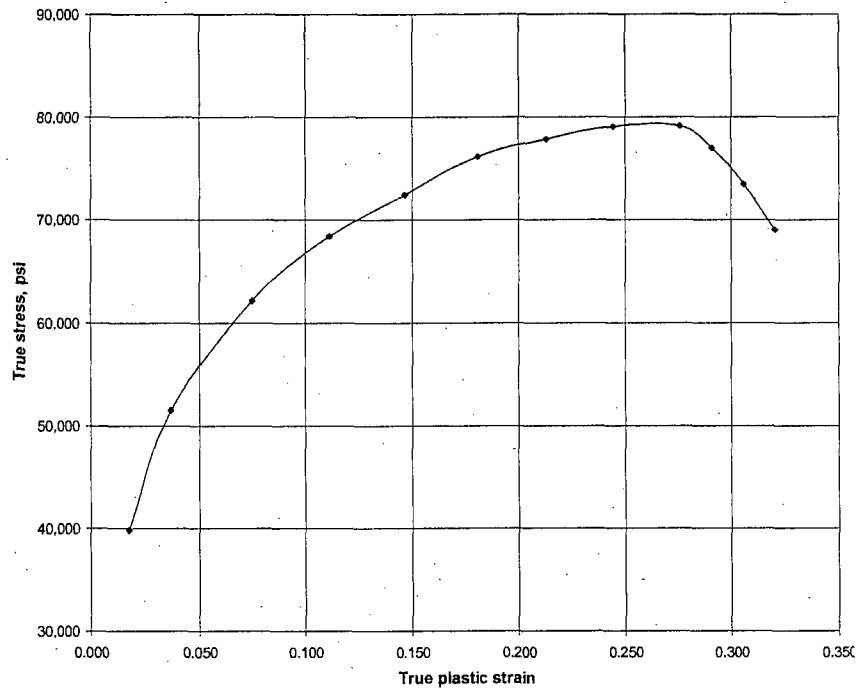
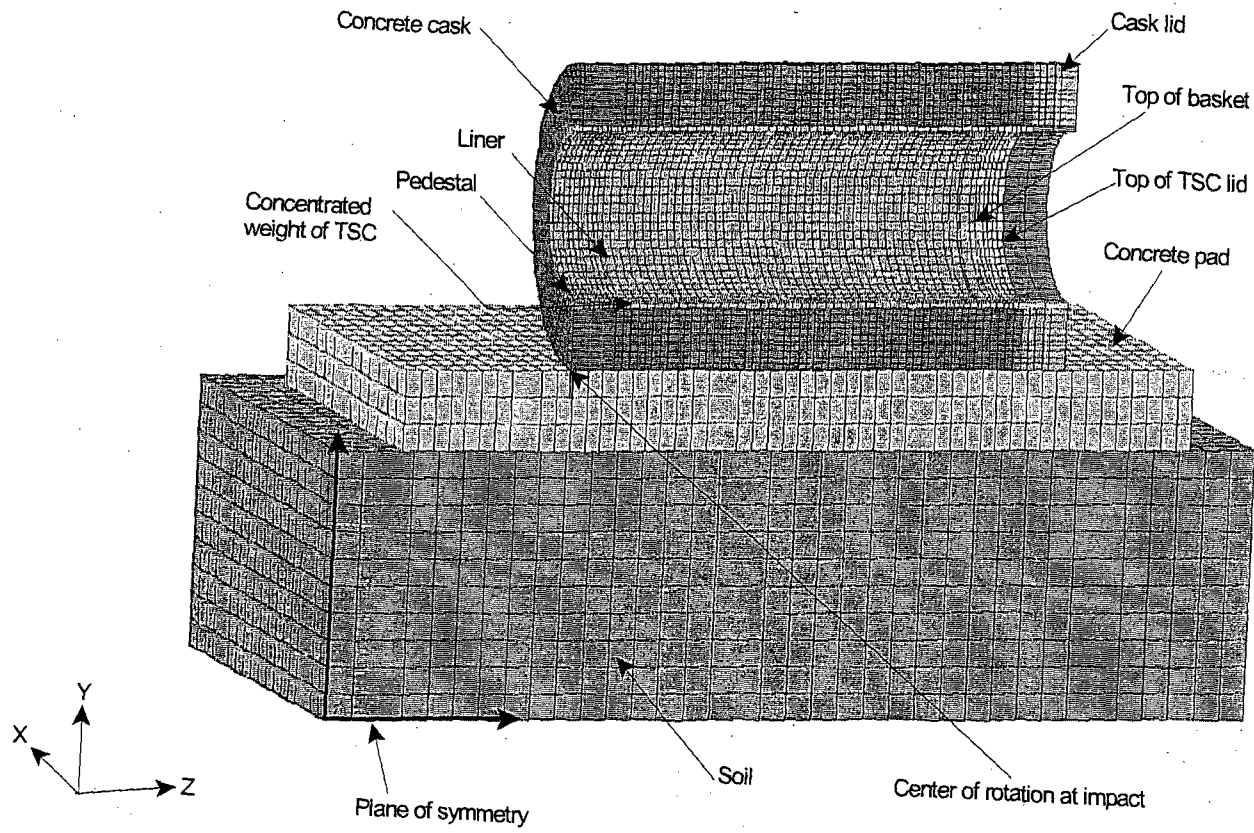


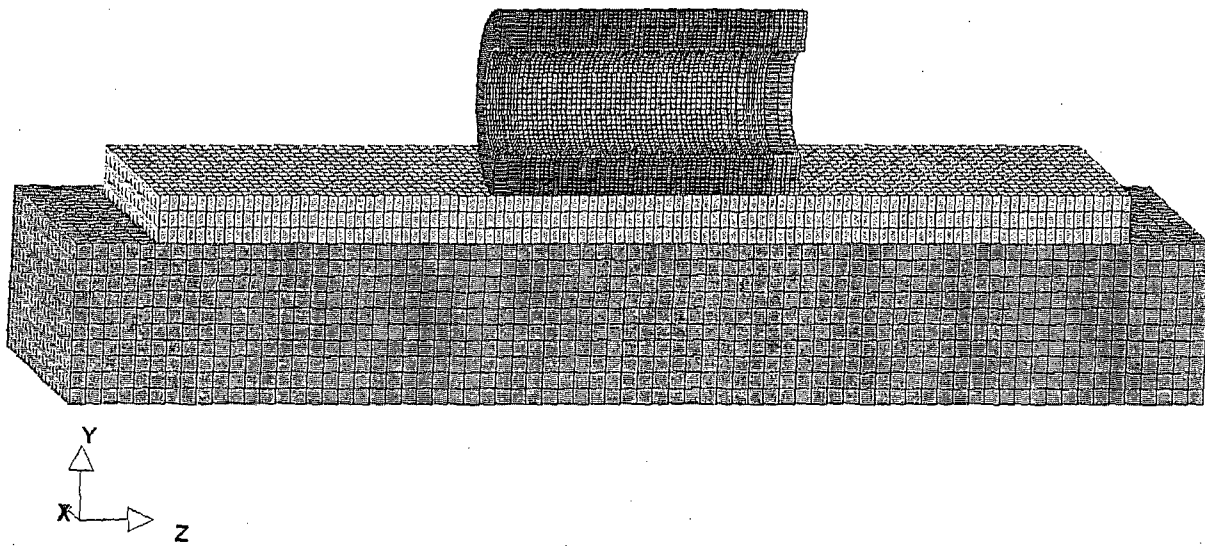


Figure 3.10.4-7 Finite Element Models for Tip-Over Evaluation

Standard Pad Model



Oversized Pad Model



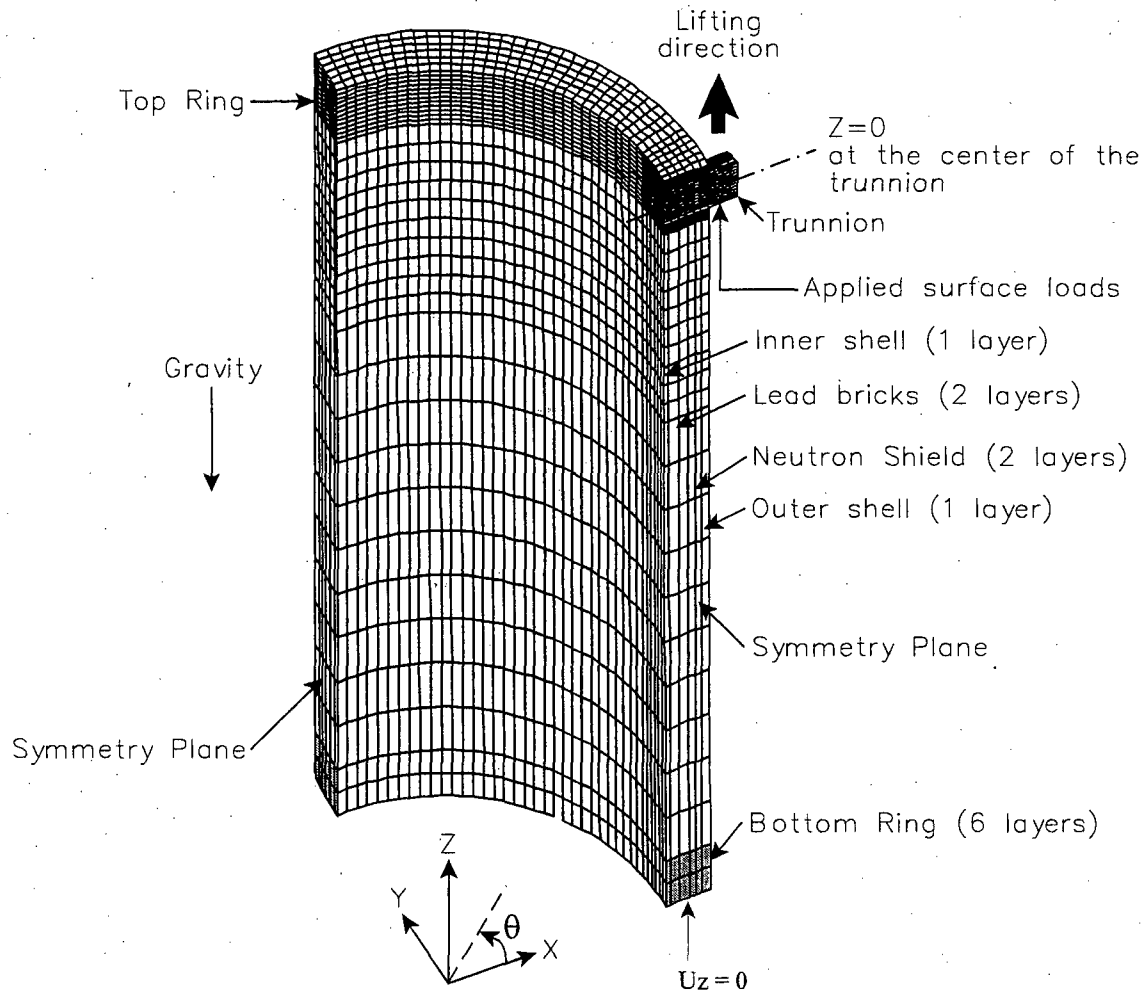
### 3.10.5 Transfer Cask Finite Element Model

The top section of the transfer cask is a solid ring made of carbon steel. A pair of trunnions, 9 inches in diameter, are mounted 180° apart on this ring. The middle section of the transfer cask is comprised of a steel inner shell, a lead layer, a neutron shield layer, and a steel outer shell. The bottom section is a solid ring made of carbon steel. A pair of rails is welded to the bottom of the solid forging. A pair of steel doors is inserted in the rails. The overall height of the transfer cask is 198.0 inches. The overall diameter of the cask is 88.0 inches. The maximum loaded weight of the transfer cask is 230,000 pounds.

A three-dimensional finite element model is used to evaluate the lifting of a fully loaded MAGNASTOR transfer cask. Because of symmetry, only one-quarter of the transfer cask is modeled, as shown in Figure 3.10.5-1. The model includes the trunnions, the top ring at the trunnion region, the inner and outer shells, the bottom, and the lead and the neutron shield between the inner and outer shells. ANSYS SOLID45 elements (8-node brick element) are used to model the transfer cask. The trunnions are partial penetration welded to the top ring. CONTAC52 elements are used to model the interface between the trunnion and the top ring. The groove welds attaching the trunnion to the top ring are represented by coupled nodes between the two components.

The total weight of the heaviest loaded transfer cask is less than 115 tons. A conservative load of 120 tons, plus a 10% dynamic load factor, is used in the model. The load used in the quarter-symmetry model is  $(240,000 \times 1.1)/4 = 66,000$  pounds. The load is applied upward at the trunnion as a "surface pressure load" whose location is determined by the lifting yoke dimensions. The magnitude of the surface pressure load is calculated so that the total upward force is equal to the load of 66,000 pounds. The model is restrained along two planes of symmetry with symmetry boundary conditions. Vertical restraints are applied to the bottom of the model to resist the force applied to the trunnion.

Figure 3.10.5-1 Finite Element Model for the Transfer Cask



### 3.10.6 Basket Stability Evaluation for Concrete Cask Tip-Over Accident Condition

This section describes the LS-DYNA models and the analyses confirming the stability of the MAGNASTOR PWR and BWR fuel baskets for the hypothetical concrete cask tip-over accident.

Confirmation that the basket does not buckle during the tip-over accident is addressed in Sections 3.7.2.1.2 and 3.7.2.2.2. Sections 3.5 through 3.7 also demonstrate that there are no other loads or stress-based failures that can contribute to instability in the MAGNASTOR basket design.

As described in Section 3.10.1.1 (PWR) and Section 3.10.2.1 (BWR), the basket geometric configuration is maintained by three features of basket component design: (1) the side and corner support weldments bolted to the fuel tubes at the basket periphery, (2) the pin-slot connections between adjacent fuel tubes, and (3) the connector pin assemblies at both ends of the basket.

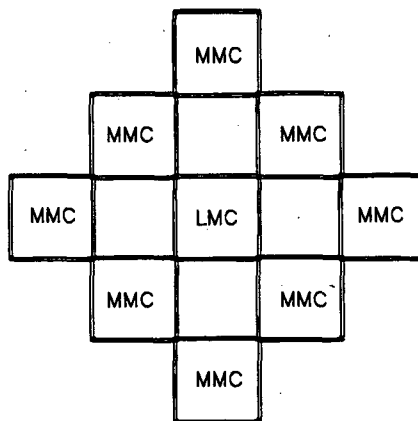
The geometric stability of the basket, addressed in this section, ensures that the fuel tubes retain their initial geometric configuration and all the pin-slot connections remain engaged after the tip-over accident. Eight pin-slot shear connections (20-inch center-to-center axially) are placed between adjacent fuel tubes for both PWR and BWR configurations, as shown in Figure 3.10.6-1. To observe the dynamic responses of the fuel tube assemblies and the pin-slot interface, a transient analysis is performed using a LS-DYNA model corresponding to a 10-inch periodic section (see Figure 3.10.6-1). The periodic model conservatively ignores the effect of tube and support weldment stiffness, multiple pins at the tube interface surface along the length of the tubes, and the connector pin assembly at both ends of the tubes. Basket geometric stability is validated using the conservative periodic model and canister shell boundary conditions representative of two axial locations along the canister shell. One location represents the maximum canister shell displacement resulting from the interaction of the basket near the middle section of the canister shell. The other axial location, corresponding to an increased acceleration and decreased canister shell displacements (since it is closer to the canister lid), is used for a sensitivity study to demonstrate that the boundary condition of the canister displacements has the governing effect on the dynamic response of the basket for stability evaluation. With the conservative periodic model, the analysis shows that all pin-slot connections (i.e., all fuel tubes) remain engaged after the tip-over event.

The safety factor for stability is based on the loading associated with the tip-over event. During the tip-over accident, lateral loading is applied to the fuel basket. The accelerations experienced

by the fuel basket are computed in Section 3.7.3.7, and the accelerations at the top of the basket are shown in Figure 3.7.3-3. Since the cask is rotating about its base, the acceleration of the basket monotonically decreases towards the base of the cask. The safety factor is defined as the factor applied to the acceleration for the basket loading in which the basket tubes maintain their geometric stability in the designed and fabricated configuration. In this evaluation, a factor of 1.5 is applied to the acceleration time history, based on the acceleration shown in Figure 3.7.3-3, for the transient evaluation of the basket using LS-DYNA. Using a factor of 1.5 confirms that the minimum safety factor for basket stability is greater than 1.5.

Since the lateral loading can be applied in an arbitrary angular direction of the basket, six basket orientations ( $0^\circ$ ,  $18^\circ$ ,  $22.5^\circ$ ,  $27^\circ$ ,  $34^\circ$  and  $43^\circ$ ) are considered in the evaluation for the PWR basket and three basket orientations ( $0^\circ$ ,  $22.5^\circ$  and  $45^\circ$ ) are considered for the BWR basket. Three-dimensional periodic finite element models are used for the evaluation, as shown in Figure 3.10.6-2 through Figure 3.10.6-7 for the PWR basket and Figure 3.10.6-8 through Figure 3.10.6-10 for the BWR basket. Half-symmetry ( $180^\circ$ ) models are used for basket orientations of  $0^\circ$  and  $45^\circ$ , and full ( $360^\circ$ ) models are used for basket orientations of  $18^\circ$ ,  $22.5^\circ$ ,  $27^\circ$ ,  $34^\circ$  and  $43^\circ$ .

The most significant condition affecting the stability of the fuel basket is gaps between adjacent fuel tubes. Specifically, those fuel tubes that are not physically attached to the side weldment or corner weldment are identified as most susceptible to instability issues. The gaps between the fuel tubes may be developed due to a lack of straightness of the tubes and/or dimensional tolerance due to fabrication. Based on the basket assembly process and tolerance, the maximum gap between adjacent tubes occurs when a single 'Least Material Condition' (LMC) tube is surrounded by eight 'Maximum Material Condition' (MMC) tubes, as shown in the following sketch. To represent this arrangement, a bounding gap of 0.025 inch (incorporated by reduction of tube width, while maintaining the tube wall thickness) is considered for three tubes for the PWR  $0^\circ$  model (see tube locations 3, 6 and 11 in Figure 3.10.1-13) and six tubes for the BWR  $0^\circ$  model (see tube locations 2, 7, 12, 14, 19 and 23 in Figure 3.10.2-13). Note tube width reduction is also considered for the corresponding tube locations in the models analyzing other basket orientations. Use of the gap size of 0.025 inch is conservative since the maximum gap size permitted during the basket assembly is limited to 0.016 inch.



Use of this approach results in the initial position of the fuel tube, in the transient evaluation, being suspended without contact between the individual tubes. While this is analytically possible, the occurrence of such gaps during fabrication is not physically possible. The assembly process, horizontal stacking, will result in minimal gaps that would generally occur along the length of the fuel tubes between points of contact. Additionally, the fuel basket design provides connector pin assemblies at the top and bottom ends of the basket that develop an assembly verification of tube-to-tube interface and act as restraints against any arbitrary motion of the interior tubes. Analyses performed neglecting the connector pin effect further maximize the condition of instability.

### **Model Description**

The models shown in Figure 3.10.6-2 through Figure 3.10.6-10 are mainly comprised of brick elements representing the fuel tubes, the fuel assembly, the pins, the support weldments, the bolts/bosses, the canister shell and the concrete cask liner.

The length of the model in the axial direction is 10 inches, which corresponds to one-half the distance between adjacent pins along the length of the basket. The corner support weldment is represented by shell elements and the shell elements are modeled along the centerline of the weldment. Since LS-DYNA takes into account the thickness of the shell element during the transient evaluation, the model must have a gap incorporated between the shell and the solid elements corresponding to a minimum value of the half-thickness of the shell element. Gaps between brick elements do not require this consideration. The bolted boss connections for attaching the support weldment to the fuel tube arrays are also modeled using brick elements. The modeling details of the bosses for the corner support weldment and side support weldment are shown in Figure 3.10.6-11 for the PWR and Figure 3.10.6-12 and Figure 3.10.6-13 for the BWR. The model allows a relative planar displacement of 1/16 inch between the support weldment and the fuel tubes by incorporating a gap of 1/16 inch on both sides of the bosses.

The pins are welded to one side of the adjacent fuel tube slots prior to the assembly of the fuel tubes to form the basket. These welds are represented by weak spring elements in the model to prevent independent arbitrary motion of the pins.

The finite element model also contains the concrete cask steel liner, which is represented by elastic brick elements with a thickness of 3.75 inches. The purpose of these elements is to impose the accelerations on the canister and basket based on the analysis results for the concrete cask tip-over accident (Section 3.7.3.7).

**Material Properties**

The mechanical properties used in the analyses are described as follows.

**Carbon Steel Fuel Tubes and Weldments:**

The fuel tubes and the corner and side weldments are represented by a piecewise linear plasticity model with the following elastic properties. Note that the maximum tube temperature is less than 700°F for the BWR basket and less than 720 °F for the PWR basket. The difference in material properties (yield and ultimate strength of SA537 carbon steel) at 700°F and 720°F is less than 1% and has an insignificant effect on the analysis results.

**Fuel tubes at 700°F (SA537, Class 1, carbon steel)**

Yield strength = 32.3 ksi

Ultimate strength = 68.4 ksi

Ultimate strain = 21%

$\nu = 0.31$  ----- Poisson's Ratio

$E = 25.5 \times 10^6$  psi ----- Modulus of Elasticity

The density corresponding to the fuel tubes was adjusted to account for the neutron absorber material.

**Side and corner weldments at 500°F (SA537, Class 1, carbon steel)**

Yield strength = 35.4 ksi

Ultimate strength =68.4 ksi

Ultimate strain = 21%

$\nu = 0.31$  ----- Poisson's Ratio

$E = 27.3 \times 10^6$  psi ----- Modulus of Elasticity

Canister Shell (SA240, Type 304/304L stainless steel)

The canister shell is represented by inelastic material with the following properties at 500°F.

Yield strength = 19.4 ksi

Ultimate strength = 63.4 ksi

$\nu = 0.31$  ----- Poisson's Ratio

$E = 25.8 \times 10^6$  psi ----- Modulus of Elasticity

Steel Inner Liner (A36 carbon steel)

The steel liner is represented by elastic material with the following properties at 500°F.

Yield strength = 29.3 ksi

Ultimate strength = 58.0 ksi

$\nu = 0.31$  ----- Poisson's Ratio

$E = 27.3 \times 10^6$  psi ----- Modulus of Elasticity

Fuel Assembly

The element representing the fuel assembly were modeled with the following inelastic properties

Yield strength = 1 ksi

$\nu = 0.49$  ----- Poisson's Ratio

$E = 1 \times 10^5$  psi ----- Modulus of Elasticity

The density for the fuel assembly corresponds to the design weight of the fuel assembly.

Boundary Conditions

Automatic surface-to-surface contact conditions are employed between the pins and the fuel tubes, between the support weldments and the fuel tubes, between the basket and the canister, and between the canister and the concrete cask. Symmetry boundary conditions are applied to all parts at the plane of symmetry (see Figure 3.10.6-2, typical). The axial displacements are restrained on both axial faces of the model.

The canister portion of the periodic model does not account for the end effects of the canister. With the rigid plates at each end of the canister, the canister shell physically restricts the motion of the tubes. To permit the canister shell elements in the periodic model to restrict the motion of the tube elements in the periodic model, the inner surface of the cask liner in the periodic model is defined based on a canister shell displacement profile corresponding to the maximum canister shell displacement during the cask tip-over accident. The nodal position of the inner surface of the liner is altered so that the displacements of the canister shell nodes in the periodic model are restricted to the same physical displacements as if the ends of the canister shell were present in the model.



The canister shell displacements are determined by the quasi-static ANSYS analysis for the canister and the basket for the cask tip-over condition. See Section 3.10.9 for a detailed description of the canister-basket models. A DLF of 1.36, in conjunction with a load factor of 1.5, is conservatively used in the canister-basket models.

To represent the accelerations applied to the periodic basket model during the tip-over, an acceleration time history is applied to the nodes of the concrete cask liner elements in the model. The acceleration data corresponds to the acceleration time history at the axial location where the maximum canister displacement occurs, with a factor of 1.5. As presented in Section 3.10.9, the maximum canister shell displacements occur at approximately 90 inches from the canister bottom. Figure 3.10.6-14(a) shows the acceleration time history corresponding to the location 86 inches from the canister bottom (with a factor of 1.5), based on the filtered acceleration time history at the top of the basket as shown in Figure 3.7.3-3. Note that the acceleration time history shown in Figure 3.10.6-14(b) corresponds to the canister shell location at 135 inches from the bottom and is used for a sensitivity study.

A velocity is applied to all the nodes of the model as an initial condition. The velocity is determined based on the location of the maximum canister shell displacements and 1.5 times the angular velocity due to the cask tip-over event (Section 3.10.4.4).

A uniform body force of 1g was applied to simulate gravity.

### **Load Cases**

The PWR and BWR basket stability evaluations are performed using the models and load conditions described in this section. As shown in Table 3.10.6-1, six base cases (P1 through P6) are considered for the PWR basket orientations of 0°, 18°, 22.5°, 27°, 34° and 43°. Additionally, Case P7 is evaluated as a sensitivity study using the canister shell displacement from the ANSYS canister-basket model in Section 3.10.9 at a section 135 inches from the bottom of the canister. The acceleration time history used in Case P7 also corresponds to the axial section 135 inches from the bottom of the canister. Case P7 uses the basket orientation of 22.5° to allow its results to be compared with Case P3 (22.5° base case).

Three base cases (B1 through B3) are evaluated for the BWR for basket orientations of 0°, 22.5° and 45°, as shown in Table 3.10.6-2. Similar to Case P7 for PWR, Case B4 is evaluated for the BWR basket as a sensitivity study for the boundary condition corresponding to a section 135 inches from the canister bottom.

### **Model Conservatism in the Periodic LS-DYNA Models**

- The models neglect any restraint developed from the connector pin assemblies at basket top and bottom ends.

- The models neglect any restraint developed by neighboring pin-slot connections (axially) in the tubes.
- The models incorporate beyond design basis maximum-minimum material conditions for the pins. A conservative tube size reduction of 0.025 inch is used for the base cases for the PWR and BWR basket models. The actual maximum fabricated assembly gap is 0.016 inch, and the prototype fabrication has shown the as-built gap is significantly less than 0.016 inch.
- The models consider boundary conditions corresponding to the maximum canister shell displacement, which occurs at a small section near the middle of the canister shell (see Figure 3.10.9-6 and Figure 3.10.9-7). Most parts of the basket are actually supported by the canister shell with less displacement (the periodic models neglect the stiffness of the basket support weldments and the fuel tube).
- The models consider the maximum displaced canister shell to be constant over the impact time history. This is also conservative because the canister shell displacement will be reduced significantly (providing more constraint to limit basket deflection) after the peak of the impact.
- The boundary condition of the canister shell displacement is determined based on conservative loading (a DLF of 1.36) as discussed in Section 3.10.9.

### **Post-Processing**

The primary output of these analyses is the resulting responses of the basket components during and after the impact. Typical responses of the basket fuel tubes are shown in Figure 3.10.6-15 and Figure 3.10.6-16 for the PWR basket and the BWR basket, respectively. These plots correspond to Case P1 and Case B1 in Table 3.10.6-1 and Table 3.10.6-2, respectively.

To further observe the response of the pin-slot connections, the change of the gap ( $x$ ) at the fuel tube corners is measured, as shown in Figure 3.10.6-17. The time history of the maximum change in  $x$ -length is obtained from the LS-DYNA analysis results for the base cases (Cases P1 through P7 and Cases B1 through B4) for the PWR basket and the BWR basket, respectively. Figure 3.10.6-18 through Figure 3.10.6-22 show the time history of the change in  $x$ -length for the location where maximum gap occurs (Point A in Figure 3.10.6-2 through Figure 3.10.6-10). The top three gap changes for each case are listed in Table 3.10.6-3 and Table 3.10.6-4 for PWR and BWR configurations, respectively. The locations of these maximum gap changes are shown in Figure 3.10.6-2 through Figure 3.10.6-10. Note that the maximum gap change for Case P7 (sensitivity study for boundary condition for PWR) is 0.112 inch (Point B of Figure 3.10.6-4), which is significantly less than the maximum gap change of the base case for 22.5 degrees (Case P3), 0.233 inch. The maximum gap change for Case B4 (sensitivity study for BWR), 0.173 inch (Point C of Figure 3.10.6-9), is also significantly less than the maximum gap change of the base case for 22.5 degrees (Case B2), 0.305 inch. This comparison shows that the canister shell profile, as opposed to the impact load, is the governing boundary condition for the basket stability evaluation. Each stability analysis orientation is performed using the maximum canister

shell displacement with the corresponding acceleration time history for the axial location of the maximum displacement from the point of rotation. All the pin-slot connections remain engaged for all the cases for both the BWR basket and PWR basket.

In order to be responsive to the requirements of 10 CFR 72.236 to provide assurance that the MAGNASTOR basket maintains stability when subject to transport accident load configurations, a specific dynamic analysis is performed. The basket and the orientation producing the worst case pin-slot displacement identified for the tip-over accident are evaluated for transport loading, with the transport cask inner shell as the boundary condition. The results summary presented in Table 3.10.6-3 and Table 3.10.6-4 identify that the BWR basket with a 22.5-degree orientation has the largest relative pin-slot displacement. Results from the governing analysis of a 30-foot side drop for the BWR basket with a 22.5-degree orientation validate basket stability for transport conditions.

A sensitivity study is performed to evaluate the effect of the gap size between the flats at tube corners. A gap of 0.016 inch (fabrication tolerance) is used as compared to the 0.025 inch for the base cases, as previously discussed. The analysis is performed for the BWR configuration with a 22.5° basket orientation, and the results are compared with the results of Case B2 (base case) in Table 3.10.6-4. The maximum gap change for this sensitivity study case is 0.227 inch, which is approximately 30% less than the maximum gap change for Case B2 (0.305 inch). This indicates that the models used in the base cases for both the PWR and BWR configurations are conservative.

A typical time history of the gap at the bosses connecting the fuel tubes and the support weldment is shown in Figure 3.10.6-23. The gap time history curves correspond to the BWR basket with a 45° orientation and the locations of the bosses are shown in Figure 3.10.6-10 (Points G1 and G2). The initial gap size is 0.0625 inch in the model. At Point G1, the gap starts to close at approximately 0.01 second. Note that the distance in the time-history plot in Figure 3.10.6-23 is measured by two nodes with 0.02-inch difference in the axial direction of the basket, which is perpendicular to the gap (i.e., the distance=0.02 inch when the gap is closed). At Point G2, the boss oscillated back and forth. At approximately 0.02 second, the "stop" moved to the opposite direction for 0.0625 inch (the gap at the opposite side is closed) and, therefore, the gap shown on Figure 3.10.6-23 is approximately 0.125 inch  $[(0.0625+0.0625)^2+0.02^2]^{1/2}$ .

### Summary

The evaluations provided in this section confirm that the PWR and BWR baskets maintain their configuration during a cask tip-over accident event. As previously discussed, a 1.5 factor is applied to the loading used for the periodic LS-DYNA for stability evaluation. The same factor was also used (in addition to a DLF of 1.36) for loading of the three-dimensional canister-basket model to determine the canister shell displacements as the boundary condition of the periodic LS-DYNA models. Considering all the conservatism in the periodic models, as previously described, it is concluded that the factor of safety for the PWR and BWR basket stability for the cask tip-over accident is considerably greater than 1.5 (and greater than acceptance criteria of 1.1, as defined in the following discussion).

The acceptance criteria for basket stability evaluation is established based on the acceptance criteria of the Collapse Load Analysis as discussed in ASME Code Subsection III, Appendix F. Section F-1341.3 states that the load should not exceed 90% of the analysis collapse load. The criterion for the minimum safety factor for the basket stability evaluation is considered to be 1.1 (1/0.9).

Figure 3.10.6-1 Basket Pin-Tube Slot Connections at Fuel Tube Corners

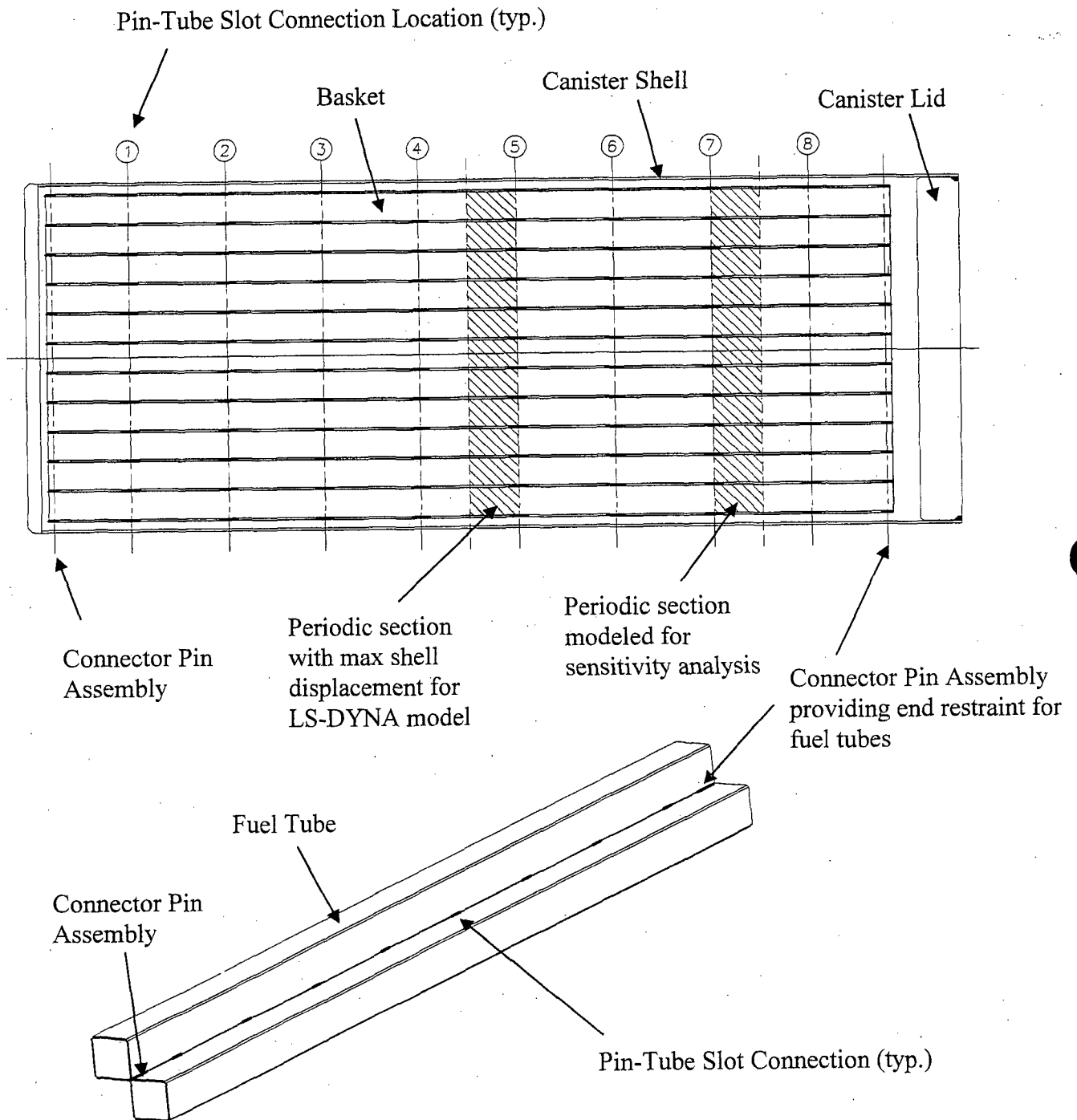


Figure 3.10.6-2 PWR Basket Finite Element Model for Concrete Cask Tip-Over Accident – 0° Basket Orientation

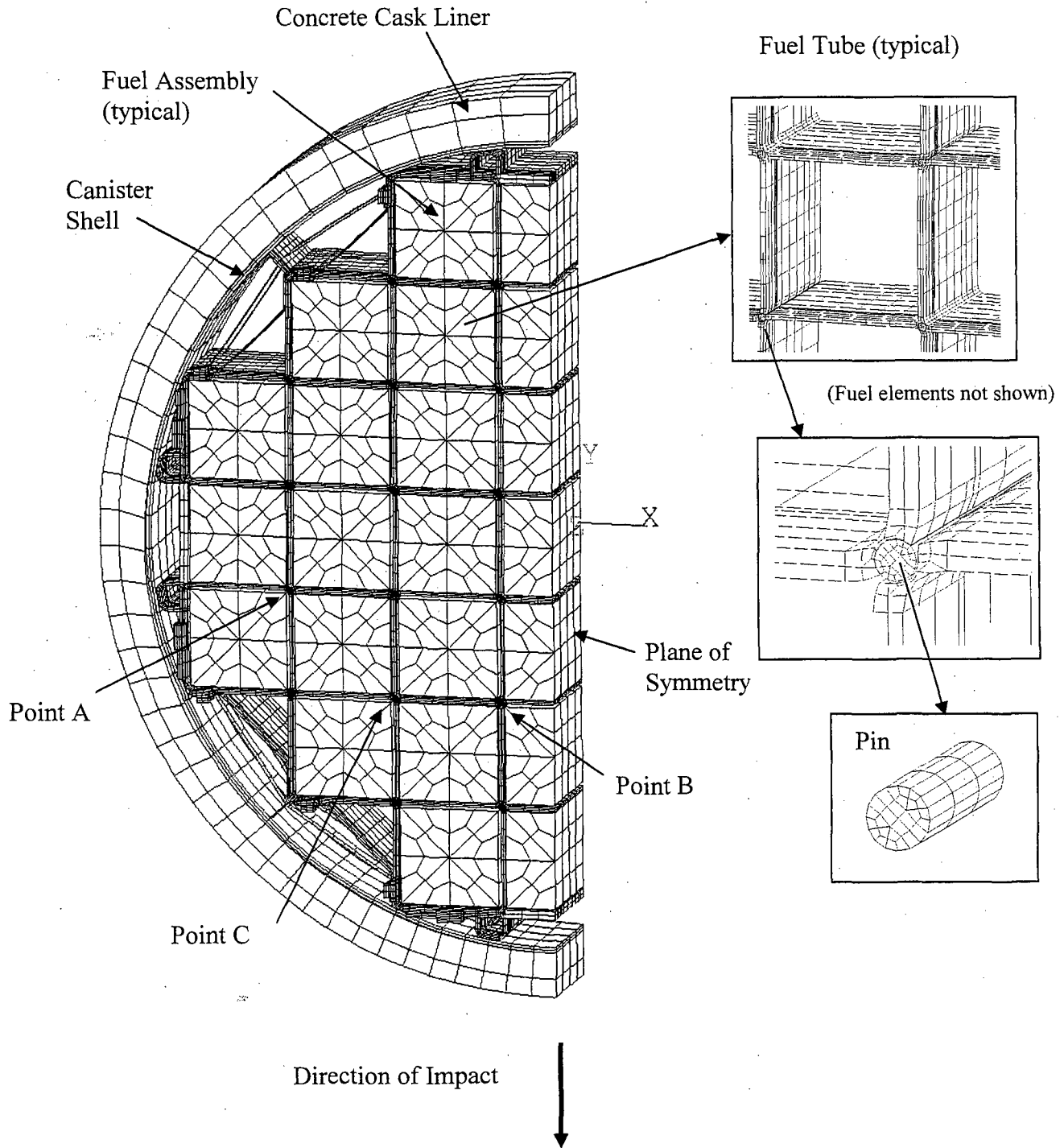


Figure 3.10.6-3 PWR Basket Finite Element Model for Concrete Cask Tip-Over Accident – 18° Basket Orientation

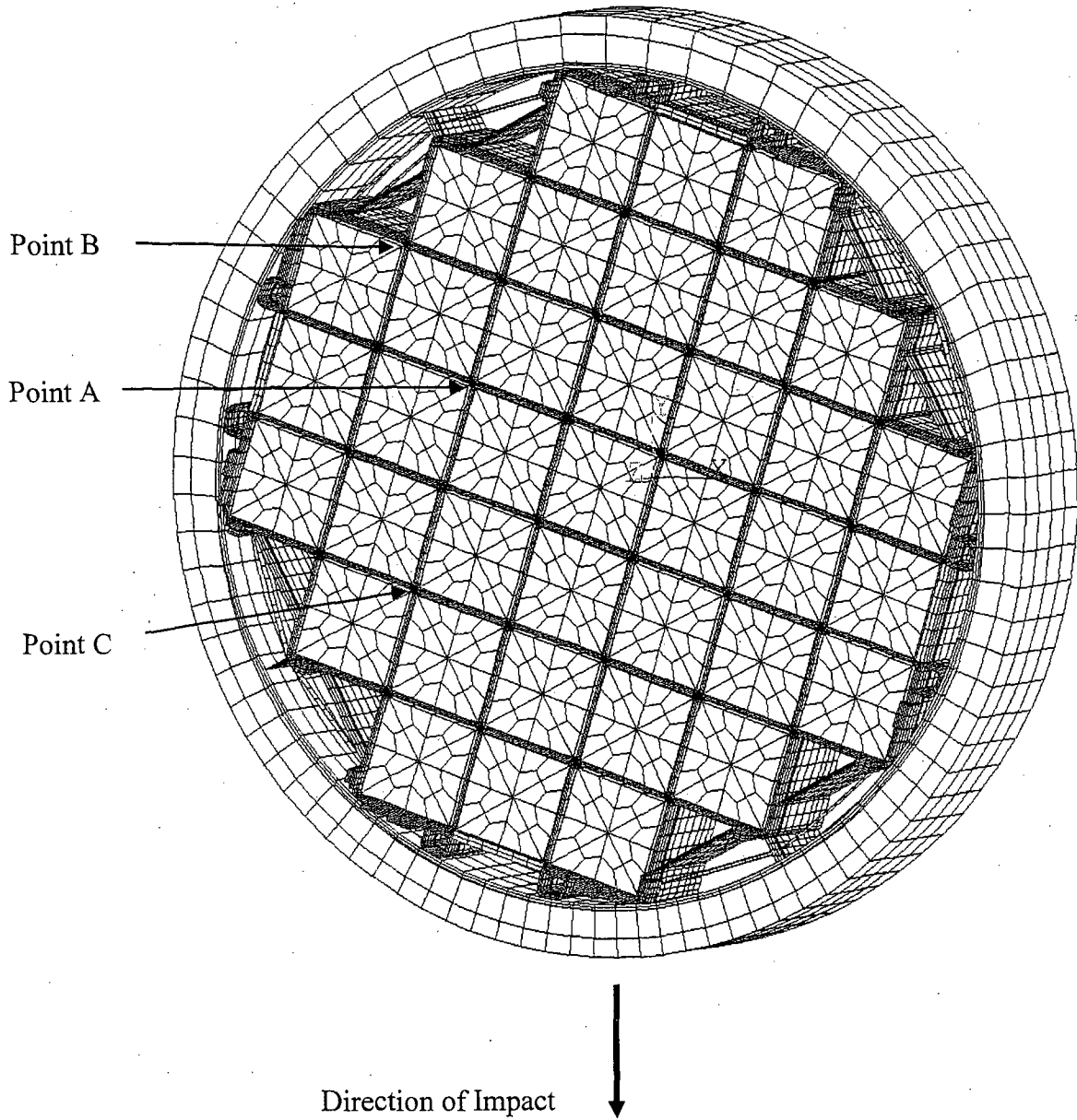


Figure 3.10.6-4 PWR Basket Finite Element Model for Concrete Cask Tip-Over Accident – 22.5° Basket Orientation

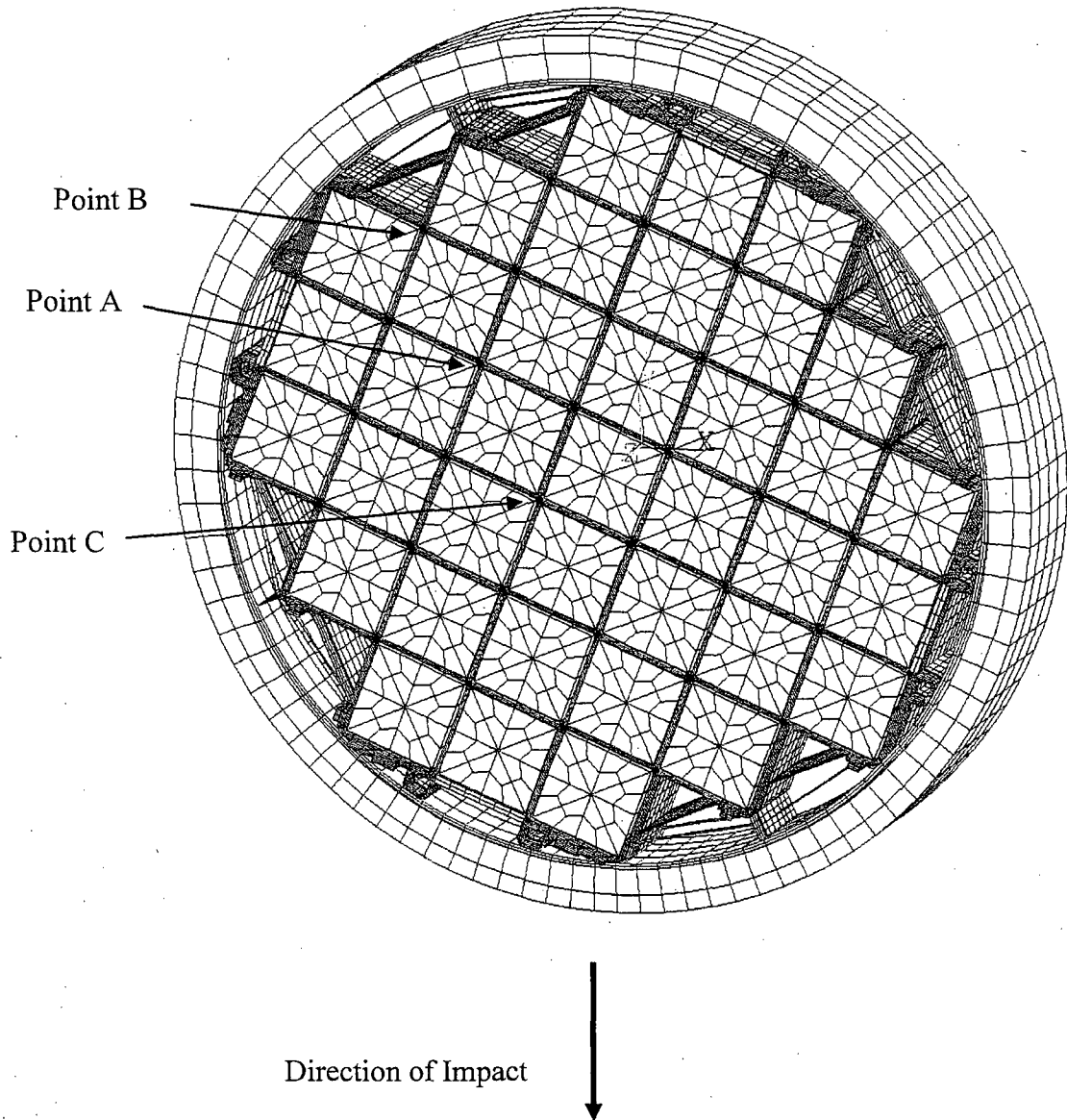




Figure 3.10.6-5 PWR Basket Finite Element Model for Concrete Cask Tip-Over Accident – 27° Basket Orientation

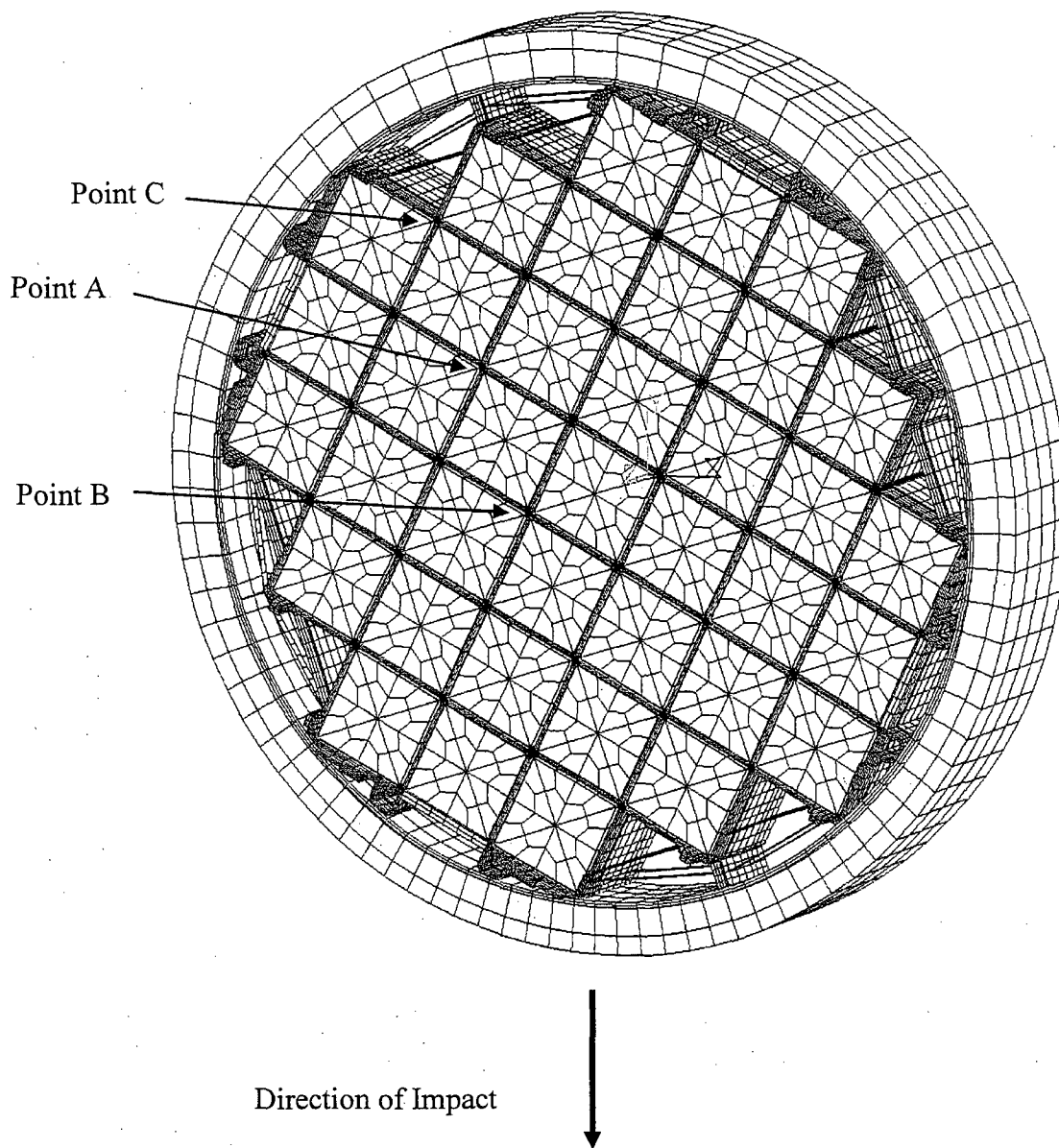


Figure 3.10.6-6 PWR Basket Finite Element Model for Concrete Cask Tip-Over  
Accident - 34° Basket Orientation

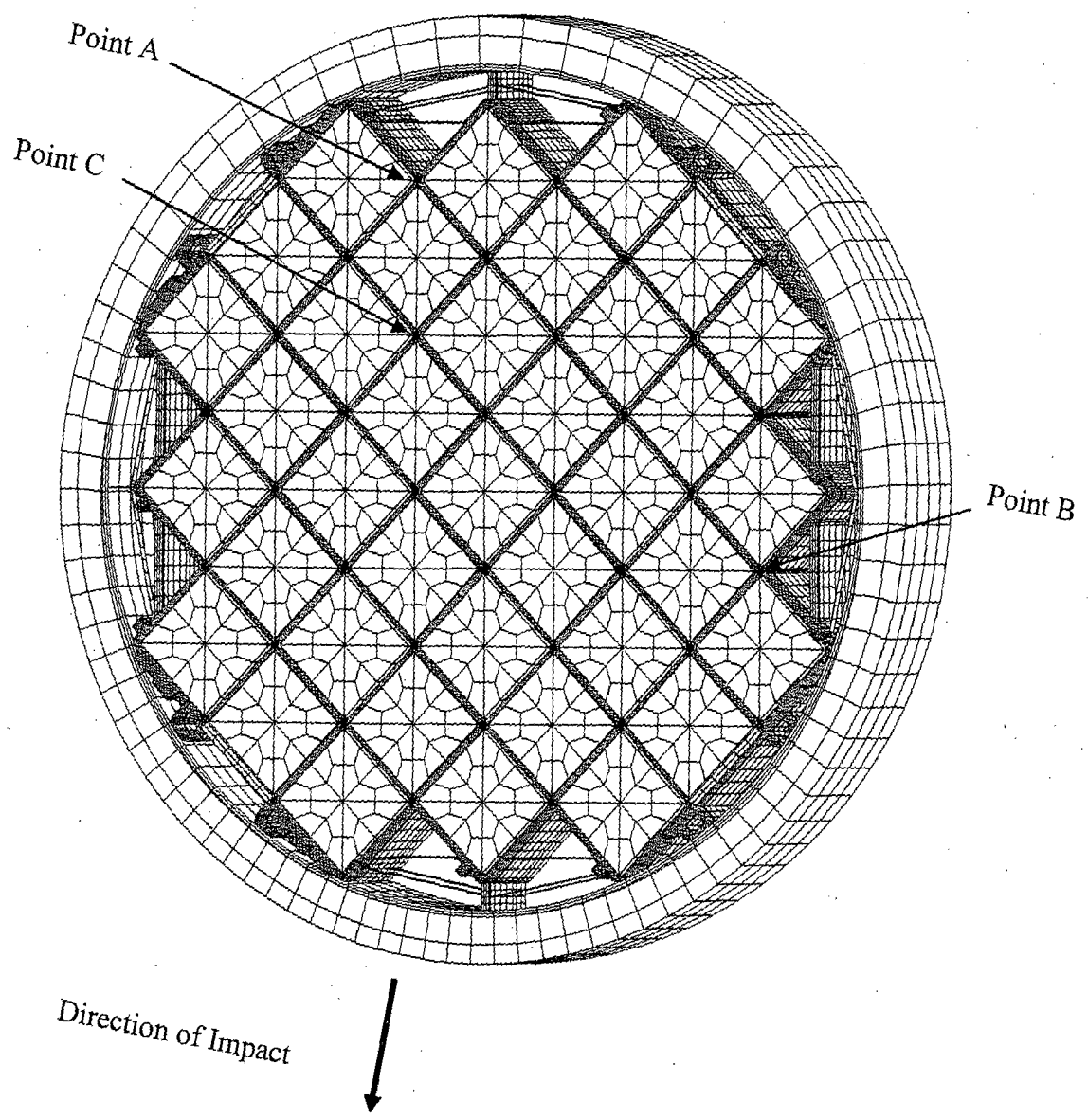


Figure 3.10.6-7 PWR Basket Finite Element Model for Concrete Cask Tip-Over Accident – 43° Basket Orientation

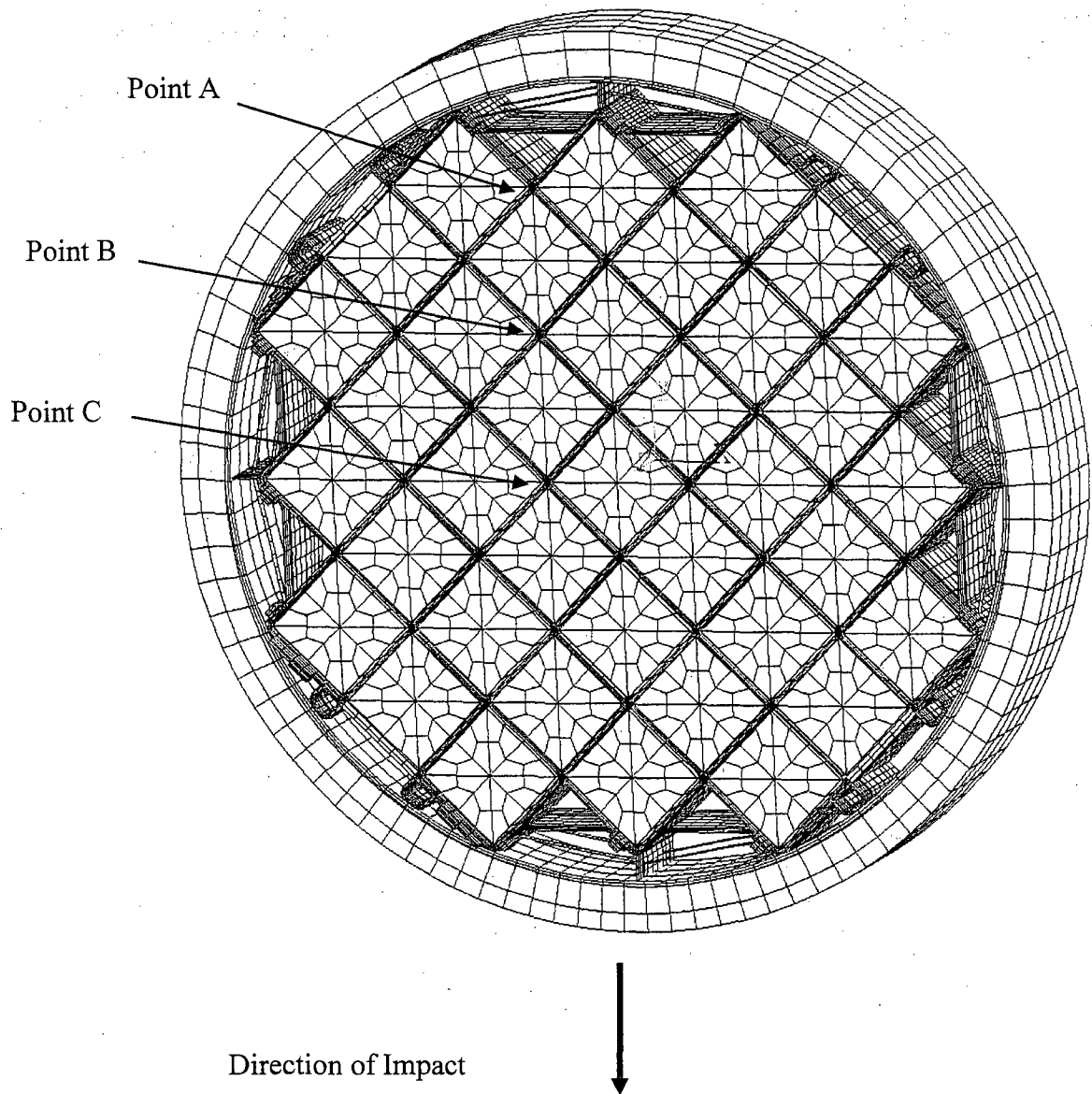
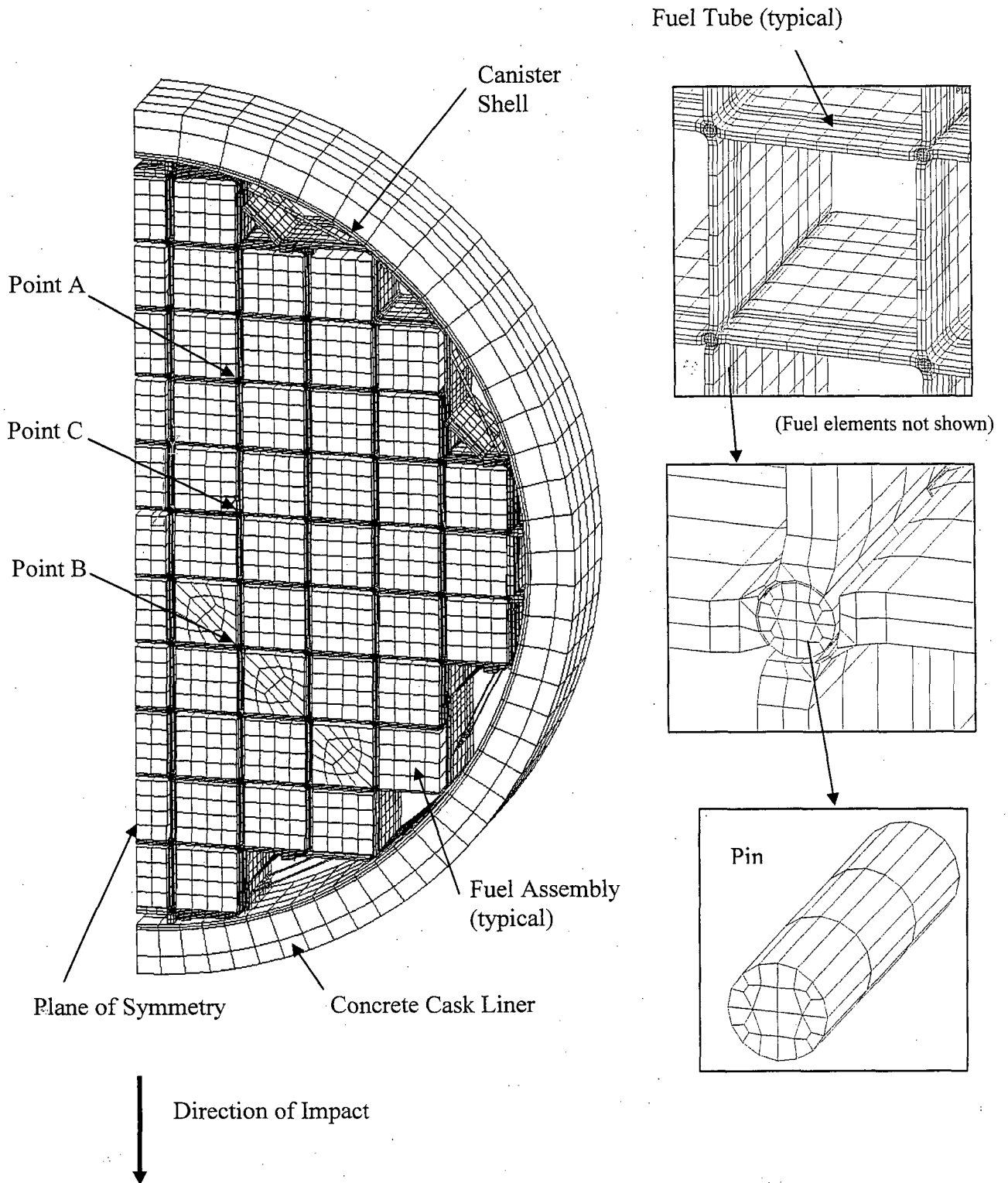


Figure 3.10.6-8 BWR Basket Finite Element Model for Concrete Cask  
Tip-Over Accident – 0° Basket Orientation



**Figure 3.10.6-9 BWR Basket Finite Element Model for Concrete Cask Tip-Over Accident – 22.5° Basket Orientation**

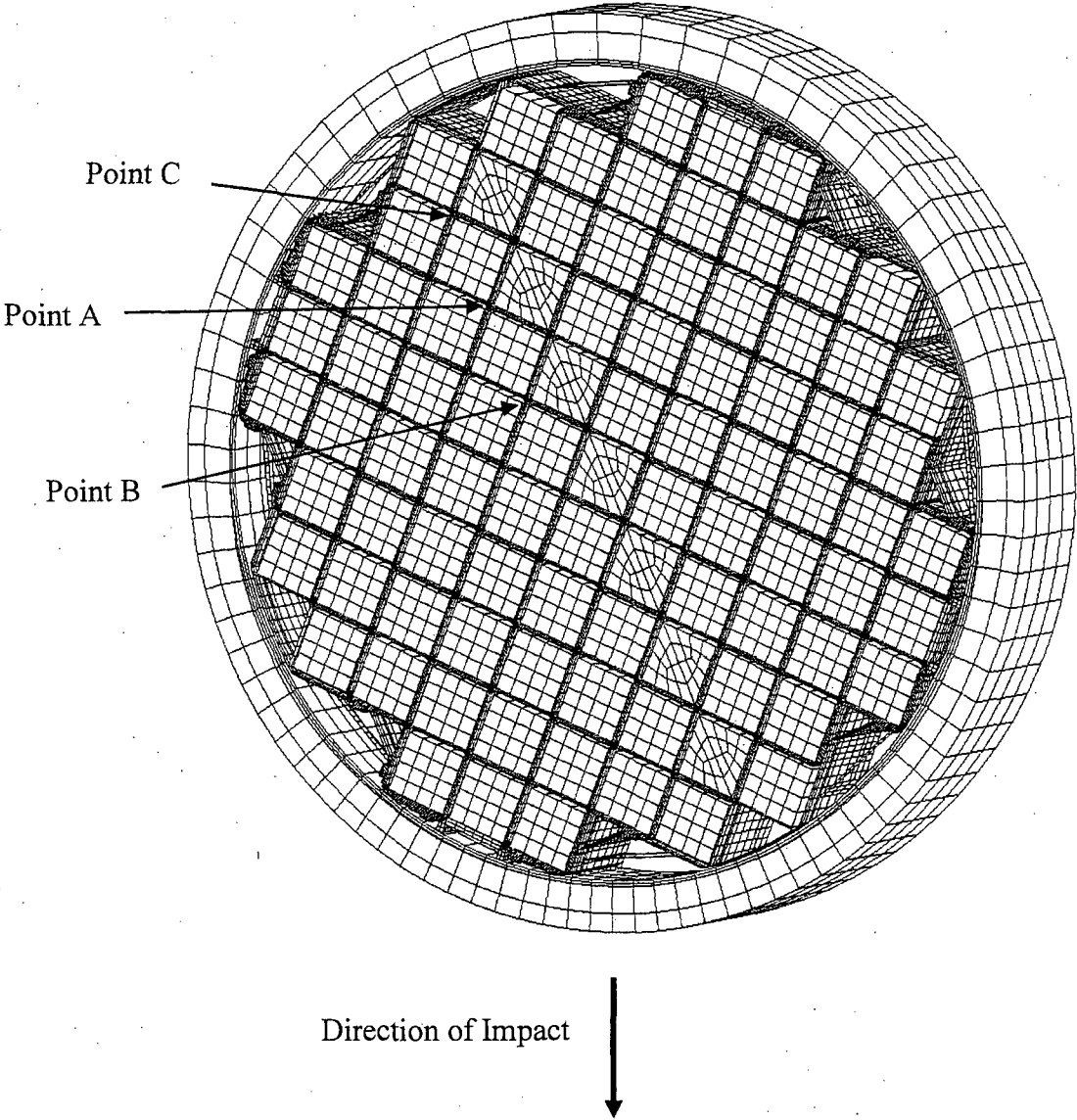


Figure 3.10.6-10 BWR Basket Finite Element Model for Concrete Cask Tip-Over Accident – 45° Basket Orientation

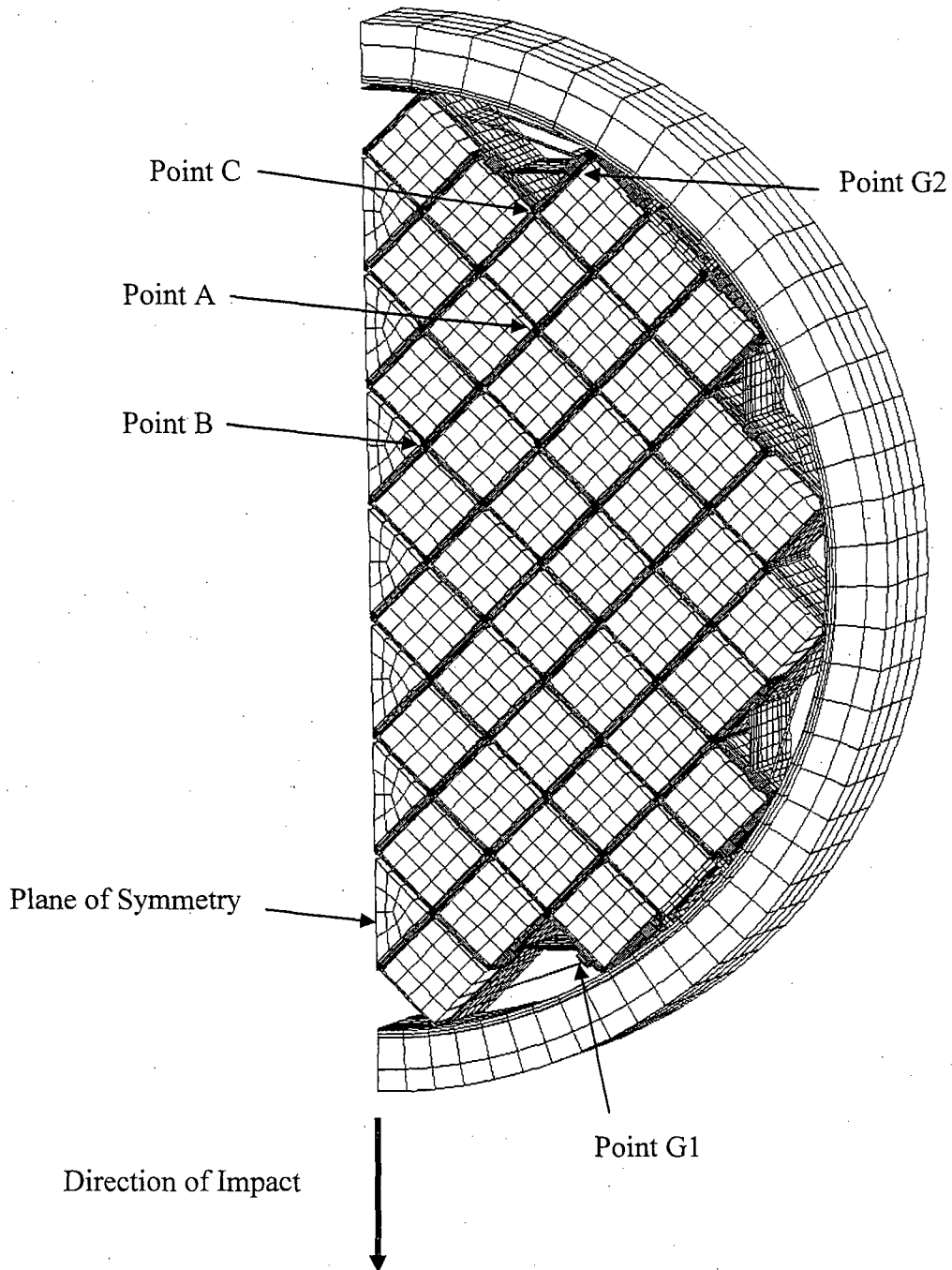


Figure 3.10.6-11 PWR Basket Finite Element Model – Boss Connection for Corner and Side Support Weldment

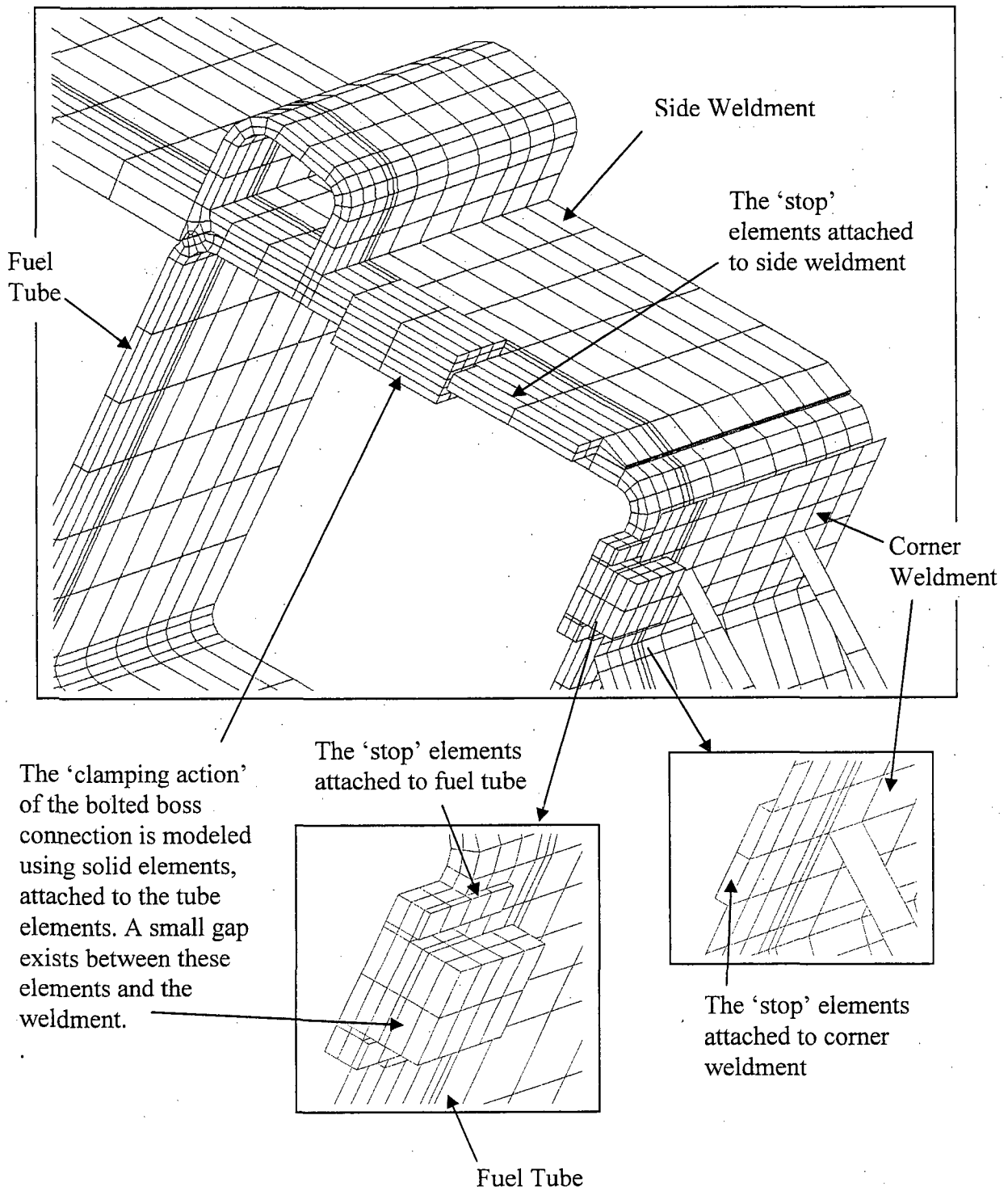
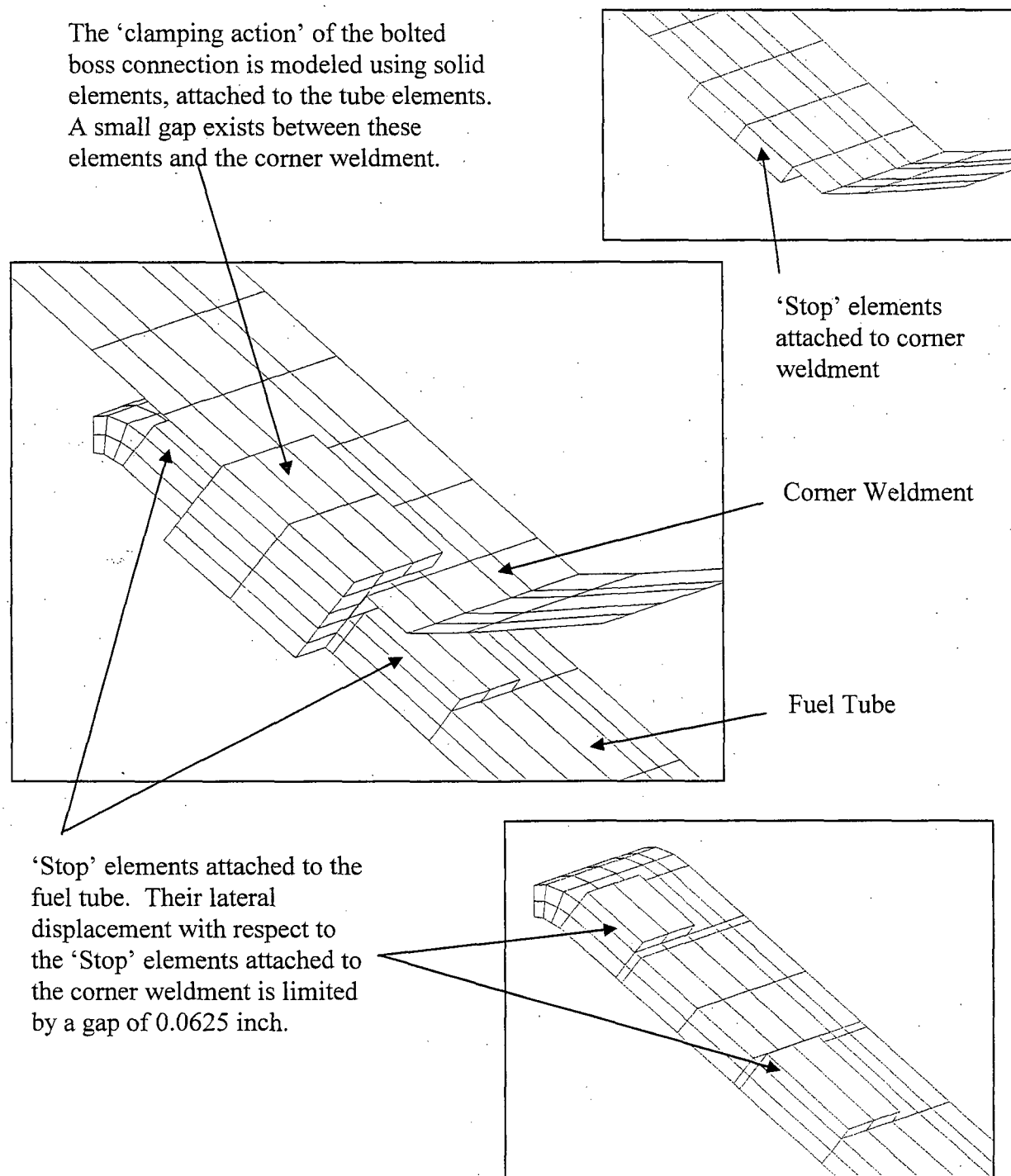


Figure 3.10.6-12 BWR Basket Finite Element Model – Boss Connection for Corner Support Weldment





**Figure 3.10.6-13 BWR Basket Finite Element Model – Boss Connection for Side Support Weldment**

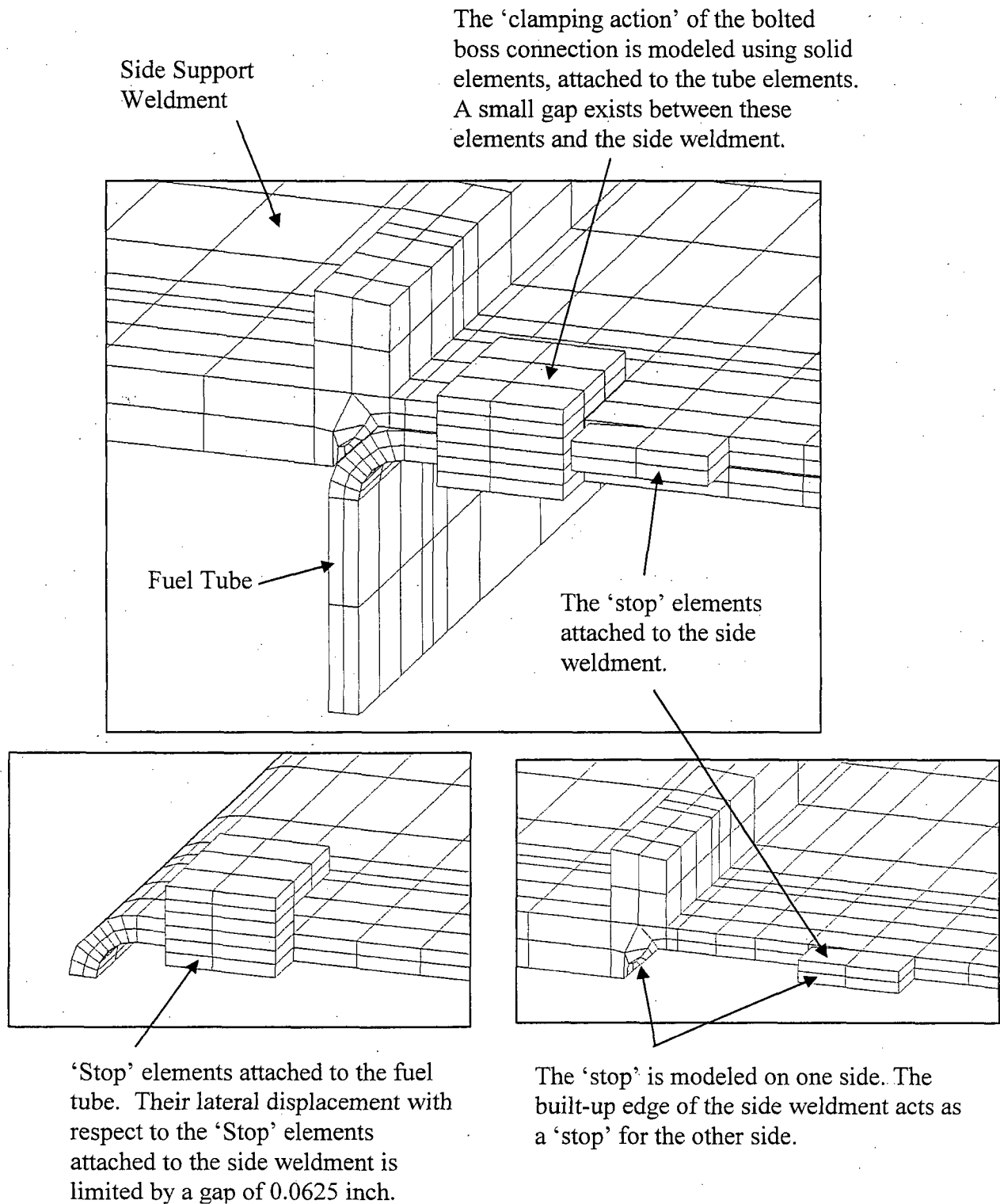
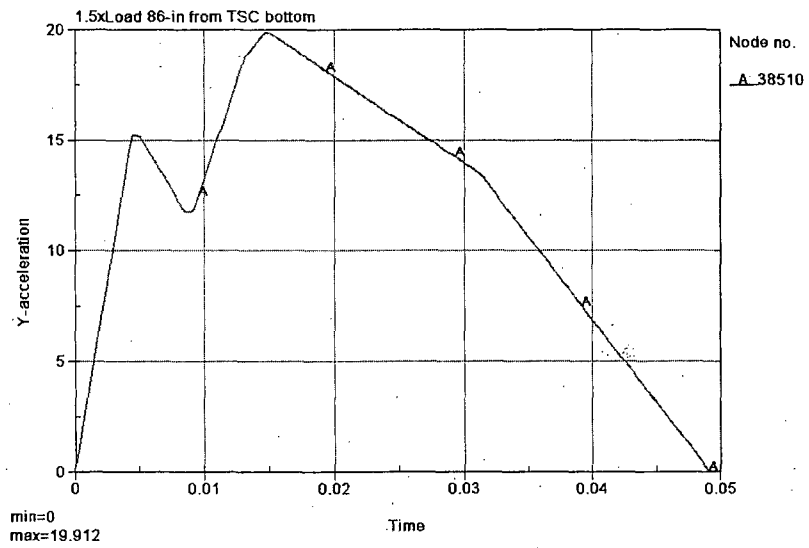


Figure 3.10.6-14 Acceleration Time History for Basket Stability Evaluation

(a)  $1.5 \times$  acceleration at 86 inches from TSC bottom



(b)  $1.5 \times$  acceleration at 135 inches from TSC bottom

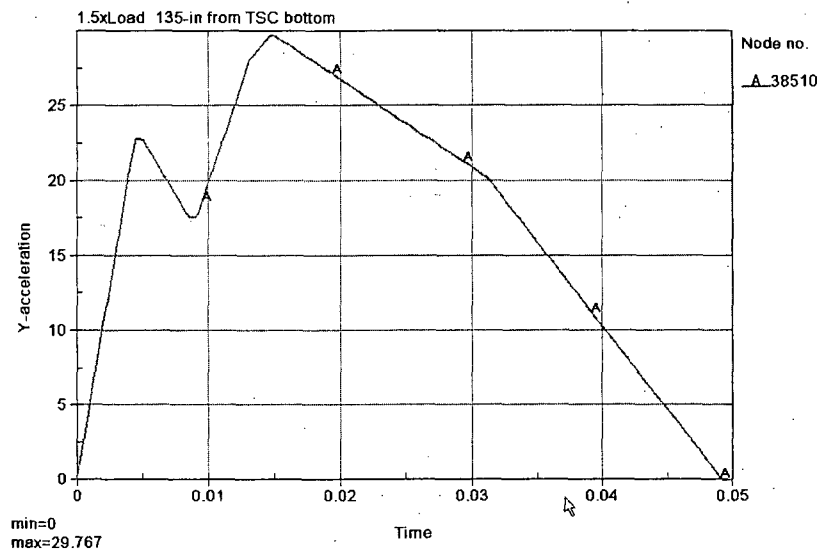
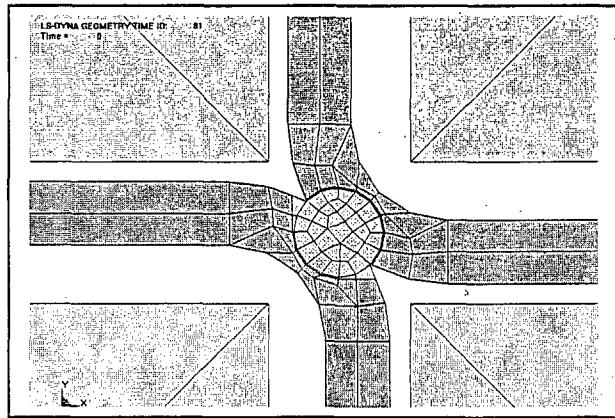
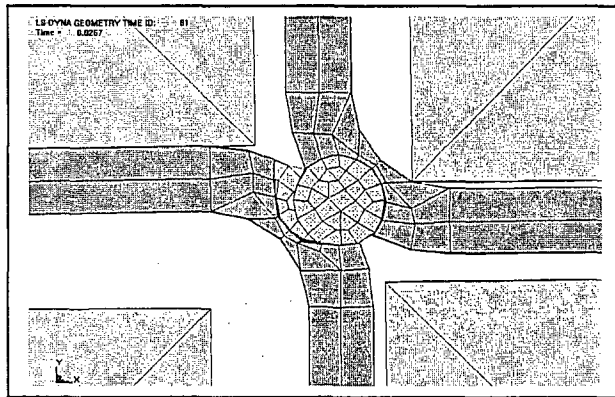


Figure 3.10.6-15 Typical Response of PWR Basket Fuel Tubes Pin-Slot Connections

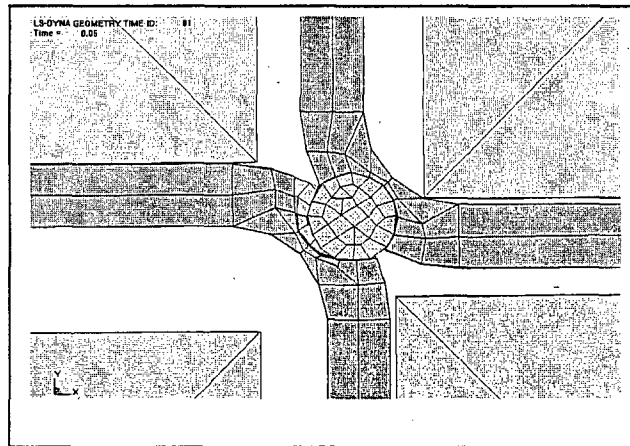
Time:0.0 sec.



Time:0.025 sec.



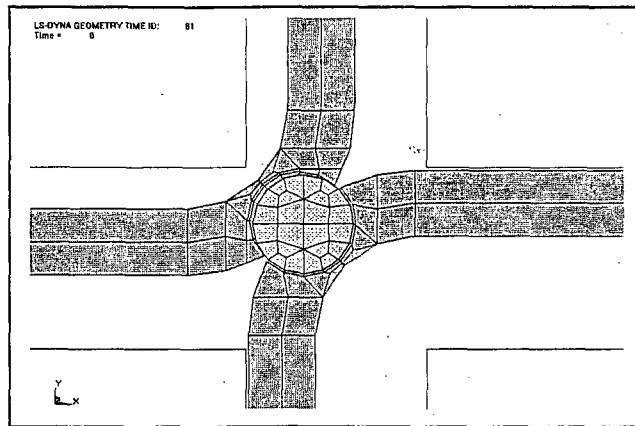
Time:0.050 sec.



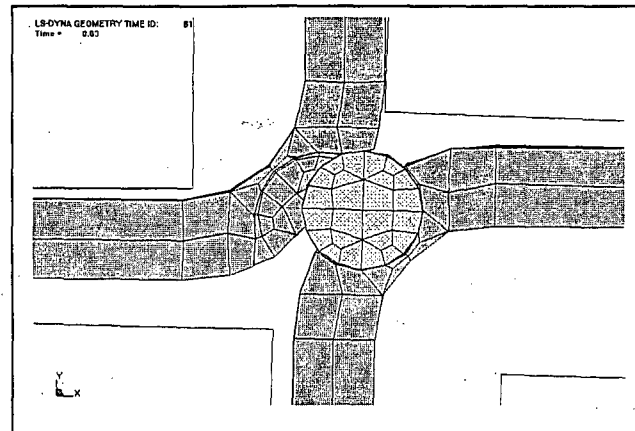
Note: See Figure 3.10.6-2 for Pin-Slot Location (Point A).

Figure 3.10.6-16 Typical Response of BWR Basket Fuel Tubes Pin-Slot Connections

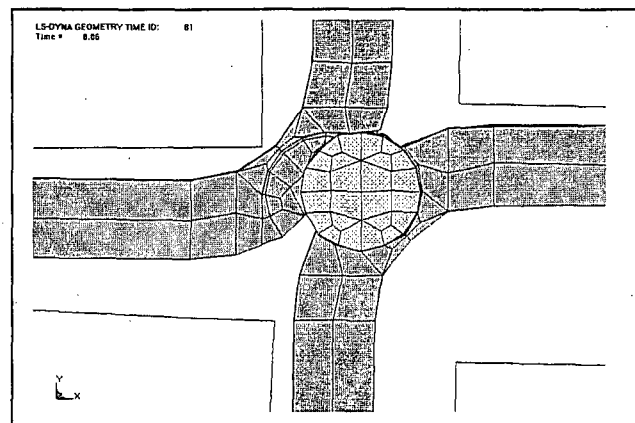
Time:0.0 sec.



Time:0.03 sec.

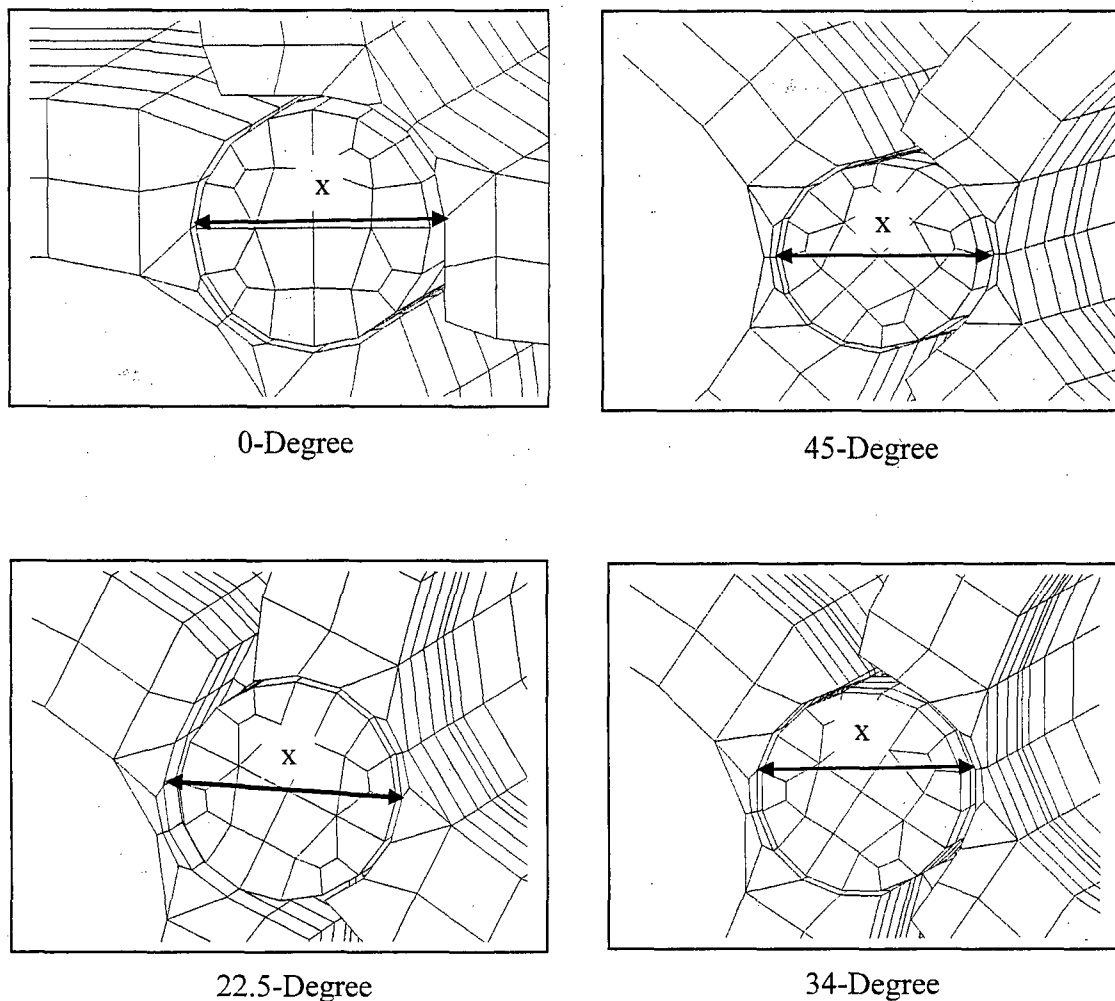


Time:0.06 sec.



Note: See Figure 3.10.6-9 for Pin-Slot Location (Point A).

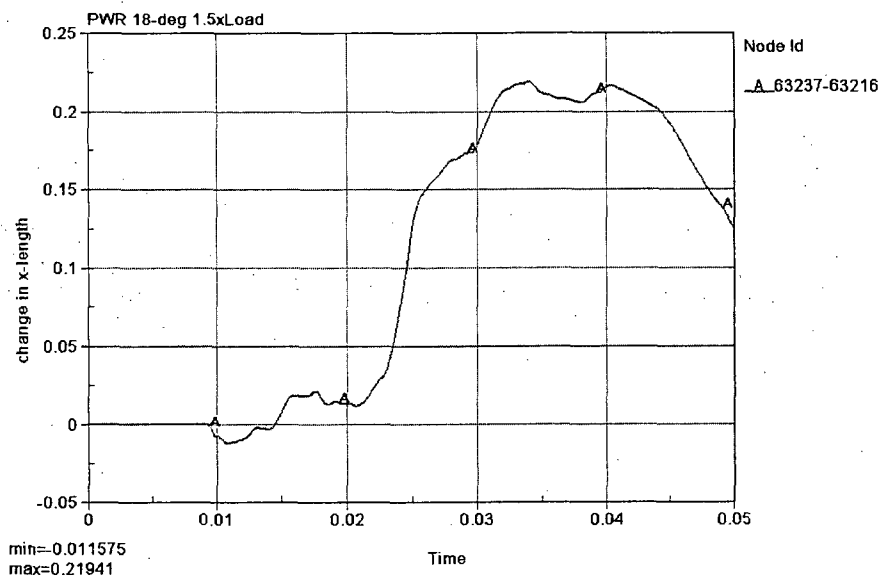
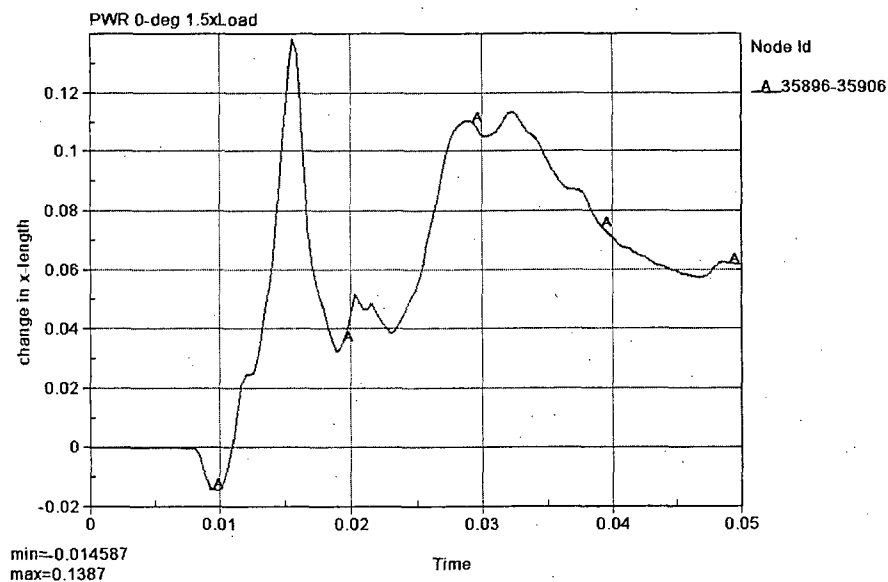
Figure 3.10.6-17 Typical Gap Measurement at Fuel Tube Corners



Note:

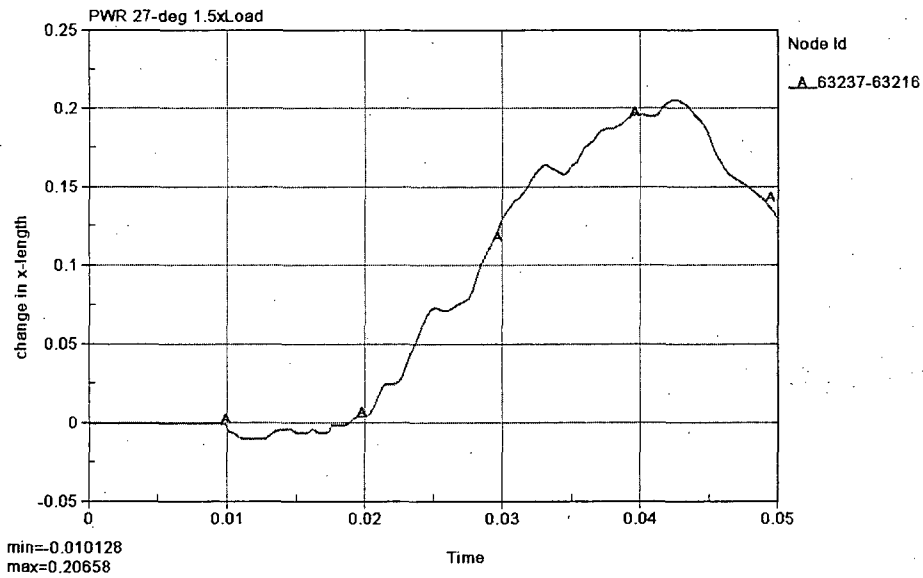
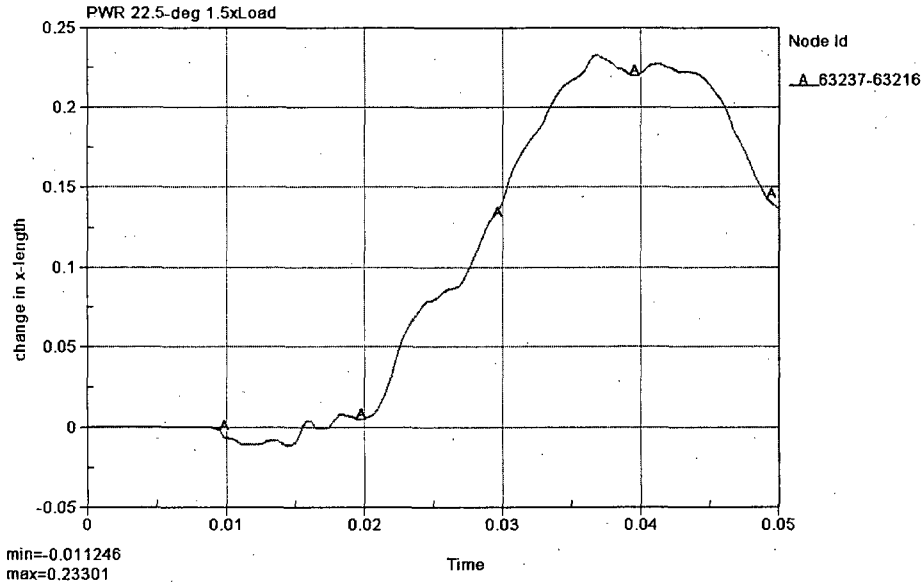
“x” is the measured gap size at the fuel tube corners. The plots of time history of the maximum gap size changes (‘change in x-length’) for the PWR and the BWR basket are shown Figure 3.10.6-18 through Figure 3.10.6-22.

Figure 3.10.6-18 Time History of Maximum Gap Change at Fuel Tube Corner –  
PWR Basket 0° and 18° Orientation



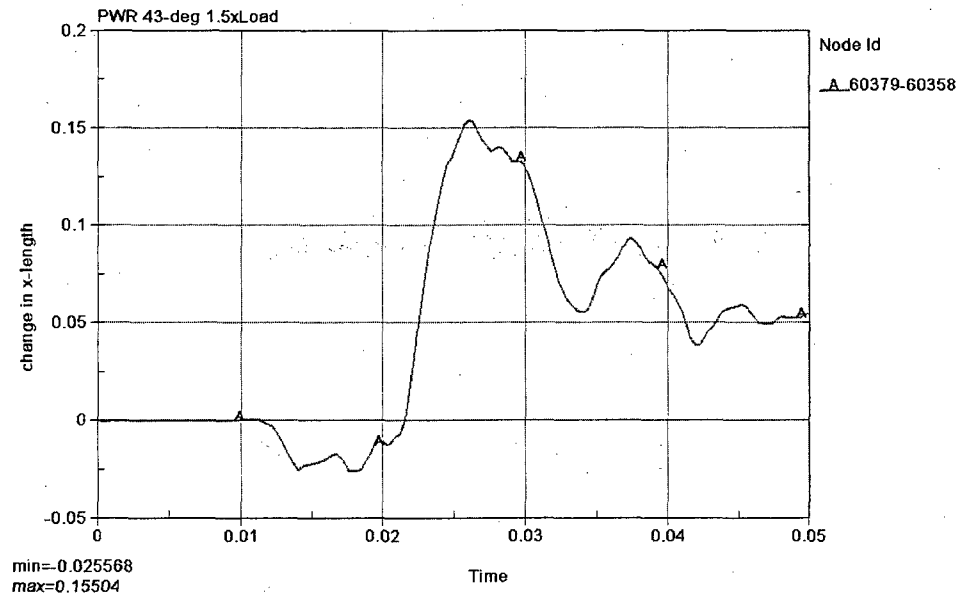
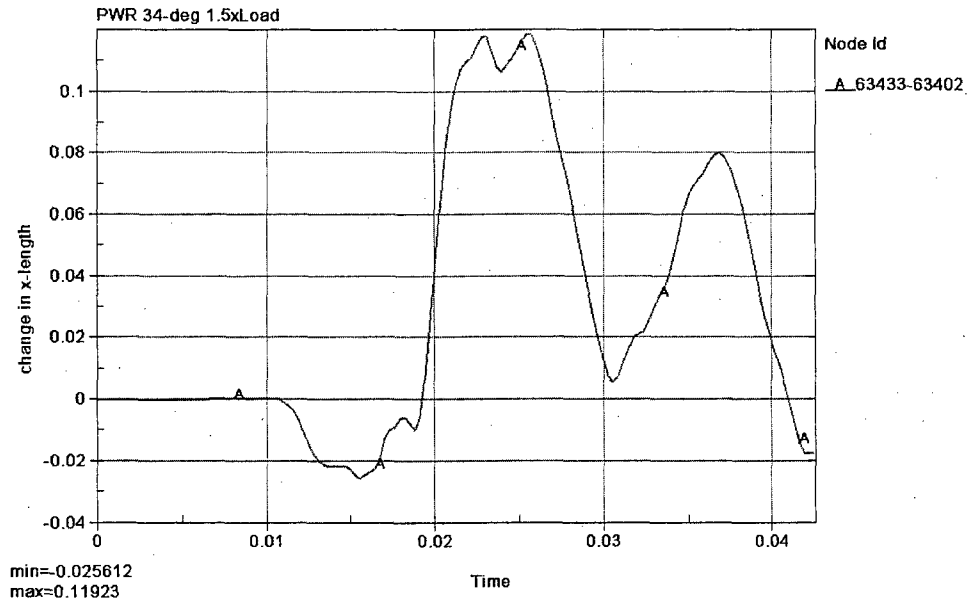
Note: See Figure 3.10.6-2 and Figure 3.10.6-3 for locations of fuel tube corners (Point A).

Figure 3.10.6-19 Time History of Maximum Gap Change at Fuel Tube Corner –  
PWR Basket 22.5° and 27° Orientation



Note: See Figure 3.10.6-4 and Figure 3.10.6-5 for locations of fuel tube corners (Point A).

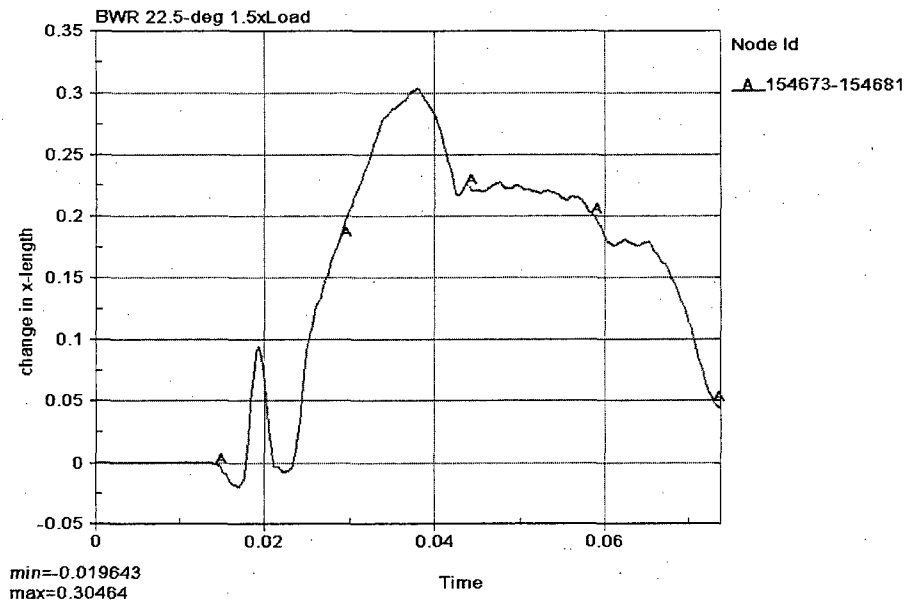
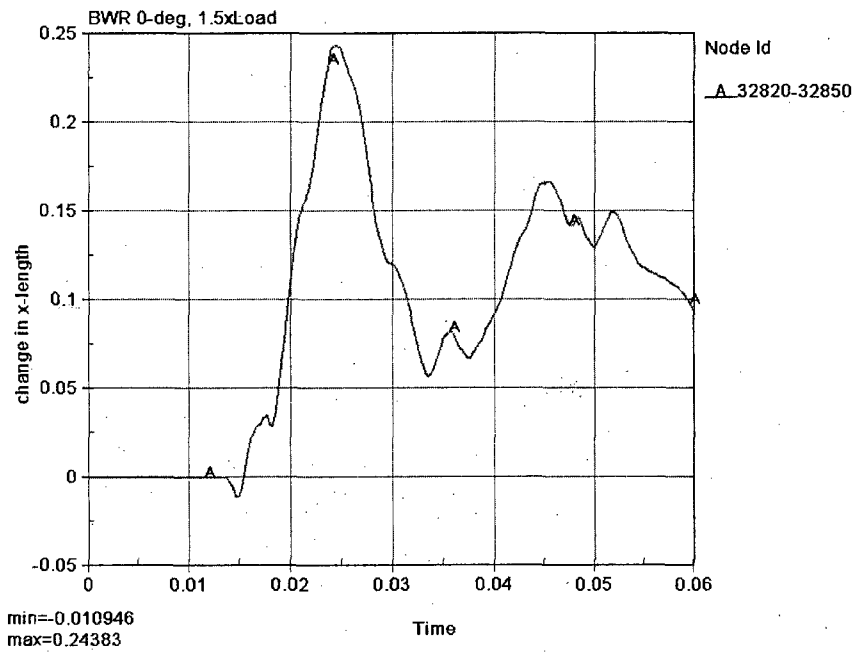
Figure 3.10.6-20 Time History of Maximum Gap Change at Fuel Tube Corner –  
PWR Basket 34° and 43° Orientation



Note: See Figure 3.10.6-6 and Figure 3.10.6-7 for locations of fuel tube corners (Point A).

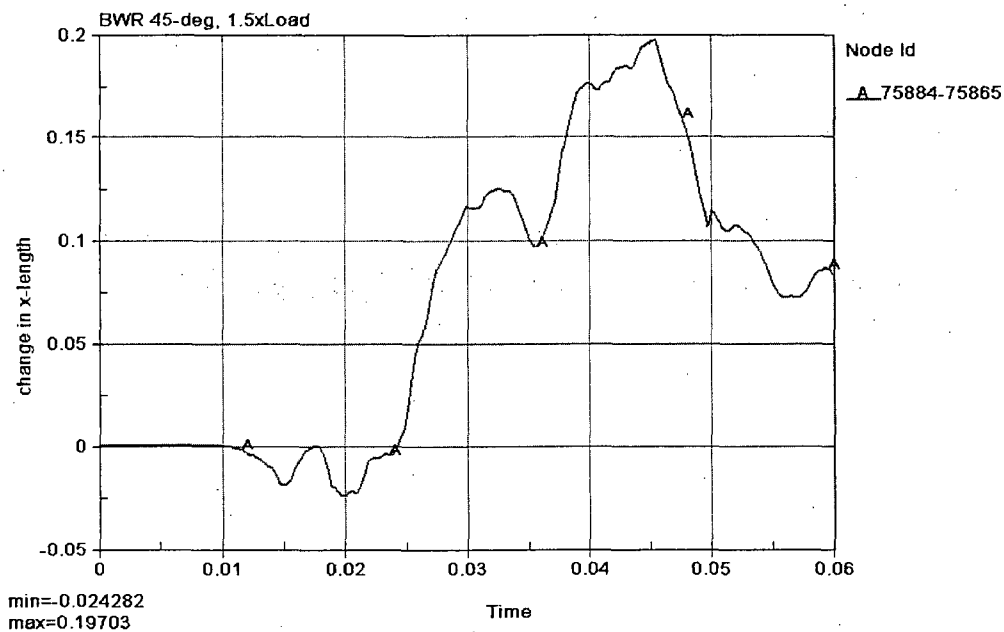


Figure 3.10.6-21 Time History of Maximum Gap Change at Fuel Tube Corner –  
BWR Basket 0° and 22.5° Orientation



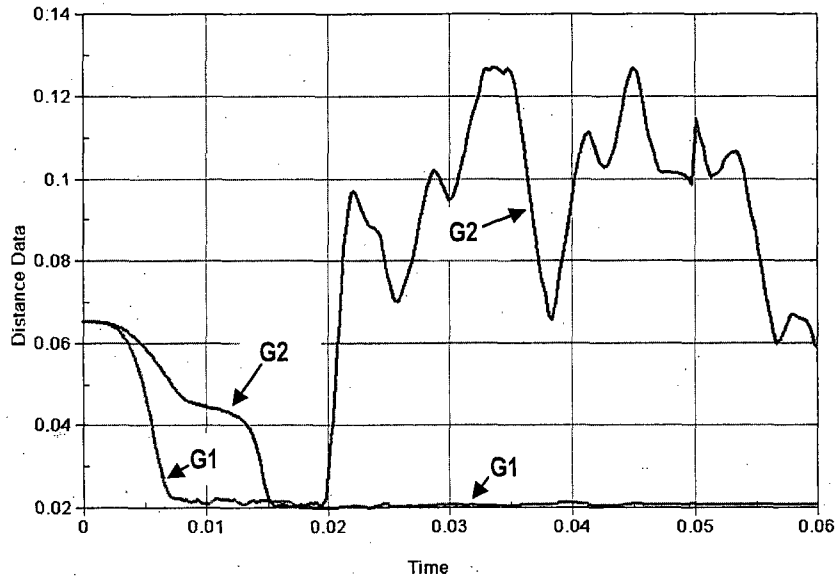
Note: See Figure 3.10.6-8 and Figure 3.10.6-9 for locations of fuel tube corners (Point A).

Figure 3.10.6-22 Time History of Maximum Gap Change at Fuel Tube Corner – BWR Basket 45° Orientation

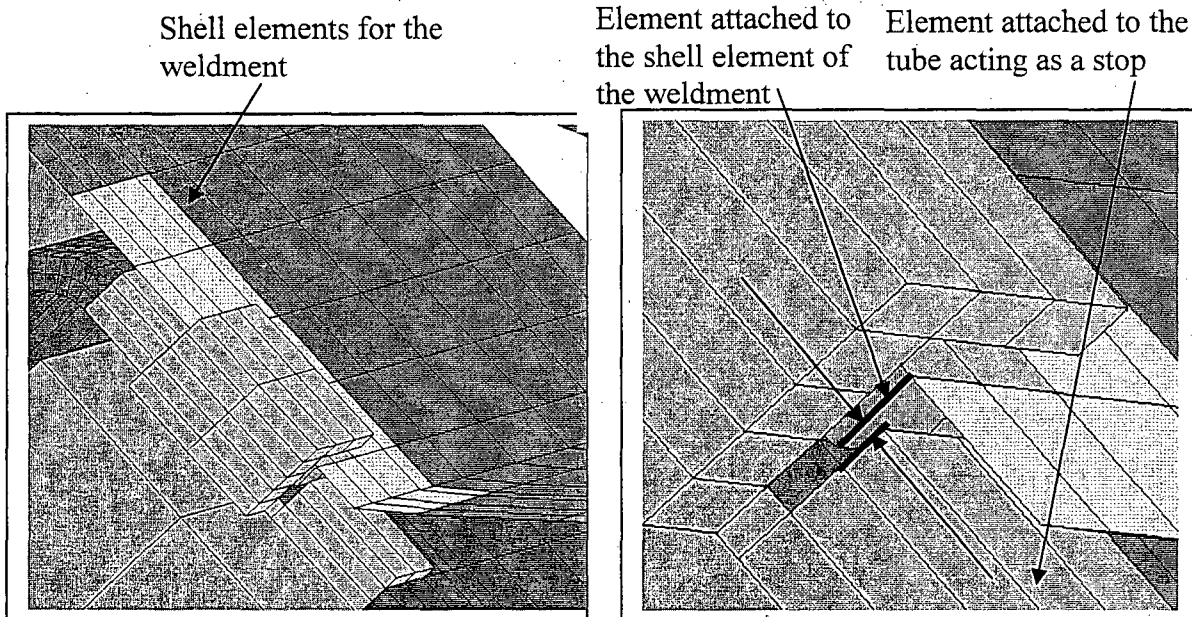


Note: See Figure 3.10.6-10 for location of fuel tube corner (Point A).

Figure 3.10.6-23 Typical Time History of Gap at Boss for BWR Support Weldments



The locations of the measured gap for "G1" and "G2" are shown in Figure 3.10.6-10.



The gap is measured between the edge of the element attached to the tube and the edge of the element attached to the shell element of the weldment.

Table 3.10.6-1 Load Cases Evaluated for PWR Fuel Basket Stability

| Case | Basket Orientation | Model Cross-Section | Remarks                        |
|------|--------------------|---------------------|--------------------------------|
| P1   | 0                  | 180°                | Base Case                      |
| P2   | 18                 | 360°                | Base Case                      |
| P3   | 22.5               | 360°                | Base Case                      |
| P4   | 27                 | 360°                | Base Case                      |
| P5   | 34                 | 360°                | Base Case                      |
| P6   | 43                 | 360°                | Base Case                      |
| P7   | 22.5               | 360°                | Sensitivity Study <sup>a</sup> |

<sup>a</sup> Sensitivity study for boundary conditions using canister shell displacement at 135 inches from canister bottom and the associated acceleration time history.

**Table 3.10.6-2 Load Cases Evaluated for BWR Fuel Basket Stability**

| <b>Case</b> | <b>Basket Orientation</b> | <b>Model Cross-Section</b> | <b>Remarks</b>                 |
|-------------|---------------------------|----------------------------|--------------------------------|
| B1          | 0                         | 180°                       | Base Case                      |
| B2          | 22.5                      | 360°                       | Base Case                      |
| B3          | 45                        | 180°                       | Base Case                      |
| B4          | 22.5                      | 360°                       | Sensitivity Study <sup>a</sup> |

<sup>a</sup> Sensitivity study for boundary conditions using canister shell displacement at 135 inches from canister bottom and the associated acceleration time history.

**Table 3.10.6-3 Summary of Maximum Gap Changes at Pin-Slot Connections  
for PWR Basket**

| Case | Basket Orientation | Max Gap Change at Pin-Slot Connection (inch) |                         |                         |
|------|--------------------|--|-------------------------|-------------------------|
|      |                    | Location A <sup>a</sup>                      | Location B <sup>a</sup> | Location C <sup>a</sup> |
| P1   | 0                  | 0.139  | 0.136                   | 0.126                   |
| P2   | 18                 | 0.219  | 0.165                   | 0.144                   |
| P3   | 22.5               | 0.233  | 0.194                   | 0.127                   |
| P4   | 27                 | 0.207  | 0.139                   | 0.120                   |
| P5   | 34                 | 0.119  | 0.104                   | 0.103                   |
| P6   | 43                 | 0.155  | 0.148                   | 0.111                   |
| P7   | 22.5               | 0.086  | 0.112                   | 0.080                   |

<sup>a</sup> Note: See Figure 3.10.6-2 through Figure 3.10.6-7 for locations for Cases P1 through P6, respectively. See Figure 3.10.6-4 for locations for Case P7.

**Table 3.10.6-4 Summary of Maximum Gap Changes at Pin-Slot Connections for BWR Basket**

| Case | Basket Orientation | Max Gap Change at Pin-Slot Connection (inch) |                         |                         |
|------|--------------------|--|-------------------------|-------------------------|
|      |                    | Location A <sup>a</sup>                      | Location B <sup>a</sup> | Location C <sup>a</sup> |
| B1   | 0                  | 0.244  | 0.164                   | 0.160                   |
| B2   | 22.5               | 0.305  | 0.279                   | 0.265                   |
| B3   | 45                 | 0.197  | 0.129                   | 0.122                   |
| B4   | 22.5               | 0.170  | 0.088                   | 0.173                   |

<sup>a</sup> Note: See Figure 3.10.6-8 through Figure 3.10.6-10 for locations for Cases B1 through B3, respectively. See Figure 3.10.6-9 for locations for Case B4.

### 3.10.7 Fuel Tube Plastic Analysis for Concrete Cask Tip-Over Accident Condition

This section describes the LS-DYNA models for the fuel tubes in the PWR and BWR fuel baskets and the analyses to evaluate any possible permanent deformation of the fuel tubes for the hypothetical concrete cask tip-over accident.

#### Model Description

As shown in Figure 3.10.7-1, a three-dimensional half-symmetry model is constructed to represent a half cross-section of a PWR fuel tube using the LS-DYNA program. The model for the BWR fuel tube is similar to that for the PWR fuel tube. The model contains a cross section of the fuel tube and a rigid block through which the displacement is applied to the top of the fuel tube.

#### Material Properties

Piecewise linear plastic properties corresponding to 700°F are used for the carbon steel fuel tubes.

#### Boundary Conditions

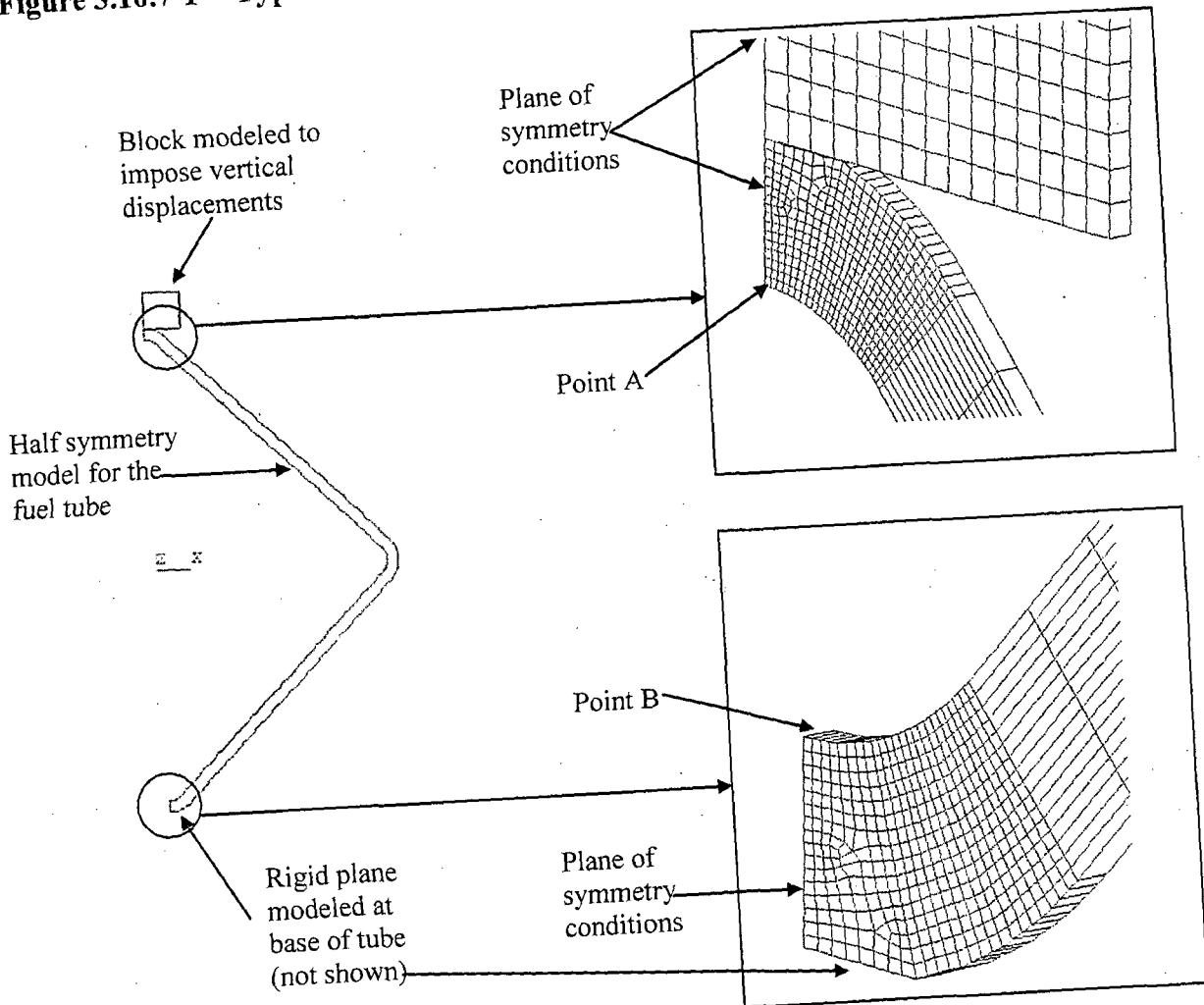
Automatic surface-to-surface contact conditions are employed between the block imposing the displacement and the top of the fuel tube. The motion at the bottom of the fuel tube is limited by the definition of a rigid plane. Symmetry boundary conditions are applied to the plane of symmetry (see Figure 3.10.7-1, typical). The vertical displacement of the block is specified as a triangular shaped time history with the maximum displacement of 0.294 inch for the PWR fuel tube and 0.34 inch for the BWR fuel tube. The displacement for the PWR tube corresponds to the maximum diagonal displacements of the fuel tubes for the tip over condition as evaluated in Section 3.7.2.1.2. For the BWR configuration, the displacement corresponds to the BWR evaluation using LS-DYNA in Section 3.10.6. The duration of the motion is 0.045 seconds which reflects the duration of the impact in the tip-over accident. The analysis is continued until a time of 0.060 seconds to obtain the final deformed shape of the fuel tube.

#### Post-processing

The permanent deformation of the fuel tubes is determined by computing the difference in the vertical displacements of Point A and Point B (Figure 3.10.7-1) in the final deformed shape. The maximum permanent diagonal displacement of the fuel tubes is computed to be 0.008 inch and 0.004 inch for the PWR and BWR fuel tubes, respectively.



Figure 3.10.7-1 Typical Finite Element Model for the Basket Fuel Tube Displacement



**3.10.8 Basket Pin-Slot Connection Evaluation for Concrete Cask Tip-Over Accident Condition**

As part of the stability evaluation for the BWR and PWR fuel baskets for the hypothetical concrete cask tip-over accident, this section describes the structural evaluation for the basket pin-slot connections subjected to maximum shearing conditions using the finite element models presented in Section 3.10.6.

The three-dimensional half-symmetry finite element models for the 0° basket orientation, as shown in Figure 3.10.8-1 (BWR) and Figure 3.10.8-3 (PWR), are used for the evaluation. These models are associated with the maximum shear forces at the pin-slot connections, based on the quasistatic analyses for BWR and PWR baskets for the tip-over accident as documented in Section 3.7.2. The models are constructed using the same modeling methodology as used for the models presented in Section 3.10.6. To more accurately solve for the stress/strain at the pin-slot connections, the pin-slot connection associated with the largest shear load is modeled with a finer mesh, as shown in Figure 3.10.8-2 (BWR) and Figure 3.10.8-4 (PWR). The LS-DYNA program is used to perform transient (time history) analyses to simulate the side impact condition of the cask tip-over accident. The unfiltered acceleration time history at the top of the basket (Figure 3.7.3-3) is conservatively used in the BWR evaluation. The maximum filtered acceleration is 26.4g and the unfiltered acceleration at the same time is 32.3g, which results in a load factor of 1.22 (32.3/26.4). The unfiltered acceleration with a factor of 1.1 is used for the PWR analysis for additional conservatism (the resulting load factor for PWR is 1.1 × 1.22, or 1.34). The calculated maximum plastic strains at this pin-slot connection are shown in the following table. See Figure 3.10.8-5 and Figure 3.10.8-6 for locations of the maximum strains in the pin and the tube slots, as well as the time history of the maximum plastic strain, for the BWR and the PWR basket, respectively.

| Basket Type | Maximum Plastic Strain |       |
|-------------|------------------------|-------|
|             | Tube Slot              | Pin   |
| BWR         | 15.4%                  | 8.4%  |
| PWR         | 16.5%                  | 15.4% |

As shown in the table, the calculated maximum plastic strains at the pin-slot connection for all of the analyzed cases are well below the material ultimate true strain of the SA 537 carbon steel (21%). Also note that the analysis results show that the plastic strain in the tube slot or pin occurs in localized regions and the majority of the material remains elastic. The pins remain completely enclosed in the tube slots and allow transfer of shear and bearing loads between adjacent fuel tubes during the cask tip-over accident. Therefore, the pin-slot connections of the

BWR and PWR fuel baskets are structurally adequate for the concrete cask tip-over accident condition.

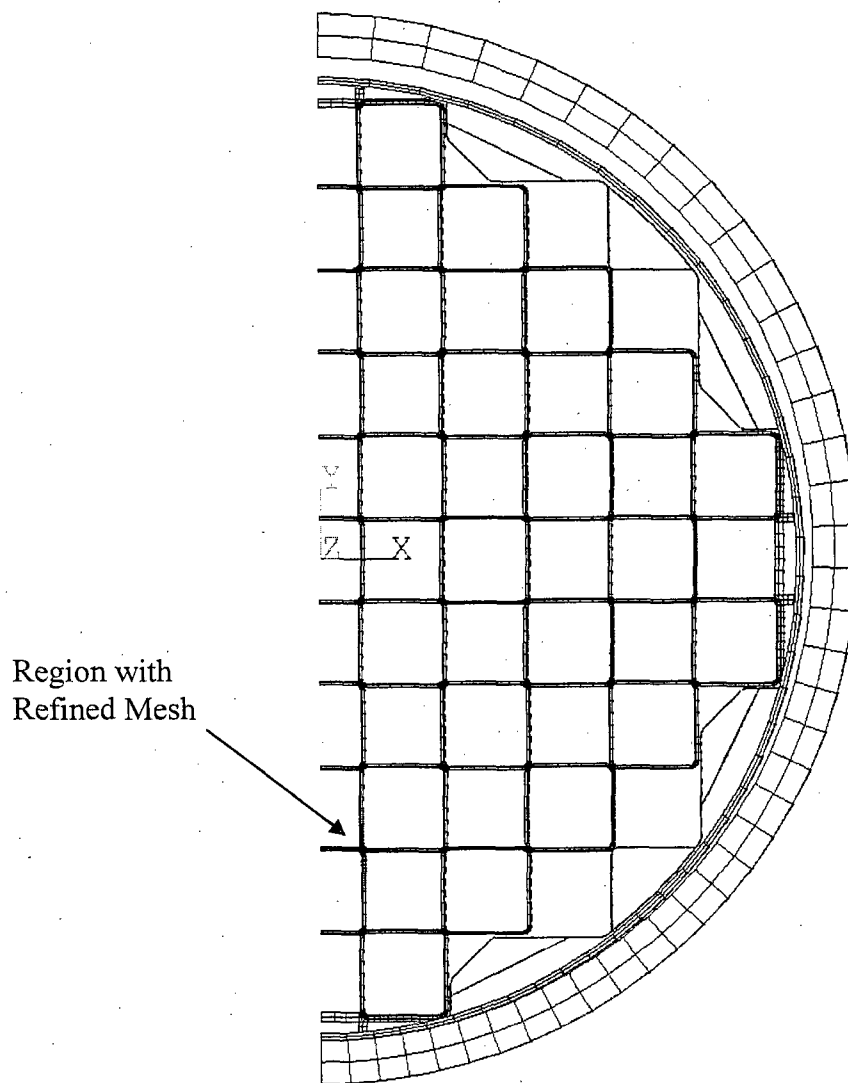
In addition, sensitivity studies are performed for the BWR basket to evaluate the effect of increased acceleration on the response of the basket in terms of stability. Three cases are considered as shown in the following table. The factor is applied to the unfiltered acceleration time history used for the base case of the BWR evaluation.

| Case No. | Factor for the Acceleration Applied to the Model |
|----------|--|
| 1        | 2.0  |
| 2        | 3.0  |
| 3        | 4.0  |

The failure mode is defined as the pin moved out of the fuel tube slot. For Case 1 and Case 2, the analysis results indicate that all pins remain enclosed in the tube slots. At the end of the solution, the pin moved into the inner surface of the fuel tube slot for approximately 0.03 inch and 0.05 inch for Case 1 and Case 2, respectively. This displacement is insignificant compared to the size of the pin and tube slot and does not result in shear failure of the material or the disengagement of the pin and fuel tube slot. However, for Case 3, when the G-load is increased by 4 times, the pin penetrates through the tube wall at the region with minimal thickness. It is observed that bulking in the fuel tube wall is initiated with Case 3 loads. Therefore, it can be concluded that the factor of safety is greater than 3 (factor used for Case 2) for the BWR basket in terms of shear failure in the pin-slot connections. A similar factor of safety is expected for the PWR basket because the shear forces at the pin-slot connections are similar for the BWR and PWR baskets based on the quasi-static analyses presented in Section 3.7.2.

**Figure 3.10.8-1 BWR Basket Finite Element Model – Location of Pin-Slot Connection with Refined Mesh**

See Figure 3.10.8-2 for details for region with refined mesh.



(Fuel elements not shown for Clarity)

**Figure 3.10.8-2 BWR Basket Finite Element Model – Pin-Slot Connection with Refined Mesh**

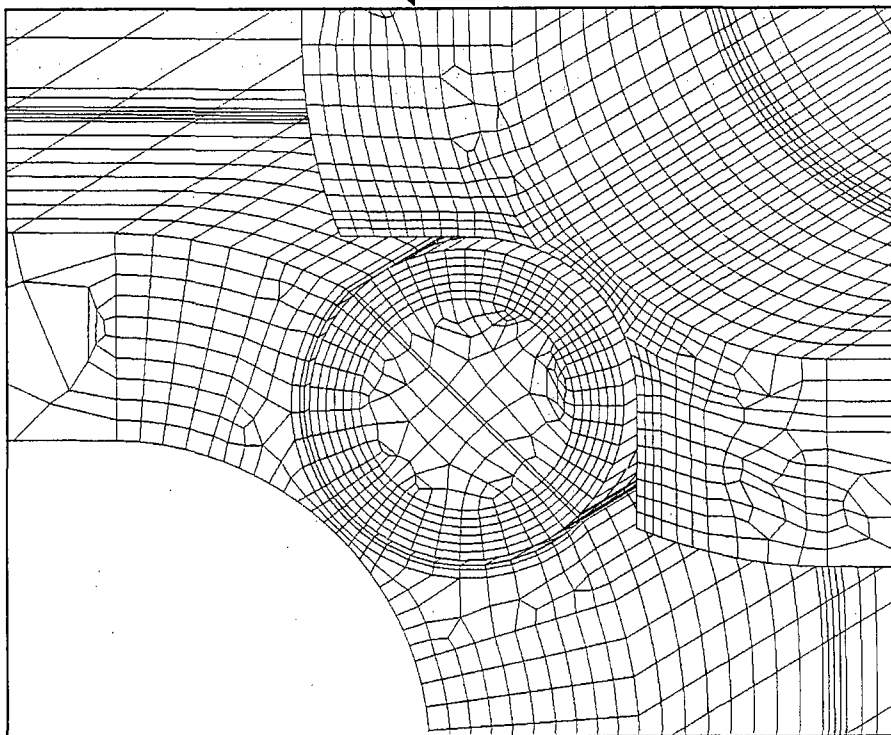
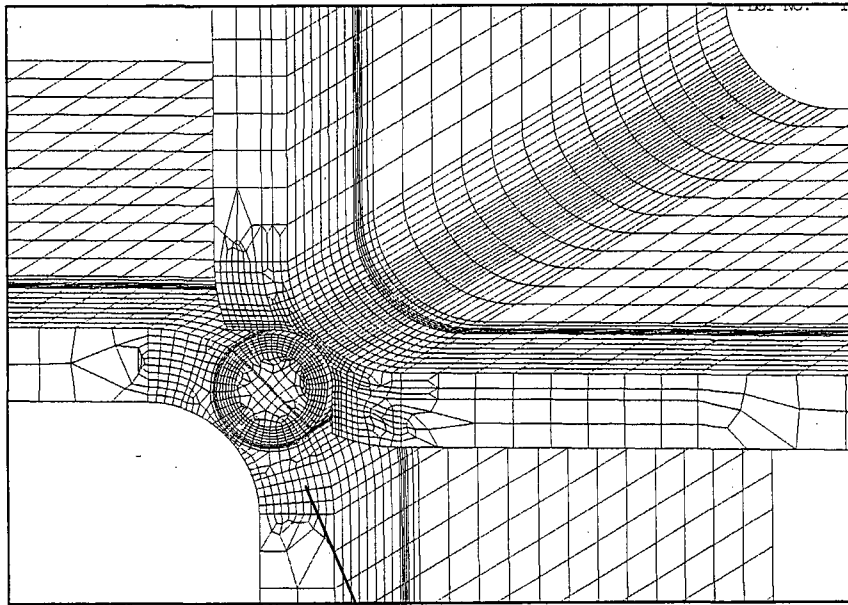
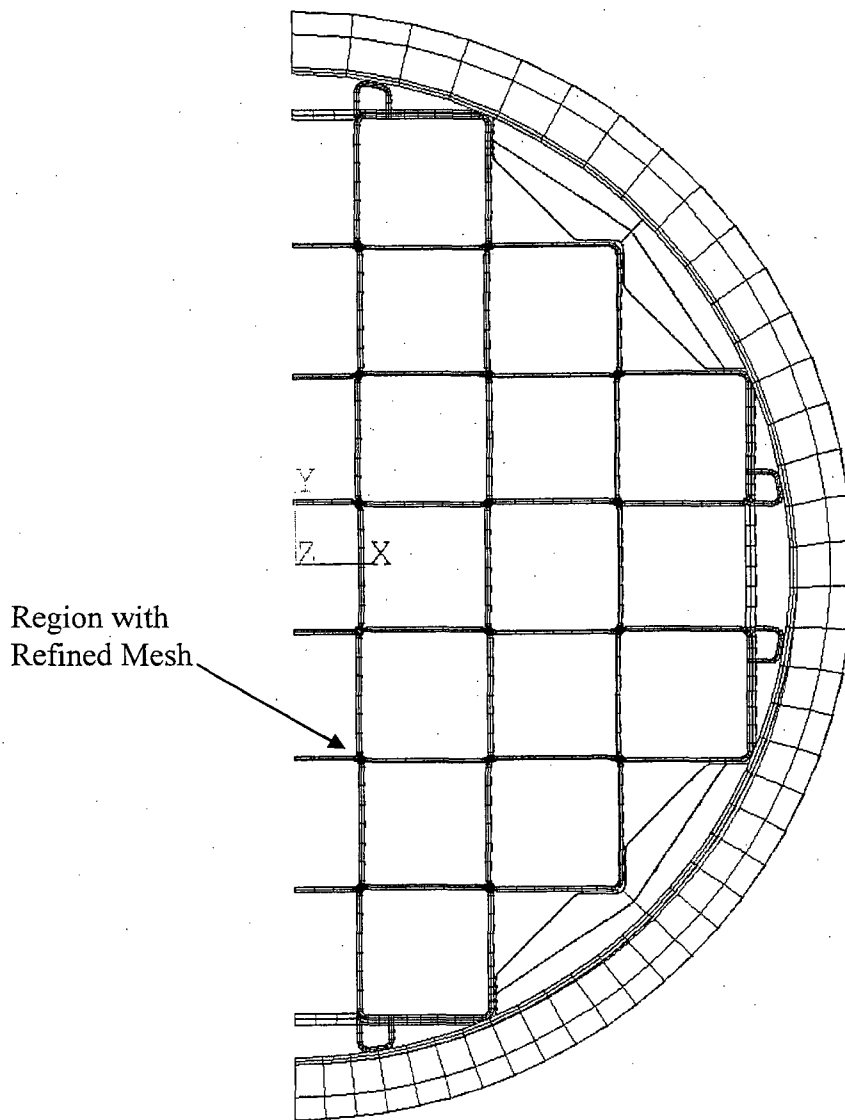


**Figure 3.10.8-3 PWR Basket Finite Element Model – Location of Pin-Slot Connection with Refined Mesh**

See Figure 3.10.8-4 for details for region with refined mesh.



(Fuel elements not shown for Clarity)

**Figure 3.10.8-4 PWR Basket Finite Element Model – Pin-Slot Connection with Refined Mesh**

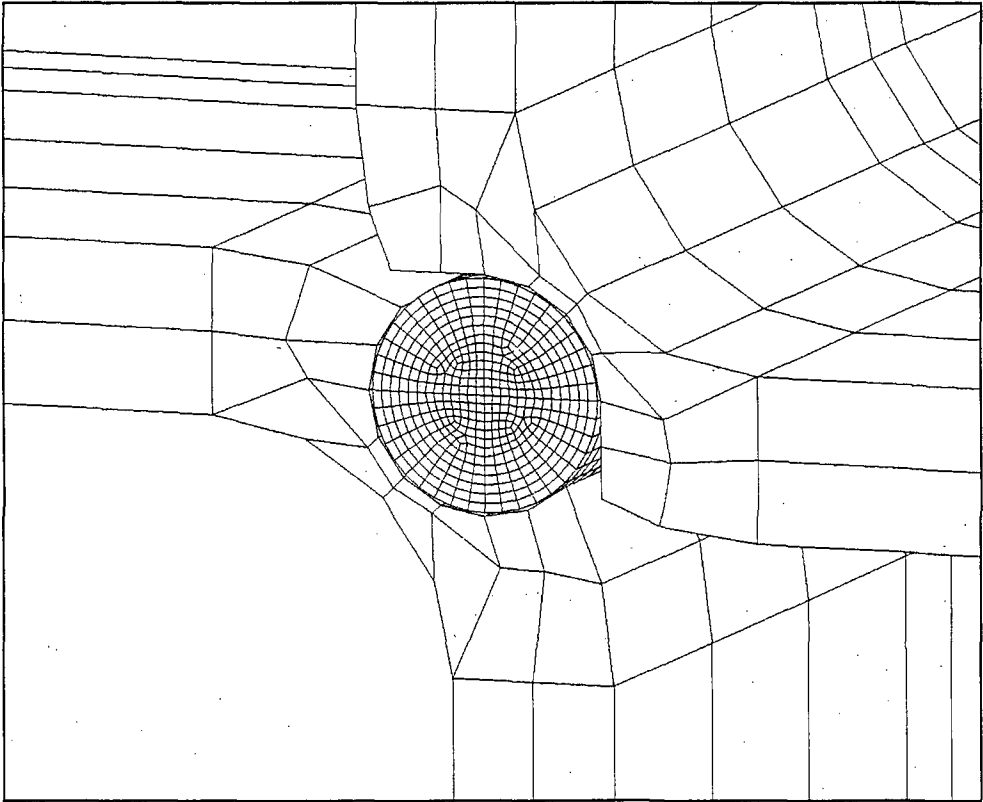
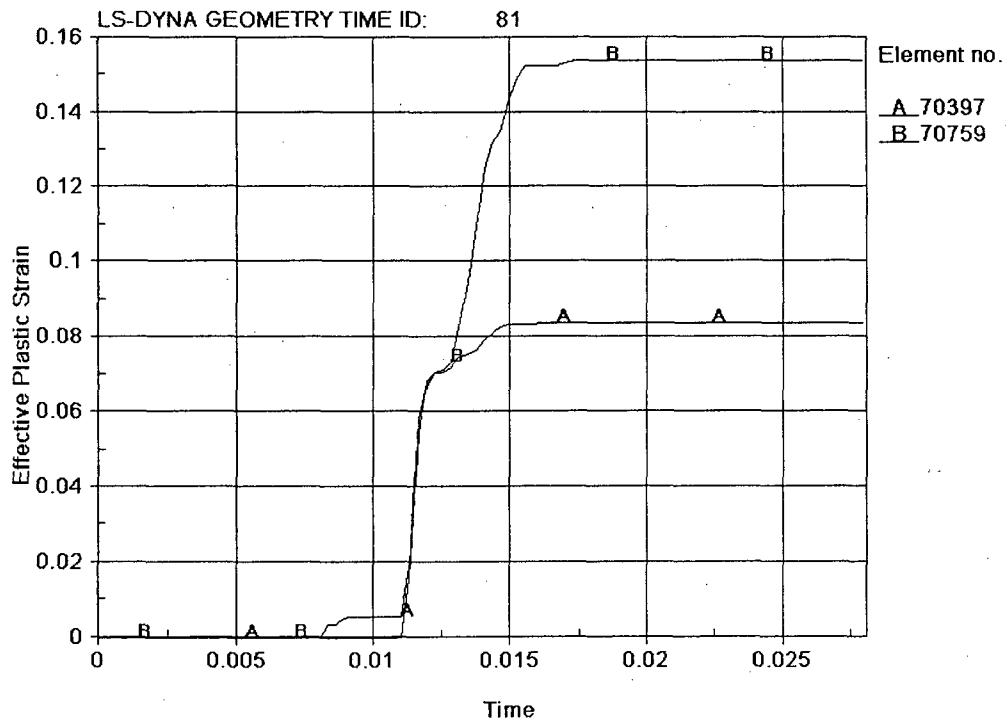
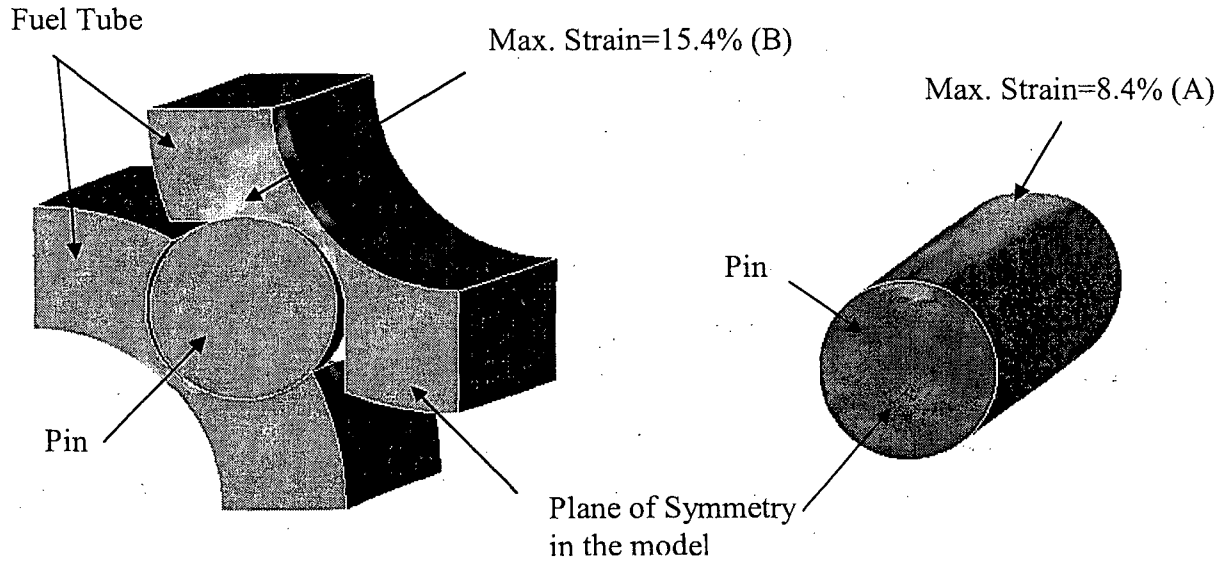


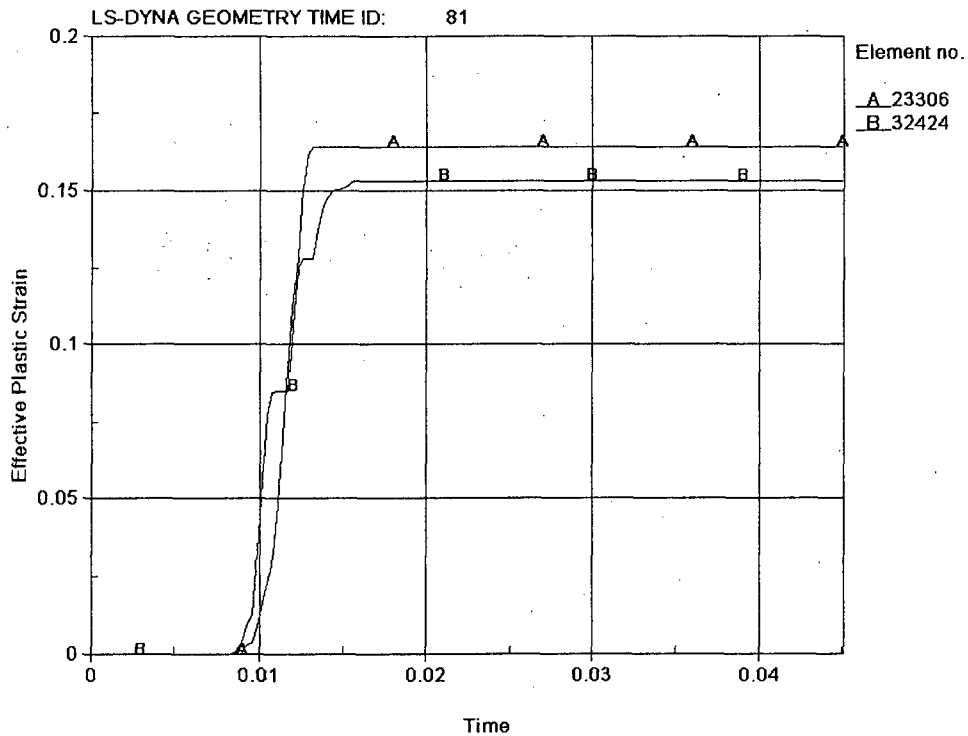
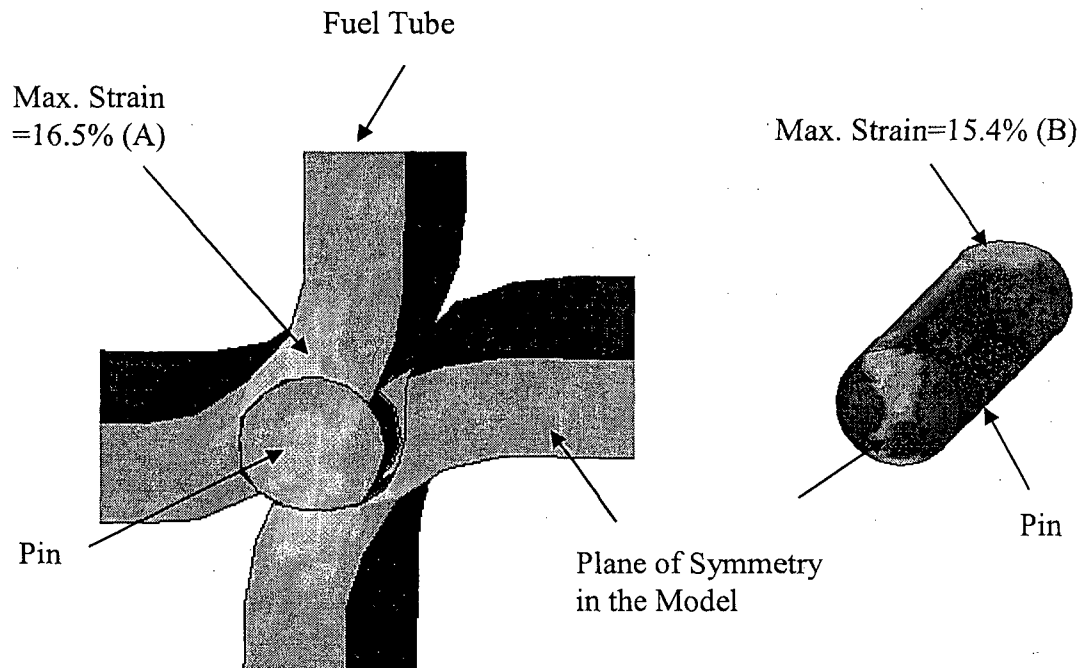
Figure 3.10.8-5 BWR Basket Pin-Slot Connection Plastic Strain – Cask Tip-over Condition



Time History of Plastic Strain at Points A and B



Figure 3.10.8-6 PWR Basket Pin-Slot Connection Plastic Strain



Time History of Plastic Strain at Points A and B  
Strain=15.4% (B)

### 3.10.9 TSC-Basket Finite Element Models

This section describes the TSC-Basket finite element models used to calculate the TSC shell displacements used as the boundary conditions in the LS-DYNA basket stability evaluation (Section 3.10.6). The finite element model includes the details of the basket and canister to account for the interaction between the basket and the canister shell, as well as the effect of the different basket orientations during the side impact of the cask tip-over condition.

To be consistent with the basket stability evaluation presented in Section 3.10.6, the canister shell displacements due to the cask tip-over condition are determined in this Section for six basket orientations, 0°, 18°, 22.5°, 27°, 34° and 45°, for the PWR configuration and three basket orientations, 0°, 22.5° and 45°, for the BWR configuration. Four finite element models are used to determine the canister shell displacements for basket orientations of 0°, 22.5°, 34° and 45° for PWR and three models are used for basket orientations of 0°, 22.5° and 45° for BWR. The shell displacements for the PWR 18° and 27° cases are determined by linear interpolation of the finite element analysis results (e.g., the shell displacements for 18° are determined based on the shell displacements of the 0° and 22.5° cases). Half-symmetry models are used for 0° and 45° cases and full 360° three-dimensional models are used for 22.5° and 34° models. Symmetry boundary conditions are applied at the plane of symmetry for the 0° and 45° models.

The PWR 45° model is shown in Figure 3.10.9-1 and Figure 3.10.9-2. The PWR 22.5° model (canister not shown for clarity) is presented in Figure 3.10.9-3. The BWR 45° and 22.5° models are shown in Figure 3.10.9-4 and Figure 3.10.9-5, respectively. The canister shell, canister lid and bottom plate, basket fuel tubes, and basket side and corner support weldments are modeled explicitly using ANSYS SOLID45 and/or SHELL63 elements. Note that the support weldments are modeled with four pieces axially with a gap of 0.25 inch between the adjacent pieces. This is slightly conservative since it reduces the stiffness of the support weldments in the model and results in slightly larger displacements of the basket and, consequently, slightly larger displacements of the canister shell. The interface between the canister shell and the standoffs at the concrete cask liner is simulated by the CONTAC52 elements, as shown in Figure 3.10.9-1 and Figure 3.10.9-4. A stiffness of  $3.0 \times 10^6$  psi is used for the gap elements representing the stiffness of the standoffs (carbon steel S-beam). A sensitivity study has been performed to assess the effect of the gap stiffness on the canister shell displacements. The sensitivity analysis uses one-half of the gap stiffness for the standoff, and the results indicate an insignificant (0.2%) change of the maximum canister shell displacement. A buckling evaluation was performed, per NUREG/CR-6322 [9], for the standoff at the concrete cask steel liner for the impact load from the canister during the cask tip-over accident. The evaluation results show that the standoff will not buckle with a minimum safety factor of 1.8.

The interface between the canister shell and the basket is modeled using CONTA175 and TARGE170 elements. The CONTA175 elements are 3-D node-to-surface contact elements and are modeled at the basket (support weldment) nodes adjacent to the inner surface of the canister shell. The TARGE170 elements are modeled at the canister shell inner surface, representing the target surface for the CONTA175 elements. CONTAC52 elements are used for the interface between basket components (e.g., surfaces between fuel tubes, between fuel tube and support weldments). The connector pin assemblies at both ends of basket are modeled using COMBIN40 elements, with a gap of 0.03 inch (to allow a maximum relative movement of 0.03 inch in all transverse directions of the basket). The intermediate pin-tube slot connections are located every 20 inches axially. The pins are not modeled explicitly. COMBIN40 elements are also used to represent the pin-tube slot interface, where a relative movement of 0.016 inch is modeled, based on the fabrication tolerance on the gap between fuel tubes. The bolts connecting the support weldments and the fuel tubes are modeled with LINK10 elements. The associated bosses are modeled using COMBIN40 elements with a gap of 0.0625 inch.

Symmetry boundary conditions are applied at the plane of symmetry for the 0° and 45° models. The material properties for the canister and the basket components are identical to those used in the PWR and BWR basket models and the canister model presented in Section 3.10.1 through Section 3.10.3 for the evaluation of the concrete cask tip-over accident.

The model considers a tapered inertia load of 60g at the top of the canister and 1g at the base of the concrete cask. As shown in Figure 3.7.3-3, the peak g-load at top of the canister is 29.5g based on the cask tip-over analysis. Therefore, the applied inertia load to the model includes a load factor of 1.5 and a conservative DLF of 1.36 ( $60 = 29.5 \times 1.5 \times 1.36$ ).

Maximum radial displacements of the canister shell occur at approximately 90 inches from the TSC bottom. The shell displacements at the cross-section with the maximum displacement are shown in Table 3.10.9-1 and Table 3.10.9-2 for PWR and BWR configurations, respectively. The canister shell displacements at 135 inches from the canister bottom are also presented (for sensitivity studies). Figure 3.10.9-6 and Figure 3.10.9-7 show the representative contour plots of the lateral (UZ) displacement of the canister shell for the PWR and BWR configurations, respectively. These displacement contours correspond to the cases with a 45° basket orientation, where the maximum lateral displacement occurs. The canister shell displacements shown in Table 3.10.9-1 and Table 3.10.9-2 are used as the boundary condition for the basket stability evaluation in Section 3.10.6.

Figure 3.10.9-1 PWR Canister-Basket Finite Element Model for Concrete Cask  
Tip-Over Accident – 45° Basket Orientation

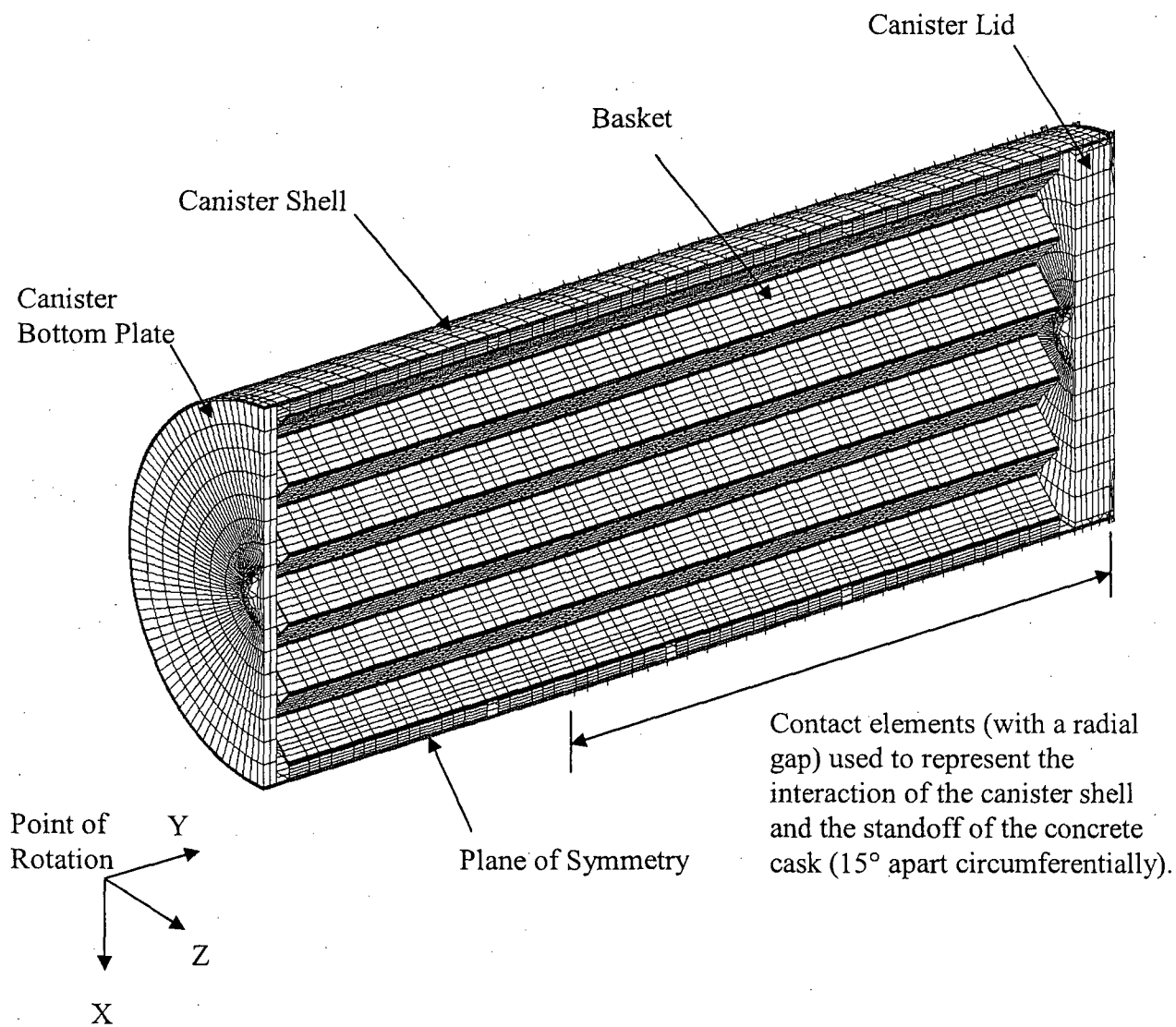
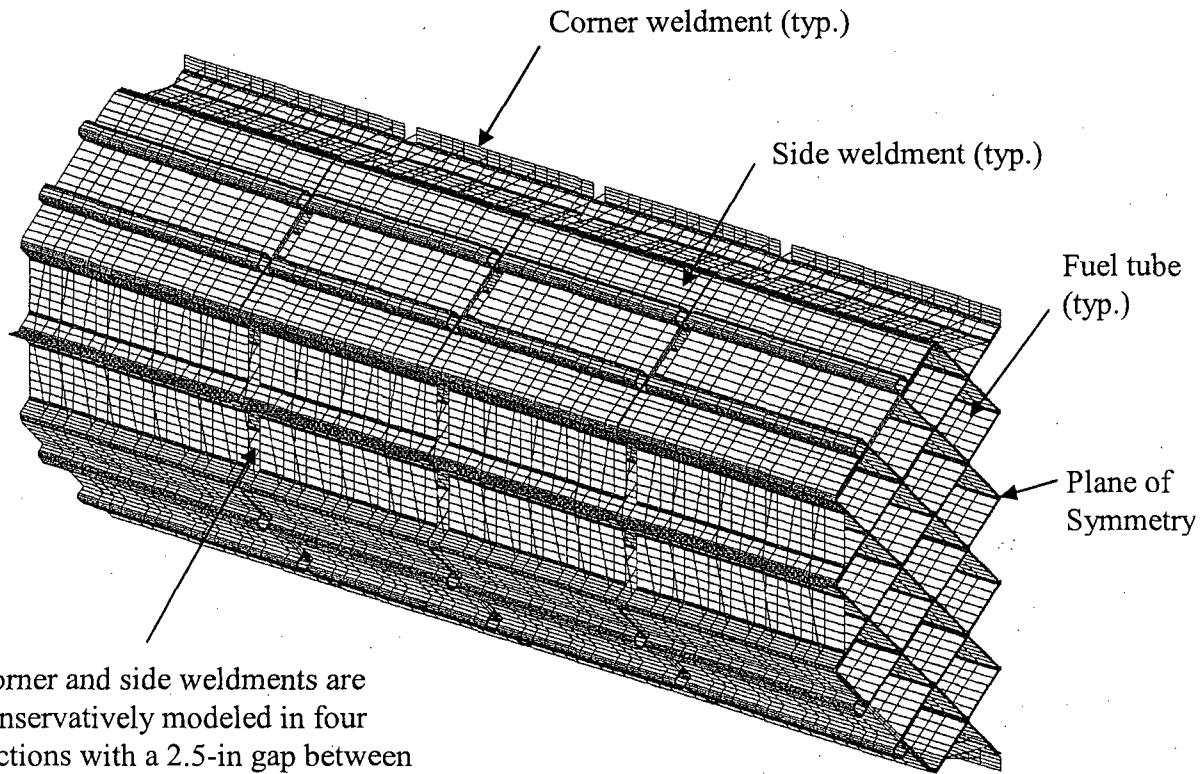


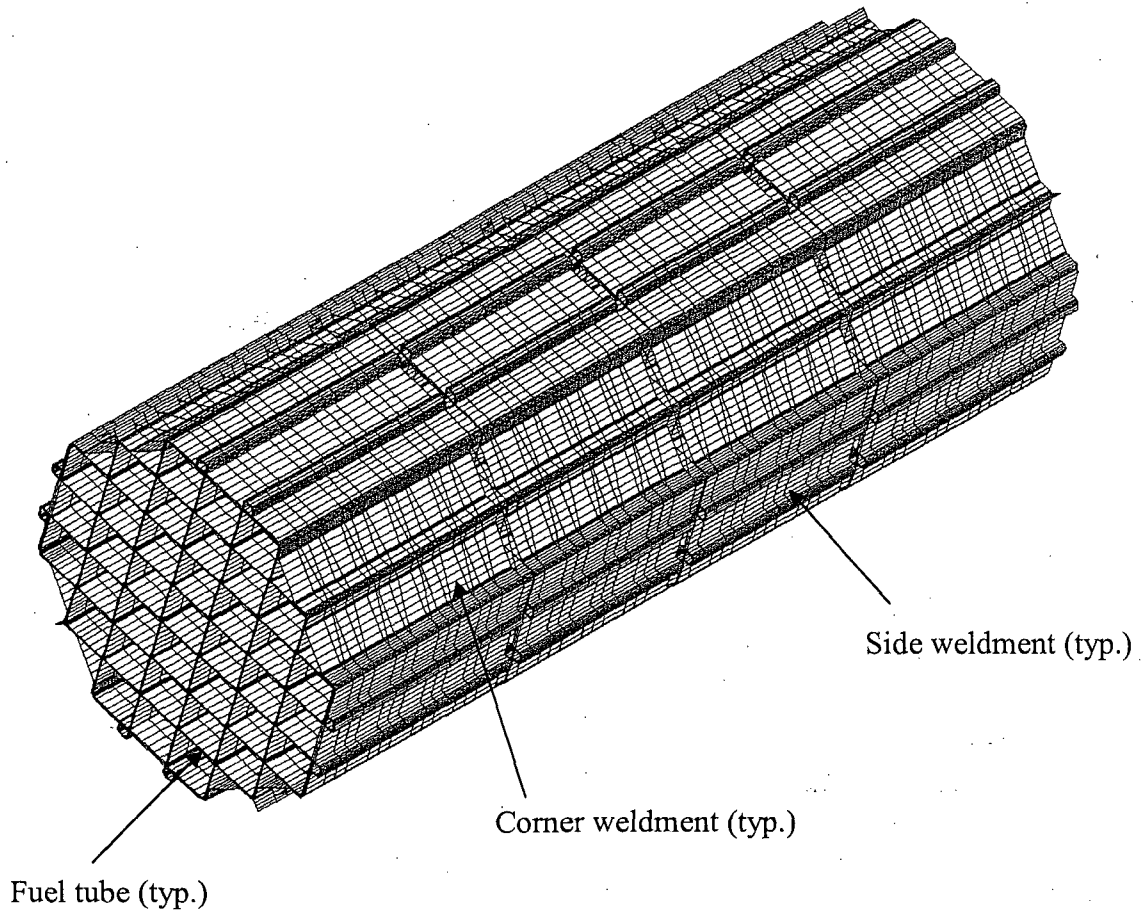
**Figure 3.10.9-2 PWR Canister-Basket Finite Element Model for Concrete Cask  
Tip-Over Accident – Basket Elements - 45° Basket Orientation**



Corner and side weldments are conservatively modeled in four sections with a 2.5-in gap between adjacent sections (typ.).

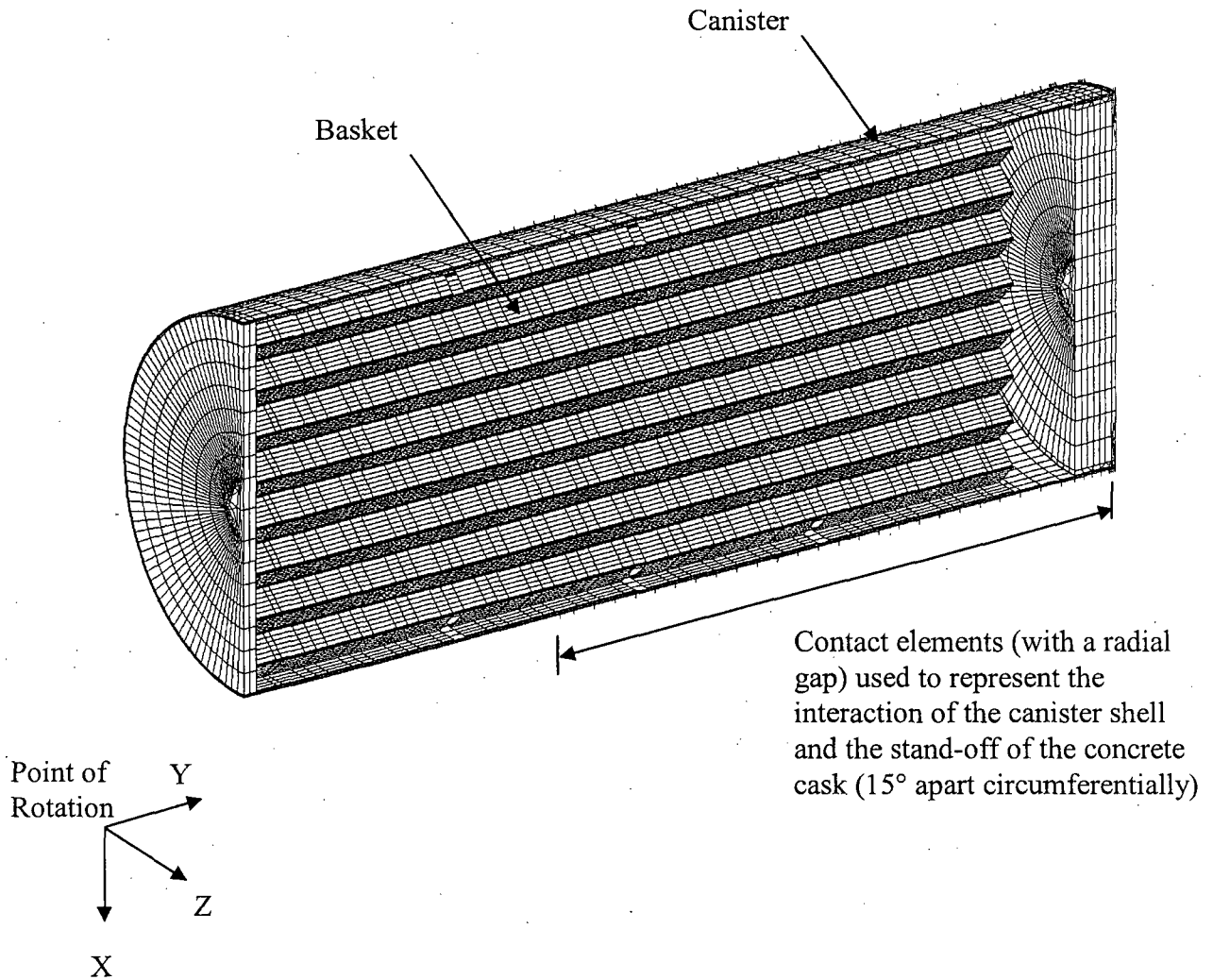
(Canister elements not shown for clarity)

Figure 3.10.9-3 PWR Canister-Basket Finite Element Model for Concrete Cask  
Tip-Over Accident – Basket Elements – 22.5° Basket Orientation

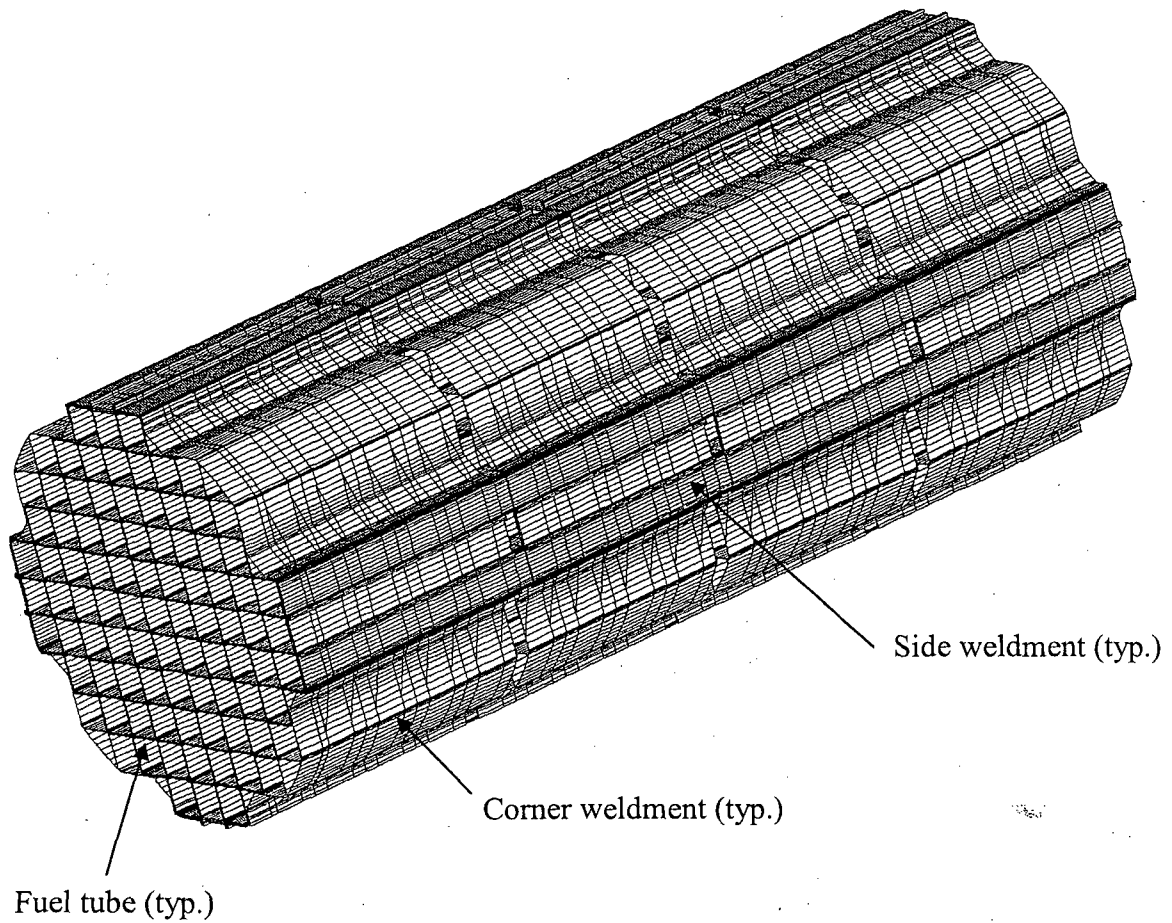


(Canister elements not shown for clarity)

Figure 3.10.9-4 BWR Canister-Basket Finite Element Model for Concrete Cask  
Tip-Over Accident – 45° Basket Orientation



**Figure 3.10.9-5 BWR Canister-Basket Finite Element Model for Concrete Cask  
Tip-Over Accident – Basket Elements – 22.5° Basket Orientation**



(Canister elements not shown for clarity)



Figure 3.10.9-6 PWR Canister Shell Lateral Displacement Contour –  
45° Basket Orientation

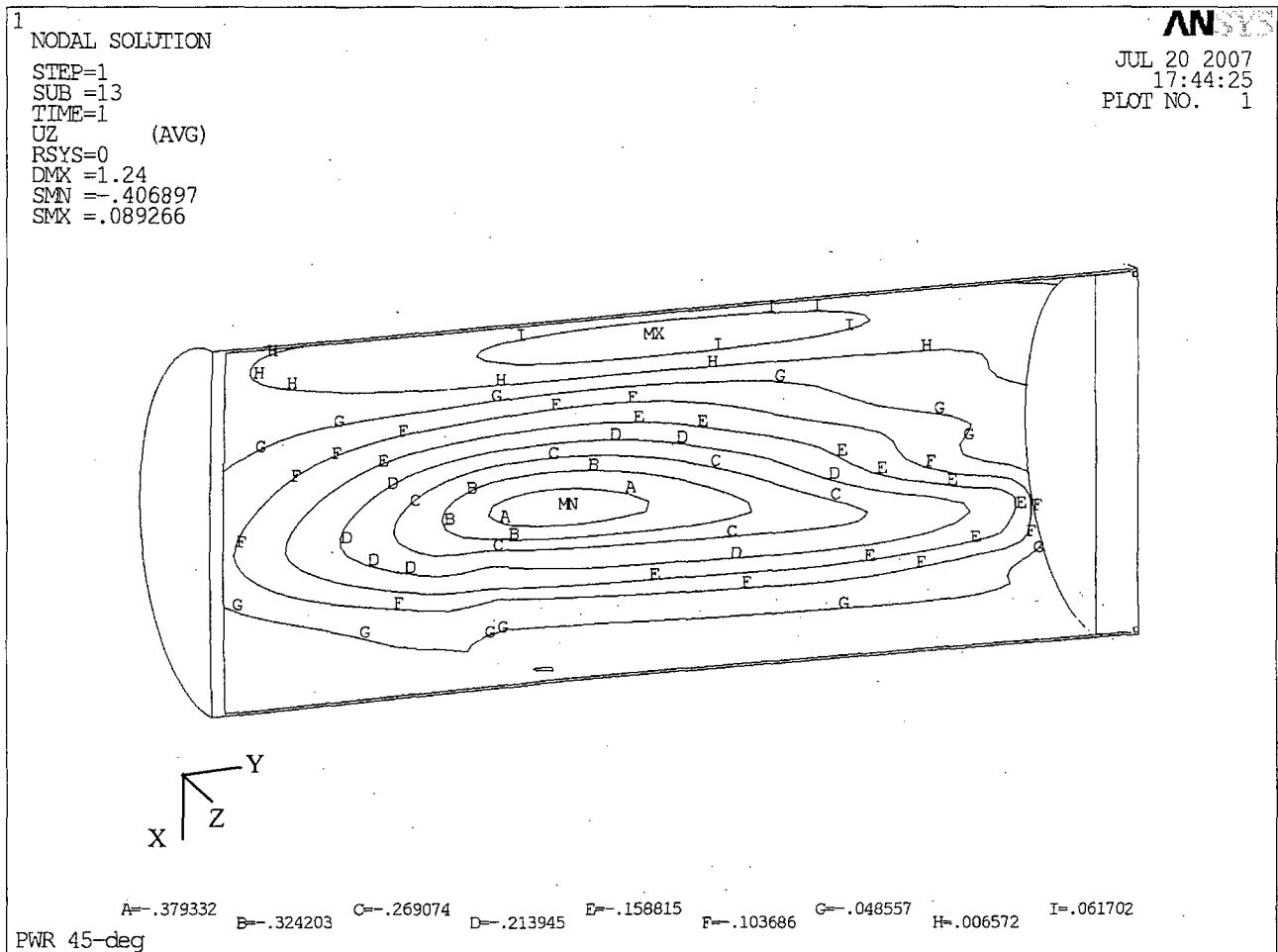
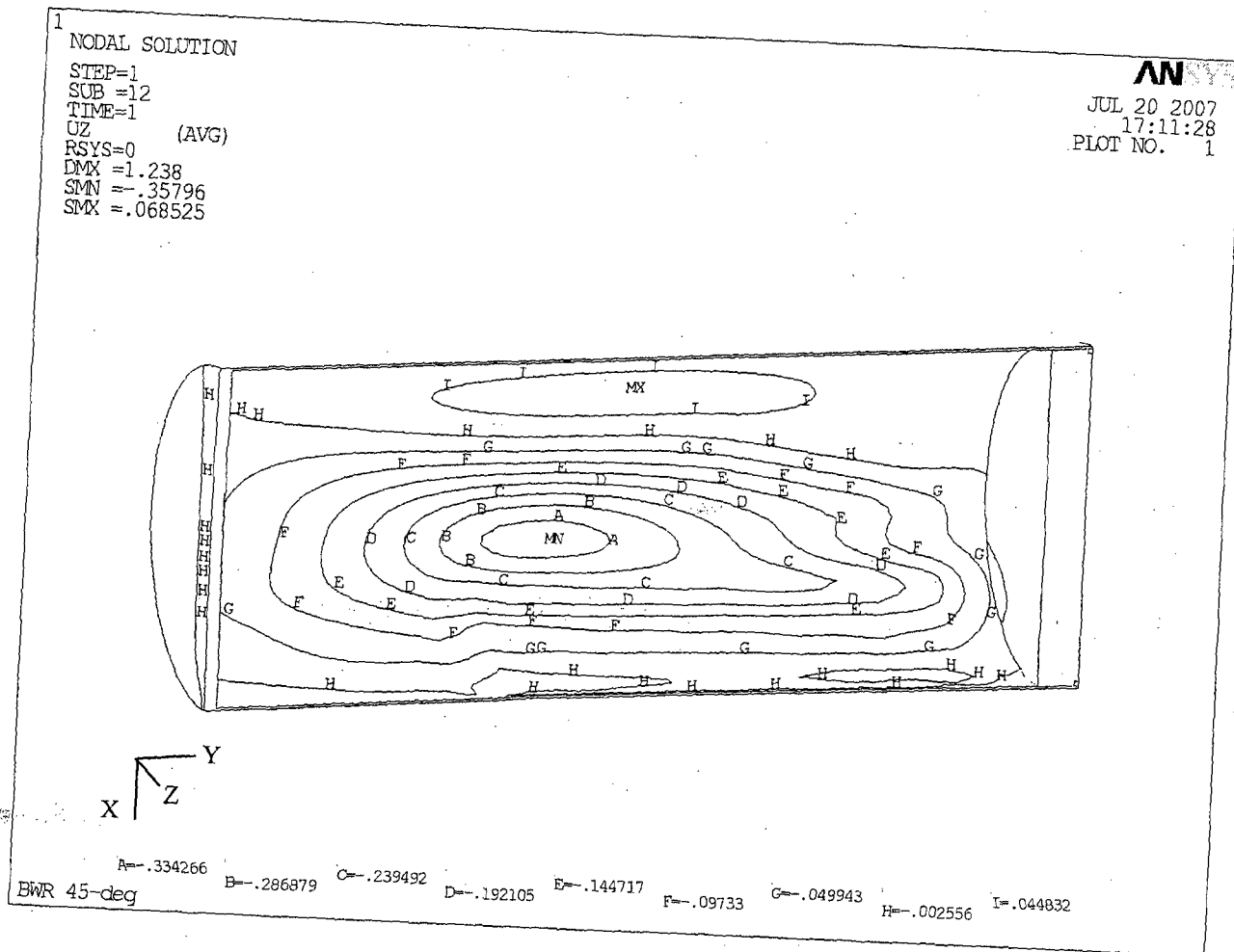


Figure 3.10.9-7 BWR Canister Shell Lateral Displacement Contour -  
45° Basket Orientation



**Table 3.10.9-1 Canister Shell Displacements Used as Boundary Conditions for the LS-DYNA Models for PWR Basket Stability Evaluation**

**Canister Shell Radial Displacement (inch)**

| Basket Orientation<br>Angle | 0°     | 18°    | 22.5°  | 27°    | 34°    | 45°    | 22.5°<br>(135 in) |
|-----------------------------|--------|--------|--------|--------|--------|--------|-------------------|
| 0°                          | 0.000  | 0.000  | 0.000  | 0.000  | 0.000  | 0.000  | 0.000             |
| 15°                         | 0.029  | 0.011  | 0.007  | 0.019  | 0.038  | 0.024  | 0.003             |
| 30°                         | 0.096  | 0.035  | 0.020  | 0.062  | 0.127  | 0.100  | 0.020             |
| 45°                         | 0.206  | 0.186  | 0.180  | 0.196  | 0.219  | 0.211  | 0.194             |
| 60°                         | 0.368  | 0.318  | 0.300  | 0.328  | 0.371  | 0.362  | 0.258             |
| 75°                         | 0.292  | 0.372  | 0.394  | 0.423  | 0.480  | 0.507  | 0.275             |
| 90°                         | 0.091  | 0.239  | 0.274  | 0.269  | 0.258  | 0.286  | 0.217             |
| 105°                        | -0.105 | -0.019 | 0.000  | -0.009 | -0.027 | 0.021  | -0.016            |
| 120°                        | -0.216 | -0.217 | -0.218 | -0.209 | -0.198 | -0.236 | -0.186            |
| 135°                        | -0.242 | -0.283 | -0.295 | -0.311 | -0.339 | -0.414 | -0.232            |
| 180°                        | -0.174 | -0.144 | -0.137 | -0.186 | -0.262 | -0.280 | -0.156            |
| 225°                        | -0.242 | -0.233 | -0.230 | -0.255 | -0.293 | -0.414 | -0.128            |
| 240°                        | -0.216 | -0.205 | -0.200 | -0.219 | -0.247 | -0.236 | -0.130            |
| 255°                        | -0.105 | -0.087 | -0.080 | -0.073 | -0.058 | 0.021  | -0.073            |
| 270°                        | 0.091  | 0.114  | 0.121  | 0.148  | 0.193  | 0.286  | 0.034             |
| 285°                        | 0.292  | 0.293  | 0.295  | 0.318  | 0.356  | 0.507  | 0.140             |
| 300°                        | 0.368  | 0.304  | 0.284  | 0.322  | 0.381  | 0.362  | 0.211             |
| 315°                        | 0.206  | 0.245  | 0.255  | 0.232  | 0.197  | 0.211  | 0.249             |
| 330°                        | 0.096  | 0.099  | 0.100  | 0.084  | 0.058  | 0.100  | 0.084             |
| 345°                        | 0.029  | 0.010  | 0.006  | 0.005  | 0.004  | 0.024  | 0.013             |

Note: Radial displacements are reported at the canister shell section where the maximum displacement occurs, except the last column, which corresponds to shell displacements at 135 inches from the canister bottom for a sensitivity study.

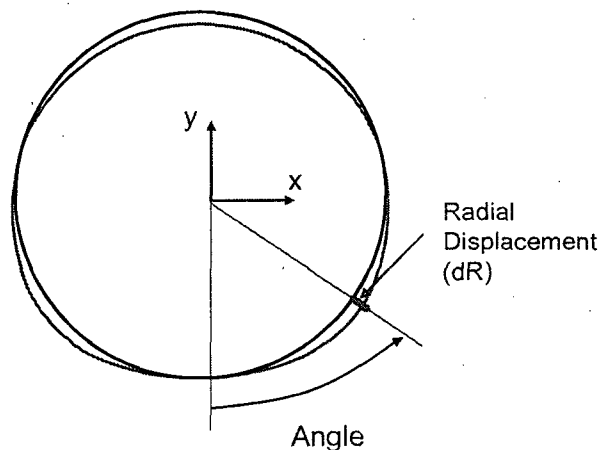
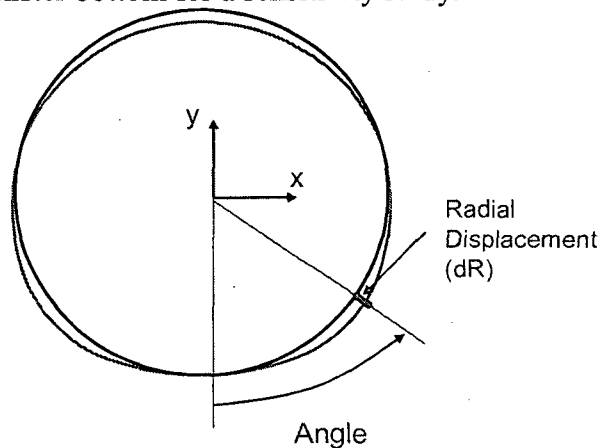


**Table 3.10.9-2 Canister Shell Displacements Used as Boundary Conditions for the LS-DYNA Models for BWR Basket Stability Evaluation**

**Canister Shell Radial Displacement (inch)**

| Basket Orientation<br>Angle | 0°     | 22.5°  | 45°    | 22.5°<br>(135-in) |
|-----------------------------|--------|--------|--------|-------------------|
| 0°                          | 0.000  | 0.000  | 0.000  | 0.000             |
| 15°                         | 0.025  | 0.066  | 0.024  | 0.078             |
| 30°                         | 0.093  | 0.095  | 0.098  | 0.087             |
| 45°                         | 0.202  | 0.205  | 0.213  | 0.171             |
| 60°                         | 0.342  | 0.366  | 0.361  | 0.349             |
| 75°                         | 0.372  | 0.444  | 0.440  | 0.352             |
| 90°                         | 0.126  | 0.279  | 0.261  | 0.174             |
| 105°                        | -0.084 | 0.052  | -0.029 | -0.032            |
| 120°                        | -0.217 | -0.298 | -0.245 | -0.251            |
| 135°                        | -0.260 | -0.372 | -0.356 | -0.256            |
| 180°                        | -0.195 | -0.224 | -0.276 | -0.154            |
| 225°                        | -0.260 | -0.320 | -0.356 | -0.201            |
| 240°                        | -0.217 | -0.285 | -0.245 | -0.190            |
| 255°                        | -0.084 | -0.130 | -0.029 | -0.118            |
| 270°                        | 0.126  | 0.142  | 0.261  | 0.027             |
| 285°                        | 0.372  | 0.396  | 0.440  | 0.228             |
| 300°                        | 0.342  | 0.418  | 0.361  | 0.357             |
| 315°                        | 0.202  | 0.217  | 0.213  | 0.215             |
| 330°                        | 0.093  | 0.152  | 0.098  | 0.159             |
| 345°                        | 0.029  | 0.076  | 0.024  | 0.084             |

Note: Radial displacements are reported at the canister shell section where the maximum displacement occurs, except the last column, which corresponds to shell displacements at 135-in from canister bottom for a sensitivity study.



## Chapter 4 Thermal Evaluation

### Table of Contents

|       |   |         |
|-------|---|---------|
| 4     | THERMAL EVALUATION .....  | 4-1     |
| 4.1   | Discussion .....  | 4.1-1   |
| 4.2   | Thermal Properties of Materials .....   | 4.2-1   |
| 4.3   | Technical Specifications for Components .....   | 4.3-1   |
| 4.4   | Normal Storage Conditions.....  | 4.4-1   |
| 4.4.1 | Thermal Analysis Models .....   | 4.4-1   |
| 4.4.2 | Test Model .....  | 4.4-24  |
| 4.4.3 | Maximum Temperatures for PWR and BWR Fuel Configurations.....   | 4.4-25  |
| 4.4.4 | Maximum Internal Pressures for PWR and BWR TSCs .....   | 4.4-28  |
| 4.5   | Off-Normal Storage Events .....   | 4.5-1   |
| 4.6   | Accident Events .....   | 4.6-1   |
| 4.6.1 | Analysis of Maximum Anticipated Ambient Heat Load .....   | 4.6-1   |
| 4.6.2 | Fire Accident.....  | 4.6-1   |
| 4.6.3 | Full Blockage of Concrete Cask Air Inlets.....  | 4.6-3   |
| 4.6.4 | Maximum TSC Internal Pressure for Accident Events.....  | 4.6-3   |
| 4.7   | References.....   | 4.7-1   |
| 4.8   | Thermal Evaluation Detail.....  | 4.8-1   |
| 4.8.1 | Benchmark of the Two-Dimensional Axisymmetric Methodology for TSC<br>Thermal Analyses For MAGNASTOR .....                               | 4.8.1-1 |
| 4.8.2 | Methodology to Compute the Porous Media Constants .....   | 4.8.2-1 |
| 4.8.3 | Benchmark Evaluation of the Two-Dimensional Axisymmetric<br>Methodology for Annular Cooling in the Concrete Cask for<br>MAGNASTOR ..... | 4.8.3-1 |

## List of Figures

|               |  |          |
|---------------|--|----------|
| Figure 4.1-1  | Definition of the Preferential Loading Pattern for PWR Fuel .....  | 4.1-4    |
| Figure 4.4-1  | Two-Dimensional Model of Concrete Cask Loaded with PWR TSC .....   | 4.4-32   |
| Figure 4.4-2  | Computational Mesh for the Two-Dimensional Axisymmetric CFD<br>Model of the Concrete Cask .....                | 4.4-33   |
| Figure 4.4-3  | Axial Power Distribution for the PWR Fuel Assembly .....   | 4.4-34   |
| Figure 4.4-4  | Axial Power Distribution for the BWR Fuel Assembly .....   | 4.4-35   |
| Figure 4.4-5  | PWR Peak Fuel Cladding Temperature versus TSC Internal Pressure .....  | 4.4-36   |
| Figure 4.4-6  | Two-Dimensional Finite Element Model of the PWR Fuel Basket .....  | 4.4-37   |
| Figure 4.4-7  | Two-Dimensional Finite Element Model of the BWR Fuel Basket .....  | 4.4-38   |
| Figure 4.4-8  | 14×14 PWR Fuel Assembly Two-Dimensional Model .....  | 4.4-39   |
| Figure 4.4-9  | 10×10 BWR Fuel Assembly Two-Dimensional Model .....  | 4.4-40   |
| Figure 4.4-10 | Neutron Absorber Model for PWR Fuel Tube .....   | 4.4-41   |
| Figure 4.4-11 | BWR Fuel Tube Configuration with Channel and Neutron Absorber .....  | 4.4-42   |
| Figure 4.4-12 | BWR Fuel Tube Configuration with Channel, but without the Neutron<br>Absorber .....                            | 4.4-43   |
| Figure 4.4-13 | Two-Dimensional Model of Transfer Cask Loaded with a PWR TSC .....   | 4.4-44   |
| Figure 4.4-14 | Temperature (°F) Distribution for the Concrete Cask and TSC Containing a<br>Design Basis PWR Heat Load .....   | 4.4-45   |
| Figure 4.4-15 | Air Velocity (m/s) in the Concrete Cask Annulus for the Design Basis<br>PWR Heat Load .....                    | 4.4-46   |
| Figure 4.4-16 | Three-Dimensional ANSYS Model of the PWR Canister for Vacuum<br>Drying Condition .....                         | 4.4-47   |
| Figure 4.4-17 | Detailed View of the Three-Dimensional ANSYS Model of the PWR<br>Canister for Vacuum Drying Condition .....    | 4.4-48   |
| Figure 4.4-18 | Three-Dimensional ANSYS Model of the BWR Canister for TFR Vacuum<br>Drying Analyses .....                      | 4.4-49   |
| Figure 4.4-19 | Detailed View of the Three-Dimensional ANSYS Model of the BWR<br>Canister for TFR Vacuum Drying Analyses ..... | 4.4-50   |
| Figure 4.8-1  | Two-Dimensional Model of the 24 PWR Assembly Thermal Test<br>Configuration .....                               | 4.8.1-7  |
| Figure 4.8-2  | ANSYS Model for Determination of the Benchmark Basket Thermal<br>Properties .....                              | 4.8.1-8  |
| Figure 4.8-3  | Temperature Profile from the Benchmark Cask Cavity Inner Surface .....   | 4.8.1-9  |
| Figure 4.8-4  | Axial Power Distribution Curve for the 15×15 PWR Fuel Assembly .....   | 4.8.1-9  |
| Figure 4.8-5  | Temperature Contours for the Benchmark Cask Thermal Test .....   | 4.8.1-10 |
| Figure 4.8-6  | Cross-Sectional View of the Three-Dimensional Fluent Model of a<br>17×17 PWR Fuel Assembly .....               | 4.8.2-5  |
| Figure 4.8-7  | Three-Dimensional FLUENT Model of a Fuel Assembly Grid .....   | 4.8.2-6  |
| Figure 4.8-8  | Three-Dimensional FLUENT Quarter-Symmetry Model for the Flow<br>Around the Grid .....                          | 4.8.2-7  |
| Figure 4.8-9  | Cross-Sectional View of the Three-Dimensional FLUENT Model of a<br>10×10 BWR Fuel Assembly .....               | 4.8.2-8  |

**List of Figures (cont'd)**

Figure 4.8-10 Two-Dimensional Axisymmetric FLUENT Model of the VSC-17 ..... 4.8.3-6  
Figure 4.8-11 ANSYS Model for Effective Properties Calculation ..... 4.8.3-7  
Figure 4.8-12 Temperature Profiles for the Canister Surface ..... 4.8.3-8  
Figure 4.8-13 Temperature Profiles for the Concrete Liner Surface ..... 4.8.3-9

List of Tables

|              |   |        |
|--------------|---|--------|
| Table 4.1-1  | Summary of Thermal Design Conditions for Storage for the MAGNASTOR.....   | 4.1-5  |
| Table 4.1-2  | Maximum Allowable Material Temperatures.....  | 4.1-6  |
| Table 4.4-1  | Effective Thermal Conductivities for 14×14 PWR Fuel Assemblies for Helium Backfill.....   | 4.4-51 |
| Table 4.4-2  | Effective Thermal Conductivities for 10×10 BWR Fuel Assemblies for Helium Backfill.....   | 4.4-51 |
| Table 4.4-3  | Maximum Component Temperatures for Normal Condition Storage of Design Basis PWR and BWR Heat Loads.....   | 4.4-52 |
| Table 4.4-4  | Helium Mass Per Unit Volume for MAGNASTOR TSCs.....   | 4.4-52 |
| Table 4.4-5  | Maximum Fuel Temperature for Water Phase – PWR  |        |
| Table 4.4-6  | Maximum Fuel Temperature for Water Phase – BWR .....  | 4.4-53 |
| Table 4.4-7  | Maximum Fuel Temperature for Helium Phase – PWR.....  | 4.4-54 |
| Table 4.4-8  | Maximum Fuel Temperature for Helium Phase – BWR .....   | 4.4-54 |
| Table 4.4-9  | Durations and the Temperature at the End of the Duration for the First Vacuum Stage (PWR).....  | 4.4-55 |
| Table 4.4-10 | Durations and the Temperature at the End of the Duration for the First Vacuum Stage (BWR) .....   | 4.4-55 |
| Table 4.4-11 | Durations and the Temperature at the End of the Duration for the Second Vacuum Stage (PWR).....   | 4.4-56 |
| Table 4.4-12 | Durations and the Temperature at the End of the Duration for the Second Vacuum Stage (BWR) .....  | 4.4-56 |
| Table 4.4-13 | TFR to Concrete Cask (PWR) Transfer Times and Temperatures .....  | 4.4-57 |
| Table 4.4-14 | TFR to Concrete Cask (BWR) Transfer Times and Temperatures.....   | 4.4-57 |
| Table 4.4-15 | Durations Allowed and the Maximum PWR Fuel Clad Temperatures for the Operation Using Reduced Vacuum Times, Reduced Cooling Time and Eight Hours of Handling ..... | 4.4-58 |
| Table 4.4-16 | Durations Allowed and the Maximum BWR Fuel Clad Temperatures for the Operation Using Reduced Vacuum Times, Reduced Cooling Time and Eight Hours of Handling.....  | 4.4-59 |



## 4 THERMAL EVALUATION

This section presents the thermal design and analyses of MAGNASTOR<sup>®</sup> for normal conditions and off-normal and accident events of storage. Results of the analyses demonstrate that with the design basis contents, MAGNASTOR meets the thermal performance requirements of 10 CFR 72 [1], NUREG-1567 [20], and NUREG-1536 [22].

#### 4.1 Discussion

MAGNASTOR consists of a TSC, concrete cask, and a transfer cask. In long-term storage, the fuel is loaded in a basket structure positioned within the TSC. The TSC is placed in the concrete cask, which provides passive radiation shielding, structural protection and natural convection cooling. The transfer cask is used to handle the TSC. The thermal performance of the concrete cask containing a loaded TSC with design basis fuel, and the performance of the transfer cask containing a loaded TSC with design basis fuel are evaluated in this chapter.

The thermal evaluation considers normal conditions and off-normal and accident events of storage. Each of these conditions can be described in terms of the environmental temperature, use of solar insolation, and the condition of the air inlets as shown in Table 4.1-1. The evaluation of the different phases of the transfer operation is accomplished by altering the properties of the medium in the canister to correspond to water or helium.

In order for the heat from the stored spent fuel assemblies to be rejected to the ambient via the concrete cask or the transfer cask, the decay heat from the spent fuel assemblies is transferred to the TSC surface. The MAGNASTOR baskets for the PWR and the BWR fuel assemblies use all three heat transfer modes—radiation, conduction and convection—to transfer the heat to the TSC surface. The basket design enhances convection heat transfer. Helium is used as the backfill gas in the TSC because its thermal conductivity is better than other allowable backfill gases. The basket is comprised of full-length carbon steel tubes that provide a significant path for conduction heat transfer. Radiation is a significant mode of heat transfer in the fuel region and between the outer surface of the basket and the TSC shell.

The significant thermal design feature of the concrete cask is the passive convective airflow around the outside of the TSC. Cool (ambient) air enters at the bottom of the concrete cask through four air inlets. Heated air exits through the four air outlets in the upper concrete cask body. Radiant heat transfer occurs from the TSC shell to the concrete cask liner, which then transmits heat to the annular airflow. Conduction through the concrete cask, although not significant, is included in the analytical model. Natural circulation of air through the concrete cask annulus, in conjunction with radiation from the TSC surface, maintains the fuel cladding temperature and all component temperatures below their design limits.

The MAGNASTOR design basis heat load is 35.5 kW for 37 PWR fuel assemblies. The PWR fuel basket can accommodate a uniform heat load of 959 W per assembly, or a preferential loading pattern as shown in Figure 4.1-1. The preferential loading pattern identified in Figure 4.1-1 defines three values of heat generation that place the fuel assemblies with the maximum

heat generation rate in an intermediate region of fuel storage locations. Analyses are performed using the two-dimensional axisymmetric model with the same fluid resistances and material properties for both the preferential and uniform loading patterns. Calculated maximum fuel temperature is the same for both loading configurations. The maximum temperatures at the radial location of the center of a preferential loaded fuel assembly with the 1.2 kW heat load is determined to be 689°F. At this same radial location, the calculated temperature for the uniform heat load is 684°F. This small increase is a localized bounding temperature response due to the localized increased heat generation for the preferential loading configuration.

The identical maximum fuel cladding temperature calculated for both loading configurations, resulting from identical total heat and small differences in inner region heat (4%), demonstrates efficiencies in the alternate PWR preferential loading configuration. Placement of the highest heat load for the preferential loading configuration in an intermediate radial location balances system performance. The thermal loading basis for the PWR analyses in this chapter uses the preferential loading since it represents the system loading with maximum heat concentration. The BWR fuel basket can accommodate 87 fuel assemblies with a uniform design basis total heat load of 33 kW, or 379 watts, per assembly.

The thermal evaluation applied different component temperature limits and allowable stress limits for long-term conditions versus short-term conditions. Normal storage operation is considered to be a long-term condition. Off-normal and accident events are considered to be short-term conditions. Thermal evaluations are performed for the design basis PWR and BWR fuels for all design conditions. The maximum allowable material temperatures for long-term and short-term conditions are provided in Table 4.1-2.

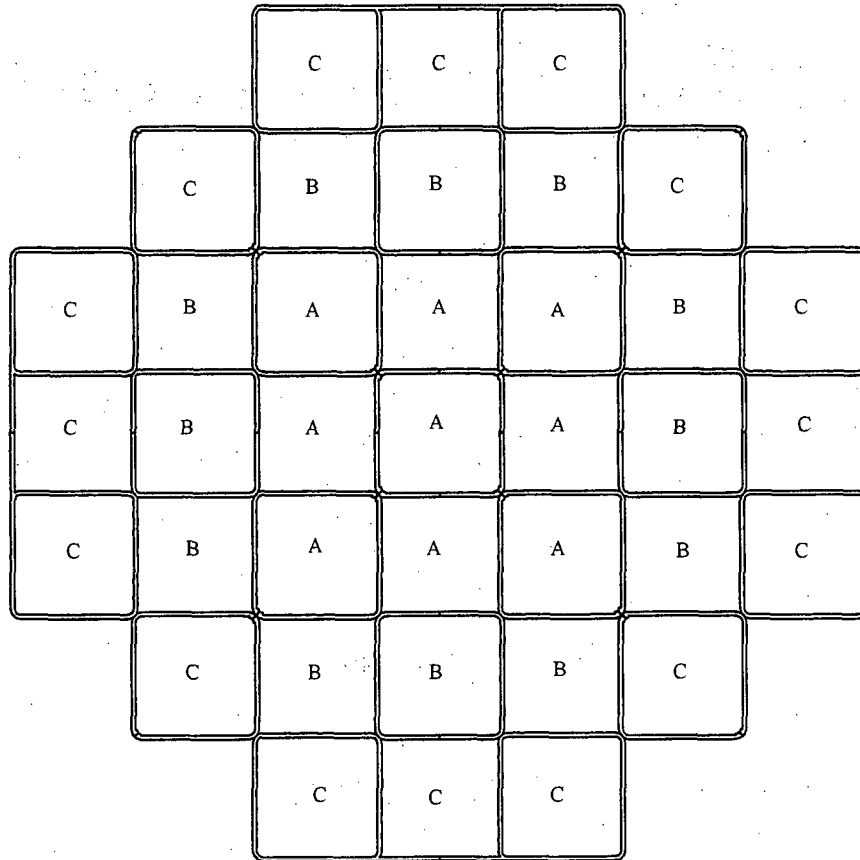
During normal conditions of storage and off-normal and accident events, the concrete cask must reject the decay heat from the TSC to the environment without exceeding the system components temperature limits. In addition, to ensure fuel rod integrity for normal conditions of storage, the spent fuel must be maintained at a sufficiently low temperature in an inert atmosphere to preclude thermally induced fuel rod cladding deterioration. To preclude fuel degradation, the maximum cladding temperature under normal conditions of storage and canister transfer operations is limited to 752°F (400°C) per ISG-11 [2]. The maximum cladding temperature for off-normal and accident events is limited to 1,058°F (570°C). For the structural components of the storage system, the thermally induced stresses, in combination with pressure and mechanical load stresses, are limited to the material allowable stress levels.

Thermal evaluations for normal conditions of storage and canister transfer operations are presented in Section 4.4. The finite element method is used to compute the effective properties

for the basket, neutron absorber and fuel region. The thermal solutions for the concrete cask and transfer cask are obtained using finite element and finite volume methodologies. Thermal models used in the evaluation of normal and transfer conditions are described in Section 4.4.1.

A summary of the thermal evaluation results for normal conditions of storage is provided in Table 4.4-3 for the PWR and the BWR cases. Table 4.4-5 through Table 4.4-14 contain the maximum fuel cladding temperatures for the different phases of the transfer operations for the PWR and BWR cases. Thermal evaluation results for off-normal and accident events are presented in Sections 4.5 and 4.6, respectively. The results demonstrate that the calculated temperatures are less than the allowable fuel cladding and component temperatures for all normal (long-term) storage conditions and for short-term events. As shown in Chapter 3, the thermally induced stresses, combined with pressure and mechanical load stresses, are also within allowable limits.

Figure 4.1-1 Definition of the Preferential Loading Pattern for PWR Fuel



| Zone Identification                 | A     | B    | C    |
|-------------------------------------|-------|------|------|
| Maximum Heat Load per Assembly (kW) | 0.922 | 1.20 | 0.80 |
| Total Number of Fuel Assemblies     | 9     | 12   | 16   |

**Table 4.1-1 Summary of Thermal Design Conditions for Storage for the MAGNASTOR**

| Condition                               |                       | Environmental Temperature (°F) | Solar Insolation <sup>a</sup> | Condition of Concrete Cask Inlets |
|---|-----------------------|--------------------------------|-------------------------------|-----------------------------------|
| Normal                                  |                       | 76 <sup>b</sup>                | Yes                           | All inlets open                   |
| Off-Normal<br>- Half Air Inlets Blocked |                       | 76                             | Yes                           | Half inlets blocked               |
| Off-Normal<br>- Severe Heat             |                       | 106                            | Yes                           | All inlets open                   |
| Off-Normal<br>- Severe Cold             |                       | -40                            | No                            | All inlets open                   |
| Accident<br>- Extreme Heat              |                       | 133                            | Yes                           | All inlets open                   |
| Accident<br>- All Air Inlets Blocked    |                       | 76                             | Yes                           | All inlets blocked                |
| Accident<br>- Fire                      | During Fire           | 1475                           | Yes                           | All inlets open                   |
|   | Before and After Fire | 76                             | Yes                           | All inlets open                   |

<sup>a</sup> Solar Insolation per 10 CFR 71 [3]:  
Curved Surface: 400 g cal/cm<sup>2</sup> (1475 Btu/ft<sup>2</sup>) for a 12-hour period.  
Flat Horizontal Surface: 800 g cal/cm<sup>2</sup> (2950 Btu/ft<sup>2</sup>) for a 12-hour period.

<sup>b</sup> Maximum average annual temperature in the 48 contiguous United States is 75.6°F. [25]

**Table 4.1-2 Maximum Allowable Material Temperatures**

| Material  | Temperature Limits (°F)    |                        | Reference  |
|---|----------------------------|------------------------|--|
|   | Long Term                  | Short Term             |  |
| Concrete  | 200(B)/300(L) <sup>a</sup> | 350                    | ACI-349 [4]<br>NUREG-1567 [20]                       |
| Fuel Clad   |                            |                        |  |
| PWR Fuel  | 752                        | 752/1,058 <sup>b</sup> | ISG-11 [2] and                                       |
| BWR Fuel  | 752                        | 752/1,058 <sup>b</sup> | PNL-4835 [5]   |
| NS-4-FR   | 300                        | 300                    | JAPC [6]   |
| Chemical Copper Lead  | 600                        | 600                    | Baumeister [7]                                       |
| ASME SA693 17-4PH Type 630 Stainless Steel                  | 650                        | 800                    | ASME Code [8]<br>ARMCO [9]                           |
| ASME SA240 Type 304 Stainless Steel                         | 800                        | 800                    | ASME Code [8]  |
| ASME SA537 Class 1 Carbon Steel                             | 800                        | 700/1,000 <sup>c</sup> | ASME Code [8]<br>ASME Code Case<br>N-707 [26]        |
| ASTM A588 Carbon Steel                                      | 700                        | 700                    | ASME Code Case<br>N-71-17 [10]<br>ASTM Standard [19] |
| ASTM A350 LF2 Carbon Steel                                  | 700                        | 700                    | ASTM Standard [19]                                   |
| ASTM A36 Carbon Steel                                       | 700                        | 700                    | ASME Code Case<br>N-71-17 [10]<br>ASTM Standard [19] |
| ASME SA695 Type B Grade 40 and<br>SA696 Type C Carbon Steel | 800                        | 800                    | ASME Code [8]  |

<sup>a</sup> B and L refer to bulk temperature and local temperature, respectively.

<sup>b</sup> 752°F TSC transfer operations; 1,058°F off-normal and accident events.

<sup>c</sup> 700°F TSC transfer operations; 1,000°F off-normal and accident events.

## 4.2 Thermal Properties of Materials

Material properties used in the analytical model are separated into two categories. One category represents materials specified in the design that are explicitly represented in the model and are tabulated in Chapter 8. The second category represents effective properties of the basket, neutron absorber and fuel region, which are calculated using the thermal models presented in Section 4.4.1.



### 4.3 Technical Specifications for Components

The three major components of MAGNASTOR must be maintained within their safe operating temperature ranges: the concrete cask, the transfer cask, and the TSC with fuel basket. The safe operating ranges for these components are from a minimum temperature of -40°F to the maximum temperatures defined in Table 4.1-2.

The criterion for the safe operating range of the lead in the transfer cask is maintaining the lead temperature below its melting point of 620°F [7]. The maximum operating temperature limit of the NS-4-FR neutron shield material in the transfer cask has been determined by the manufacturer and ensures the stability of the material. The temperature limits for the steel components of the fuel basket and the TSC are defined by ASME Code Section II, Part D [8] and ASME Code Case N-707 [26]. The temperature limits for the steel components of the transfer cask and the concrete cask are defined by ASTM Standards [19]. The temperature limits for concrete are defined by ACI-349 [4] and NUREG-1567 [20].

#### 4.4 Normal Storage Conditions

The finite element and finite volume methods are used to evaluate the thermal performance of MAGNASTOR for normal conditions of storage. The general-purpose finite element analysis program ANSYS [11] is used to perform analyses requiring radiation and conduction. The Computational Fluid Dynamic (CFD) program FLUENT [12], which is based on finite volume methods, is used to perform analysis that includes conduction, radiation and convection. In FLUENT, convection of heat is simulated through motion of fluid, as well as by the specification of a film coefficient for a surface boundary condition.

##### 4.4.1 Thermal Analysis Models

Analysis models used for the thermal evaluation of both the PWR and BWR design configurations are described in the following sections. The methodology inherent in the models conservatively reflects the heat transfer performance provided by the MAGNASTOR design.

The designs for both the PWR and the BWR fuel systems utilize the same method of passive heat rejection to transfer the decay heat from the fuel assemblies to the ambient environment. The TSC is a closed system, whereas the concrete cask and the transfer cask are open to the environment. Internal to the TSC, the decay heat is transferred from the fuel assemblies in each of the fuel tubes to the TSC shell by three modes of heat transfer: convection, conduction and radiation. The fuel baskets designed for PWR and BWR fuel assemblies permit the helium backfill gas to flow up the fuel tubes containing the fuel assemblies and carry the heat away from the fuel assemblies. The region in the TSC just above the fuel basket allows the helium flow upward from the fuel tubes to combine and flow through the downcomer regions formed between the TSC shell and the basket side weldments. The gas exiting the downcomer regions at the bottom of the fuel basket enters a region below the basket tubes. The flow of the helium upward in the fuel basket and downward in the downcomer regions is driven by the buoyancy forces created by the effect of the heated helium rising up through the fuel tubes. To increase the buoyancy force, the density of the helium is increased by raising the helium backfill pressure. Since the fuel tubes are full-length carbon steel tubes, they provide a path for conduction of heat. While the tubes are not welded together, the effect of the gap between the tubes is mitigated by the use of the helium backfill. The side and corner weldments of the fuel basket, which support the fuel basket during a side impact, also provide a path of heat conduction. While a gap is considered between the side and corner weldments and the TSC shell for analysis purposes, the heat transfer across the gap is provided by the radiation from the weldments and conduction through the helium gap to the TSC shell. Radiation is also a mode of heat transfer, which allows heat from the interior of the fuel assembly to be transferred to the outer pins of the fuel assembly.

Additionally, since the fuel assemblies are assumed to be in the center of each fuel tube, radiation also contributes to the heat transfer from each fuel assembly to the fuel tube wall. Radiation is also taken into account for all gaps, such as those between the tubes. Additionally, radiation contributes to the heat being transferred from the outer basket surface to the TSC shell.

As the heat is being transferred to the TSC shell, the airflow up the annulus region between the TSC and the concrete cask carbon steel liner is removing heat from the TSC outer surface and rejecting it to the ambient environment. This annulus airflow is also driven by the buoyancy of the heated air. The air entering the air inlets at the base of the concrete cask provides a supply of cooler air into the annulus region. The heated air rises and exits the air outlets. Since the TSC shell faces the concrete cask liner, it radiates heat to the liner, which allows heat from the liner to be transferred to the annulus airflow. The liner also serves to distribute the heat along the length of the liner. Heat not rejected into the airflow is conducted through the concrete cask wall to the outer surface. At the surface, both convection and radiation modes of heat transfer reject the heat to the ambient.

Due to the convection of the fuel decay heat into the downcomer, the temperature distribution along the length of the TSC shell inner surface is not uniform, but increases monotonically from the base of the TSC to an elevation near to the top of the basket. This indicates that the heat flux due to the heated helium along the TSC wall is not uniform, and that this heat flux actually can be considered to be a boundary condition to the airflow in the annulus region of the concrete cask. For this reason, it is more efficient to consider a model in which both the TSC fuel basket and fuel region are considered in conjunction with the airflow in the annulus region of the concrete cask. The model used to represent the TSC and the concrete cask is a two-dimensional axisymmetric model, which is described in Section 4.4.1.1.

The fuel basket and fuel regions inside the TSC are modeled as homogeneous regions incorporating all modes of heat transfer. Effective thermal conductivities are used to represent the conduction and radiation in the fuel region and fuel basket, which require a two-step modeling process. A series of two-dimensional planar models is generated to determine the effective conductivities for the fuel assembly (Section 4.4.1.3) and the neutron absorber (Section 4.4.1.4). Using the effective conductivity for the fuel region and the neutron absorber, the effective conductivity for the fuel basket is determined using the two-dimensional fuel basket model as presented in Section 4.4.1.2.

The flow of helium in the fuel region is affected by the wetted perimeter associated with the fuel pins. To represent the flow of helium in the fuel region, which is represented as a homogenized entity, porous media is used in the modeling. The porous media model allows the effect of the reduced flow area of the fuel rods and the fuel assembly grids to be considered in representing

the momentum of the helium flow by including a pressure drop based on the geometry of the fuel assembly, i.e., the pitch of the fuel rods, the fuel rod diameter, and the fuel assembly grid geometry. Additional fluid flow analyses are required to determine the constants inherent in the porous media use for flow between cylindrical-shaped fuel rods and for fuel assembly grids. The determination of porous media constants is presented in Section 4.8.2. The flow of helium in the downcomer regions in the TSC does not require special consideration of effective flow conditions. To confirm that the use of a two-dimensional model for the TSC is an acceptable and conservative methodology, a benchmark is provided in Section 4.8.1.

The thermal evaluation for the transfer conditions is performed using the two-dimensional axisymmetric models of the transfer cask and TSC, as presented in Section 4.4.1.5. Similar to the model of the concrete cask and TSC, the fuel basket and fuel assemblies inside the TSC in the transfer cask are modeled as homogeneous regions using effective thermal properties.

#### **4.4.1.1 Two-Dimensional Axisymmetric Concrete Cask and TSC Models**

This section describes the finite volume models used to evaluate the thermal performance of the concrete cask and TSC for the PWR and BWR fuel configurations. As shown in Figure 4.4-1, the two-dimensional axisymmetric concrete cask and TSC model includes the following:

- Concrete cask, including lid, liner, pedestal and stand
- Air in the air inlets, the annulus and the air outlet
- TSC shell, lid and bottom plate
- Basket with fuel and neutron absorber
- Helium internal to the TSC

The fuel basket, fuel and neutron absorber are modeled as homogeneous regions with effective properties. The effective thermal conductivities for the TSC internals in the radial and axial directions are determined using the two-dimensional models as detailed in Section 4.4.1.2.

The two-dimensional axisymmetric concrete cask and TSC model is used to perform computational fluid dynamic analyses to determine the component temperature, the mass flow rate, velocity and temperature of the airflow in the annulus region, as well as for the helium flow internal to the TSC. Since the concrete cask and its components are contained in the model, the temperature distributions in the concrete and the concrete cask steel liner are also determined. Two models are generated for the evaluations—the PWR system and the BWR system, respectively. These models are identical, except for differences in dimensions of the downcomer regions and the effective properties of the TSC internals. Figure 4.4-2 shows an overall view of the cells employed in the model representing both the concrete cask and the TSC containing a design basis fuel heat load.

### **Modeling of the Concrete Cask**

The concrete cask body has four air inlets at the bottom and four air outlets at the top. Since the configuration is symmetrical, it can be simplified into a two-dimensional axisymmetric model by using equivalent dimensions for the air inlets and outlets, which are assumed to extend around the concrete cask periphery. The vertical air gap is an annulus, with a radial width of 3.5 inches. This radial dimension of the air annulus between the TSC shell and the concrete cask liner is modified to a smaller effective value to account for the reduction of the airflow cross-sectional area due to the standoffs welded to the liner. The bottom ends of the standoffs are more than 63 inches from the bottom of the TSC, which means that for over 30% of the length of the annulus, the standoffs do not exist. The model conservatively represents them as being the full length of the TSC. The additional axial conductance from the standoffs is conservatively neglected. Thermal radiation across the annulus gap is considered in the model, and the emissivities of the TSC surface and the concrete cask liner are reported in Chapter 8. Heat being radiated to the concrete cask liner is transferred into the annulus by convection, as well as being conducted through the concrete cask wall.

The most significant mechanism for rejecting heat into the environment is through the movement of air up through the annulus. The airflow in the vertical annulus is modeled as transitional turbulent flow using the  $k-\omega$  turbulence model in FLUENT [12]. This determination was made through the use of a thermal test of PWR canistered fuel contained in a vertical concrete cask, which is described in EPRI Report TR-100305 [21] and provides a description of the test canister, the concrete cask, the fuel assemblies, and the boundary conditions employed in a series of tests. The total heat load of the fuel used in the tests was 14.9 kW. Extensive temperature measurements were made for the basket, fuel, canister and concrete cask for each test conducted. The thermal test of interest employed the vacuum condition for the canister. This test was selected since it removed the influence of convection inside the canister and simplified the thermal model inside the canister. FLUENT was used to perform a two-dimensional steady-state axisymmetric analysis of the system described in [21] using two turbulent flow models: a low Reynold's number turbulence model (low Re  $k-\epsilon$ ) and a transitional turbulence model ( $k-\omega$ ). Technical details for these turbulence models are contained in the documentation for FLUENT. The thermal models and boundary conditions used in the analyses are detailed in Section 4.8.3. Results for the temperature profiles for the canister surface and the concrete liner surfaces for both turbulence models are shown in Figure 4.8-11 and Figure 4.8-12. The results indicate that both turbulence models yield conservative predictions for the temperature profiles and that both the low Reynold's number  $k-\epsilon$  and the  $k-\omega$  models are appropriate for use in the analysis of air flow up through the annulus between the canister and the concrete cask. Since the use of the  $k-\omega$  model provides conservative results for the canister shell and concrete cask for a test

corresponding to 14.9 kW, the use of the  $k-\omega$  model is also considered to be appropriate for analyses having larger heat loads. As the heat load is increased, the turbulence in the annulus air flow is also expected to increase. The results of the analysis for the thermal tests are considered as validation for the use of the  $k-\omega$  turbulence model for the annulus region of MAGNASTOR.

The mesh corresponding to the annulus for the analysis is shown in Figure 4.4-2. Increased cell density is used in the annulus region adjacent to the wall to allow the  $y^+$  at the wall to be on the order of unity, ensuring proper turbulence modeling.

The TSC model is included with the concrete cask model as shown in Figure 4.4-1. Boundary conditions at the edges of the model to the ambient are applied to the concrete cask surfaces. The heat flux being transferred from the helium internal to the TSC through the TSC shell and into the air annulus region is not considered to be a boundary condition for the concrete cask since all of these components are included in the same model. The boundary conditions applied to the outer surface of the concrete cask include the following.

- Solar insolation to the outer surfaces of the concrete cask.
- Natural convection heat transfer at the outer surfaces of the concrete cask.
- Radiation heat transfer at the concrete cask outer surfaces.

### **Solar Insolation**

The solar insolation on the concrete cask outer surfaces is considered in the model. The incident solar energy is applied based on 24-hour averages as shown:

$$\text{Side surface: } \frac{1475\text{Btu/ft}^2}{24\text{hrs}} = 61.46\text{Btu/hr} \cdot \text{ft}^2$$

$$\text{Top surface: } \frac{2950\text{Btu/ft}^2}{24\text{hrs}} = 122.92\text{Btu/hr} \cdot \text{ft}^2$$

### **Natural Convection**

Natural convection heat transfer at the outer surfaces of the concrete cask is evaluated by using the heat transfer correlation for vertical and horizontal plates. This method assumes a surface temperature and then estimates Grashof (Gr) or Rayleigh (Ra) numbers to determine whether a heat transfer correlation for a laminar flow model or for a turbulent flow model should be used. Since Grashof or Rayleigh numbers are much higher than the values defining the transition from laminar to turbulent flow, correlation for the turbulent flow model is used as shown in the following.

Side surface (Kreith) [13]:

$$Nu = 0.13(Gr \cdot Pr)^{1/3} \quad \text{for } Gr > 10^9$$

$$h_c = Nu \cdot k_f / H_{vcc}$$

Top surface (Incropera) [14]:

$$Nu = 0.15Ra^{1/3} \quad \text{for } Ra > 10^7$$

$$h_c = Nu \cdot k_f / L$$

where:

|           |       |  |
|-----------|-------|--|
| Gr        | ----- | Grashof number   |
| $h_c$     | ----- | Average natural convection heat transfer coefficient   |
| $H_{vcc}$ | ----- | Height of the concrete cask                            |
| $k_f$     | ----- | Conductivity   |
| L         | ----- | surface characteristic length,<br>L = area / perimeter |
| Nu        | ----- | Average Nusselt number                                 |
| Pr        | ----- | Prandtl number   |
| Ra        | ----- | Rayleigh number  |

All material properties required in these equations are evaluated based on the film temperature defined as the average value of the surface temperature and the ambient temperature.

**Radiation Heat Transfer**

The radiation heat transfer between the outer surfaces of the concrete cask and the ambient environment is evaluated in the model by calculating an equivalent radiation heat transfer coefficient.

$$h_{rad} = \frac{\sigma(T_1^2 + T_2^2)(T_1 + T_2)}{\frac{1}{\epsilon_1} + \frac{1}{\epsilon_2} + \frac{1}{F_{12}} - 2} \quad [14]$$

where:

|                             |       |  |
|-----------------------------|-------|--|
| $h_{rad}$                   | ----- | Equivalent radiation heat transfer coefficient                       |
| $F_{12}$                    | ----- | View factor  |
| $T_1$ & $T_2$               | ----- | Surface ( $T_1$ ) and ambient ( $T_2$ ) temperatures                 |
| $\epsilon_1$ & $\epsilon_2$ | ----- | Surface ( $\epsilon_1$ ) and ambient ( $\epsilon_2=1$ ) emissivities |
| $\sigma$                    | ----- | Stefan-Boltzmann Constant  |

At the concrete cask side, an emissivity for a concrete surface of  $\epsilon_1 = 0.9$  is used and a calculated view factor ( $F_{12}$ ) = 0.182 [14] is applied. The view factor is determined by conservatively

assuming that the cask is surrounded by eight casks. At the cask top, an emissivity,  $\epsilon_1$ , of 0.8 is conservatively used (emissivity for concrete is 0.9), and a view factor,  $F_{12}$ , of 1 is applied.

### **Modeling of the TSC**

The TSC is a closed system designed so that pressurized helium can circulate inside the TSC and transfer heat from the fuel in the basket to the TSC shell. Circulating helium is modeled as laminar flow inside the TSC. Additionally, the basket permits heat to be conducted from the interior regions of the basket to the periphery of the basket, then radiated and convected to the TSC shell surface. The stiffeners at the periphery of the basket do provide a path of conduction to the TSC shell, even though a small gap exists between the stiffeners and the TSC shell. The heat conduction through these stiffeners is neglected in the evaluation, which is considered to be conservative. Radiation is modeled in the fuel assemblies, as well as in gaps in the basket. Heat transfer to the TSC lid and bottom plate is considered in the analysis, but it is not a major contributor to the heat-rejection process. Two separate models are generated—one for the PWR fuel configuration and one for the BWR fuel configuration. The differences between the two models are in the dimensions of the basket region and the effective properties derived for each basket and fuel region.

The TSC region consists of the following: the TSC shell, the TSC bottom plate, the TSC lid, the fuel basket region, and the helium-filled volume outside the fuel basket region. The fuel basket region is subdivided into three sections to reflect the location of the active fuel region with the associated heat generation and the fuel regions above and below the active fuel regions. These three separate regions are shown in Figure 4.1-1.

The cross-section of the flow path for the helium in the fuel basket and TSC significantly changes between the flow up through the basket region and the flow down in the downcomer region next to the TSC shell. For the flow up through the basket, the outline of the cross-sectional area is comprised of the area between the square basket tubes and circular fuel pins. Additionally, as the helium flows up through the basket tube, the fuel assembly grids will provide resistance to the flow. In the downcomer region, the exterior boundary is circular, while the interior boundary is the edge of the square fuel tubes. This is also an irregular-shaped area. In a two-dimensional representation of these areas, the concept of the hydraulic diameter is employed, which is commonly used to determine an equivalent cross-sectional area for a cross-section with complex shapes.

To account for the resistance to flow in the fuel region in the basket due to the wetted perimeter of the fuel region in the basket, the porous media option for fluids is used. The resistance to flow due to the fuel pins and the fuel assembly grids is represented in terms of a pressure drop



included in the momentum equations for each cell in the model associated with porous media. The expression for the pressure drop used in FLUENT is given by:

$$\frac{\Delta P}{L} = \frac{\mu}{\alpha \cdot \varepsilon} V + C \left( \frac{1}{2} \rho V^2 \right)$$

where:

|               |       |   |
|---------------|-------|---|
| $\Delta P/L$  | ----- | pressure drop per unit length (Pa/m)  |
| $V$           | ----- | superficial fluid velocity (m/s)  |
| $\mu$         | ----- | fluid viscosity (kg/m-s)  |
| $\rho$        | ----- | fluid density (kg/m <sup>3</sup> )  |
| $1/\alpha$    | ----- | viscous flow resistance (m <sup>-2</sup> )  |
| $\varepsilon$ | ----- | porosity factor, which is the ratio of the cross-sectional area of the flow, to the cross-sectional area of the porous media region in the FLUENT model |
| $C$           | ----- | inertial resistance factor (m <sup>-1</sup> )   |

In this expression, the viscosity is input as a temperature-dependent material property for the helium, and the density is computed during the solution based on the ideal gas law. The permeability is based on the geometry of the fuel rods and the fuel assembly grid. Since the velocities are on the order of 0.03 m/s or less, the second term comprised of  $V^2$  is considered to be insignificant as compared to the first term. Therefore, the calculation for the inertial resistance factors is neglected. Details of the calculation of the viscous flow resistance factors are contained in Section 4.8.2. The values used for the evaluation are based on the bounding fuel parameters.

The downcomer region of the TSC does not use a porous media model. The areas of the downcomer regions are calculated to be 600 inches<sup>2</sup> and 550 inches<sup>2</sup> for the PWR and the BWR fuel baskets, respectively. These areas are used to calculate the effective outer diameter of the fuel basket region, which serves as the radial boundary for the porous media region for the fuel.

Due to the large cross-section for the flow up through the fuel basket, the helium velocity is expected to be sufficiently low to correspond to laminar flow. In the downcomer region, the gas velocities would result in the flow being in a transitional regime. Conservatively, all helium flow in the TSC is taken to be laminar.

The porous media representation of the fuel basket region incorporates orthotropic effective thermal conductivities. The axial conductance in the fuel basket region is due to the significant cross-sectional area of the fuel tubes and the fuel assemblies. The in-plane conductance is associated with the conductance of the fuel tubes, as well as the effective conductivities of the

fuel assembly and neutron absorber. The effective conductivity of the fuel basket region is determined in two steps. Separate effective thermal conductivities for the two-dimensional fuel assembly and the neutron absorber are computed for the axial and the in-plane directions using two finite element models. Details for these models are described in Section 4.4.1.3 for the fuel assemblies and Section 4.4.1.4 for the neutron absorber. In these sections, both the PWR and the BWR effective properties calculations are performed.

The resulting conductivities for the fuel assemblies and neutron absorber are then used in a single two-dimensional planar model of the cross-section of the basket, which is used to determine the axial and in-plane conductivities for the fuel basket region associated with the porous media. This model is described in Section 4.4.1.2. The effective conductivity for the porous media model uses two conductivities ( $k_f$  and  $k_s$ ), as identified in the following equation.

$$K_{\text{eff}} = \epsilon \times k_f + (1 - \epsilon) \times k_s$$

where:

|            |       |  |
|------------|-------|--|
| $\epsilon$ | ----- | porosity factor  |
| $k_f$      | ----- | thermal conductivity of the helium   |
| $k_s$      | ----- | thermal conductivity associated with the solid portion of the porous media model |

### **Heat Generation**

The heat generation for the fuel is applied to the active fuel region of the TSC model (see Figure 4.4-1) for the PWR and the BWR fuel assemblies. The maximum design basis heat loads to be considered for the PWR and the BWR fuel basket configurations are 35.5 kW and 33 kW, respectively.

For the PWR fuel basket, two patterns of heat generation are considered. A uniform loading of 35.5 kW or 959 W in each fuel location is considered. The axial power distribution for PWR fuel, as shown in Figure 4.4-3, is included in applying the heat generation. An optional heat generation pattern, as shown in Figure 4.1-1 is also considered and has the same total heat load of 35.5 kW. The application of the heat generation for this condition incorporates an axial distribution and a radial distribution. The area over which each fuel assembly heat load is distributed in Figure 4.1-1 is determined on the basis of the cross-section of the fuel tubes containing the specific heat loads identified as A, B and C in Figure 4.1-1. The heat generation values specified in Figure 4.1-1 are considered to be the maximum permissible heat generation in each fuel location. It is noted that maximum fuel assembly heat load in Figure 4.1-1 is 25% greater than the heat load for the uniform condition. The fuel heat load in the center of the basket in Figure 4.1-1, Zone A, at 0.922 kW is only 4% less than the uniform heat loading at

0.96 kW per assembly. The use of hotter assemblies in the Zone B ring results in slightly more flow in the Zone B region with the higher heat load, but simultaneously presents a bounding condition over the uniform loading of the entire basket since the edge of Zone A temperatures are increased by the influence from the higher heat in Zone B. An analysis using a 40 kW preferential loading with a more aggressive annular turbulence model (K- $\epsilon$ ) and a reduced flow resistance showed that the preferential heat distribution increased the maximum fuel temperatures by 6°F. With the reduction of the maximum heat load to 35.5 kW, the 6°F difference in maximum fuel cladding temperature will decrease, but will still produce temperatures equal to or greater than the uniform heat load configuration.

For the BWR fuel basket, only a uniform thermal loading pattern is considered. The design basis heat load for BWR fuel is 33 kW, which corresponds to a maximum heat load of 379 watts for each of the 87 fuel assemblies. The axial power distribution for the BWR fuel is shown in Figure 4.4-4. For some BWR fuel assembly enrichments, the five fuel locations in the center of the BWR basket will not be loaded. In this configuration, the fuel assembly decay heat is limited to 379 watts. Fuel storage locations not containing a fuel assembly will have an effective fuel cell insert installed to prevent the helium flow from bypassing the fuel locations containing fuel assemblies. The configuration with a partially loaded fuel basket containing BWR fuel assemblies with a maximum heat load of 379 watts per assembly is considered to be bounded by the fully loaded BWR fuel basket configuration. Temperatures obtained from analyses performed using the maximum heat load in conjunction with a fully loaded BWR basket are considered to bound the results for a partially loaded basket.

### **Pressure of the Helium Backfill**

To drive the convection internal to the TSC, it is necessary to increase the density of the helium. Since the free volume in the TSC remains constant, the density of the backfill gas can be increased by backfilling the TSC to a range of pressures and temperatures that would result in an increase in the density. In the MAGNASTOR design, the TSC is pressurized to 7 atm (gauge) for the helium backfill for normal conditions. Since the gas in the model is characterized as an ideal gas, the increased density in the analysis can be indirectly obtained by specifying a pressure in the TSC region. For the PWR normal condition, the density of helium in the TSC associated with a pressure of 7 atm (g) is (0.76g/liter). It is important to assess the effect of the helium density on the performance of the system. The evaluation of the sensitivity of the peak fuel temperature to the pressure is performed using the PWR model described in this section. The condition requiring a change is the pressure that is applied to the TSC region of the model. The results of the model solutions for pressures of 1 atm (g), 3 atm (g), 5 atm (g) and 7 atm (g) are shown as a graph in Figure 4.4-5. As shown in Figure 4.4-5, the variation of the peak cladding

temperature with the pressure specified inside the TSC is a nonlinear function. The peak cladding temperature decreases sharply when the pressure increases from 1 atm to 3 atm. Subsequent increases in the pressure to 5 atm and 7 atm do not result in the same rate of decrease of the clad temperature as for the 1 atm and 3 atm cases. The model of the TSC in the concrete cask has two regions of convection separated by a TSC shell. Heat can only be transferred through the shell from the TSC internal region to the annulus region outside the TSC. The flow characteristics in the annulus region are primarily affected by the total heat generation being transferred through the TSC shell, as well as the geometry of the annulus. As the pressure (and the associated mass) of the gas in the TSC is increased, the buoyancy force inside the TSC is increased. This increases the mass flow rate of the TSC gas so that the ability to reject heat from the fuel is also increased. This would tend to reduce the maximum clad temperature. However, the flow in the annulus is not expected to be significantly affected by the velocity of the gas internal to the TSC. Therefore, regardless of the buoyancy force inside the TSC, the maximum clad temperature is limited by the shell temperature, which is controlled by the annulus flow. At some pressure level, an increase in the TSC pressure (and mass) of the gas would not significantly decrease the fuel clad temperature, which would imply a reduced derivative of the clad temperature with respect to the pressure. This is the characteristic of the curve in Figure 4.4-5, which implies that further increase in the pressure does not result in a significant reduction of the clad temperature. There is an advantage in operating in this regime of the curve in that the sensitivity of the clad temperature due to a reduction in the helium density is reduced. This evaluation demonstrates that even with a 10% loss of density, the peak clad fuel temperatures for the design basis heat load remain under 752°F (400°C). The calculated maximum temperatures from this evaluation show that there is an acceptable 10 psig tolerance for the minimum helium backfill pressure.

### **Mesh Sensitivity Evaluation**

With respect to the sensitivity of the calculated fuel cladding, concrete cask and TSC temperatures to the number of divisions of the finite volume cells, this need only be addressed for the regions containing fluid flow. For the solid regions, such as the concrete or the steel components, the sensitivity evaluation of cell refinement is not required.

There are two fluid regions in the model: the airflow annulus region outside the TSC, and the helium region inside the TSC. Each of these fluid regions uses a different fluid flow model. The TSC internal flow is modeled utilizing a laminar flow model; the airflow in the annulus region is modeled using a turbulent flow model.

In the concrete cask annulus region, the modeling accuracy of the turbulent flow depends not on the usual refined mesh near the wall, as for a laminar flow condition, but on the value of  $y^+$ , as

previously discussed. The cell divisions in the annulus region have been set to permit the  $y^+$  to be less than unity, which is acceptable according to FLUENT documentation. Therefore, further refinement of the annulus region would not provide a more accurate temperature result.

For the helium flow in the TSC (laminar flow), the largest velocities are in the downcomer regions and, essentially, the entire heat load must be transferred to the TSC shell. The focus of the sensitivity evaluation is the number of cell divisions in the downcomer region. The largest velocity gradients in the downcomer regions occur in the radial direction, not in the axial direction. To determine the sensitivity of the radial divisions in the downcomer region, the number of radial divisions modeled was increased by a factor of two. The axial divisions in the downcomer region remain the same. The mesh refinement in the air annulus and in the concrete cask remains unchanged. The condition used in the evaluation corresponded to the normal condition using a uniform heat loading of 40 kW, which bounds the design basis condition for the 35.5 kW. The results of this evaluation showed that the maximum fuel temperature changed by less than 1°F for the increased refinement mesh. The temperature of the TSC shell showed a decrease of 2°F for the mesh with the increased refinement. This indicates that the maximum fuel temperature is relatively insensitive to the mesh refinement in the downcomer region.

### **Heat Transfer by Radiation**

Thermal radiation in all fluid (air and helium) regions has been considered in the model, specifically the following.

- Thermal radiation across the air annulus between the TSC shell and the concrete cask liner.
- Thermal radiation across the air gap above the TSC lid and in the isolated air region below the pedestal of the concrete cask.
- Thermal radiation across the helium downcomer region between the fuel basket and the TSC shell.

The discrete ordinates (DO) radiation model in FLUENT is used to solve the radiative heat transfer equation with emissivity values applied on the solid material surfaces.

Radiation in the porous media fuel region is modeled by using equivalent thermal conductivities that include the effects of heat transfer by radiation. The model of the porous media region in FLUENT is enclosed by a vertical wall that separates the porous region from the downcomer. The wall is comprised of two sides; one side facing the inner surface of the canister and the other facing the interior region of the porous media. An emissivity corresponding to electroless nickel is applied to the side facing the canister surface. On the side of the wall facing the interior region of the porous media, an emissivity of zero is applied to avoid incorporating the radiation already taken into account using the effective properties for the basket.

#### 4.4.1.2 Two-Dimensional Fuel Basket Models

The purpose of the two-dimensional fuel basket model is to determine the effective thermal conductivity of the basket region in the axial and radial directions. The effective conductivities are used in the two-dimensional axisymmetric concrete cask and TSC models, and the two-dimensional axisymmetric transfer cask and TSC models. Two types of media are considered in the TSC: helium and water. The fuel assemblies and neutron absorbers in the fuel basket model are shown as homogeneous regions with effective thermal properties, which are determined by the two-dimensional fuel assembly models and the two-dimensional fuel tube models described in Sections 4.4.1.3 and 4.4.1.4, respectively. The analyses performed in Section 4.4.1.3 identify that the PWR fuel assembly with the minimum conductivity is the 14×14. The properties of the PWR 14×14 fuel assembly are used in the evaluation of the effective properties for the PWR basket in this section. For the BWR assembly, the bounding fuel assembly type is the 10×10, which is used to determine the effective properties for the BWR basket.

Since the effective properties for the fuel basket correspond to the basket region, which is comprised of full-length fuel tubes, it is only necessary to consider a cross-section of the basket with a two-dimensional planar model. Due to symmetry of the basket designs, only a 1/8-section model is required for the PWR and the BWR fuel baskets. ANSYS is used to perform the conduction analysis using the models shown in Figure 4.4-6 for the PWR fuel basket and Figure 4.4-7 for the BWR fuel basket. The models include only radiation and conduction heat transfer. Radiation heat transfer is incorporated into the effective properties for the fuel assemblies and the neutron absorbers. Each fuel basket model takes into account the size of the cells in the basket – i.e., those cells formed directly by the fuel tube, and those cells formed by adjacent fuel tubes. The neutron poison is contained only on the inner surface of the basket tubes. The exterior tubes, which form the boundary of the downcomer region, may not have neutron absorbers on the adjacent surface of the interfacing fuel tubes. In the condition where the neutron absorber sheet is not required for criticality control, aluminum plates may be installed as an alternative to maintain thermal properties. The PWR and BWR fuel basket models evaluated in this section use the conductivity of the neutron poison defined in Chapter 8.

Additionally, it is conservatively assumed for both the PWR and BWR fuel baskets that a gap between the fuel tubes exists for the full length of the tube without any contact, as shown in Figure 4.4-6 and Figure 4.4-7. The gap between the fuel tubes is modeled as being 0.01 inch, and the conduction through the gap is based on the presence of either helium or water, depending on the condition.

The effective thermal conductivity ( $K_{\text{eff}}$ ) of the fuel basket region in the radial direction is determined by considering the basket region as a solid cylinder with heat generation.

Considering the temperature at the center of the TSC to be  $T_{max}$ , the effective thermal conductivity ( $K_{eff}$ ) is shown:

$$K_{eff} = \frac{Q}{4\pi H(T_{max} - T_o)} = \frac{Q}{4\pi H\Delta T} \quad [15]$$

where:

- Q ----- total heat generated by the fuel (Btu/hr)
- H ----- length of the active fuel region (in)
- $T_o$  ----- boundary temperature of the basket
- $\Delta T$  -----  $T_{max} - T_o$  (°F)

The value of  $\Delta T$  is obtained from thermal analysis using the two-dimensional models shown in Figure 4.4-6 and Figure 4.4-7, with the boundary temperature constrained to be  $T_o$ . The effective conductivity ( $K_{eff}$ ) is then determined by using the stated expression. The analysis is repeated by applying different boundary temperatures so that temperature-dependent conductivities can be determined.

#### 4.4.1.3 Two-Dimensional Fuel Assembly Models

The two-dimensional fuel assembly models include the fuel pellets, cladding, and the media occupying the space between fuel rods. The media is considered to be helium for storage conditions, and water or helium for transfer conditions. The two-dimensional finite element models of the fuel assemblies are used to determine the effective conductivities for the PWR and BWR fuel assemblies. The effective conductivities are used in the two-dimensional fuel basket models described in Section 4.4.1.2. For the PWR fuel assemblies, four separate types are considered: 14×14, 15×15, 16×16 and 17×17. For the BWR fuel assemblies, four separate types are considered: 7×7, 8×8, 9×9 and 10×10. For the BWR fuel assembly, a fuel channel is considered since it may be present and it will result in bounding fuel cladding temperatures. Therefore, it is only necessary to address a single fuel configuration for each of the fuel assembly types.

The two-dimensional fuel assembly models include the fuel pellets, cladding, media between fuel rods, media between the fuel rods and the inner surface of the fuel tube (PWR), or between the fuel rods and the inner surface of the fuel channel (BWR), and a gap between the fuel pellets and cladding. The media are considered to be helium for storage, and water or helium for transfer conditions. Modes of heat transfer modeled include conduction and radiation between individual fuel rods for the steady-state condition. ANSYS PLANE55 conduction elements and MATRIX50 radiation elements are used to model conduction and radiation. (Radiation is not considered for the water condition.) Radiation elements are defined between fuel rods and

between the fuel rods and the fuel tube (PWR) or the fuel channel (BWR). A typical PWR fuel assembly finite element model is shown in Figure 4.4-8, which corresponds to the 14×14 fuel assembly. The BWR fuel assembly model only considers the region up to the inner surface of the channel, and a typical BWR fuel assembly is shown in Figure 4.4-9, which corresponds to the 10×10 fuel assembly.

The effective conductivity for the fuel is determined by using an equation defined in a Sandia National Laboratory Report [15]. The equation is used to determine the maximum temperature of a square cross-section of an isotropic homogeneous fuel with a uniform volumetric heat generation. At the boundary of the square cross-section, the temperature is constrained to be uniform. The expression for the temperature at the center of the fuel is given by:

$$T_c = T_e + 0.29468 (Qa^2 / K_{eff})$$

where:

|           |       |  |
|-----------|-------|--|
| $T_c$     | ----- | the temperature at the center of the fuel (°F)                                   |
| $T_e$     | ----- | the temperature applied to the exterior of the fuel (°F)                         |
| $Q$       | ----- | volumetric heat generation rate (Btu/hr-in <sup>3</sup> )                        |
| $a$       | ----- | half length of the square cross-section of the fuel (inch)                       |
| $K_{eff}$ | ----- | effective thermal conductivity for the isotropic homogeneous fuel (Btu/hr-in-°F) |

Volumetric heat generation (Btu/hr-in<sup>3</sup>) based on the design heat load is applied to the pellets. The effective conductivity is determined based on the heat generated and the temperature difference from the center of the model to the edge of the model. Temperature-dependent effective properties are established by performing multiple analyses using different boundary temperatures. The effective conductivity in the axial direction and the effective density of the fuel assembly are calculated on the basis of the material area ratio. The effective specific heat is computed on the basis of a weighted mass average.

For the PWR fuel assemblies, the 14×14 fuel assembly is shown to have the effective properties that correspond to the minimum values, as shown in Table 4.4-1 for both fuel tube configurations.

For the BWR fuel assemblies, the 10×10 fuel assembly is shown to have the effective properties that correspond to the minimum values, as shown in Table 4.4-2.



#### 4.4.1.4 Two-Dimensional Neutron Absorber Models

The two-dimensional neutron absorber model is used to calculate the effective conductivities of the neutron absorber, the neutron absorber retainer, and the fuel channel (for BWR only). These effective conductivities are used in the two-dimensional fuel basket models (Section 4.4.1.2). A total of three neutron absorber models is required: one PWR model (for the PWR 14×14) and two BWR models—one with the neutron absorber plate and channel, and one with the channel but without the neutron absorber plate, corresponding to the enveloping configurations of the 10×10 BWR fuel assembly.

The configurations shown in the neutron absorber models in Figure 4.4-10 and Figure 4.4-11 for PWR and BWR fuel, respectively, incorporate the neutron absorber (and the channel for the BWR). The configuration shown in Figure 4.4-12 is for the BWR fuel tube with the channel, but without the neutron absorber.

As shown in Figure 4.4-10, the PWR fuel tube model includes the neutron absorber, the stainless steel retainer, and the gaps between the neutron absorber and the stainless steel retainer and the surface of the fuel tube. Two conditions of media are considered in the gaps: helium and water.

ANSYS PLANE55 conduction elements and LINK31 radiation elements are used to construct the model. The model consists of four layers of conduction elements and two sets of radiation elements (radiation elements are not used for the water condition) that are defined at the gaps (two for each gap). The thickness of the model (x-direction) is the distance measured from the outside surface of the stainless steel retainer to the inside surface of the fuel tube (assuming the neutron absorber is centered between the retainer and the fuel tube, and there is no contact for the length of the basket). The gap size between the neutron absorber and the adjacent surfaces is 0.002 inch.

The BWR fuel assemblies may include a fuel channel, as compared to the PWR assemblies, which have no fuel channel. Therefore, two effective conductivity models are necessary for the BWR: one model with the neutron absorber plate (a total of six layers of materials) and a fuel channel; and the other model with a fuel channel, but with a gap replacing the neutron absorber plate (a total of two layers of materials).

As shown in Figure 4.4-11, the first BWR neutron absorber model includes the fuel channel, the retainer, the neutron absorber and associated gaps. As shown in Figure 4.4-12, the second BWR neutron absorber model includes the fuel channel and the gap between the fuel channel and the fuel tube surface.

Heat flux is applied at the left side of the model (retainer for PWR model and fuel channel for BWR model), and the temperature at the right boundary of the model is specified. The heat flux

is determined based on the design heat load. The maximum temperature of the model (at the left boundary) and the temperature difference ( $\Delta T$ ) across the model are calculated by the ANSYS model. The effective conductivity ( $K_{xx}$ ) is determined using the following formula.

$$q = K_{xx} (A/L) \Delta T$$

or

$$K_{xx} = q L / (A \Delta T)$$

where:

|            |       |   |
|------------|-------|---|
| $K_{xx}$   | ----- | effective conductivity (Btu/hr-in-°F) in X direction in Figure 4.4-10 through Figure 4.4-12 |
| $q$        | ----- | heat rate (Btu/hr)  |
| $A$        | ----- | area (in <sup>2</sup> )   |
| $L$        | ----- | length (thickness) of model (in)  |
| $\Delta T$ | ----- | temperature difference across the model (°F)  |

The temperature-dependent conductivity is determined by varying the temperature constraints at one boundary of the model and solving for the temperature difference. The effective conductivity for the parallel path (the Y direction in Figure 4.4-10) is calculated by the following.

$$K_{yy} = \frac{\sum K_i t_i}{L}$$

where:

|       |       |   |
|-------|-------|---|
| $K_i$ | ----- | thermal conductivity of each layer (Btu/hr-in-°F) |
| $t_i$ | ----- | thickness of each layer (in)                      |
| $L$   | ----- | total length (thickness) of the model (in)        |

#### **4.4.1.5 Two-Dimensional Transfer Cask and TSC Model for Operations Involving 24-Hour Cooling**

During the transfer condition, the TSC in the transfer cask is subjected to four separate conditions.

- The water phase when the lid is being welded to the TSC.
- The drying phase during which helium is present while vacuum drying to remove moisture from the TSC.
- The helium backfilled phase when the TSC closure is completed and the transfer cask cooling water system is operating (24 hours of cooling).

- The operation of transferring the helium-backfilled TSC into the concrete cask with the transfer cask annulus circulating water cooling system drained.

In this section, analyses are performed to support the use of 24-hour cooling after the drying phase and prior to loading of the canister into the concrete cask. The use of the 24-hour cooling permits the maximum time for the drying phase and the maximum time to transfer the canister into the concrete cask. Section 4.4.1.6 describes the evaluation of an alternate system drying operational cycle permitting the cool time to be minimized and the loading of the canister into the concrete cask to be limited to eight hours.

The first step is considered to be steady-state conditions for all heat loads. For vacuum drying operations, there is no time limit for the PWR basket with heat loads less than or equal to 25 kW, and no time limit for the BWR basket with heat loads less than or equal to 29 kW. The time in vacuum drying is administratively controlled for the PWR basket with heat loads greater than 25 kW, and for the BWR basket with heat loads greater than 29 kW, to ensure the maximum fuel cladding temperature is less than the allowable temperature. For high heat loads greater than 25 kW for the PWR basket and greater than 29 kW for the BWR basket, the 24-hour helium-backfilled phase is needed for both systems. The maximum time allowed for loading the helium-backfilled TSC into the concrete cask without operating the transfer cask annulus circulating water cooling system is determined by transient analyses. During the operational sequence of TSC loading, an annulus circulating water cooling system may be used to flow water through the annulus to cool and maintain a specified temperature for the TSC external shell. Other than using the pool to cool the system, alternative cooling methods, including TSC preparations on a pool shelf partially submerged or placement in an equivalent immersion method, may also be used. The annulus cooling methods, when used, are designed to accommodate design basis heat loads without additional heat rejection from the transfer cask to the environment.

#### **Evaluation of the Water Phase**

The model that includes water in the TSC treats the entire cavity as though it is filled with water. Since it is necessary to remove some water from the TSC during the closure lid welding operation, the water level in the TSC may be below the top of the fuel basket. The fuel tubes are designed with holes in the sides to permit the water to flow from the center of the TSC to the downcomer region of the TSC. The two-dimensional axisymmetric transfer cask and TSC models are used to evaluate the transfer operation for PWR fuels and BWR fuels. The components comprising the transfer cask and TSC model are shown in Figure 4.4-13 for the PWR configuration. The BWR model is identical to the PWR model except for a slight difference in the dimensions. The TSC portion of the model is identical to the model employed in Section 4.4.1.1, with the exception that one of the conditions in the transfer operations uses

water in the TSC instead of helium. The model for the TSC, described in Section 4.4.1.1, uses effective properties for the fuel basket region. For the water condition, the methodology described in Sections 4.4.1.2, 4.4.1.3, and 4.4.1.4 is used to determine the effective properties for the fuel basket region. For the condition of water in the TSC, no contribution due to radiation was considered; only conduction was taken into account for the effective properties. The porous media constants for the fuel basket region need not be recomputed since they are dependent on the fuel assembly and fuel basket geometry only. However, during the analytical evaluation of the water phase, the pressure drop in the fuel basket region due to the water requires the use of the viscosity, which is input as a material property. Since the maximum water temperature in the TSC is significantly below 212°F, the water is expected to remain in the liquid state, and the use of properties for the liquid state is acceptable. The transfer cask and the water annulus between the transfer cask and the TSC are also included in the model. The transfer cask is represented by effective properties. The transfer cask wall is comprised of four different materials: 1) a carbon steel inner shell; 2) a lead gamma shield layer; 3) an NS-4-FR neutron absorber layer; and 4) a carbon steel outer shell. Effective thermal conductivity for the transfer cask in the radial direction treats the four different cask wall materials as being in series. The effective thermal conductivity for the transfer cask wall in the axial direction treats the four different cask wall materials as being in parallel. The model also contains the shield doors of the transfer cask. While the inlets to the transfer cask are tubes in the side walls of the transfer cask, they are included in the model as straight sections parallel to the annulus. The following conditions are applied to the model for the steady-state evaluation of the water condition.

- The outer surfaces of the transfer cask are considered to be adiabatic and without the application of solar insolation.
- The inlet water temperature for the annulus between the TSC and the transfer cask is specified to be 100°F.
- The driving force for the water flow in the annulus between the TSC and the transfer cask is natural convection.
- The heat generation internal to the TSC is modeled as 15, 20, 25, 30 and 35.5 kW for PWR fuels. The heat loads in Regions A, B and C, as defined in Figure 4.1-1, are factored based on the heat load for heat loads other than 35.5 kW. For the heat load of 35.5kW, the heat loads in Region A, B and C are 0.922 kW, 1.20 kW and 0.80 kW, respectively. The heat generation internal to the TSC is modeled as 15, 20, 25, 30 and 33 kW for BWR fuels with a uniform heat distribution.
- The flow in the TSC and in the annulus region is treated as being laminar for both the water and helium conditions of the TSC.
- Radiation heat transfer is removed from the solution.

### **Evaluation of the Drying Phase-Vacuum Drying System**

A Vacuum Drying System (VDS) is used to evacuate and dry the TSC cavity by vaporization and removal of the water vapor and other gases from the cavity through the vent and drain port openings. During the vacuum drying phase, convection is not considered in the TSC cavity region. Conduction helium properties are utilized during the low-pressure drying process [27].

The transfer cask model used for the thermal transient analysis is comprised of a three-dimensional ANSYS model, as shown in Figure 4.4-16 and Figure 4.4-17 for PWR fuel and Figure 4.4-18 and Figure 4.4-19 for BWR fuel. Both PWR and BWR models do not contain the canister lid and bottom and, conservatively, neglect any heat being rejected in the axial direction. During the vacuum drying phase, the annulus circulating water cooling system is a normal operating system that allows the heat from the canister to be rejected in the same manner as for the water phase. The transfer annulus circulating water cooling system is an operational convenience and not a safety-related system, since the transfer cask can be placed back into the spent fuel pool at any point in time during the transfer operation without resulting in thermal shock to the transfer cask system. Maximum temperature on the canister outer diameter from the water phase analysis is applied to the canister surface for each heat load.

Effective properties for the PWR and BWR fuel region and the neutron absorber for the helium inside the canister are employed, and they are described in Sections 4.4.1.3 and 4.4.1.4, respectively. These two models are used to determine the allowable time in vacuum, depending on the heat load, to ensure that the fuel cladding temperature limit of 752°F (400°C) is not exceeded. For a heat load less than or equal to 25 kW for PWR fuel and less than or equal to 29 kW for BWR fuel, there is no time limit for the vacuum drying process. The steady-state fuel cladding temperature remains below 752°F (400°C). For heat loads greater than the unlimited vacuum time loadings, vacuum time limits are defined to meet system dry criteria. If system dry criteria are not met, operations are required to return to system cooling. For heat loads greater than 25 kW for PWR fuel and greater than 29 kW for BWR fuel, drying operations can continue following 24 hours of cooling the TSC, either with the annulus cooling system or returning the transfer cask and TSC to the spent fuel pool. TSC cooling is facilitated by backfilling the TSC cavity with helium to a pressure of 7 atmospheres (gauge). The backfilled helium will establish a convective heat transfer flow regime, thereby reducing the fuel cladding and system component temperatures.

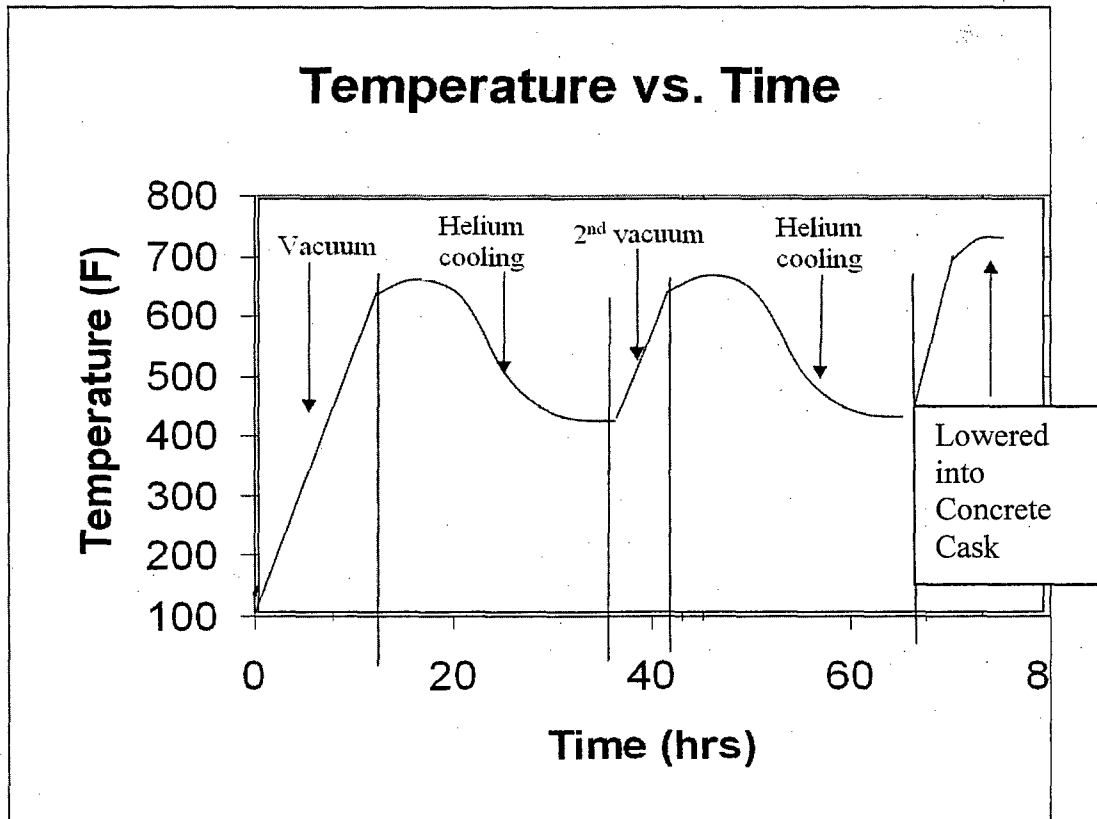
Transient analyses are performed to determine the maximum system temperature following the backfill helium condition for heat loads greater than 25 kW for PWR fuel and greater than 29 kW for BWR fuel. Analyses are performed for the 35.5 kW PWR and the 33 kW BWR design basis heat loads using the same two-dimensional FLUENT model used for analysis of the water

phase condition with modified material properties and boundary conditions. The initial temperature field of the transient evaluation to simulate the helium backfill condition is obtained from the analysis results at the end of the vacuum drying process (ANSYS results) for the respective heat load.

The FLUENT model used to analyze the cooldown transient defines the locations at which initial temperatures are required from the ANSYS results. For each node in the FLUENT model, there are eight node points in the circumferential direction in the ANSYS 45-degree symmetry model to compute the average temperature for the respective locations. The ANSYS model employs linear temperature shape functions across each element, so that interpolation between nodes and within an element provides temperatures that are consistent with the nodal temperature in the ANSYS results. The peak temperatures, which occur at the center line of the model, are transferred to the respective FLUENT node locations as initial temperatures in order to provide an upper bounding initial condition, conserving system heat provided to the FLUENT model.

The design basis heat load provides bounding temperatures and minimum times for vacuum and the longest time for helium cooling when needed. With the identification of the temperature after the backfill condition, the time in vacuum for the potential cooling cycles can be determined, since the temperature time history will follow the same time dependency as for the initial vacuum condition.

The following diagram presents the system thermal transient history representative of vacuum drying followed by a postulated system cooling cycle of 24 hours, followed by a second system vacuum drying that is again followed by a second 24-hour cooling period preceding the TSC transfer to the concrete cask. It is noted that the 24-hour cooling period returns the system to a steady-state condition for the design basis heat load, providing a bounding operating cycle for all heat loads less than the design basis. Similarly, cooling the system for a period of 24 hours provides maximum canister transfer time from the transfer cask to the concrete cask when the water is drained from the annulus cooling system. Additional analyses defining system response to these conditions are addressed in the following discussions.



### Mesh Sensitivity Evaluation

The vacuum drying operation uses a three-dimensional ANSYS model to determine the thermal response of the fuel, shown in Figure 4.4-16 and Figure 4.4-18 for PWR and BWR fuel, respectively. Sensitivity of the mesh density is performed for the PWR design basis heat load of 35.5 kW. The finite element model uses an ANSYS element with a linear shape function for calculating the temperature within each element and uses a minimum of six elements in the fuel assembly cross-section plane. Temperature variation in the fuel region is expected to be parabolic since the heat generation is constant within any specified axial cross-section. Using a minimum of six elements permits development of an analytical parabolic distribution. To confirm the adequacy of the mesh density for the axial divisions, the number of elements in the model shown in Figure 4.4-16 was doubled, and the transient condition using design basis heat was rerun. The maximum fuel clad temperature was determined to be 633°F, as compared to 634°F for the solution with one-half the element density (shown in Table 4.4-9). The results from this mesh sensitivity evaluation validate that the maximum fuel temperature is relatively insensitive to mesh refinement in the fuel region.

### **Evaluation of the Helium Phase**

Following the completion of drying and final cavity evacuation, the TSC is backfilled and pressurized with helium to establish the cavity atmosphere for the normal condition of storage. The transfer cask and TSC remain in this helium phase condition until the TSC is placed into the concrete cask. During the helium phase, the transfer cask annulus cooling system will be used until the TSC preparations for transfer to the concrete cask are completed. Steady-state analyses for heat loads of 15, 20, 25, 30 and 35.5 kW for PWR fuel, and with heat loads of 15, 20, 25, 30 and 33 kW for BWR fuel, are performed using the model for the helium phase. The evaluation of this condition is performed to determine the initial condition for the operation in which the TSC is placed into the concrete cask with the transfer cask annulus cooling system drained.

### **Evaluation of Moving the TSC into the Concrete Cask**

The transfer cask is used to load the TSC into the concrete cask. During this phase, there is no active auxiliary cooling of the transfer cask. The annulus is filled with ambient air and this operation is time-limited to control the fuel cladding temperature to less than 752°F (400°C). The thermal performance of the transfer cask in this operation is evaluated for four conditions. Two transient conditions are for the PWR fuels with heat loads of 25 kW and 35.5kW, and two cases are for the BWR fuels with heat loads of 25 kW and 33 kW. The initial conditions for the four analyses are obtained from the steady-state analyses with water in the transfer cask annulus described in the preceding section (Evaluation of the Helium Phase) for the corresponding heat load.

#### **4.4.1.6 Two-Dimensional Transfer Cask and TSC Model for Operations Involving Minimum Cooling Time and a Loading Time of Eight Hours**

Operational experience can lead to enhancement in the draining, vacuum drying and welding operations to minimize the need for maximum times for drying and loading operations or the potential need for cycles in the vacuum drying phase. Operational experience will reduce loading times and reduce staff radiation exposure. The following discussion presents the operational controls to be implemented.

Even with the absence of additional cycles for vacuum or the use of the 24-hour cool time, the TSC in the transfer cask is still subjected to four separate operational boundary conditions.

- The water phase when the lid is being welded to the TSC.
- The drying phase during which helium is present while vacuum drying to remove moisture from the TSC.



- The helium-backfilled phase is minimized to seven hours or less. It is during this time when the TSC port covers are completed and the transfer cask annulus circulating water cooling system is operating.
- The eight hours for the operation of transferring the helium-backfilled TSC into the concrete cask with the transfer cask annulus circulating water cooling system drained.

Regardless of the time in the vacuum drying or loading operation, the response of the canister and transfer cask in the water phase (inside the canister) is not affected. With cooling water in the annulus, the time to remain in this condition is not altered from the system analyses or results reported in Section 4.4.1.5 for the water phase.

Without the additional cool time (of 24 hours), the initial temperatures of the canister and fuel are significantly increased upon entering the loading phase (where the water in the annulus is drained and replaced by air). Reducing the time in the vacuum phase, as compared to the times shown in Table 4.4-9 (PWR) and Table 4.4-10 (BWR), the temperatures at the start of the condition leading to the transfer of the canister to the concrete cask can be reduced to a level that allows eight hours for the transfer loading time.

To determine the vacuum and cool time limits, the models and their results described in Section 4.4.1.5 are used. The temperature time histories computed for the heat loads identified in Table 4.4-9 (PWR) and Table 4.4-10 (BWR) are used to identify the maximum clad temperatures at the end of the reduced vacuum times for the individual heat loads. The transient analyses for the condition of the helium backfill, in conjunction with water in the annulus as described in Section 4.4.1.5 identify the temperature increase expected for the range of heat loads for the fuel clad upon backfilling the canister with helium. Analyses in Section 4.4.1.5 identify that the maximum increase in the temperature of the fuel for the bounding PWR and BWR heat loads is 44°F and 34°F, respectively. The 44°F PWR increase and the 34°F BWR increase corresponding to the design basis heat bound the temperature for all other possible heat loads of the PWR or BWR fuel assemblies. The maximum temperature increase is conservatively added to the maximum fuel clad temperature occurring at the end of the reduced time in vacuum. This temperature is used to confirm that an additional eight hours for the canister in the transfer cask with air in the annulus is equal to, or less than, the maximum fuel clad temperatures determined in Section 4.4.1.5.

#### **4.4.2      Test Model**

MAGNASTOR is conservatively designed by analysis. Therefore, no physical model is employed for thermal analysis. The benchmark provided in Section 4.8.1 provides confirmation that the analysis methodology employed for the MAGNASTOR design is conservative.

#### 4.4.3 Maximum Temperatures for PWR and BWR Fuel Configurations

##### Normal Conditions of Storage

The temperature distribution and maximum component temperatures for MAGNASTOR for normal conditions of storage are provided in this section. System components containing PWR and BWR fuels are addressed separately. The temperature distributions for the BWR design basis fuel are similar to those of the PWR design basis fuel and are, therefore, not presented.

The temperature distribution for the concrete cask and the TSC containing the PWR design basis fuel for normal conditions of storage, with a uniform heat load, is shown in Figure 4.4-14. The air velocity distribution in the annulus between the TSC and the concrete cask liner for the normal conditions of storage for PWR fuel is shown in Figure 4.4-15. The maximum component temperatures for the normal conditions of storage for the PWR and BWR design basis fuel are shown in Table 4.4-3. It is noted that these system thermal performance results are based on an average annual ambient temperature of 76°F at sea level pressure and standard air density properties. Site-specific conditions are to be evaluated to assure thermal margins are maintained for steady-state storage conditions at the intended MAGNASTOR ISFSI site.

As shown in Figure 4.4-14, the peak fuel temperature for the normal storage condition occurs near the top of the fuel basket and, based on the uniform spacing of the isotherms at the centerline of the TSC, the temperature varies monotonically from the TSC bottom to the peak near the top of the fuel basket. This is indicative that the dominant mode of heat rejection from the fuel is by convection due to the helium flow circulating within the TSC.

The calculated temperatures at the TSC surface for the normal storage condition are higher than the concrete liner or surface, indicating that radiation heat transfer occurs across the concrete cask to TSC annulus. As shown in Table 4.4-3, the maximum local temperature in the concrete can reach 271°F for PWR design basis fuel, which is less than the 300°F allowable temperature. It is noted that the temperature difference between the average outlet temperature and the design basis normal ambient of 76°F for the PWR design basis heat load of 35.5 kW is calculated to be 85°F. Similar analysis for the BWR design basis heat load of 33 kW is calculated to be 79°F.

##### Transfer Condition for 24-Hour Cooling and Multiple Vacuum Drying Cycles

The maximum component temperatures for MAGNASTOR during the transfer operation are reported in this section for operational procedures using 24 hours of cooling. The transfer operation is comprised of four separate phases: the water phase, the drying phase, the helium phase, and the TSC transfer phase. The water phase and the helium phase are not time limited due to the normal use of the transfer cask annulus cooling water system, partially submerged

loading conditions, or an equivalent immersion system. The transfer cask annulus cooling system is an operational convenience and not a safety-related system, since the transfer cask can be placed back into the spent fuel pool at any point in time during the transfer operation without resulting in thermal shock to the transfer cask system. The annulus cooling water system maintains the canister shell at a temperature significantly lower than the temperature corresponding to the normal conditions of storage. The maximum temperatures for the water phase are listed in Table 4.4-5 and Table 4.4-6 for PWR fuel and BWR fuel, respectively. The maximum temperatures for the helium phase are listed in Table 4.4-7 and Table 4.4-8 for PWR fuel and BWR fuel, respectively. Table 4.4-9 and Table 4.4-10 present times for the vacuum drying for heat loads greater than 25 kW for PWR fuel and greater than 29 kW for BWR fuel that are administratively controlled to maintain the fuel cladding temperature below the 752°F limit. If additional vacuum drying is required for heat loads requiring administrative controls to meet the specified cavity dryness criteria, additional drying cycles can be performed following 24 hours of cooling the TSC, either with the annulus cooling water system or by returning the transfer cask and TSC to the spent fuel pool. Table 4.4-11 and Table 4.4-12 show the second vacuum time and maximum fuel temperatures at the end of the duration for PWR fuel and BWR fuel, respectively. Note that the PWR fuel cladding temperatures shown in Table 4.4-5 through Table 4.4-10 are bounded by the PWR fuel cladding temperatures for the normal storage steady-state conditions in Table 4.4-3. Therefore, the normal condition design bases PWR heat load fuel cladding and component temperatures, such as for the fuel basket and the TSC, bound the maximum temperatures for any phase of the transfer condition for the fuel basket and TSC components.

The time for TSC transfer to the concrete cask is administratively limited to ensure that the maximum fuel cladding temperature is bounded by the design bases heat load normal condition storage temperature.

Table 4.4-13 and Table 4.4-14 show the duration and the maximum fuel temperature at the end of the TSC placement in the concrete cask for both PWR fuel and BWR fuel, respectively. The time duration for the transfer operation is determined by modeling the water material properties in the annulus as air, as described in Section 4.4.1.5.

The off-normal condition for use of the annulus cooling system corresponds to loss of cooling by the annulus cooling system. This can occur during the water phase or the drying phase of transfer operations. If loss of cooling occurs during the water phase, a conservative energy balance treating the canister surface as being adiabatic shows that the canister temperature can be maintained for 13 hours without exceeding 212°F. If the water phase exceeds this time limit, the cask is to be returned to the spent fuel pool or the cooling water system is restarted. In the event

of loss of cooling occurring during the vacuum drying phase, the canister is first backfilled with 7 atm (gauge) helium, and then is returned to the pool. The time limit for this backfilling and returning to the spent fuel pool or starting the cooling water system is four hours.

The loading procedures in Chapter 9 provide operational sequence alternatives and time limitations if the annulus cooling system is not operating. In all cases, the final corrective action is to backfill the TSC with helium to 7 atm gauge pressure and return the system to the spent fuel pool or restart the cooling water system. These operational sequences, time limits and corrective actions will ensure that the fuel cladding and system component temperatures do not exceed design allowable values.

### **Transfer Condition for Minimum Cooling Time and Eight Hours of Canister Transfer**

The maximum component temperatures for MAGNASTOR during the transfer operation are reported in this section for operational procedures using the minimum cooling time and eight hours of canister transfer (as determined by the evaluation in Section 4.4.1.6). The transfer operation is comprised of four separate phases: the water phase, the drying phase (reduced time as compared to the evaluations in Section 4.4.1.5), the helium phase (minimized cooling time), and the TSC transfer phase (limited to eight hours). The water phase and the helium phase permit indefinite time due to the normal use of the transfer cask annulus cooling water system, partially submerged loading conditions, or an equivalent immersion system. The annulus cooling water system maintains the canister shell at a temperature significantly lower than the temperature corresponding to the normal conditions of storage. The maximum temperatures for the water phase are listed in Table 4.4-5 and Table 4.4-6 for PWR fuel and BWR fuel, respectively.

Heat load-dependent vacuum drying times reported in Table 4.4-9 and Table 4.4-10 confirm that for the same heat loads, the PWR fuel clad temperatures bound the BWR fuel clad temperatures. The temperatures reported in Table 4.4-15 and are for the maximum PWR and BWR clad temperatures, respectively, at the end of the reduced vacuum time, the reduced cool time, and the eight hours of loading. These results confirm that the maximum clad temperatures have significant margin relative to the 752°F fuel clad temperature limit.

For system operations that are outside the sequence presented in Table 4.4-15 or Table 4.4-16, as a result of equipment failure or some other event that extends drying and transfer operations, 24 hours of cool time will be implemented for cycles of vacuum drying and prior to transferring the canister into the concrete cask.

#### 4.4.4 Maximum Internal Pressures for PWR and BWR TSCs

The maximum TSC internal operating pressures for normal conditions of storage are calculated in the following sections for the TSCs containing PWR and BWR design basis fuel assemblies.

##### Maximum Internal Pressure for the TSC Containing PWR Fuel

The internal pressure of a TSC containing PWR fuel assemblies is a function of fuel type, burnup, initial enrichment, cool time, fuel condition (failure fraction), presence or absence of nonfuel hardware, TSC length, and the backfill gases in the TSC. Gases included in the pressure evaluation of a TSC containing PWR fuel include fuel rod fission, decay and backfill gases, gas generated by the nonfuel hardware components (assembly control components contain boron as the absorber material), and TSC backfill gases. Each of the PWR fuel types is separately evaluated to determine a bounding pressure for a TSC containing PWR fuel assemblies.

Fission gases include all fuel material generated gases, including helium generated by long-term actinide decay. Based on detailed SAS2H calculations, the quantity of fission and decay gases rises as burnup and cool time are increased and enrichment is decreased. The maximum gas available for release is conservatively calculated based on 70,000 MWd/MTU burnup cases at an enrichment of 1.9 wt %  $^{235}\text{U}$  and a cool time of 40 years for maximum fissile material assemblies in each major PWR fuel class. For other PWR fuel assembly types, fission and decay gases are determined by ratioing the fissile material mass to the maximum fissile material mass assemblies.

Fuel rod backfill pressure varies significantly among the PWR fuel types. Based on a literature review, a 500 psig backfill is assigned to Westinghouse and CE core fuel types. A maximum backfill pressure of 435 psig is assigned to B&W core assemblies. Backfill gas quantities are based on the fresh fuel free volume between the fuel pellet stack and the fuel rod cladding, including the plenum volume, and a backfill temperature of 68°F.

Burnable poison rod assemblies (BPRAs) placed within the TSC may contribute additional gas quantities due to n-alpha reaction of  $^{10}\text{B}$  during in-core operation. A portion of the neutron poison population is formed by  $^{10}\text{B}$ . Other neutron poisons, such as gadolinium and erbium, do not produce a significant amount of helium nuclides (alpha particles). The principal BPRAs in use include the Westinghouse Pyrex (borosilicate glass) and WABA (wet annular burnable absorber) configurations, as well as B&W BPRAs and shim rods used in CE cores. The CE shim rods replace standard fuel rods to form a complete assembly array. The quantity of helium available for release from the BPRAs is directly related to the initial boron content of the fuel rods and the release fraction of gas from the matrix material. The gas released from either of the low-temperature, solid matrix BPRA materials is likely to be limited, but no release fractions

were available in open literature. Consequently, a 100% release fraction is applied. Initial boron content in the Westinghouse and B&W BPRAs is based on a uniform absorber concentration of  $0.0063 \text{ g/cm}^{10}\text{B}$ . The maximum number of poison rods is 16 for Westinghouse  $14 \times 14$  fuel assemblies, 20 for Westinghouse and B&W  $15 \times 15$  fuel assemblies, and 24 for Westinghouse and B&W  $17 \times 17$  fuel assemblies. The length of the absorber rods is conservatively taken as the active fuel length. CE core shim rods are modeled at  $0.0126 \text{ g/cm}^{10}\text{B}$  for 16, 12, and 12 rods applied to CE-manufactured  $14 \times 14$ ,  $15 \times 15$ , and  $16 \times 16$  fuel assemblies, respectively.

Under normal operating conditions, the helium backfill for a TSC containing PWR fuel assemblies is at a maximum average gas temperature of  $465^\circ\text{F}$  and a pressure of 103 psig. Nominal helium densities for both PWR and BWR fuel types are shown in Table 4.4-4. Maximum system backfill pressure at operating conditions is set by the use of the operating procedures documented in Chapter 9. This approach ensures that an acceptable helium density is established in the canister prior to sealing. Free volumes inside the two classes of TSCs containing PWR fuel are 10,000 and 10,400 liters. The free volumes do not include PWR fuel assembly and nonfuel hardware components, since these vary for each assembly type. The free volume of the TSC is obtained by subtracting the assembly volume (with BPRA, TP or CEA insert). For the Westinghouse BPRAs, the Pyrex volume is employed since it displaces more volume than the WABA rods.

The TSC internal pressure is determined by summing the partial pressures of the TSC helium backfill gas and the released gases from the fuel and the poison rods. The partial pressure due to the fuel and neutron poison rod gases is determined by the ideal gas correlation ( $PV=nRT$ ) and the applicable rod release fractions and failure rates. For normal conditions, a 1% rod failure fraction is applied. For failed fuel rods, the releasable molar quantity of the fission and actinide decay gas is 30%, with 100% of the rod backfill gas being released. The normal condition average temperature of the gases released from the fuel rods and neutron poison inserts is conservatively set to  $485^\circ\text{F}$  (525 K) in the partial pressure calculation.

The TSC is evaluated for normal condition pressure for each of the PWR fuel types, with insert. The maximum normal condition pressure for a TSC containing PWR fuel assemblies is 104 psig. At a 1% rod failure fraction, the quantity of gas released from the fuel and neutron poison rods is minimal, resulting in no significant effect on system pressure.

The calculated maximum pressure of 104 psig allows for a 6 psig tolerance on the TSC helium backfill prior to reaching the 110 psig system pressure used in the Chapter 3 normal condition structural evaluations. Significantly higher pressure margins exist in the off-normal and accident pressures. Off-normal and accident pressures were calculated at 114 psig (10% fuel failure and off-normal thermal conditions) and 201 psig (100% fuel failure, see Section 4.6.4), and these

calculated values are significantly lower than the established pressure limits of 130 psig for off-normal and 250 psig for accident condition pressures that are used in the structural calculations.

### **Maximum Internal Pressure for the TSC Containing BWR Fuel**

Maximum internal pressures are determined for the BWR fuel in the same manner as those documented for the TSC containing PWR fuel. Primary differences for the BWR evaluations, versus those for the PWR, include a rod backfill gas pressure of 132 psig, a maximum burnup of 60,000 MWd/MTU used to generate fission gases, and the absence of neutron poison gases (no nonfuel hardware in the BWR system). The 132 psig rod backfill pressure used in this analysis is significantly higher than the 6 atmosphere (g) maximum pressure reported in open literature. Free volumes, without fuel assemblies, in the TSC containing BWR fuel types are 9,900 and 10,300 liters.

A bounding normal condition average temperature of 525 K is used for the partial pressure analysis of the fuel rod gases. The maximum normal condition pressure for a TSC containing BWR fuel is 104 psig.

The calculated maximum pressure of 104 psig allows for a 6 psig tolerance on the TSC helium backfill prior to reaching the 110 psig system pressure employed in the Chapter 3 normal condition structural evaluations. Significantly higher pressure margins exist in the off-normal and accident pressures. Off-normal and accident pressures were calculated at 110 psig (10% fuel failure and off-normal thermal conditions) and 158 psig (100% fuel failure, see Section 4.6.4) and are conservatively bounded by the 130 psig off-normal and 250 psig accident condition pressures that were employed in the structural calculations.

### **TSC Backfill Helium Tolerances**

Due to measurement and instrument uncertainties in the canister backfill operation, a range of allowed helium backfill density (g/liter) is determined in this section.

Any increase in backfill density is limited by the associated rise in pressure, which in turn is limited to the structural analysis inputs (110 psig for the limiting normal condition). As documented in the pressure evaluations, a 6 psi tolerance is acceptable prior to reaching system pressures employed in the structural analysis. Assuming a constant temperature, which is conservative as increased backfill density would enhance heat transfer and increase system pressure, and applying the ideal gas law make backfill density directly proportional to pressure. Relying on a 6 psi tolerance on a nominal pressure of 103 psig (118 psia) allows for a 5% increase in backfill density.

A decrease in backfill density is limited by thermal constraints. Lower helium density reduces convective heat capability of the system and, thereby, raises fuel clad temperature. Thermal analysis in Section 4.4.1.1 states that a 10% decrease in backfill density is acceptable while remaining below the maximum allowed clad temperature limit of 752°F.

Table 4.4-4 lists the pressure and temperature limited upper and lower bound helium backfill densities.



Figure 4.4-1 Two-Dimensional Model of Concrete Cask Loaded with PWR TSC

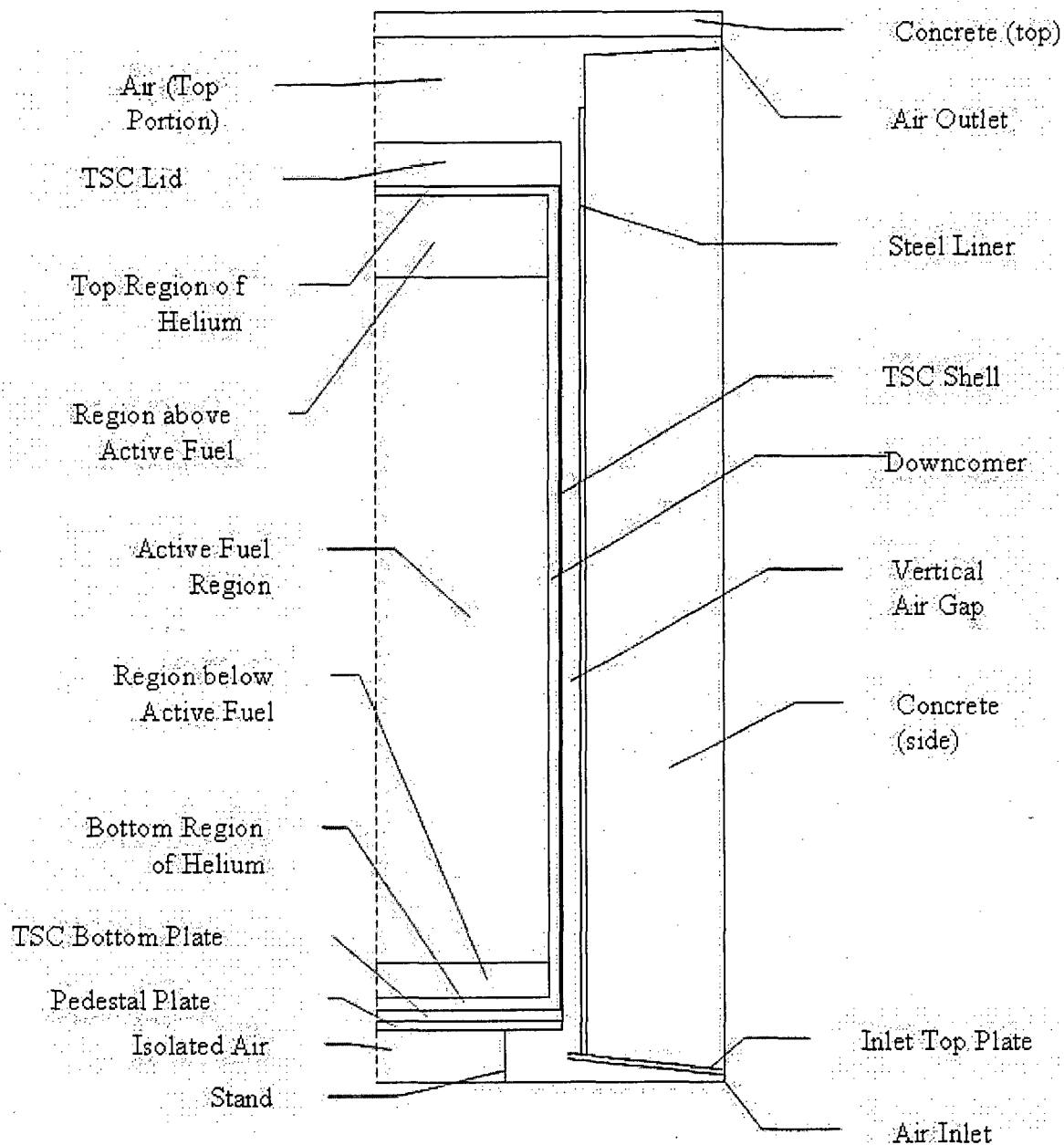


Figure 4.4-2 Computational Mesh for the Two-Dimensional Axisymmetric CFD Model of the Concrete Cask

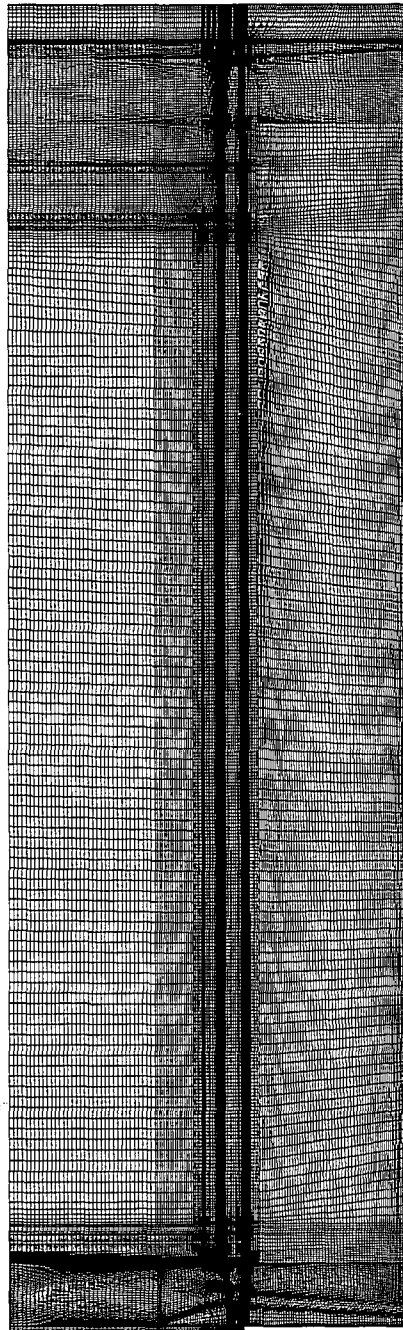


Figure 4.4-3 Axial Power Distribution for the PWR Fuel Assembly

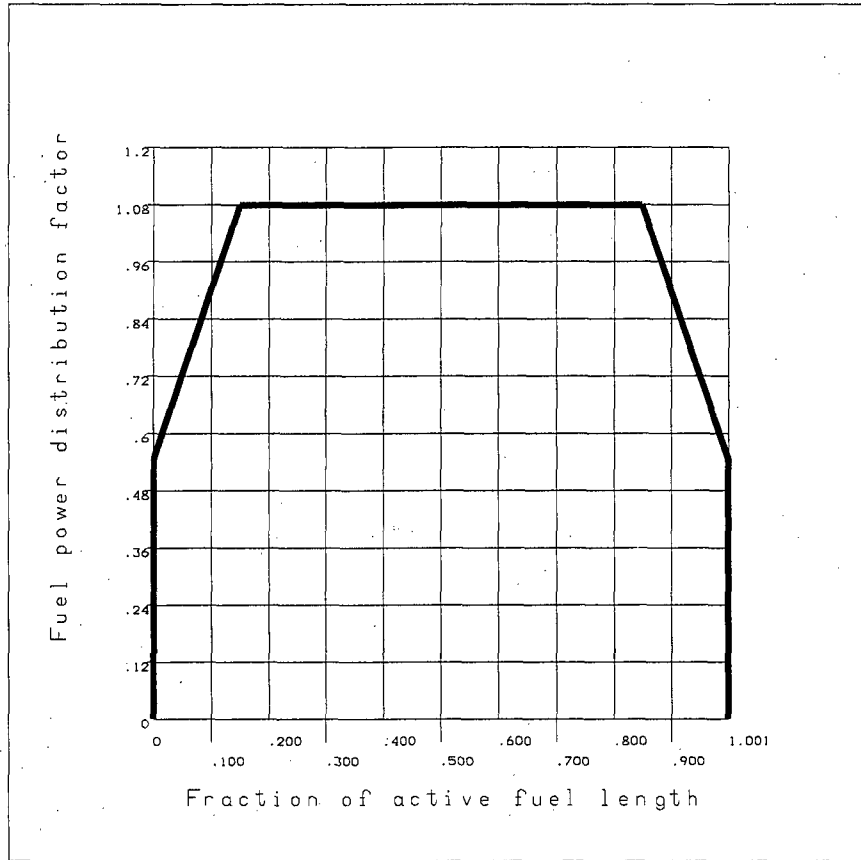


Figure 4.4-4 Axial Power Distribution for the BWR Fuel Assembly

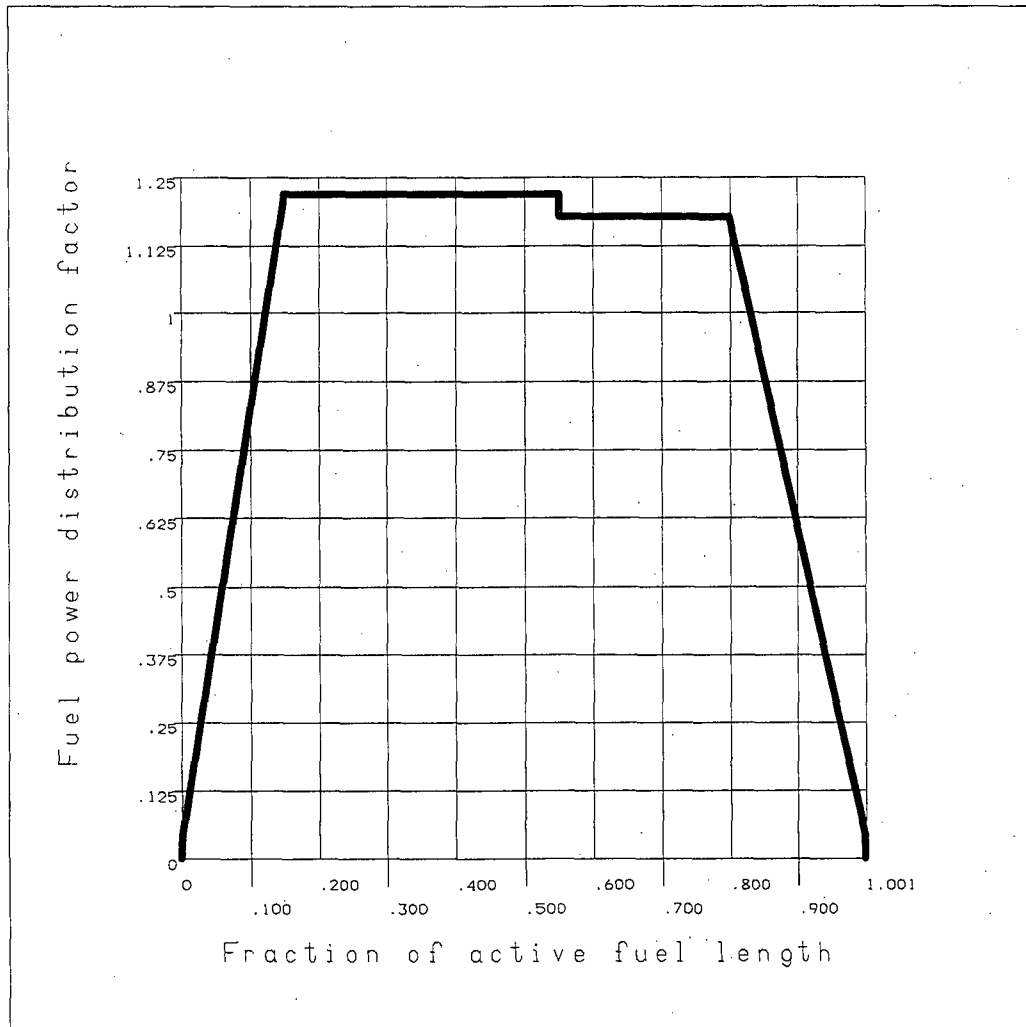


Figure 4.4-5 PWR Peak Fuel Cladding Temperature versus TSC Internal Pressure

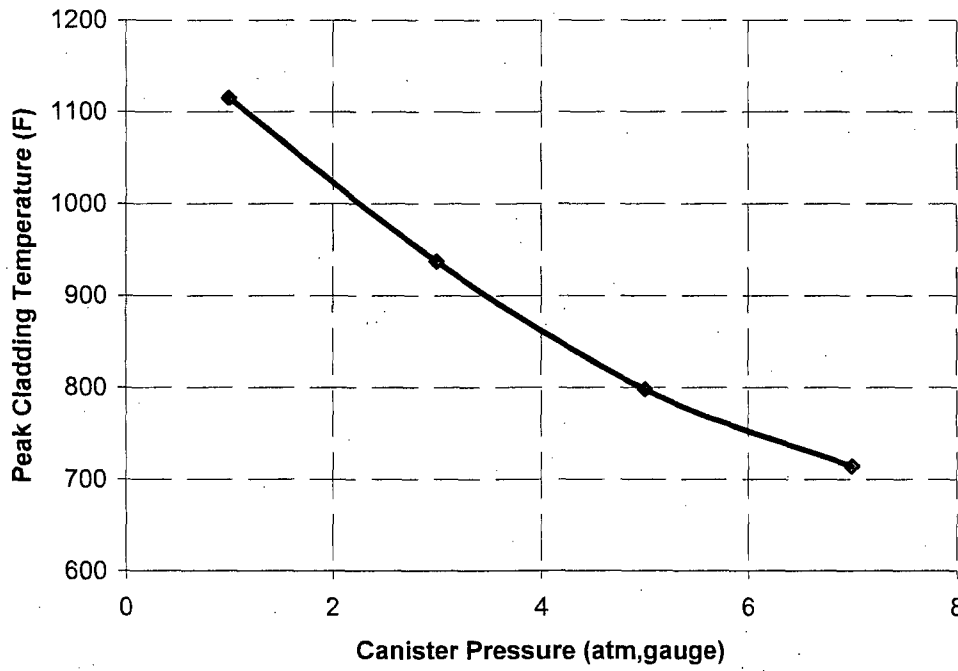


Figure 4.4-6 Two-Dimensional Finite Element Model of the PWR Fuel Basket

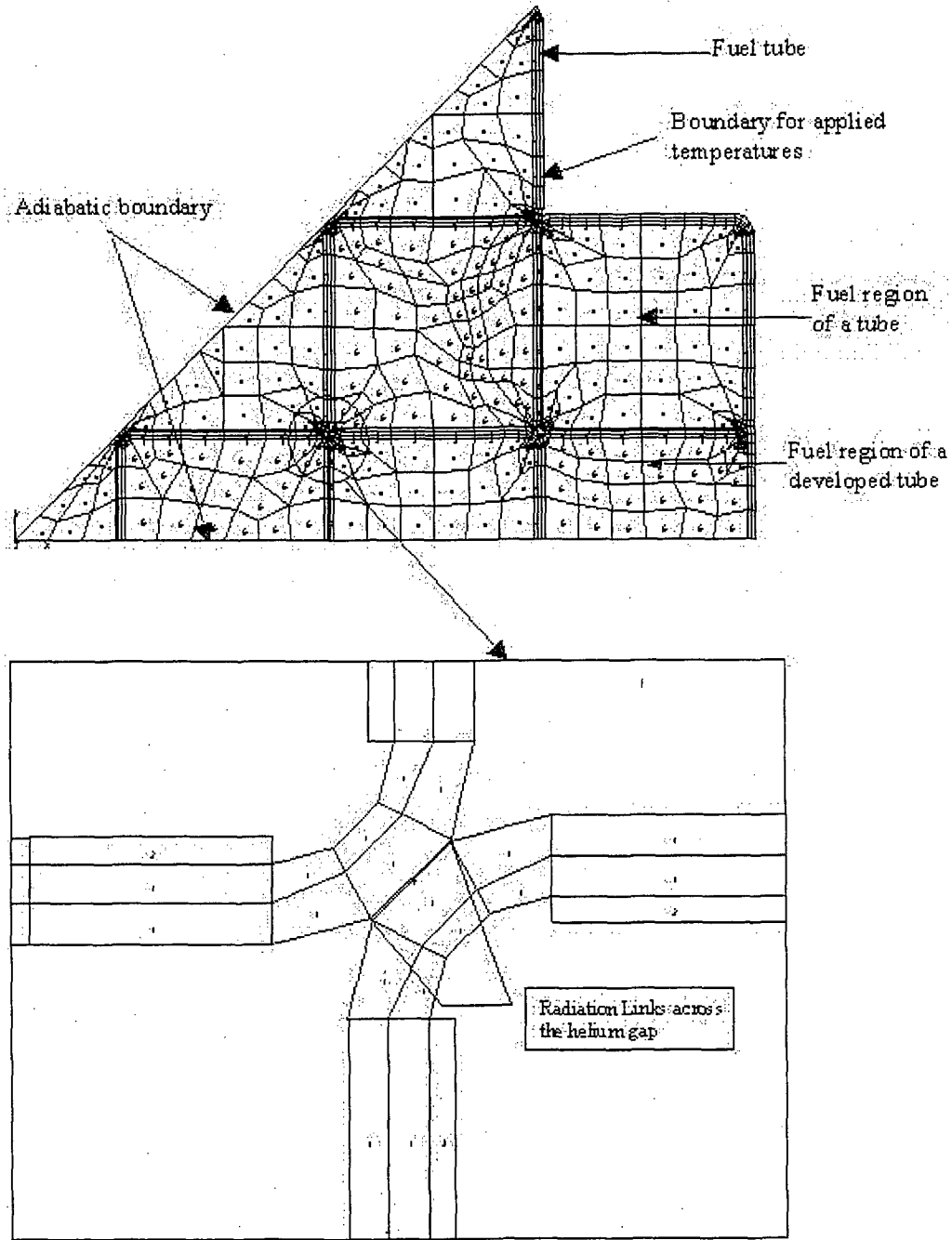


Figure 4.4-7 Two-Dimensional Finite Element Model of the BWR Fuel Basket

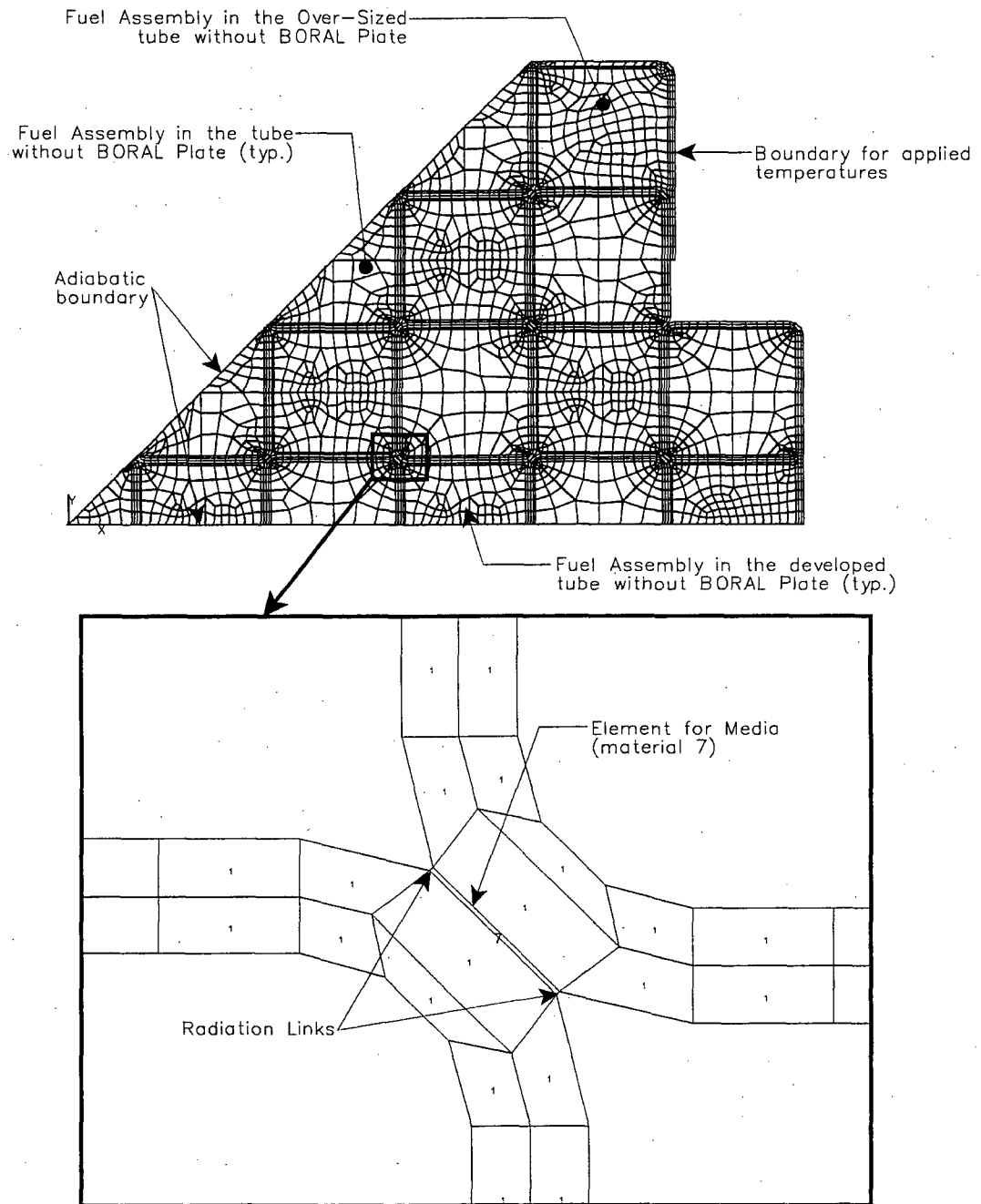
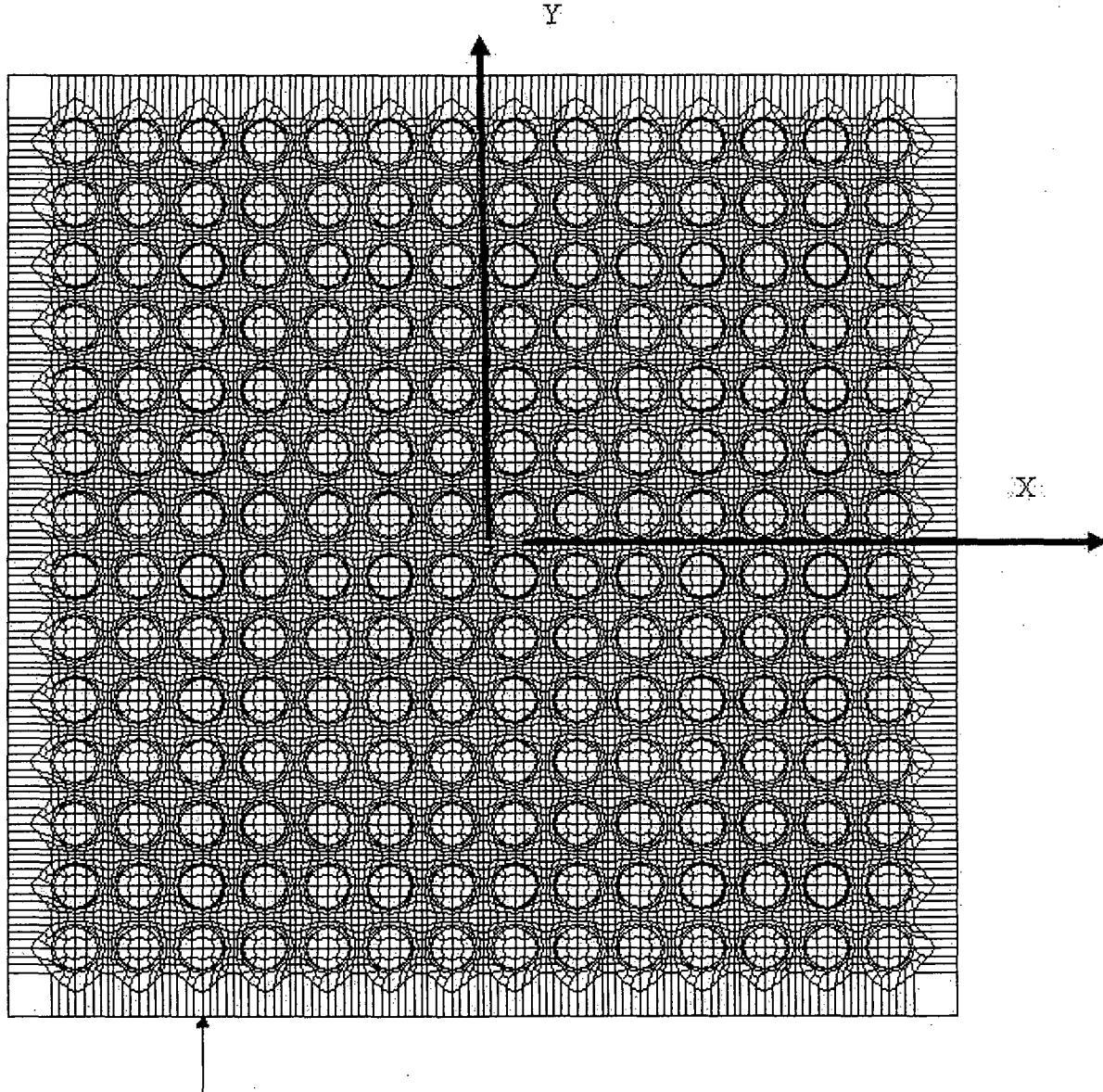


Figure 4.4-8 14×14 PWR Fuel Assembly Two-Dimensional Model

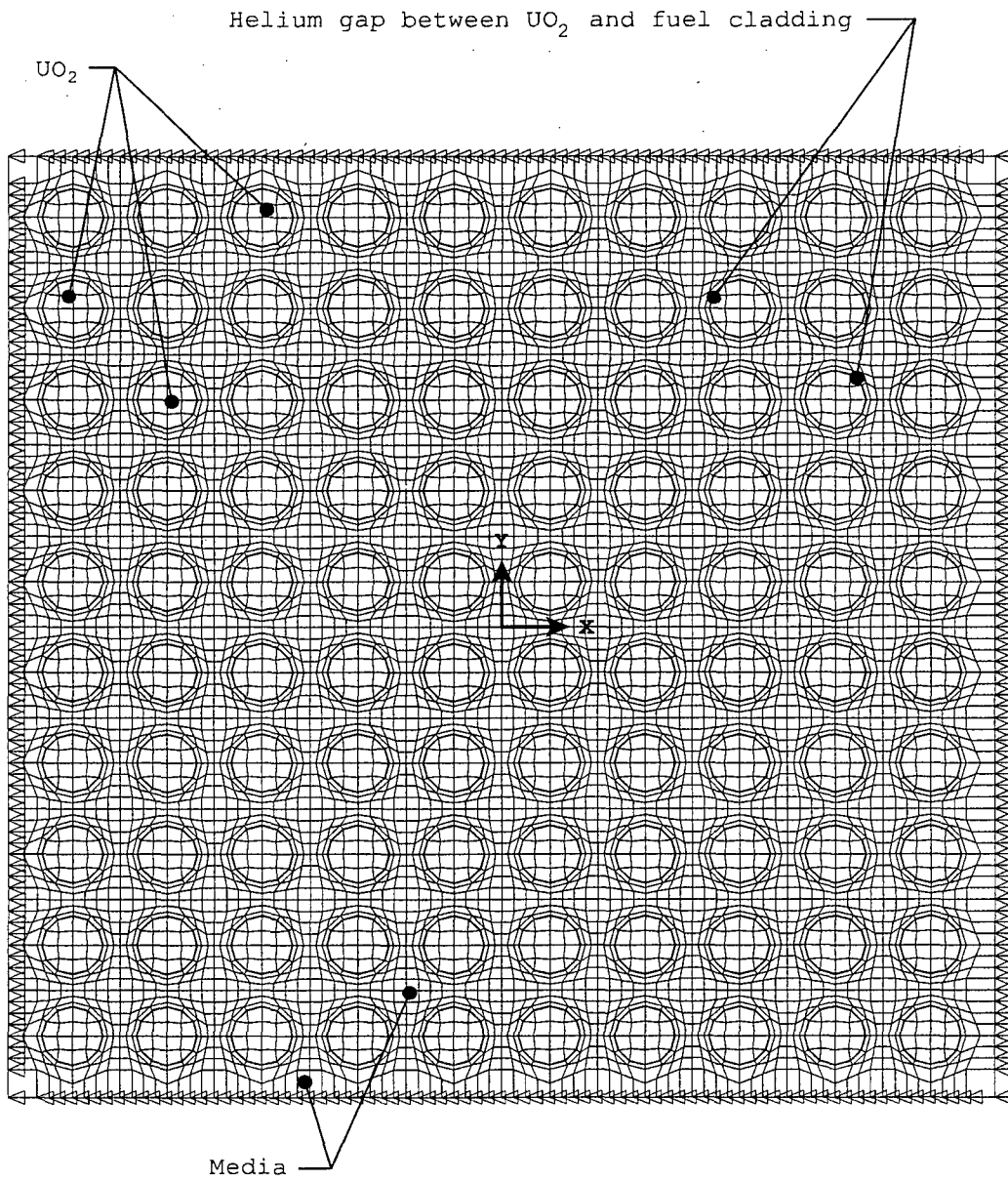


Temperature boundary condition applied along the edge of the model.

Note: X and Y correspond to the in-plane directions of the fuel assembly, while Z is out of the plane and corresponds to the axial direction of the fuel assembly.

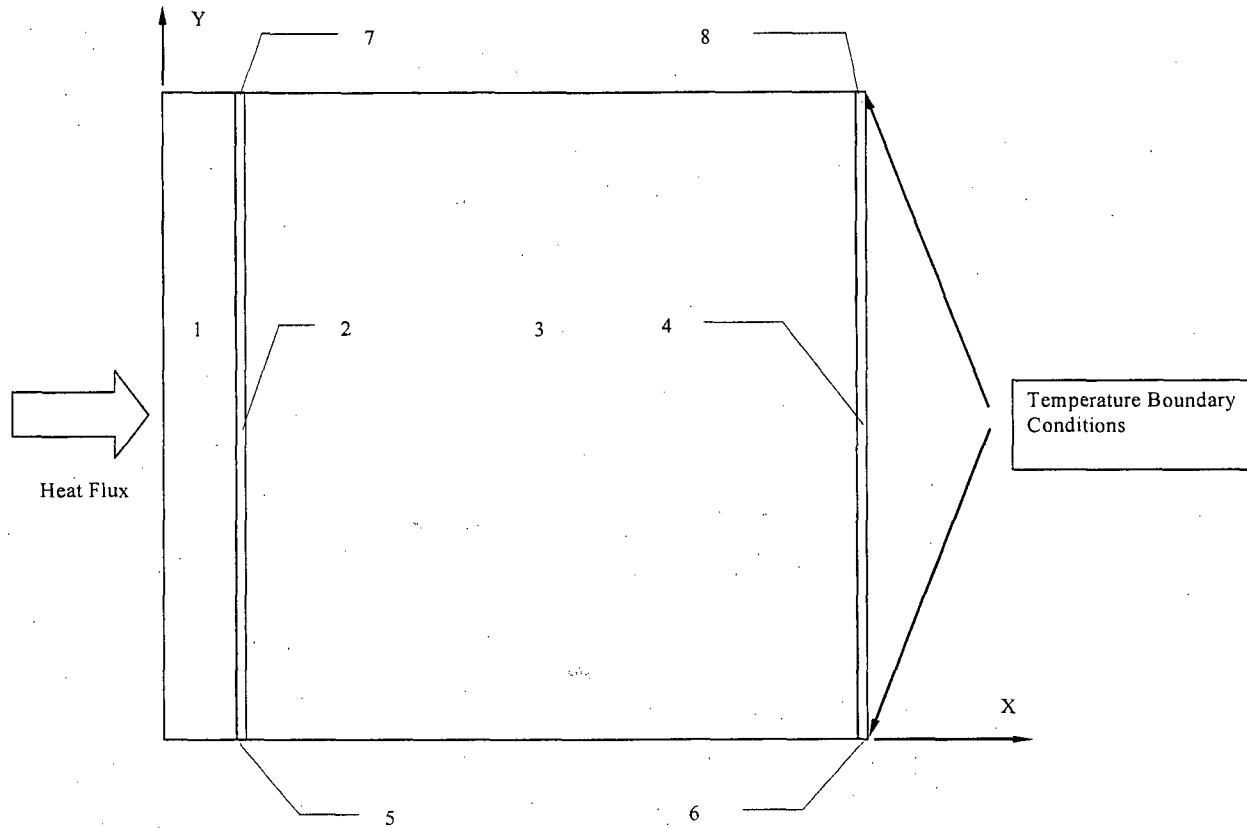


Figure 4.4-9 10×10 BWR Fuel Assembly Two-Dimensional Model



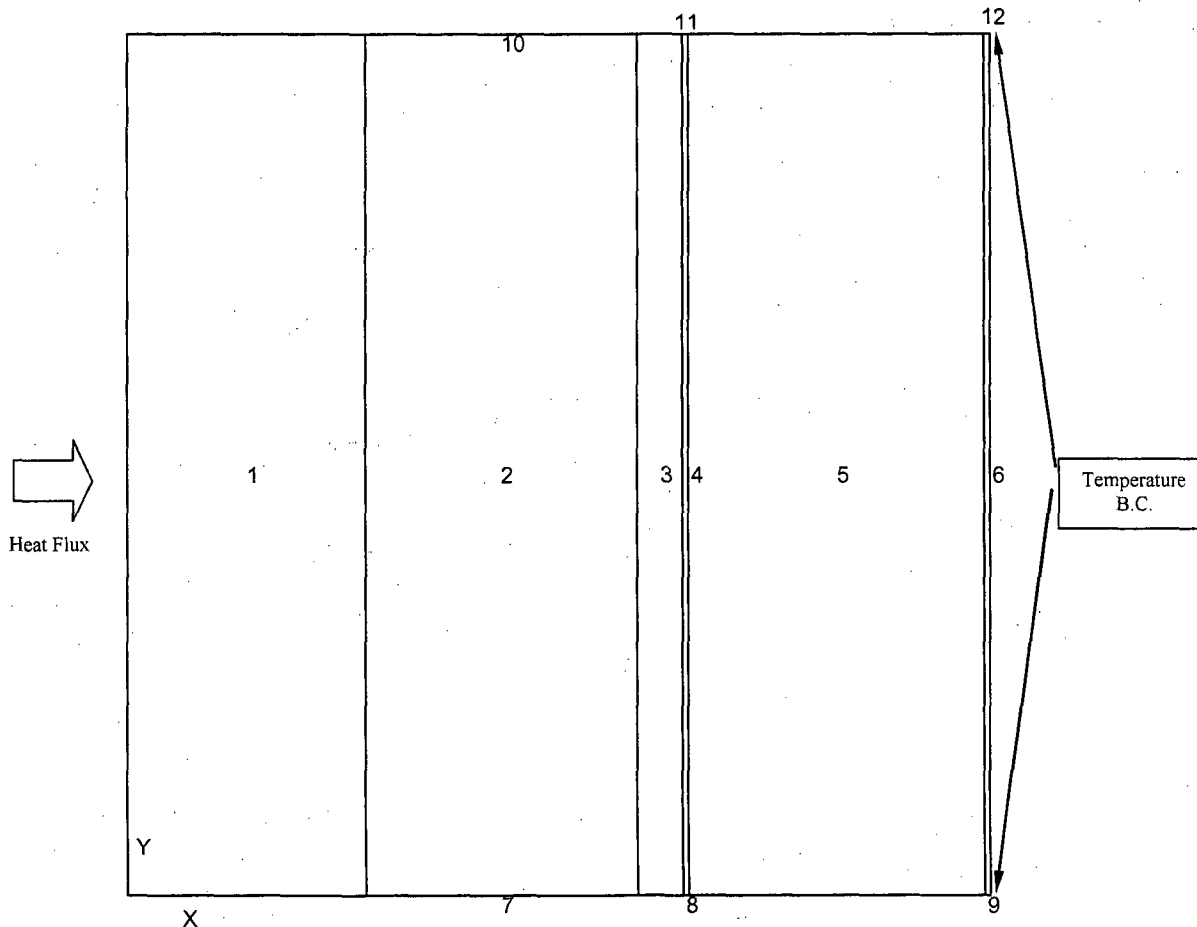
◁ Fixed Temperature Boundary Condition

Figure 4.4-10 Neutron Absorber Model for PWR Fuel Tube



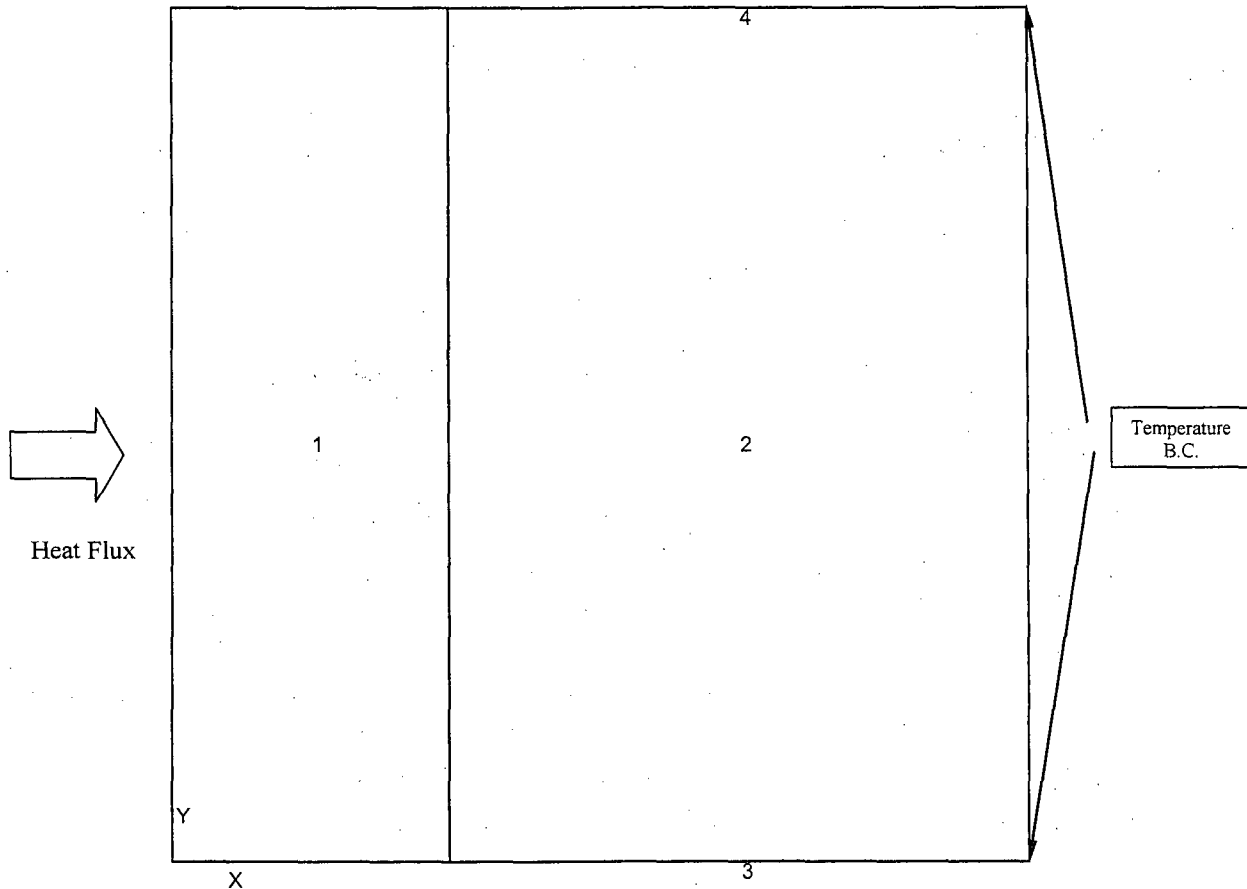
| Element Number | Description   |
|----------------|---|
| 1              | Stainless Steel Retainer Strip                                    |
| 2              | Media - Helium or water   |
| 3              | Neutron Absorber  |
| 4              | Media - Helium  |
| 5,7            | Radiation Links (between stainless steel and neutron absorber)    |
| 6,8            | Radiation Links (between aluminum and nickel plated carbon steel) |

Figure 4.4-11 BWR Fuel Tube Configuration with Channel and Neutron Absorber



| Element Number | Description   |
|----------------|---|
| 1              | Zirconium-based alloy (BWR fuel channel)                            |
| 2, 4, 6        | Media – Helium or water   |
| 3              | Stainless Steel Retainer Strip                                      |
| 5              | Neutron Absorber  |
| 7, 10          | Radiation Links (between zirconium-based alloy and stainless steel) |
| 8, 11          | Radiation Links (between stainless steel and aluminum)              |
| 9, 12          | Radiation Links (between aluminum and nickel-plated carbon steel)   |

Figure 4.4-12 BWR Fuel Tube Configuration with Channel, but without the Neutron Absorber



| Element Number | Description  |
|----------------|--|
| 1              | Zirconium-based alloy (BWR fuel channel)                                       |
| 2              | Media --- Helium or water  |
| 3, 4           | Radiation Links (between zirconium-based alloy and nickel-plated carbon steel) |

Figure 4.4-13 Two-Dimensional Model of Transfer Cask Loaded with a PWR TSC

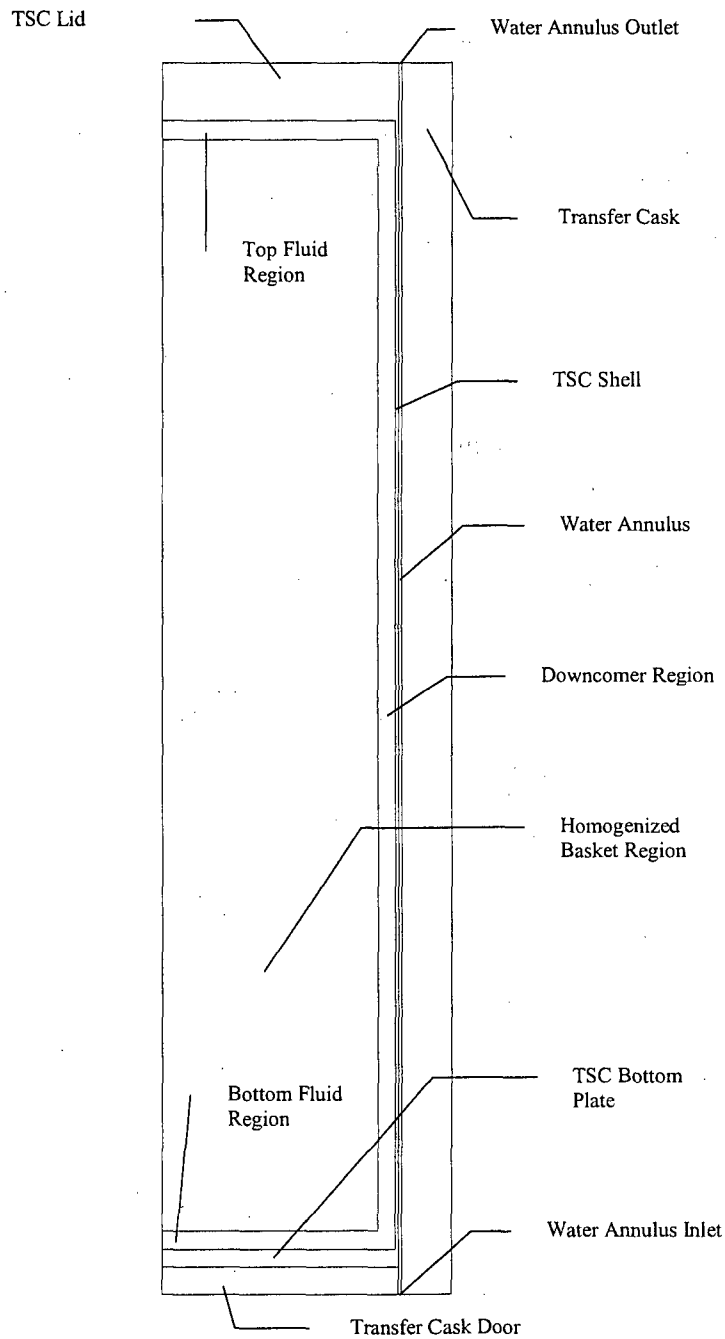


Figure 4.4-14 Temperature (°F) Distribution for the Concrete Cask and TSC  
Containing a Design Basis PWR Heat Load

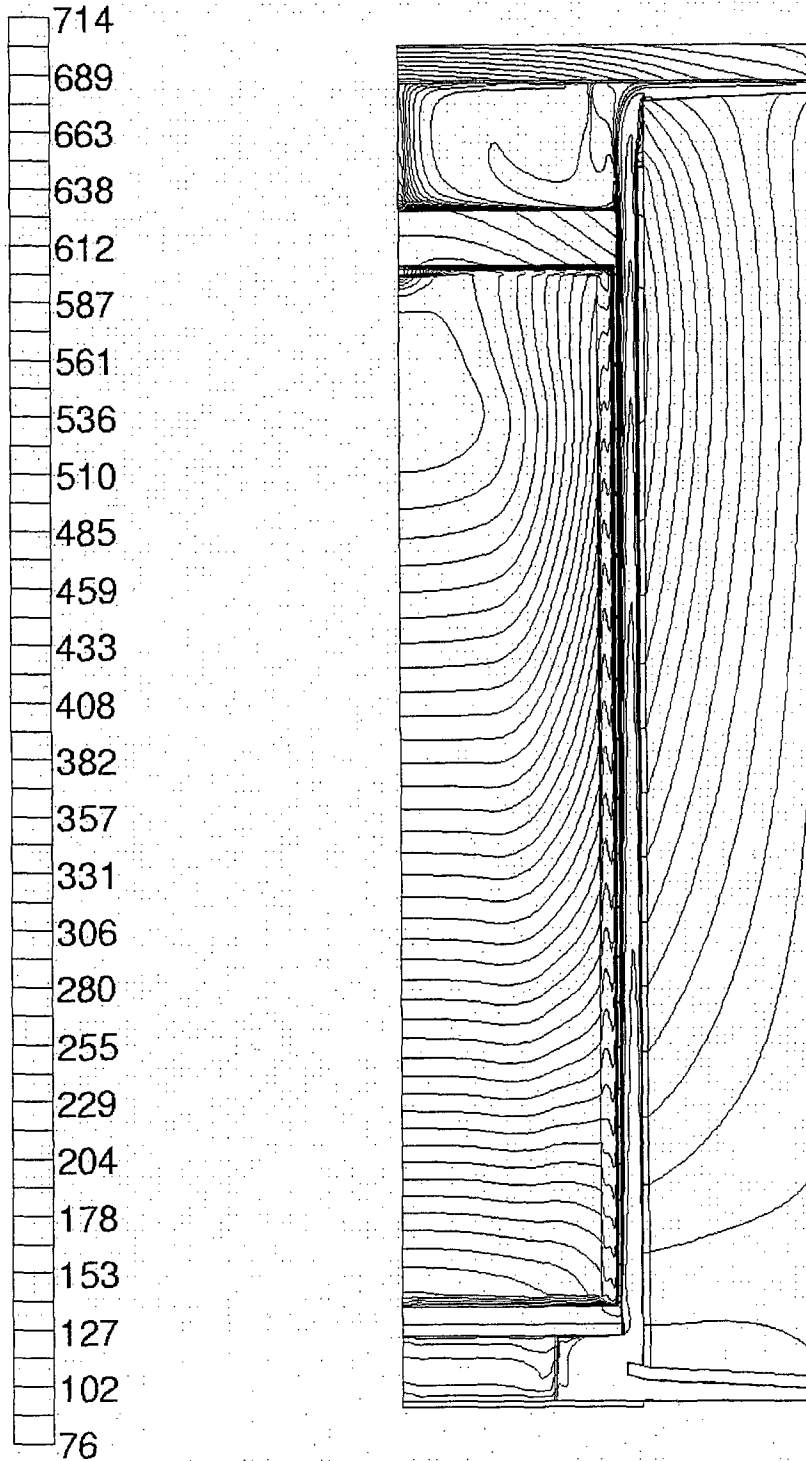


Figure 4.4-15 Air Velocity (m/s) in the Concrete Cask Annulus for the Design Basis PWR Heat Load

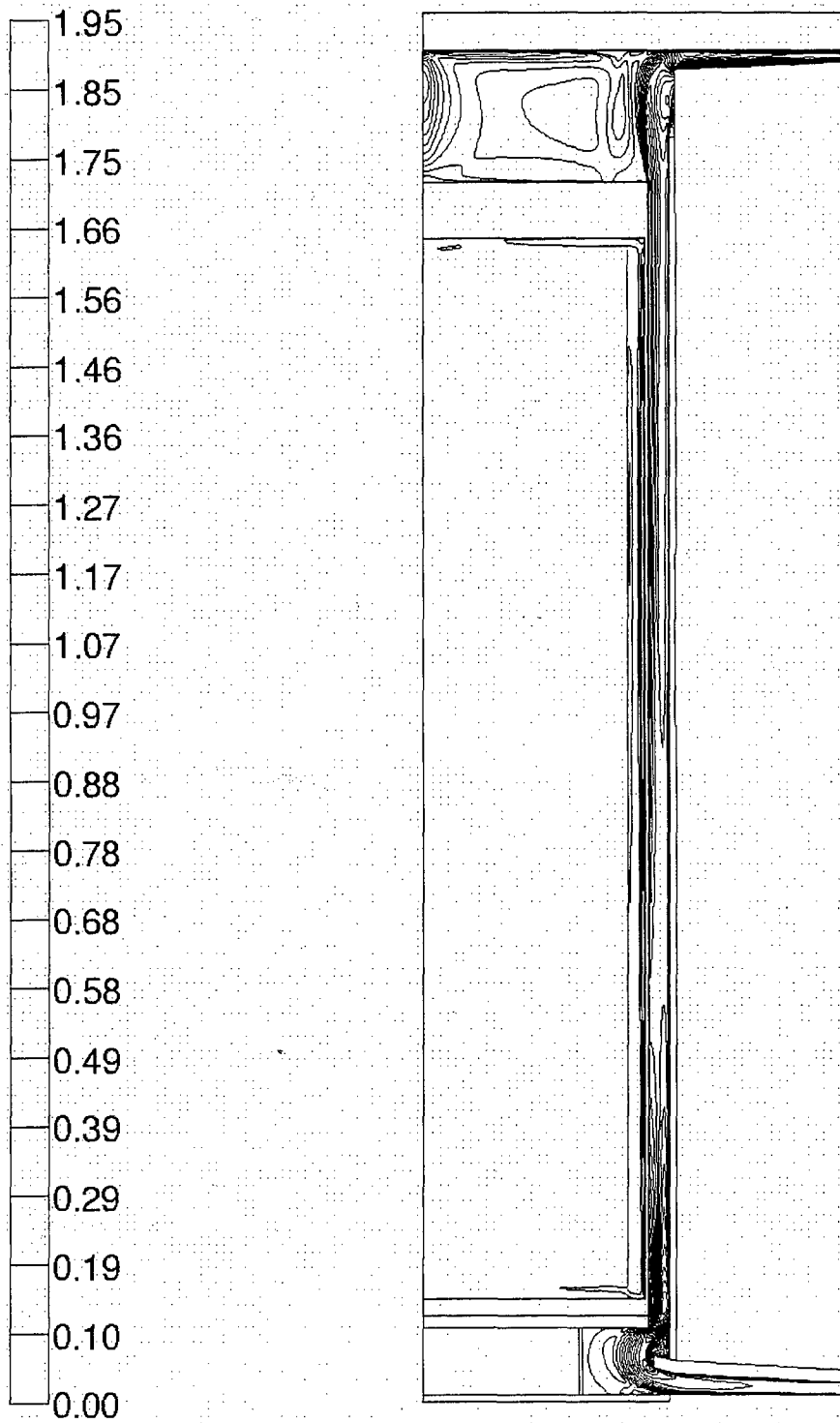


Figure 4.4-16 Three-Dimensional ANSYS Model of the PWR Canister for Vacuum Drying Condition

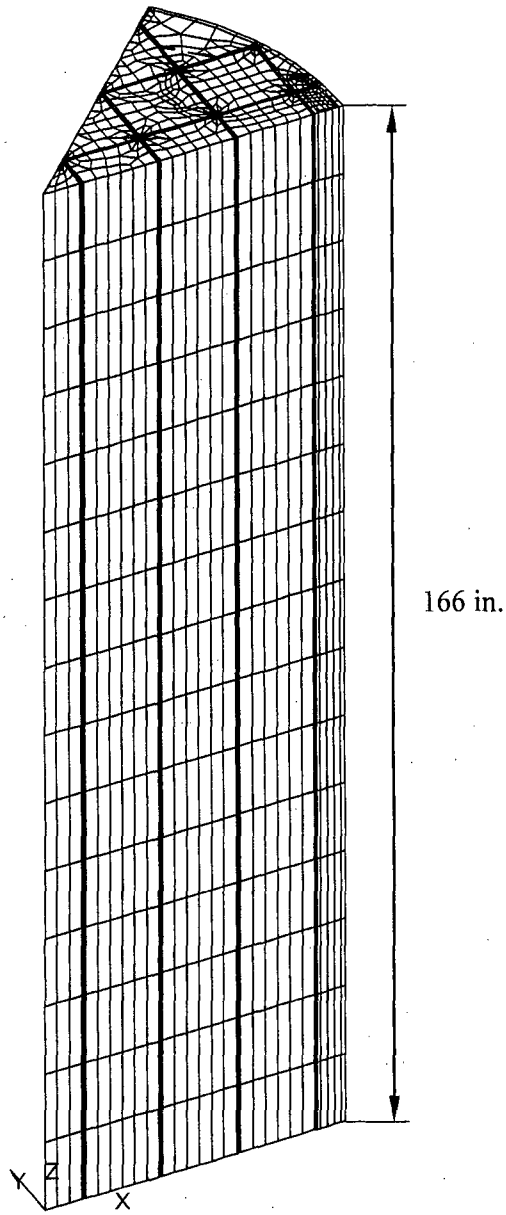




Figure 4.4-17 Detailed View of the Three-Dimensional ANSYS Model of the PWR Canister for Vacuum Drying Condition

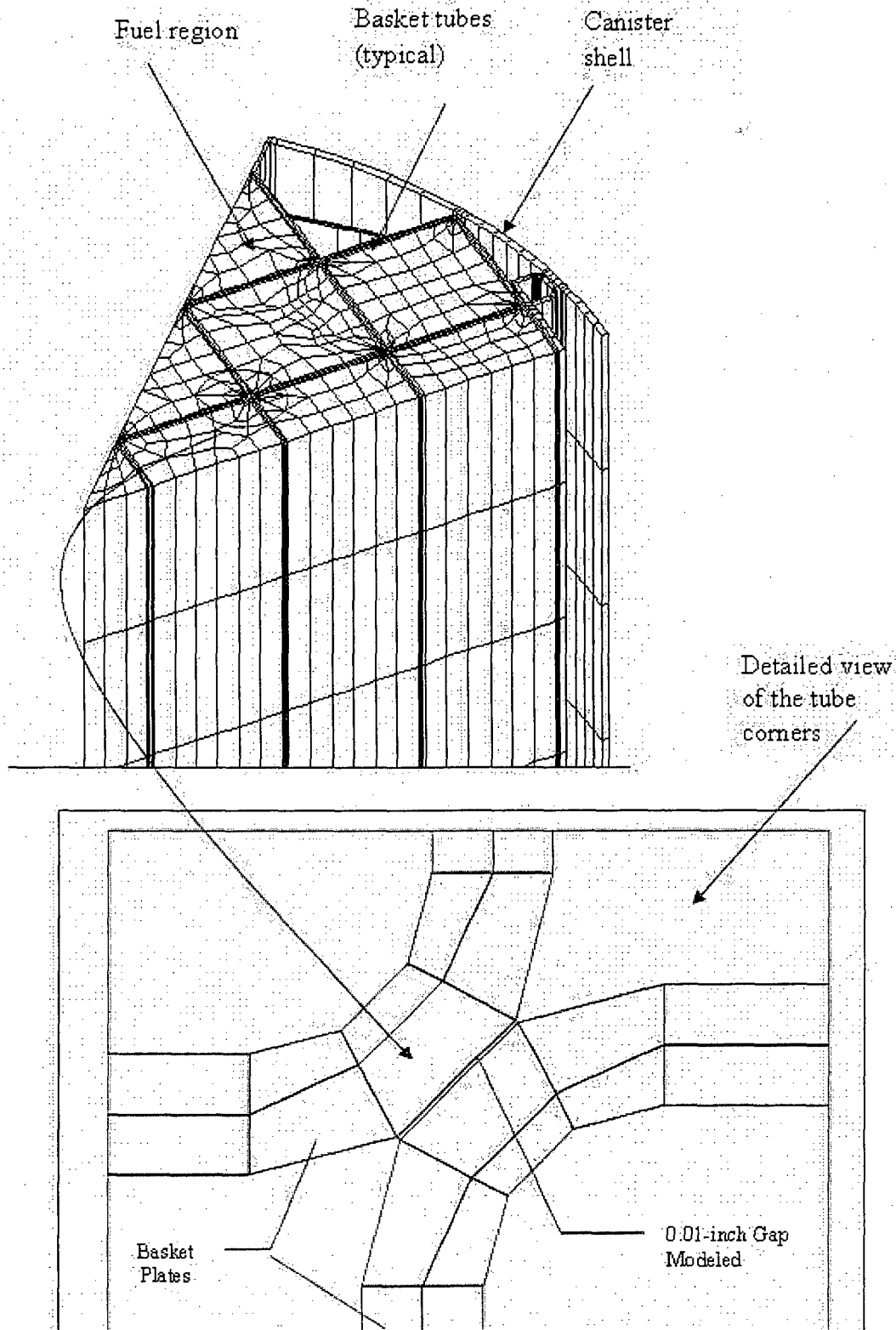


Figure 4.4-18 Three-Dimensional ANSYS Model of the BWR Canister for TFR Vacuum Drying Analyses

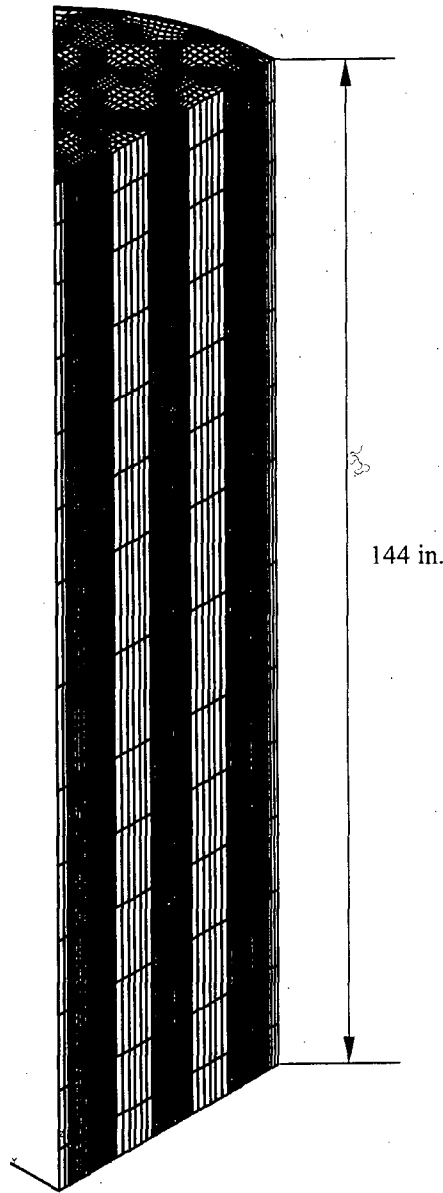
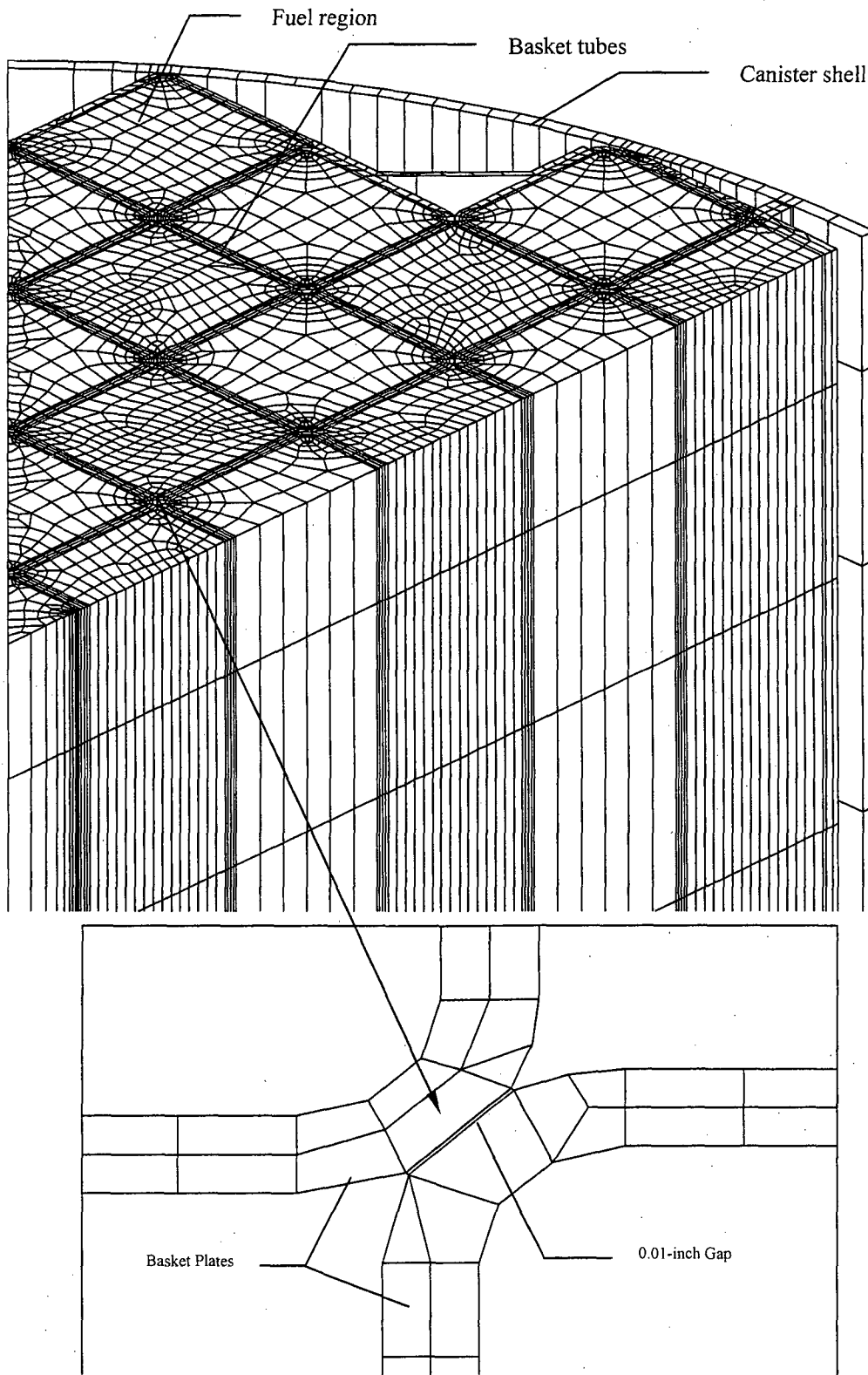


Figure 4.4-19 Detailed View of the Three-Dimensional ANSYS Model of the BWR  
Canister for TFR Vacuum Drying Analyses



**Table 4.4-1 Effective Thermal Conductivities for 14×14 PWR Fuel Assemblies for Helium Backfill**

For fuel assemblies in fuel tubes with the neutron absorber:

| Conductivity <sup>a</sup><br>(Btu/hr-in-°F) | Temperature (°F) |       |       |       |
|---|------------------|-------|-------|-------|
|   | 228              | 421   | 619   | 819   |
| K <sub>xx</sub>                             | 0.019            | 0.025 | 0.035 | 0.045 |
| K <sub>yy</sub>                             | 0.019            | 0.025 | 0.035 | 0.045 |
| K <sub>zz</sub>                             | 0.172            | 0.155 | 0.146 | 0.143 |

For fuel assemblies in positions without the neutron absorber:

| Conductivity <sup>a</sup><br>(Btu/hr-in-°F) | Temperature (°F) |       |       |       |
|---|------------------|-------|-------|-------|
|   | 227              | 419   | 615   | 815   |
| K <sub>xx</sub>                             | 0.020            | 0.027 | 0.037 | 0.049 |
| K <sub>yy</sub>                             | 0.020            | 0.027 | 0.037 | 0.049 |
| K <sub>zz</sub>                             | 0.169            | 0.152 | 0.143 | 0.140 |

**Table 4.4-2 Effective Thermal Conductivities for 10×10 BWR Fuel Assemblies for Helium Backfill**

| Conductivity <sup>a</sup><br>(Btu/hr-in-°F) | Temperature (°F) |       |       |       |
|---|------------------|-------|-------|-------|
|   | 192              | 394   | 597   | 801   |
| K <sub>xx</sub>                             | 0.021            | 0.028 | 0.039 | 0.053 |
| K <sub>yy</sub>                             | 0.021            | 0.028 | 0.039 | 0.053 |
| K <sub>zz</sub>                             | 0.176            | 0.161 | 0.152 | 0.151 |

<sup>a</sup> K<sub>xx</sub> and K<sub>yy</sub> correspond to the in-plane directions and K<sub>zz</sub> corresponds to the axial direction in the basket.

**Table 4.4-3 Maximum Component Temperatures for Normal Condition Storage of Design Basis PWR and BWR Heat Loads**

| Component                | PWR         | BWR         | Allowable Temperature (°F) |
|--------------------------|-------------|-------------|----------------------------|
| Fuel Cladding            | 714         | 682         | 752                        |
| Fuel Basket <sup>a</sup> | 714         | 682         | 800                        |
| TSC Shell                | 457         | 431         | 800                        |
| Concrete                 | 271 (local) | 243 (local) | 300 (local)                |
|                          | 160 (bulk)  | 153 (bulk)  | 200 (bulk)                 |

**Table 4.4-4 Helium Mass Per Unit Volume for MAGNASTOR TSCs**

| Fuel Type | Helium Density (g/liter) |             |             |
|-----------|--------------------------|-------------|-------------|
|           | Nominal                  | Lower Bound | Upper Bound |
| PWR       | 0.763                    | 0.694       | 0.802       |
| BWR       | 0.774                    | 0.704       | 0.814       |

<sup>a</sup> The maximum fuel cladding temperature is conservatively used.

**Table 4.4-5 Maximum Fuel Temperature for Water Phase – PWR**

| Heat Load (kW) | T <sub>max</sub> of Fuel (°F) | T <sub>max</sub> of Canister OD (°F) |
|----------------|-------------------------------|--------------------------------------|
| 35.5           | 130                           | 113                                  |
| 30             | 126                           | 111                                  |
| 25             | 121                           | 110                                  |
| 20             | 118                           | 108                                  |
| 15             | 114                           | 106                                  |

**Table 4.4-6 Maximum Fuel Temperature for Water Phase – BWR**

| Heat Load (kW) | T <sub>max</sub> of Fuel (°F) | T <sub>max</sub> of Canister OD (°F) |
|----------------|-------------------------------|--------------------------------------|
| 33             | 126                           | 113                                  |
| 30             | 124                           | 112                                  |
| 25             | 120                           | 110                                  |
| 20             | 117                           | 108                                  |
| 15             | 113                           | 106                                  |

**Table 4.4-7 Maximum Fuel Temperature for Helium Phase – PWR**

| Heat Load (kW) | T <sub>max</sub> of Fuel (°F) | T <sub>max</sub> of Canister OD (°F) |
|----------------|-------------------------------|--------------------------------------|
| 35.5           | 432                           | 120                                  |
| 30             | 400                           | 118                                  |
| 25             | 363                           | 115                                  |
| 20             | 319                           | 112                                  |
| 15             | 282                           | 109                                  |

**Table 4.4-8 Maximum Fuel Temperature for Helium Phase – BWR**

| Heat Load (kW) | T <sub>max</sub> of Fuel (°F) | T <sub>max</sub> of Canister OD (°F) |
|----------------|-------------------------------|--------------------------------------|
| 33             | 410                           | 117                                  |
| 30             | 387                           | 116                                  |
| 25             | 351                           | 114                                  |
| 20             | 314                           | 111                                  |
| 15             | 275                           | 109                                  |

**Table 4.4-9 Durations and the Temperature at the End of the Duration for the First Vacuum Stage (PWR)**

| Heat Load (kW) | Vacuum Duration (hours) | $T_{max}$ at Steady State or at the End of the Duration (°F) |        |
|----------------|-------------------------|--|--------|
|                |                         | Fuel   | Basket |
| 15             | No limit                | 509  | 483    |
| 20             | No limit                | 627  | 599    |
| 25             | No limit                | 739  | 709    |
| 30             | 32                      | 636  | 608    |
| 35.5           | 24                      | 634  | 606    |

**Table 4.4-10 Durations and the Temperature at the End of the Duration for the First Vacuum Stage (BWR)**

| Heat Load (kW) | Vacuum Duration (hours) | $T_{max}$ at Steady State or at the End of the Duration (°F) |        |
|----------------|-------------------------|--|--------|
|                |                         | Fuel   | Basket |
| 15             | No limit                | 441  | 428    |
| 20             | No limit                | 543  | 528    |
| 25             | No limit                | 641  | 625    |
| 29             | No limit                | 717  | 700    |
| 30             | 44                      | 641  | 624    |
| 33             | 33                      | 630  | 613    |



**Table 4.4-11 Durations and the Temperature at the End of the Duration for the Second Vacuum Stage\* (PWR)**

| Heat Load (kW) | Helium Backfill Duration (hours) | T <sub>max</sub> of Fuel/Basket at the End of the Helium Backfill (°F) | Second Vacuum Duration (hours) | T <sub>max</sub> of Fuel/Basket at the End of the Second Vacuum (°F) |
|----------------|----------------------------------|--|--------------------------------|--|
| 35.5           | 24                               | 454  | 11                             | 635  |

\* For the cases with heat load higher than 25 kW, the duration and temperatures at the end of the duration shown in this table can be conservatively used.

**Table 4.4-12 Durations and the Temperature at the End of the Duration for the Second Vacuum Stage\* (BWR)**

| Heat Load (kW) | Helium Backfill Duration (hours) | T <sub>max</sub> of Fuel/Basket at the End of the Helium Backfill (°F) | Second Vacuum Duration (hours) | T <sub>max</sub> of Fuel/Basket at the End of the Second Vacuum (°F) |
|----------------|----------------------------------|--|--------------------------------|--|
| 33             | 24                               | 432  | 16                             | 630  |

\* For the cases with heat load larger than 29 kW, the duration and temperatures at the end of the duration shown in this table can be conservatively used.

Table 4.4-13 TFR to Concrete Cask (PWR) Transfer Times and Temperatures

| Heat Load<br>(kW) | Allowed<br>Duration<br>(hours) | T <sub>max</sub> of Fuel/Basket at the End of the<br>Transfer from TFR to Concrete Cask<br>(°F) |
|-------------------|--------------------------------|---|
| 25                | 48                             | 703   |
| 35.5              | 22                             | 701   |

Table 4.4-14 TFR to Concrete Cask (BWR) Transfer Times and Temperatures

| Heat Load<br>(kW) | Allowed<br>Duration<br>(hours) | T <sub>max</sub> of Fuel/Basket at the End of the<br>Transfer from TFR to Concrete Cask<br>(°F) |
|-------------------|--------------------------------|---|
| 25                | 65                             | 700   |
| 33                | 32                             | 703   |

**Table 4.4-15 Durations Allowed and the Maximum PWR Fuel Clad Temperatures for the Operation Using Reduced Vacuum Times, Reduced Cooling Time and Eight Hours of Handling**

| Heat Load (kW)      | [1]<br>Vacuum Time <sup>(1)</sup> (Hour) | [2]<br>T <sub>max</sub> of Fuel at the End of the Vacuum (°F) | [3]<br>Minimum Helium Cooling Time (Hour) | [4]<br>T <sub>max</sub> of Fuel During the Helium Cooling (°F) | Transfer Time Allowed (Hour) | [5]<br>T <sub>max</sub> of Fuel at the End of the Duration (°F) |
|---------------------|--|---|---|--|------------------------------|---|
| 35.5 <sup>(2)</sup> | 15                                       | 543   | 7   | 587  | 8                            | 701   |
| 30 <sup>(2)</sup>   | 19                                       | <543  | 7   | <587   | 8                            | <701  |
| 25 <sup>(3)</sup>   | 50                                       | 661   | 0   | 661  | 8                            | 703   |
| 20 <sup>(3)</sup>   | No limit                                 | 582   | 0   | <661   | 8                            | <703  |
| 15 <sup>(3)</sup>   | No limit                                 | 475   | 0   | <661   | 8                            | <703  |

- (1) Maximum fuel temperature started at 212°F.
- (2) For heat loads of 30 kW and 35.5 kW, the response of the fuel temperature due to the helium backfill (performed at the end of the vacuum) is determined by the transient analysis (of helium in the canister) using a heat load of 35.5 kW. This evaluation shows that the clad temperature will increase by 44°F and then returns to the maximum vacuum temperature (column [2]) of 543°F in seven hours. By restricting the maximum vacuum temperature to 543°F, the peak temperature during the cooling phase is limited to 587°F. By limiting the clad temperature to 543°F (column [2]), the eight hours of transfer time will result in temperatures in column [5] of 701°F or less.
- (3) For heat loads less than 25 kW, the response of the fuel temperature due to the helium backfill (performed at the end of the vacuum) is determined by the transient analysis (of helium in the canister) using a heat load of 25 kW. This evaluation shows that the clad temperature will not increase over the value shown in column [2]. By restricting the maximum vacuum temperature to 661°F (or less), the eight hours of transfer time will result in temperatures in column [5] of 703°F or less, which is based on the transient evaluation of air in the annulus using a heat load of 25 kW. The difference between the column [2] and the column [4] temperatures indicates that additional margin exists for the maximum temperature at the end of the transfer operation.

**Table 4.4-16 Durations Allowed and the Maximum BWR Fuel Clad Temperatures for the Operation Using Reduced Vacuum Times, Reduced Cooling Time and Eight Hours of Handling**

| Heat Load (kW)    | [1]<br>Vacuum Time <sup>(1)</sup> (Hour) | [2]<br>T <sub>max</sub> of Fuel at the End of the Vacuum (°F) | [3]<br>Minimum Helium Cooling Time (Hour) | [4]<br>T <sub>max</sub> of Fuel During the Helium Cooling (°F) | Transfer Time Allowed (Hour) | [5]<br>T <sub>max</sub> of Fuel at the End of the Duration (°F) |
|-------------------|--|---|---|--|------------------------------|---|
| 33 <sup>(2)</sup> | 26                                       | 601   | 6   | 635  | 8                            | 703   |
| 30 <sup>(2)</sup> | 31                                       | <601  | 6   | <635   | 8                            | <703  |
| 29 <sup>(2)</sup> | 34                                       | <601  | 6   | <635   | 8                            | <703  |
| 25 <sup>(3)</sup> | No limit                                 | 641   | 0   | <678   | 8                            | 700   |
| 20 <sup>(3)</sup> | No limit                                 | 543   | 0   | <678   | 8                            | <700  |
| 15 <sup>(3)</sup> | No limit                                 | 441   | 0   | <678   | 8                            | <700  |

- (1) Maximum fuel temperature started at 212°F.
- (2) For heat loads, 29 kW, 30 kW and 33 kW, the response of the fuel temperature due to the helium backfill (performed at the end of the vacuum) is determined by the transient analysis (of helium in the canister) using a heat load of 33 kW. This evaluation shows that the clad temperature will increase by 34°F and then returns to the maximum vacuum temperature (column [2]) of 601°F in six hours. By restricting the maximum vacuum temperature to 601°F, the peak temperature during the cooling phase is limited to 635°F. By limiting the clad temperature to 601°F (column [2]), the eight hours of transfer time will result in temperatures in column [5] of 703°F or less.
- (3) For heat loads of 25 kW or less, the response of the fuel temperature due to the helium backfill (performed at the end of the vacuum) is determined by the transient analysis (of helium in the canister) using a heat load of 25 kW. This evaluation shows that the clad temperature will not increase over the value shown in column [2]. By restricting the maximum vacuum temperature to 678°F (or less), the eight hours of transfer time will result in temperatures in column [5] of 700°F or less, which is based on the transient evaluation of air in the annulus using a heat load of 25 kW. The difference between the column [2] and the column [4] temperatures indicates that additional margin exists for the maximum temperature at the end of the transfer operation.

**4.5 Off-Normal Storage Events**

This section evaluates postulated off-normal storage events that might occur once during any calendar year of operation. The actual occurrence of any of these events is, therefore, infrequent. The concrete cask and TSC model described in Section 4.4.1.1 is used for the evaluation of the concrete cask and TSC for the off-normal events: severe ambient temperature conditions (106°F and -40°F) and the half-blocked air inlets condition. The evaluation of the off-normal events for variations in the ambient temperature only requires a change to the boundary condition temperature. For the half-blocked air inlets condition, the air inlet condition is modified to permit only half of the air flow into the inlet. The design basis heat loads of 35.5 kW and 33 kW are used in the evaluations of the concrete cask and TSC containing PWR and BWR fuels, respectively.

The principal component temperatures for each of the off-normal events, discussed previously, are summarized in the following tables, along with the allowable temperatures. Note that the maximum fuel cladding temperatures are conservatively used as the maximum fuel basket temperatures. As the tables show, the component temperatures for the concrete cask and TSC containing PWR and BWR fuels are within the allowable values for the off-normal storage events.

**Principal Component Temperatures – Off-Normal Storage of PWR Fuel**

| Component     | 106°F Ambient, Maximum Temperatures (°F) | -40°F Ambient, Maximum Temperatures (°F) | 76°F Ambient/Half Blocked Air Inlets Temperatures (°F) | Allowable Temperature (°F) |
|---------------|--|--|--|----------------------------|
| Fuel Cladding | 752                                      | 603                                      | 717  | 1,058                      |
| Fuel Basket   | 752                                      | 603                                      | 717  | 1,000                      |
| TSC Shell     | 485                                      | 336                                      | 459  | 800                        |
| Concrete      | 311                                      | 118                                      | 274  | 350                        |

**Principal Component Temperatures – Off-Normal Storage of BWR Fuel**

| Component     | 106°F Ambient, Maximum Temperatures (°F) | -40°F Ambient, Maximum Temperatures (°F) | 76°F Ambient/Half Blocked Air Inlets Temperatures (°F) | Allowable Temperature (°F) |
|---------------|--|--|--|----------------------------|
| Fuel Cladding | 719                                      | 569                                      | 684  | 1,058                      |
| Fuel Basket   | 719                                      | 569                                      | 684  | 1,000                      |
| TSC Shell     | 459                                      | 312                                      | 433  | 800                        |
| Concrete      | 282                                      | 93                                       | 246  | 350                        |

There are no adverse consequences due to these off-normal events. The maximum component temperatures are less than the allowable temperature limits.

**Off- Normal Event TSC Internal Pressures**

Off-normal event TSC internal pressures are evaluated using the method and inputs documented in the normal condition pressure evaluations (Section 4.4.4). The off-normal event TSC internal pressure analysis considers a 10% rod failure fraction and a TSC backfill temperature at 495°F and a pressure of 106 psig. The higher backfill temperature, and associated pressure, is the result of the “severe heat” off-normal thermal evaluation. The maximum TSC internal pressures calculated for off-normal events are 114 psig for the PWR system and 110 psig for the BWR system.

## 4.6 Accident Events

This section presents the evaluations of the thermal accident design events, which address very low probability events that might occur once during the lifetime of the ISFSI or hypothetical events that are postulated because their consequences may result in the maximum potential impact on the surrounding environment. Three thermal accident events are evaluated in this section: maximum anticipated heat load, fire accident and full blockage of the air inlets. The maximum TSC internal pressure for the bounding accident conditions is evaluated in Section 4.6.4.

The concrete cask and TSC model described in Section 4.4.1.1 is used for the evaluation of the concrete cask and TSC for these thermal accident events.

### 4.6.1 Analysis of Maximum Anticipated Ambient Heat Load

This section evaluates the concrete cask and the TSC for the postulated accident event of an ambient temperature of 133°F. A steady state condition is considered in the thermal evaluation of the system for this accident event.

Using the same methods and thermal models described in Section 4.4.1.1 for the normal conditions of storage, thermal evaluations are performed for the concrete cask and the TSC with its contents for this accident condition. All boundary conditions in the model are the same as those used for the normal condition evaluation, except that an ambient temperature of 133°F is used. The maximum calculated temperatures of the principal PWR and BWR cask component, with the corresponding allowable temperatures, are as follows.

| Component     | PWR<br>Maximum<br>Temp (°F) | BWR<br>Maximum<br>Temp (°F) | Allowable<br>Temp. (°F) |
|---------------|-----------------------------|-----------------------------|-------------------------|
| Fuel Cladding | 786                         | 753                         | 1,058                   |
| Fuel Basket   | 786                         | 753                         | 1,000                   |
| TSC Shell     | 510                         | 483                         | 800                     |
| Concrete      | 347                         | 317                         | 350                     |

Note that the maximum fuel cladding temperatures are conservatively considered to be the maximum basket temperatures. This evaluation shows that the component temperatures are within the allowable temperatures for the extreme ambient temperature conditions.

### 4.6.2 Fire Accident

A fire may be caused by flammable material or by a transport vehicle. While it is possible that a transport vehicle could cause a fire while transferring a loaded storage cask at the ISFSI, this fire

will be confined to the vehicle and will be rapidly extinguished by the persons performing the transfer operations or by the site fire crew. Fuel in the fuel tanks of the concrete cask transport vehicle and/or prime mover (maximum 50 gallons) is the only flammable liquid that could be near a concrete cask, and potentially at, or above, the elevation of the surface on which the cask is supported. The fuel carried by other onsite vehicles or by other equipment used for ISFSI operations and maintenance, such as air compressors or electrical generators, is considered not to be within the proximity of a loaded cask on the ISFSI pad. Site-specific analysis of fire hazards will evaluate the specific equipment used at the ISFSI and determine any additional controls required.

The analyzed area is a 15×15-foot square, less the 136 in-diameter footprint of the concrete cask, corresponding to the center-to-center distance of the concrete casks on the ISFSI pad. The potential depth (D) of the 50-gallon pool of flammable liquid is calculated as follows.

$$D = \frac{50 \times 231}{15 \times 15 \times 144 - 3.14 \times 128^2 / 4} = 0.6 \text{ in.}$$

With a burning rate of 5 in/hr, the fire would continue for 7.2 minutes. The fire accident evaluation in this section conservatively considers an 8-minute fire. The temperature of the fire is taken to be 1,475°F, which is specified for the fire accident event in 10 CFR 71.73c [3].

The fire condition is an accident event and is initiated with the concrete cask in a normal operating steady-state condition. To determine the maximum temperatures of the concrete cask components, the two-dimensional axisymmetric model of the concrete cask and TSC for the PWR configuration described in Section 4.4.1.1 is used to perform a transient analysis. The PWR configuration is considered to bound the BWR configuration due to the higher initial temperatures of the normal condition.

The initial condition of the fire accident transient analysis is based on the steady-state analysis results for the normal condition of storage, which corresponds to an ambient temperature of 100°F in conjunction with solar insolation (as specified in Section 4.4.1.1). The fire condition is implemented by applying a boundary temperature condition of 1,475°F at the air inlet and the lower surface of the steel plate forming the top of the air inlet for eight minutes. This boundary condition temperature is applied as a stepped boundary condition. During the eight-minute fire, solar insolation is also applied to the outer surface of the concrete cask. At the end of the eight minutes, the temperature at the inlet is reset to the ambient temperature of 100°F. The cooldown phase is continued for an additional 10.7 hours to observe the maximum TSC shell temperature and the average temperature of the TSC contents.



The maximum fuel temperature increased by less than 3°F, thus remaining well below the accident event temperature limit of 1,058°F. The maximum temperature of the TSC shell increases to 512°F due to the fire condition. The limited duration of the fire, the large thermal capacitance of the concrete cask, and the minimal thermal conductivity limit the local region where the concrete temperatures exceed 300°F to less than 10 inches above the top surface of the air inlets. These results confirm that the operation of the concrete cask is not adversely affected during and after the fire accident condition.

#### **4.6.3 Full Blockage of Concrete Cask Air Inlets**

This section evaluates the concrete cask for the transient condition of full blockage of the air inlets at the normal storage condition temperature (100°F).

The accident temperature conditions are evaluated using the concrete cask and TSC thermal models described in Section 4.4.1.1. The transient analysis assumes initial normal storage conditions, with the sudden loss of convective cooling of the TSC. This is simulated by removing the inlet and outlet conditions from the model. Heat is then rejected from the TSC to the concrete cask liner only by radiation and convection. The loss of convective cooling to the ambient environment results in a sustained heat-up of the TSC and its contents and the concrete cask. The maximum fuel cladding temperature, maximum basket temperature, and the maximum concrete bulk temperature remain less than the allowable accident temperatures for approximately 72 hours after the initiation of the event. However, the internal pressure in the TSC cavity will reach the analyzed maximum pressure condition of 250 psig in approximately 58 hours after the initiation of a complete blockage event.

The evaluation demonstrates that there are no adverse consequences due to this accident, provided that debris is cleared from at least two air inlets within 58 hours based on the steady-state evaluation of the half-blocked air inlet condition in Section 4.5.

#### **4.6.4 Maximum TSC Internal Pressure for Accident Events**

Accident event pressures are evaluated with the method and inputs documented in the normal condition pressure evaluation (Section 4.4.4). System conditions incorporated in the accident analysis are an increased rod failure fraction and an increase in the average gas temperature of the TSC. A 100% rod failure fraction is applied in the system pressure calculation in conjunction with normal system temperatures. The second accident pressure evaluation applies the bounding thermal accident TSC average gas temperature to a TSC with a 1% (normal condition) fuel failure fraction. The bounding thermal accident, and associated pressure increase, is the result of the air inlets full blocked thermal evaluation. The average TSC gas

temperature applied in the thermal accident pressure evaluation is a conservative 684°F compared to 677°F calculated for this condition. Maximum calculated TSC internal pressures for the PWR and BWR systems are documented as follows.

| <b>System</b> | <b>100%<br/>Fuel Failure</b> | <b>Inlets<br/>Blocked</b> |
|---------------|------------------------------|---------------------------|
| PWR           | 201 psig                     | 129 psig                  |
| BWR           | 158 psig                     | 129 psig                  |

#### 4.7 References

1. 10 CFR 72, "Licensing Requirements for the Independent Storage of Spent Nuclear Fuel and High Level Radioactive Waste and Reactor-Related Greater than Class C Waste," Code of Federal Regulations, US Government, Washington, DC.
2. ISG-11, Revision 3 – "Cladding Considerations for the Transportation and Storage of Spent Fuel," US Nuclear Regulatory Commission, Washington, DC, November 17, 2003.
3. 10 CFR 71, "Packaging and Transportation of Radioactive Material," Code of Federal Regulations, US Government, Washington, DC.
4. ACI-349-85, "Code Requirement for Nuclear Safety Related Concrete Structures and Commentary," American Concrete Institute, Farmington Hills, MI.
5. PNL-4835, Johnson, A.B., and Gilbert, E.R., "Technical Basis for Storage of Zirconium-based alloy-Clad Fuel in Inert Gases," 1985.
6. "NS-4-FR Fire Resistant Neutron and/or Gamma Shielding Material" - Product Technical Data, The Japan Atomic Power Company, Tokyo, Japan.
7. Standard Handbook for Mechanical Engineers, Baumeister T. and Mark, L.S., 7<sup>th</sup> Edition, New York, McGraw-Hill Book Co., 1967.
8. ASME Boiler and Pressure Vessel Code, Section II, Part D, "Properties," American Society of Mechanical Engineers, New York, NY, 2001 Edition with 2003 Addenda.
9. ARMCO Product Data Bulletin No. S-22, "17-4PH, Precipitation Hardening Stainless Steel," ARMCO, Inc., 1988.
10. ASME Code Case N-71-17, "ASME Boiler and Pressure Vessel Code, Code Cases - Boilers and Pressure Vessels," American Society of Mechanical Engineers, New York, NY, 1996.
11. ANSYS, Revision 6.0, ANSYS INC, Canonsburg, PA
12. FLUENT, Revision 6.1, Fluent Inc, Lebanon, NH
13. "Principles of Heat Transfer," Krieth F., Bohn M.S., Fifth Edition, West Publishing Company.
14. "Fundamentals of Heat and Mass Transfer," F.P. Incropera and D.P. DeWitt, 1981.
15. "A Method for Determining the Spent-Fuel Contribution to Transport Cask Containment Requirements," TTC-1019, UC-820, Sandia 90-2406, Sanders, T. L., et al., November 1992.
16. EPRI NP-5128, "The TN-24P PWR Spent-Fuel Storage Cask: Testing and Analyses," Pacific Northwest Laboratory, Virginia Power Company and EG&G, Idaho National Engineering Laboratory, April 1987.
17. "A Physical Introduction to Fluid Mechanics," 1st Edition, Alexander J. Smits, 2000.
18. "Fluid Mechanics," 2<sup>nd</sup> Edition, Frank M. White, 1979.

19. "Annual Books for ASTM Standards," Section 1, Volume 01.04, American Society for Testing and Materials, West Conshohocken, PA.
20. "NUREG-1567, Standard Review Plan for Spent Fuel Dry Storage Facilities," US Nuclear Regulatory Commission, Washington, DC, March 2000.
21. EPRI TR-100305, "Performance Testing and Analyses of the VSC-17 Ventilated Concrete Cask," Pacific Northwest Laboratory, Virginia Power Company and EG&G, Idaho National Engineering Laboratory, May 1992.
22. "NUREG-1536, Standard Review Plan for Dry Cask Storage Systems", US Nuclear Regulatory Commission, Washington, DC January, 1997.
23. DOE/ET/47912-3, NAC-C-8129, "Domestic Light Water Reactor Fuel Design Evaluation," Volume III, September 1981.
24. DOE/RW-0184, Office of Civilian Radioactive Waste Management, "Characteristics of Spent Fuel, High-Level Waste, and Other Radioactive Wastes Which May Require Long-Term Isolation," Volume 3, December 1987.
25. ASHRAE Handbook, "Fundamentals," American Society of Heating, Refrigeration, and Air Conditioning Engineers, Atlanta, GA, 1993.
26. ASME Boiler and Pressure Vessel Code, Case N-707, "Use of SA-537, Class A Plate for Spent-Fuel Containment Internals in Non-pressure Retaining Applications Above 700°F (370°C)", Section III, Division 3.
27. "The Properties of Gases and Liquids," Bruce E. Poling, etc., 5<sup>th</sup> Edition, McGraw Hill, 2001.

**4.8            Thermal Evaluation Detail**

This section contains thermal evaluation detail not found in the preceding sections.

#### **4.8.1 Benchmark of the Two-Dimensional Axisymmetric Methodology for TSC Thermal Analyses For MAGNASTOR**

In this section, a benchmark evaluation is performed. A thermal evaluation using two-dimensional modeling methodology is performed for a system for which a thermal test has been conducted. Convection, conduction and radiation within the confinement boundary are considered in this evaluation. The thermal test is described in EPRI NP-5128 [16]. The results of the thermal evaluation using the two-dimensional methodology performed in this section show that the two-dimensional methodology is conservative and, therefore, acceptable for use in the thermal evaluation of MAGNASTOR.

##### **4.8.1.1 Introduction**

The thermal design of MAGNASTOR involves all three modes of heat transfer to reject heat from the fuel into the ambient. The most dominant mode of heat transfer is by convection, which involves helium removing heat from the fuel assembly as it flows up through the fuel tubes and transferring the heat to the TSC shell as it flows down through the basket weldment (downcomer) region. The heat transferred to the TSC shell is then rejected into the concrete cask annulus airflow and transported to the ambient environment. The design of the concrete cask annulus to permit airflow between the TSC and the concrete cask to transfer heat to the ambient is in numerous licensed spent fuel storage system designs. The most significant difference with the MAGNASTOR design is the inclusion of convection in the TSC as a means of removing heat from the fuel assemblies.

The geometry of the MAGNASTOR fuel basket is an array of square tubes in a cylindrical outer boundary, the TSC shell. This implies that the flow of the helium upward in the basket is through a complex cross-section of squares, less the circular cross-sections of the fuel rods. The downward flow of the helium on the outside of the fuel basket next to the TSC shell is also through an area with a complex cross-section, since the outer boundary is circular and the inner boundary of the downcomer is the outer perimeter of the square array of fuel tubes. While this has the characteristics of a three-dimensional system, it is evaluated as a two-dimensional axisymmetric system. Even as a three-dimensional system, the complex flow area for the fuel region is impractical to be incorporated into a fluid flow analysis with detailed modeling for each fuel rod. Additionally, due to the design of the fuel basket and the range of fuel temperatures expected, conduction and radiation heat transfer throughout the fuel basket cannot be neglected. The methodology adopted for this analysis includes the determination of effective properties for thermal conduction and radiation, as well as for fluid flow resistances, which are to be

implemented in a two-dimensional axisymmetric model. The end result of the two-dimensional evaluation is to determine the maximum temperatures for the fuel rod cladding.

For this reason, a benchmark is performed to demonstrate that two-dimensional methodology is acceptable to determine the maximum fuel cladding temperatures for MAGNASTOR.

#### **4.8.1.2 Purpose**

The purpose of this section is to provide a benchmark, which demonstrates that the two-dimensional methodology employed in the MAGNASTOR thermal evaluation is conservative.

#### **4.8.1.3 Description of the Thermal Test**

In EPRI NP-5128 [16], thermal testing was performed for a vertical metal cask containing 24 PWR (15×15) assemblies with a total heat load of 20.6 kW. The variation of the heat loads between the assemblies was less than 6%, which can be approximated as a uniform heat load. The basket contained in the cask during testing was comprised of an array of 24 square slots in which the basket walls were constructed of aluminum. While there were a series of tests performed, the test of interest for this evaluation was the test corresponding to vertical orientation of the cask in which the cask was backfilled with nitrogen to one atmosphere. Axial profiles of the temperature data were obtained in the tests for the inner surface of the cask, as well as for various radial locations in the basket. Temperature data was not obtained for the center of any fuel assembly, but rather on the basket.

#### **4.8.1.4 FLUENT Model Description**

The two-dimensional axisymmetric model for this evaluation only needs to consider the cavity of the metal cask. Modeling of the cask wall and surface is not considered necessary since the temperatures at the cask inner surface from the test are being applied as the boundary conditions for the model. The various regions of the model are shown in Figure 4.8-1. Regions 2 through 5 comprise the full length of the basket of the cask. Regions 2 through 4 represent the fuel in the basket, and Region 3 corresponds to the 144-inch active fuel region. Region 5 is considered to be within the length of the basket, but outside the length of the fuel assembly. Regions 1, 6 and 7 correspond to the backfill gas, nitrogen. For Regions 1, 6 and 7, it is only necessary to input the material properties for nitrogen to simulate the flow of nitrogen in the cask cavity. The gas is modeled as an ideal gas in FLUENT and all regions in the model utilized laminar flow conditions.

#### **4.8.1.4.1 Effective Properties for the Basket and Fuel Regions**

For the regions corresponding to the basket, effective properties are employed in the analysis. To account for the flow resistance of the wetted perimeter of the fuel and the fuel assembly grids, the porous media option in FLUENT is used. The determination of the porous media constants depends on the radius assigned to the basket region, which also must be associated with the effective cross-section area of the downcomer region. The cross-section for the downcomer region is used to compute the outer radius of the basket region in the two-dimensional axisymmetric model (Regions 2 through 5). Calculation of these constants for the porous media is described in Section 4.8.2. The methodology applied for this benchmark follows the same methodology described for the MAGNASTOR TSC model in Section 4.4.1.1.

The effective thermal properties for the basket region are computed using an ANSYS model shown in Figure 4.8-2. This model contains the aluminum basket and the fuel regions, which are modeled with homogeneous orthotropic thermal conductivities. To determine the temperature-dependent effective thermal conductivity of the basket region, a series of temperatures is applied to the boundary of the model. Solutions for each boundary condition determine the maximum temperature of the basket and the associated change in temperature from the boundary to the maximum temperature location. The effective thermal conductivities are determined using the same expression employed for MAGNASTOR in Section 4.4.1.2.

#### **4.8.1.4.2 Boundary Conditions**

The outer edges of the model correspond to the inner surface of the cask cavity. The following boundary conditions were applied to the model.

##### **Temperature Specification**

To remove any uncertainties in the model due to the cask wall conductance, the convection condition at the cask surface, or the variations in the ambient conditions, the temperatures from the test corresponding to the inner surface of the cavity were applied to the outer surface of the model. The temperature profile is shown in Figure 4.8-3.

##### **Heat Generation**

The total heat load applied to Region 3 of the model in Figure 4.8-1 was 20.6 kW. The heat generation was assumed to be uniformly distributed over the radial direction from the basket centerline to the outer radius of the porous media region (Region 3). In the axial direction, the power distribution as shown in Figure 4.8-4 was applied, which shows a peaking factor of 1.2.



**Buoyancy**

Since the backfill gas was specified as an ideal gas, the only condition required to enact buoyancy as a driving force for the nitrogen is to set the gravity acceleration as  $-9.8 \text{ m/sec}^2$ .

**Cavity Pressure**

To be consistent with the boundary conditions used in the analyses for MAGNASTOR, a pressure was applied to the cavity region. For the benchmark, the pressure in the cavity was set to zero (gauge).

**4.8.1.5 Analysis Results**

The temperature contour corresponding to the applied conditions is shown in Figure 4.8-5. The distribution of the contours along the centerline shows the maximum temperature is close to the top of the basket, which is characteristic of baskets in which the dominant heat transfer is by convection. The maximum basket temperature reported in the thermal test was  $232^\circ\text{C}$ , as compared to a maximum basket temperature of  $233^\circ\text{C}$  obtained from the analysis. This indicates that the analysis temperature is  $1^\circ\text{C}$  conservative with respect to the test data.

**4.8.1.6 Application of the Benchmark to the MAGNASTOR Evaluation**

The benchmark thermal test cask contained PWR assemblies and was backfilled with nitrogen. The force driving the movement of the backfill gas is buoyancy. A common metric employed to compare buoyancy driven systems is the Rayleigh Number (Ra), which can be computed for both systems. The Ra is expressed as follows.

$$Ra = (\rho^2 \beta g \Delta T L^3 / \mu^2) \times Pr \quad [14]$$

where:

|            |       |   |
|------------|-------|---|
| $\rho$     | ----- | density ( $\text{kg/m}^3$ )   |
| $\beta$    | ----- | coefficient of expansion (1/K)  |
| $g$        | ----- | gravitational constant = $9.8 \text{ m/sec}^2$  |
| $\Delta T$ | ----- | temperature difference = max. centerline<br>temperature - basket bottom temperature (K) |
| $L$        | ----- | height of basket (m)  |
| $\mu$      | ----- | viscosity ( $\text{N-sec/m}^2$ )  |
| $Pr$       | ----- | Prandtl number  |

Using the data from the benchmark thermal test and the analysis of the normal condition for MAGNASTOR, the Ra of the backfill gas can be computed for each analysis.

| Design    | Gas $T_{ave}$<br>(K) | $\rho$<br>(kg/m <sup>3</sup> ) | $\beta$ (1/K) | $\Delta T$<br>(K) | $\mu$<br>(N-sec/m <sup>2</sup> ) | Pr    | L (m) | Ra                    |
|-----------|----------------------|--------------------------------|---------------|-------------------|----------------------------------|-------|-------|-----------------------|
| MAGNASTOR | 520                  | 0.7501                         | 1/520         | 222               | $2.63 \times 10^{-5}$            | 0.668 | 4.420 | $1.97 \times 10^{11}$ |
| Benchmark | 426                  | 1.213                          | 1/426         | 142               | $2.30 \times 10^{-5}$            | 0.703 | 4.076 | $4.33 \times 10^{11}$ |

Note:  $T_{ave}$  is the average gas temperature (helium for MAGNASTOR and nitrogen for the benchmark) used to evaluate the properties in this table.

As indicated by the preceding table, the Ra for MAGNASTOR is the same order of magnitude as that for the benchmark. This indicates that the buoyancy forces driving the flow in the benchmark are essentially identical to the buoyancy force in the MAGNASTOR design.

Additionally, both models employ a laminar flow model inside the cavity. While the benchmark cask thermal test design stores 24 PWR fuel assemblies and the MAGNASTOR PWR design can store 37 PWR fuel assemblies, the arrays of both designs are comprised of square slots of nearly the same dimensions. The geometry of the flow area in the basket region is similar for both, since PWR fuel assemblies occupy a square slot in a square design. This is indicated in the following table, which contains the slot dimensions. These values indicate that the porous media parameters would also be similar, and in both analyses, the porous media parameters are computed using the same methodology.

| Design    | Fuel Assembly<br>Width (inch) | Slot Size (inch) |
|-----------|-------------------------------|------------------|
| MAGNASTOR | 8.426                         | 8.86/8.76        |
| Benchmark | 8.304                         | 8.99             |

This indicates the high degree of similarity of both configurations. Additionally, in both designs, the downcomer region is comprised of a circular outer boundary and an inner boundary consisting of a series of edges of squares.

In both designs, the basket is formed of plates (or tubes for MAGNASTOR), which also serve as conductors to the periphery of the basket. In the benchmark evaluation and in the MAGNASTOR evaluation, the porous media material is modeled to represent the conduction in the basket as well, since the basket plates were not modeled explicitly. The conductivity for the porous media region represents the radial conductance, as well as the axial conductance of the baskets. The method used to compute the effective thermal conductivities for both baskets was identical.

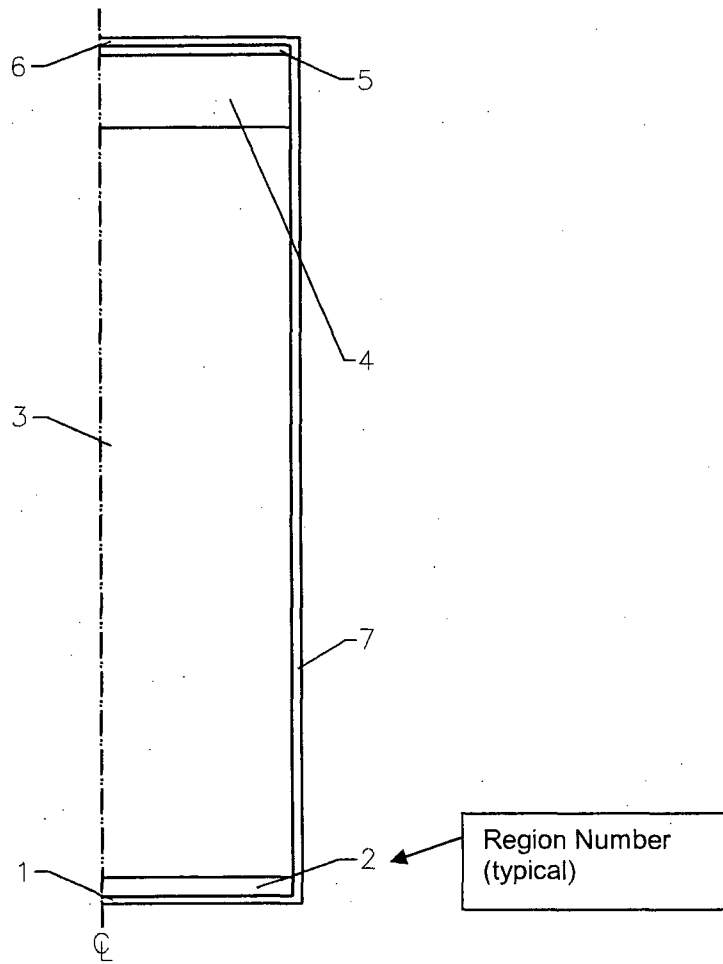
The reported results of the thermal test indicate that the two-dimensional modeling using FLUENT is conservative, since the FLUENT simulation of the benchmark predicted a higher temperature than the reported test data. It is important to note that the thermal boundary conditions for the FLUENT analysis of the benchmark thermal test employed the temperatures from the benchmark test directly, which eliminates any uncertainties in the analysis due to the

conduction through the benchmark cask body, convection from the cask surface, or variations in the ambient conditions over the cask. The analysis associated with the thermal test focused only on the convection internal to the cask cavity. This confirms that the axisymmetric modeling, in conjunction with the use of porous media material characterization, is an acceptable methodology for the computation of maximum fuel cladding temperatures.

#### **4.8.1.7      Conclusions**

In this section, a thermal evaluation has been performed for the thermal test described in EPRI N-5128 [16]. The analysis results indicate that the two-dimensional axisymmetric modeling methodology incorporating effective thermal properties and the flow resistance in the fuel region is acceptable to determine a bounding maximum fuel temperature. The benchmark also confirms the use of the hydraulic diameter for the representation of the nonaxisymmetric downcomer region, as well as the use of orthotropic properties for the basket conductance.

Figure 4.8-1 Two-Dimensional Model of the 24 PWR Assembly Thermal Test Configuration



| Region Number | Description                                   | Dimension (mm) |
|---------------|---|----------------|
| 1             | Bottom nitrogen region                        | 45             |
| 2             | Region below active fuel region in the basket | 152            |
| 3             | Active fuel region                            | 3658           |
| 4             | Region above active fuel region in the basket | 248            |
| 5             | Basket region without fuel                    | 18             |
| 6             | Top nitrogen region                           | 29             |
| 7             | Equivalent radial gap (downcomer region)      | 64             |

Figure 4.8-2 ANSYS Model for Determination of the Benchmark Basket Thermal Properties

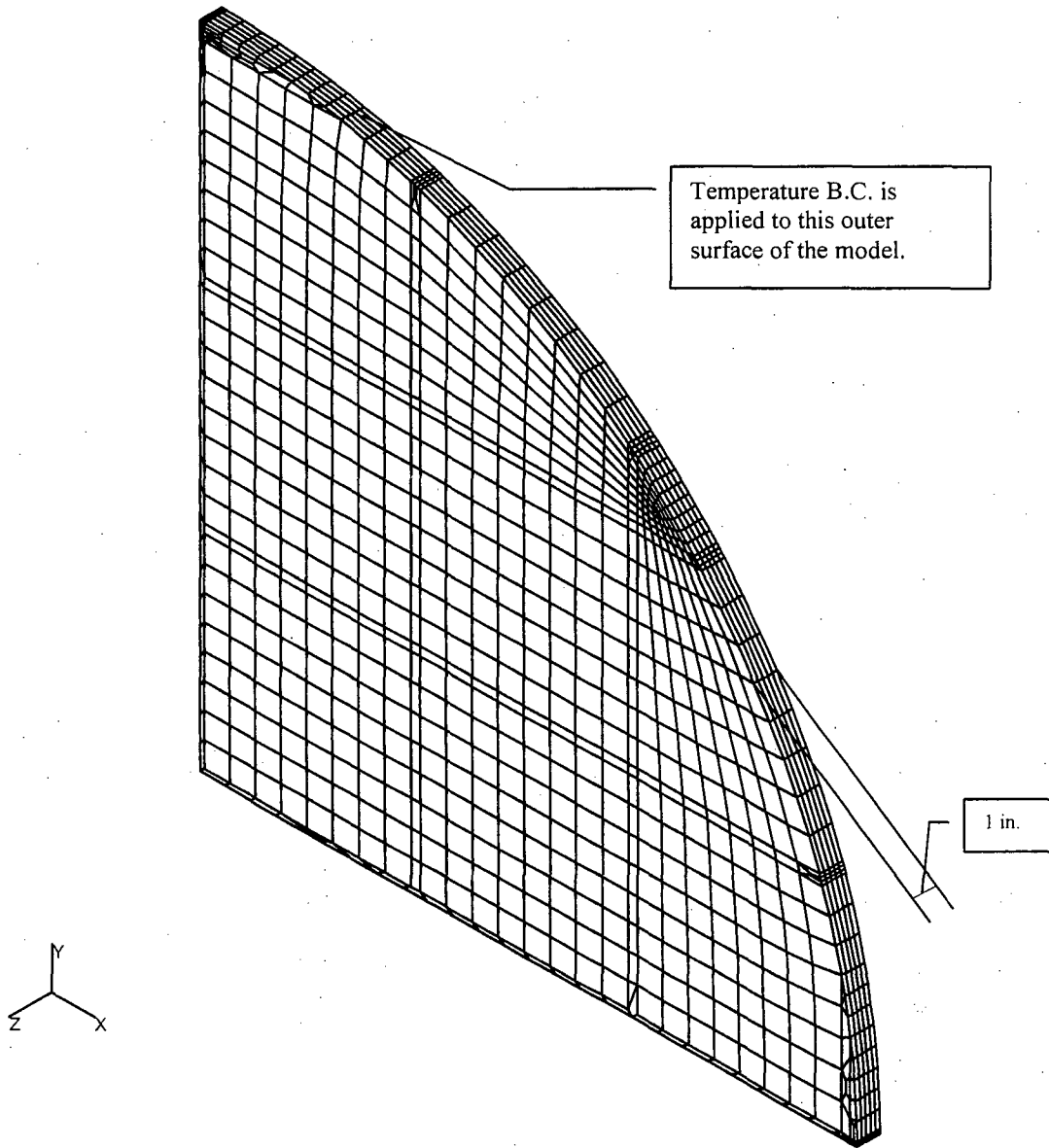


Figure 4.8-3 Temperature Profile from the Benchmark Cask Cavity Inner Surface

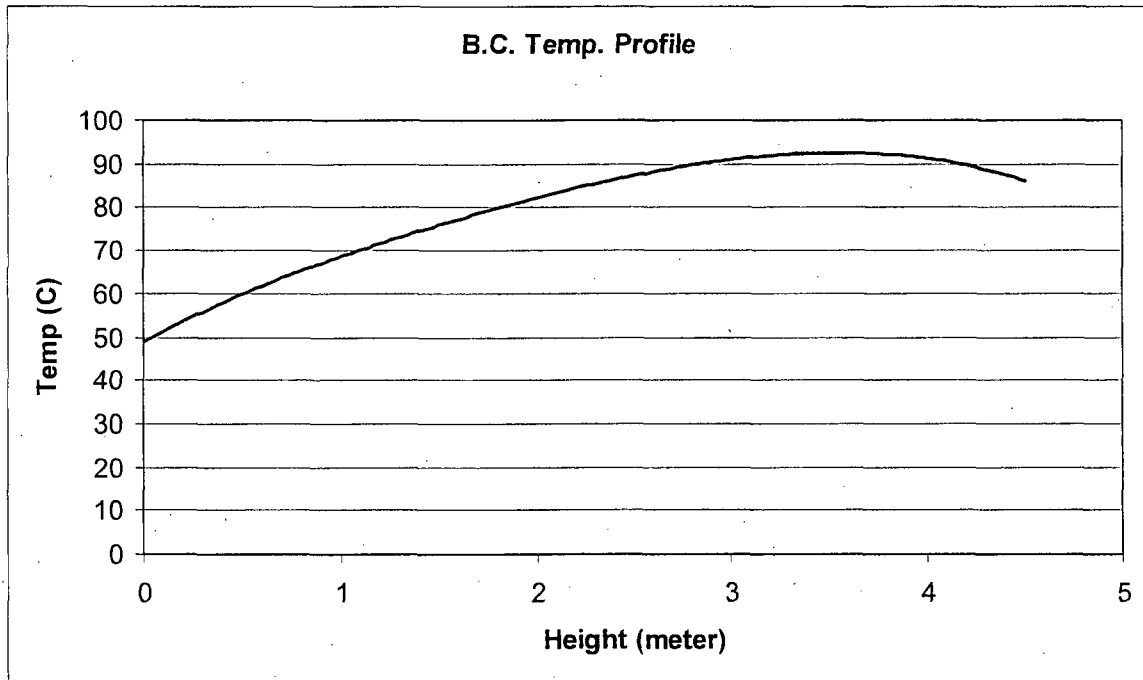


Figure 4.8-4 Axial Power Distribution Curve for the 15x15 PWR Fuel Assembly

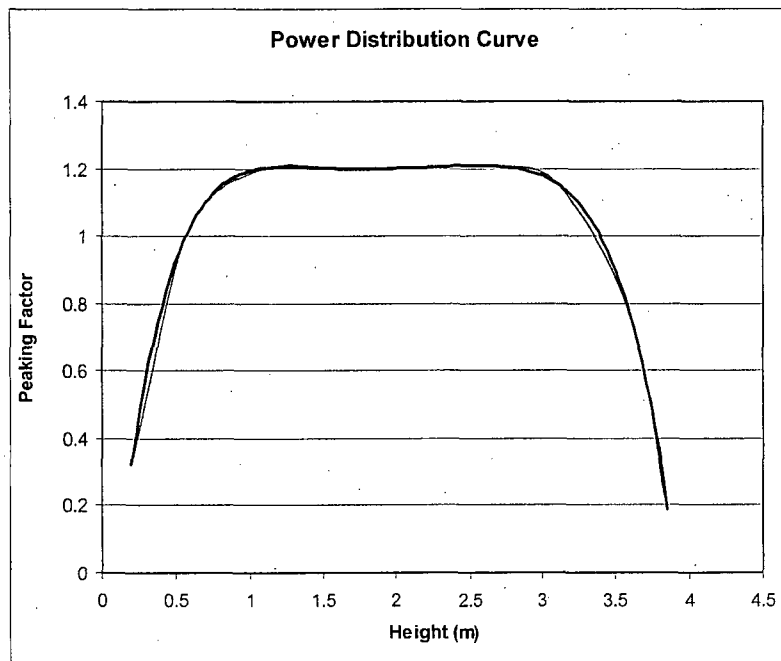
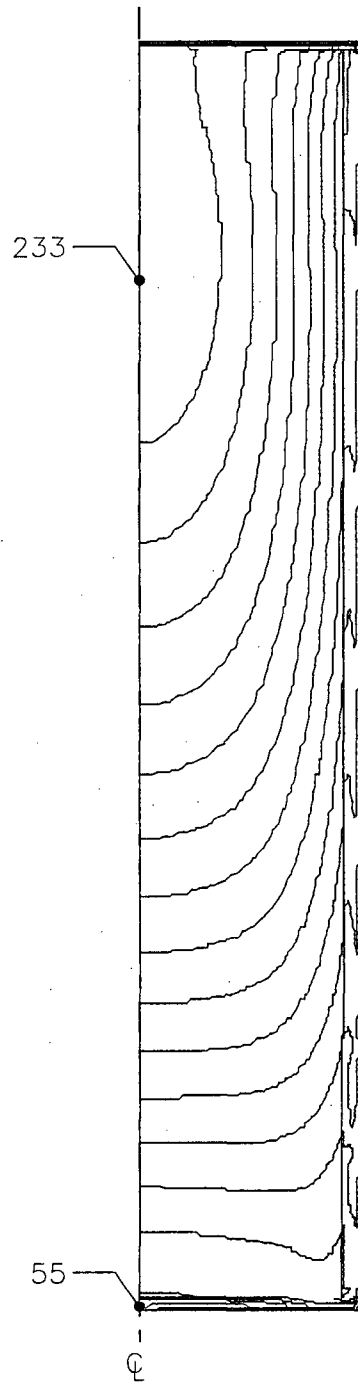


Figure 4.8-5 Temperature Contours for the Benchmark Cask Thermal Test



**4.8.2 Methodology to Compute the Porous Media Constants**

This section presents the methodology used to determine the porous media constants, which will simulate the flow resistance due to the fuel assembly and fuel assembly grids to be taken into account for the basket tube/fuel region of the two-dimensional axisymmetric TSC model.

To simulate the flow resistance in the porous media models, the following FLUENT porous media pressure drop [12] is employed.

$$\frac{\Delta P}{L} = \frac{\mu}{\alpha \epsilon} V + C \left( \frac{1}{2} \rho V^2 \right)$$

where:

|              |       |   |
|--------------|-------|---|
| $\Delta P/L$ | ----- | pressure drop per unit length (Pa/m)          |
| $V$          | ----- | superficial fluid velocity (m/s)              |
| $\mu$        | ----- | the fluid viscosity (kg/m-s)                  |
| $\rho$       | ----- | fluid density (kg/m <sup>3</sup> )            |
| $\alpha$     | ----- | permeability parameter (m <sup>2</sup> )      |
| $C$          | ----- | inertial resistance factor (m <sup>-1</sup> ) |

In this representation, the pressure drop for the porous media consists of two terms: one being proportional to the velocity and the other proportional to the velocity squared. Since the velocities are on the order of 0.03 m/s in the porous media region, the contribution due to the V<sup>2</sup> term is neglected. The pressure drops for the fuel rods and the fuel assembly grids are taken into account in the first term. For the first term, the viscosity ( $\mu$ ) is obtained from the material properties defined for the gas, while the factor ( $\alpha$ ), referred to as the permeability, is computed on the basis of laminar flow. The purpose of this section is to determine an  $\alpha$  for the BWR and the PWR fuel assemblies, which represents not only the resistance for the axial flow along the fuel rods, but also the additional resistance through the fuel assembly grids. The porous cells in the FLUENT program are 100% open in the porous media model [12]. Therefore, the factor for V must include the porosity factor with the values specified for 1/ $\alpha$ . The input of 1/ $\alpha$  into FLUENT is adjusted based on the porosity of the porous media [12]. The permeability for the BWR and the PWR fuel assemblies is determined separately. Separate models are considered for the spacing, size of the fuel rods, and the number of fuel rods in the PWR and the BWR fuel assemblies.

**Permeability ( $\alpha$ ) for the PWR Fuel Assembly**

For the PWR fuel assembly, the configuration that is considered to provide a bounding value for  $\alpha$  is the 17x17 fuel assembly. The calculation for the 1/ $\alpha$  for the entire PWR fuel assembly requires three FLUENT models. A quarter-symmetry model of the cross-section of the 17x17



fuel assembly is generated using FLUENT and the cross-section of the model is shown in Figure 4.8-6. The length of this fuel assembly model is 0.20 m in the axial direction, and consists of approximately 1.3 million cells. The purpose of this model is to determine the pressure drop per unit length  $(\Delta P/L)_{\text{ROD}}$  along the fuel rod. For this reason, only the momentum equation is required to be solved. A velocity (U) for the gas entering the model is specified to be 0.03 m/s, which represents the velocity observed in the canister evaluation. Since the flow is considered to be laminar, the actual value used in the evaluation is not significant. Using the  $\Delta P/L$  determined from the three-dimensional model, the  $1/\alpha$  for the fuel rods is computed by

$$1/\alpha_{\text{ROD}} = (\Delta P/L)_{\text{ROD}} / (\mu U)$$

A second three-dimensional model is generated to determine the pressure drop of the gas through a 60 mm-long fuel assembly grid. A periodic model of a single cell is considered, which is shown in Figure 4.8-7, and consists of approximately 199,000 cells. The length of the model is 60 mm, which represents the full length of the 60 mm grid. The boundary conditions on the axial faces used in the fuel rod model are applied to each end of the periodic model of the fuel assembly grid. The model result is the determination of the average pressure at the outlet end of the grid, which is determined by computing the area averaged pressure acting on the outlet. This is used to compute the pressure drop per unit length  $(\Delta P/L)_{\text{GRID}}$ , which is used to compute the  $1/\alpha_{\text{GRID}}$  for the fuel assembly grid by

$$1/\alpha_{\text{GRID}} = (\Delta P/L)_{\text{GRID}} / (\mu U)$$

Since the grid model is periodic, it simulates the condition in which the fuel assembly grid extends for the entire width of the basket slot region. This is not the geometry of the PWR fuel assembly grid in the basket, but rather there is a minimum of a 0.17-inch gap between the largest PWR fuel assembly and the smallest basket slot in the PWR basket. As the helium gas flows vertically up through the fuel rods, gas will not only flow through the fuel assembly grid, but also around the grid. To determine the distribution of the flow, a third three-dimensional quarter-symmetry FLUENT model consisting of approximately 332,500 cells is developed, as shown in Figure 4.8-8. A porous region with a length of 9.37 inches represents a section of fuel rods of 9.37 inches prior to the fuel assembly grid, and a section corresponding to a length of 9.37 inches is modeled after the fuel assembly grid. Both of these regions use the porous media constants determined for the bounding PWR fuel rod configuration. The bounding configuration was identified in two DOE reports ([23] and [24]) for the configuration with the largest combined grid length for all PWR assemblies. As shown in Figure 4.8-8, a nonporous gas region with a thickness of 0.17 inch is modeled in parallel with the region representing the fuel assembly grid. The porous media data for this model uses the results of the calculation of the porous media just for the fuel assembly grid. From the solution of the momentum equation, the

effective  $1/\alpha_{\text{EFF}}$  corresponding to the pressure drop  $(\Delta P/L)_{\text{EFF}}$  over the axial region containing the fuel assembly grid is computed using

$$1/\alpha_{\text{EFF}} = (\Delta P/L)_{\text{EFF}} / (\mu U)$$

The pressure drop is the difference between the averaged pressure on the outlet surface (area averaged) and the inlet, which is set to zero. To combine the permeabilities into a single quantity, the pressure drops over all the grids  $[(\Delta P/L)_{\text{EFF}}]$  are added to the pressure drop  $[(\Delta P/L)_{\text{ROD}}]$  over the remaining length of the fuel assembly (total fuel assembly length less the length of the fuel assembly grids) to calculate the total pressure drop due to fuel assembly grids and the fuel rods. Using an expression similar to the ones above, the  $1/\alpha$  for the PWR fuel assembly is computed to be

$$1/\alpha_{\text{PWR}} = (\Delta P_{\text{tot}}/L_{\text{tot}}) / (\mu U) = 462,087 \text{ 1/m}^2$$

### **Permeability ( $\alpha$ ) for the BWR Fuel Assembly**

For the BWR fuel assembly, the configuration that is considered to provide a bounding value for  $\alpha$  is the 10×10 fuel assembly. The calculation for the  $1/\alpha$  for the entire BWR fuel assembly requires two FLUENT models. A quarter-symmetry model of the fuel rods of the 10×10 fuel assembly was generated using FLUENT, and the cross section of the model is shown in Figure 4.8-. The length of this fuel assembly model is 0.20 m in the axial direction, and consists of approximately 0.6 million cells. The walls of this model correspond to the BWR channel. This assumes that no helium gas flow is occurring between the BWR channel and the wall of the fuel tube. The model in Figure 4.8- does not contain any water tubes that are present in the BWR fuel assembly design. This is considered to be conservative since the cross-sectional area for flow is reduced by not considering gas flow through the water tubes.

This model is used to determine the pressure drop per unit length  $(\Delta P/L)_{\text{ROD}}$  along the fuel rod, as was performed for the PWR fuel. A velocity ( $U$ ) for the gas entering the model was specified to be 0.03 m/s, which represents the velocity observed in the canister evaluation. Since the flow is considered to be laminar, the actual value employed in the evaluation is not significant. Using the  $\Delta P/L$  determined from the three dimensional model the  $1/\alpha$  for the fuel rods is computed by

$$1/\alpha_{\text{ROD}} = (\Delta P/L)_{\text{ROD}} / (\mu U)$$

For the fuel assembly grid for the BWR, the pressure drop determined for the PWR fuel assembly grid was used. The evaluation of the effect of the grid for the PWR corresponds to a 17×17 fuel assembly which would inherently have more obstructions for flow as compared to a worst case 10×10 BWR fuel assembly. The pressure drop across the PWR fuel assembly grid is therefore considered to bound the pressure drop associated with the fuel assembly grid for the BWR design.

To combine the permeabilities into a single quantity, the pressure drop over multiple grids is computed. The bounding configuration was identified in references [23] and [24] for the configuration with the largest combined grid length for all BWR assemblies. The combined pressure drop was calculated by adding  $((\Delta P/L)_{\text{GRID}})$  to the pressure drop  $((\Delta P/L)_{\text{ROD}})$  over the remaining length of the fuel assembly (total fuel assembly length less the total length of the fuel assembly grids). The  $1/\alpha$  for the entire BWR fuel assembly is computed to be

$$1/\alpha_{\text{BWR}} = (\Delta P_{\text{tot}}/L_{\text{tot}}) / (\mu U) = 566,550 \text{ 1/m}^2$$

Figure 4.8-6 Cross-Sectional View of the Three-Dimensional Fluent Model of a 17x17 PWR Fuel Assembly

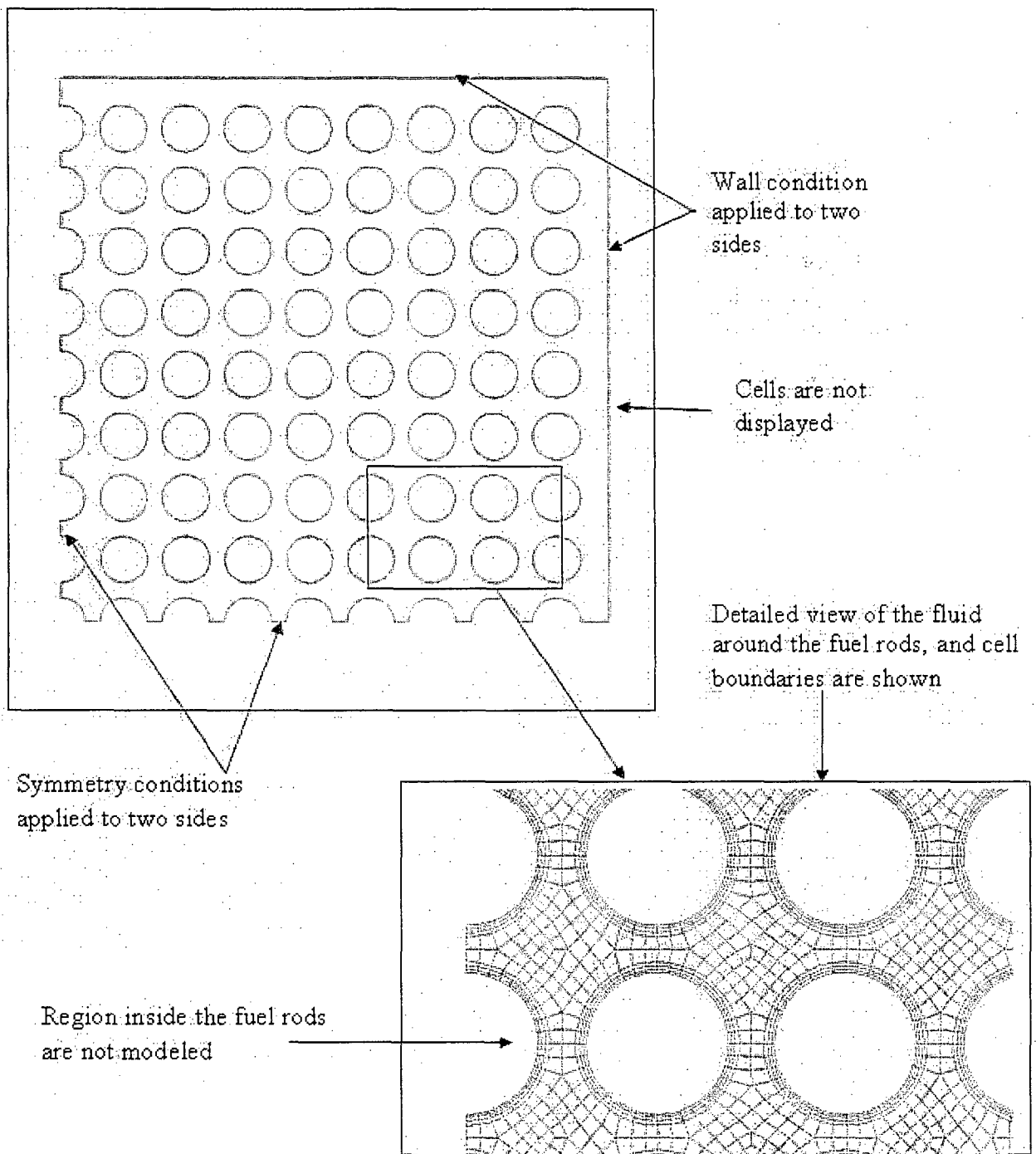


Figure 4.8-7 Three-Dimensional FLUENT Model of a Fuel Assembly Grid

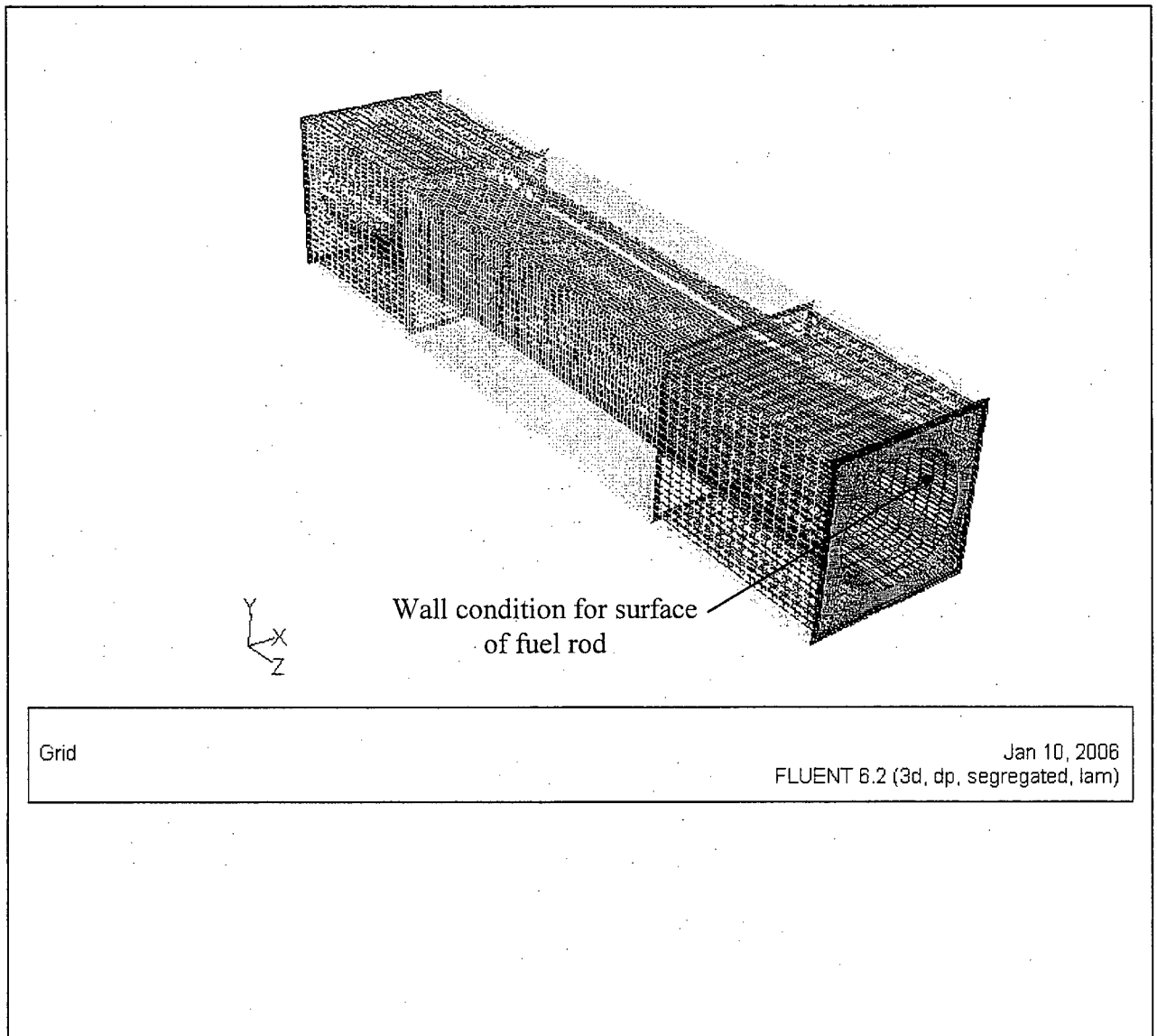


Figure 4.8-8 Three-Dimensional FLUENT Quarter-Symmetry Model for the Flow Around the Grid

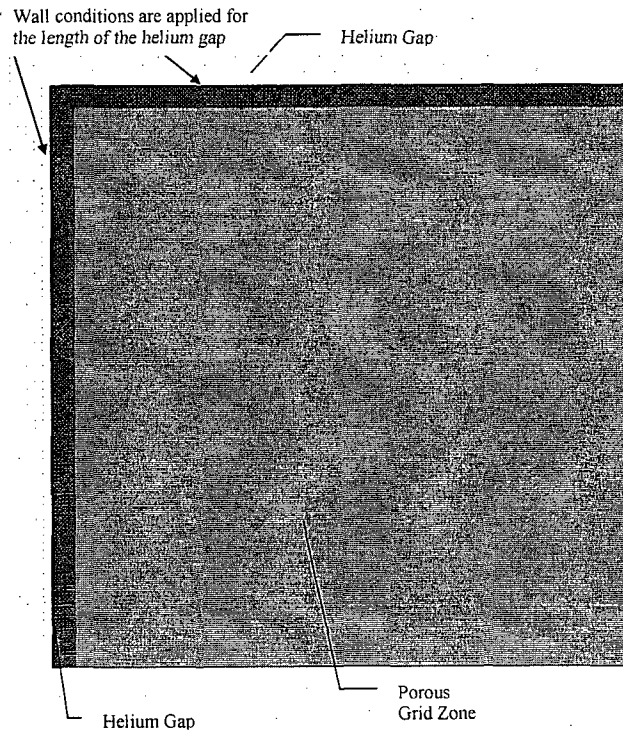
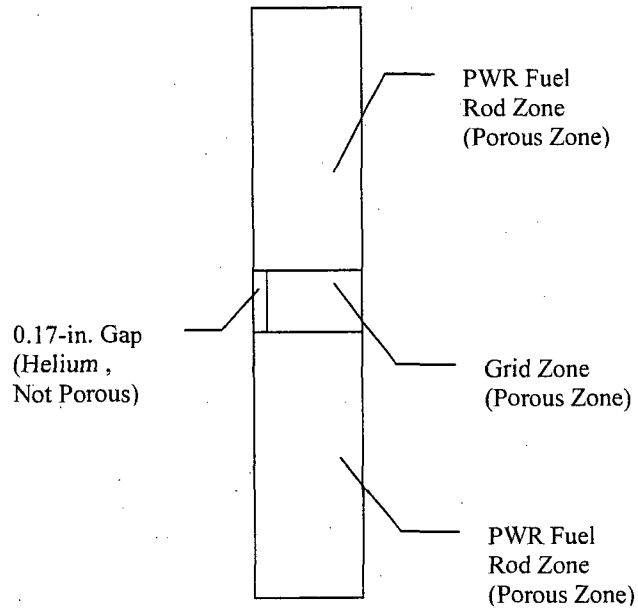
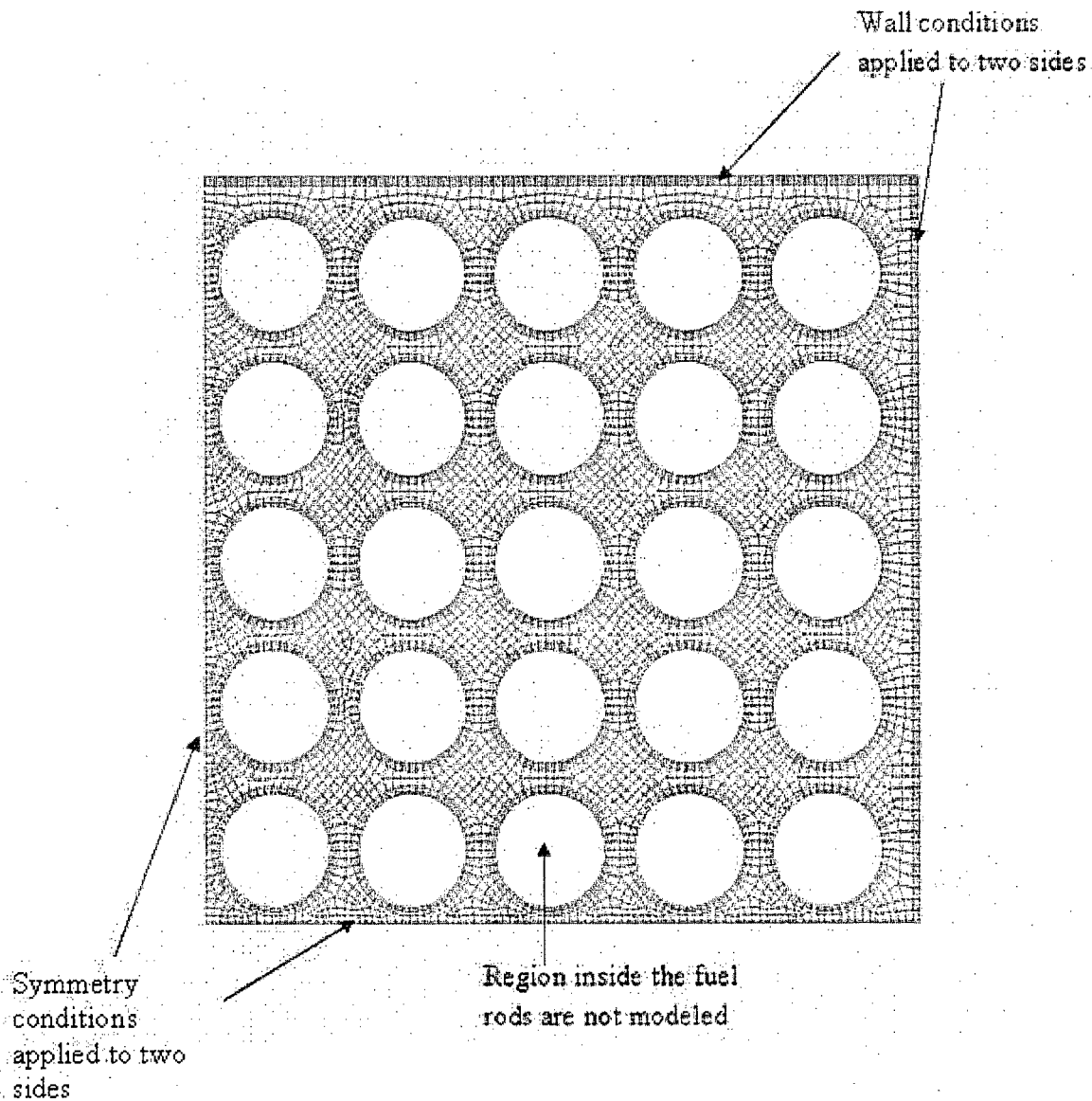


Figure 4.8-9 Cross-Sectional View of the Three-Dimensional FLUENT Model of a 10×10 BWR Fuel Assembly



### 4.8.3 Benchmark Evaluation of the Two-Dimensional Axisymmetric Methodology for Annular Cooling in the Concrete Cask for MAGNASTOR

In this section, a benchmark evaluation is performed to evaluate the adequacy of the  $k-\omega$  and the low Reynold's (low Re)  $k-\epsilon$  turbulent flow models that can be used in the evaluation of the flow in the annulus between the canister and the concrete cask. A thermal evaluation using two-dimensional modeling methodology is performed for a system for which a thermal test has been conducted. The thermal test is described in EPRI TR-100305 [21]. The results of the thermal evaluation using the two-dimensional methodology performed in this section show that both turbulent flow models provide conservative temperatures for the canister surface and the concrete cask liner. This thermal benchmark evaluation confirms that the use of the  $k-\omega$  turbulence model, in conjunction with the two-dimensional methodology, is conservative and, therefore, acceptable for use in the thermal evaluation of MAGNASTOR.

#### 4.8.3.1 Introduction

The thermal design of MAGNASTOR rejects heat from the canister surface to the ambient environment via convection and radiation. Ambient air enters the base of the concrete cask, removes heat via convection from the canister surface, as well as from the surface of the concrete liner, and exits the top of the concrete cask through radial outlets. Radiation of heat from the canister surface to the concrete liner also occurs, which allows the heat to then be convected into the annulus region or conducted through the thickness of the concrete cask. The annulus region is axisymmetric, with the exception of the air inlet and the air outlet, thus lending itself to representation by a two-dimensional axisymmetric model. While the air inlet and air outlet are rectangular in shape, the cross-sectional area of the air inlet and air outlet in an axisymmetric model can vary radially to account for the constant cross-sectional area in the actual test article. A single height for the inlets and outlets can be used, provided the modeled height does not represent more cross-sectional area than the actual inlet and outlet. An important consideration for the analysis of the annulus air flow is the identification of the turbulent flow models. Two models are available:  $k-\omega$  and low Re  $k-\epsilon$  turbulent flow models, which are described in the FLUENT documentation [12]. Selection of the turbulent flow model for MAGNASTOR is based on the thermal test data provided in EPRI TR-100305 [21].

#### 4.8.3.2 Purpose

The purpose of this section is to provide a thermal benchmark, which will demonstrate that the  $k-\epsilon$  turbulent flow model used in the MAGNASTOR thermal evaluation is conservative.



#### **4.8.3.3      Description of the Thermal Test**

In EPRI TR-100305 [21], thermal testing was performed for a vertical concrete cask loaded with a canister containing 17 PWR fuel assemblies with a total heat load of 14.9 kW. The basket contained in the cask during testing was comprised of 17 square slots in which the basket walls were constructed of carbon steel. A series of thermal tests were performed that corresponded to different canister conditions, as well as different air inlet and air outlet conditions. To minimize the uncertainty introduced by other thermal behavior, either inside the canister or outside the canister, the test using the vacuum condition with fully opened vents was employed. This test was conducted inside a large structure, which removed the uncertainty of solar insolation affecting the surface temperatures. Additionally, the method and location in which the inlet temperatures were measured were also documented. Axial profiles of the temperatures for the canister surface, as well as the concrete liner surface, were provided in the results published for the thermal test. The temperature profile provides the basis for the comparison of the performance of the different turbulent flow models.

#### **4.8.3.4      Fluent Model Description**

The FLUENT two-dimensional axisymmetric model of the VSC-17 is comprised of the canister and the concrete cask. The definition of the regions and the cells comprising the model is shown in Figure 4.8-9. Since the vacuum condition is being modeled in the canister, the only region to support fluid flow is the air annulus region between the canister and the concrete liner. The edge of the model corresponds to the outer surface of the concrete cask. The model contains the same changes in direction in the air inlet and the air outlet as exist in the concrete cask used in the thermal test. The heights of the air inlet and air outlet for each segment are selected to allow the physical cross-sectional area to bound the area contained in the FLUENT model.

There are two parameters of interest that influence the heat rejection into the annulus region. Since the heat is being radiated from the canister to the inner liner of the concrete cask, the emissivity of the two facing surfaces (the outer surface of the canister and the inner surface of the liner of the concrete cask) can directly influence the heat transfer. In this evaluation, an emissivity value of 0.7 was used for the carbon steel surfaces. More important is the selection of one of the turbulent flow models for the air flow up through the annulus region: a transitional turbulent flow model ( $k-\omega$  model) or a low Re turbulent flow model (low Re  $k-\epsilon$  model). In FLUENT, either turbulent flow model can be selected. Unlike the specification of emissivity as a property of the surface, the use of a particular turbulence model defines certain requirements for the cells adjacent to the wall. The radial size of the cell divisions near the wall is typically compared to a dimensionless quantity defined as  $y^+$  [12]. Guidelines contained in Reference 12

recommend using a  $y^+$  of near unity for the transitional model ( $k-\omega$ ) and for the low Re  $k-\epsilon$  model. This implies that the near wall cell divisions for the models are significantly refined near the wall.

#### **4.8.3.5 Effective Properties for the Basket and Fuel Region**

For the regions corresponding to the basket, effective properties are employed in the analysis. The effective thermal properties for the basket region are computed using an ANSYS model shown in Figure 4.8-10. In Reference 21, the description of the basket indicates that a cylindrical shell (connected to the outer basket tubes) forms part of the surface facing the inner surface of the canister. Outside of the axial locations that do not have the cylindrical shell, the outer surface of the outer basket slots faces the inner surface of the canister shell directly. The model shown in Figure 4.8-10 models the cylindrical shell for the full length of the basket. The cylinder shell, where it does exist in the canister used in the thermal test, provides an additional radiation shield that reduces the effectiveness of the radiation heat transfer from the outer basket tubes to the canister shell. This would result in higher basket temperatures in the analyses. In the FLUENT model in Figure 4.8-9, there is a gap between the outer radius of the cylindrical shell and the inner surface of the canister. Between these two surfaces, radiation is simulated using conduction properties that have a cubic temperature dependency.

The basket cross-section model contains the carbon steel basket and the fuel regions, which are modeled with homogeneous orthotropic thermal conductivities. To determine the temperature-dependent effective thermal conductivity of the basket region, a series of temperatures is applied to the boundary of the model (as shown in Figure 4.8-10). Solutions for each boundary condition determine the maximum temperature of the basket and the associated change in temperature from the boundary to the maximum temperature location. The effective thermal conductivities are determined using the same expression employed for MAGNASTOR in Section 4.4.1.2.

#### **4.8.3.6 Boundary Conditions**

The outer edges of the model correspond to the outer surface of the concrete cask. Two cases are presented in this section to assess the performance of each turbulent flow model. The boundary conditions employed for each model were identical, with the exception of the selection of the turbulent flow model.

#### **Temperature Specification**

The edge of the model includes not only the air inlet and the air outlet, but also the remainder of the concrete cask surface. For the air inlets, the average temperature of the test recorded ambients for the vacuum test for the fully opened inlets (Run No. 6 in [21]) was applied as the

temperature for the air inlet in the model. For the remainder of the concrete cask surface, a temperature of 26°C was used for computation of the heat transfer by natural convection from the side and top of the concrete cask. A film coefficient was also specified for the bottom surface of the model to maximize the heat transfer to the base, thereby reducing the heat flux to the canister surface.

### **Heat Generation**

The total heat load applied to the active fuel region of the model was 14.9 kW, and a user specified function reflected the power profile curve for the fuel in EPRI TR-100305 [21]. The power distribution has a peaking factor of 1.2. The heat generation was assumed to be uniformly distributed over the radial direction from the basket centerline to the outer radius of the porous media region.

### **Buoyancy**

Since the annulus gas was specified as an ideal gas, the only condition required to enact buoyancy as a driving force for the air is to set the gravity acceleration as  $-9.8 \text{ m/sec}^2$ .

An additional parameter that must be specified is the “operating” density at the air inlet. Since the annulus gas is being treated as an ideal gas, the “operating” density was specified to be the density of the gas at the inlet temperature for a site elevation of 1,400 m.

#### **4.8.3.7 Analysis Results**

The temperature profiles for the two turbulent flow models for the canister surface and for the concrete cask liner surface are shown in Figure 4.8-11 and Figure 4.8-12, respectively. The results confirm that both turbulent flow models conservatively predict the temperatures on both the canister surface and the concrete liner surface. The temperature profiles for the low Re k- $\epsilon$  model provided a slight improvement over the k- $\omega$  turbulent flow model.

#### **4.8.3.8 Application of the Benchmark to the MAGNASTOR Evaluation**

The primary purpose of the preparation of this benchmark is to confirm the selection of the turbulent flow model, and for this reason, the vacuum test in EPRI TR-100305 [21] was selected, which minimized the uncertainties of the thermal behavior internal to the canister. The air flow in the annulus is primarily controlled by the height, the radial thickness of the annulus and the heat load. Since the test in EPRI TR-100305 [21] employed actual fuel assemblies, the height of the annulus in the thermal test and in the MAGNASTOR design are sufficiently similar. The thicknesses of the annulus region for the thermal test and for the MAGNASTOR are 3 inches and 3.75 inches, respectively. A metric for buoyancy-driven flows for vertical parallel surfaces is a

modified Rayleigh's number in which the standard Rayleigh number is factored by the ratio (D/L) of the gap thickness (D) and the length (L). Since D/L is actually larger for the MAGNASTOR design, this would indicate that the modified Rayleigh number is larger for MAGNASTOR, resulting in increased convection. Likewise, the design basis heat load for MAGNASTOR is 35.5 kW, as compared to the thermal test using 14.9 kW. Increased heat load would only increase the level of turbulence in the annulus region.

#### **4.8.3.9      Conclusions**

In this section, a thermal evaluation has been performed for the thermal test described in EPRI TR-100305 [21]. The analysis results indicate that the two-dimensional axisymmetric modeling methodology using the k- $\omega$  turbulent flow model is acceptable to determine a bounding maximum fuel temperature and bounding concrete temperatures. The benchmark also confirms the use of the operating density associated with the ambient temperature for the concrete cask.

Figure 4.8-9 Two-Dimensional Axisymmetric FLUENT Model of the VSC-17

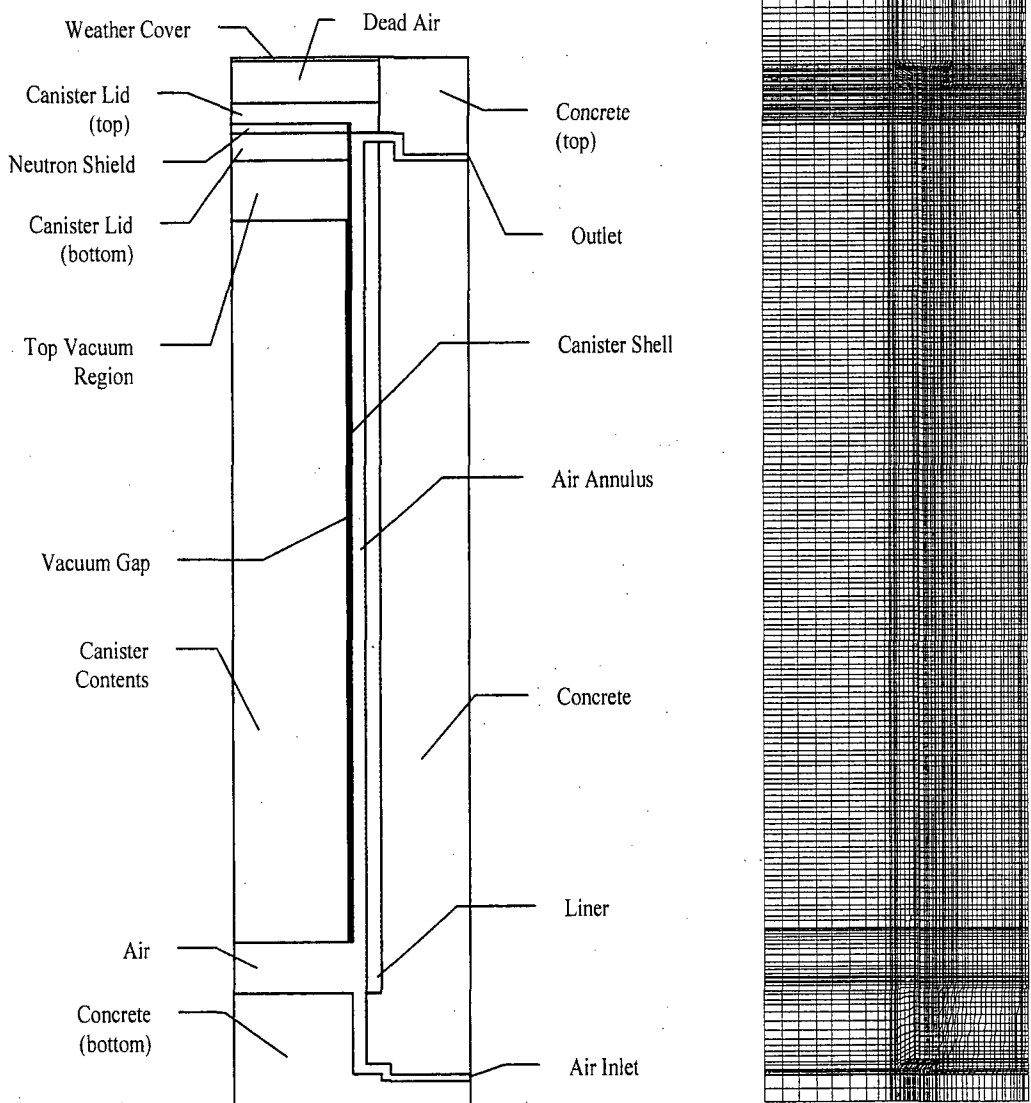


Figure 4.8-10 ANSYS Model for Effective Properties Calculation

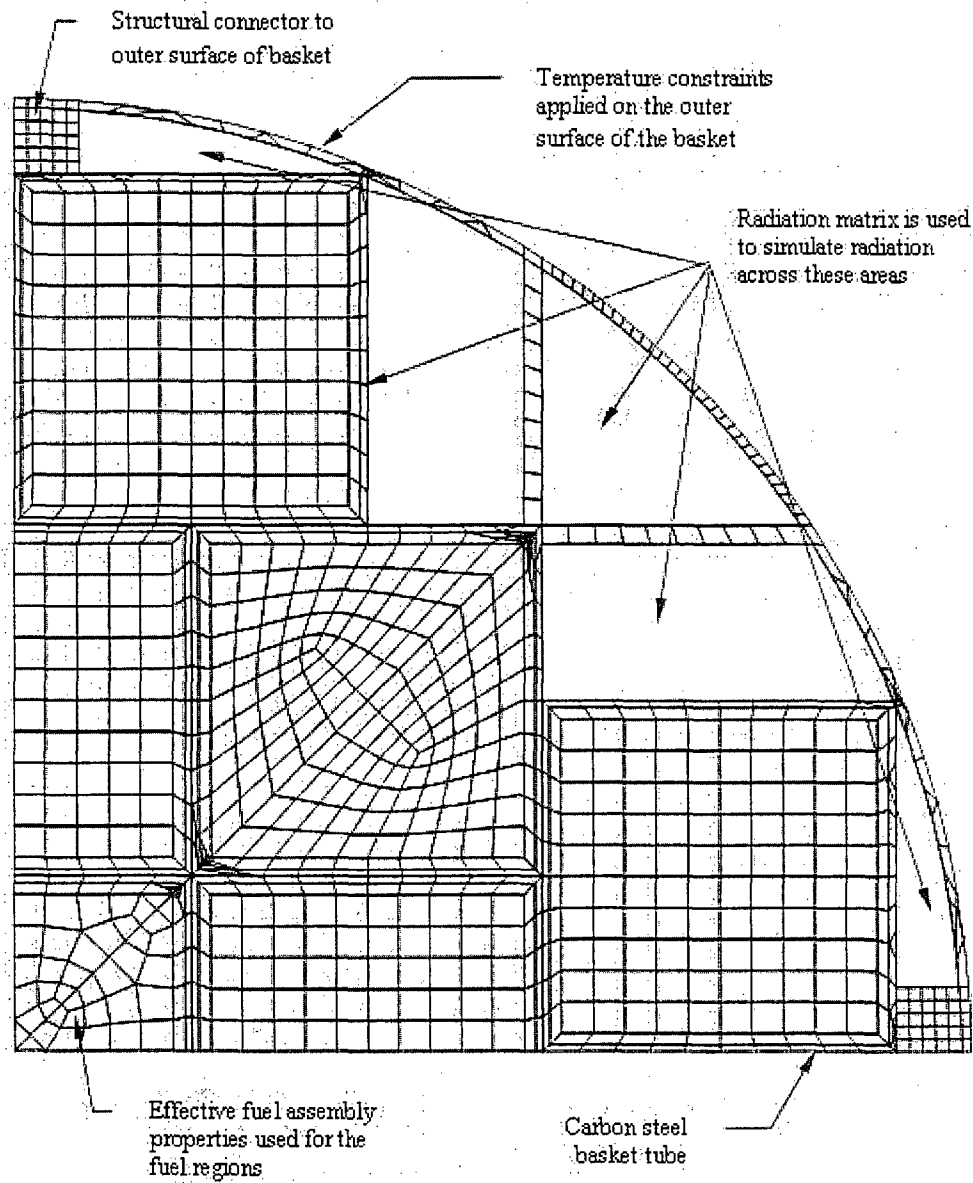


Figure 4.8-11 Temperature Profiles for the Canister Surface

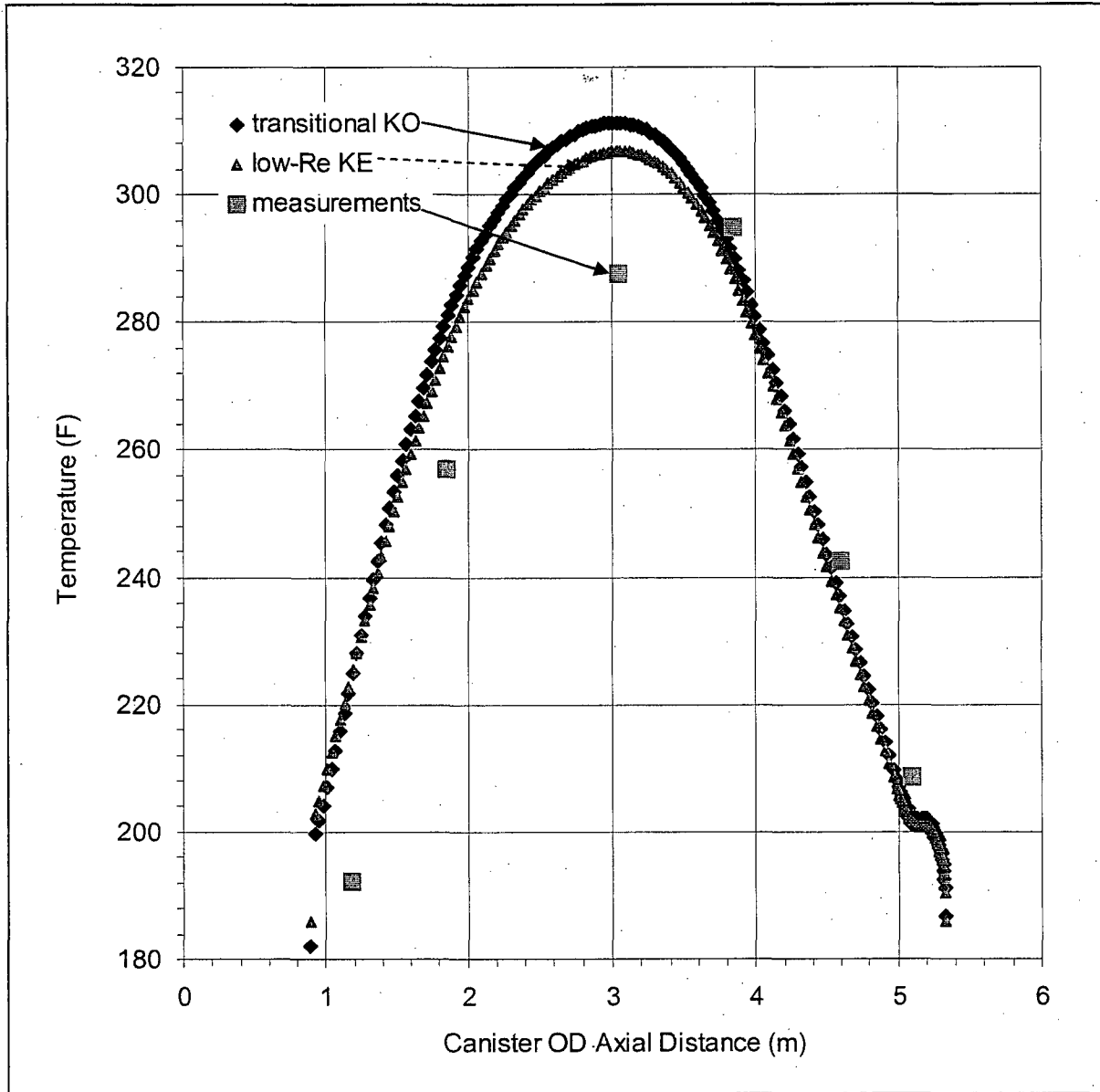


Figure 4.8-12 Temperature Profiles for the Concrete Liner Surface

